Handbook on the Physics and Chemistry of Rare Earths
Vol. 37
edited by K.A. Gschneidner, Jr., J.-C.G. Bünzli and V.K. Pecharsky

ISSN: 0168-1273/DOI: 10.1016/S0168-1273(07)37035-9

Chapter 235

LANTHANIDE NEAR-INFRARED LUMINESCENCE IN MOLECULAR PROBES AND DEVICES

Steve COMBY and Jean-Claude G. BÜNZLI
École Polytechnique Fédérale de Lausanne (EPFL), Laboratory of Lanthanide Supramolecular Chemistry, BCH 1402, CH-1015 Lausanne, Switzerland
E-mail: jean-claude.bunzli@epfl.ch

Contents

List of abbreviations

8-Q	8-hydroxyquinolinate
aad	adamantylideneadamantane-1,2-dioxetane
ac	acetate
acac	acetylacetonate
AMP	amplifying waveguide spiral
ba	benzoylacetonate
bath	monobathophenantholine
BCP	bathocuproine
bdc	1,4-benzenedicarboxylate
bdc-F_4	2,3,5,6-tetrafluoro-1,4-benzenedicarboxylate
bppz	2,3-bis-(2-pyridyl)pyrazine
bptz	3,6-bis-(2-pyridyl)tetrazine
bpy	2,2′-bipyridine
bpym	2,2′-bipyrimidine
bpypz	3,5-di(2-pyridyl)pyrazolate
BSA	bovine serum albumin
btfa	benzoyltrifluoroacetonate
CD	circular dichroism
CL	chemiluminescence
CN	coordination number
CoP	(cyclopentadienyl)tris(diethylphosphito)cobaltate(I) anion
CPL	circularly polarized luminescence
CSA	cationic surfactant
cw	continuous wave
cyclam	1,4,8,11-tetraazacyclotetradecane
cyclen	1,4,7,10-tetraaza-dodecane
dam	diantipyrylmethanate
daphm	diantipyrylphenylmethanate
dapm	diantipyrylpropylmethanate
dbm	dibenzoylmethanate
DEDMS	diethoxydimethylsilane
DEMS	diethoxymethylsilane
dithi	2-dithienyl-2,2′-bipyridazine
dme	1,2-dimethoxy-ethane

dmf	dimethylformamide
dmp	dipivaloylmethanate
dmso	dimethylsulfoxide
DNA	deoxyribonucleic acid
dnm	dinaphthoylmethanate
do3a	1,4,7,10-tetraaza-cyclododecane-N,N',N''-triacetate
dota	1,4,7,10-tetraaza-cyclododecane-N,N',N'',N'''-tetraacetate
dotma	1R,4R,7R,10R-$\alpha,\alpha',\alpha'',\alpha'''$-tetramethyl-1,4,7,10-tetraaza-cyclododecane-1,4,7,10-tetra-acetate
dotp	1,4,7,10-tetraazacyclododecane-1,4,7,10-tetrakis-methylene-phosphonate
dpa	pyridine-2,6-dicarboxylate (dipicolinate)
dpga	diphenylguanidine
dpm	dipivaloylmethanate
dppm	bis(diphenylphosphinomethane)
dtpa	diethylenetrinitrilopentaacetate
dtta	diethylenetriaminetetraacetate
ECL	electrochemically generated luminescence
edta	ethylenediamine-N,N',N'',N'''-tetraacetate
ELISA	enzyme-linked immunosorbent assay
ESA	excited state absorption
ET	electron transfer
Etonium	1,2-ethanediaminium, N,N'-bis[2-(decyloxy)-2-oxo-ethyl]-N,N,N',N'-tetramethyl-dichloride
ETU	energy transfer up-conversion
fac	facial
FAU	Faujasite
fod	6,6,7,7,8,8,8-heptafluoro-2,2-dimethyl-3,5-octadionate
fwhh	full width at half height
fx	fluorexon
had	hexaaza-triphenylene
HBS	HEPES-buffered saline buffer
hCG	human chorionic gonadotropin
HEPES	N-(2-hydroxyethyl)-piperazine-N'-2-ethanesulfonic acid
hesa	hexylsalicylate
hfa	hexafluoroacetylacetonate
HOMO	highest occupied molecular orbital
HPLC	high performance liquid chromatography
HSA	human serum albumin
HSAB	hard and soft acid and base theory
IgG	immunoglobulin G
im	imidazole
ITO	indium tin oxide
IUPAC	Internationl Union of Pure and Applied Chemistry
LB	Langmuir–Blodgett
LCD	liquid crystal display
LD	laser diode
LED	light emitting diode
LF	ligand field
LLCT	ligand-to-ligand charge transfer state
LMCT	ligand-to-metal charge transfer state
LUMO	lowest unoccupied molecular orbital
MBBA	N-(p-methoxybenzylidene)-p-butylaniline
MCD	magnetic circular dichroism
MDMO-PPV	polyl[2-methoxy-5-(3′,7′-dimethyl-octyloxy)]-p-phenylene vinylene
mgl	1-deoxy-1-(methylamino)glucitol
MLCT	metal-to-ligand charge transfer state
MMA	methylmethacrylate
MOF	metal–organic framework (coordination polymer)
MRI	magnetic resonance imaging
NASI	N-acryloxysuccinimide

NIR	near infrared
NIT2py	4,4,5,5-tetramethyl-2-(2′-pyridyl)-4,5-dihydro-1*H*-imidazol-1-oxyl 3-oxide
NMR	nuclear magnetic resonance
nta	nitrilotriacetate
NTA	4,4,4-trifluoro-1-(2-naphthyl)-1,3-butanedionate
OEP	octaethylporphyrinate
OLED	organic light emitting diode
Otf	trifluoromethanesulfonate
ox	oxalate
PAN	1-(2-pyridylazo)-2-naphthol
PAR	1-(2-pyridylazo)resorcinol
pbs	bis(perfluorobutylsulfonyl)imide, $[C_4F_9SO_2]_2N$
Pc	phthalocyanine
pdon	1,10-phenanthroline-5,6-dione
PEDOT	poly(3,4-ethylene dioxythiophene)
PEG	polyethyleneglycol
PET	photoinduced electron transfer
phen	1,10-phenanthroline
PMMA	polymethylmethacrylate
pms	bis(perfluoromethylsulfonyl)-aminate or bis(trifluoromethanesulfonyl)-imide (Tf_2N)
poa	perfluorooctanoylacetate
pom	perfluorooctanoylmethanate
POM	polyoxometalates
pos	bis(perfluorooctylsulfonyl)-aminate
PS	Phthalexon S
PSS	polystyrene sulfonate
PVK	poly-(*N*-vinylcarbazole)
PVV	poly(phenylene–vinylene)
py	pyridine
P-FiPMA	polyhexafluoroisopropylmeth-acrylate
qb	4-(4-(3-triethyoxysilylpropoxy)-phenylazo)-phenyl-diphenyl phosphine oxide
Quin	2-methyl-8-hydroxyquinolinate
RTIL	room temperature ionic liquid
SAP	square antiprism
SHE	standard hydrogen electrode
SOMO	single occupied molecular orbital
stta	mono-thio-thenoyltrifluoro-acetonate
tbo	trimethylenebis(oxamide)
TBP	tetrabenzoporphyrinate
TEOS	tetraethyl orthosilicate
Tf_2N	bis(trifluoromethanesulfonyl)-imide or bis(perfluoromethylsulfonyl)-aminate (pms)
TGA	thermogravimetric analysis
thf	tetrahydrofuran
TMA	tetramethylammonium
TMOS	tetramethoxysilane
topo	trioctylphosphine oxide
Tos	tosylate
Tp^H	hydridotris(1-pyrazolyl)borate
TPD	*N*,*N*-diphenyl-*N*,*N*-bis(3-methylphenyl)-[1,1′-biphenyl]-4,4′-diamine
tpen	tetrakis(2-pyridylmethyl)-ethylenediamine
TPP	tetraphenylporphyrinate
tppo	triphenylphosphine oxide
tpy	2,2′:6′,2″-terpyridine
Tris	2-amino-2-(hydroxymethyl)-propane-1,3-diol
Trp	tryptophan
TSAP	twisted square antiprism
tta	thenoyltrifluoro-acetylacetonate
TTP	tetra-*para*-tolylporphyrinate
UPT	up-converting phosphor technology
WDM	wavelength division multiplexer
Wt%	weight percent
YAG	yttrium aluminum garnet
YLF	yttrium lithium fluoride
XO	xylenol orange

1. Outline and scope of the review

Trivalent lanthanide ions offer a wide variety of opportunities to spectrochemists in that their $[Xe]4f^N$ electronic configuration generates numerous electronic levels, up to 3432 for Gd^{III}, for instance. These ions display three types of electronic transitions. Charge transfer transitions, both ligand-to-metal (LMCT) and metal-to-ligand (MLCT), are allowed by Laporte's selection rule. Their energy is usually high, so that they appear in the UV above 40 000 cm^{-1}, except for the ions which may be relatively easily either reduced to their +2 state (Sm^{III}, Eu^{III}, Tm^{III}, Yb^{III}), or oxidized to their +4 state (Ce^{III}, Pr^{III}, Tb^{III}). In these cases, the broad charge transfer transitions may occur at energies as low as 30 000 cm^{-1}. To illustrate this point, energies of the 2p(O)–4f LMCT transitions are plotted in fig. 1, using data from the Phosphor Handbook (Shionoya and Yen, 1999). From a practical viewpoint, LMCT transitions are used to pump energy into the lamp phosphors containing Eu^{III} or Tb^{III}, for instance. The second kind of transitions corresponds to the promotion of a 4f electron into the 5d sub-shell; such transitions are also allowed by the parity rule, resulting in sizeable oscillator strengths with absorption coefficients in the range 10^{-2}–10^{3} M^{-1} cm^{-1}, that is, comparable to those of the charge transfer transitions. Their energy depends largely upon the metal environment because 5d orbitals are external and they interact directly with ligand orbitals; however, these transitions are also quite energetic and only those of Ce^{III}, Pr^{III} and Tb^{III} are commonly observed below 50 000 cm^{-1}. Energies of the 4f–5d transitions in calcium fluoride matrix are reported in fig. 1, from literature data compiled by Dorenbos (2003). Finally, lanthanide trivalent ions display sharp f–f transitions, involving the rearrangement of the electrons in the 4f sub-shell and are therefore forbidden, which explains their faint intensities, with absorption coefficients smaller than 10 M^{-1} cm^{-1} and even often smaller than 1 M^{-1} cm^{-1}. These transitions are quite narrow and the barycenter of the ligand-field split bands is fairly insensitive to the metal ion environment. As a consequence, they are easily recognizable and therefore lanthanide ions are ideal candidates for optical probes.

Most of the lanthanide trivalent ions are luminescent, either fluorescent (Pr^{III}, Nd^{III}, Ho^{III}, Er^{III}, Yb^{III}) or phosphorescent (Sm^{III}, Eu^{III}, Gd^{III}, Tb^{III}, Dy^{III}, Tm^{III}) or both. Their emission covers the entire spectrum (0.3–3 μm), from UV (Gd^{III}) to visible (e.g. blue Tm^{III}, green Tb^{III}, orange Sm^{III}, or red Eu^{III}), and NIR spectral ranges (see below). The Stokes shifts are extremely small since the rearrangement of the electrons in the 4f sub-shell does not lead to much change in the chemical bond lengths, contrary to what is observed with organic compounds or d-transition metal ions; the configurational coordinate diagrams of fig. 2 depicts these two situations; when the excited state potential energy curve is displaced with respect to the ground level curve, vertical excitation following the Franck–Condon principle leads to vibrationally excited states and the same is valid for deexcitation, resulting in broad band spectra. The contrary holds for Ln^{III} ions and therefore the emission bands are narrow and the radiated colors are rather pure, so that they may be used in trichromatic phosphors for lighting

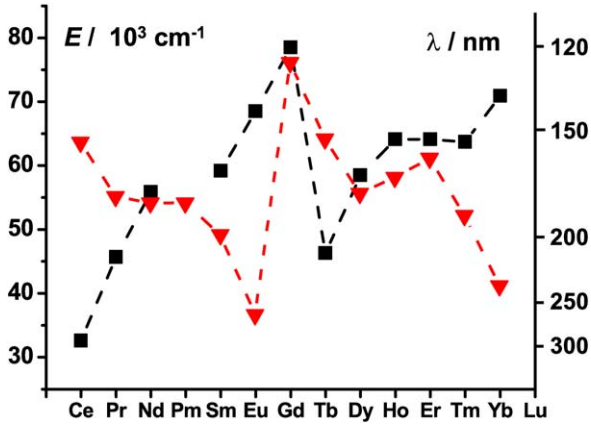

Fig. 1. Energy of the 2p(O)–4f LMCT transitions (▼) (Shionoya and Yen, 1999) and of the 4f–5d transitions of Ln^{III} ions in a CaF_2 matrix (■) (Dorenbos, 2003).

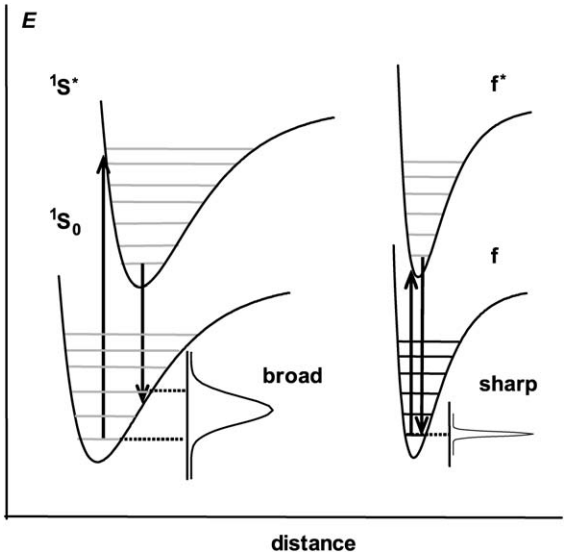

Fig. 2. Sharp emission from Ln^{III} ions due to the small offset of the electronic levels as shown from the configurational coordinate diagram (right); as a comparison, the case of an organic molecule is depicted on the left ($^1S_0$ = singlet ground state, $^1S^*$ = singlet excited state).

purposes. Two ions, La^{III} and Lu^{III}, have no f–f transitions and are not luminescent, while Ce^{III} displays an intense d–f emission which can be tuned from 290 to 500 nm. Ions in other oxidation states are also luminescent, but in this review we restrict ourselves to trivalent ions.

Initially, interest for NIR emission of lanthanide ions stemmed from the development of optical fibers, lasers and amplifiers for telecommunication (Kido and Okamoto, 2002; Kuriki et al., 2002) and there are a wealth of theoretical and technical papers published in this area. Up-conversion processes have also been the subject of intense investigations (Auzel, 2004). These two areas of research and development mostly deal with purely inorganic compounds or, more recently, with luminescent polymers; they will not be covered in this chapter, with the exception of the latter, which will be partly described.

The large attention noted presently for NIR-emitting molecular compounds originates from needs in medical diagnostic. Imaging technologies developed over the past thirty years, such as magnetic resonance imaging, X-ray or nuclear tomography, have revolutionized clinical medicine. Several parameters influence the final result, resolution, depth penetration, availability of biocompatible and targeted probes, as well as the detection threshold of the latter (Weissleder, 2001). During the past decade, *in vivo* optical detection of tumors by means of near infrared photons has gained momentum (Becker et al., 2001; Kim et al., 2004; Weissleder et al., 1999) because it represents a non-invasive technique allowing the exploration of deeper tissues, the investigation range extending from a few mm up to 20 cm (Weissleder and Ntziachristos, 2003). Indeed, biological tissues have very low absorption coefficients above 700 nm and, in addition, the absorption of water, a major component of biological tissues, diminishes drastically above 900 nm. The development of targeted NIR fluorophores coupled to peptides prompted applications in clinical situations where other imaging techniques are not an option. Until now, most of these clinical applications have made use of organic dyes as probes for NIR imaging and differentiation between the target and background fluorescence has been achieved by molecular switches or beacons (protease-triggered NIR probes) which can be activated *in vivo* by a suitable biochemical reaction (Weissleder, 2001).

An alternate strategy would be to resort to bioprobes incorporating NIR-emitting lanthanide ions (Dossing, 2005; Faulkner et al., 2005). Similarly to the visible-emitting Ln^{III} ions, which are well-known optical probes (Bünzli, 2004; Bünzli, 2005; Bünzli and Piguet, 2005), the main advantages of these ions lie in their easily recognizable atom-like spectra and large Stokes shifts when they are excited through the ligand levels. In addition, time-resolved luminescence allows one to achieve a high signal-to-noise ratio since the lifetimes of the Ln^{III} emissive states are substantially longer than those of organic material. Synthetic strategies are now at hand to insert Ln^{III} ions in a variety of molecular and supramolecular assemblies (Piguet and Bünzli, 1999) which control and even enhance their photophysical properties through the so-called sensitization process since f–f transitions have too small oscillator strengths to yield an efficient excitation path (Bünzli and Piguet, 2005).

In this review, we mainly concentrate on molecular, NIR-emitting compounds containing Nd^{III}, Er^{III}, or Yb^{III}; discrete molecular edifices containing other ions emitting in this range but less relevant to the problematic dealt with here, namely Pr^{III}, Sm^{III}, Dy^{III}, Ho^{III}, and Tm^{III}, have been far less studied and will only be mentioned when relevant. After a brief introduction on the photophysics of near-infrared emitting trivalent lanthanide ions, we describe the various synthetic strategies proposed for encapsulating these ions into molecular edifices and making use of macrocyclic or acyclic ligands or of d-transition metal complexes. Novel approaches

resorting to inorganic clusters, inorganic–organic hybrids (coordination polymers), nanoparticles, or ionic liquids will also be outlined. The chapter ends by a short overview on potential applications, including medical imaging and by a critical evaluation of the chromophores for sensitizing NIR-emitting trivalent lanthanide ions. Separation between the description of NIR-emitting molecular complexes and applications is not always unambiguous, so that in several instances, the motivation for and requirements of applications are described in section 3 rather than in section 4.

Literature is covered up to the end of September 2006.

2. Photophysics of near-infrared emitting trivalent lanthanide ions

The photophysics of the NIR-emitting lanthanide ions is not fundamentally different from that of the UV or visible-emitting ions. Intrinsically, f–f transitions are weak and the main objectives of synthetic chemists tailoring adequate environments for luminescent lanthanide ions is firstly to increase the amount of energy which can be pumped into the excited states and secondly to minimize radiationless deactivation processes. For the free ions, the latter are more efficient if the energy gap between the lowest ligand-field sub-level of the excited state and the highest electronic level of the ground state is small. This is unfortunately the case for most of the NIR-emitting ions.

2.1. *Near-infrared transitions*

Formally, the NIR spectral range starts at 750 nm and many trivalent lanthanide ions display transitions with wavelengths longer than 750 nm, including, for instance, the red emitter Eu^{III} which has a weak transition around 820 nm originating from the $^5D_0$ level ($^5D_0 \rightarrow {}^7F_6$) and several other weak transitions between 2 and 2.6 μm assigned to transitions between the ^7F_J sublevels (Carnall et al., 1962). However, known practical applications of NIR luminescence often make use of radiation around 1.32 and 1.55 μm, the so-called telecommunication windows, in which silica is particularly transparent. Praseodymium, neodymium, and possibly dysprosium, cover the first wavelength. Erbium is ideally suited for the second, in particular erbium-doped amplifiers compensate for losses in optical fibers. Neodymium is of course also well known for its 1.06 μm laser line used in the yttrium aluminum garnet (YAG) laser either as spectroscopy light source or for nuclear fusion. For biological tissues, the spectral range of interest is approximately 0.85–1.1 μm, where light transmission is maximized. For these reasons, we shall mostly concentrate on ions emitting sizable luminescence above 850 nm and below 1.6 μm, even if some applications rely on laser lines with longer wavelength, e.g. the holmium transition around 2.1 μm for medical applications. Some relevant electronic levels of NIR-emitting Ln^{III} ions are reported in fig. 3, where the luminescent levels are indicated by black down triangles when the transition terminates on one of the sub-levels of the ground state while other transitions are designated by arrows. A list of the main NIR transitions can be found in table 1. With the exception of Pr^{III} and Sm^{III}, the NIR-emitting ions are fluorescent. Several of them have complex photophysical properties (Tanabe, 2002), featuring emission in both visible and NIR spectral

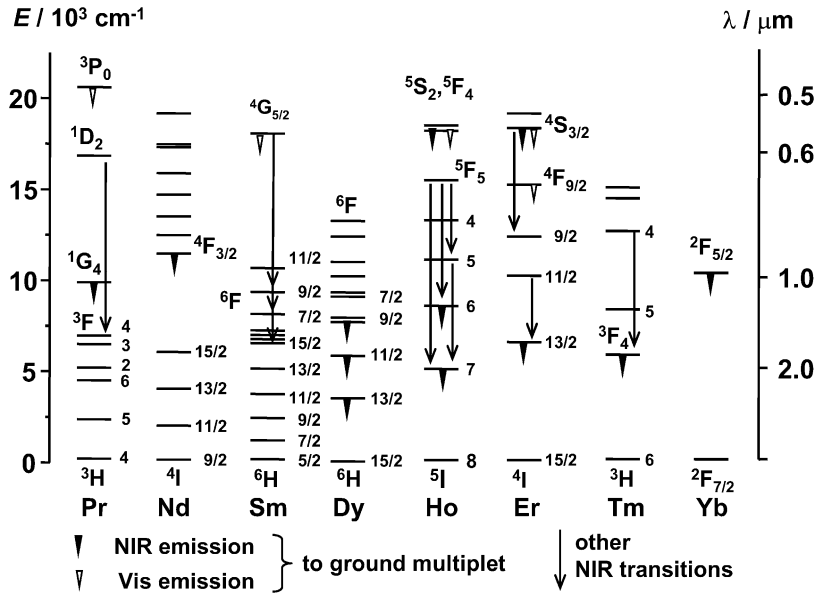

Fig. 3. Partial energy diagrams of NIR-emitting trivalent lanthanide ions. Energies are for the aquo-ions (Carnall et al., 1968; Carnall, 1979).

ranges, that have been thoroughly studied in inorganic matrices (Crosswhite and Moos, 1967; Dieke, 1968) and in solid state materials for the development of lasers (Reisfeld and Jorgensen, 1977), up-conversion devices (Auzel, 2004), optical amplifiers (Kuriki et al., 2002) or organic light emitting diodes (Kido and Okamoto, 2002).

As for the ions of prime interest for this review, Nd^{III} displays fluorescence in three distinct spectral ranges: 0.87–0.92, 1.06–1.09, and 1.32–1.39 μm ($^4F_{3/2} \rightarrow {}^4I_{9/2}$, $^4I_{11/2}$, $^4I_{13/2}$ transitions), the second line being the well known laser line produced by Nd:YAG lasers, which can be doubled (532 nm, green light, e.g. for laser pointers), tripled (355 nm, blue) or quadrupled (266 nm); these lasers enter in a variety of analytical and industrial applications and can reach extremely high powers (up to 20 MW in nuclear fusion machines). The YAG matrix can also be co-doped with other trivalent lanthanide ions, providing a whole range of other interesting emission lines. The longer wavelength line of Nd^{III} occurs in the middle of the first telecommunication window and has drawn attention for amplification of the 1.3 μm signals. Er^{III} has a more complicated photophysics with several emission lines both in the visible (from the $^4S_{3/2}$ excited level) and in the NIR range, in addition to having up-conversion capability (Auzel, 2004); the main line of significance here is however the $^4I_{13/2} \rightarrow {}^4I_{15/2}$ transition around 1.54 μm on which most fiber optic telecommunication amplifiers are based (Weber et al., 1998). Recently, another IR line has been evidenced in yttrium oxide matrix, at 1.75 μm, assigned to the $^4S_{3/2} \rightarrow {}^4I_{9/2}$ transition from Er^{III} in a C_2 site (Zhang et al., 2004).

Table 1
Properties of the main NIR-emitting trivalent lanthanide ions

Ln	G[a]	I[b]	F[c]	λ (μm)	E (cm^{-1})	Comment
Pr	$^3H_4$	$^1D_2$	$^3F_4$	1.01–1.04	9890–9600	
		$^1G_4$	$^3H_5$	1.30–1.33	7700–7540	Telecom line
		$^1D_2$	$^1G_4$	1.44	6940	
Nd	$^4I_{9/2}$	$^4F_{3/2}$	$^4I_{9/2}$	0.87–0.92	11 500–10 870	
			$^4I_{11/2}$	1.06–1.09	9430–9170	Laser line
			$^4I_{13/2}$	1.32–1.39	7575–7195	Telecom line
			$^4I_{15/2}$	1.84–1.86	5410–5375	
Sm	$^6H_{5/2}$	$^4G_{5/2}$	$^6F_{1/2}$	0.88	11 385	
			$^6F_{7/2}$	1.02–1.04	9790–9660	
			$^6F_{9/2}$	1.16–1.17	8630–8570	
Dy	$^6H_{15/2}$	$^6H_{9/2}$, $^6F_{11/2}$	$^6H_{15/2}$	1.28–1.34	7810–7575	Telecom line
		$^6H_{11/2}$	$^6H_{15/2}$	1.7–1.8	5880–5555	
		$^6H_{13/2}$	$^6H_{15/2}$	2.89–3.02	3460–3310	
Ho	$^5I_8$	$^5F_5$	$^5I_7$	0.98–0.99	10 250–10 100	
			$^5I_6$	1.48–1.51	6760–6630	
			$^5I_5$	2.39–2.45	4180–4090	
		$^5I_5$	$^5I_7$	1.63–1.68	6120–5965	
		$^5I_6$	$^5I_8$	1.16–1.19	8650–8370	
		$^5I_7$	$^5I_8$	1.98–2.10	5050–4760	Laser line, medical applications
Er	$^4I_{15/2}$	$^4I_{13/2}$	$^4I_{15/2}$	1.54–1.60	6500–6250	Telecom line
		$^4S_{3/2}$	$^4I_{9/2}$	1.7	5880	Laser line
		$^4I_{11/2}$	$^4I_{13/2}$	2.7	3700	Laser line
Tm	$^3H_6$	$^3F_4$	$^3H_6$	1.75–1.90	5730–5260	
		$^3H_4$	$^3H_5$	2.33	4290	
Yb	$^2F_{7/2}$	$^2F_{5/2}$	$^2F_{7/2}$	0.96–1.03	10 400–9710	

[a]Ground level.
[b]Initial level.
[c]Final level.

Finally, Yb^{III} possesses a single emission line in the range 0.98–1.03 μm, owing to its extremely simple electronic structure with one unpaired electron. Typical spectra of these three NIR-emitting ions are presented in fig. 4.

Among the other NIR-emitting ions, Pr^{III} has two main NIR bands at 1.04 μm ($^1D_2 \rightarrow {}^3F_4$) and 1.3 μm ($^1G_4 \rightarrow {}^3H_5$), the latter being used in telecommunications for amplification of the 1.3 μm signals; it is also often a component of solid state optical materials in view of its ability of generating up-conversion, that is blue emission from its $^3P_0$ level upon two- or three-photon pumping of the $^1G_4$ or $^1D_2$ state. Trivalent samarium Sm^{III} features three spin-forbidden NIR emission lines from the $^4G_{5/2}$ excited state to sublevels of the first excited spectroscopic term, namely ^6F_J with $J = 9/2$, 7/2, and 5/2; emission from the same excited level to the ground multiplet yields lines in the visible range, between 560 and 650 nm, and one NIR line at 710 nm ($^4G_{5/2} \rightarrow {}^6H_{11/2}$). Less well known Dy^{III} exhibits three NIR emission bands, one

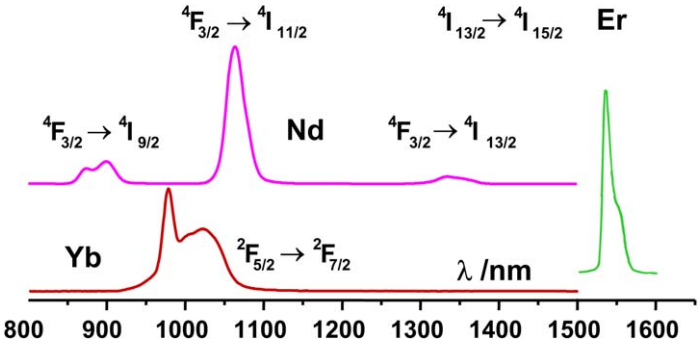

Fig. 4. Typical NIR emission spectra of Nd^{III}, Er^{III}, and Yb^{III}.

around 1.34 μm ($^6H_{9/2}$, $^6F_{11/2} \rightarrow {}^6H_{15/2}$) which has been considered as a third candidate for amplification of the 1.3-μm signals (Page et al., 1997), one ($^6H_{11/2} \rightarrow {}^6H_{15/2}$) at 1.75 μm, and another one at longer wavelength, $^6H_{13/2} \rightarrow {}^6H_{15/2}$ around 2.9 μm. In addition, dysprosium presents yellow emission from the $^4F_{9/2}$ excited level down to the ground multiplet.

One of the lanthanide ions with the richest spectroscopic properties is Ho^{III}, including up-conversion, and only a few of its features are reported in fig. 3; one emission line is close to the second telecommunication window ($^5F_5 \rightarrow {}^5I_6$, 1.5 μm) while another, at 2.1 μm ($^5I_7 \rightarrow {}^5I_8$) has generated several medical applications in laser surgery for ophthalmic treatments or for enucleating the prostate for instance (Kuo et al., 2002). The lasers are Q-switched Ho:YAG systems directly pumped into the $^5I_7$ level, Tm^{III} being used as sensitizer thanks to its $^3F_4 \rightarrow {}^3H_6$ line at 1.8–1.9 μm, itself pumped by a diode laser. Ho^{III} emits a second NIR line around 2.2–2.3 μm ($^5I_4 \rightarrow {}^5I_6$). With similar purposes, a multi-wavelength laser system has been proposed for precise and efficient tissue ablation under water and was realized by coupling two laser lines, from Ho^{III} at 2.1 μm and Er^{III} at 2.79 μm into a zirconium fluoride optical fiber (Pratisto et al., 1995). In addition to the transition mentioned above, Tm^{III} displays another NIR line at 1.4–1.5 μm, arising from the $^3H_4 \rightarrow {}^3F_4$ transition.

2.2. *Sensitization processes*

The emissive properties of a lanthanide ion are governed by the facility with which its excited state(s) can be populated and the nonradiative deactivation paths minimized. Most of the electronic transitions of the trivalent Ln^{III} ions involve a redistribution of electrons within the 4f sub-shell. Electric dipole selection rules forbid such transitions but these rules are relaxed by several mechanisms. An important one is the coupling with vibrational modes, where a molecular vibration temporarily changes the geometric arrangement around the metal ion and, therefore, its symmetry. Other mechanisms which cause a breakdown of the selection rules are the *J*-mixing and the mixing with opposite-parity wavefunctions, such as 5d orbitals, ligand orbitals or charge transfer states. The coupling between the perturbating states and the 4f wavefunctions depends on the strength of the interaction between the 4f orbitals and the surrounding ligands; in view of the shielding of the 4f orbitals, the degree of mixing

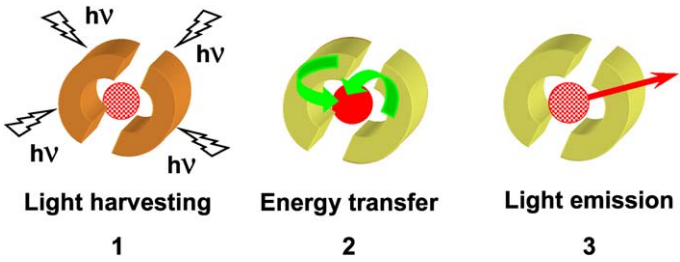

Fig. 5. Schematic representation of the sensitization process of lanthanide luminescence via the surroundings of the metal ion.

remains small, and so are the oscillator strengths of the f–f transitions. As a consequence, even if many lanthanide-containing compounds display a good quantum yield, direct excitation of the Ln^{III} ions rarely yields highly luminescent materials. Indirect excitation, termed sensitization or antenna effect, and discovered by Weissman (1942) has to be used. It proceeds in three distinct steps (fig. 5). Firstly, light is absorbed by the immediate environment of the Ln^{III} ion through the attached organic ligands (chromophores) or the inorganic matrix in case of solid state compounds such as lamp phosphors. Secondly, energy is transferred onto one or several excited states of the metal ion, and, thirdly, de-excitation processes take over and the metal ion emits its characteristic spectrum.

Sensitization via ligand-to-metal charge transfer states or d-transition metal ions can also be envisaged. Charge transfer states essentially operate for Sm^{III}, Eu^{III}, and Yb^{III}; they are often used when these ions are inserted into inorganic matrices and their energy has to be carefully tuned. Indeed, if such LMCT states lie at high enough energy, they can transfer energy into the excited 4f-states; however, when their energy is close to the energy of the emitting level, they act as efficient quenchers of the 4f-luminescence. The second excitation mode relies on energy transfer from a d-transition metal ion. For instance, Cr^{III} is a known activator of the Nd^{III} luminescence in YAG lasers (Seltzer, 1995) and, more recently, this excitation mode has stirred interest for the sensitization of NIR luminescence in molecular complexes (Shavaleev et al., 2005) and for increasing the apparent lifetimes of Nd^{III} and Yb^{III} (Imbert et al., 2003). Sensitization via ligand states is still the commonest strategy and numerous ligands have been designed to meet the stringent requirements pertaining to efficient energy transfers to the Ln^{III} ions.

Although often discussed and modeled in terms of a simple ligand(S_1) $\rightarrow$ ligand(T_1) $\rightarrow$ Ln^* energy flow which can be optimized by adjusting the energy gap between the lowest ligand triplet state and the Ln^{III} emitting level (Archer et al., 1998; Gutierrez et al., 2004; Latva et al., 1997), sensitization of trivalent lanthanide ions is an exceedingly complex process involving several mechanisms and numerous rate constants (de Sá et al., 2000; Gonçalves e Silva et al., 2000; Gonçalves e Silva et al., 2002). The various contributions to the ligand-to-lanthanide ion energy transfer rates W_{ET} may be described within the frame of Judd–Ofelt theory (Judd, 1962; Ofelt, 1962) by eqs. (1)–(3) in which J is the total angular momentum quantum number of the lanthanide ion while α specifies a 4f spectroscopic term; G is the

degeneracy of the ligand initial state and S_L is the electric dipole strength associated with the transition $\phi \rightarrow \phi'$ in the ligand. The quantities $\langle \| \| \rangle$ are reduced matrix elements of the unit tensor operators $U^{(\lambda)}$ (Carnall et al., 1997), and R_L is the distance from the metal ion nucleus to the region of the ligand molecule in which the ligand donor (or acceptor in case of back transfer) state is localized (Malta et al., 1999). The first set of equations describes the contribution of the dipole-2^λ pole mechanism:

$$W_{ET}^{mp} = \frac{2\pi}{\hbar}\frac{e^2 S_L}{(2J+1)G} F \sum_\lambda \gamma_\lambda \left\langle \alpha' J' \left\| U^{(\lambda)} \right\| \alpha J \right\rangle^2, \quad \lambda = 2, 4, \text{ and } 6, \tag{1a}$$

$$\gamma_\lambda = (\lambda + 1)\frac{\langle r^\lambda \rangle^2}{(R_L^{(\lambda+2)})^2} \left\langle 3 \left\| C^{(\lambda)} \right\| 3 \right\rangle^2 (1 - \sigma_\lambda)^2, \tag{1b}$$

$\langle r^\lambda \rangle$ is the radial expectation value of r^λ for 4f electrons, $C^{(\lambda)}$ is a Racah tensor operator, and

$$F = \frac{1}{\hbar \Delta A_L}\sqrt{\frac{\ln 2}{\pi}} \exp\left[-\left(\frac{\Delta E}{\hbar \Delta A_L} \right)^2 \ln 2 \right], \tag{1c}$$

where ΔE is the energy difference between the ligand donor level and the lanthanide ion acceptor level and ΔA_L is the band width at half height of the ligand transition.

The second equation characterizes the dipole–dipole mechanism:

$$W_{ET}^{dp} = \frac{2\pi}{\hbar}\frac{e^2 S_L}{(2J+1)G R_L^6} F \sum_\lambda \Omega_\lambda^{e.d.} \left\langle \alpha' J' \left\| U^{(\lambda)} \right\| \alpha J \right\rangle^2, \quad \lambda = 2, 4, \text{ and } 6. \tag{2}$$

The third equation represents the exchange mechanism:

$$W_{ET}^{ex} = \frac{8\pi}{3\hbar}\frac{e^2 (1 - \sigma_0)^2}{(2J+1)R_L^4} F \left\langle \alpha' J' \| S \| \alpha J \right\rangle^2 \sum_m \left| \left\langle \phi \left| \sum_k \mu_z(k) s_m(k) \right| \phi' \right\rangle \right|^2, \tag{3}$$

where S is the total spin operator of the metal ion, μ_z is the z component of the electric dipole operator, s_m ($m = 0, \pm 1$) is a spherical component of the spin operator for the ligand electrons, and σ_0 is a distance-dependent screening factor (Gonçalves e Silva and Malta, 1997). The first term in eq. (3) implies a R_L^{-4} dependence, but the last term depends exponentially on the donor–acceptor distance (e^{-R_L}) and this term dominates the overall distance dependence. While the second (Förster) and third (Dexter) mechanisms are well known and documented in the literature, contribution from the multipolar mechanisms are often ignored, despite that they account for a great share of the energy transferred from the surroundings to the lanthanide ions. Dexter's (or exchange) mechanism, involves a double electron transfer and requires a good overlap between the ligand and metal orbitals, while in Förster's (or dipole–dipole) mechanism, the dipole moment associated with the $^3T^*$ state couples with the dipole moment of the 4f orbitals (fig. 6). Due to their respective dependence upon the donor–acceptor distance, Dexter's and the multipolar mechanisms operate at shorter distances than the dipole–dipole mechanism. They are therefore preferred mechanisms for energy transfer from the ligands to the metal ion, whereas dipole–dipole transfers are the main operating mechanisms in metal-to-metal energy transfer processes.

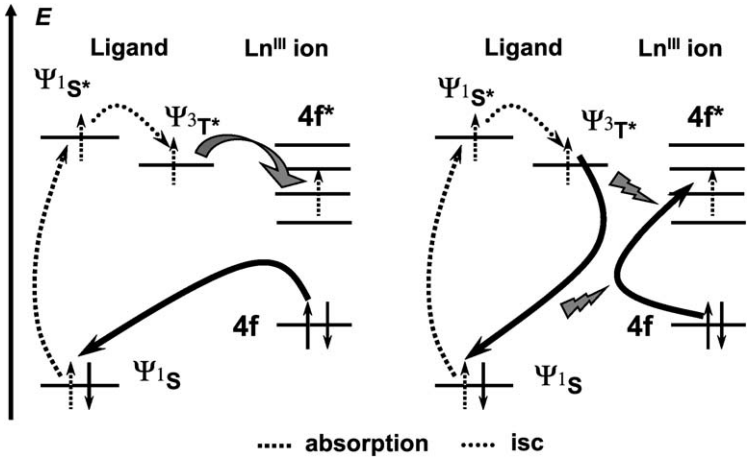

Fig. 6. Schematic representation of Dexter (exchange, left) and Förster (dipole–dipole, right) mechanisms for energy transfer.

When the mechanism is purely dipole–dipolar (Förster mechanism), simplified eqs. (4b) and (4c) allow an estimate of the efficiency of transfer between the donor and the acceptor:

$$\eta_{\text{et}} = 1 - (\tau_{\text{obs}}/\tau_0), \tag{4a}$$

$$\eta_{\text{et}} = \frac{1}{1 + (R_{\text{DA}}/R_0)^6}, \tag{4b}$$

where τ_{obs} and τ_0 are the lifetimes of the donor in presence and in absence of acceptor, respectively, R_{DA} is the distance between the donor and the acceptor and R_0 is the critical distance for 50% transfer, which depends on (i) an orientation factor κ having an isotropic limit of 2/3, (ii) the quantum yield Q_{D} of the donor (in absence of the acceptor), (iii) the refractive index n of the absorption (and emitting) medium, and (iv) the overlap integral J between the emission spectrum of the donor and the absorption spectrum of the acceptor:

$$R_0^6 = 8.75 \times 10^{-25}\left(\kappa^2 \cdot Q_{\text{D}} \cdot n^{-4} \cdot J\right). \tag{4c}$$

Considering the above discussion, the fine tuning of the ligand-to-Ln^{III} transfer process requires the adjustment of several parameters; a comprehensive discussion is not given here, more detailed descriptions being available elsewhere. Both singlet and triplet states of the ligand may transfer energy onto the metal ion (fig. 7) and this transfer may be phonon-assisted; however, since the singlet state is short lived, this process is often not efficient, except in the case of ions such as Nd^{III} or Er^{III}. Classical qualitative considerations on the ligand-to-metal energy transfer thus take solely the energy of the triplet state into consideration. Or, rather, the energy of the lowest triplet state $^3T^*$ since elaborate ligands presently designed usually feature several triplet states (as well as several overlapping $^1S^*$ states). Rules of thumb are that efficient intersystem crossing (isc) from the singlet excited state of the ligand to the triplet state

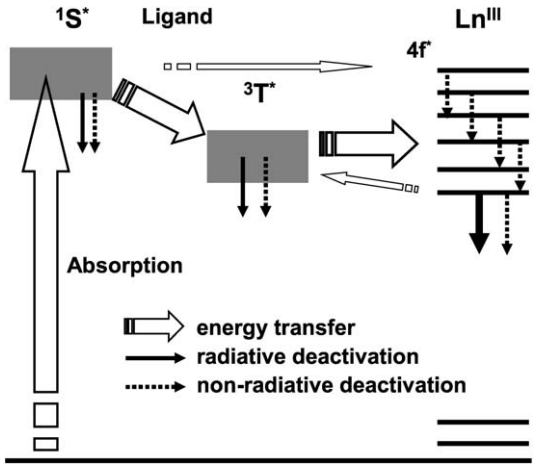

Fig. 7. Simplified diagram showing the main energy flow paths during sensitization of lanthanide luminescence. From (Bünzli and Piguet, 2005), reproduced by permission of the Royal Society of Chemistry.

with the lowest energy occurs when $\Delta E(^1S^*–^3T^*)$ is around 5000 cm^{-1} while high yield transfers from the triplet state to the excited levels of the Ln^{III} ions require $\Delta E(^3T^*–\Gamma^*_{Ln})$ in the range 2500–5000 cm^{-1}. When the latter energy gap is larger, the transfer efficiency drops and when it is smaller, back transfer processes become sizeable and reduce the overall efficacy of the transfer process.[1] A simple experiment to assess if the triplet state is implied in the energy transfer is to measure the metal-centered luminescence in absence and in presence of oxygen which is a good quencher of triplet states. If the rate of quenching by oxygen is larger than the rate of the $^3T^*–\Gamma^*_{Ln}$ transfer, which is often the case, then the metal-centered luminescence weakens considerably upon bubbling oxygen into the solution. On the other hand, non quenching does not necessarily means that the triplet state is not involved in the energy transfer mechanism, but can simply point to the rate of transfer being larger than the rate of oxygen quenching (often estimated around 10^7 s^{-1}).

2.3. *Erbium sensitization by ytterbium and/or cerium*

One of the big challenges in photonic materials is the design of an efficient, low-noise amplifier operating at the eye-safe telecommunication wavelength of 1.55 μm, a reason why the spectroscopy of Er^{III} has been investigated in details. Three main wavelengths can be used to pump energy into Er^{III}, 800 nm ($^4I_{9/2}$), 980 nm ($^4I_{11/2}$), and 1.48 μm (upper ligand-field sublevels of the $^4I_{13/2}$ level). The most favorable is the second one, which is used to pump erbium-doped optical amplifiers displaying large gain efficiency and having a quantum-limited noise level of only 3 dB. Three electronic levels are implied in the amplification process. First,

[1] When evaluating the energy differences, one should take the 0-phonon transitions of $^1S^*$ and $^3T^*$ into account and not the maximum of the band envelope.

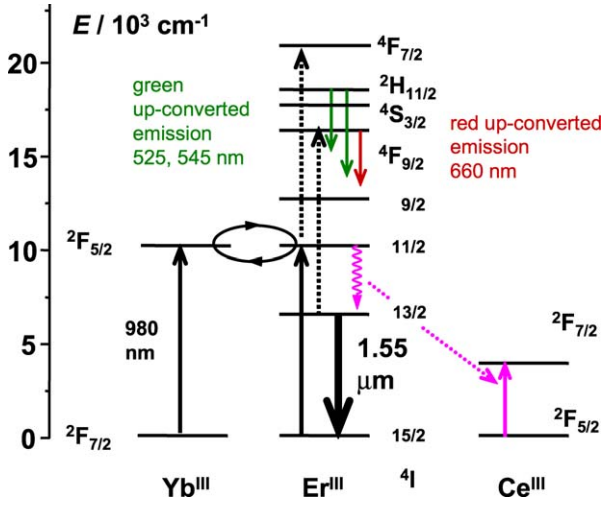

Fig. 8. Transitions of interest for Er^{III} and its sensitizers. Internal nonradiative deactivations are not shown for clarity. Dotted arrows represent up-conversion processes. Adapted from (Le Quang et al., 2005).

an electron is promoted into the $^4I_{11/2}$ level, which either de-activates nonradiatively to the metastable $^4I_{13/2}$ level or absorbs a second photon to reach the $^4F_{7/2}$ level (excited state absorption, ESA). This up-conversion phenomenon is responsible for a significant reduction in the efficiency of the Er^{III} emission, especially that the $^4I_{13/2}$ level may also absorb a photon to reach the red-emitting $^4F_{9/2}$ state. Since Yb^{III} also displays absorption at 980 nm, but with better cross section, it can be used as Er^{III} sensitizer. Alternatively, Ce^{III} may play a similar role in accelerating the population feeding of $^4I_{13/2}$ from $^4I_{11/2}$ through coupling with its $^2F_{7/2} \leftarrow {}^2F_{5/2}$ transition (fig. 8).

2.4. *The special case of ytterbium*

Trivalent ytterbium is a special ion within the lanthanide series in that it possesses only two electronic 4f levels. The fluorescent $^2F_{5/2}$ level lies at around 10 000 cm^{-1} above the $^2F_{7/2}$ ground state. Consequently, ligands with excited (triplet) states having energies around 12–15 000 cm^{-1} are required for sensitizing its NIR luminescence. In this respect, porphyrins are suitable and have been extensively used (*vide infra*, section 3.1.1). On the other hand, antenna effects with ligands having excited states of much higher energy have been observed and there has been some debate regarding the mechanism of this sensitization process. One tempted explanation is that population of the Yb($^2F_{5/2}$) level is achieved by energy transfer from the triplet state *in a phonon-assisted process* (Crosby and Kasha, 1958). Indeed, in [Yb(dbm)$_3$] for instance (dbm is dibenzoylmethanate) the energy difference between Yb($^2F_{5/2}$) state and dbm($^3\pi\pi^*$) is about 13 000 cm^{-1} and direct efficient transfer via exchange or dipole–dipole mechanism is not too plausible. In the phonon-assisted process, the chelate $^3\pi\pi^*$ state transfers energy on high energy vibrational levels of the chelate coupled to the $^2F_{5/2}$ excited state.

The relatively large change in the lowest $^*\pi \leftarrow \pi$ absorption band of the ligand upon complexation, both in energy and intensity, is consistent with a strong vibrational coupling. In more modern terms, this explanation can be translated into a single-configurational coordinate picture, in which the abscissa coordinate Q represents the main expansion coordinate of the $^*\pi \leftarrow \pi$ excitation, that is essentially the breathing mode of the chelate ring ($\approx$1200 cm^{-1}). The states are double, coupled metal–ligand states and are therefore doubly labeled; in the following, bold labels refer to excited states. Excitation leads to the coupled state $^2F_{7/2}$–$^{\mathbf{1}}\mathbf{S_1}$, which relaxes first to $^2F_{7/2}$–$^{\mathbf{3}}\mathbf{T_1}$ by isc and to $^{\mathbf{2}}\mathbf{F_{5/2}}$–$^1S_0$; the latter state can then emit NIR light to reach the ground state $^2F_{7/2}$–$^1S_0$. Using Huang–Rhys theory within the Franck–Condon approximation, H. Güdel and collaborators have calculated that the rate constant of the nonradiative ($^2F_{7/2}$–$^{\mathbf{3}}\mathbf{T_1}$) $\rightarrow$ ($^{\mathbf{2}}\mathbf{F_{5/2}}$–$^1S_0$) process in $[Yb(dpa)_3]^{3-}$ (dpa is dipicolinate) is seven orders of magnitude larger than for $^{\mathbf{3}}\mathbf{T_1} \rightarrow {}^1S_0$ in the free ligand, so that the nonradiative process leading to excitation of the Yb^{III} ion is quite plausible (Reinhard and Güdel, 2002). In the case of $[Yb(tta)_3(H_2O)_2]$, an efficiency of unity ($\pm$15%) has been calculated for the $^3T_1 \rightarrow {}^2F_{5/2}$ energy transfer (Venchikov and Tsvirko, 2000). If they have energy comparable to the energy of the lowest triplet state, MLCT states could also be involved in such a phonon-assisted energy transfer.

Another theory put forward is that excitation goes through a long-range electron transfer and involves the divalent oxidation state of ytterbium (deW. Horrocks et al., 1997; Supkowski et al., 1999). This suggestion was motivated by the observation that the 980-nm emission of Yb^{III} is detected in codfish parvalbumin in which the two bound Ca^{II} ions have been replaced with Yb^{III} ions. This calcium-binding protein contains a single tryptophan (Trp) unit which, on the basis of modeling from the known structure of carp parvalbumin, is found to be approximately equidistant from the two metal ion sites with the nearest indole ring atom 8–11 Å from a metal ion site. Excitation of tryptophan at 290 nm results in the NIR luminescence from Yb^{III}. In fact, the intensity of the singlet state emission of Trp in Ln^{III}-loaded codfish parvalbumin is almost constant for all Ln^{III} ions, except Eu^{III} and Yb^{III} (Breen et al., 1985). At the time, the authors proposed an energy transfer mechanism involving overlap of tryptophan emission with a ligand-to-metal charge-transfer band. However, upon re-examination of the absorption spectra, no such LMCT band could be observed, either for Eu^{III}-bound parvalbumin or for the Yb^{III} complex. As a consequence, the electron transfer mechanism depicted in fig. 9 was proposed.

The ground state of the indole sub-unit cannot reduce Yb^{III}, but the excited state Trp* can. The driving force, ΔG_{Ln} for the forward electron transfer (ET) may be estimated with the equation:

$$\Delta G_{Ln} = E\left(Ln^{III}/Ln^{II}\right) + E_{Trp^*} - E\left(Trp^{\cdot+}/Trp\right). \tag{5}$$

The reduction potential of the tryptophan radical cation is estimated to be 1.13 eV, while the energy of Trp in its excited singlet state is 3.9 eV. The reduction potential of the protein-bound metal ion corresponds to the reduction potential ($-$1.05 V for Yb^{III}/Yb^{II}) plus a correction of $-$0.18 eV to account for the larger binding constant for Ln^{III} ions to parvalbumin ($\approx$100 times that of Ln^{II} ions). These values yield a driving force for Yb^{III} of $\Delta G = -1.54$ eV

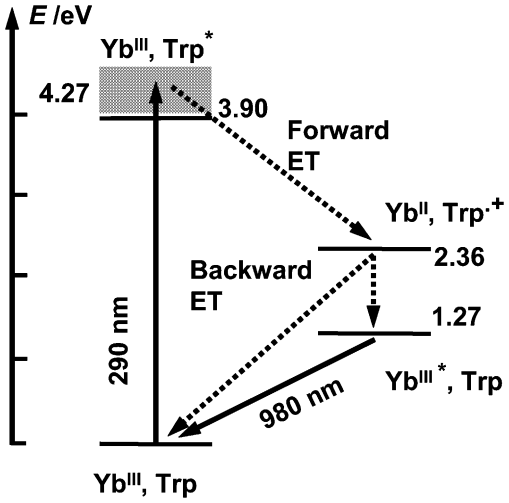

Fig. 9. Proposed electron-transfer mechanism for the sensitization of Yb^{III} luminescence by the excited state of tryptophan (Trp). Figures are energies of the states in eV. Redrawn from (deW. Horrocks et al., 1997).

($-148.6\ \mathrm{kJ\,mol^{-1}}$). The reduction of Yb^{III} by tryptophan in its excited singlet state (the forward electron transfer process in fig. 9) produces the tryptophan radical cation $Trp^{\cdot+}$ and Yb^{II}. The former is a strong oxidant, triggering the electron to return onto tryptophan, yielding Yb^{III*} and ground state Trp. The Gibbs free energy of the electron transfer back reaction, $\Delta G = E(Ln^{III}/Ln^{II}) - E(Trp^{\cdot+}/Trp)$ amounts to -2.36 eV ($-227.7\ \mathrm{kJ\,mol^{-1}}$) and since it is larger than the energy of the $^2F_{5/2}$ state (1.27 eV, 122.5 kJ $\mathrm{mol^{-1}}$), trivalent ytterbium is thus produced in either the ground or excited state. The fraction of excited Yb^{III*} ions formed results in near-infrared luminescence at about 980 nm (deW. Horrocks et al., 1997).

This mechanism is thought to be operative in coordination compounds as well (Beeby et al., 2002c), although in some instances, a fraction of the Yb^{III} ions is probably excited via the LMCT state.

2.5. *Quantum yields and radiative lifetimes*

In addition to mastering the various processes leading to electronic excitation of the lanthanide ions, one has to prevent excited states to de-excite via nonradiative processes. The overall deactivation rate constant, which is inversely proportional to the observed lifetime τ_{obs}, is given by:

$$k_{obs} = k^{rad} + \sum_n k_n^{nr} = k^{rad} + \sum_i k_i^{vibr}(T) + \sum_j k_j^{pet}(T) + \sum_k k_k'^{nr}, \tag{6}$$

where k^r and k^{nr} are the radiative and nonradiative rate constants, respectively; the superscript vibr points to vibrational processes while pet refers to photo-induced electron transfer

processes (De Silva et al., 2000); the rate constants k' are associated with the remaining deactivation paths. The quantum yield is defined as being the number of emitted photons divided by the number of absorbed photons. For an Ln^{III} ion, the intrinsic quantum yield, i.e. the quantum yield obtained by direct excitation into the 4f* levels is simply given by:

$$Q_{Ln}^{Ln} = \frac{\tau_{obs}}{\tau_{rad}} \tag{7}$$

in which $\tau_{rad} = 1/k^{rad}$ is the radiative lifetime of the Ln^{III} ion, that is the inverse of its deactivation rate constant in absence of any quenching and/or nonradiative deactivation processes.

Deactivation through vibrations is especially effective and represents a major concern in the design of both inorganic and organic edifices. Multi-phonon processes are temperature dependent and the deactivation rate constant is also very sensitive to the metal–ligand distance since the interaction is of multipole–multipole nature, wherein the dipole–dipole component is predominant (Hüfner, 1978). In aqueous solutions, interaction with water, both in the inner and outer coordination spheres of the Ln^{III} ion, leads to a severe quenching of the metal luminescence via O–H vibrations. Although detrimental to the design of highly luminescent edifices, this phenomenon can be used to assess the number of water molecules q interacting in the inner coordination sphere and several approximate phenomenological equations have been proposed, based on the assumptions that O–D oscillators do not contribute to deactivation and that all the other deactivation paths are the same in water and in deuterated water, and can henceforth be assessed by measuring the lifetime in the deuterated solvent: (Beeby et al., 1999; Supkowski and deW. Horrocks, 2002):

$$q = A \times (k_{H_2O} - k_{D_2O} - B) - C, \tag{8}$$

where A, B, and C are phenomenological Ln-depending parameters determined using series of compounds with known hydration numbers. Parameter A describes the inner sphere contribution to the quenching, parameter C the outer sphere contribution of closely diffusing water molecules, while the corrective factor B, which has the same units as k, accounts for the presence of other de-activating vibrations (e.g. N–H or C–H oscillators). Such relationships, which exist for Nd^{III} (Faulkner et al., 2001), Sm^{III} (Kimura and Kato, 1995), Eu^{III} (Supkowski and deW. Horrocks, 2002), Tb^{III} (Beeby et al., 1999), Dy^{III} (Kimura and Kato, 1995), and Yb^{III} (Beeby et al. 1999), are to be used with care and with the right calibration, given the hypotheses implied. They are nevertheless quite useful and can be extended to other solvents, for instance alcohol. Of interest to this review are the relationships for solvation of Yb^{III} in water and methanol (Beeby et al., 1999), in which the rate constants are expressed in μs^{-1}:

$$q_{Yb} = 1 \times (k_{H_2O} - k_{D_2O} - B), \quad \text{with } B \text{ between } 0.1 \text{ and } 0.3\ \mu s^{-1}, \tag{9a}$$

$$q_{Yb} = 2.0 \times (k_{CH_3OH} - k_{CD_3OD} - B), \quad \text{with } B \text{ between } 0.05 \text{ and } 0.1\ \mu s^{-1}. \tag{9b}$$

Establishing q for Nd^{III} is more problematic. For instance, an A factor of 342 ns (rate constants are expressed in ns^{-1}) can be calculated from lifetime data of the perchlorate salt (table 2), assuming $q = 9$. A similar value is reported for nitrate, 360 ns (Beeby and Faulkner, 1997),

Table 2
Illustration of the energy gap law with respect to quenching of the Ln^{III} luminescence

Ln	ΔE (cm^{-1})	Nb of phonons, n		τ (μs)[a]		Reference
		OH	OD	H_2O	D_2O	
Gd	32 100	9	15	2300	n.a.	(Bünzli, 1989)
Tb	14 800	4	7	467	3800	(Bünzli, 1989)
				431	4600	(Kimura and Kato, 1995)
Eu	12 300	3–4	5–6	108	4100	(Bünzli, 1989)
Yb	10 250	3	4.5	n.a	3.95[b]	(Beeby et al., 1997)
				0.17[c]	5	(Ermolaev and Sveshnikova, 1979)
Dy	7850	2–3	3–4	2.6	42	(Kimura and Kato, 1995)
Sm	7400	2	3	2.7	60	(Kimura and Kato, 1995)
Er	6600	2	3	n.a.	0.369	[d]
Nd	5400	1–2	2–3	0.031	0.143	(Beeby and Faulkner, 1997; Lis et al., 2001)

[a]In dilute solutions of perchlorate salts, at room temperature.
[b]Ytterbium triflate.
[c]Estimated from quantum yield.
[d]Erbium triflate 0.5 M, measured in the authors' laboratory (2006).

while the following equation has been established based on measurements on 4 polyaminocarboxylates (edta, nta, dtpa, and a phosphinate-substituted cyclen, H_4**27c**, see section 3.1.4 below):

$$q_{Nd} = 130 \times (k_{H_2O} - k_{D_2O}) - 0.4. \tag{10a}$$

However, this equation does not yield acceptable results in the case of cryptates for instance (Faulkner et al., 2001) and must be used with extreme care. The corresponding equation for methanol solvation is (Beeby et al., 2002a):

$$q_{Nd} = 290 \times (k_{CH_3OH} - k_{CD_3OD}) - 0.4, \tag{10b}$$

but again it has to be used with much caution. The main problem in establishing such a relationship for Nd^{III} is inherent to the presence of C–H vibrations in organic ligands. These vibrations are efficient quenchers even if they lie in the second coordination sphere or even further, so that calibration becomes tricky unless their contribution to the quenching can be established precisely.

The best way to minimize vibration-induced deactivation processes is to design a rigid metal-ion environment, free of high-energy vibrations and protecting the Ln^{III} ion from solvent interaction. Such an environment also contributes to reduce collision-induced deactivation in solution. Further protection may be gained by inserting the luminescent edifice into micelles, a strategy used in some bioanalyses.

Finally, both photo-induced electron transfer from the ligand to the metal ion, resulting in a reduction of Ln^{III} into Ln^{II} with a concomitant quenching of the metal-centered luminescence, and energy back transfer (see fig. 7) have to be avoided by an adequate ligand design positioning the LMCT and triplet states sufficiently away from the emissive state.

In the case of ligand sensitization, the overall quantum yield of a lanthanide-containing molecular edifice is given by

$$Q_{\mathrm{Ln}}^{\mathrm{L}} = \eta_{\mathrm{sens}} \cdot Q_{\mathrm{Ln}}^{\mathrm{Ln}} = \eta_{\mathrm{sens}} \cdot \frac{\tau_{\mathrm{obs}}}{\tau_{\mathrm{rad}}} \tag{11}$$

$$\text{or} \quad \eta_{\mathrm{sens}} = Q_{\mathrm{Ln}}^{\mathrm{L}} \cdot \frac{\tau_{\mathrm{rad}}}{\tau_{\mathrm{obs}}}, \tag{11a}$$

whereby $Q_{\mathrm{Ln}}^{\mathrm{L}}$ and $Q_{\mathrm{Ln}}^{\mathrm{Ln}}$ are the overall and intrinsic quantum yields resulting from indirect and direct excitation, respectively, while η_{sens} represents the efficacy with which electromagnetic energy is transferred from the surroundings onto the metal ion; τ_{obs} is the experimental lifetime of the metal excited state (measured upon direct excitation) and τ_{rad} is its radiative lifetime.

The intrinsic quantum yield $Q_{\mathrm{Ln}}^{\mathrm{Ln}}$ essentially depends on the energy gap between the lowest lying excited (emissive) state of the metal ion and the highest sublevel of its ground multiplet. The smaller this gap, the easier is its closing by nonradiative deactivation processes, for instance through vibrations of bound ligands, particularly those with high energy vibrations such as O–H, N–H, or C–H. With the assumption that the de-activating phonons involved have the same energy, the rate temperature-dependent constant $W(T)$ for the quenching of a single excited level is described by the following expression (Hüfner, 1978):

$$W(T) = W(0)\left[\frac{\exp(\hbar\omega_i/kT)}{\exp(\hbar\omega_i/kT) - 1}\right]^{\Delta E/\hbar\omega_i}, \tag{12a}$$

where $\hbar\omega_i$ is the energy of the de-activating vibration (at maximum of band envelope) and ΔE the energy gap between the $\mathrm{Ln}^{\mathrm{III}}$ excited state and the terminal low-lying state, $W(0)$ is the spontaneous rate at 0 K, all the vibrations being in their fundamental state. At low temperature, this term dominates the nonradiative deactivation process since $\hbar\omega_i \gg kT$ and therefore eq. (12a) reduces to:

$$W(T) = W(0) = C_1 \cdot \exp(-C_2 \cdot \Delta E/\hbar\omega_i), \tag{12b}$$

with C_1 and C_2 being empirical parameters characteristic of the $\mathrm{Ln}^{\mathrm{III}}$ environment. In practice, the excited level possesses several crystal-field sublevels, the population of which is in thermal equilibrium. The latter is reached in times short compared to the multiphonon decay time, but since phonon-induced decay rates are significantly slower for the upper levels in view of the larger energy gaps, depopulation of the lower crystal field sub-level is the major contribution to the deactivation process. As a result, the observed lifetime and the quantum yields diminish considerably. A rule of thumb is that radiative de-excitation will compete efficiently with multi-phonon processes if the energy gap is more than 6 quanta of the highest energy vibration present in the molecule.

Multiphonon deactivation is also caused by interaction with alcohol or other vibrations of the solvents, as illustrated in table 3, where $\mathrm{Nd}^{\mathrm{III}}$ lifetime data are reported for various salts in methanol, dmso and their deuterated analogs. One can estimate the rate constant k_{nr} of the deactivation process assuming that the radiative rate is not affected by deuteration $k^{\mathrm{nr}} =$

Table 3
Lifetimes (ns) of the Nd($^4F_{3/2}$) level for solutions of Nd^{III} salts in various solvents. Uncertainties are ±10% for $\tau < 100$ ns and ±5% for $\tau > 100$ ns (Beeby and Faulkner, 1997)

Salt	H_2O	D_2O	CH_3OH	CH_3OD	CD_3OD	dmso	dmso-d_6
$Nd(ClO_4)_3{\cdot}xH_2O$	30	143	43	191	385	1726	6200
$NdCl_3{\cdot}xH_2O$	29	147	68	245	478	1692	7880
$Nd(NO_3)_3{\cdot}6H_2O$	29	152	70	290	476	1700	9020
$Nd(ac)_3{\cdot}H_2O$	41	158	131	322	517	1148	2329

$k_{obs} - k^{rad}$. From the data for $Nd(NO_3)_3 \cdot xH_2O$ in methanol, the relative changes in k^{nr} induced by substituting O–H and C–H by O–D and C–D are therefore equal to $\Delta k = 1.1 \times 10^7\ s^{-1}$ and $1.3 \times 10^6\ s^{-1}$, respectively. Taking into account that there are three C–H groups per O–H, this means that O–H vibrations are de-activating the Nd($^4F_{3/2}$) level about 30 times more efficiently than C–H vibrations; this is due to the facts that O–H oscillators are closer to the Nd^{III} ion and that their energy is larger when compared to C–H oscillators (Beeby and Faulkner, 1997). Selected relevant lifetime data for solutions in water and deuterated water are given in table 2, illustrating the quenching effect of O–H vibrations.

Within the frame of the simplified energy transfer model ($^1S^* \rightarrow {}^3T^* \rightarrow Ln^*$), eq. (11) can be developed as follows:

$$Q_{Ln}^{L} = \eta_{isc} \cdot \eta_{et} \cdot Q_{Ln}^{Ln}, \tag{13}$$

with η_{isc} representing the efficacy of the intersystem crossing process and η_{et} the effectiveness of the $^3T^* \rightarrow Ln$ transfer. When excitation of $^3T^*$ leads to a relatively large expansion of the Ln–L distance, energy transfer occurs as long as the higher vibrational levels of the triplet state are populated, that is the transfer stops when the lowest vibrational level is reached and triplet state phosphorescence takes over. On the other hand, if the Ln–L expansion is small, transfer is feasible as long as the triplet state is populated. If the rate constant of the transfer is large with respect to both radiative and nonradiative deactivation of $^3T^*$, the transfer then becomes very efficient ($\eta_{sens} \approx 1$, eqs. (11)). In order to compare the efficiency of chromophores to sensitize Ln^{III} luminescence, both the overall and intrinsic quantum yields have to be determined experimentally. If general procedures are well known for both solutions (Chauvin et al., 2004) and solid state samples (de Mello et al., 1997), measurement of Q_{Ln}^{Ln} is not always easy in view of the very small absorption coefficients of the f–f transitions. This quantity can in principle be estimated differently, from eq. (7), if the radiative lifetime is known. The latter is related to Einstein's expression for the rate of spontaneous emission A from an initial state $|\Psi J\rangle$ characterized by a J quantum number to a final state $|\Psi' J'\rangle$:

$$A\left(\Psi J, \Psi' J'\right) = \frac{64\pi^2}{3h} \cdot \frac{\tilde{\nu}_0^3}{(2J+1)} \cdot \left[\frac{n(n^2+2)^2}{9} \cdot P_{ed} + n^3 \cdot P_{md}\right], \tag{14}$$

where $\tilde{\nu}$ is the energy of the transition, n the refractive index, h is Planck's constant (6.63×10^{-27} erg s), and P_{ed} and P_{md} are the oscillator strengths of the electric dipole and magnetic

Table 4
Selected Judd–Ofelt intensity parameters for Ln^{III} ions in units of 10^{-20} cm^2

Ln	Matrix/anion/solvent	Ω_2	Ω_4	Ω_6	Reference
Nd	YAG	0.37	2.29	5.97	(Kaminski and Li, 1974)
	Aquo ion	2.25	4.08	9.47	(Carnall et al., 1983)
	ClO_4^-/CH_3CN	1.2	7.7	9.8	(Bünzli and Vuckovic, 1984)
	$[Nd(dpa)_3]^{3-}/H_2O$	7.13	3.78	13.21	(Mondry and Starynowicz, 1995)
Er	YAG	1.43	1.64	1.28	(Wang et al., 1993)
	Aquo ion	1.34	2.19	1.88	(Carnall et al., 1983)
	$ErCl_3 \cdot 6H_2O$/EtOH	5.0	2.5	0.6	(Keller et al., 1982)
	$[Er(tta)_3]$/MeOH	34.7	1.3	2.7	(Isobe and Misumi, 1974)
Yb	Aquo ion	0.93	1.76	1.89	(Carnall et al., 1965)
	$LiNO_3$–KNO_3 melt	13.1	2.32	1.55	(Carnall et al., 1978)

dipole contributions to the transitions. According to Judd–Ofelt theory:

$$P_{\text{ed}} = e^2 \sum_{\lambda=2,4,6} \Omega_\lambda \left|\left\langle J \left\| U^\lambda \right\| J' \right\rangle\right|^2, \tag{15}$$

with Ω_λ representing the Judd–Ofelt parameters (Judd, 1962; Ofelt, 1962) and U^λ doubly reduced matrix elements which are tabulated (Nielson and Koster, 1963).[2] Selected values of Ω_λ parameters for Nd^{III}, Er^{III}, and Yb^{III} are reported in table 4.

The magnetic dipole contribution can be calculated from:

$$P_{\text{md}} = \frac{4\pi^2 e^2 h}{3m^2c^2} \cdot \frac{\tilde{\nu}_0^3}{(2J+1)} \cdot \left|\left\langle J \| L + 2S \| J' \right\rangle\right|^2, \tag{16}$$

where $L + 2S$ is the spin–orbit operator which can be evaluated according to published methods (Carnall et al., 1965), and e, m, c have their usual meaning. Then if the excited state $|\Psi J\rangle$ relaxes to several different states $|\Psi' J'\rangle$, the radiative lifetime τ_{rad} is equal to:

$$\tau_{\text{rad}} = \frac{1}{\sum_{J'} A(\Psi J, \Psi' J')}. \tag{17}$$

The radiative lifetime can therefore be estimated from the spectral intensity that is from eqs. (14)–(17). Except for the special case of Eu^{III} for which a convenient simplified equation can be derived because one transition ($^5D_0 \rightarrow {}^7F_1$) has a pure magnetic origin (Werts et al., 2002), this calculation is not trivial and large errors can occur, including those pertaining to the hypotheses made. In particular it has been assumed that the emitting and receiving levels are really $(2J+1)$-fold degenerate or, if split by crystal field effects, that all the sublevels are equally populated. This is obviously not true and in the case of Er^{III} this may lead to errors up to 20%. If the absorption spectrum corresponding to an emission spectrum is known however, which may be the case when the luminescence transitions terminate onto the ground level, the

[2] Note that eqs. (14) through (18) are given within the frame of the cgs–esu unit system. Oscillator strengths are therefore expressed in $esu^2\,cm^2 = debye^2$ while Ω_λ parameters are in cm^2.

Table 5
Selected values of radiative lifetimes for Ln^{III} ions

Ion	Compound	Solvent	Excited state	End state	τ_{rad} (ms)	Reference
Pr	Doped in Y_2O_3	–	$^1G_4$	^3H_J	0.58	(Weber, 1968)
Nd	$[Nd(dtpa)]^{2-}$	D_2O	$^4F_{3/2}$	^4I_J	0.3–3.4	(Werts et al., 2002)
Sm	$[Sm(H_2O)_n]^{3+}$	H_2O	$^4G_{5/2}$	^6H_J	6.26[a]	(Carnall, 1979)
Eu	$[Eu(H_2O)_n]^{3+}$	H_2O	$^5D_0$	^7F_J	9.67[a]	(Carnall, 1979)
Tb	$[Tb(H_2O)_n]^{3+}$	H_2O	$^5D_4$	^7F_J	9.02[a]	(Carnall, 1979)
	$[Tb(H_2O)_n]^{3+}$	H_2O	$^5D_4$	^7F_J	5.4[b]	(Bünzli, 1989)
Dy	$[Dy(H_2O)_n]^{3+}$	H_2O	$^4F_{9/2}$	^6H_J	1.85[a]	(Carnall, 1979)
Ho	$[Ho(H_2O)_n]^{3+}$	H_2O	$^5S_2$	^5I_J	0.37[a]	(Carnall, 1979)
Er	$[Er(D_2O)_8]^{3+}$	D_2O	$^4I_{13/2}$	$^4I_{15/2}$	8.68	(Werts et al., 2002)
Yb	$[Yb(dtpa)]^{2-}$	D_2O	$^2F_{7/2}$	$^2F_{5/2}$	1.21	(Werts et al., 2002)

[a]Calculated value from spectral intensities.
[b]Recalculated from Q^{Ln}_{Ln} and τ_{obs} data reported in the reference.

radiative lifetime is equal to:

$$\frac{1}{\tau_{rad}} = 2303 \cdot \frac{8\pi c n^2 \tilde{\nu}_0^2}{N_A} \cdot \frac{(2J'+1)}{(2J+1)} \cdot \int \varepsilon(\tilde{\nu})\, d\tilde{\nu}, \tag{18}$$

where c is the speed of light in vacuo (in cm s^{-1}), $\tilde{\nu}_0$ is the frequency of the transition in cm^{-1}, n is the refractive index of the medium, N_A is Avogadro's number, $\varepsilon(\tilde{\nu})$ is the absorption spectrum of the transition in M^{-1} cm^{-1} vs wavenumbers (Werts et al., 2002).

There are two important points to be stressed here in order to correct many errors reported in the literature. Firstly, the radiative lifetime is characteristic of one emitting state. If several excited states of an Ln^{III} ion emit light, then each of them will have a characteristic radiative lifetime.

Moreover, the radiative lifetime is not a constant for a given ion and a given electronic level. Indeed, there is a dependence on the refractive index, as clearly shown by eq. (14), so that transposition of a literature value to a specific compound cannot be made directly, which explains the wide range of τ_{rad} values reported for an individual Ln^{III} ion. As an example, reported radiative lifetimes for Er^{III} range from 3 to 12 ms, even for relatively similar compounds (see table 19 below)! Another hypothesis inherent to Judd–Ofelt theory is that 4f functions do not contain contributions from 5d orbitals, which is not quite the case for Pr^{III} and Tb^{III} for instance. Selected data reported in the literature are listed in table 5.

2.6. *Multi-photon absorption and up-conversion*

Up-conversion is a process by which two photons of lower energy are subsequently converted into a luminescence photon of higher energy (typically, two IR photons giving rise to one visible photon, e.g. in Er^{III}-containing compounds). This anti-Stokes process is usually observed for ions embedded in solids and is made possible by various mechanisms, such as the now classical excited state absorption mechanism (ESA), or sequential energy transfers (ETU for

energy transfer up-conversion), or cooperative absorption by two or three metal ions. They are very well documented and reviewed (Auzel, 2004) and shall not be discussed here.

On the other hand, many ligands proposed for the sensitization of Ln^{III} luminescence have singlet excited states above 28 000 cm^{-1} (below 360 nm), which implies UV excitation. Not only does this feature results in larger costs for routine measurements (instruments, quartz cuvettes) but, in addition, when materials of biological origin are analyzed, photochemical damages can be induced. Henceforth the search was launched by several research groups for ligands able to be excited into the visible range. So far, few ligands have been found fulfilling this condition and only a handful of them can be excited above 400 nm. If, in addition, one takes into account the high transparency of biological materials above approximately 700 nm, a desirable way of exciting the ligands would be to make use of light with wavelengths larger than this limit, which means that one would then probably have to resort to two-photon absorption. This phenomenon is documented for organic molecules and a strategy for the design of molecules with large two-photon absorption cross sections has been recently developed. Indeed, oscillator strengths for two-photon absorption are usually orders of magnitude smaller than those for one-photon absorption. The concept makes use of symmetric charge transfers, from the ends of a conjugated system to the middle, or vice versa, which upon excitation are correlated, resulting in an enhanced value of the cross section for two-photon absorption. Bis(styryl)benzene derivatives with donor–π–donor, donor–acceptor–donor, and acceptor–donor–acceptor structural motifs exhibit exceptionally large values of two-photon absorption cross sections, up to about 400 times that of trans-stilbene. The combination of large two-photon absorption cross sections and high luminescence quantum yield offers potential for unprecedented brightness in two-photon luminescence imaging or enhanced photosensitivity in two-photon sensitization, respectively (Albota et al., 1998). To date, there are few examples pertaining to the subject of this review in which lanthanide luminescent molecular probes have been excited by a two-photon process. In one related example, Eu^{III} has been directly excited at 796 nm (through the $^5L_6 \leftarrow {}^7F_0$ transition, at 398 nm) in deuterated water for the purpose of using the resulting luminescence for microscopy imaging; in water the intensity is much lower. Trivalent terbium could also been excited via a three-photon process (768 nm) by the same tunable Ti:sapphire laser (Lakowicz et al., 2001). Two- and three-photon excitations of the same ions have been achieved via complexed nucleic acids, proteins, and other fluorescent chelators such as coumarin, carbostyril-124 or methyl anthranilate (Piszczek et al., 2002b). A more recent study proposed a ternary beta-diketonate complex of Eu^{III} for multiphoton excitation (Fu et al., 2005); to our knowledge, such a process has rarely been demonstrated for NIR-emitting molecular complexes.

2.7. *Synthetic strategies for ligand and complex design*

In addition to the features relevant to energy-transfer processes and minimization of nonradiative deactivation discussed above, the Ln^{III} environment in a lanthanide-containing luminescent probe must also fulfill several other requirements: high thermodynamic stability, kinetic inertness, and a saturated coordination sphere. Furthermore, in case of bio-analyses, the luminescent probe has to comply with biochemical aspects as well, especially if the probe is to be

used *in vivo*. Given the large lability of lanthanide ions and their need for high coordination numbers (Bünzli, 1998), this poses a real challenge to synthetic chemists who have come up with several strategies to meet, it which are briefly outlined below.

In aqueous solutions, the enthalpy and entropy changes upon complex formation between Ln^{III} cations and many ionic ligands is predominantly influenced by changes in hydration of both the cation and the ligand(s). Complexation results in a decrease in hydration, yielding positive entropy changes favorable to the complexation process. On the other hand, dehydration is endothermic and contribution from bond formation between the cation and the ligand(s) often does not compensate this unfavorable energy contribution to the variation in Gibbs free energy so that the overall complexation process is generally entropy driven. Therefore, it is advantageous to resort to polydentate ligands for building a coordination environment around Ln^{III} ions. During the last decades, inorganic chemists have come up with a number of imaginative strategies to insert Ln^{III} ions into functional edifices using such polydentate ligands.

2.7.1. *Linear polydentate and multifunctional ligands*

Numerous ligands fall into this category, so that we shall only mention three large classes of ligands which have produced interesting Ln^{III} complexes. Polyaminocarboxylates have played a special role in Ln^{III} coordination chemistry since publication of the crystal structure of the La^{III} complex with edta (ethylenediamine-N,N',N'',N'''-tetraacetate) definitively convinced the chemical community that Ln^{III} ions frequently possess coordination numbers larger than 6 (here 10). With log K in the range 15–20, $[Ln(edta)]^-$ complexes are quite stable and consequently, aminocarboxylate complexing units have been grafted on numerous substrates, including macrocycles, e.g. dota, 1,4,7,10-tetraaza-cyclododecane-N,N',N'',N'''-tetraacetate, with log K's in the range 23–25 (Izatt et al., 1991). Stability of these complexes arises from the combination of (i) large entropic effects due to de-solvation of the aqua-ion, (ii) charge compensation occurring upon complexation, (iii) the formation of strong ionic bonds with the carboxylate units, and (iv) the formation of stable five-membered chelate rings (Choppin, 1989).

Another efficient coordinating unit is β-diketonate. Rare earth β-diketonates have been prepared as early as 1897 by G. Urbain and they are among the most investigated Ln^{III} coordination compounds, useful in a wealth of applications, ranging from complexation agents in solvent–solvent extraction processes, to NMR shift reagents, luminescent probes for time-resolved immunoassays, and electroluminescent materials. The bidentate nature of the chelating moiety, however, leads often to hexa-coordinated tris-complexes which complete their coordination sphere by adding two water molecules; detrimental to luminescent properties, these molecules can nevertheless be easily replaced with chromophores such as phenanthroline or bipyridine leading to highly luminescent ternary complexes (Binnemans, 2005b).

Acyclic Schiff base derivatives represent a resourceful class of compartmental ligands which are prepared by self-condensation of appropriate formyl and amine precursors. The condensation reaction is simple and generally leads to the desired product in high yield. Literature data on Ln^{III} mono- and bimetallic complexes, as well as on 4f–d transition metal bimetallic entities with these derivatives are abundant and have been reviewed recently (Vigato and Tamburini, 2004). Extension to multimetallic systems and to complexes with 5f elements

is straightforward. Appropriate choice in the number and nature of the coordinating atoms ensures a well defined coordination environment so that multimetallic systems with metal ions at pre-defined distances may be designed.

2.7.2. *Macrocyclic receptors* (Sastri et al., 2003)

The idea behind the design of such ligands is to build a pre-organized cavity bearing several donor atoms generating suitable interactions with the metal ion (i.e. hard–hard or soft–soft in HSAB-theory) and with a cavity diameter well adapted to the size of the guest cation (*lock-and-key principle*). In this way, reorganization energy of the ligand upon complexation is minimized. Lanthanide macrocyclic chemistry started in the late 1960's when the need for NMR shift reagents induced the study of lanthanide phthalocyanines and porphyrins (Ng, 2001). Two other classes of macrocyclic receptors were developed soon after as model ligands for the transport of cations through biological membranes, coronands (initially, crown ethers) and cryptands which were tested with variable success with the Ln^{III} ions (Izatt et al., 1985). Indeed, the difference in ionic radius between lanthanum and lutetium amounts to only ca. 0.15 Å (for coordination number 9) while the ionic radius of two consecutive lanthanide ions differs by a mere 0.01–0.015 Å, that is a fine tuning of the receptor to accommodate a specific Ln^{III} ion is out of reach, except possibly for the selective complexation of larger versus smaller ions, or vice versa. This remark is also valid for lanthanide complexes with two series of macrocycles which were studied starting in the mid 1970's: simple calixarenes (Asfari et al., 2001; Bünzli et al., 2000; Roundhill, 1995) and cyclic Schiff base derivatives (Vigato and Tamburini, 2004).

Therefore, another strategy was developed, based on the *induced-fit* concept, which uses flexible receptors in order to optimize the interactions between the donor atoms and the metal ion. In fact, the coordination environment is built upon complexation thanks to the flexibility introduced into the complexation agent, which is now termed "predisposed ligand". These receptors are either large macrocycles able to wrap around the guest or small macrocycles fitted with pendant arms. The latter approach has proved to be very successful, particularly with calixarene (Asfari et al., 2001) and cyclen (1,4,7,10-tetraaza-dodecane) (Lukes et al., 2001) derivatives.

2.7.3. *Podands*

The induced-fit approach can also be conducted in an efficient way by designing podands. Here the functionalized pendant arms are no more attached onto a potentially coordinating macrocycle but simply on a single atom (boron, nitrogen, carbon, or transition metal ions) or a small aromatic ring such as benzene or triazine. This strategy is particularly useful when the design of a lanthanide-containing molecular edifice requires bidentate or tridentate pendant arms. Their grafting onto macrocycles is indeed not always straightforward from a synthetic point of view. Ligands with four arms are usually built from small aromatic rings, while tri-armed receptors are often engineered from a single atom. The number of donor atoms can be easily varied by changing both the number of arms and their denticity. However, these ligands are less predisposed than the macrocycles fitted with pendant arms and the orientation of the arms to put the hosting cavity together requires more conformational work, which is

detrimental to the stability of the final molecular edifice. One remedy is to profit from non-covalent interactions, such as H-bonding (Renaud et al., 1999) or π-stacking interactions, or to start from a transition-metal podate (Piguet et al., 2000) to position the arms in the right conformation prior to complexation.

2.7.4. *Self-assembly processes*

In going from pre-organized to pre-disposed receptors, one benefits from simplified synthetic procedures. The next step is to resort to metallosupramolecular chemistry and take advantage of both the high electric field generated by the Ln^{III} ions and weak intermolecular interactions to self-assemble small coordinating units around a metal ion. Application to coordination chemistry is relatively recent (Lehn, 1995). This strategy has been tested in our laboratories to produce large libraries of mono- and di-topic ligands which self-assemble with Ln^{III} ions to yield monometallic and bimetallic 4f–4f, 4f–4f′, as well as d–4f triple-helical edifices under strict thermodynamic control and with predetermined physico-chemical properties (Bünzli and Piguet, 2002). Theoretical and rational modeling of the self-assembly of these helicates is now at hand, which enables a more rational approach (Piguet et al., 2005) as well as extension to multimetallic systems (Floquet et al., 2004), so that self-assembly processes slowly emerge as a privileged strategy for the engineering of elaborate multimetallic edifices and devices.

3. NIR-emitting molecular edifices

In this section, lanthanide-containing NIR-emitting compounds are classified according to the synthetic strategy used to encapsulate the metal ion starting with macrocyclic compounds (Korovin and Rusakova, 2001), then moving to acyclic receptors before describing sensitization with transition metal ions and, finally, various other approaches leading to new materials.

3.1. *Macrocyclic ligands*

3.1.1. *Simple lanthanide porphyrinates*

Tetrapyrrole derivatives such as porphyrins or phthalocyanines (Pc) are highly stable and have exceedingly delocalized π systems. Consequently, they exhibit a wide range of intriguing optical, electrical, magnetic, and spectroscopic properties which render them useful in the fields of materials science, catalysis, biology, and medicine. Their combination with trivalent lanthanide ions has been investigated quite early, starting in the mid 1960's and leading to the isolation of $[Ln(Pc)_2]$ complexes (Ln = Pr, Nd, Er, Lu) which are now well known electrochromic materials (Ng, 2001). Regarding NIR sensitization however, no phthalocyanine complexes with metal-centered NIR luminescence have been reported yet, the initial work of Gurevich and Solev'ev in 1961 having demonstrated that no luminescence from Yb^{III} is detected, the energy of the $^3T^*$ state being lower than the energy of the $Yb(^2F_{5/2})$ excited level (Gurevich and Solev'ev, 1961). On the other hand, numerous NIR-emitting lanthanidoporphyrins have been reported, particularly with Yb^{III} in view of the favorable energy of the porphyrin triplet state. Metalloporphyrins display rich photochemical properties. Their absorption spectrum consists usually of two structured bands, in the ranges 400–425 nm ($^1S_2 \leftarrow {}^1S_0$,

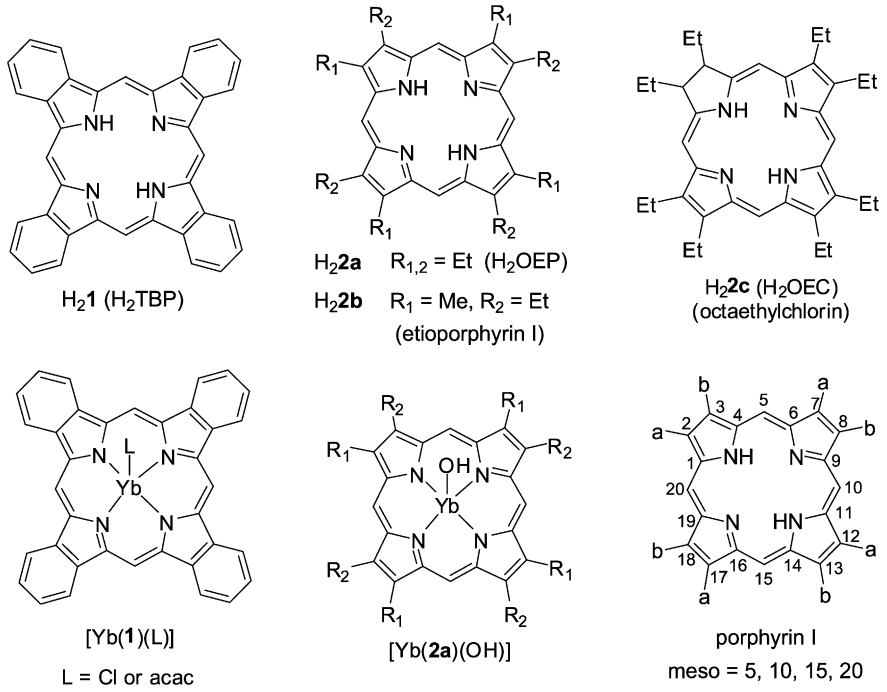

Fig. 10. Free porphyrin ligands (top) and first NIR-emitting lanthanidoporphyrins, along with the numbering adopted for porphyrins (bottom right).

Soret or B-band, $\log \varepsilon \approx 4.5$–$5.5$) and 520–650 nm ($^1S_1 \leftarrow {}^1S_0$, Q-band, $\log \varepsilon \approx 3$–$4$). Fluorescence occurs from both the Soret and Q states since the triplet state $^3T_1$ lies below $^1S_1$.

The nomenclature of porphyrins, which belong to the larger class of tetrapyrrole compounds, is sometimes obscured by historical remnants (e.g. chlorin which does not contain any chlorine substituent, see H_2**2c** in fig. 10, or 2,4-di(α-methoxyethyl)-deuteroporphyrin for H_4**4b**, see fig. 11 below). IUPAC has published nomenclature rules in 1986[3] and the numbering adopted for the ring is given in fig. 10. The 5, 10, 15, and 20 positions are commonly referred to as *meso* positions; the roman number after a name (I though IV) denotes the relative positions of substituents a and b.

Taking advantage of the fact that the triplet state of metalloporphyrins with tetrabenzoporphyrin (H_2TBP or H_2**1**, fig. 10) lies around 12 500 cm^{-1}, a team from Minsk succeeded in sensitizing Yb^{III} luminescence in solutions of [Yb(TBP)L], where L = Cl or acac (acetylacetonate), in several solvents like benzene, dimethylformamide (dmf), pyridine, quinoline or a mixture of octane and benzene (Kachura et al., 1974). Energy transfer from the porphyrin chromophore was ascertained by the excitation spectrum of the Yb^{III} luminescence being identical to the absorption spectrum of the complex. In benzene, the quantum yield of

[3] http://www.chem.qmul.ac.uk/iupac/tetrapyrrole/.

the metal-centered luminescence measured upon ligand excitation amounts to 0.5% with a $Yb(^2F_{5/2})$ lifetime equal to 12 μs. Although this quantum yield is low, only a weak phosphorescence band from the ligand was observed and the Yb^{III}-centered luminescence was not quenched by bubbling oxygen into the solution at room temperature. From the photophysical data measured on this system, the authors have estimated the rate constant of the ligand-to-Yb^{III} energy transfer to be on the order of 10^7 s^{-1}. Within experimental errors, identical data have been obtained for quantum yield, lifetime and energy transfer rate in the case of the Yb^{III} complex with octaethylporphyrin, H_2OEP or H_2**2c** (Solovev et al., 1976). The latter authors have also detected a faint luminescence from [Nd(TBP)acac] and [Nd(OEP)acac]. High energy C–H vibrations play an important role in the deactivation of the $Yb(^2F_{5/2})$ level through both inter- and intra-molecular processes (Tsvirko and Kachura, 1975). For instance, the lifetime of the $^2F_{5/2}$ level in [Yb(TBP)(acac)] increases considerably, from 12 to 72.5 μs, when benzene is substituted by carbon disulfide as solvent, removing intermolecular interactions with C–H vibrations. Regarding intramolecular C–H vibrations, the lifetime of [Yb(**2b**)(acac)] in CS_2 increases from 71 to 131 μs when etioporphyrin is deuterated four-fold at the methane bridges. Finally, replacing acac with a chloride ion in the deuterated etioporphyrin complex leads to a lifetime of 143 μs.

The photophysical processes in [Ln(TBP)acac] dissolved in ethanol and their correlation with Ln^{III} ion characteristics have been later fully investigated by picosecond transient spectroscopy (Tsvirko et al., 1986) for a number of Ln^{III} ions including Er^{III} and Yb^{III}. The non-radiative decay rates of the ligand excited states in the lanthanide-TBP complexes vary by several orders of magnitude depending on the emissive state and the Ln^{III} ion: from 2×10^{10} to 2×10^{11} s^{-1} for $^1S_1$, from 3×10^{11} to 2×10^{13} s^{-1} for $^1S_2$, and from 6×10^2 to 3×10^{10} s^{-1} for $^3T_1$. The latter deactivation rate constant decreases exponentially when the energy gap $\Delta E(^3T_1\text{–}Ln^*)$ is between 4000 and 14 000 cm^{-1} while it remains more or less constant for $\Delta E < 4000$ cm^{-1}. In [Yb(TBP)acac], the $Yb(^2F_{5/2})$ lifetime was found to be 4.5 μs that is, much smaller than the value reported in other non-protic solvents (Kachura et al., 1974).

Soon after the first attempt to sensitize NIR luminescence through the porphyrin triplet state, octaethylporphyrin complexes were synthesized with several rare earth ions (R = Y, Sm, Eu, Gd, Tb, Dy, Ho, Er, Tm, Yb, Lu), by heating free H_2OEP with metal chlorides in an imidazole melt at 210 °C for 2 h, followed by purification steps, including chromatography on a magnesium carbonate column. Chemical analysis and infrared spectroscopy ($\tilde{\nu}_{OH} = 3270$ cm^{-1}) established the chemical formula [Ln(OEP)(OH)]. Similar complexes can be prepared from lanthanide acetylacetonates (Gouterman et al., 1976). Although these complexes are not very stable, some of them dissociating readily in methanol, their photophysical properties were established: (i) f^0, f^7, and f^{14} complexes display fluorescence (0-phonon transition at 575–580 nm) and phosphorescence (0-phonon transition around 700 nm), the latter being especially strong for the Gd^{III} complex, (ii) f^2–f^6 and f^8–f^{12} compounds show essentially fluorescence from the organic ligand, both at room and low (77 K) temperature, while (iii) [Yb(OEP)(OH)] emits in three distinct spectral ranges, corresponding to the singlet and triplet state luminescence as described above, and to the $^2F_{5/2} \rightarrow {}^2F_{7/2}$ transition. While the quantum yield of the Yb^{III}-centered luminescence was not determined, simultaneous detection of ligand fluorescence and phosphorescence points to a less efficient sensitization than

in the TBP analog. The emission spectra of the two porphyrinates [Yb(TBP)(OH)]·$2H_2O$ and [Yb(OEP)(OH)]·H_2O consist in the intense electronic 4f–4f transition centered at 975 nm and in broad side-bands which are temperature dependent. Their detailed analysis allowed the determination of the ligand–field splitting of both $^2F_{5/2}$ and $^2F_{7/2}$ states (Asano-Someda and Kaizu, 2001).

Porphyrins possess several medically useful properties. The most prominent is their ability to accumulate in cancer cells, or more generally in fast growing tissues, so that they are presently being explored in a number of medical applications ranging from cancer therapy (the best known application), to cardiology, ophthalmology, or dermatology. Starting at the end of the 1970's, patients with breast, lung, prostate and skin cancer have been treated by photodynamic therapy. In this cure, a porphyrin photosensitizer is administrated via intravenous injection and localizes in the cancerous region. Visible (red) light is used to activate the sensitizer and to produce singlet oxygen, the cytotoxic agent. Results were encouraging, with almost 100% of complete or partial response. On the other hand, secondary effects developed, such as burns and skin rashes. Moreover, the early porphyrin treatments were seldom strong enough to kill the entire tumor. Finally, some porphyrins are activated by light that cannot penetrate deep enough into the tumor. Henceforth, the search for new porphyrins with a greater potency and which could be activated by light penetrating deeper in human tissues, in the near-infrared range. Haematoporphyrins accumulate more efficiently in malignant tumor than porphyrins and are therefore privileged target for photodynamic treatment of cancer. On the other hand, they have two disadvantages: (i) a high phototoxicity, which requires protection of patients from the action of light on the skin, and (ii) a low contrast of tumors caused by the masking effect of the background luminescence they generate because of a relatively low efficacy of the intersystem process. These disadvantages can be overcome, at least in principle, by the use of the 1-μm emission line of Yb^{III}, since the luminescence of the latter is distinct from the luminescence of the porphyrins and, moreover since the lifetime of the $^2F_{5/2}$ level is relatively long, time-resolved spectroscopy can increase further the signal-to-noise ratio. Therefore, efforts have been undertaken to develop suitable lanthanidoporphyrins with high quantum efficiency. One of the first reports mentioning potential application of Yb^{III} haematoporphyrins H_4**3** for the diagnosis of malignant tumors uses tetramethyl-haematoporphyrin H_2**4a**, 2,4-di(α-methoxyethyl)-deuteroporphyrin H_4**4b**, *meso*-tetra(*p*-carboxyphenyl)porphyrin H_6**4c**, and tetrasulfophenylporphyrin H_6**4e** depicted in fig. 11 (Gaiduck et al., 1989; Gaiduck et al., 1990). In view of the poor solubility of the complexes, they were introduced into phosphatidylcholine liposomes. A fiber-laser luminescence spectrometer has been especially designed to monitor the Yb^{III} luminescence from sarcoma-implanted mice. Both the central and peripheral regions of the tumors were measured, as well as surrounding healthy skin, which allowed the determination of a contrast ratio γ_S from the total emission areas S (emission from tumor) and S_0 (emission from healthy skin):

$$\gamma_S = \frac{S - S_0}{S}. \tag{19}$$

The complexes [Yb(**4a**)]$^+$ and [Yb(**4c**)]$^{3-}$ yield a contrast value $\gamma_S = 10 \pm 2$, while the two other complexes are more efficient, with γ_S values equal to 19 ± 4, and 45 ± 9 for [Yb(**4b**)]$^-$

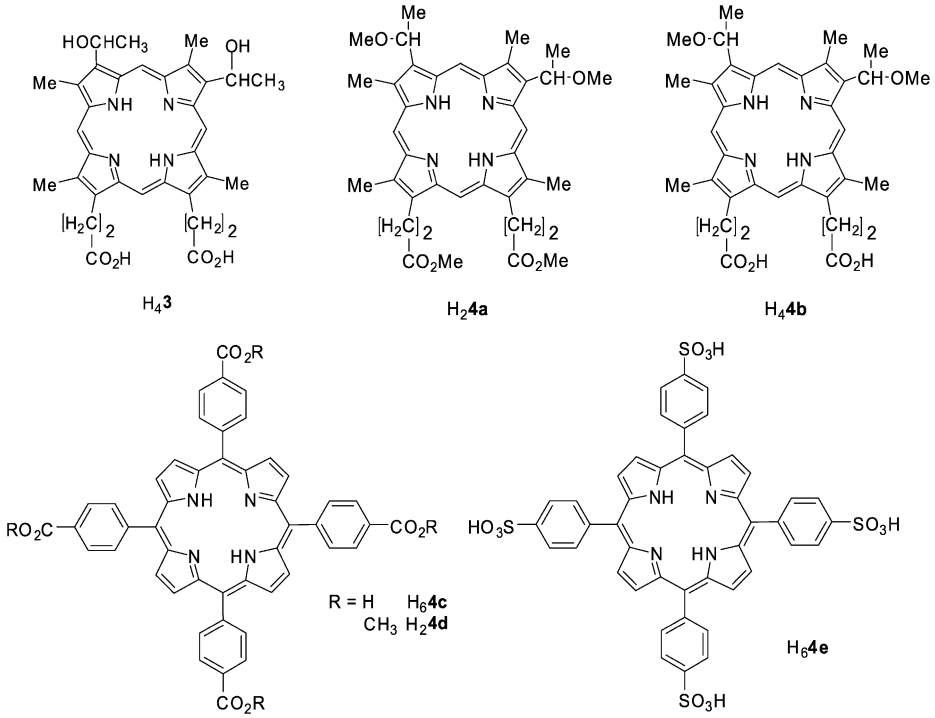

Fig. 11. Structure of haematoporphyrins used to sensitize Yb^{III} luminescence in tumors.

and $[Yb(\mathbf{4e})]^{3-}$, respectively. In addition to the lower phototoxicity of the lanthanidoporphyrinates these contrast data compare most favorably with those obtained with porphyrins alone (1.1–1.2). The detailed photophysics of these complexes has been elucidated and interpreted in terms of crystal-field theory (Gaiduck et al., 1991); in liposomes, $[Yb(\mathbf{4b})]^{-}$ displays a lifetime of the metal excited state of 1.5 μs, slightly smaller than in the solid state (1.9 μs).

Sensitization of Yb^{III} luminescence by tetraphenylporphyrinate **5c** (TTP, fig. 12) is demonstrated by a dramatic drop in the quantum yields of the $^1S_1$-level fluorescence of this species from 0.06% for [Lu(TTP)acac] to less than 3×10^{-3}% for the Yb^{III} derivative. In parallel, the quantum yield of the $^1S_2$-level fluorescence diminishes from 0.15% (Lu^{III}) to 0.01% (Yb^{III}). No quantum yield for the metal-centered luminescence is given in this initial work, but $\tau(^2F_{5/2})$ is reported to be equal to 5 μs (Tsvirko et al., 1980). The quantum yield of [Nd(TTP)acac] has been determined in benzene and is equal to 0.025% (Shushkevich et al., 1981). The latter authors have also measured the quantum yields of [Yb(OEP)acac] (0.045%) and [Yb(**2c**)acac] (0.054%) in the same solvent and undertaken a careful study of the polarization of Nd^{III} and Yb^{III} emission bands and discussed it with respect to the symmetry of the complexes. In order to improve the photophysical properties of [Er(TPP)acac] the complex has been dispersed at concentrations of 5, 17, 28, and 37 wt% into thin films of π-conjugated

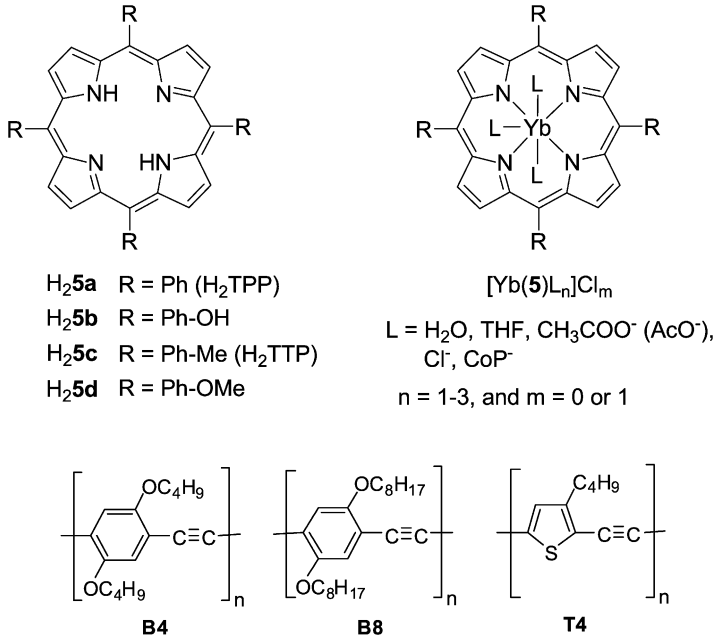

Fig. 12. (Top) [5,10,15,20-tetrakis(*p*-(R)phenyl)porphyrins] and their Yb^{III} complexes. (Bottom) π-conjugated polymers used to host [Er(TPP)acac].

polymers (fig. 12, bottom) obtained by spin coating followed by vacuum annealing. The presence of the lanthanide ion in the porphyrinate produces a strong quenching of the free base visible fluorescence and the NIR quantum yield of a solution of the parent complex 7×10^{-3} M in chloroform amounts to 0.04%. In the thin films, of thickness 500 ± 10 nm, energy transfer occurs from the π-conjugated systems because of spectral overlap between the Q absorption band of [Er(TPP)acac] with the fluorescence band of the polymers; interestingly, 5 wt% of the complex quenches 80% of the **B8** polymer fluorescence. A detailed study has been performed along the lines of Förster theory for dipole–dipolar transfer. The donor quantum yield amount to 14, 22, and 1.5% for **B4**, **B8**, and **T4**, respectively, and the critical distance for 50% transfer (eq. (4b)) was estimated to be 2.3, 2.6, and 1.4 Å, respectively. These are quite short and at such distances other mechanisms should also be operative (exchange mechanism for instance), although the authors could satisfyingly fit their data of the fractional quenching of the host luminescence versus the concentration of emitting ions by a theory derived from Förster mechanism. The relative transfer efficiency for 2 wt% of the Er^{III} complex dispersed in thin films amounts to 74 and 21% for **B4** and **T4**, when **B8** is taken as the reference, pointing to the better efficiency of the latter (Pizzoferrato et al., 2004).

In Yb^{III} tetraphenylporphyrinates, the substituent in the *para* position of the phenyl ring plays an important role in the luminescence intensity, as demonstrated for the series of complexes [Yb(**5b**)(AcO)$(H_2O)_2$], [Yb(**5c**)(thf)$(H_2O)_2$]Cl, [Yb(**5a**)(thf)$(H_2O)_2$]Cl,

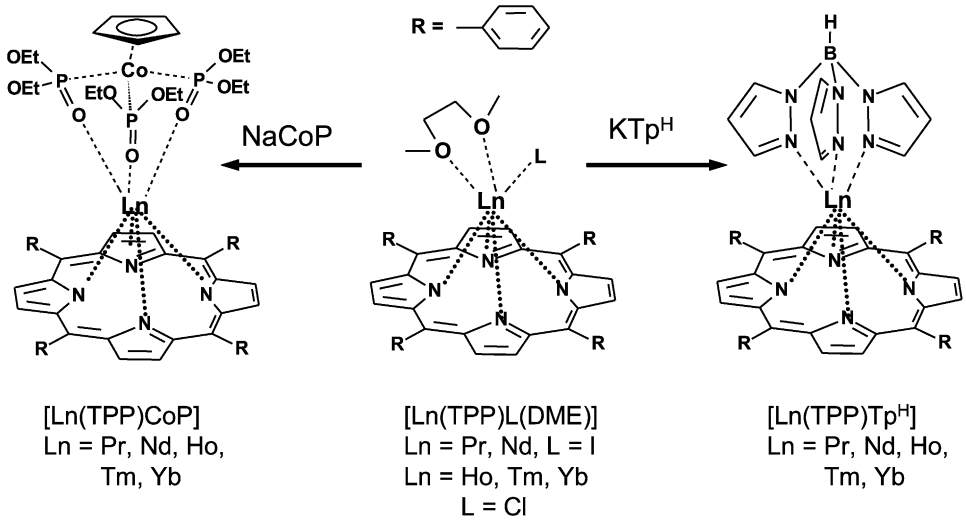

Fig. 13. High-yield syntheses of [Ln(TPP)CoP] and [Ln(TPP)Tp^H] (Foley et al., 2003).

[Yb(**5d**)$(H_2O)_3$]Cl, and [Yb(**5d**)(CoP] (fig. 12) where CoP is the cyclopentadienyl-tris(diethylphosphito)cobaltate(I) anion (see fig. 13) for which the luminescence intensity increases in the proportions 1:22:36:62:271, upon excitation at 512 nm (Meng et al., 2000). The effect of coordinated water molecules on the metal-centered fluorescence intensity is clearly seen in the more than four-fold enhancement obtained by replacing the three water molecules in [Yb(**5d**)$(H_2O)_3$]Cl by CoP; the $^2F_{5/2}$ lifetime of the latter complex (40 μs) is also much longer than lifetimes reported for other Yb^{III} porphyrinates. In addition, the cobaltate anion rigidifies the molecule, which results in a much finer structure of the ligand-field split electronic levels.

Initial synthesis of lanthanide tetraphenylporphyrinates aimed at serving as dipolar probes for nuclear magnetic resonance involved distillation of acetylacetone from a lanthanide acetylacetonate in the presence of the dianion TPP^{2-} (**5a**) to give [Ln(TPP)(acac)] in low yield, 10–30% (Wong et al., 1974). The latter arises from the necessary chromatographic purification which causes hydrolysis of the porphyrinates. A higher yield synthesis was only proposed recently, which involves nucleophilic displacement of chloride ions from anhydrous lanthanide trichloride tris(tetrahydrofuran) adducts by the TPP^{2-} dianion under the form of dilithiotetraphenylporphyrin bis(dimethoxyethane); yields up to 85% have been obtained and the crystal structures of the holmium and ytterbium porphyrinate have been solved (Foley et al., 2002). Following a similar synthetic procedure, the same authors have subsequently developed a strategy to isolate in gram quantities [Ln(TPP)L] complexes capped with multidentate ligands L such as hydridotris(1-pyrazolyl)borate (Tp^H) and CoP (Foley et al., 2003). In methylene chloride, the absorption spectra of the two series of complexes [Ln(TPP)Tp^H] and [Ln(TPP)CoP] display the characteristic Soret and *Q* bands around 425 nm and in the range 550–600 nm, respectively, these bands being slightly red-shifted in going from Tp^H

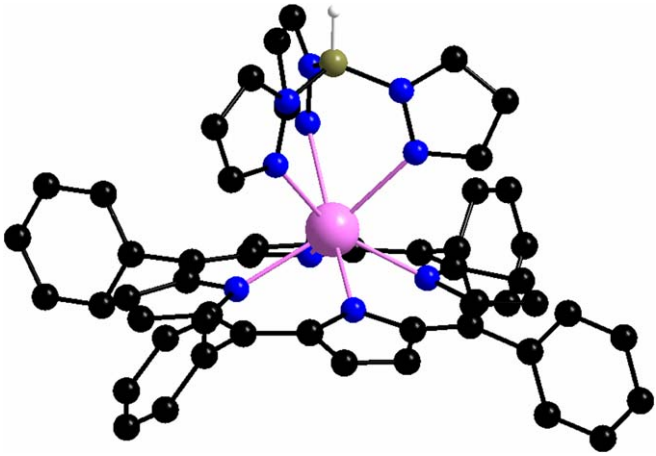

Fig. 14. Molecular structure of seven-coordinate [Yb(TPP)Tp^{H}], redrawn from (Foley et al., 2003).

to CoP. Excitation on the Soret band yields weak emission bands around 650 and 715 nm, assigned to free base H_2TPP since all the samples contain this impurity.

In addition, in the case of Nd^{III}, Er^{III}, and Yb^{III}, characteristic Ln^{III} emission is detected. Absolute quantum yields of CH_2Cl_2 solutions have been determined with respect to both H_2TPP (H_2**5a**, $Q = 11\%$) and [Zn(TPP)] ($Q = 3.15\%$ in ethanol) and amount to: 0.24, 0.09, and 3.2%, respectively, for the complexes with Tp^{H} as capping ligand, and 0.2, 0.1, and 2.4%, respectively, for those with CoP. They are small, but generally higher than the yields obtained for other complexes. This arises from the coordination environment (fig. 14) provided by both TPP^{2-} and the capping anion which effectively shields the Ln^{III} ion from interacting with solvent vibrations, particularly C–H vibrations in this case. This explanation is consistent with the quantum yield of [Yb(TPP)Tp^{H}] increasing only from 3.2 to 3.4% in going from CH_2Cl_2 to $CDCl_3$. The emission quantum yields follow the trend $Yb^{III} > Nd^{III} > Er^{III}$, in line with the energy gap law, and the nature of the capping ion does not affect much the quantum yields. Transient absorption spectra of [Nd(TPP)Tp^{H}] further revealed that excited state absorption in the spectral range 450–500 nm (between the *B* and *Q* bands) is stronger than in the case of the Yb^{III} complexes, pointing to an equilibrium population of the TPP^{2-} triplet state produced via thermally activated energy back transfer from the Nd($^4F_{3/2}$) state which lies only at about 2000 cm^{-1} below $^3T_1(TPP^{2-})$. It is noteworthy that in an earlier investigation, no Er-centered luminescence was observed for [Er(TPP)(OH)], [Er(TPP)dpm] (dpm is dipivaloylmethanate), and [Er(OEP)(OH)] solutions in methanol or methanol/ethanol mixtures. On the other hand, these compounds exhibit dual fluorescence from the $^1S_1$ and $^1S_2$ states while $^3T_1$ emission can be detected at low (77 K) temperature (Kaizu et al., 1986).

The beneficial influence of the capping ligand and of aromatic *meso* substituents on the sensitization of Yb^{III} luminescence has been further demonstrated by a systematic study (Rusakova et al., 2004a). In a first step, *n*-alkyl substituted porphyrins have been compared to aromatic- and heteroaromatic-substituted porphyrins. Subsequently, the authors test how

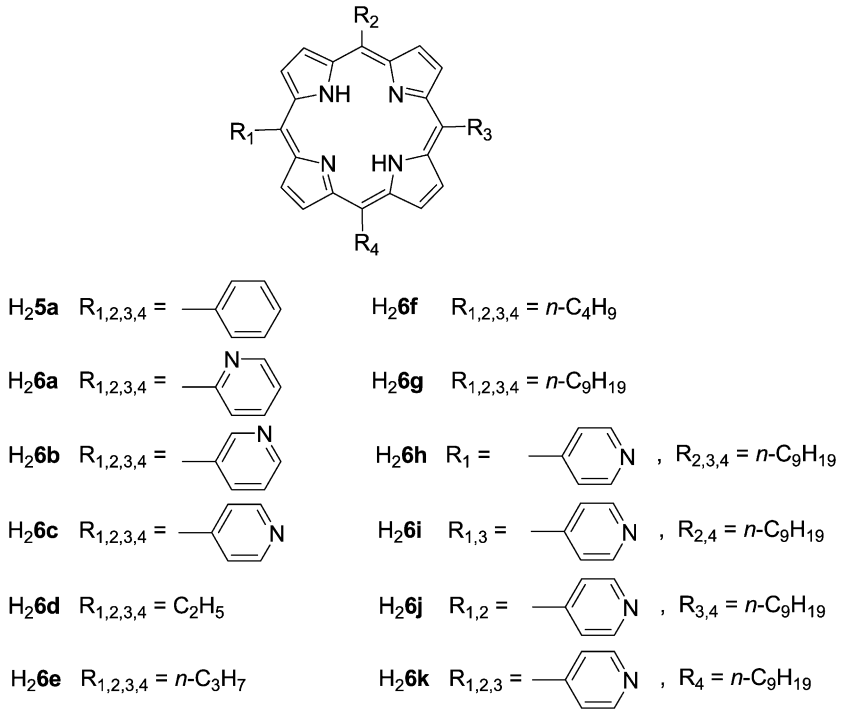

Fig. 15. Porphyrins used in a comparative study to assess the influence of the *meso* substituent and of the capping ligand on Yb^{III} luminescence (Rusakova et al., 2004a).

the nature of the capping ligand, chloride, bromide, acetylacetonate (acac), thenoyltrifluoroacetylacetonate (tta), and benzoylacetonate (ba) affects the quantum yield of the metal-centered luminescence.

Ytterbium complexes with the porphyrins described in fig. 15 were synthesized by reacting an excess of ytterbium acetylacetonate with the corresponding porphyrin in 1,2,4-trichlorobenzene, followed by chromatographic purification on an alumina column. Excitation in the Soret band around 430 nm of methanolic solutions 10^{-5}–10^{-4} M of the ytterbium porphyrinates, which have high extinction coefficients ($\log \varepsilon$ lies in the range 4.2–5.2), results in a very large decrease in the luminescence of the porphyrin fragments (600–640, and 700–720 nm) and in the observation of the $Yb(^2F_{5/2})$ emission. Excitation spectra of the 4f emission coincide with the absorption spectra of the complexes, confirming the energy transfer from the porphyrinates moieties to the metal ion, most probably via the triplet states of the porphyrins, which lie in the range 12 890–12 935 cm^{-1}. Results of the analysis of the 12 ytterbium porphyrinates are outlined in fig. 16.

Both the absolute quantum yield (determined with respect to zinc tetraphenylporphyrin in ethanol) and the product of the molar absorption coefficient at the excitation wavelength with the quantum yield, $\varepsilon \cdot Q$, which represents the overall luminescence efficiency follow the

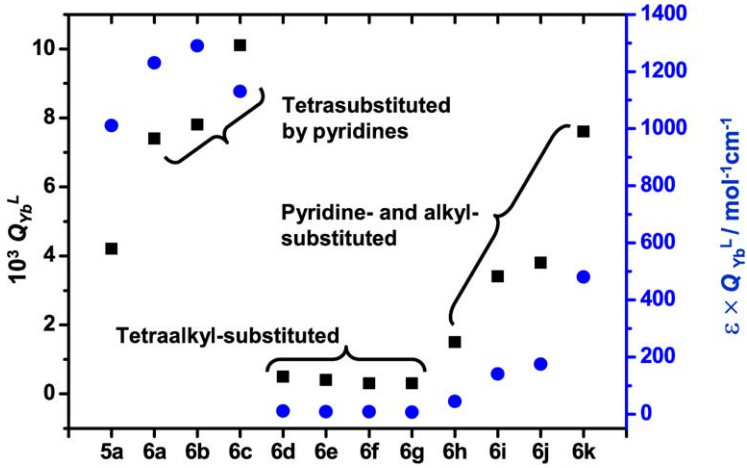

Fig. 16. Quantum yield (■, left scale) and overall luminescence efficacy $\varepsilon \cdot Q$ (●, right scale) of methanolic solutions of Yb^{III} porphyrinates with ligands depicted in fig. 15 (Rusakova et al., 2004a).

same trend. The latter is also reflected in the $^2F_{5/2}$ lifetimes which vary from about 1 μs for the alkyl-substituted porphyrinates to 12 μs for the complex with **6c**.

Porphyrinates devoid of aromatic *meso* substituents **6d–6g** have clearly very low luminescence, irrespective of the chain length which was increased from C_2 in **6d** to C_9 in **6g**. The metal-centered photophysical properties improve gradually upon successive replacement of the alkyl chains with a pyridine moiety (**6h–6k**), but the position of the substituents (e.g. $R_{1,3}$ in **6i** vs $R_{1,2}$ in **6j**) has little influence. The effects generated by the aromatic substituents increase almost linearly with the number of substitutions, the quantum yield increasing from 0.03 (**6g**) to 0.15 (**6h**), 0.36 (average of **6i**, **6j**) and 0.76% (**6k**) while the last substitution (**6c**) brings it only up to 1.0%. Among the porphyrinates tetrasubstituted by aromatic rings, the one bearing a simple phenyl group is the less effective in sensitizing the Yb^{III} luminescence. Replacement of the latter with a pyridine unit increases the quantum yield by a factor 2–2.5 depending on the position of the N atom in the ring and indicating that electronic effects are important in determining the efficiency of the ligand-to-metal energy transfer process.

Finally, photophysical properties can also be finely tuned by the nature of the capping anionic ligand. The study conducted on the four aromatic substituted porphyrinates **5a**, **6a–6c** yielded consistent results, the quantum yield of the metal-centered luminescence following the sequence acac > ba > Cl > tta > Br (see fig. 18 for the structure of the capping ligands) for all of the complexes. The surprising position of tta, which usually forms highly luminescent complexes with Ln^{III} ions, is explained by the authors as resulting from the strong Yb–O bonds generated by tta which weaken the Ln–N(porphyrinates) bonds and henceforth diminish the energy transfer efficiency. One notes, however, that the ratio $Q(\text{acac})/Q(\text{Br})$ lies in the range 1.7–2.1, indicating a relatively small effect generated by differences in the anionic capping ligand. Excitation of the porphyrinates in the Q-band of porphyrin, which appears as

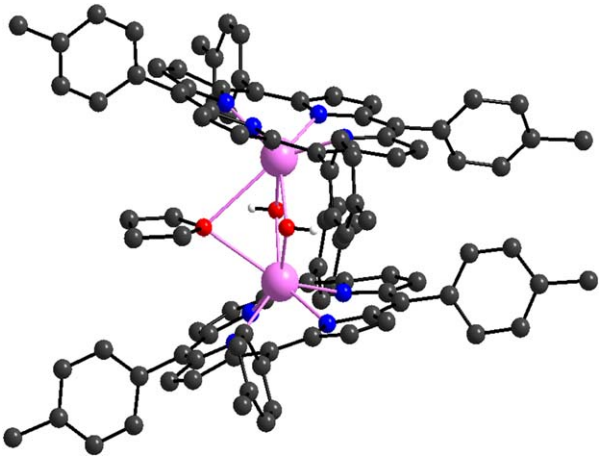

Fig. 17. Molecular structure of the dimer {[Yb(**5c**)(μ-OH)]$_2$(μ-thf)}·6H$_2$O, redrawn from (H. He et al., 2004c).

a structured four-component absorption band between 510 and 650 nm, is also feasible, but the molar absorption coefficient is one to two orders of magnitude smaller than the one of the Soret band, so that the overall luminescence efficiency is quite small (Rusakova et al., 2004a).

Further studies on the influence of the nature of the *meso* substituent in TPP^{2-} complexes have been published recently. For instance, [Ln(L)(H$_2$O)$_3$]$^+$ complexes with L = **5a**, **5c**, **5d**, and **7a–7c** (fig. 18) exhibit both porphyrinate (650 nm) and Ln^{III} NIR emission (Ln = Er, Yb) in CHCl$_3$ despite the coordination of three water molecules (H.S. He et al., 2004a). In the case of Yb^{III}, methyl and methoxy substituents enhance the metal-centered emission, but halogen substituents are detrimental to this luminescence. It is worth mentioning that halogen-substituted porphyrinates are more sensitive to hydrolysis than the others, forming hydroxyl-bridged or halogen-bridged dimers. Photophysical measurements have been performed on dilute solutions (2×10^{-5} M) so that this may well have affected intensity measurements since heavy atom substitutions usually favor intersystem crossing, and therefore are beneficial to the ligand-to-Ln^{III} energy transfer. The intensity of the Yb^{III} emission increases substantially when the three water molecules are replaced with one chloride ion and two dmf molecules (H. He et al., 2004c). Er^{III} emission was extremely weak so that no such effect was observed but, on the other hand, substitution of the coordinated water molecules by thf or dmf resulted in an increase in the luminescence intensity (H. He et al., 2004b, 2004c). Dimerization of the monoporphyrinates [Yb(TPP)(H$_2$O)$_3$]Cl complexes with **5a**, **5c**, and **5d** (fig. 18) occurred when the authors attempted to replace the three water molecules with Tp^{Me} in order to improve the photophysical properties. The dimer {[Yb(**5c**)(μ-OH)]$_2$(μ-thf)} was obtained (fig. 17), as well as four other ones, [Yb(**5a**)(μ-OH)(μ-OH$_2$)]$_2$, [Yb(**5d**)(μ-Cl)(H$_2$O)]$_2$, [Yb(**5d**)(μ-OH)]$_2$, and {[Yb(**5c**)]$_2$(μ-OH)(μ-Quin)} (Quin = 2-methyl-8-hydroxyquinolinate), depending on the reaction conditions, particularly on the solvent and on the nature of added donor molecules. The intensity of the Yb^{III} emission of [Yb(**5a**)(μ-OH)(μ-OH$_2$)]$_2$ is comparable to

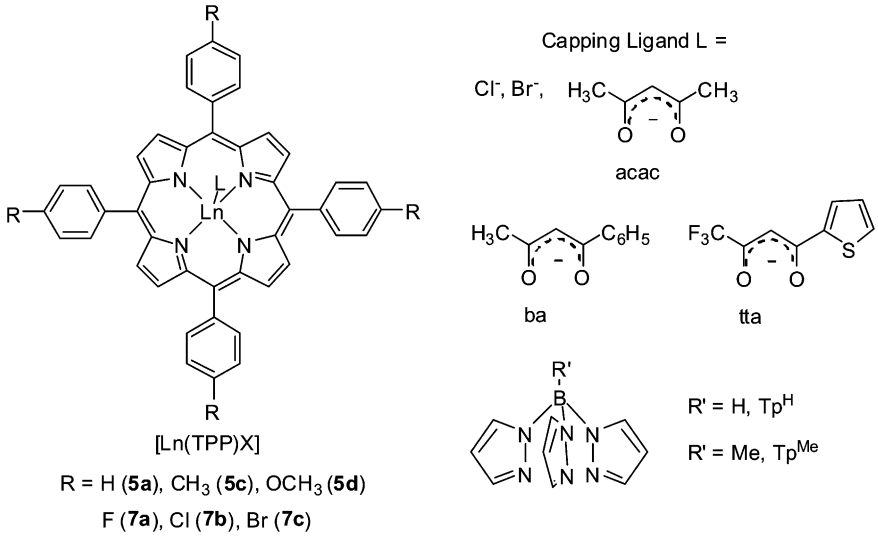

Fig. 18. Lanthanide porphyrinates with substituted TPP^{2-} and anionic capping ligand.

the one of the monoporphyrinate [Yb(**5a**)Cl$(dmf)_2$], while a substantial increase is observed for [Yb(**5d**)(μ-Cl)$(H_2O)]_2$ and {[Yb(**5c**)$]_2$(μ-OH)(μ-Quin)} (H. He et al., 2004c). Subsequently, the same authors succeeded in replacing the water molecules with capping anionic ligands such as Tp^H or CoP (fig. 18). With the former capping ligand, the relative intrinsic quantum yields Q^{Nd}_{Nd}, determined in toluene from the observed lifetimes, upon excitation in the porphyrinate Q-band at 514 nm, and assuming that the radiative lifetime is the same for all compounds, amount to 1, 0.98, 0.79, 0.31, and 0.98 for porphyrinates **5a** (reference complex), **5c**, **5d**, **7a**, and **7b**, respectively (H. He et al., 2004b).

The substituent effect on Q^{Nd}_{Nd} differs from the one on the total luminescence intensity which follows the same pattern as established for $[Yb(TPP)(H_2O)_3]^+$ in chloroform (H. Hu et al., 2004b, 2004c). The "absolute" intrinsic yield Q^{Nd}_{Nd} calculated with an estimated $\tau_{rad} = 0.25$ ms amounts to 0.33% for **5a**. Comparing this figure with the value of 0.24% for Q^{Ln}_{L} in CH_2Cl_2 (Foley et al., 2003) points to a fairly efficient sensitization of the NIR luminescence by TPP (estimated $\eta_{sens} \approx 0.7$). The solvent influence on the intensity of the Nd^{III} emission follows the trend benzene > dichloromethane > thf > chloroform > acetone > acetonitrile > dmf > methanol, that is, stronger donors probably displace the capping anion and quench the NIR luminescence via their high energy vibrations (O–H in case of methanol). For Yb^{III} complexes, both electron-donating groups (**5c**, **5d**) and halogen substituents (**7a–7c**) were found to be detrimental to the metal-centered luminescence, with respect to **5a** while the solvent dependence of the (much weaker) luminescence of the Er^{III} porphyrinates is the same as for the Nd^{III} compounds (H.S. He et al., 2004a).

A similar study has been performed on [Nd(TPP)CoP] complexes with **5a**, **5c**, **5d**, and **7a–7c** in toluene with the same conclusions as to the effects of the *meso* substituent and

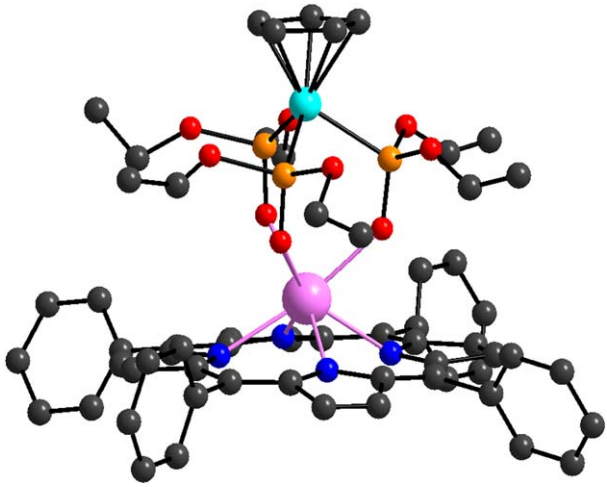

Fig. 19. Molecular structure of seven-coordinate [Er(TPP)CoP^{Me}], redrawn from (Wong et al., 2001).

solvent (H. He et al., 2004a). Metal-centered emission has also been reported for [Er(**5a**)CoP] (fig. 19), and [Yb(**5d**)CoP], the latter having $\tau_{obs} = 16$ µs (Wong et al., 2001), as compared to 20 µs for [Yb(**5d**)Tp^{H}] (H.S. He et al., 2004a).

3.1.2. *Other lanthanide porphyrinates*

N-confused porphyrins are isomers of porphyrins which contain an inverted pyrrole ring linked to the porphyrinic conjugate system through a β-carbon (fig. 20). Treatment of H_2**8** with Ln[N(SiMe$_3$)$_2$]$_3$·[LiCl(thf)$_3$]$_x$ in refluxing toluene, followed by the addition of Na(CoP^{Me}) at room temperature results in the crystallization of green complexes with formula [Ln(**8**)CoP^{Me}] (Ln = Er, Yb) in 75% yield. According to its X-ray structure, the Yb^{III} compound is eight-coordinate, being bound to the three O-atoms of the capping ligand, to the three N-atoms from the confused porphyrin, as well as to the inner C–H edge of **8** through an agostic η^2 bond. It displays a weak NIR luminescence upon excitation at 600 nm, the intensity of which is one order of magnitude smaller when compared with [Yb(**5a**)CoP]. This provides further evidence for the formation of the agostic bond, the strong quenching of the luminescence being attributed to the presence of a C–H oscillator in the inner coordination sphere (Zhu et al., 2005).

In order to simplify the synthesis of lanthanide porphyrinates fitted with a capping anionic ligand, W.K. Wong and collaborators have proposed to graft a potentially anionic pendant group on the porphyrin framework which could act as an axial ligand, much as has been done in mimicking cytochrome 450 (H. He et al., 2003). In view of its good coordination properties towards lanthanide ions and, also, its efficient sensitization of the metal-centered luminescence, a β-diketonate moiety was chosen, more precisely a diethyl malonate group. The latter was linked in *ortho* position of one of the phenyl *meso* substituent through a C_5O

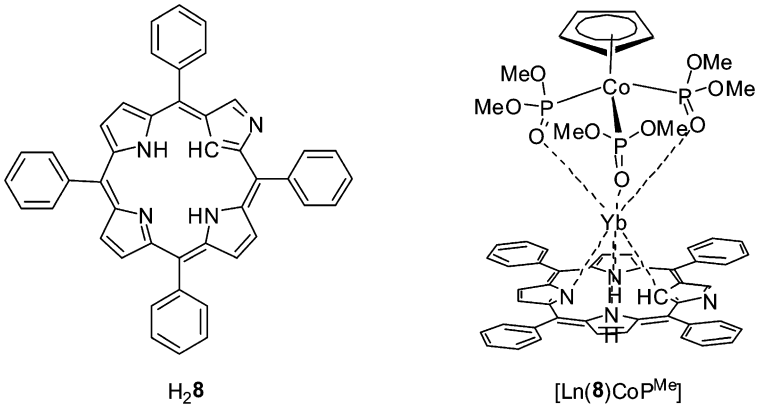

H_2**8** [Ln(**8**)CoP^{Me}]

Fig. 20. *N*-confused tetraphenyl-porphyrin and its Yb^{III} complex with a CoP capping anionic ligand.

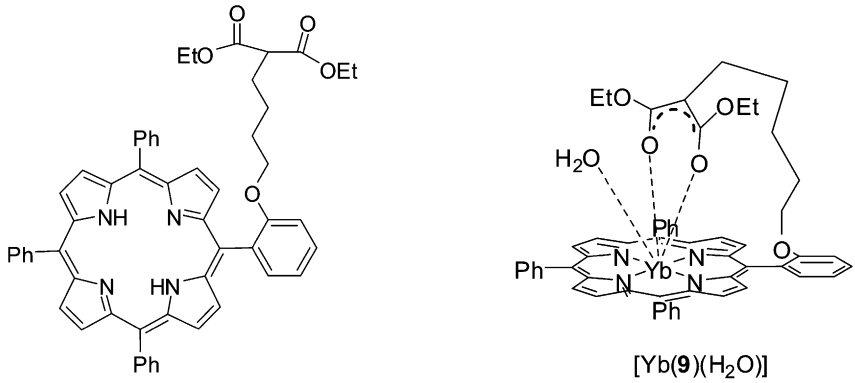

H_2**9** [Yb(**9**)(H_2O)]

Fig. 21. Diethyl malonate-appended porphyrin and its Yb^{III} complex.

alkyl chain. Air stable porphyrinates [Ln(**9**)(H_2O)] (Ln = Nd, Er, Yb) (fig. 21) were isolated and their stability has been ascribed to coordination of the malonate bidentate unit.

The three complexes display NIR luminescence in addition to porphyrinate emission at 650 nm, although Er^{III} luminescence is again faint. In addition, the Nd^{III} porphyrinate proved to be photosensitive and decomposed under irradiation by the N_2-laser (337 nm), so that its photophysical characteristic could not be determined. The lifetime of the Yb($^2F_{5/2}$) level amounts to 2.43 μs, that is about ten times smaller than for [Yb(**5d**)Tp^H]. Replacement of the water molecule with dmf when the porphyrinate is dissolved in this solvent results in an increase in the intensity of the metal-centered luminescence.

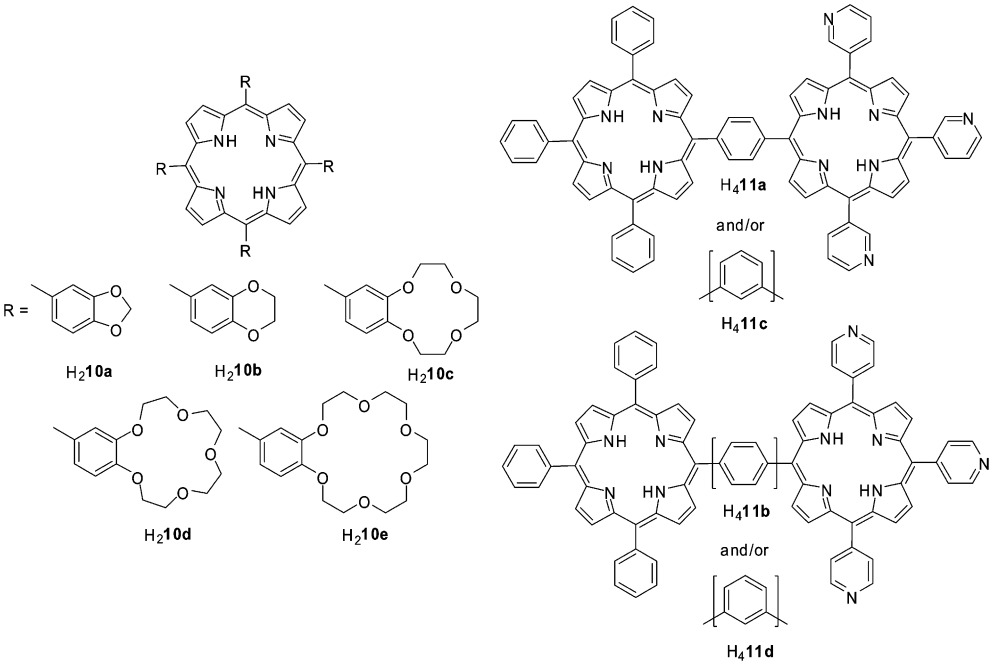

Fig. 22. Crown-ether derivatized porphyrins (left) and bis(porphyrins) (right).

The four *meso* positions of porphyrin have been substituted with several O-containing cycles, including benzodioxolan, benzodioxane, benzo-12-crown-4, benzo-15-crown-5, and benzo-18-crown-6 ethers (fig. 22) in an attempt to determine the influence of coordinated alkali ions on the Yb^{III} photophysical properties (Korovin et al., 2001). The triplet state in the [Yb(**10**)(acac)] complexes lies in the range 13 775–13 955 cm^{-1} and upon excitation at 532 nm, the $^5F_{5/2} \rightarrow {}^2F_{7/2}$ transition is seen for all five complexes.

The quantum yields of the metal-centered luminescence Q^L_{Yb} (determined in dmf at room temperature with respect to [Zn(**5a**)]) increase from 0.13% for **10a** and **10b**, to 0.19% (**10c**), and 0.27% (**10d**), while it is slightly smaller (0.25%) for **10e**; in parallel, τ_{obs} ($^2F_{5/2}$) ranges from 3.4 to 5.9 μs. Similarly, the ligand-centered luminescence decreases by 8–13%, confirming the ligand-to-metal energy transfer. Complexation of alkali-metal ions, Na^I with **10c**, K^I with **10d**, and Cs^I with **10e** results in changes in the absorption spectra of the Yb^{III} porphyrinates. They are assigned to the formation of sandwich-type dimers in which two porphyrinates encapsulate eight alkali cations: IR spectra clearly point to the coordination of the alkali cations. A concomitant increase in Q^L_{Yb} results: from 0.19 to 0.28% for **10c**, from 0.27 to 0.98% for **10d**, and from 0.25 to 0.70% for **10e**. The four-fold increase for K^I reflects the better stability of the K(benzo-15-crown-5)$_2$ complex with respect to the other alkali complexes.

The same group has also prepared bis(porphyrins) with the purpose of modeling electron-transfer processes (Korovin et al., 2002f). The four asymmetric bis(porphyrins) described in the right part of fig. 22 have been synthesized; one of the porphyrinic ring bears pyridine *meso* substituents since this moiety is favorable to the sensitization of Yb^{III} luminescence as depicted in fig. 16. The Soret band of the bis(porphyrins) is split by 7–11 nm, which suggests a positioning of the two porphyrin rings intermediate between parallel and perpendicular conformations. The bimetallic Yb^{III} bis(porphyrinates) were obtained from $Yb(acac)_3$ and the free bases in 1,2,4-trichlorobenzene, under argon atmosphere. The quantum yields Q_{Yb}^{L} (measured in dmf) of the compounds with **11a** (0.41%) and **11b** (0.54%) are larger than with **11c** (0.27%) and **11d** (0.35%). That is, 1,3-pyridyl *meso* substituents induce a more efficient sensitization than 1,4-pyridyl moieties, as does the *para* linkage of the two porphyrin units on the central benzene anchor. The quantum yields are comparable to the one determined for **5a**, but smaller than those for the porphyrinates with **6b** and **6c**. Model calculations explain the better luminescence of monoporphyrinates as opposed to bis(porphyrinates) by the absence of Yb···Yb interaction in the former. In the dimer, calculations yield Yb···Yb distances of 12.0 Å for complexes with **11a** and **11c**, and 10.8 Å for the compounds with **11b** and **11d**.

In summary, despite the adequate match between the energies of the porphyrinate triplet state and the $Yb(^2F_{5/2})$ level, the reported quantum yields to date for complexes in organic solvent are usually much smaller than 1%, with three exceptions, [Yb(**6c**)(acac)] (1.01% in methanol), [Yb(**5a**)Tp^H] (3.2% in CH_2Cl_2), and [Yb(**5a**)CoP] (2.4% in CH_2Cl_2), and protic solvents dramatically decrease these figures. Nevertheless, some applications of NIR-emitting lanthanidoporphyrinates have been proposed (see section 4), including the imaging of cancerous cells described above (Gaiduck et al., 1990), so that interest for these complexes remains high.

3.1.3. *Derivatized coronands and cryptands*

A coronand is a cyclic molecule containing several donor atoms in its ring. An archetypal example is the class of cyclic ethers termed crown ethers which contain the repeating –CH_2–CH_2–O– motif and were proposed by C.J. Perdersen in 1967. Other examples include *N*-containing aza crown ethers and cyclic Schiff base derivatives. The interaction of simple, neutral coronands with Ln^{III} ions in water is often weak, and the resulting coronates are amenable to axial interaction with solvent molecules so that they have often been derivatized in order to increase their coordination properties as well as their functionalities. Another strategy to overcome this problem is to include two amine bridgeheads in the cycle and graft an addition polydentate chain to yield cryptands (Sastri et al., 2003). In this section, we deal with the latter two classes of ligands, including cyclic Schiff bases. Cyclen derivatives and substituted calixarenes are discussed separately, in view of their special importance in lanthanide coordination chemistry.

With respect to heavier lanthanide ions such as Yb^{III}, 15-crown-5 has the most adequate cavity size (Bünzli and Pilloud, 1989) and Korovin has fitted this crown ether with an anilinoacridine chromophore which displays cytostatic and/or antiviral activity. If anilinoacridines alone, bearing a hydroxyl or a carboxylic acid substituent in *ortho*, *meta*, or *para* position (fig. 23), are reacted with ytterbium trinitrate, they yield 1:1 complexes with the *ortho*- and

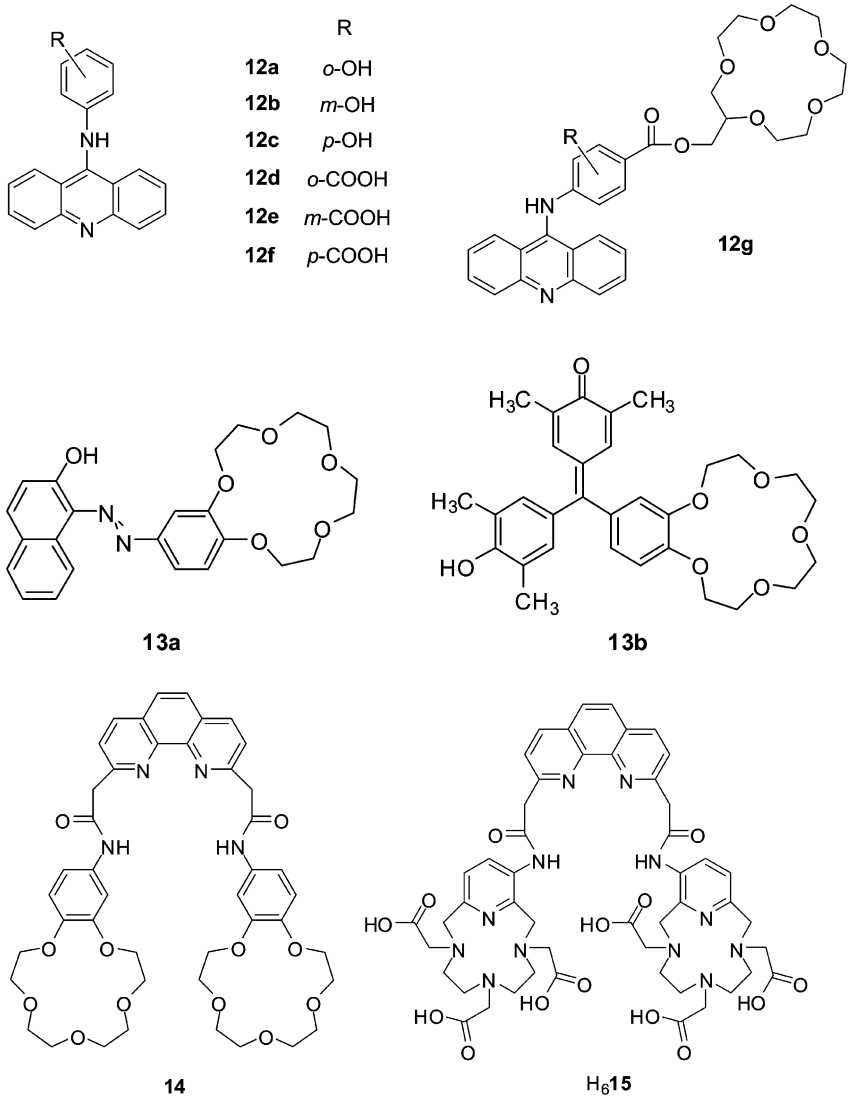

Fig. 23. Derivatized 15-crown-5 and benzo-15-crown-5 ethers, as well as a bis(azacyclic) ligand used to sensitize Nd^{III} and Yb^{III} luminescence (Korovin and Rusakova, 2004; Korovin et al., 2002c, 2002d, 2002e; Rusakova et al., 2004b).

meta-substituted ligands whereas the two *para*-substituted ligands **12c** and **12f** lead to the formation of 1:2 (metal:ligand) complexes. Upon complexation, the broad fluorescence band of the chromophore appearing in the range 460–540 nm is quenched to an extent of 85–90%, pointing to energy transfer onto the metal ion. The quantum yields of the metal-centered lu-

minescence in water–ethanol mixtures is the highest for the 1:2 complex while remaining extremely low: 0.0026 and 0.0034% for **12c** and **12f**, respectively (Korovin et al., 2002a). This is understandable because several water molecules still interact in the inner coordination sphere. The latter interaction is somewhat reduced in 1:1 nitrato complexes with macrocyclic ligand **12g** and the quantum yield increases substantially to reach 0.022% (Korovin et al., 2002e). This still low quantum yield arises from the insufficient protection of the Yb^{III} ion by the crown ether: since nitrate ions are displaced by water molecules, axial interaction with the solvent can still occur. Moreover, the energy of the triplet state of the acridine chromophore is around 21 000 cm^{-1} which is too high for an efficient sensitization.

Benzo-15-crown-5 ether has been derivatized with several light-harvesting chromophores with the aim of sensitizing NIR luminescence from Nd^{III} and Yb^{III} in protic solvents. For instance, dyes 1-phenylazo-2-naphthol (cf. **13a**, fig. 23) and xylenol blue (**13b**) with triplet states lying at approximately 16 270 and 15 850 cm^{-1}, respectively, have been fused to the polyether macrocycle. The resulting ligands form 1:1 complexes with lanthanide trinitrates, as expected (Bünzli, 1987), and they display a reasonably intense luminescence. The quantum yields determined upon excitation at 532 nm with respect to [Zn(**5a**)] amount to 0.66 and 0.88% for the Yb^{III} complexes with **13a** and **13b**, respectively, and to 0.09 and 0.12% for the corresponding complexes with Nd^{III}. According to an initial report (Korovin et al., 2002c), measurements have been carried out in methanol, but in a subsequent paper, the authors report the same figures for solutions in deuterated water (Korovin and Rusakova, 2004). Anyway, whichever the solvent was, the quantum yields for the macrocyclic Yb^{III} complexes are 5–8 times larger than those reported for the complexes with the chromophoric units alone.

Another sensitizing substituent used in conjunction with benzo-15-crown-5 units is 1,10-phenanthroline, which has been linked through its 2 and 9 positions to two macrocycles to yield **14**. The latter forms bimetallic 2:1 complexes with lanthanide nitrates; the quantum yields measured under the same experimental conditions as above, except for the solvent, acetone, are however smaller, 0.39% (Yb^{III}) and 0.067% (Nd^{III}), due the higher energy of the phenanthroline triplet state (Korovin et al., 2002d). On the other hand, bimetallic complexes with H_6**15** are much more stable ($\log K \approx 17$) and they provide a tighter environment for the first coordination sphere of the metal ion: [Ln_2(**15**)] complexes display the highest quantum yields reported so far for Nd^{III} and Yb^{III} compounds in water: 0.085 and 0.53%, respectively. Lifetime data measured both in water (0.72 μs for Nd^{III} and 4.55 μs for Yb^{III}) and deuterated water (1.34 μs for Nd^{III} and 8.86 μs for Yb^{III}) point to a relatively weak effect of water molecules on the radiationless de-excitation process: using Beeby's phenomenological equation (9a) for Yb^{III} (Beeby et al., 1999), one gets $q \approx 0.1$ (without applying the second-sphere correction). Data reported for complexes with the ligands depicted on fig. 23 clearly show the importance of optimizing the ligand-to-metal energy transfer process while simultaneously minimizing nonradiative deactivation of the metal-centered excited states.

Lanthanide chemistry with Schiff bases is quite extensive and numerous acyclic, cyclic, monometallic and polymetallic (4f–4f′, 4f–5f, 4f–nd) complexes have been synthesized and studied, in particular with compartmental ligands, owing to the ability of the latter to bind two or more metal ions in close proximity. Asymmetrization of these ligands also provides important diversification of the coordinating sites (Vigato and Tamburini, 2004). On the other

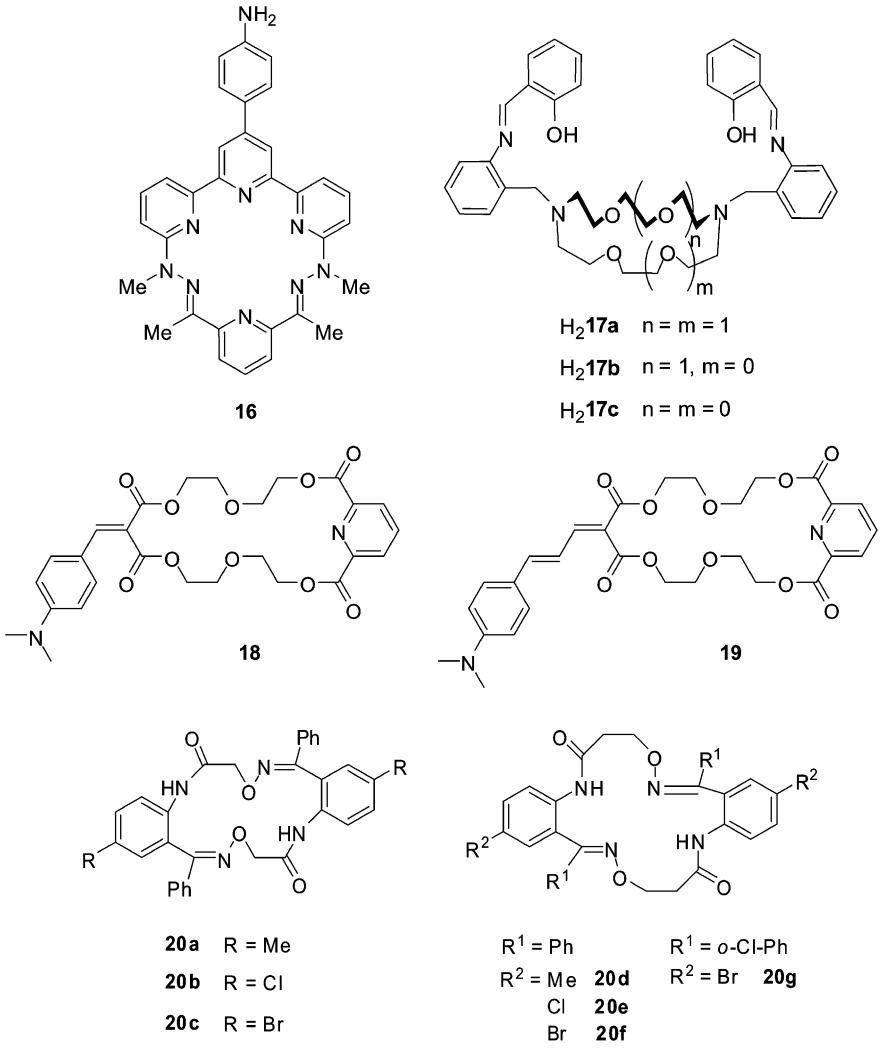

Fig. 24. Coronands and cyclic Schiff bases.

hand, there are only a few examples of sensitization of lanthanide NIR luminescence by such ligands. Interestingly, the complexes with ligand **16** (fig. 24) can be prepared in methanol by template-directed condensation of the terpyridine subunit with 2,6-diacetylpyridine in presence of $LnCl_3$ (Hall et al., 1998). The triplet state of this ligand has too low an energy (0-phonon transition at 18 400 cm^{-1} in EtOH/MeOH glass at 77 K) to sensitize Eu^{III} and Tb^{III} luminescence, but luminescence from $[Yb(H\mathbf{16})]^{4+}$ is detected in water, methanol and in their deuterated analogs. From the lifetimes determined at pH (resp. pD) ≈ 5–5.5, 0.32 and 9.1 μs,

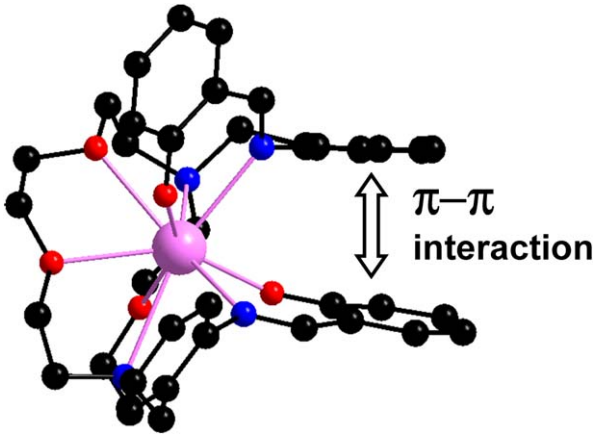

Fig. 25. Molecular structure of [Ce(**17b**)]$^{+}$, redrawn from (Gonzales-Lorenzo et al., 2003).

the hydration number q could be estimated to 2.8 ± 0.2. In presence of 0.1 M NaCl, the hydration number becomes smaller, 2.2 ± 0.2 (Beeby et al. 1999) consistent with the X-ray structure of the Eu^{III} complex which reveals two water molecules and one chloride ion bound in the inner coordination sphere. Upon increasing the pH (resp. pD), the Yb($^2F_{5/2}$) lifetime becomes longer and q decreases to eventually reach zero, which is tentatively explained by the successive formation of μ-hydroxo and μ-oxo dimers.

The three Schiff-base bibracchial lariat ethers H_2**17a–c** derivatives have been designed for their ability to form a cryptand-like cavity upon reaction with Ln^{III} ions, the size of which can be tuned by varying the number of –CH_2–CH_2–O– units in the macrocycle. The two 2-salicylaldiminobenzyl pendant arms fold in such a way that π–π interactions between aromatic rings result in the formation of a cryptand-like cavity, as demonstrated by the X-ray structure of the Ce^{III} complex with **17b** depicted on fig. 25 (Gonzales-Lorenzo et al., 2003). The triplet state of the di-anionic receptor is located at 18 750 cm^{-1} (0-phonon component measured on the Gd^{III} complex) so that sensitization of the NIR luminescence is not optimum; nevertheless, Nd^{III} emission could be detected.

The smaller receptor H_2**17c** is better suited for the complexation of heavier lanthanide ions. The [Ln(**17c**)]$^{+}$ complexes with Ln = Ho, Er are isostructural, as shown by X-ray structure determination and have essentially the same molecular arrangement as [Ce(**17b**)]$^{+}$, except for a smaller coordination number, 8, due to the reduced sized of the macrocycle (Gonzales-Lorenzo et al., 2005). Both Er^{III} and Yb^{III} complexes are emissive in the NIR range in acetonitrile and methanolic solutions. Determination of the lifetime of the Yb($^2F_{5/2}$) level in methanol (2.92 μs) and deuterated methanol (4.65 μs) leads to $q_{CH_3OH} \approx 0.2$ using eq. (9b) so that the induced cavity formed upon reaction of H_2**17c** with the smaller lanthanide ions is as protective as the one formed by H_2**17b** with the larger Ln^{III} ions. Lifetimes for Er^{III} are shorter, 0.42 μs in methanol for instance. The series of ligands H_2**17a–c** provides an original way of forming stable complexes in organic solvents, especially that the induced cavity can

be somewhat tuned to the size of the lanthanide ion. With respect to sensitization of Ln^{III} NIR luminescence however, the triplet states of these molecules, around 19 000 cm^{-1}, have too high energies to produce efficient ligand-to-metal energy transfers.

The two macrocyclic ligands **18** and **19** (fig. 24) were prepared with the hope of challenging the properties of Er^{III} *tris*(8-hydroxyquinolinate) [Er(8-Q)$_3$] which, at the time, was considered for producing organic electroluminescent diodes emitting in the 1.5 μm range. The idea was to extend the absorption edge of [Er(8-Q)$_3$] located at around 460 nm. Indeed, ligand **19** displays an absorption band at 550 nm. Unfortunately, the corresponding Er^{III} complex is four times less luminescent than the complex with ligand **18** the absorption edge of which is similar to the one of 8-hydroxyquinolinate. In absence of quantitative photophysical data (quantum yields, lifetimes), a convincing explanation could not be given (Meinardi et al., 2003).

Ligands **20a–c** form stable 1:1 complexes with lanthanide nitrates in dmf, with log K in the range 4.4–4.9. Determination of the hydration number q by lifetime measurements points to values close to two, so that it was inferred that the macrocyclic ligand is not completely bound to the metal ions. Nevertheless, the Yb^{III} compounds display NIR luminescence upon ligand excitation, despite a triplet state located at high energy (21 250–21 800 cm^{-1}): quantum yields amount to 0.007, 0.041, and 0.003% for complexes with **20a**, **20b**, and **20c**, respectively, while the corresponding lifetimes are 0.2, 1.1, and 0.4 μs. The heavy atom effect may be responsible for the larger values of the latter two quantum yields, although one would have expected the values for the chloro- and bromo-substituted ligands being inverted (Pavlovsky et al., 2004). Replacement of nitrate with chloride leads to smaller values of quantum yield and lifetime for **20a** (0.005%, 0.1 μs) and **20b** (0.030%, 0.8 μs) while the quantum yield of **20c** becomes larger, (0.006%) despite a small shortening in the lifetime to 0.3 μs (Rusakova et al., 2005). Expansion of the 16-membered cycle to 18 atoms results in a large improvement in quantum yields by factors 7, 6, and 21 for the nitrato complexes with **20d**, **20e**, and **20f**, respectively. It is noteworthy that the quantum yield of the nitrato complex [Yb(NO$_3$)$_3$(**20e**)] reaches 0.23% (lifetime = 2.4 μs). A similar effect is observed for the chloro complexes with **20d** and **20f** the quantum yields of which increase by factors seven and eight, while [YbCl$_3$(**20e**)] displays a two-fold reduction in quantum yield compared with [YbCl$_3$(**20b**)]. Finally, *ortho* substitution of the phenyl groups of **20f** by chlorine also increases the quantum yields of both chloro (0.09%, lifetime = 1.3 μs) and nitrato (0.19%, lifetime = 1.9 μs) complexes two to threefold with respect to the unsubstituted compounds; unfortunately, such a substitution has not been probed for **20e** (Rusakova et al., 2005).

The series of ligands **21** derived from 2,6-substituted pyridines (fig. 26) was designed to determine the influence of the number of aromatic chromophoric fragments (between one and four) on the NIR luminescence properties of Nd^{III}. Ligands **21a–e** have been prepared by templated condensation of pyridine-2,6-dicarboxyaldehyde and the corresponding diamine in methanol with Nd(NO$_3$)$_3$·6H$_2$O as the templating agent. With respect to the complex with **21c** taken as reference, the luminescence intensity in dmf is approximately twice as large for complexes with ligands having two (**21a**) and three (**21d**, **21f**, **21g**) aromatic chromophores, while it is distinctively larger for those having four such units (**21b**, factor 4.3, and **21e**, factor 4.8). It is noteworthy that other modifications in the cyclic ligands such as the nature of the

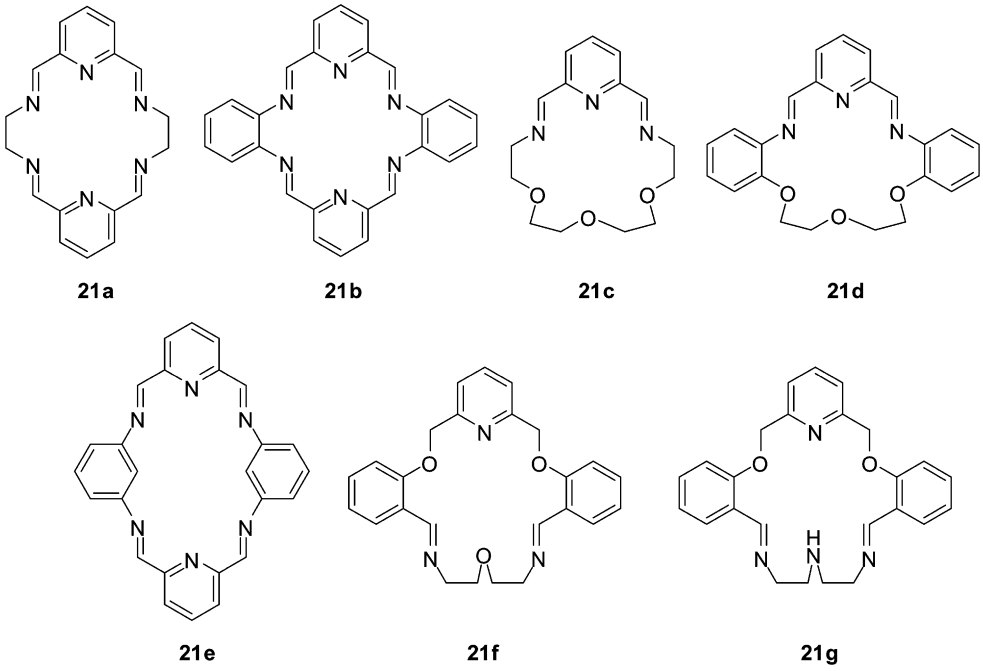

Fig. 26. Aza and oxaza macrocycles.

donor atoms (oxygen versus secondary and/or tertiary amines) have little influence on the overall luminescence intensity (Korovin et al., 2003).

In order to test the behaviour of lanthanide luminescent molecular complexes as optical amplifiers for polymer-based waveguides working in the NIR range, Reinhoudt and collaborators have synthesized *m*-terphenyl-based pre-organized hemispherands and used Eu(III) as a model for studying the effects of the organic ligands on the metal-centered luminescence. The macrocyclic ligands reduce the solvent coordination, as demonstrated for the Eu^{III} complexes with **22a**, $q_{CH_3OH} = 1.9 \pm 0.5$, and **22c**, $q_{CH_3OH} \approx 1$ (Wolbers et al., 1997c), so that these authors subsequently synthesized ligand **22b** (fig. 27) for the sensitization of Nd^{III} with the hope of reducing further solvent interaction in the inner coordination sphere (Wolbers et al., 1997b). Lifetime measurements on a solution of the Eu^{III} complex with the dioxolane-decorated ligand **22b** at a concentration of 10^{-4} M in methanol and deuterated methanol yield essentially the same lifetimes (1.42 and 1.56 ms, respectively) so that q_{CH_3OH} is indeed close to zero for this ion. Unfortunately, NIR emission of [Nd(**22b**)] is extremely weak in non-deuterated methanol, with a lifetime shorter than 0.2 μs, whereas it amounts to 0.5 μs in fully deuterated methanol, indicating that solvent molecules still coordinate to this larger lanthanide ion, contrary to Eu^{III}.

Further investigations were therefore undertaken with ligands **22c** and **22d**, which sensitize both visible- and NIR-emitting Ln^{III} ions (Wolbers et al., 1998b). Due to the fact that the en-

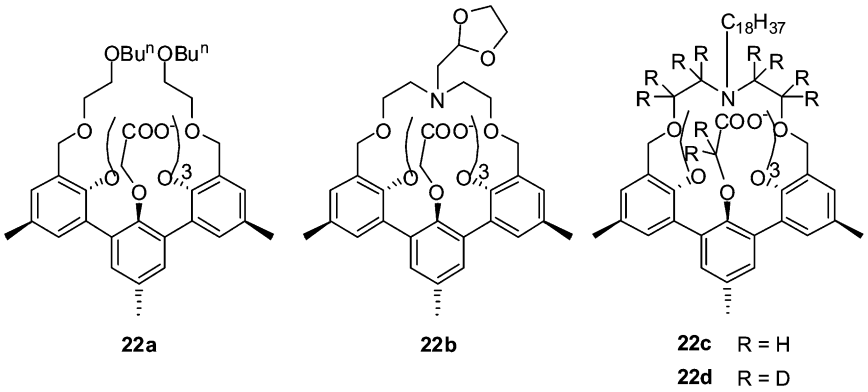

Fig. 27. Hemispherands designed by D.N. Reinhoudt (Wolbers et al., 1997b, 1998b).

ergy gap between $^1G_4$ and $^3F_4$ ($\approx$3000 cm^{-1}) is resonant with a C–H vibration, the Pr($^1G_4 \rightarrow {}^3H_5$) transition could not be observed. On the other hand, Nd^{III}, Er^{III} and Yb^{III} luminescence was detected for complexes with **22a**, **22c** and **22d**, its intensity increasing in the same order. For Nd^{III}, lifetime determination in both non-deuterated and deuterated methanol revealed that solvent molecules still interact in the first coordination sphere of the complexes with **22c** and **22d**. Partial deuteration of ligand **22c** resulted in an increase in the luminescence intensity in deuterated methanol by a factor 2.3 while the lifetime increased from 0.79 to 0.89 μs. From these data, the authors estimated the rate constant for quenching by the C–H modes of the ligand to be 142 ms^{-1}, as compared to 21 ms^{-1} for Yb^{III} (determined from the luminescence lifetimes of 16 and 24 μs in methanol and deuterated methanol), and 6 ms^{-1} for Sm^{III}, emphasizing the large role played by these vibrations in the quenching of Ln^{III} NIR luminescence. The Er^{III} complexes yield a relatively broad emission band in deuterated *n*-butanol, which is of interest for telecommunication applications, although its intensity is very weak and the associated lifetime quite short, 0.8 μs (Wolbers et al., 1998b).

Cryptands have been somewhat deceptive for both coordination chemistry (Sastri et al., 2003) and photophysical properties of the resulting lanthanide complexes despite some commercial uses (Mathis, 1998), in particular of Lehn's Eu^{III} cryptate with cryptand **23a** (fig. 28). The latter has been tested for the sensitization of the NIR luminescence of Nd^{III} and Yb^{III}. Characteristic emission from these two ions is seen upon excitation of the bipyridyl chromophores at 355 nm. Emission from Yb^{III} is reported to be much more intense than the one from Nd^{III} and the authors propose that the excitation mechanism depicted in fig. 9 is operative in this case since no transient absorption corresponding to the formation of the triplet state could be detected (Faulkner et al., 2001). Analysis of lifetime measurements in both water ($\tau(^2F_{5/2}) = 0.52$ μs) and deuterated water (5.21 μs) gives a hydration number $q = 1.5$. Since fitting the luminescence decays to a double exponential function did not improve noticeably the resulting fit, the authors concluded that the non-integer value does not reflect an equilibrium between two different hydration states but, rather, that the distance of close approach of two water molecules is longer: note that comparable experiments on Eu^{III} and Tb^{III}

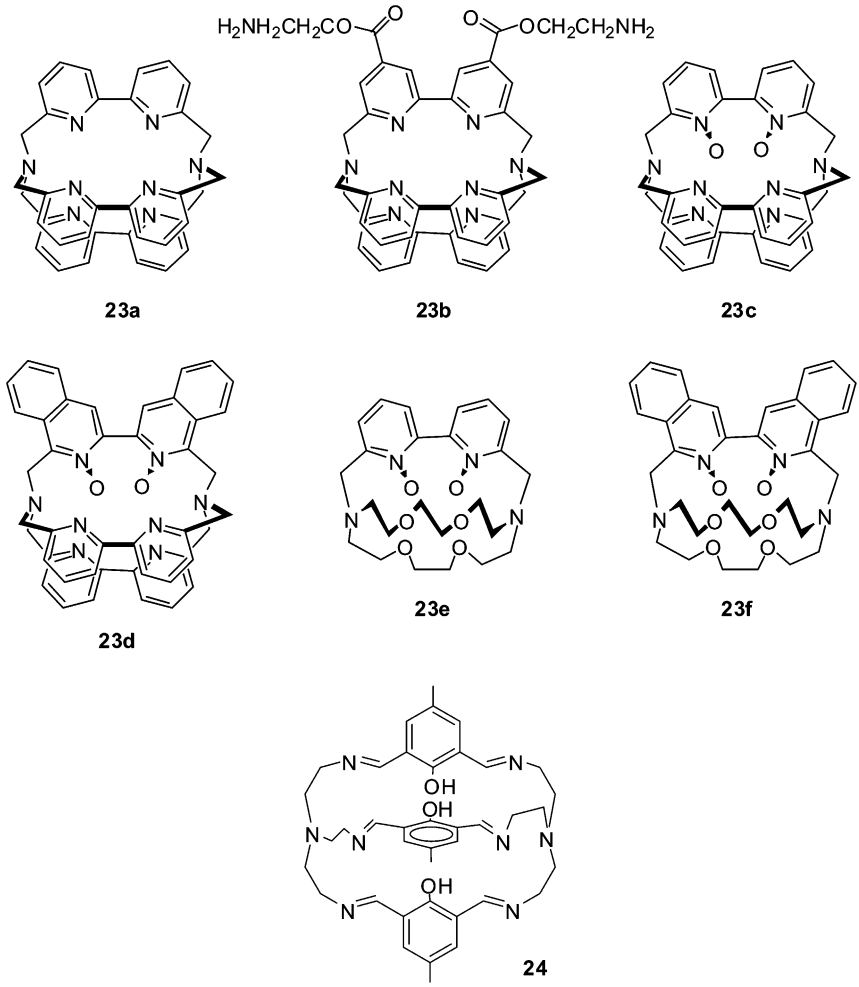

Fig. 28. Some cryptands proposed for the sensitization of NIR luminescence.

cryptates yield $q \approx 2$. Establishing q for the Nd^{III} cryptate proved to be more difficult since no reliable parameters A, B, and/or C (see eqs. (8) and subsequent discussion above) are published to date. The authors tried to calibrate a relationship by measuring the relevant data for complexes with edta, nta, dtpa, and a cyclen derivative for which $q = 2, 2, 1$, and 0, respectively. When applied to the present case, eq. (10a) yielded $q \approx 0.5$, a value obviously too low, that was explained by the absence, in the cryptate, of a large number of C–H oscillators in the vicinity of the Nd^{III} ion. The Nd^{III} cryptate possesses indeed a relatively long lifetime, 0.1 μs in water and 0.3 μs in deuterated water.

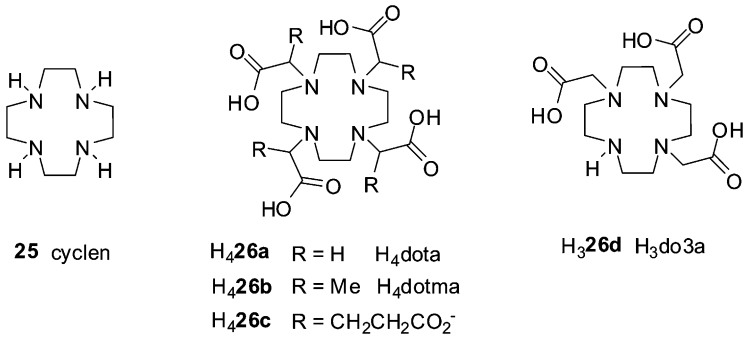

Fig. 29. Basic ligands derived from cyclen.

Following this study, Korovin and coworkers tested cryptands **23b–f** which are used in time-resolved luminescent immunoassays (Mathis, 1993) for the sensitization of Yb^{III} luminescence (Korovin et al., 2002b). From the lifetimes determined in both water and deuterated water, one calculates that the hydration number varies from ≈2 (**23b**), to ≈1.5 (**23a**, **23e**), and finally to ≈1 (**23c**, **23d**, **23f**). Quantum yields were not determined, but luminescence intensities relative to the cryptate with **23a** (in water, at room temperature) point to cryptands **23c** and **23d** being the best sensitizers of the Yb^{III} luminescence with a seven-fold enhancement, while cryptates with **23e** and **23b** are only 1.5- to 1.8-times more luminescent.

The iminocryptate **24**, which can be prepared by a one-pot template reaction, was initially designed for the simultaneous complexation of two 4f ions (Platas et al., 2000) or one 4f ion and one 3d (e.g. Zn^{II}, Cu^{II}) ion (Rodriguez-Cortinas et al., 2002). Sensitization of Nd^{III} and Yb^{III} was also observed, particularly in the 4f–Zn^{II} heterodimetallic cryptates, for which the crystal field splitting of the 4f levels could be interpreted in terms of a distorted C_3 local symmetry.

3.1.4. *Derivatized cyclens*

One of the most studied classes of macrocyclic ligands in lanthanide coordination chemistry is without any doubt the molecules derived from cyclen **25**, a 12-membered ring bearing four amino functions, 1,4,7,10-tetraaza-dodecane (fig. 29). In particular, its tetra-carboxylic derivative H_4dota (H_4**26a**) was synthesized in 1976 by a German chemist, H. Stetter from the University of Aachen, who isolated complexes with divalent transition metal and alkaline-earth cations (Stetter and Frank, 1976). The tetra-carboxylic acid has pK_a values of 11.1, 9.69, 4.84, and 3.95 (in solutions with $\mu = 0.1$ M KCl). Three years later, a young Belgian chemist, Jean François Desreux from the University of Liège, discovered that $dota^{4-}$ forms highly stable complexes with lanthanide ions, with $\log K_1$ in the range 25–28, and that these complexes are also highly kinetically inert.

At that time, the medical industry was looking for good contrast agents able to enhance the sharpness of magnetic resonance images and trivalent gadolinium was an obvious candidate in view of its 7/2 spin. However, Gd^{III} is toxic (the lethal dose, LD_{50}, for gadolinium chloride

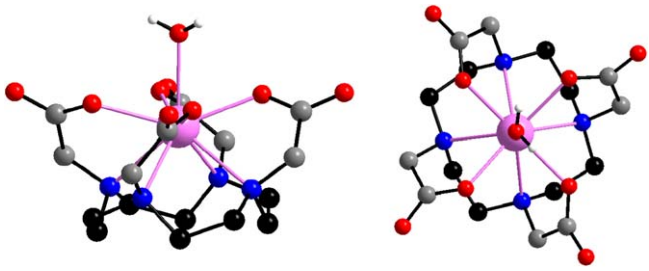

Fig. 30. Two views of the structure of $[Gd(dota)]^-$ showing the encapsulation of the metal ion by the four pendant arms (left) and the C_4 symmetry (right, top view). Redrawn from (Chang et al., 1993).

is 0.4 mmol kg^{-1} for mice) because its ionic radius is almost equal to that of Ca^{II}, resulting in replacement of the latter in a number of calcium-dependent systems. Many proteins exhibit a binding affinity up to 1000-fold higher for Gd^{III} compared with Ca^{II} in view of the higher charge density of the former cation. As a consequence, Gd^{III} had to be inserted into a very stable and highly inert complex before being injected to patients. Henceforth the choice of $dota^{4-}$ was made by a French company, Guerbet SA, which filed a patent in 1988 for meglumine gadoterate, $[Gd(dota)(H_2O)]^-(mgl)^+$, under the registered trade mark Dotarem™ (meglumine is 1-deoxy-1-(methylamino)glucitol, $MeHN–(CH_2)–(CHOH)_4–(CH_2OH)$.

The structure of $[Gd(dota)]^-$ is shown in fig. 30. The coordination cavity is achieved by the four nitrogen atoms of the ring and by four additional oxygen donor atoms located on each dangling arm. With respect to the commonly observed 9-coordination of the trivalent lanthanide ions in aqueous solution, one position remains free for interaction with water, an essential feature in the design of contrast agents. The four carboxylate groups are folded, yielding a monocapped square antiprismatic coordination (SAP) with a twist angle of about 40° that is close to the ideal value of 45°. In fact, in solution, two species coexist, which are in slow exchange on the NMR time scale. These species differ in the position of the bound acetates relative to the macrocycle, with the major isomer, denoted M and which predominates for Nd–Lu complexes with dota, having the square antiprismatic geometry illustrated above. The other isomer, m, possesses a twisted square antiprismatic coordination geometry (TSAP), with a twist angle ranging between 15° and 30°. It is of prime importance to note that the SAP isomer bears one coordinated water molecule (coordination number CN = 9), while the TSAP isomer is devoid of water coordination (CN = 8). The relative concentration of the two isomers depends of the specific ligand: if the M isomer predominates for dota complexes (for Yb^{III}, the ratio is about 4:1) the situation is reverse for dotma compounds for which the m isomer is the most abundant.

The formation of the $[Ln(dota)(H_2O)]^-$ species is rather slow since it corresponds to considerable stiffening of the ligand. Detailed kinetic studies unveiled the following reaction mechanism (Wu and deW. Horrocks, 1995; Lincoln, 1997):

$$Ln^{3+}(aq) + H_2dota^{2-}(aq) \leftrightarrows [Ln(H_2dota)(H_2O)_5]^+(aq), \quad K \approx 10^6\ M^{-1}. \tag{20}$$

In a first step, intermediate species form rapidly upon mixing the lanthanide ion with H_4dota. Both excited state luminescence lifetime determinations for the Eu^{III} complex (Chang et al., 2001) and molecular mechanics calculations are consistent with a structure in which the lanthanide ion is coordinated to four carboxylate groups, well away from the nitrogen atoms of the macrocycle, two of which are protonated. This intermediate may react with a hydroxide group to form monoprotonated neutral species in a rapid equilibrium.

$$[Ln(H_2dota)(H_2O)_5]^+(aq) + OH^- \leftrightarrows [Ln(Hdota)(H_2O)_5](aq) + H_2O. \quad (21)$$

Finally, the monoprotonated species rearrange into the final product:

$$[Ln(Hdota)(H_2O)_5](aq) \leftrightarrows [Ln(dota)(H_2O)]^- + 4H_2O + H^+. \quad (22)$$

The rate of conversion of $[Ln(H_2dota)(H_2O)_5]^+(aq)$ into $[Ln(dota)(H_2O)]^-$ is pH-dependent and ranges from 7.2×10^{-4} to 7.9×10^{-2} s^{-1} for Ln = Eu as the pH is raised from 3.8 to 5.8; similar values are obtained for Ln = Gd. Dissociation of the Gd-dota complex is also very slow and its half-life in a 0.1 M solution of hydrochloric acid is larger than one month.

The usual dose for a MRI experiment is 0.1 mmol kg^{-1}, there are few side effects and excretion is reasonably fast (75% in 3 h). Given these properties, the cyclen framework has been also used for designing potential luminescent bioprobes emitting either in the visible or in the NIR spectral ranges. Since luminescence probes do not necessarily require four chromophores, a common synthetic pathway is to start from H_3do3a (H_3**26d**, fig. 29), or from its analog with protected carboxylic acid groups, now commercially available, and to derivatize the remaining secondary amine function with the desired chromophore. Another framework with interesting properties is H_8dotp (fig. 31). Its complexes have been studied in details with regard to their solution and magnetic properties, and their potential as high-resolution NMR shift reagents for protein structure determination. The thulium complex $[Tm(dotp)]^{5-}$ induces a particularly large paramagnetic shift. The thermodynamic stability constants with the first half of the lanthanide series (La–Gd) are in the range $\log K = 28.9$–29.6, as determined by a competitive method with the dye arsenazo III (Sherry et al., 1996). They are slightly larger than those for $[Ln(dota)]^-$ and the complexes display only one isomer in solution, on the NMR time scale, as opposed to two for $[Ln(dota)]^-$, see above. The only drawback of the dotp complexes is the larger negative charge, which may be a problem for *in vivo* applications, by increasing substantially the osmotic pressure. This is a reason why phosphinic acid derivatives (fig. 31) are often preferred since their complexes bear only one negative charge, similarly to dota complexes.

The first study using a cyclen derivative to sensitize the NIR emission of Yb^{III} appeared in 1997. David Parker (Beeby et al., 1997) found that the tetrabenzyl phosphinate complex $[Yb(\mathbf{27c})]^-$ which, according to X-ray and relaxometry investigations, contains no bound water (Aime et al., 1997), displays a longer $Yb(^2F_{5/2})$ lifetime (4.5 μs in H_2O) than [Yb(**27d**)] (1.87 μs in H_2O). In deuterated water, the lifetime of $[Yb(\mathbf{27c})]^-$ increases to 8.9 μs; using eq. (9a) without the second sphere correction, one gets $q \approx 0.1$, that is the residual quenching effect can be assigned to a contribution from closely diffusing, unbound water molecules ("outer-sphere" effect). The Nd^{III} complex with **27c** has a lifetime of 0.16 μs in water and 0.33 μs in deuterated water (Faulkner et al., 1999), and use of eq. (10a) yields indeed $q \approx 0$.

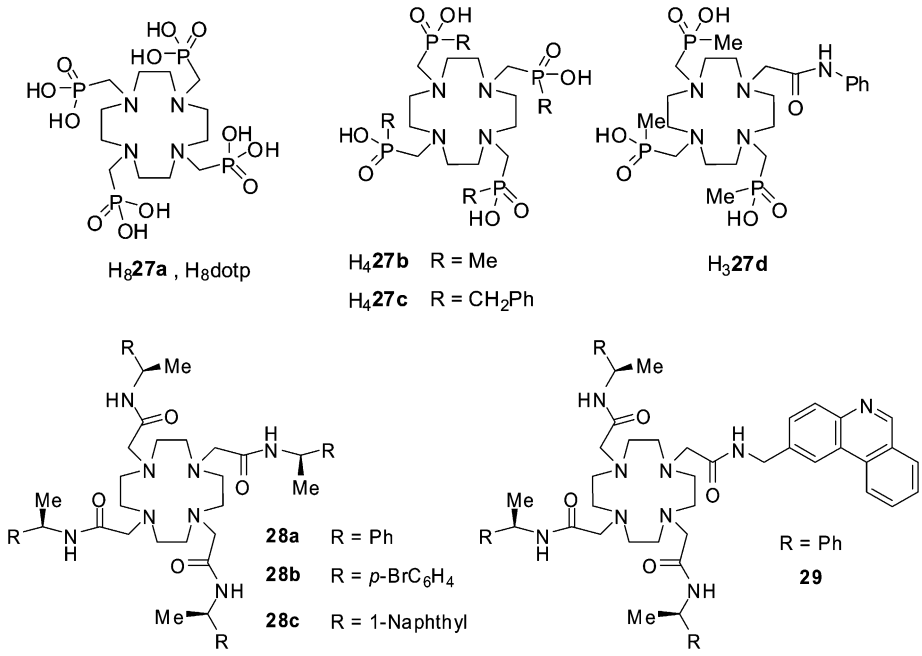

Fig. 31. Phosphonic and phosphinic acid derivatives of cyclen (top), and tetraamide derivatives (bottom).

The shorter lifetime of the related mono-amide triphosphinate complex [Yb(**27d**)] (6.7 μs in D_2O) leads to $q \approx 0.4$ (without the correction) or $q \approx 0.15$ if the correction in eq. (9a) is taken into account. This apparent hydration number can be explained by the presence of a hydrogen bonded water molecule, as demonstrated for the Eu^{III} and Tb^{III} complexes (Aime et al., 1996). On the other hand, the lifetimes of the related complexes with the tetraamide ligands **28a–c** (fig. 31) are much shorter (0.7–0.8 μs in H_2O and 5.0–7.5 μs in D_2O) reflecting the presence of bound water molecules, in line with known crystal structures with other lanthanide ions. The rate of water dissociation in $[Ln(\mathbf{28a})(H_2O)]^{3+}$ is 500-fold faster for Ln = Yb, compared to Eu, as ascertained by NMR data: $k_{dis} = (1.9 \pm 0.7) \times 10^6\ s^{-1}$ ($\Delta G^0 = 34.6 \pm 2.6\ kJ\ mol^{-1}$). The rate constants for the decay of the Yb($^2F_{5/2}$) excited level amount to $1.6 \times 10^5\ s^{-1}$ ($\tau_{obs} = 6.25$ μs) in D_2O and $1.4 \times 10^6\ s^{-1}$ ($\tau_{obs} = 0.71$ μs) in H_2O at room temperature, that is close to the water exchange rate constant. Therefore, single exponential decays are observed at this temperature. At lower temperature, a single decay is still observed for the D_2O solution, but in water, the decay becomes bi-exponential, the faster process being ascribed to the 9-coordinate monohydrated species and the slower one to the 8-coordinate non-hydrated complex (Batsanov et al., 1999).

The quenching effect of proximate OH, NH, and CH vibrations on Yb^{III} luminescence (see eq. (9a)) has been determined by measuring the rate constants for the depopulation of the $^2F_{5/2}$ state of complexes with $edta^{4-}$, $dtpa^{5-}$, $(\mathbf{H16})^+$ (fig. 24), $(\mathbf{26a})^{4-}$, $(\mathbf{26c})^{4-}$ (fig. 29),

Table 6
Comparison between actual (q) and calculated (q_{corr}) hydration states for Yb^{III} complexes with cyclen derivatives (Beeby et al., 1999)

Complex	q[a]	Δk_{obs} (μs^{-1})[b]	$A \times \Delta k_{corr} = q_{corr}$[c]
[Yb(**27c**)]$^{-}$	0	0.11	0
[Yb(**27b**)]$^{-}$	0	0.24	0.04
[Yb(**26a**)]$^{-}$	0.8[d]	0.50	0.30
[Yb(**26c**)]$^{-}$	0	0.74	0.54
[Yb(**28a**)]$^{3+}$	1	1.27	1.07
[Yb(**28c**)]$^{3+}$	1	1.00	0.80
[Yb(**28b**)]$^{3+}$	1	1.17	0.97
[Yb(H**16**)]$^{4+}$	3	2.98	2.78
[Yb(**27d**)]	0	0.38	0.18

[a] As determined by NMR or X-ray diffraction.
[b] $\Delta k_{obs} = k_{H_2O} - k_{D_2O}$.
[c] $A = 1$ μs; $\Delta k_{corr} = \Delta k_{obs} - 0.20\ \mu s^{-1}$, except for **27c**.
[d] Taking into account the 4:1 *M*:*m* isomer proportion.

(**27b**)$^{4-}$, (**27c**)$^{4-}$, (**27d**)$^{3-}$, and **28a–c** (fig. 31) in both water and deuterated water (Beeby et al., 1999). Deuterated analogs have been synthesized as well, particularly for replacing the N–H group in the amide ligands **28** with N–D functions, and for substituting some of the ring CH_2 groups of dota. In fact NH/ND exchange does occur rapidly on the experimental timescale and double exponential decays were observed for the cationic complexes with amides **28**. The main results for the evaluation of the effect of proximate water molecules are reported in table 6.

Given the uncertainty of ±15% affecting the lifetime measurements, an average uncertainty of ±0.3 can be assigned to the q_{corr} values. Except in the cases of the anionic complexes with (**26a**)$^{4-}$ and (**26c**)$^{4-}$, agreement between the values calculated from the lifetimes and the values estimated from other data is good. In fact, additional corrections should apply, in particular for the presence of N–H oscillators in the tetraamide complexes (0.06 μs^{-1}) and for the CH oscillators (0.088 μs^{-1}). Equation (9a), in which B is set to 0.25 μs^{-1} and C to 0, takes these contributions partially into account.

Circularly polarized luminescence (CPL) from chiral molecular systems is the emission analog of circular dichroism (CD) and as such reflects the chirality of the excited state in the same manner as CD probes reflect the chirality of the ground state (Riehl and Muller, 2005). For lanthanide ions, large CPL (and/or CD) signals are expected for f–f transitions obeying magnetic dipole selection rules, in particular $\Delta J = 0, \pm 1$; Eu($^5D_0 \rightarrow {}^7F_1$), Tb($^5D_4 \rightarrow {}^7F_4$, $^5D_4 \rightarrow {}^7F_5$), Dy($^4F_{9/2} \rightarrow {}^6H_{11/2}$), Yb($^2F_{5/2} \rightarrow {}^2F_{7/2}$) emissions are typical examples. Recent advances in instrumentation permit the detection of very small differences in the intensity of left versus right circular polarization, opening the field for measurements of Yb^{III} complexes. In CPL, results are usually reported in term of the dissymmetry ratio g_{lum}:

$$g_{lum} = \frac{\Delta I(\lambda)}{(1/2) I(\lambda)} = \frac{2[I_L(\lambda) - I_R(\lambda)]}{I_L(\lambda) + I_R(\lambda)}, \tag{23}$$

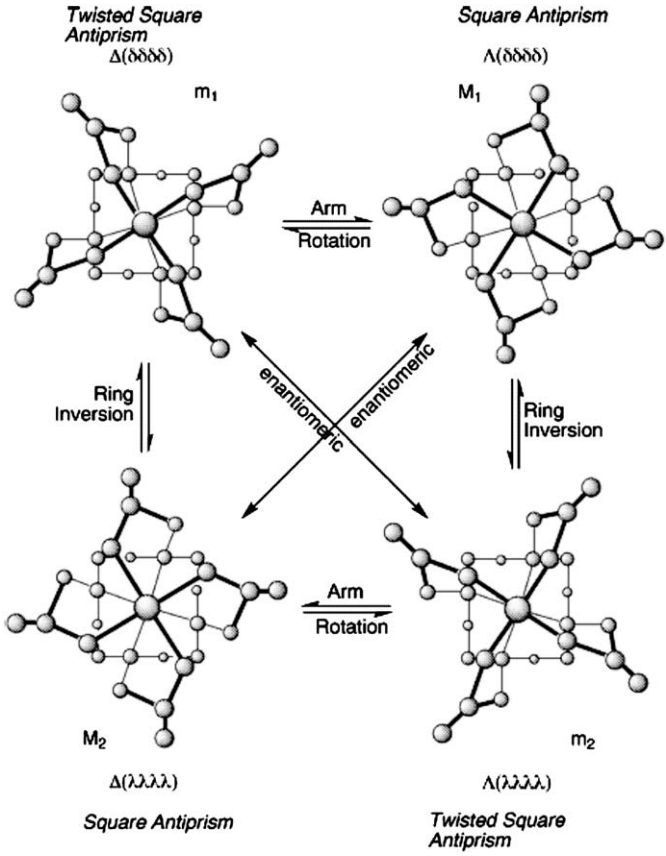

Fig. 32. Schematic representation of the isomers of cyclen-based complexes, with chirality and potential exchange mechanisms between them. From (Dickins et al., 1998), reproduced with permission of the Royal Chemical Society (RSC) on behalf of the Centre National de la Recherche Scientifique (CNRS).

in which R and L stands for right polarized and left polarized emission intensity, respectively. The dissymmetry factor provides useful information concerning the structural changes that take place on the timescale of the light emission. Complexes with cyclen derivatives display rich chiral properties, induced both by the positioning of the arms, indicated by Δ for a clockwise or by Λ for an anti-clockwise arrangement, and the cycle which can adopt two enantiomeric conformations in the complex, $\lambda\lambda\lambda\lambda$ or $\delta\delta\delta\delta$ in each 5-member chelate ring according to Corey and Bailar's classification (fig. 32). The ring inversion of $[Yb(dotma)]^-$ (fig. 29), $\Lambda(\lambda\lambda\lambda\lambda) \leftrightarrows \Lambda(\delta\delta\delta\delta)$, in methanol, is a slow process on the NMR timescale and the equilibrium is in favor of the m isomer over the M form (in a proportion of about 13:1), with $K(298) = 0.075$, $\Delta H^0 = -4\ \mathrm{kJ\,mol^{-1}}$, $\Delta S^0 = -35\ \mathrm{J\,K^{-1}\,mol^{-1}}$. The NIR CD spectrum of the $^2F_{5/2} \leftarrow {}^2F_{7/2}$ transition shows several well-resolved transitions with a very high

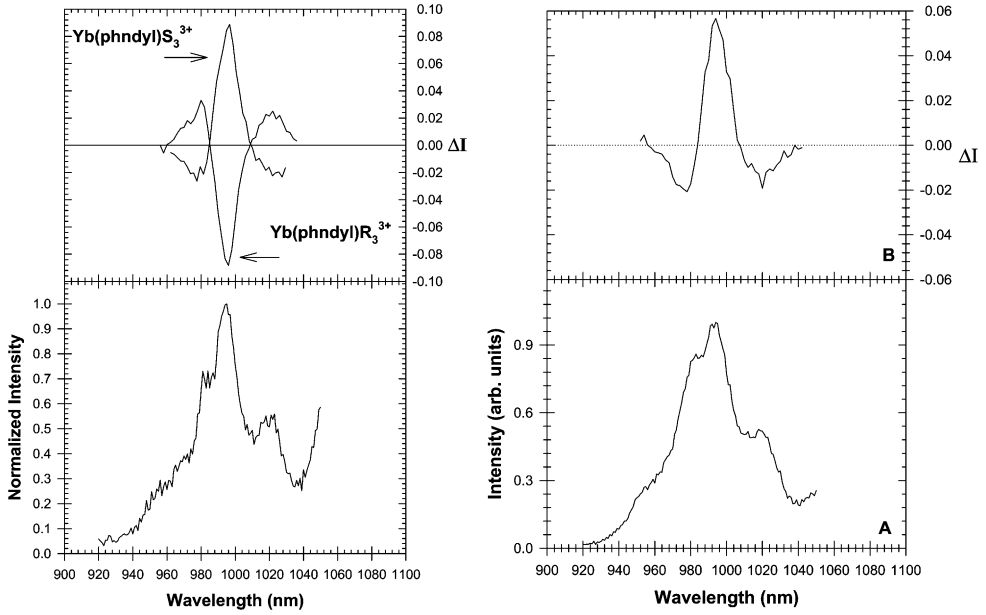

Fig. 33. Total luminescence spectra (B) and circularly polarized spectra (A) of the Yb($^2F_{5/2} \rightarrow {}^2F_{7/2}$) transition for [Yb(*S*-**29**H)]$^{4+}$, [Yb(*R*-**29**H)]$^{4+}$ 1 mM in D_2O (left) and [Yb(*S*-**28b**)]$^{3+}$ 0.5 mM in D_2O (right). Reproduced with permission from (Maupin et al., 1998). Note: phndylR$_3$ and phndylS$_3$ correspond to *R*-**29**H$^+$ and *S*-**29**H$^+$, respectively.

dissymmetry factors. The ligand field splitting and population of the LF sub-levels have been determined as a function of temperature (Di Bari et al., 2000a).

In the first study of CPL emission of optically active Yb^{III} complexes with tetra-amide derivatives of cyclen, the authors have selected ligands **28b** and **29** (fig. 31), the latter bearing a phenanthridyl chromophore for better sensitization of the Yb^{III} luminescence when it is protonated (Maupin et al., 1998). The two enantiomers *R* and *S*, with each chiral amine having the same conformation produce C_4-symmetrical complexes with, as a consequence, a splitting of the Yb^{III} levels into three ($^2F_{5/2}$) and four ($^2F_{7/2}$) ligand-field sub-levels. This splitting is reflected in the total emission spectrum of [Yb(**29**H)] 1 mM in D_2O containing trifluoroacetic acid; as required by symmetry, two opposite CPL spectra are obtained for the two complexes with the two enantiomers and the dissymmetry factors calculated for the three main peaks of the spectra $|g_{lum}|$ are >0.1, that is analogous to those reported for similar complexes with Eu^{III} and Tb^{III}. The sign pattern in the CPL spectrum of [Yb(*S*-**28b**)]$^{3+}$ is identical to the one displayed by [Yb(*S*-**29**H)]$^{4+}$ while the dissymmetry factor is somewhat smaller (fig. 33). This is evidence that the replacement of one of the chiral amines with the achiral phenanthridyl group does not change the C_4 arrangement around the central metal ion.

Further studies reported similar CPL spectra for [Yb(**28a**)]$^{3+}$, as compared to [Yb(**28b**)]$^{3+}$ (Dickins et al., 1999), with dissymmetry factor g_{lum} for the peak corresponding to the maximum of luminescence (at 995 nm) of −0.18 (Maupin et al., 2000). A quantitative comparison with the CD spectrum for which the absorption dissymmetry factor $g_{abs} = -0.11$ is difficult in view of the spectral overlap of various transitions from differently populated LF sub-levels, as demonstrated in a previously cited study (Di Bari et al., 2000a). However, such a comparison is useful to verify the sign of the CPL emission:

$$g_{abs} = \frac{\Delta\varepsilon}{(1/2)\varepsilon} = \frac{2(\varepsilon_L - \varepsilon_R)}{\varepsilon_L + \varepsilon_R}. \tag{24}$$

C_4-symmetric species are prime targets for developing useful correlations between CPL spectra and chemical structure, and the sign (and magnitude) of the CPL signals have been correlated to the degree of helical twist of the complex, the strength of the ligand field, and the polarisability of the axial donor group (Di Bari et al., 2000b; Dickins et al., 2003; Lisowski et al., 2004). The local helicity at the lanthanide center can also be related to the angle between the electric dipole and magnetic dipole transition moments and therefore to the rotary strength of a given transition; however, most of the CPL studies associated with this correlation have been performed on Eu^{III} and Tb^{III} C_4-symmetrical species (Riehl and Muller, 2005).

As mentioned above, the phenanthridyl chromophore is more efficient in sensitizing Yb^{III} emission when it is protonated, so that [Yb(**29**H)]$^{4+}$/[Yb(**29**)]$^{3+}$ can act as a switchable luminescent couple in function of pH. In fact this corresponds to two different mechanisms for the sensitization of Yb^{III} luminescence (Beeby et al., 2002c). As depicted in fig. 9, a rapid, sequential electron exchange mechanism is thought to be responsible for the sensitization of Yb^{III} luminescence at least when both electron transfer steps are thermodynamically feasible, which is the case here. Indeed the triplet state energies are ≈22 000 cm^{-1} for the phenanthridine chromophore and ≈21 300 cm^{-1} for the phenanthridinium moiety and both have negligible overlap with the $^2F_{5/2}$ excited state. Since the rate of the backward electron transfer $Yb^{II} \rightarrow Yb^{III*}$ is fast, one can simplify the mechanism by writing:

$$\text{Phen}^* + \text{Yb}^{III} \xrightarrow{k_{et}} \text{Phen} + \text{Yb}^{III*} \xrightarrow{k_{lum}} \text{Phen} + \text{Yb}^{III} + h\nu. \tag{25}$$

Therefore, the intensity of the emitted light is given by:

$$I(t) \propto \frac{k_{et}}{k_{lum} - k_{et}} \cdot \left(e^{-k_{et}t} - e^{-k_{lum}t}\right). \tag{26}$$

From eq. (26), one sees that if $k_{et} \gg k_{lum}$, the growth of the metal-centered luminescence will mirror the decay of the triplet state, k_T, while the decay of the metal-centered luminescence will be determined by $k_{obs} = k_{lum}$. On the other hand, if $k_{et} \ll k_{lum}$, that is when the energy transfer step is rate determining, the observed decay rate constant will reflect the decay of the triplet state, $k_{obs} = k_T$, and therefore k_{obs} will depend on the degree of aeration of the solution; the growth of the Yb^{III}-centered luminescence will be independent of the presence of oxygen but conversely it will depend on the nature of the solvent. The kinetics of the energy transfer has been investigated by time-resolved luminescence of the metal

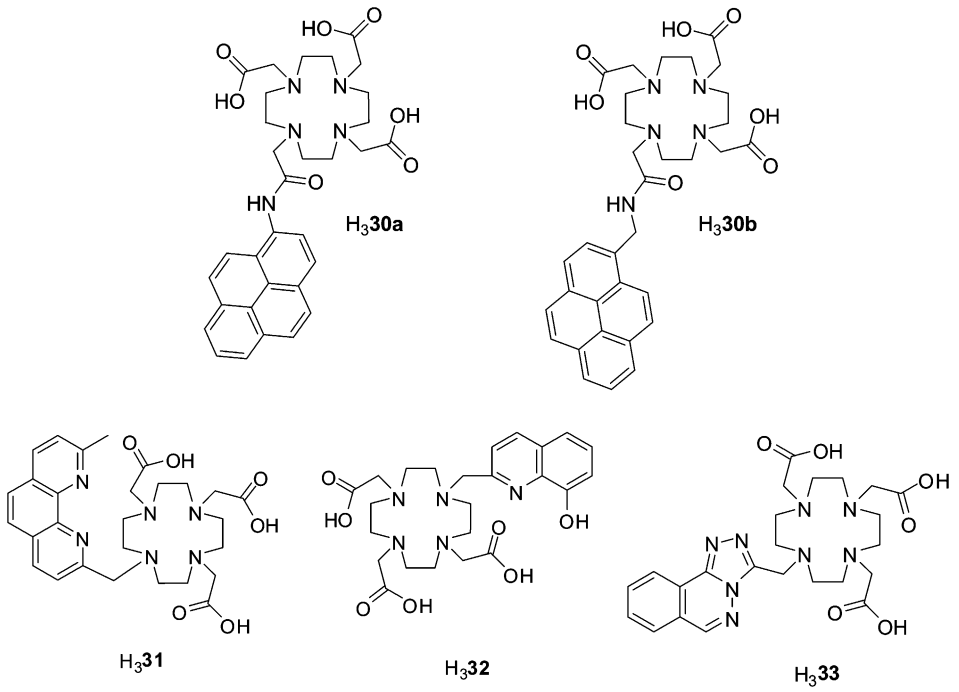

Fig. 34. Chromophore-appended dota ligands.

ion, as well as by fluorescence and triplet–triplet absorption data for the phenanthridine chromophore in both acidic and neutral water and deuterated water. In addition, it was established that the presence of oxygen decreased the luminescence intensity of Yb^{III} by a factor 4–5 for the protonated complex while it did not affect the non-protonated compound. Since it is well established that oxygen does not quench directly lanthanide excited states, the effect of oxygen on the metal-centered luminescence reveals a quenching of the triplet state. From these data, the authors could establish that the protonated complex $[Yb(\mathbf{29}H)]^{4+}$ follows a classical behaviour with direct sensitization of the Yb^{III} luminescence through energy transfer from the triplet state. The profile of the time-resolved luminescence for the un-protonated complex $[Yb(\mathbf{29})]^{3+}$ which is the major species for pH > 6 is very different, with a luminescent decay independent of aeration, pointing to a sensitization mechanism following the double electron transfer depicted in fig. 9. A similar investigation for $[Nd(\mathbf{29}H)]^{4+}$ ruled out the latter mechanism for the sensitization of Nd^{III} (Beeby et al., 2001), which is in line with Nd^{II} not being readily accessible in water ($E^0_{red} < -2.5$ V).

Other chromophores have been grafted onto the dota framework (fig. 34). Both pyrene-sensitized Nd^{III} and Yb^{III} emissions have been observed with ligands $H_3\mathbf{30a}$ and $H_3\mathbf{30b}$; lifetime determinations in H_2O and D_2O led to $q_{Nd} = 0.8$ and 1.0, respectively, while data for Yb^{III} yielded 1.1 and 0.5, respectively. Interestingly, quantum yields for [Ln(**30a**)] in which

the pyrene chromophore is directly bound to the amide coupling group are 1.6-fold larger than for [Ln(**30b**)] in which the pyrene sensitizing group is linked by a methylene spacer. In line with this observation, the rise time in complexes with H_3**30b** is longer (70 ns for Nd^{III} and 125 ns for Yb^{III}) than in complexes with H_3**30a** (<5 ns for Nd^{III} and 15 ns for Yb^{III}), implying a less efficient energy transfer with increasing separation of the chromophore and the metal ion (Faulkner et al., 2004).

A way of expelling the interacting water molecule out of the first coordination sphere is to use a bidentate pendant chromophore such as *o*-phenanthroline in ligand H_3**31**, which will saturate the coordination sphere of the metal ion. As a matter of fact, the hydration number of [Eu(**31**)] proved to be zero and the antenna is reasonably efficient in sensitizing the europium luminescence ($Q^{L}_{Eu} = 30\%$ in D_2O as determined with respect to $[Ru(bpy)_3]^{2+}$ in aerated water, $Q = 2.8\%$). Despite a close to 1 value of η_{sens} for the Er^{III} complex, the quantum yield in D_2O remains extremely weak for this compound, $Q^{L}_{Er} = 5 \times 10^{-4}\%$, in line with the difficulty of preventing nonradiative deactivation for this ion (Quici et al., 2004). The complex with 8-hydroxyquinoline-fitted ligand H_3**32** also emits a weak Er^{III} luminescence in water at pH 7, but no quantitative data are at hand (Rizzo et al., 2004). Lifetimes only are reported for [Ln(**33**)] (Ln = Nd, Eu, Er, Yb) in H_2O and D_2O ($q_{Eu} = 0.9$) and the Er^{III} luminescence in water is said to be very weak (Burton-Pye et al., 2005).

Instead of grafting a coordinating chromophore on the macrocyclic framework, which sometimes requires the recourse to relatively complicated synthetic routes, another strategy was tested, which forms ternary complexes in situ. An example is pyrene acetic acid H**34** (fig. 35) which reacts with [Ln(**26d**)$(H_2O)_2$] to form kinetically labile ternary complexes [Ln(**26d**)(**34**)$(H_2O)_x$], Ln = Nd, Yb (Faulkner et al., 2004). Metal-centered luminescence occurs upon pyrene excitation. However, according to lifetime measurements for Yb^{III}, 0.72 and 2.52 μs in H_2O and D_2O, respectively, and the use of eq. (9a), $q = 0.9$, which suggests that a pyrene acetic acid molecule is coordinated to the metal center expelling one water molecule, but not the second one. That is, the ternary complex does not represent an improvement over [Yb(**30a**)].

Another potential ancillary ligand is tetrathiafulvalene carboxylic acid H**35a**. Indeed, the sulfur-based heterocycle tetrathiafulvalene is a highly efficient electron donor which can be oxidized sequentially to the radical cation and dication and which is incorporated in various materials applications. Ligand H**35a** effectively acts as a sensitizer for Yb^{III} luminescence and lifetime measurements on [Yb(**35a**)$_3$] in methanol (0.50 μs) and deuterated methanol (3.67 μs) point to $q_{CH_3OH} = 3.25$ (cf. eq. (9b)), whereas the ternary complex [Yb(**26d**)(**35a**)] has $q_{CH_3OH} = 0.2$ ($\tau_{H_2O} = 2.02$ μs, $\tau_{D_2O} = 3.49$ μs). In the latter, sensitization occurs through the double electron redistribution mechanism outlined in fig. 9, as substantiated by electrochemical data leading to an estimated $\Delta G \approx 2.37$ eV for the electron back transfer (Faulkner et al., 2002). S.J.A. Pope has further screened several other mono- and di-anionic ligands, **35b–e** (fig. 35); all of the ternary complexes [Ln(**26d**)(**35b–e**)] (Ln = Nd, Yb) are emissive, some of them weakly, while luminescence from Er^{III} species is faint which prevented lifetime determination. Lifetimes for methanolic solutions are in the range 1.4–2 ms for Yb^{III} and **35a**, **c**, **e** while no emission is observed for **35b**; for Nd^{III}, lifetimes range from 108 to 237 ns for **35a–e**. From the q_{MeOH} values deduced from lifetime data for Yb^{III}, carboxylates appear to

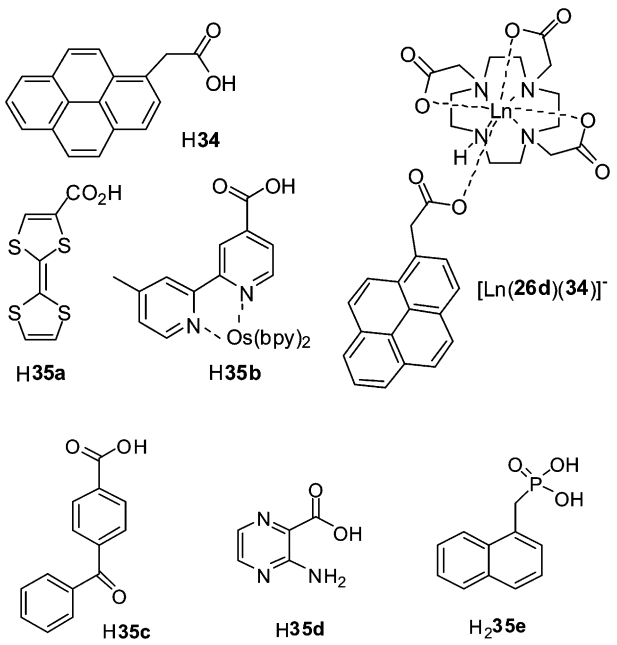

Fig. 35. Ancillary chromophoric ligands for the formation of ternary complexes.

behave as monodentate ligands and their replacement with phosphate anions is quite easy; by contrast, phosphonate derivatives are more robust, being bound in a bidentate fashion (Pope et al., 2006). Altogether, however, it seems that the strategy of producing ternary complexes in situ has not yielded better sensitization efficacy compared to 1:1 complexes with octa- or nona-dentate ligands.

Finally, there are also some reports of Nd^{III} and Yb^{III} bimetallic complexes in which two cyclen moieties are coupled together by a chromophoric unit (fig. 36). Korovin and Rusakova have screened a series of seven dyes, with triplet state energy in the range 13 750–14 320 cm^{-1}, for their ability to sensitize Nd^{III} and/or Yb^{III} luminescence. The best one proved to be phthalexon S, with quantum yields in D_2O of 0.41% for Yb^{III} and 0.025% for Nd^{III} and consequently, ligand H_7**36** was synthesized by a Mannich reaction involving phenol red, do3a, and formaldehyde in 1:3:3 proportion (Korovin and Rusakova, 2002). Complexes with 2:1 Ln:L stoichiometry (Ln = Nd, Yb) are soluble in water and both the quantum yields and lifetimes are noticeably larger than those for the 1:1 complexes with the dye, or with do3a. For the bimetallic Yb^{III} complex, $Q^{L}_{Yb} = 1.45\%$ in D_2O measured with respect to [Zn(TPP)], which is indeed one of the largest quantum yields reported for an ytterbium complex in solution. The corresponding lifetime amounts to 12.6 μs and decreases to 6.8 μs in H_2O which corresponds, according to eq. (9a), to $q \approx 0$, a surprising result at first, but the inexistent hydration may be traced back to the lipophilicity of the linkage unit. The corresponding data for Nd^{III} are $Q^{L}_{Nd}(D_2O) = 0.23\%$, $\tau_{H_2O} = 0.75$ μs and $\tau_{D_2O} = 1.45$ μm. Under the same

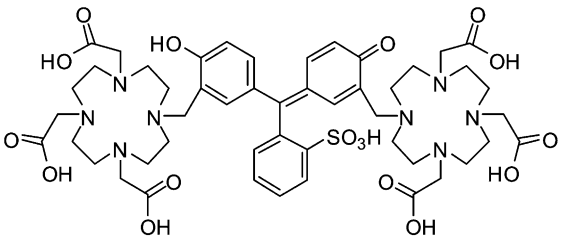

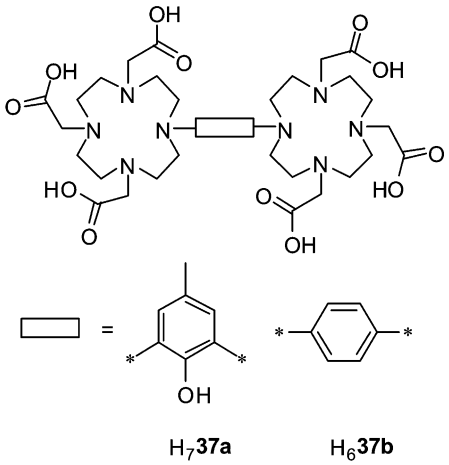

Fig. 36. Cyclen-based ditopic ligands for bimetallic complexes.

excitation conditions (532 nm), luminescence for the bimetallic Er^{III} complex could only be observed in dmso-d_6 ($\tau = 1.8$ μs) (Korovin and Rusakova, 2004).

Reaction of the ditopic ligand H_7**37a** with ytterbium triflate yields a well defined, kinetically stable bimetallic complex. Its photophysical properties demonstrate that two different Yb^{III} environments are present on the luminescence timescale. For instance, luminescence decays upon excitation at 337 nm are bi-exponential, with lifetimes of 0.51 and 1.67 μs in water and 1.17 and 4.95 μs in D_2O. The corresponding q values are 0.3 and 1.0 (eq. (9a)). There are essentially two possibilities, either the formation of one bimetallic complex with two different binding sites or the co-existence of two forms of the complex in solution. From a coordination viewpoint, a reasonable assumption if the first hypothesis is valid would be that both sites are 8-coordinate, by the seven donor atoms of each macrocycle and by either a water molecule or a phenol oxygen, since the bulk of the macrocycles prevents the two metal ions from sharing the latter donor atom (Pope et al., 2003b). When the phenol linkage group is replaced with a simpler p-xylene unit in H_6**37b**, the $Yb(^2F_{5/2})$ decay is a single exponential function corresponding to lifetimes of 1.45 μs in water and 6.07 μs in deuterated water, hence

to $q = 0.4$ (eq. (9a)). The two binding sites are now equivalent, as further demonstrated by the NMR spectrum and the hydration is close to zero, with a somewhat unusual coordination number of 7, again possibly due to the hydrophobicity of the coupling group (Pope et al., 2003a).

3.1.5. *Derivatized calixarenes and resorcinarenes*

Calix[*n*]arenes are a family of macrocycles prepared by condensation reactions between *n* *para*-substituted phenols and *n* formaldehyde molecules under either base or acid catalysis. Different sizes of the macrocycles can be obtained ($n = 4$–20) (Stewart and Gutsche, 1999) depending on the exact experimental conditions, which were mastered in the 1960's (Gutsche, 1998), but the most common receptors are those with $n = 4, 6, 8$ (macrocycles with an odd number of phenol units are more difficult to synthesize). We use here the simplified nomenclature in which the number of phenolic units is indicated between square brackets and *para* substituents are listed first.[4] Calixarenes, which can be easily derivatized both on the *para* positions of the phenolic units and on the hydroxyl groups, have been primarily developed for catalytic processes and as biomimics, but it was soon realized that they can also easily encapsulate metal ions and the first complexes with d-transition metal ions were isolated in the mid-1980's (Olmstead et al., 1985). Jack Harrowfield characterized the first lanthanide complex with a calixarene in 1987, a bimetallic europium complex with *p-tert*-butylcalix[8]arene (Furphy et al., 1987).

Calix[4]arenes can adopt several conformations. The most usual one is when the four alkyl substituents are on the same side, resulting in a cone conformation, stabilized by strong hydrogen bonds between the intra-annular OH groups. Initially, the rim bearing the alkyl substituents was termed "upper rim"; however, to avoid potential confusions, the current practice is to name it "wider rim". The other conformers are the partial cone one in which one alkyl substituent lies opposite to the three other ones, the 1,2-alternate and the 1,3-alternate. Most of the lanthanide complexes with calix[4]arene derivatives contain the ligand in the cone conformation. The calixarene framework can be regarded as a platform with two rims onto which functional groups can be separately grafted to modify either the coordination behaviour or the lipophilicity, which is important for solubility. The size of the induced cavity can be modulated both by adjusting the number *n* of phenolic units and/or the size of the pendant-arm substituents. Simple calix[*n*]arenes bearing no substituent on the narrower rim and *p-tert*-butyl groups on the wider rim form complexes with lanthanide ions with the following Ln:L stoichiometry: 2:2 for $n = 4$ and 5, 1:2 for $n = 6$, but one ligand molecule is not coordinated, and 2:1 for $n = 8$ (Bünzli et al., 2000). Some 1:1 complexes with the latter are also known (Bünzli and Besançon, 2005), and this stoichiometry is often seen with derivatized calix[4]arenes. When phenol is replaced with resorcinol, similar cyclic compounds are obtained, which have the same four conformational possibilities as calix[4]arene, but which are more fluxional in absence of intra-annular OH groups (fig. 37).

[4] *p-tert*-Butylcalix[4]arene for instance is 5,11,17,23-tetra-4-*tert*-butyl-25,26,27,28-tetrahydroxycalix[4]arene or for a complete description, pentacyclo[19.3.1.13,7.19,13.115,19]octacosa-1(25),3,5,7(28),9,11,13(27),15,17,19(26),21,23-dodecaene-25,26,27,28-tetrol, 5,11,17,23-tetrakis(1,1-dimethylethyl).

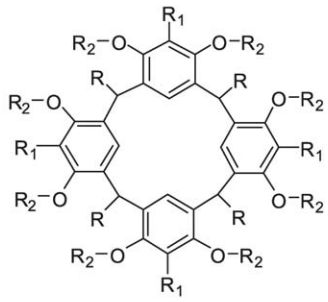

	R	R_1	R_2
H_8**38a**	C_6H_5	CH_2-N(C_2H_5)$_2$	H
H_8**38b**	CH_3	CH_2-N(C_2H_5)$_2$	H
H_8**38c**	CH_3	H	H
38d	CH_3	H	$COCH_3$
H_8**38e**	C_6H_5	H	H
38f	C_6H_5	H	$COCH_3$
38g	CH_3	Br	$COCH_3$

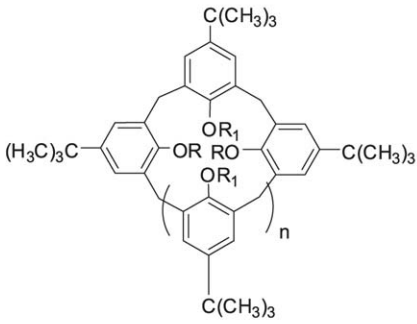

	n	R_1	R
H_4**39a**	1	H	H
39b	1	CH_3	R_1
39c	1	$H_2CHC{=}CH_2$	R_1
H_4**39d**	1	CH_2COOH	R_1
39e	1	CH_2COOCH_3	R_1
H_2**39f**	1	$CH_2CONHC_6H_5$	H
H_8**40**	5	H	H

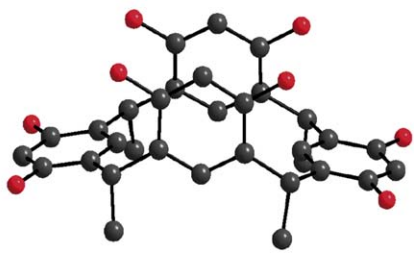

H_8**38c**

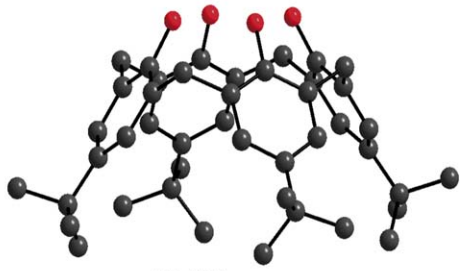

H_4**39a**

Fig. 37. (Top) Formulae of calix[4]resorcinarenes; (middle) formulae of calix[n]arenes; (bottom) X-ray structures of (left) calix[4]resorcinarene (MacGillivray et al., 2001) and (right) *p-tert*-butylcalix[4]arene (Ungaro et al., 1985).

Shevchuk and coworkers have performed systematic investigations of Nd^{III} and Yb^{III} 1:1 complexes with a series of calix[4]resorcinarenes and calix[4]arenes. A first study aimed at establishing an analytical procedure for the determination of these two ions in organic solvents. The intrinsic luminescence of the ligand is quenched when Yb^{III} chloride is added to the so-

Table 7
Quantum yields (Yb^{III}) or partial quantum yields (Nd^{III}) for 1:1 complexes of Ln^{III} chlorides with calix[4]resorcinarenes and calix[4]arenes measured upon ligand excitation (290 nm) at room temperature

Ligand	Solvent	E_T (cm^{-1})	Q_{Nd} (%)[a]	Q_{Yb} (%)	Refs.
H_8**38a**	dmf (Nd)[b]	18 400	0.028 (0.053)	0.095	[c]
H_8**38b**	Ethanol (Yb)	19 000	0.013 (0.027)	0.086	
H_8**38c**		18 800	0.043 (0.075)	0.068	
38d		19 500	0.026 (0.049)	0.061	
H_8**38e**		18 200	0.065 (0.107)	0.037	
38f		18 500	0.056 (0.084)	0.033	
38g		19 000	0.012 (0.026)	0.026	
H_4**39a**	dmf		0.080	0.120	[d]
39b			0.090	0.180	
39c			0.060	0.090	
H_4**39d**		20 600–23 500	0.180	0.220	
39e			0.070	0.120	
H_2**39f**			0.240	0.610	

[a]Determined taking into account only the $^4F_{3/2} \rightarrow {}^4I_{11/2}$ transition (1.06 μm). Values in parentheses take into account the two transitions $^4F_{3/2} \rightarrow {}^4I_{11/2}$, $^4I_{9/2}$.
[b]Whether measurements were performed in dmf or ethanol is not clear.
[c](Shevchuk et al., 1998b, 1999).
[d](Shevchuk et al., 1998a; Korovin and Rusakova, 2001).

lution and the maximum of metal-centered luminescence for macrocycles H_8**38a** and H_8**38b** occurs when a 1:1 stoichiometric ratio is reached. The nature of the solvent has a large influence on the luminescence intensity, the best ones being dmf for the first complex and ethanol for the second, with an approximate 12-fold increase in luminescence intensity over water. The presence of the phenyl group in H_8**38a** is beneficial to the sensitization process and linear relationships were obtained in the concentration ranges 0.1–10 μg ml^{-1} and 0.5–5 μg ml^{-1}, for H_8**38a** and H_8**38b**, respectively. The estimated detection limit for the Yb^{III}/H_8**38a**/dmf system is 0.09 μg ml^{-1}, but other Ln^{III} ions interfere (Shevchuk et al., 1997). The quantum yields of the Yb^{III} complexes with the calix[4]resorcinarenes reported in fig. 37, which possess triplet states between 17 700 and 19 500 cm^{-1} as determined from the phosphorescence spectra of the Lu^{III} solutions, range from 0.026% for **38g** to 0.095% for H_8**38a** in ethanol (for a detailed listing, see table 7). The influence of the various substituents is not clear, for instance the exchange of the phenyl group by a methyl group does not produce the same change in the pairs H_8**38a/b**, **38c/e**, and **38d/f**, and surprisingly, the introduction of a bromine substituent in **38g** decreases the quantum yield with respect to **38d**, possibly pointing to a sensitization mechanism involving the singlet state of the ligand since the presence of the bromine substituent increases the efficiency of the isc process; as a consequence, the population of the singlet state decreases. However, the reported quantum yields, measured on 10^{-4} M solutions with respect to [Zn(TPP)], should be considered with some care since the authors did not establish the speciation in these solutions (Shevchuk et al., 1998b). A study conducted on Nd^{III} solutions

Table 8
Partial quantum yields[a] of Nd^{III} and quantum yields of Yb^{III} luminescence upon ligand excitation (300 nm) in homo- and hetero-bimetallic complexes with *p-tert*-butylcalix[8]arene in dmf, at room temperature (Korovin et al., 2000)

Compound	Q_{Nd} (%)	Compound	Q_{Yb} (%)	Compound	Q_{Nd} (%)	Compound	Q_{Yb} (%)
Nd_1Nd_1	0.088	Yb_1Yb_1	0.432	$Nd_{1.8}Tb_{0.2}$	0.207	$Yb_{1.95}Nd_{0.05}$	0.522
$Nd_{1.8}Sm_{0.2}$	0.185	$Yb_{1.9}Sm_{0.1}$	0.629	$Nd_{1.5}Tb_{0.5}$	0.135	$Yb_{1.9}Nd_{0.1}$	0.503
$Nd_{1.5}Sm_{0.5}$	0.152	$Yb_{1.8}Sm_{0.2}$	0.612	Nd_1Tb_1	0.042	$Yb_{1.8}Nd_{0.2}$	0.374
Nd_1Sm_1	0.052	$Yb_{1.5}Sm_{0.5}$	0.534	$Nd_{0.2}Tb_{1.8}$	0.011	$Yb_{1.8}Pr_{0.2}$	0.007
$Nd_{1.8}Eu_{0.2}$	0.177	Yb_1Sm_1	0.356	$Nd_{1.8}Yb_{0.2}$	0.012	$Yb_{1.8}Dy_{0.2}$	0.021
$Nd_{1.5}Eu_{0.5}$	0.105	$Yb_{1.8}Eu_{0.2}$	0.078	$Nd_{1.5}Yb_{0.5}$	0.005	$Yb_{1.8}Ho_{0.2}$	0.012
Nd_1Eu_1	0.057	$Yb_{1.8}Tb_{0.2}$	0.051	$Nd_{0.2}Yb_{1.8}$	0.003		
$Nd_{0.2}Eu_{1.8}$	0.007	$Yb_{1.5}Tb_{0.5}$	0.014				

[a]Determined taking into account the two $^4F_{3/2} \rightarrow {}^4I_{11/2}$, $^4I_{9/2}$ transitions only.

led to similar conclusions with quantum yields in the range 0.026 to 0.107% (Shevchuk et al., 1999). In addition, the number of bound dmf molecules in the inner coordination sphere was assessed by measurement of the luminescence intensity in various dmf/dmf-d_7 mixtures; it amounts to one for H_8**38a**, H_8**38b**, and **38g**, and to two for the other ligands.

The higher energy of the triplet states in calixarenes **39a–f** (fig. 37), 20 600–23 500 cm^{-1}, allows sizeable sensitization of Eu^{III} and Tb^{III} luminescence. Compared with calix[4]resorcinarenes, better quantum yields are also obtained for the Nd^{III} and Yb^{III} 1:1 complexes (table 7), 0.06–0.24%, and 0.09–0.61%, respectively. However, the solvent is not the same, dmf as compared to ethanol, which may explain the difference. As for the calix[4]resorcinarene complexes, the speciation in solution has not been established, but in this case, the 1:1 complexes have been isolated and gave satisfactory elemental analyses (Korovin and Rusakova, 2001; Shevchuk et al., 1998a). The best quantum yields are obtained with H_2**39f** which bears two phenylamide chromophores on the narrower rim and these substituents are directly coordinated onto the lanthanide ion, which understandably increases the efficiency of the energy transfer process.

When reacted with lanthanide nitrates in dmf or dmso in presence of a base such as triethylamine, *p-tert*-butylcalix[8]arene (H_8**40**) can host two different Ln^{III} ions at a quite short distance (≈3.8 Å) by adopting a chair-like configuration (Bünzli et al., 2000). The mechanism of energy transfer between Ln^{III} ions can therefore be tested by inserting two different metal ions in the macrocycle (Froidevaux and Bünzli, 1994). Korovin and coworkers have synthesized two series of $Nd_{2-x}Ln_x$ (Ln = Nd, Sm, Eu, Tb, Yb) and $Yb_{2-x}Ln_x$ (Ln = Pr, Nd, Sm, Eu, Dy, Ho, Yb) complexes with H_8**40** and determined the corresponding quantum yields in dmf (table 8). The Nd^{III} luminescence is enhanced by a factor 2–2.5 with respect to [Nd_2(H_2**40**)$(dmf)_5$] by the presence of ions such as Sm^{III}, Eu^{III}, and Tb^{III}, when they are in small quantity ($x = 0.2$). Increasing their molar fraction to 0.5 systematically lowers the luminescence intensity and when $x = 1$, the luminescence intensity is smaller than the one displayed by the homobimetallic species. On the other hand, Yb^{III} acts as an efficient quencher of the Nd^{III} luminescence. In the case of Yb^{III}, most of the Ln^{III} ions quench the $^2F_{5/2}$ luminescence, except Nd^{III} ($x = 0.05$–0.1), Sm^{III} ($x = 0.5$–1.0), and Tb^{III} ($x = 0.2$–0.5) which

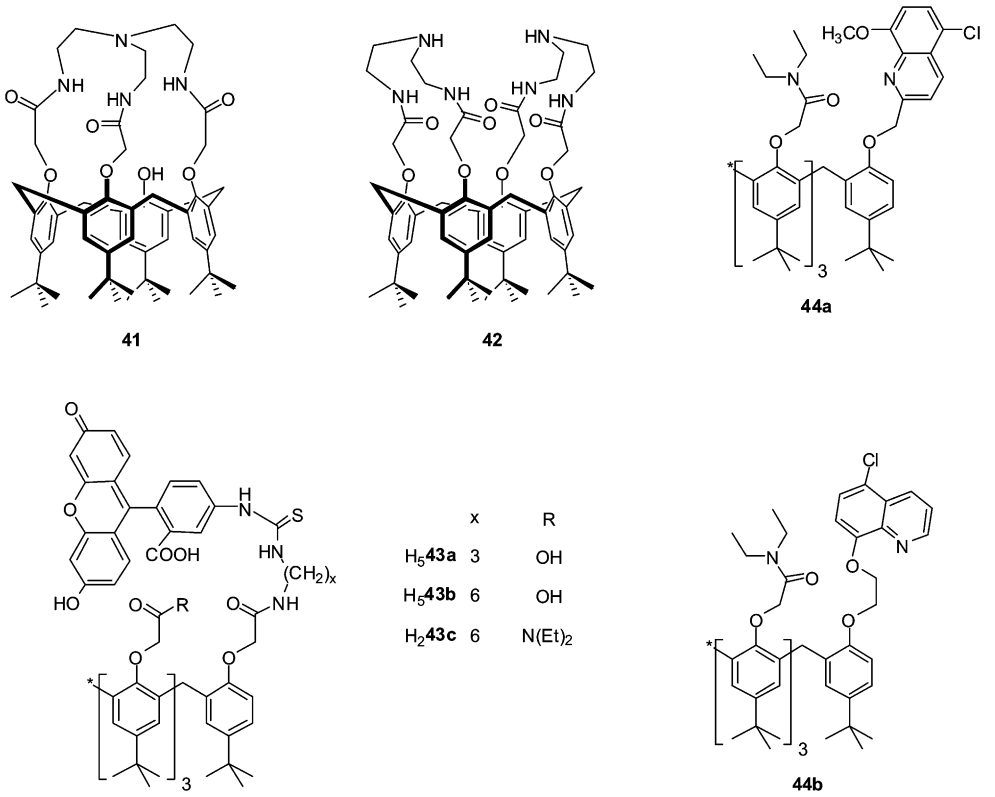

Fig. 38. Calix[4]azacrowns (top left), calix[4]arenes fitted with fluorescein (bottom left) and with chloroquinoline (top right, bottom right).

cause some enhancement. Both intra- and intermolecular energy transfers occur, the latter being less important as demonstrated by measuring the variation of the luminescence intensity in mixtures of homobimetallic complexes (Korovin et al., 2000).

The calix[4]azacrowns **41** and **42** (fig. 38), capped with aminopolyamide bridges bind Ln^{III} ions and form both 1:1 and 1:2 (Ln:L) complexes with stability constants in the ranges $\log \beta_1 \approx 5$–6 and $\log \beta_2 \approx 10$–11 in acetonitrile for **42**, while the stability of the complexes with **41** is about two orders of magnitude smaller. Hydration numbers around 1 were found for the Eu^{III} and Tb^{III} complexes, but the ability of the ligands to sensitize Ln^{III} luminescence is very weak, except in the Tb^{III} complex with **42**. No Er^{III} luminescence could be evidenced, but some Nd^{III} emission was recorded, which is 12 times larger with ligand **42** than with receptor **41** (Oueslati et al., 2006).

To improve the photophysical properties of the calixarene receptors, the team of D. Reinhoudt has covalently grafted one adequate chromophore, fluorescein, on the narrower rim of calix[4]arene via either a propyl (H_5**43a**) or a hexyl (H_5**43b**) bridge; simultaneously strongly

coordinating carboxylic acid or diethylamide groups were introduced on the remaining three phenolic functions. In fact, receptors **43a–c** (fig. 38) were designed so that the resulting 1:1 complexes are sufficiently lipophilic and therefore can dissolve in organic solvents, a prerequisite for the preparation of thin films by spin-coating or for their introduction into polymer layers as active optical components.

The intrinsic triplet yield of fluorescein, which absorbs in the green part of the visible spectrum (515 nm), is only 2% but the presence of the lanthanide ion increases considerably the efficacy of the intersystem crossing rate. In complexes of the three NIR-emitting lanthanide ions with dtpa-fluorescein for instance, the fluorescence intensity of the chromophore is reduced by 65–85%, pointing to an enhanced isc process (Hofstraat et al., 1998). Nd^{III} and Yb^{III} luminescence is sensitized by exciting both at 310 (phenolic groups) and 515 nm (fluorescein), the latter excitation mode yielding more intense luminescence, while Er^{III} only emits upon excitation of the fluorescein. Although Yb^{III} luminescence is sensitized by both ligands H_5**43a** and H_5**43b**, the authors only fully tested Nd^{III} and Er^{III} complexes in both aerated and de-aerated methanol-d_4 and dmso because they were interested in developing devices for telecommunication purposes.[5] No significant change in luminescence intensity was detected upon removal of oxygen, which implies a strong interaction between the chromophore and the lanthanide ion, in line with a substantial red shift observed in the absorption spectrum of fluorescein upon complexation. Indeed, fluorescein contains a deprotonated carboxylic acid group under the experimental conditions used and can fold over the lanthanide ion and coordinate to it, protecting it from further solvent interaction. Moreover this observation allows one to estimate the rate of ligand to metal energy transfer being larger than 3×10^8 s^{-1} in the two solvents. Lifetimes for the Er^{III} complexes are 0.8–0.9 μs in methanol-d_4 and 1.6–1.7 μs in dmso. On the basis of the other measured photophysical properties (molar absorption coefficients, energy transfer rates, triplet yields), a rough calculation was made of the gain which may be reached using the calixarene-based materials as the medium for optical amplifiers. For a 2-μm core waveguide doped with the Er^{III} calixarene complexes, a 1.7-dB cm^{-1} gain would be obtainable with only 1.4-mW pumping, which would mean a significant improvement over inorganic glass-based Er-doped fiber amplifiers, despite the lifetimes being shorter by approximately three orders of magnitude. It is noteworthy that the length of the alkyl chain connecting fluorescein to the calix framework does not play a decisive role in the values of the lifetimes, but the overall luminescence is more intense for the Nd^{III} complex with H_5**43a** compared to the one with H_5**43b**. Based on the only photophysical parameter reported, the Nd($^4F_{3/2}$) lifetime, receptor **43c** appears to be less interesting than the two tricarboxylic ligands (Hofstraat et al., 1998; Wolbers et al., 1998a). In inorganic optical amplifiers, sensitization of the Er^{III} luminescence is often achieved by co-doping Yb^{III} in the matrix because this ion has a broad charge-transfer absorption band and, additionally, it efficiently transfers energy onto erbium. In organic matrices, the excitation efficiency of Yb^{III} is largely increased by the antenna effect (by 3–4 orders of magnitude). Since calixarenes **43** (see fig. 38) were shown to be reasonably good hosts for Er^{III} luminescence, the Dutch team at Twente has tried to combine both advantages by designing ditopic bis(calixarene) ligands with various coupling groups (fig. 39). Another motivation

[5] On the other hand, no NIR emission was detected for Pr^{III}.

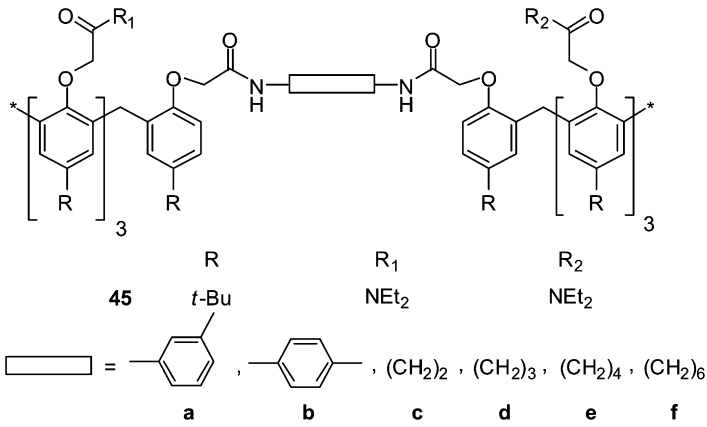

Fig. 39. Bis-calix[4]arenes (Wolbers et al., 1997a).

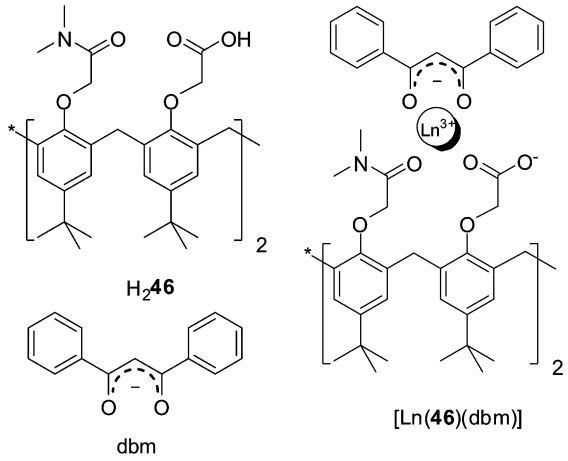

Fig. 40. Ternary complex with an amide-acid calixarene and dbm (Hebbink et al., 2001a).

was the study of metal-to-metal energy transfer, which was performed for [NdEu(**45b**)] in several solvents. The lifetime of the Eu($^5D_0$) level is shorter in the heterobimetallic NdEu complex than in the EuEu compound in chloroform, acetonitrile, and thf, which is indicative of a $Eu^{III} \rightarrow Nd^{III}$ energy transfer. The yield of transfer, calculated as $100(1 - \tau_{obs}/\tau_0)$ where τ_0 is the lifetime in absence of energy acceptor, i.e. in the EuEu compound, amounts to about 50–65% (Wolbers et al., 1997a).

Another chromophore, 8-alkoxy-5-chloroquinoline, was appended to the narrower rim of a calix[4]arene triamide, **44a** and **44b** (see fig. 38). If Nd^{III}, Er^{III}, and Yb^{III} nitrates are added to acetonitrile solutions of these receptors, quenching of the methoxyquinoline luminescence oc-

curs and is accompanied by a sizeable increase in the metal-centered luminescence; however, no quantitative data were reported (Casnati et al., 2003).

Although this strategy has not been much tested, the appended chromophoric arm can be replaced by the formation of a ternary complex with an adequate strongly coordinating antenna, e.g. dibenzoylmethanate (fig. 40), as seen previously for cyclen-based complexes. Deuterated dichloromethane solutions of [Ln(**46**)(dbm)] (Ln = Nd, Er, Yb) exhibit the typical emission spectra of these ions upon excitation of the dbm antenna at 360 nm. Lifetimes are in the microsecond range, 0.9, 1.3, and 12.5 μs for Nd^{III}, Er^{III}, and Yb^{III}, respectively (Hebbink et al., 2001a).

3.2. *Acyclic ligands*

3.2.1. *Beta-diketonates and related chelates*

From the first synthesis of rare-earth β-diketonates in 1897 by Urbain until now, hundreds of different complexes formed by reaction between Ln^{III} ions and β-diketone derivatives have been described in the literature. Interest for this type of complexes comes from their potential application in numerous and diverse domains. These complexes can be used for example as extractants in solvent–solvent extraction processes or as active compounds for the development of chelate lasers or liquid lasers. But they can also find applications in NMR as shift reagents or as electroluminescent materials in organic light-emitting diodes (OLEDs) (Binnemans, 2005b).

In presence of lanthanide ions, β-diketonates generally form neutral tris complexes, [Ln(β-diketonate)$_3$], the delocalization of the negative charge of the ligand leading to the formation of stable six-membered chelate rings. Since lanthanide ions frequently adopt coordination numbers of 8 or 9 in solution, the coordination sphere of the lanthanide ion in these six-coordinate complexes is not complete. Therefore the presence of one or several molecules of solvent in the first coordination sphere is often observed, giving complexes of general formula [Ln(β-diketonate)$_3$(solv)$_n$], with solv = H_2O, dmf, dmso and n = 1–3. Stable ternary complexes [Ln(β-diketonate)$_3$(L)$_n$] can also be formed in presence of bidentate (n = 1) Lewis bases (L) such as 2,2′-bipyridine or 1,10-phenanthroline, or monodentate (n = 2) ones such as triphenylphosphine oxide (tppo) or tri-*n*-octylphosphine oxide (topo). Additionally, apart from tris complexes, tetrakis complexes with general formula [Ln(β-diketonate)$_4$]$^-$ can be obtained in which the lanthanide ion is surrounded by four β-diketonate ligands and which are more luminescent than the tris complexes.

As it is well known, sensitization of Ln-centered luminescence can be achieved via an intramolecular energy transfer upon excitation of organic ligands, instead of using direct excitation of the weak Ln^{III} absorption bands. This phenomenon now called “antenna effect” or “luminescence sensitization” has first been observed in 1942 by Weissman for europium(III) complexes formed with salicylaldehyde and with β-diketonates, more particularly benzoylacetonate (ba, **48a**), dibenzoylmethanate (dbm, **48b**) and *meta*-nitrobenzoylacetonate (**47a**, fig. 41) (Weissman, 1942).

At the end of the 1950’s, Crosby and Kasha reported the rather exceptional case of near-infrared luminescence of trivalent ytterbium ion in an 1:3 (Ln:L) chelate occurring after intramolecular energy transfer between the organic ligand, in this case dbm (**48b**), and the lan-

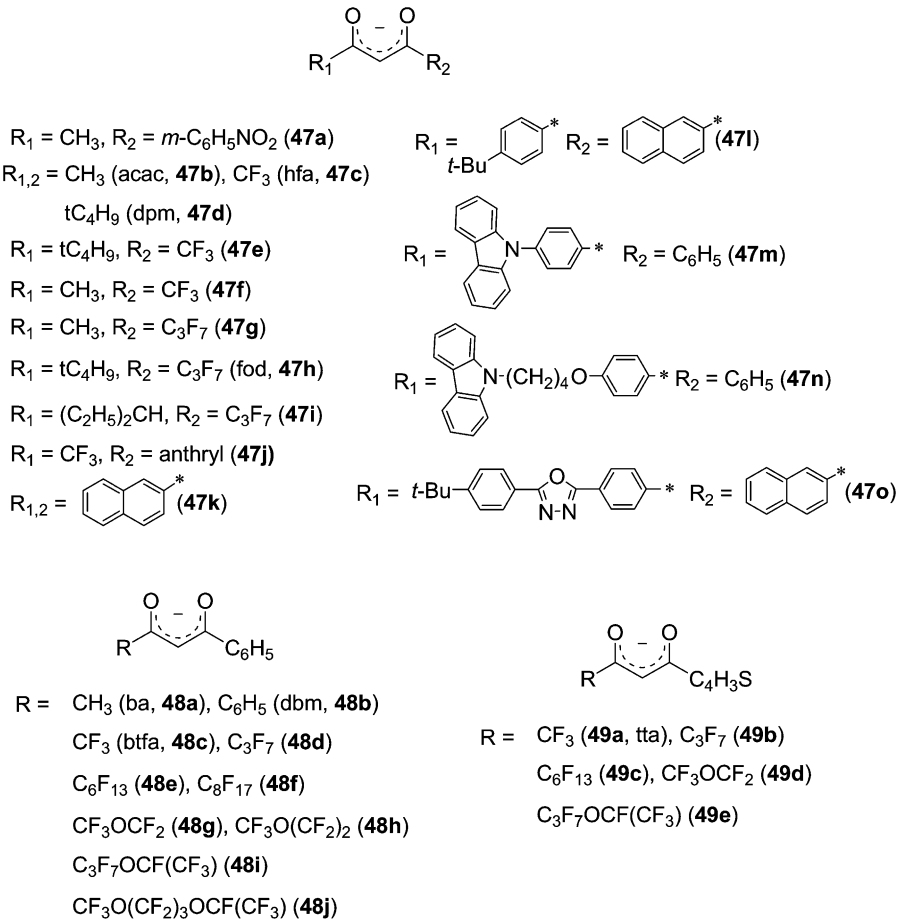

Fig. 41. β-Diketonate ligands.

thanide ion. At 77 K, in a 1:1:1 mixture of ethyl ether, isopentane, absolute ethanol and under excitation in the absorption band of the β-diketonate at 365 nm, an intense luminescence emission at 971 $\pm$ 4 nm corresponding to the $^2F_{5/2} \rightarrow {}^2F_{7/2}$ transition of the Yb^{III} ion was observed. The efficiency of the intramolecular energy transfer is quite remarkable given that the triplet $^3\pi\pi^*$ state of the chelate lies at 20 500 cm^{-1}, that is at about 10 000 cm^{-1} above the $^2F_{5/2}$ acceptor level of the Yb^{III} ion (Crosby and Kasha, 1958). This opened new perspectives in the understanding and determination of ligand-field effects in Yb^{III} complexes. Indeed, until this work, emission spectra were most of the time unavailable for ytterbium so that only the splitting of the upper $^2F_{5/2}$ level could be determined. Ligand-field calculations are easily achievable with tris(β-diketonates), the symmetry around the ion being well defined. As a consequence new calculations performed by Perkins showed good agreement

between the experimentally observed Yb^{III} energy levels and those calculated according to the electrostatic ligand-field theory (Perkins and Crosby, 1965). After these first studies, interest in β-diketonate complexes emitting near-infrared light died out until Meshkova and her Ukrainian research group published a series of works at the end of the 1980's and beginning of the 1990's. At this time determination of lanthanide impurities in compounds of other lanthanides became necessary since high-purity lanthanide compounds were extensively used in advanced materials.

Determination of lanthanide ions with a fairly low detection limit of 10^{-5}–10^{-6} wt% is achieved with Ln^{III} β-diketonates. Relying on this fact new, rapid, selective, and highly sensitive analytical methods essentially based on the luminescence properties of these complexes have been developed. After a preliminary work on Sm^{III} and Eu^{III} chelates (Topilova et al., 1989), interest focused on NIR-emitting lanthanides, more particularly on Nd^{III} and Sm^{III} ions since they are often present as impurities in lanthanide oxides. A first study dealt with the determination of trace amounts in europium oxide using thenoyltrifluoroacetonate (tta, **49a**, fig. 41) and diantipyrylpropylmethane, dapm, see fig. 44 below (Meshkova and Rusakova, 1990). Mixing these ligands with lanthanide ions in ethanol yields 1:3:1 (Ln:tta:dapm) complexes which are precipitated and put into suspension in a 0.5% solution of gelatin. Under excitation in the absorption bands of tta or dapm at 340 or 270 nm, respectively, luminescence is observed at 878 and 903 nm for Nd^{III} ($^4F_{3/2} \rightarrow {}^4I_{9/2}$ transition) and at 950 nm for Sm^{III} ($^4G_{5/2} \rightarrow {}^6F_{5/2}$ transition). In order to obtain a better sensitivity the Eu^{III} luminescence has to be masked, the band at 820 nm ($^5D_0 \rightarrow {}^7F_6$) being quite close to the Nd^{III} $^4F_{3/2} \rightarrow {}^4I_{9/2}$ transition. One way to achieve this consists in reducing Eu^{III} into Eu^{II}, which is not luminescent in this spectral range, using Jones reducing agent since other lanthanides are not reduced with amalgamated zinc. However Eu^{II} is quite sensitive to traces of oxygen and it is necessary to stabilize the europium ion in its bivalent oxidation state. For this purpose the authors suggested to isolate Eu^{II} ions from the solution by addition of sulfate and precipitation of $EuSO_4$. Optimizing the different parameters, such as solution pH, contact time with the reducing agent, and sulfate ion concentration finally allowed to reach detection limits of 3.2×10^{-4} and 2.2×10^{-4} wt% for Nd^{III} and Sm^{III}, respectively. A series of fluorine-containing β-diketonates, with an ether function in the fluorinated alkyl chain (**48d**, **48g–i** and **49b**, **49d**, **49e**) were synthesized to improve the detection limit of Nd^{III} in lanthanide sesquioxides Ln_2O_3 (Ln = Y, La, Gd, Lu). By analyzing the $^4F_{3/2} \rightarrow {}^4I_{11/2}$ (1.06 μm) transition of Nd^{III} in complexes formed with ligands **48g**, **48h**, or **49d** and dapm, a detection limit of 5×10^{-5} wt% was achieved. A complete study of the photophysical properties of a large series of this kind of Nd^{III} β-diketonates was also performed (Topilova et al., 1991).

Meshkova et al. have investigated the influence of the substituents grafted on ligands **47b**, **c**, **e**, **g**, **i**, **48a–h**, and **49a**, **b**, **d**, **e** on the optical characteristics of Nd^{III} in tris β-diketonates and related ternary complexes with 1,10-phenanthroline or other organic bases (Meshkova et al., 1992b; Rusakova et al., 1992b; Rusakova et al., 1992a). Samples were measured as suspensions in aqueous ethanol containing 0.5% of gelatin to stabilize the suspended particles. The luminescence properties of the Nd^{III} complexes, namely intensities, quantum yields, and lifetimes increase in going from symmetrical to asymmetrical β-diketonates. For example the quantum yield of the tris complex with symmetrical dbm (**48b**) is 0.031% whereas replac-

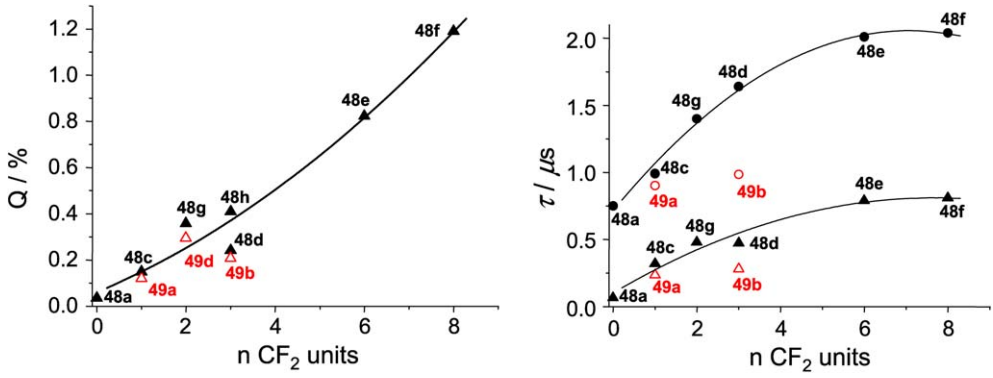

Fig. 42. (Left) Partial luminescence quantum yields ($^4F_{3/2} \rightarrow {}^4I_{11/2}$ transition) of Nd^{III} tris(β-diketonates). (Right) Luminescence lifetimes of tris and ternary Nd^{III} complexes as a function of the fluorinated radical chain length. Filled and opened triangles stand for tris complexes with benzoylacetonate and thienylacetonate derivatives, respectively; filled and opened circles for the corresponding ternary complexes formed with phen.

ing one phenyl with a CH_3 (**48a**) or a CF_3 (**48c**, btfa) group gives quantum yields of 0.036 and 0.149%, respectively. The same trend is observed when fluorine-containing ligands are used compared to non-fluorinated ones. Additional enhancement of the luminescence quantum yields and lifetimes can be achieved by lengthening the chain of the fluorinated residue, as can be visualized on fig. 42 for benzoyl and α-thienyl acetonate derivatives. However branching of the fluorinated chains, even if they are lengthened, causes a decrease in the spectroscopic properties of the complexes; a potential explanation is the steric hindrance becoming considerable and resulting in a lengthening of the Ln–O bonds and consequently in a weaker Nd^{III}–diketonate interaction.

Moreover β-diketonates featuring an aryl residue, in this case a phenyl group, have better luminescent properties than the corresponding complexes with alkyl or thienyl substituents. This arises from the additional stabilization brought by the formation of a single π-electronic conjugation chain between the aryl ring and the six-member ring of the enolic tautomer. Another way to enhance the luminescent characteristics of these complexes consists in introducing an oxygen atom, that is, an ether function, in the fluorinated radical chain. This effect can be explained by the flexibility of the C–O–C bond ensuring better shielding of the central ion from quenching action of water molecules. An alternative hypothesis tested was the coordination of a fluorine atom belonging to the terminal trifluoromethyl group. However, conformational analysis of La^{III} and Nd^{III} perfluoro-β-diketonates done both by molecular mechanics calculations and by NMR spectroscopy clearly showed no evidence of additional coordination of a fluorine atom (Meshkova et al., 1998). As a consequence, the increase in luminescence properties of Ln^{III} β-diketonates with the elongation of the fluorinated radical chain was explained by the enhanced lipophilicity of these ligands, which form a highly hydrophobic shell around the Ln^{III} ion, thus eliminating strong luminescence quenchers such as OH oscillators, both from the inner and outer coordination spheres. This assumption was

Table 9
Luminescence properties (lifetimes and intrinsic quantum yields) of Nd^{III} β-diketonates with dbm derivatives ($\tau_0(Nd) = 0.25$ ms)

Complex	τ (μs)	Q_{Nd}^{Nd} (%)
[Nd(dbm)$_3$(phen)]	0.707 (62.9%)	
	21.5 (37.1%)	8.6
[Nd(dbm)$_3$(bath)]	0.670 (52.3%)	
	20.2 (47.7%)	8.1
[Nd(**47n**)$_3$(bath)]	0.803 (28.6%)	
	14.0 (71.4%)	5.60
[Nd(**47k**)$_3$(bath)]	0.845 (11.6%)	
	24.5 (88.4%)	9.81
[Nd(**47m**)$_3$(bath)]	0.864 (7.8%)	
	24.2 (92.2%)	9.69
[Nd(**47o**)$_3$(bath)]	0.994 (6.7%)	
	24.9 (93.3%)	9.95

confirmed with fluorinated ligands possessing much higher lipophilicity and lower surface tension than the corresponding un-fluorinated β-diketonates.

In an effort to sensitize Nd^{III} and Er^{III}, J.G. Kang and coworkers have designed the asymmetrical β-diketonate **47j** (fig. 41) bearing an anthracene antenna. In dmf, the fluorescence of the latter has a quantum yield of 3.62% in the Gd^{III} tetrakis compound $[Gd(\mathbf{47j})_4]^-$, which is drastically reduced to 0.89 and 1.70% in the Nd^{III} and Er^{III} complexes, indicating energy transfer onto these ions. Indeed, NIR emission is seen, with lifetimes equal to 0.83 μs (Nd^{III}) and 1.53 μs (Er^{III}). Similar effects are observed in chloroform and 2-methyltetrahydrofuran (Nah et al., 2006). Recently, L.F. Yang et al. studied a series of novel β-diketonates formed with dbm derivatives, featuring functionalized aromatic moieties (see fig. 41, ligands **47k–47o**) (L.F. Yang et al., 2006). The absorption spectra of the free ligands measured in CH_2Cl_2 display strong absorption bands between 300–400 nm, attributed to intramolecular π–π^* transition. The absorptions of the dbm derivatives are red-shifted compared to the 342 nm band of dbm, the largest shift (about 33 nm) being observed for ligands **47m** and **47o**, due to the extended conjugation system. This additional conjugation is also responsible for the lowering of the singlet state energy of the ligands from 433 nm for dbm to 507 nm for **47o**. However, in the case of ligand **47n**, introduction of a donor carbazole group on the dbm framework through a flexible chain does not influence the π system of the molecule. Phosphorescence spectra of the Gd^{III} complexes allowed the determination of the triplet states energy, which is between 20 410 and 18 520 cm^{-1}.

All the ternary Nd^{III} complexes, [Nd(β-diket)$_3$(bath)], formed with these ligands and with bath (monobathophenanthroline) exhibit the characteristic metal-centered NIR luminescence. The photophysical properties of these chelates are compared to those of [Nd(dbm)$_3$(phen)] in table 9.

All the luminescence decays are biexponential, but since the complexes are quite hygroscopic, the shortest lifetime has been attributed by the authors to hydrated species and therefore only the longer lifetime has been taken into consideration. The longest lifetime is ob-

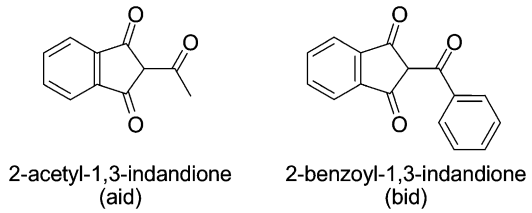

Fig. 43. Cyclic β-diketones.

served for [Nd(**47o**)$_3$(bath)] with a value of 24.9 μs, which is almost 2-fold larger than the smaller one, 14.0 μs, observed for [Nd(**47n**)$_3$(bath)].

Measurements on complexes formed with cyclic β-diketones (fig. 43) demonstrated that for identical molar absorption coefficient values, higher luminescence intensities were observed for cyclic β-diketonates compared to aliphatic ones. This indicates a more efficient energy transfer to the Nd^{III} ion on account of the rigid structure of these cyclic β-diketonates in which the central ion is well shielded from interaction with water molecules.

To complete the study on Nd^{III} β-diketonates, ternary complexes formed with various organic bases (fig. 44) have also been considered. Addition of a second ligand results in all cases in an enhancement of the luminescence properties compared to the corresponding tris complexes since water molecules are removed from the first coordination sphere of the Ln^{III} ion. For example, lifetimes are 2–3 times longer when 1,10-phenanthroline is used as ancillary ligand (fig. 42). Luminescence intensities are also enhanced, up to 6-fold, depending on the organic base used. However this increase is less important for β-diketonates containing long fluorinated alkyl chains or for cyclic ligands because of their higher lipophilicity. Changes occurring in luminescence intensities as a function of the nature of the organic base acting as ancillary ligand (fig. 44) have been investigated and the luminescence enhancements observed in going from tris to ternary complexes are summarized on fig. 45 for the most representative β-diketonates (see fig. 41 for formulae).

The solvent also influences the luminescence intensity and the largest enhancement was achieved with dmso or dmf, which are known to coordinate strongly to Ln^{III} ions and thus favor the removal of water molecules from the first coordination sphere. Smaller enhancements were observed when ethanol or a protic solvent was used. The amount of solvent used for producing the suspensions is also crucial and the authors showed that the maximal luminescence intensity occurs for a concentration of the solvent of 20 vol%, above which the suspension decomposes thus leading to decreasing intensities.

In summary, this series of studies on Nd^{III} β-diketonates demonstrate that luminescence properties are enhanced when the fluorinated chain is lengthened. As a consequence, attempts have been made to use the benzoylacetonate derivatives **48e** and **48f** in luminescence determination of lanthanides in order to improve the sensitivity of the method. Luminescence intensities for Nd^{III} and Yb^{III} chelates formed with **48e** and **48f** are higher by a factor 1.2–1.6 than those observed for the ternary complexes formed with tta and phen. Although highly sensitive detection of Nd^{III} and Yb^{III} can also be achieved using tris complexes only, ternary

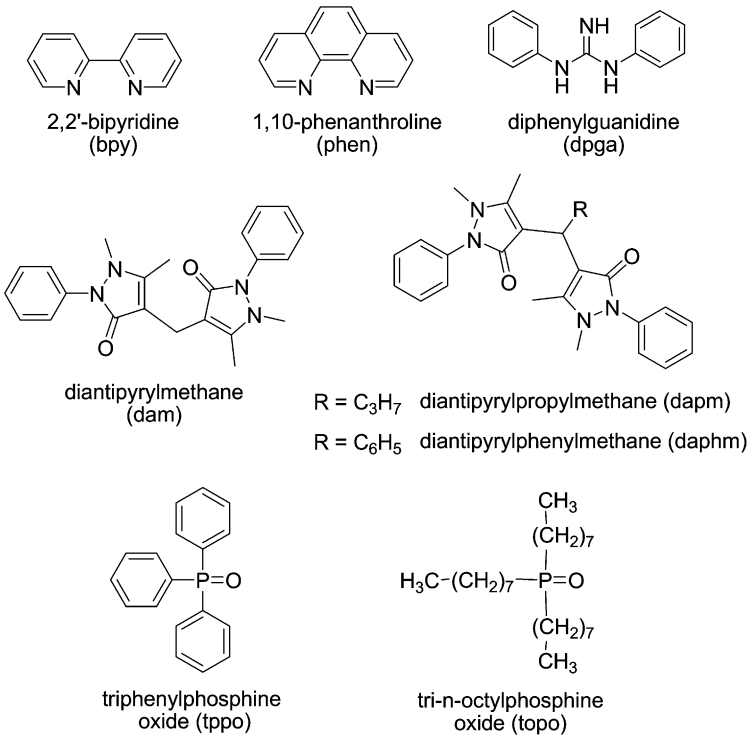

Fig. 44. Organic bases used as second ligand in ternary β-diketonate complexes.

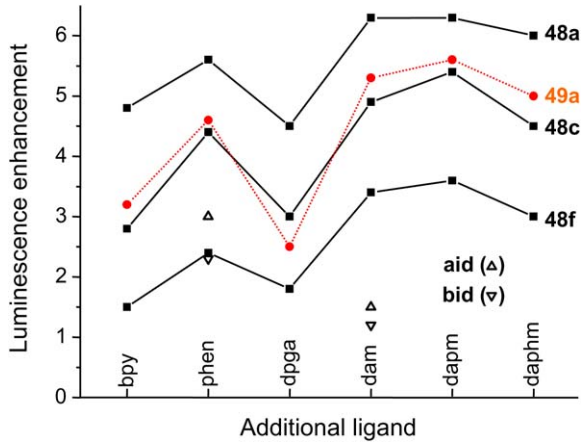

Fig. 45. Enhancement factors of the luminescence intensity between some tris(β-diketonates) and their corresponding ternary complexes.

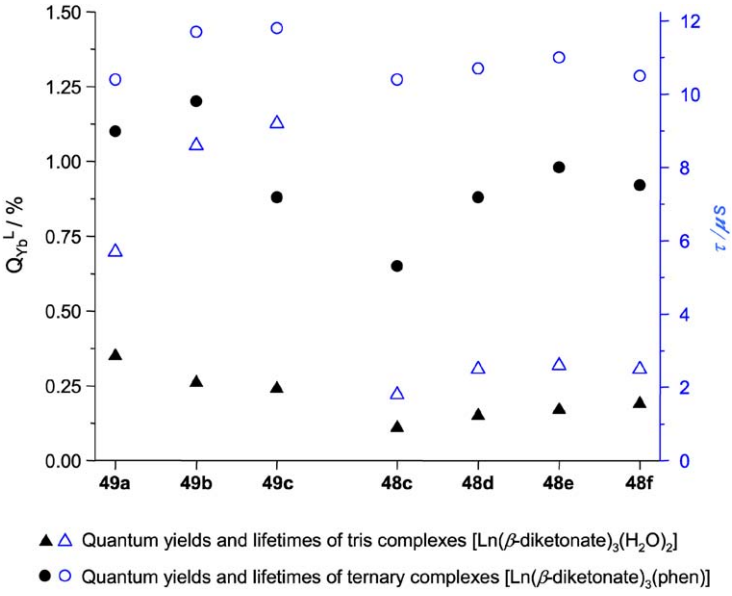

Fig. 46. Quantum yields (▲, ●, left scale) and lifetimes (△, ○, right scale) of Yb^{III} β-diketonates in toluene.

complexes are preferentially used. Detection limits are as low as 3×10^{-5} and 7×10^{-5} wt% for Nd^{III} and Yb^{III}, respectively (Meshkova et al., 1997).

The luminescence properties of Yb^{III} β-diketonates generally parallel the trends observed for Nd^{III} complexes. For instance, an increase in luminescence intensity was observed in going from thienyl to benzoyl derivatives, from fluorine-free to fluorine-containing β-diketonates and in this case with increasing fluorinated alkyl chain length. However replacement of a CF_2 unit with an ether function leads to a small decrease of the luminescence intensity contrary to what was observed for Nd^{III} chelates. Adding dmso or dmf to the suspension also results in sizeable increase in luminescence intensity. When compared to Nd^{III}, however, the Yb^{III} complexes seem to be more stable since concentration of dmso or dmf can be increased up to 80 vol% before partial decomposition of the suspended complexes. Studies on ternary complexes were also performed and the luminescence enhancement observed in going from tris to ternary complexes is similar to what was reported for their Nd^{III} analogs. The greatest enhancement was observed for the complex formed with **48c** and topo, the ratio $I_{ternary}/I_{tris}$ reaching seven (Bol'shoi et al., 1997; Topilova et al., 1997).

This work was followed by a more detailed study including determination of quantum yields and lifetimes for the Yb^{III} β-diketonates formed with fluorinated benzoyl (**48c–j**, fig. 41) and thienyl (**49a–e**) derivatives of acetylacetonate and for their corresponding ternary complexes with phen (Meshkova et al., 1999; Tsvirko et al., 1999). Complexation of 1,10-phenanthroline induces 3- to 6-fold increases in quantum yields, which amount to 0.11–0.35% for the tris complexes while they reach 0.65–1.20% for the ternary complexes (fig. 46). A par-

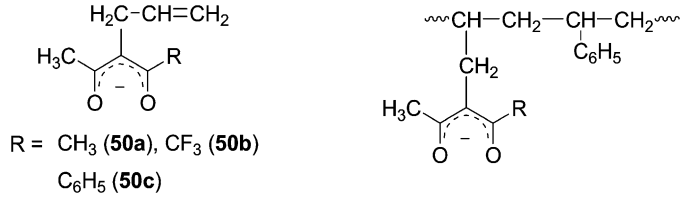

Fig. 47. Allyl-derivatized β-diketonates (left) and copolymer formed with styrene (right).

allel evolution is observed for the lifetimes, as expected since lifetimes increase when phenanthroline is used as second ligand. However the increase is less important in complexes with thienyl derivatives, for which enhancement factors of 1.5–1.8 were observed, compared to enhancement factors of 4–6 for benzoyl derivatives. Analysis of these data (fig. 46) gives useful information about the role played in deactivation processes by the main and secondary ligands. As seen in section 2.5, the sensitization efficacy of the ligand can be written as:

$$\eta_{\text{sens}} = Q_{\text{Ln}}^{\text{L}} \cdot \frac{\tau_{\text{rad}}}{\tau_{\text{obs}}}. \tag{11a}$$

Assuming $\tau_{\text{rad}} \approx 1$ ms (see table 5) the authors estimate $\eta_{\text{sens}} > 0.6$. As a consequence, the low quantum yield values are explained mainly by deactivation of the Yb^{III} excited state occurring through high-frequency vibrational modes of both ligand and solvent. In order to minimize these vibrational deactivations, allyl derivatives **50a–c** (fig. 47) of ligands **47b**, **47f**, and **48a** (fig. 41) have been synthesized and luminescence intensities of Nd^{III} and Yb^{III} complexes have been studied either in their monomeric form or in their co-polymeric form with styrene or methylmethacrylate (MMA) (Meshkova, 2000).

It turned out that incorporation of tris complexes into the polymeric chain is difficult, the predominant complex then becoming the less luminescent 1:2 (Ln:L) species. Despite this, the luminescence intensities in Nd^{III} and Yb^{III} complexes attached to styrene are one order of magnitude higher than those observed in solutions of tris complexes formed with the corresponding β-diketonates, derivatized or not. This can be explained by the rigid structure of the copolymer and also by the important decrease in the energy losses due to thermal deactivations, the molecular mass of the Ln^{III} copolymers being significantly larger when compared to the tris complexes. Compound [Ln(**50c**)$_3$-styrene]$_n$ displays the best luminescence with an intensity 2–5 times higher with respect to the corresponding diketonates with **50a** and **50b**. Such copolymeric compounds can be useful for the luminescence determination of lanthanides in highly quenching environments. To fully understand the nonradiative deactivation processes occurring in Yb^{III} β-diketonates, the luminescence characteristics of dibenzoylmethanate and thenoyltrifluoroacetonate, as well as their deuterated analogs dbm-d_1 and tta-d_1 (fig. 48) were studied in toluene and partly in carbon tetrachloride and dmso-d_6 (Tsvirko et al., 2001). Complexes of general formula, [Yb(β-diketonate)$_3$(H_2O)$_2$] are formed in solvents with low coordinating ability like toluene, the two water molecules remaining in the first coordination sphere of the metal ion. The contribution of these water molecules to nonradiative deactiva-

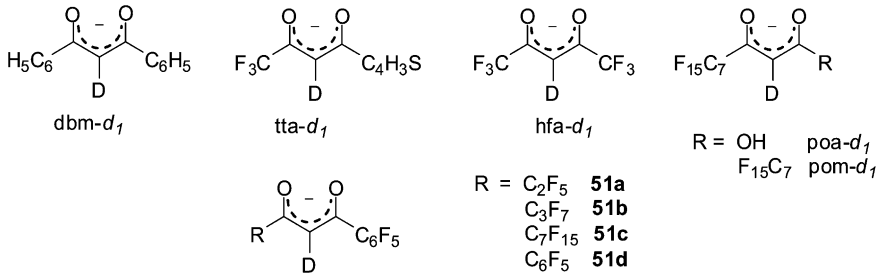

Fig. 48. Some deuterated β-diketonates.

tion considerably exceeds the total contribution of all the other de-activating groups. This is why little or no increase in luminescence is observed upon deuteration of the central CH group of the ligands. On the other hand, the replacement of H_2O by D_2O in tris Yb^{III} complexes with tta (**49a**, fig. 41) leads to a ≈1.5-fold increase in the luminescence quantum yield, demonstrating that the exclusion of the water molecules from the inner coordination sphere is essential for optimized luminescence properties. This can be easily achieved (i) by using a solvent like dmso or better, dmso-d_6, with much superior coordinating properties towards Ln^{III} ions than toluene, (ii) by forming ternary complexes through the addition of an organic base, like 1,10-phenanthroline or trioctylphosphine oxide. Following the first strategy, using dmso-d_6 as solvent instead of toluene, yielded [Yb(β-diketonate)$_3$(dmso-d_6)$_2$] complexes with quantum yields 18–32 times larger than the hydrated complexes. For example [Yb(tta)$_3$(H_2O)$_2$] has a quantum yield of 0.12% and a lifetime of 1.19 μs, whereas the respective values for [Yb(tta)$_3$(dmso-d_6)$_2$] are 2.14% and 27.3 μs. Such an increase was also observed in presence of phen but to a lesser extent, with quantum yield and lifetime for [Yb(tta)$_3$(phen)] reaching 1.60% and 15.8 μs, respectively.[6]

Once water molecules are removed, deuterating the central C–H group of the β-diketone further increases the quantum yields and lifetimes by approximately 17% in the ternary complexes. Another source of nonradiative deactivation that should not be neglected comes from diffusing solvent molecules in the second sphere which contain high-frequency C–H vibrations. As a consequence, replacement of toluene with carbon tetrachloride leads to a further slight increase in the luminescence lifetimes of [Yb(dbm-d_1)$_3$(phen)] and [Yb(tta-d_1)$_3$(phen)] (table 10).

Nonradiative deactivation of the Yb($^2F_{5/2}$) excited state occurs through vibrational states of surrounding molecular groups. Since the contributions of these molecular groups to the overall nonradiative deactivation rate constant are known to be additive, the following equation can be written:

$$\frac{1}{\tau_{obs}} = k^{rad} + k^{nr} \approx k^{rad} + k(\text{diket}) + k(\text{CH, CD}) + k_\alpha + k_\beta, \tag{27}$$

[6] The same authors had previously reported different values for [Yb(tta)$_3$(H_2O)$_2$] ($Q^L_{Yb} = 0.35\%$, $\tau = 6.7$ μs) and [Yb(tta)$_3$(phen)] ($Q^L_{Yb} = 1.11\%$, $\tau = 10.4$ μs) (Meshkova et al., 1999; Tsvirko et al. 1999, 2001).

Table 10
Quantum yields and lifetimes of the $^2F_{5/2} \rightarrow {}^2F_{7/2}$ transition of Yb^{III} in β-diketonate complexes (Tsvirko et al., 2001)

Complex	dbm		tta	
	Q^L_{Yb} (%)	τ (μs)	Q^L_{Yb} (%)	τ (μs)
[Yb(β-diketonate)$_3$(H_2O)$_2$][a]	0.023	1.0	0.12	1.16
[Yb(β-diketonate)$_3$(phen)][a]	0.59	10.3	1.60	15.8
[Yb(β-diketonate-d_1)$_3$(phen)][a]	0.69	12.1	1.86	18.6
[Yb(β-diketonate-d_1)$_3$(phen)][b]	0.69	13.6	2.14	22.8
[Yb(β-diketonate)$_3$(dmso-d_6)][c]	0.73	17.4	2.14	27.3
[Yb(β-diketonate-d_1)$_3$(dmso-d_6)][c]	1.26	30.1	6.10	71.8

[a]Solution in toluene.
[b]Solution in CCl_4.
[c]Solution in dmso-d_6.

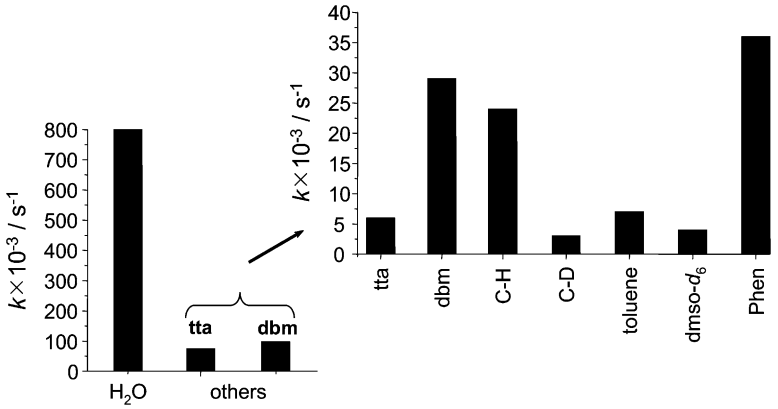

Fig. 49. Nonradiative deactivation rate constants of Yb^{III} ion in tris or ternary β-diketonate complexes for various molecular groups (Tsvirko et al., 2001).

where k^{rad} is the radiative rate constant for the $^2F_{5/2} \rightarrow {}^2F_{7/2}$ transition while the rate constants for nonradiative deactivation are denoted as follows: k(diket) is associated with the β-diketonate anions, except for the central CH group, k(CH) and k(CD) correspond to deactivation through vibrations from the central CH and CD bonds; finally, k_α is the rate constant associated with neutral ligands or solvent molecules L coordinated to the central ion, and k_β includes contributions from solvent molecules in the second coordination sphere. Making use of the data reported in table 10 and assuming $k^{rad} \approx 1000\ s^{-1}$, Tsvirko et al. have been able to estimate the different contributions of each molecular groups (fig. 49). It is noteworthy that the contribution of coordinated water molecules ($k^{nr}_{H_2O} \approx 8 \times 10^5\ s^{-1}$) greatly exceeds the total contribution of all remaining molecular groups ($k^{nr}_{tot} \approx 7.3 \times 10^4\ s^{-1}$ for [Yb(tta)$_3$phen]

or 9.6×10^4 s^{-1} for [Yb(dbm)$_3$phen] in toluene. The next largest contribution comes from the β-diketonates themselves, with tta quenching less ($k_{diket} + k_{CH} = 3 \times 10^4$ s^{-1}) than dbm (5.3×10^4 s^{-1}).

Thus if one wants to improve the overall quantum yield of β-diketonate complexes, removal of coordinated water molecules is absolutely necessary. By means of the estimated nonradiative deactivation rate constants, calculations showed that removal of these water molecules allows one to reach a maximum quantum yield of 2.6% in toluene for the Yb^{III}-tta complex. However, water molecules are usually replaced with a coordinating secondary ligand, such as phenanthroline, which also contributes to the nonradiative deactivation ($k_{phen} \approx 3.6 \times 10^4$ s^{-1}), but to a much lesser extent than water molecules. Further improvement can be reached by deuteration of the central C–H group in the β-diketonate: in [Yb(tta-d_1)$_3$(phen)] for instance, deactivation due to C–H oscillators occurs eight times faster when compared to C–D oscillators.

By taking advantage of the keto–enol equilibrium, [Yb(hfa-d_1)$_3$] was prepared in methanol-d_4 and its luminescence properties were determined in several solvents, methanol-d_4, thf-d_8, PO(OMe)$_3$, and dmso-d_6. Emission intensity is the largest in the latter solvent, by a factor 2.5 with respect to deuterated methanol and the Yb($^2F_{5/2}$) lifetime reaches 66 µs, as compared to 10 µs in methanol-d_4 (Kim and Park, 2003).

Further enhancement of luminescence properties is possible through halogenation of the C–H group. With this improvement, the maximum theoretical quantum yield achievable (without water molecules and secondary ligand) is 14%, corresponding to a Yb($^2F_{5/2}$) lifetime of 140 µs (Tsvirko et al., 2001).

Quenching of the Er($^4I_{13/2}$) luminescence by O–H and C–H vibrations has been quantified for tris and tetrakis complexes with hexafluoroacetylacetonate (hfa) presenting various degrees of hydration and deuteration (Winkless et al., 2006). Hydrated [Er(hfa)$_3$(H$_2$O)$_2$], Cs[Er(hfa)$_4$] and Cs[Er(hfa)$_4$] dissolved in CD$_3$OD show single exponential decay with lifetimes of 100 ns, 1.8, and 1.6 µs, respectively. When [Er(hfa)$_3$(H$_2$O)$_2$] is dried under vacuum (1 mbar), the decay becomes bi-exponential with associated lifetimes of 132 ns (17%) and 1.8 µs (83%), demonstrating the large effect of O–H vibrations. The lifetime of the tetrakis complex is still quite short and reflects the quenching effect of the four C–H oscillators which are at a distance of about 4.7 Å from the erbium ion. When this compound is almost fully deuterated (98%), its decay is bi-exponential, with lifetimes of 11 µs (96.4%) and 106 µs (3.64%). The latter is assigned to ions with no hydrogen atoms in their coordination sphere and surrounded by nearest neighbour molecules with no hydrogen atoms. The population analysis based on the contribution of the two exponential to the fluorescence decay points to Er^{III} sites for which the 160 nearest hydrogen atoms are fully deuterated, that is to Er^{III} sites surrounded by 40 fully deuterated $[Er(hfa)_4]^-$ entities. This corresponds to a fully deuterated shell with 20 Å diameter. This figure is comparable to the one calculated for Er^{III} 8-hydroxyquinolinates by the "continuous medium approximation" (Quochi et al., 2006), about 30 Å.

Kazakov and coworkers determined the influence of water on the luminescence of [Ln(β-diketonate)$_3$(H$_2$O)$_2$] in toluene (Ln = Nd, Sm, Tb, Dy, and Yb) (Voloshin et al., 2000c; Voloshin et al., 2000d). Addition of water quenches the NIR luminescence of the Nd^{III} and

Yb^{III} chelates with ligands **48c** and **49a** whereas the opposite effect, i.e. an enhancement of the luminescence, is observed for the corresponding Sm^{III} complexes and for Tb^{III} diketonates with **47b** and **48c**. This behavior was explained by significant concentration quenching due to formation of dimers $[Ln(\beta\text{-diketonate})_3(H_2O)_n]_2$ occurring at high concentrations of chelate. These dimers have lower luminescence properties compared to monomers since quenching is caused by deactivation of the ligand excited state before the $L \rightarrow Ln$ energy transfer and by cross-relaxation in the Ln^{III} ions. Addition of water causes dissociation of the poorly luminescent dimers to give more luminescent monomers.

The effect of fluorination of the alkyl chains of deuterated β-diketonates, as well as of the deuterated solvent on Nd^{III} luminescence is described in several papers and the main results are reported in table 11. Generally speaking, the more fluorine substituents on the alkyl chains, the largest the intrinsic quantum yield Q_{Nd}^{Nd}, e.g. the series acac-d_1–hfa-d_1–pom-d_1 in dmso-d_6 for which the quantum yield increases from 0.8 to 1.1, and 3.2%, respectively. Some care has to be exercised in interpreting these data since values for the same compound may vary widely. This is demonstrated by Q_{Nd}^{Nd} data for hfa-d_1 in thf-d_8 which varies from 0.5 to 1.5% depending on the authors. One reason could be concentration at which measurements have been carried out. Too low a concentration leads to dissociation of the complex, while larger concentration induces quenching. For instance, Y. Hasegawa and collaborators have shown that the quantum yield of $[Nd(pom\text{-}d_1)_3]$ in dmso-d_6 is fairly constant at $\approx$3.2% in the concentration range 1–7×10^{-2} M while it drops to $\approx$1.2% for a 0.3 M solution. Similarly, the quantum yield of $[Nd(hfa\text{-}d_1)_3]$ in the same solvent drops from 2.5% for a 10^{-2} M solution to 0.6% at 0.5 M, a range overlapping the values reported in table 11. For the systems tested, concentration quenching occurs through collisions and is therefore diffusion controlled. Assuming pure dipole–dipole interaction of the colliding molecules, the estimated critical distance for 50% transfer, R_0, is 11.7 Å, while the average distance between molecules in a 0.1 M solution is around 14 Å (Hasegawa et al., 1996b). Thus the large emission efficiency of the pom chelate is due to the suppression of cross relaxation as nonradiative energy transfer by maintaining the distance between Nd^{III} ions at the limit of the diffusional collision. As far as solvents are concerned, dmso-d_6 is the best, the quantum yield in this medium being at least two times larger than in the other tested solvents. A last point of interest is the comparison between symmetrical and asymmetrical ligands, the latter having the tendency to induce a stronger luminescence. The improvement in quantum yield is relatively modest when asymmetry arises from different fluorinated alkyl chains grafted on the acac substrate or when it is closer to the inner coordination sphere of the metal ion, compare for instance symmetric pom-d_1 with asymmetric poa-d_1. However, in the latter case, the oscillator strength of the hypersensitive transition is 2.5 times higher, so that the solution is more luminescent (Iwamuro et al., 1998). It is noteworthy that tetrakis chelates have much larger Ω_2 parameter than tris analogs (cf. data for btfa); the corresponding parameter for $[Er(btfa)_4]^-$ amounts to 26.1×10^{-20} cm^2 and simulations on $[Sm(btfa)_4]^-$ dissolved in methylmethacrylate, a precursor of PMMA, demonstrate the feasibility of an optical amplifier working at 650 nm, a wavelength corresponding to the absorption minimum of PMMA. Based on the data collected, a gain of 20 dB is predicted for a 60-cm fiber (Koeppen et al., 1997).

Table 11
Judd–Ofelt parameter Ω_2, Nd($^4F_{3/2}$) lifetimes and quantum yields of various fluorinated tris(β-diketonates). See fig. 48 for ligand formulae

Diketonate	Solvent	Ω_2 (10^{-20} cm^2)	τ ($^4F_{3/2}$) (μs)	Q^{Nd}_{Nd} (%)[a]	Q^{L}_{Nd} (%)[b]	Refs.
acac-d_1	dmso-d_6	22.2	3.3	0.8	n.a.	c,d
tfa-d_1	dmso-d_6	19.1	5.7	1.1	n.a.	c
hfa-d_1	acetone-d_6	16.3	1.71	0.4	n.a.	c,d,e
	methanol-d_4	14.8	0.70	≈0.1	n.a.	c,e
	thf-d_8	17.5	2.33	0.5	n.a.	c,e
		23.8	1.9	0.7	n.a.	g
		23.8	2.1	1.51	0.30 (20)	f
	dmf-d_7	n.a	2.86	0.6	n.a.	c,e
	dmso-d_6	9.2	6.3	1.1	n.a.	c,e
btfa[h]	acetone-d_6	61.6	417[i]	n.a.	n.a.	j
pom-d_1	methanol-d_4	2.2	1.6	0.7	n.a.	c
	dmso-d_6	1.4	14.5	3.2	n.a.	c
poa-d_1	methanol-d_4	22.3	1.4	0.7	n.a.	g
	acetone-d_6	18.0	1.7	0.8	n.a.	g
	thf-d_8	19.3	2.5	0.8	n.a.	g
51a	thf-d_8	26.5	2.7	1.34	0.30 (22)	f
51b	thf-d_8	26.9	2.4	1.29	0.30 (23)	f
51c	thf-d_8	30.4	4.5	1.70	0.42 (25)	f
51d	thf-d_8	31.3	2.8	1.44	0.52 (35)	f

[a]Intrinsic total quantum yield ($^4F_{3/2} \rightarrow {}^4I_J$, J = 9/2, 11/2, 13/2) under excitation at 585 nm.
[b]Quantum yield upon ligand excitation (350–395 nm), $\eta_{sens} = 100 \times Q^{L}_{Nd}/Q^{Nd}_{Nd}$ in parentheses.
[c](Hasegawa et al., 1998).
[d](Hasegawa et al., 1996c).
[e](Hasegawa et al., 1996a).
[f](Iwamuro et al., 2000b).
[g](Iwamuro et al., 1998).
[h]Tetrakis chelate.
[i]Radiative lifetime.
[j](Koeppen et al., 1997).

Sulfur-containing asymmetric β-diketonates, such as mono-thio-thenoyltrifluoroacetonate (stta, **52**, fig. 50), give intensely colored, air and moisture stable complexes [Ln(stta)$_3$(tppo)$_2$] (Ln = Nd, Yb) which emit in the near-infrared (Voloshin et al., 2001b). However thio substitution results in lower thermal stability and lower luminescence efficiency for Nd^{III} and Yb^{III} chelates when compared to the diketonates obtained with the non-sulfonated analog tta. Despite this, the advantage of stta chelates lies in their ability to sensitize Ln^{III} emission with visible blue light (465 nm) whereas the corresponding tta complexes have to be excited with UV light.

Bis(perfluoroalkylsulfonylaminates) bear some resemblance with diketonates and their Nd^{III} complexes with alkyl chain length ranging from 1 to 8 have been measured in deuterated acetone and dmso, as well as in un-deuterated acetone. While all these complexes

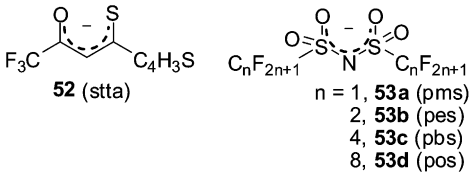

Fig. 50. Mono-thio-thenoyltrifluoroacetonate (stta) and bis(perfluoroalkylsulfonyl)aminate.

have identical quantum yield of 3.3% in dmso-d_6, [Nd(pos)$_3$] (fig. 50) is the most luminescent in acetone-d_6 ($\tau = 13$ µs, $Q_{\mathrm{Nd}}^{\mathrm{Nd}} = 3.2\%$) and un-deuterated acetone ($\tau = 12$ µs, $Q_{\mathrm{Nd}}^{\mathrm{Nd}} = 3.0 \pm 0.5\%$), the order of the quantum yields being [Nd(pos)$_3$] > [Nd(pbs)$_3$] > [Nd(pes)$_3$] > [Nd(pms)$_3$]. The identical quantum yields (and lifetimes) in dmso-d_6 most probably arise from the replacement of the ligands with dmso molecules. Coordination of three pos ligands to Nd^{III} builds a relatively symmetric environment around the metal ion, so that Judd–Ofelt parameter Ω_2 is small, 0.1×10^{-20} cm^2 (Hasegawa et al., 2000; Yanagida et al., 2000a).

Strong erbium luminescence with a full-width at half-maximum of 100 nm is also generated by the ternary complex [Er(pos)$_3$phen] upon excitation in the ancillary ligand band at 333 nm. With respect to direct Er^{III} excitation into the $^2H_{11/2}$ level at 520 nm, the photoluminescence signal increases by a factor 20 (Van Deun et al., 2004b).

Very few studies are available on the near-infrared luminescence of praseodymium diketonates in solution. One of these deals with the influence of the ligand triplet state energy on the luminescence of the Pr^{III} chelates formed with ligands **47b**, **d**, **h**, **48c**, and **49a** (Voloshin et al., 2001a). For Pr^{III}, emission can take place from three different levels, $^3P_0$ (green), $^1D_2$ (red and NIR) and $^1G_4$ (NIR); in addition some papers report luminescence from $^3P_1$ as well. On the other hand, emission from $^1G_4$ is rarely seen in solution, contrary to solid state, as shown for the trinitrate [Pr(NO$_3$)$_3$(X$_2$O)$_6$] (X = H, D) in dmso and dmso-d_6 which emits light only from $^3P_1$, $^3P_0$, and $^1D_2$ (Sveshnikova and Timofeev, 1980). The studied β-diketonates can be classified into three groups depending on the energy of the triplet state $E(^3\pi\pi^*)$, larger, approximately equal, or smaller than $E(^3P_0)$. Chelates formed with ligands **47b**, **d**, and **h** belong to the first group ($E(^3\pi\pi^*) > {}^3P_0$) and as a consequence they emit blue and red light from both $^3P_0$ and $^1D_2$ excited states. The second group includes ligand **48c** which fulfils the condition $E(^3\pi\pi^*) \approx E(^3P_0)$ and displays very weak luminescence from this excited state which is depopulated by metal-to-ligand energy back transfer. However red and near-infrared emission from unquenched $^1D_2$ state is clearly observed at 605, 890, and 1060 nm. The energy corresponding to the latter band also matches the energy of the $^1G_4 \rightarrow {}^3H_4$ transition, but the assignment could not be ascertained. The chelate with ligand **49a** belongs to the third group, $E(^3P_0) > E(^3\pi\pi^*) \geqslant E(^1D_2)$. Excitation of [Pr(**49a**)$_3$(H$_2$O)$_2$] at 365 nm results in red and near-infrared luminescence of Pr^{III} originating only from the $^1D_2$ level. In dmso, luminescence in the near-infrared is more intense than the red luminescence, with partial quantum yields of <0.18% (1060 nm) and 0.006% (605 nm). It results from this study that emission

of Pr^{III} in organic chelates from two and/or one excited state(s) can be tuned by choosing a ligand with a triplet state having the appropriate energy relative to the $^3P_0$ and $^1D_2$ levels.

In an attempt to sensitize Er^{III} luminescence by partial energy transfer from Yb^{III}, these two ions have been co-crystallized in a 1:1 ratio to yield $[Er_{1/2}Yb_{1/2}(\mathbf{47c})_3(tppo)_2]$. The molar ratio Er:Yb has been ascertained by energy dispersion X-ray spectroscopy and their photophysical properties were studied in reference to those of their monometallic analogs, $[Er(\mathbf{47c})_3(tppo)_2]$ and $[Yb(\mathbf{47c})_3(tppo)_2]$ (Zhong et al., 2006). The luminescence measurements have been performed at room temperature on bulk microcrystalline powders under excitation at 355 nm. At this wavelength, tppo does not absorb much, so that one can consider that the excitation energy goes mainly into the hfa levels. The triplet state of the latter is located at 22 200 cm^{-1} and is almost resonant with the Er^{III} $^4F_{5/2}$ (22 100 cm^{-1}), $^4F_{7/2}$ (20 400 cm^{-1}), and $^2H_{11/2}$ (19 100 cm^{-1}) levels, which ensures a sizeable energy transfer efficiency. Erbium emission at 1530 nm is effectively observed in pure $[Er(\mathbf{47c})_3(tppo)_2]$ and is enhanced in the Er–Yb co-crystallized complex (about two to three-fold), with a concomitant decrease of the Yb^{III} luminescence intensity at 980 nm when compared to $[Yb(\mathbf{47c})_3(tppo)_2]$. Therefore, Yb^{III} contributes to the Er^{III} emission by energy transfer from the $Yb(^2F_{5/2})$ level to (probably) the resonant $Er(^4I_{11/2})$ excited state. Due to the larger absorption cross-section of Yb^{III} ions at 980 nm compared to Er^{III}, a usual method to improve the pumping efficiency of Er^{III} ions consists in using an Yb-based 980 nm semiconductor laser diode (LD). Thus excitation of the Er–Yb co-crystallized complex at 980 nm with an LD source also exhibited significant near-infrared luminescence enhancement (two to three-fold) for the Er^{III} ion with respect to the pure monometallic complex. In fact indirect excitation of the Er^{III} ions occurs via energy transfer from the $^2F_{5/2}$ level of the Yb^{III} ion to the $^4I_{11/2}$ Er^{III} level, before subsequently decaying to a lower level, $^4I_{13/2}$, from which near-infrared emission takes place ($^4I_{13/2} \rightarrow {}^4I_{15/2}$ transition). However the efficiency of this process is modest, as demonstrated by lifetime measurements. All luminescence decays obtained under excitation at 355 nm proved to be single exponential functions from which $Yb(^2F_{5/2})$ lifetimes equal to 89.1 and 83.7 μs could be extracted for $[Yb(\mathbf{47c})_3(tppo)_2]$ and co-crystalline $[Er_{1/2}Yb_{1/2}(\mathbf{47c})_3(tppo)_2]$, respectively, while the lifetime of $Er(^4I_{13/2})$ remains the same at ≈61 μs. Using eq. (4a), the slight decrease in Yb^{III} lifetime translates into an efficiency of about 6% only for the Yb → Er energy transfer. Calculated quantum yields of 0.43 and 0.44% for Er^{III} and 4.5 and 4.2% for Yb^{III}, in pure and co-crystallized complexes, respectively, were obtained using eq. (7) with radiative lifetimes of 14 ms (Er^{III}) and 2 ms (Yb^{III}).

So far in most of the afore-mentioned studies the β-diketonates played the role of both coordination and sensitization unit. This is also true for the second ligand in ternary complexes, but this ligand may be more specifically designed so that the photophysical functionality becomes more important. Apart from the widely used phenanthroline, luminescence sensitization has been achieved using organic dyes with large absorption cross sections. One example is Nile red (fig. 51), which reacts with β-diketonates $[Ln(\mathbf{47h})_3(solv)]$ (Ln = Er, Yb) in benzene yielding NIR luminescent solutions (Werts et al., 1999b).

Another example is IR5 with a triplet state energy at ≈7700 cm^{-1} closely matching the acceptor $^4I_{13/2}$ level of the Er^{III} ion at 6500 cm^{-1} (H.S. Wang et al., 2004). Moreover, excitation in the near-infrared spectrum is compatible with optical communication applications based on

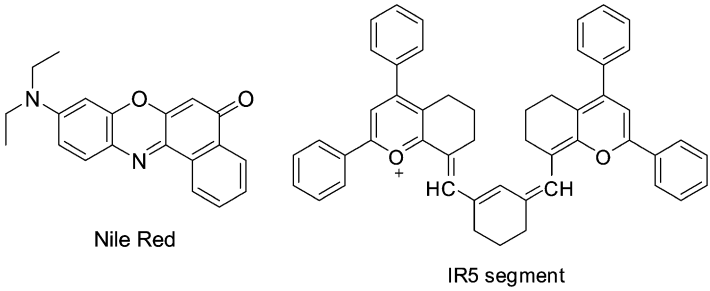

Fig. 51. Organic dyes used in ternary β-diketonate complexes.

silica fibers, in which a 980 nm semiconductor laser diode is typically used as pumping source. In view of the involved organic synthesis procedures needed to obtain an IR5-functionalized ligand, the authors decided in favor of ternary complexes formed by ion association of an anionic tetrakis β-diketonate, in this case [Er(**47c**)$_4$]$^-$, with the IR5 basic dye which possesses a large cationic segment (fig. 51). Luminescence of a bulk powdered sample of [Er(**47c**)$_4$IR5] has been studied at two different wavelengths using as excitation sources, an Ar^+ laser with (488 nm) and a 980 nm semiconductor LD. Upon excitation at both wavelengths two-fold and ten-fold luminescence enhancements were observed when compared to the parent anionic K[Er(**47c**)$_4$] complex, respectively. Indirect excitation mechanisms for the investigated complex are deduced to be mainly $^1S_2 \rightarrow {}^1S_1 \rightarrow {}^3T_1 \rightarrow Er^{III}(^4I_{13/2})$ for 488 nm excitation and $^1S_1 \rightarrow {}^3T_1 \rightarrow Er^{III}(^4I_{13/2})$ for 980 nm excitation. In the former case, $^1S_2$ deactivates to $^1S_1$ rather than to $^3T_2$ since the internal conversion $S_2 \rightarrow S_1$ takes place extremely fast compared to the intersystem crossing from $^1S_2$ to $^3T_2$. Regarding the interest for applications in telecommunications, the efficient sensitization of the Er^{III} luminescence in [Er(**47c**)$_4$IR5] complex pumped at 980 nm let foresee its possible incorporation into polymers or hybrid inorganic–organic matrices for the fabrication of planar amplifiers. Use of a long-wavelength source for excitation is advantageous both for optical devices and medical imaging.

On the other hand, highly luminescent ternary complexes formed with bpy or phen can only be excited by UV radiation. To circumvent this drawback, S. Faulkner and M.D. Ward (Shavaleev et al., 2003c) have synthesized new compounds in which the diimine ligand, 3,6-bis(2-pyridyl)tetrazine (bptz, fig. 52), plays simultaneously the role of a coordinating and sensitizing group. Contrary to other N,N'-bidentate ligands such as bpy and phen, the absorption maximum of the tetrazine unit lies at relatively low energy (18 200 cm^{-1}, $\approx$550 nm). In order to maximize the sensitization process, the chromophoric unit has been directly coordinated to the metal center, which is further bound to three thenoyltrifluoroacetonate anions. Reaction of the potentially bis-bidentate bridging ligand bptz with two equivalents of various Ln^{III} complexes [Ln(tta)$_3$(H$_2$O)$_2$] (Ln = La, Nd, Gd, Er, and Yb) in aqueous ethanol yielded either monometallic complexes [Ln(tta)$_3$(bptz)] (Ln = La, Nd) or bimetallic entities [{Ln(tta)$_3$}$_2$(μ-bptz)] (Ln = Gd, Er, Yb) (fig. 52). It is not well understood yet why the larger lanthanides ions only give monometallic species while the smaller lanthanides give bimetallic complexes, since the stepwise binding constants corresponding to the association of one and

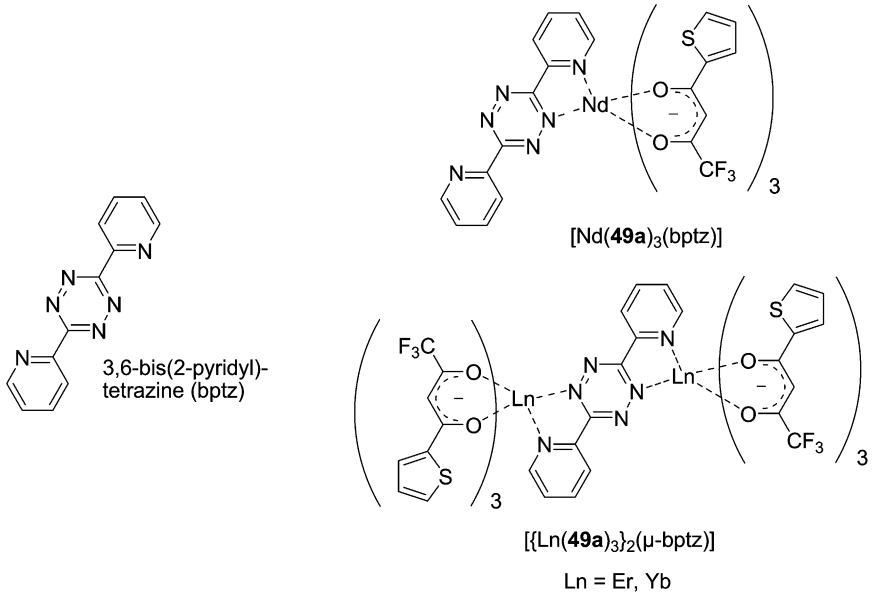

Fig. 52. Monometallic and bimetallic Ln^{III} complexes formed with 2,6-bis(2-pyridyl)-tetrazine (bptz).

two $Ln(tta)_3$ units, respectively, are similar for La and Yb, amounting to ca. $K_1 = 10^6\ M^{-1}$ and $K_2 = 10^5\ M^{-1}$. Excitation of the complexes formed with near-infrared emitting Ln^{III} ions has been performed both on tta and bptz ligands at 337 and 520 nm, respectively. For the Nd^{III} monometallic complex in solution in CH_2Cl_2, single exponential decays were observed under both excitation wavelengths, with lifetimes amounting to 0.76 and 0.78 μs, respectively. This clearly indicates that the ternary complex does not dissociate in dichloromethane since excitation on the bptz ligand leads to NIR luminescence only if the complex $[Nd(tta)_3(bptz)]$ remains intact. In solid state, absence of solvent-based quenching results in a longer lifetime ($\tau = 1.25$ μs).

Under excitation of the Er^{III} and Yb^{III} bimetallic complexes at 337 nm bi-exponential decays were obtained resulting from the dissociation of the bimetallic complex into the monometallic species. According to the binding constants, 11% dissociation is expected, but further dissociation yielding free bptz and $[Ln(tta)_3(solv)]$ is also envisaged by the authors. Therefore three distinct luminescent species are present in solution; however the best fit is obtained using a two-component model indicating that bimetallic and monometallic complexes have similar lifetimes. For the Yb^{III} ion the lifetimes are 13.3 and 1.0 μs. The longer-lived emission is assigned both to the bi- and monometallic complex and the shorter-lived emission to solvated $Yb(tta)_3$. The bimetallic Er^{III} complex shows similar behavior, i.e. under 337 nm excitation a longer-lived emission (1.70 μs) corresponding to intact $[\{Er(tta)_3\}_2(\mu\text{-bptz})]$ and to some $[Er(tta)_3(bptz)]$ while the shorter lifetime (0.15 μs) is attributed to the solvated $Er(tta)_3$. The lifetimes of solid samples of $[\{Yb(tta)_3\}_2(\mu\text{-bptz})]$ and $[\{Er(tta)_3\}_2(\mu\text{-bptz})]$

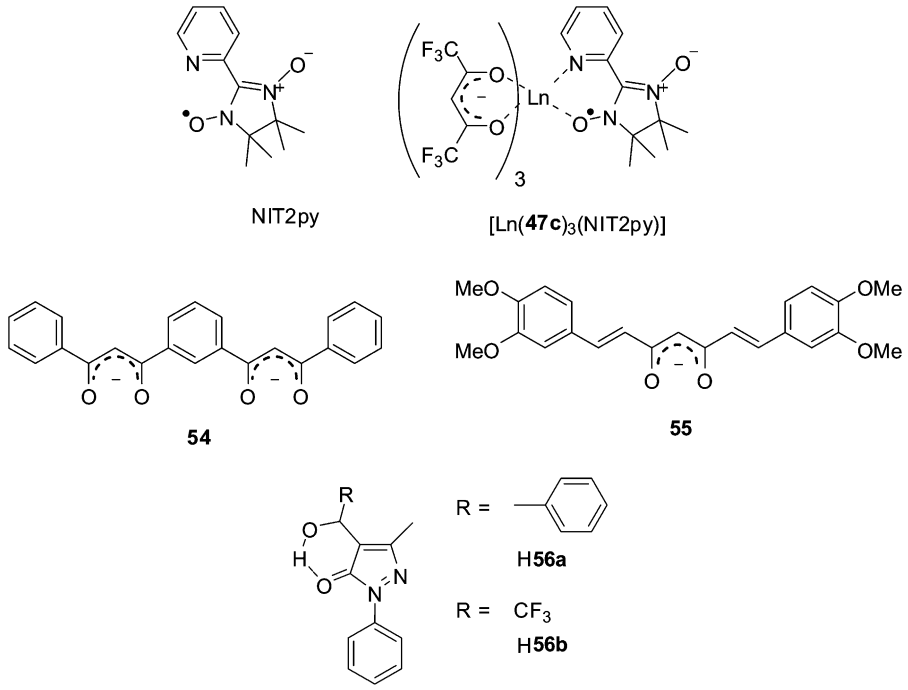

Fig. 53. (Top) Ligand 4,4,5,5-tetramethyl-2-(2′-pyridyl)-4,5-dihydro-1*H*-imidazol-1-oxyl-3-oxide (NIT2py) and its ternary complexes with hfa (**47c**). (Middle) Bis(diketonate) and non-phenolic derivatives of natural curcumin. (Bottom) Pyrazolones.

are 14.1 and 2.0 μs, respectively. Intrinsic quantum yields have also been calculated from the observed and radiative lifetimes (assumed to be 0.25, 14 and 2 ms, respectively) and amount to 0.3, 0.012, and 0.7% for Nd^{III}, Er^{III}, and Yb^{III}, respectively.

Recently, sensitization of the NIR luminescence of Nd^{III}, Tm^{III}, and Yb^{III} was achieved through energy transfer from the single occupied molecular orbital π^* (SOMO) of the nitroxide radical of ligand NIT2py (see fig. 53) (Kaizaki et al., 2005). This ligand was used as secondary ligand for the formation of ternary complexes [Ln(**47c**)$_3$(NIT2py)] with tris-hexafluoroacetylacetonate chelates (Ln = Nd, Sm, Eu, Tm, Yb, and Lu) (fig. 53). In the solid state at 15 K, Ar^+ laser excitation (514.5 nm) of the Nd^{III} and Yb^{III} complexes leads to the observation of their typical NIR luminescence. More unusual is the NIR luminescence exhibited by the Tm^{III} complex at 10 000 cm^{-1} ($^3H_4 \rightarrow {}^3H_6$) and 12 500 cm^{-1} ($^3F_3 \rightarrow {}^3H_6$). On the contrary, [Eu(**47c**)$_3$(NIT2py)] only gives the intraligand doublet–doublet luminescence of the SOMO π^* excited state, probably due to its lower lying position compared to the emissive 4f energy levels of Eu^{III} ions.

So far only diketonates containing one binding site have been investigated. One way to increase the luminescence is to develop ligands containing multiple binding sites, such as

1,3-bis(3-phenyl-3-oxopropanoyl)benzene (H_2**54**, fig. 53) which consists in two conjugated benzoyl β-diketone sites linked by a 1,3-phenylene spacer (Bassett et al., 2004). Reaction of H_2**54** with $LnCl_3 \cdot 6H_2O$ in a 3:2 ratio in the presence of triethylamine leads to the formation of a single species, the triple-stranded helicates $[Ln_2(\mathbf{54})_3 \cdot nH_2O]$ (Ln = Nd, Sm, Eu) with high molar absorption coefficients ($\approx 1.3 \times 10^5$ $M^{-1}\,cm^{-1}$). Excitation in the ligand absorption band (358 nm) of a dmf-d_7 solution of $[Nd_2(\mathbf{54})_3]$ yielded three narrow bands corresponding to the typical Nd^{III} $^4F_{3/2} \rightarrow {}^4I_{9/2}$, $^4I_{11/2}$ and $^4I_{13/2}$ transitions. Analyzing the emission decay monitored at 1054 nm resulted in a lifetime of 1.5 μs which can be compared to the reported lifetime of 2.86 μs for $[Nd^{III}(hfa)_3(solv)]$ in dmf-d_7 (Hasegawa et al., 1996a). Taking into account a radiative lifetime of 270 μs, the intrinsic quantum yield of the Nd^{III} ion is 0.6%.

Lanthanide complexes formed with most of the β-diketonates, like acac, dbm or tta, have relatively high energy triplet excited states (20 000–25 000 cm^{-1}) compared to the principal emissive states of NIR emitting Ln^{III} ions. In order to allow a better sensitization of Ln^{III} luminescence, efforts have been made in the synthesis of ligands possessing triplet states that are more energetically suitable. Following this idea a non-phenolic analog of curcumin (**55**, fig. 53) was synthesized (Seltzer et al., 2005). Curcumin (bis(4-hydroxy-3-methoxyphenyl)-1,6-heptadiene-3,5-dione) is a natural product with an enolic form functionally similar to substituted β-diketonates in terms of metal complexation, but with more extensive π-electron conjugation and consequently longer wavelength absorption and lower triplet state energy ($\sim$14 000 cm^{-1} for the enolate form in dioxane). Since the absorption spectrum of the non-phenolic curcuminoid in methanol solution is almost similar to the one of natural curcumin, the authors reasonably assume that the energy of the triplet states of **55** and curcumin are similar. Excitation of $[Yb(\mathbf{55})_3(phen)]$ at 418 nm results in the typical Yb^{III} emission. In order to determine if the sensitization occurs through an intramolecular energy transfer or via photo-induced electron transfer (PET) mechanism, the free enthalpy ΔG^0 of the electron transfer reaction has been calculated and compared with the values obtained for tryptophan and dbm, for which PET mechanism is known to be favored. In the case of ligand **55**, fluorescence sensitization occurs exclusively through intramolecular energy transfer. It is also the case for the Nd^{III} ternary complex since no divalent oxidation state is available for neodymium. Even if the phenanthroline unit is not involved in the sensitization process, excitation being performed at 418 nm, luminescence enhancement in going from the tris complex to the ternary compound is nevertheless observed because of the exclusion of water molecules from the first coordination sphere of the Ln^{III} ion.

3.2.1.1. *Chemiluminescence (CL)* Chemiluminescence can be generated by decomposition of adamantylideneadamantane-1,2-dioxetane (aad), which is an energy-rich four-member cyclic peroxide. It decomposes into adamantanone, produced both as its singlet and triplet excited states. The resulting chemiluminescence spectrum consists of a broad-band extending from 350 to 550 nm, which overlaps the absorption spectrum of thenoyltrifluoroacetonate in $[Ln(tta)_3(H_2O)_2]$ (Ln = Nd, Yb). Singlet–singlet energy transfer from adamantanone onto tta is followed by the usual energy migration to the triplet state of the β-diketonate and the 4f levels, so that NIR emission matching the photoluminescence spectra is observed in toluene (Voloshin et al., 2000b). The rate constants for the quenching of aad chemiluminescence are

7.9×10^9 and 8.9×10^9 s^{-1} for Nd^{III} and Yb^{III}, respectively. Both the above-described intermolecular mechanism, as well as an intramolecular pathway in the ternary complex with aad which forms in solution, are responsible for the observation of NIR luminescence in these systems. Addition of water to the toluene solutions quenches the NIR luminescence, while it enhances the visible CL emission of the corresponding solution of Eu^{III} and Tb^{III} (Voloshin et al., 2000c). Neodymium and ytterbium tris(benzoyltrifluoroacetonates) display the same CL as tta complexes, although for Yb^{III} its intensity is about 2.5 times lower than for the tta chelate. On the other hand, almost no CL is detected for acetylacetonate complexes (Voloshin et al., 2000a). Thermal or photochemical decomposition of aad also triggers CL from [Pr(dpm)$_3$] and Pr(fod)$_3$], both in the visible (from the $^3P_1$, $^3P_0$, and $^1D_2$ levels) and in the NIR at 850 nm ($^1D_2 \rightarrow {}^3F_2$ transition) and 1100 nm ($^1D_2 \rightarrow {}^3F_4$ transition). The excited chelate [Pr(fod)$_3$]* also initiates decomposition of aad by branched quantum chain reaction (Kazakov et al., 1998).

3.2.1.2. *Electroluminescence* Lanthanide β-diketonates are extensively used for the design of electroluminescent devices or for the development of optical amplifiers in telecommunications. These applications are not specifically reviewed here, but some of them will be presented in section 4.

3.2.1.3. *Pyrazolones* 4-Acyl-pyrazolones H**56** (fig. 53, bottom) are a class of heterocyclic ligands bearing similarities with β-diketonates. These ligands are mainly known as extractants for a variety of metals, including 4f-elements. Langmuir–Blodgett film-forming properties of A[Ln(**56a**)$_4$], where A = *N*-alkyl-4-(2-(4-(dimethylamino)phenyl)ethenyl)pyridinium and Ln = La, Nd, Dy, Yb are comparable to those of hemicyanine iodide but the lanthanide complexes display largely enhanced second-order hyperpolarizability as determined from second harmonic generation experiments (Huang et al., 1995). Attention was drawn to these lanthanide complexes in 1998, when it was demonstrated that the ternary Tb^{III} complex with the 4-isobutyryl derivative and triphenylphosphine oxide (tppo) possesses a much higher green electroluminescence intensity than aluminum tris(8-hydroxyquinolinate), [Al(8-Q)$_3$] (Gao et al., 1998). Reaction of $Ln(NO_3)_3 \cdot xH_2O$ with H**56a** and KOH in a 1:1 mixture of ethanol and water yields air-stable 8-coordinate tris complexes [Ln(**56a**)$_3$(H$_2$O)(EtOH)] for the entire lanthanide series. The Nd^{III} compound crystallizes in the triclinic $P\bar{1}$ space group and the coordination environment of the metal ion is fairly close to a square antiprismatic geometry. A 5×10^{-4} M solution in acetonitrile (Nd^{III}) displays NIR luminescence at 0.88 and 1.06 μm upon excitation at 337 nm. Similarly the $^1D_2 \rightarrow {}^3F_4$ emission from Pr^{III} is detected for solutions of the complexes with both **56a** and **56b** in dmso, although it is much weaker than Nd^{III} fluorescence, especially in the case of the second complex (Pettinari et al., 2002).

3.2.2. *Quinolinates*

8-Hydroxyquinoline (8-quinolinol or 8-HQ) and its halogenated derivatives (see fig. 54) are bidentate ligands possessing good coordination properties towards a wide range of metal ions, including rare earths. For a long time, 8-HQ has been essentially used as reagent for gravimetric analysis; the first report for Ln^{III} analysis appeared in 1936 (Pirtea, 1936).

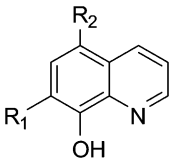

H**57a** $R_{1,2}$ = H
H**57b** R_1 = Cl, R_2 = H
H**57c** $R_{1,2}$ = Cl
H**57d** $R_{1,2}$ = Br
H**57e** $R_{1,2}$ = I

Fig. 54. 8-Hydroxyquinoline-based ligands.

In view of the poor solubility of metal hydroxyquinolinates in aqueous media, 8-HQ also found applications as extraction reagent. These first two applications only take advantage of the coordination properties of the bidentate ligand, but 8-HQ also possesses useful photophysical properties, with a triplet state located around 17 100 cm^{-1} (585 nm). For instance, the Al^{III} tris(8-hydroxyquinolinate) complex [Al(8-Q)$_3$] exhibits intense green electroluminescence and is certainly the most investigated quinoline-based chelate. Indeed, interest in [Al(8-Q)$_3$] complexes started in 1987 when C.W. Tang and S.A. Van Slyke demonstrated its usefulness as active medium in organic light emitting diodes (OLEDs) operating in the visible region around 510 nm (Tang and Van Slyke, 1987). Moreover, [Al(8-Q)$_3$] is commonly used as the electron transport/emitting layer in electroluminescent devices and much effort is still focused on the optimization of its performance, particularly its luminescence efficiency and long-term stability. Optical devices based on organic materials emitting in the visible region are well known and are routinely incorporated in electroluminescent devices. NIR-emitting lanthanide chelates based on 8-hydroxyquinoline have also attracted much attention during the last decade because of their potential use as active components in optical amplifiers or OLEDs operating at telecom wavelengths. Current optoelectronic devices are often composed of silica optical fibers which have two main windows in their transmission loss spectra in the 1.3 and 1.5 μm wavelength regions. The 1.5 μm window is one of the standard telecommunication windows, therefore Er^{III} chelates have been extensively tested for this purpose since the Er($^4I_{13/2} \rightarrow {}^4I_{15/2}$) transition has the right wavelength. Moreover, use of organic materials instead of traditional inorganic optoelectronic components offers some advantages, such as solution processing, flexibility and low cost. W.P. Gillin and R.J. Curry were first to demonstrate that replacement of the [Al(8-Q)$_3$] chelate with its Er^{III} analog is achievable from a technological point of view, yielding a 1.5 μm light source which can be integrated directly within silicon devices (Curry and Gillin, 1999; Gillin and Curry, 1999).

After this first report of NIR electroluminescence using Er^{III} hydroxyquinolinate, H. Suzuki et al. investigated the luminescence characteristics of this complex under different sample forms which can further be used as NIR emissive materials. Three types of samples have been prepared: vacuum-deposited thin-films, doped spin-coated IR polymer films and doped polymer microparticles (Suzuki et al., 2003). Typical NIR luminescence of the Er^{III} ion was observed at 1.55 μm for each sample form and with higher intensities when excitation was performed in the ligand absorption bands instead of directly in the Er^{III} excited levels. This clearly indicates that sensitization of Er^{III}-centered luminescence occurs through ligand-to-metal energy transfer. For the doped monodispersed PMMA microparticles the lower lumi-

nescence intensity is explained by the lower chelate concentration and by the host polymer PMMA which has a much larger absorption cross section than the other two materials in this spectral range. A great advantage of the [Er(8-Q)$_3$] chelate that makes it suitable for application in optical amplifier is its luminescence bandwidth, which is, for each sample form, larger than those of Er^{III} in various inorganic glass matrices exhibiting optical amplification. Indeed large bandwidth is necessary to get a wide gain bandwidth for optical amplification. Luminescence bandwidths ranging from 79 nm for the vacuum-deposited thin-film to 97 nm for doped PMMA microparticles have been obtained, which compare favorably with bandwidths of 7.94 nm in pure silica fiber and 63.8 nm in fluorohafnate glass. The larger bandwidths originate from the more inhomogeneous nature of the sample, including the Er^{III} chelate and/or the polymer matrices. For a better understanding of the emission process occurring in this kind of material, time-resolved studies have been performed on Er^{III} tris(8-hydroxyquinolinate) under the form of powder, thin-film blend with polycarbonate, evaporated film, and in solution in dmso-d_6 (Magennis et al., 2003). In all the cases, the $^4I_{13/2} \rightarrow {}^4I_{15/2}$ transition displays biexponential decays with mean luminescence lifetimes of 0.2 μs for the powder, 0.6 μs for the thin-film blend, 1.03–1.37 μs for evaporated film depending on the film thickness, and 2.7 μs in solution. For the solution, a rise time of ca. 30 ns has also been observed. The biexponential decays reflects the presence of different local environments around the Er^{III} ions and is attributed to the different numbers of solvent molecules that can be coordinated to tris complexes. It is noteworthy that longer lifetimes have been obtained in solution than in the solid state. This is due to the replacement of bound water or methanol molecules with more coordinating dmso-d_6 molecules, which possess vibrations with much lower energy and thus provide less efficient quenching of the Er^{III} luminescence. By assuming a radiative lifetime $\tau_{rad} = 8$ ms, which the authors report as being an average of radiative lifetimes published for erbium complexes, and taking into account the mean lifetimes $\tau_{mean} = A_1 \cdot \tau_1 + A_2 \cdot \tau_2$, where A_i are the pre-exponential factors, luminescence quantum yield have been estimated to ca. 0.002% for the powder, 0.005% for the thin-film blend with polycarbonate, 0.01% for evaporated film and 0.03% for solution in dmso-d_6. These small quantum yields suggest that the low efficiency of 0.01% estimated by R.J. Curry and W.P. Gillin for an [Er(8-Q)$_3$] based OLED device may actually be close to the maximum efficiency achievable when such an Er^{III} organic chelate is used as the emissive material (Curry et al., 2000).

The 1:3 stoichiometry of lanthanide 8-hydroxyquinolinates was taken for granted for a long time until R. van Deun et al. became interested in the relationship between the structure of these compounds and their luminescence and discovered that three types of 8-hydroxyquinolinates and of their halogenated derivatives can be isolated depending on the experimental conditions: (i) hydrated tris complexes [Ln(**57**)$_3 \cdot x$H$_2$O], (ii) tetrakis complexes [ALn(**57**)$_4$] and (iii) trimeric complexes [Ln$_3$(**57**)$_8$B], where A and B are monovalent cation and anion, respectively (Van Deun et al., 2004a). Monomeric anhydrous tris complexes could not be obtained from syntheses in solutions. The syntheses of lanthanide 8-hydroxyquinolinates were repeated following the most frequently used synthetic procedures found in literature and instead of 1:3 complexes, mixtures of different species were obtained in most of the cases. The first procedure, listed as method A in table 12, consists in mixing an ethanolic solution of the ligand and an aqueous solution of Ln^{III} nitrate, to which a slight

Table 12
Summary of the synthetic procedures commonly used in literature to yield rare-earth quinolinates (Van Deun et al., 2004a)

Method (year)	Ligand (solvent)	LnX_3 (solvent)	Base	Complexes
A (1971)	H**57a** (EtOH) H**57c**, **d**, **e** (EtOH)	$Ln(NO_3)_3$ (H_2O)	NH_4OH	tris/trimeric tris/tetrakis
B (2001)	H**57** (H_2O/MeOH, 20/80)	$LnCl_3$ (H_2O)	–	trimeric (>90%)
C (1957)	H**57a**, **b** (acetone) H**57c**, **d**, **e** (acetone)	$LnCl_3$ (H_2O)	$CH_3CO_2NH_4$	trimeric tris/tetrakis
D (2004)	H**57** (EtOH)	$LnCl_3$ (EtOH)	NaOH	tetrakis

excess of an ammonium hydroxide solution is added, thus causing the precipitation of the complex. Elemental analyses of the complexes lead to the conclusion that they correspond to the general formula $[Ln(\mathbf{57})_3 \cdot xH_2O]$. However the presence of another, trimeric species $[Ln_3(\mathbf{57})_8(solv)]^+$ is suggested by mass spectrometry and confirmed by X-ray analysis of Er^{III} single crystals. In this trimeric complex, the two peripheral erbium ions each coordinate to four 8-hydroxyquinolinate ligands. An additional hydroxide anion is bound to one of the peripheral erbium ions, while a water molecule is coordinated to the other one. Each ligand coordinates in a bidentate fashion and bridges the erbium ions via the oxygen atom except for two peripheral ligands. The synthetic method B, which is the most currently used method to produce active emitting materials for OLEDs, resulted in the formation of pure trimeric complexes (in >90% yields). The last method investigated (method C, see table 12) uses ammonium acetate as a base leading for ligands **57a** and **57b** to the formation of trimeric species in which the two peripheral erbium ions are both surrounded by four ligands and linked to the central erbium ion, this latter being coordinated to six oxygen atoms and to one acetate counterion (fig. 55, right).

With halogen-disubstituted ligands, a mixture of tris and tetrakis complexes is obtained, but no longer the trimeric species. In the tris complex, erbium coordination consists of three bidentate 8-hydroxyquinolinates and two water molecules, the latter forming strong hydrogen bonds with the oxygen atoms of two ligands of a second tris complex and thus leading to the formation of dimerized tris complexes (fig. 55, upper left). To summarize, ligands **57a** and **57b** form primarily trimeric complexes, while disubstituted ligands **57c**, **57d**, and **57e** yield tris/tetrakis mixtures.

New synthetic routes have therefore been developed in order to improve the purity of the precipitates. Thus pure tetrakis complexes (see fig. 55, bottom) could be isolated using ligand **57** in ethanol with a large excess of sodium ions in slightly basic conditions (method D, table 12), whereas method B seems to be the more appropriate synthetic way to obtain pure trimeric complexes. Pure tris complexes could not be isolated; however mixtures with up to 75% of tris complex could be obtained by using as little ammonium hydroxide as possible and a mixture of dichloromethane and water as biphasic solvent (improved A method).

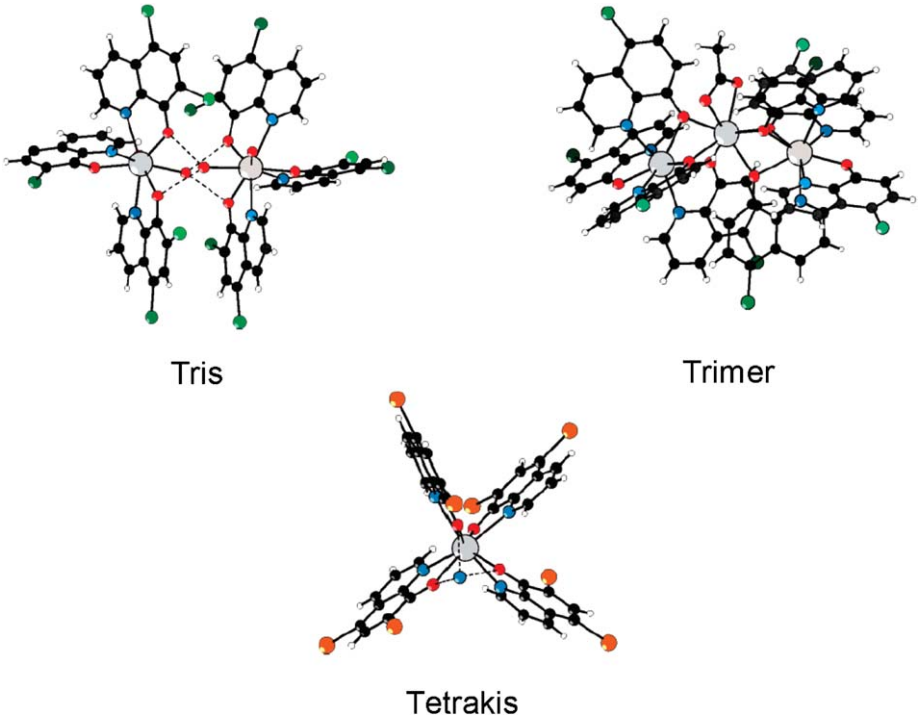

Fig. 55. The three types of structures observed for rare-earth 8-hydroxyquinolinates. Reproduced with permission from (Van Deun et al., 2004a).

Before these findings, Van Deun et al. had investigated the luminescence properties of Er^{III} tris-8-hydroxyquinolinate complexes in dmso upon ligand excitation around 400 nm (Van Deun et al., 2003a). Since dmso molecules coordinate to the Er^{III} ion expelling the water molecules from the first coordination sphere, the most efficient quencher in such complexes is the aromatic C–H stretching vibration, which is located at 3060 cm^{-1}. As a consequence, the second overtone almost matches the energy of the Er($^4I_{13/2} \rightarrow {}^4I_{15/2}$) transition (≈6500 cm^{-1}). Thus by substituting the aromatic proton with a heavy atom the stretching frequency should be significantly lowered, so that higher overtones would be required for efficient quenching, a process less likely to occur. Indeed, halogen substitution of the 5,7-hydrogen atoms in the quinoline moiety results in an increase of the luminescence intensity by not less than 30%, with lifetimes going from 1.2 μs for the unsubstituted ligand **57a** to 1.9 and 1.8 μs for ligands **57c** and **57d**, respectively. However, it has to be noted that the tris complex has been synthesized according to method A (see table 12) and thus most likely consisted of a mixture of tris and tetrakis species. In fact, the emission intensity of trimeric and tetrakis species with the same ligand is almost identical, whereas the tris species, due to coordinated solvent molecules, are less luminescent. Taking this observation into account, pure tetrakis complexes

have been synthesized with disubstituted ligands and showed a luminescence enhancement of 50% instead of 30% (Van Deun et al., 2004a). Lifetimes of the tris and tetrakis complexes with ligand **57c** amount to 2.2 and 2.3 μs, respectively, whereas lifetime of pure $[Er(\mathbf{57a})_4]^-$ is 1.5 μs.

More recently, a fourth type of structure with general formula $[Er_3(\mathbf{57a})_9]$ has been elucidated by X-Ray analysis (Artizzu et al., 2005). In this trimetallic complex, each erbium ion presents a distorted antiprismatic geometry; the two outer ions being bound by four nitrogen and four oxygen atoms while the inner ion is coordinated to one nitrogen and seven oxygen atoms. The overall structure is strengthened by π–π stacking interactions occurring between quinolinate anions. Mass spectrometry and UV–vis–NIR spectroscopy clearly show that the structure of the trimetallic complex is maintained in dmso solution. Two bands are observed in the diffuse reflectance spectrum, a first one around 1.5–1.55 μm assigned to the $^4I_{13/2} \leftarrow {}^4I_{15/2}$ transition and a second one near 1.68 μm corresponding to the absorption of the first overtone of the stretching mode of the aromatic quinolinate C–H groups. As a consequence, Er^{III} luminescence quenching in the $[Er_3(\mathbf{57a})_9]$ complex is also only due to the aromatic C–H vibrations of the ligand. Despite the presence of two distinct sites in the complex, nearly single exponential decay was observed within the available dynamic range. This can be explained by the fact that the Er^{III}–Er^{III} energy migration occurs much faster (10-ns time scale) than the Er^{III} nonradiative decay time, 2.2 μs for a crystalline sample; as a result, the excitation energy migrates and is delocalized over the three ions, so that only an average emission spectrum is observed.

The quenching of the NIR-emitting $Er(^4I_{13/2})$ level induced by resonant dipolar interaction between the metal ion and high frequency vibrations of the organic ligand has been modeled by means of a "continuous medium approximation" using the erbium quinolinate complexes described above (Artizzu et al., 2005; Van Deun et al., 2004a) as test compounds (Quochi et al., 2006). In this model, the quenching process is assumed to follow Förster's mechanism with a $1/r^6$ dependence on the dipole–dipole distance and the discrete acceptor distribution (i.e. C–H, C–C, C–O vibrations) is replaced with a continuous and homogeneous distribution ρ_A, representing an average acceptor density. The non-radiative rate constant can therefore be estimated as

$$k_{nr} = \frac{k_r}{(2\pi n)^4 R_{min}^3} \int F_D(\lambda)\alpha_A(\lambda)\lambda^4 \, d\lambda \cong \frac{\lambda_{em}^4}{(2\pi n)^4} \cdot \frac{k_r \langle \alpha_A \rangle_{Er}}{R_{min}^3}, \tag{28}$$

where n is the refractive index, R_{min} is the minimum distance between the Er^{III} ion and the acceptor (calculated from the crystal structure), $F_D(\lambda)$ is the normalized Er^{III} emission spectrum, $\alpha_A = \sigma_A \rho_A$ is the vibrational absorption coefficient of the acceptor distribution where σ_A is the absorption cross section. The radiative rate constant k_r is given by the Strickler–Berg expression:

$$k_r = 8\pi n^2 c \int \frac{\sigma_E(\lambda)}{\lambda^4} \, d\lambda \tag{29}$$

in which $\sigma_E(\lambda)$ is the emission cross section. Therefore, k_{nr} depends on two spectroscopic quantities only: the radiative rate constant k_r and the vibrational absorption averaged over the

Er^{III} emission, $\langle\alpha_A\rangle_{Er}$. The model works well (within $\pm 10\%$) because R_{min} is relatively large ($\approx$3.4 Å for the chosen hydroxyquinolinate). In $[Er_3(\mathbf{57a})_9]$ for instance, $\tau_r = 5 \pm 0.5$ ms and $\langle\alpha_A\rangle_{Er} = 1 \pm 0.3$ cm^{-1}; with $n \approx 1.5$, the calculated non-radiative lifetime becomes $\tau_{nr} = 2.6$ µs, in reasonably good agreement with the experimental value of 2.3 µs. One way of decreasing the influence of the vibrational quenching is to increase R_{min}; however, assuming $\langle\alpha_A\rangle_{Er} \approx 1$ cm^{-1}, one sees that R_{min} should be larger than 30 Å for k_{nr} to be smaller than k_r. Another mean is the reduction of the vibrational absorption $\langle\alpha_A\rangle_{Er} = \langle\sigma_A\rangle_{Er} \cdot \rho_A$, which is achievable by using halogenated ligands and by reducing the density of vibrational quenching groups. Again, for k_{nr} to be smaller than k_r, one can calculate that $\langle\sigma_A\rangle_{Er}$ should be smaller than 5×10^{-4} cm^{-1}, a value two thousand times smaller than the one measured for the unsubstituted complexes. Such values, however, are close to the ones calculated for fluorinated polymers.

8-Hydroxyquinolinates are also well-suited for the sensitization of Nd^{III} luminescence since their triplet state emission centered at $\approx$585 nm overlaps the Nd^{III} absorption band with the highest transition probability ($^2G_{7/2}$, $^4G_{5/2} \leftarrow {}^4I_{9/2}$). Examples are the series of neodymium complexes formed with 8-hydroxyquinolinate-based ligands **57** depicted on fig. 54 (Iwamuro et al., 1999; Iwamuro et al., 2000a). Excitation performed on the absorption band of the ligand (425 nm for ligand **57a** and 447 nm for ligands **57c**, **d**, **e**) leads to the typical Nd^{III} luminescence at 890, 1070 and 1350 nm. As for the corresponding Er^{III} complexes, substitution of the hydrogen atoms in the 5- and 7-position of the 8-hydroxyquinoline by halogen atoms leads to an increase in the luminescence quantum yields in dmso-d_6 by more than a factor of two: $Q^L_{Ln} = 0.4$, 1.0, 1.0, and 0.9% for ligands **57a**, **c**, **d**, and **e**, respectively (Iwamuro et al., 2000a). Intrinsic quantum yields and lifetimes have also been measured and follow the same trend, i.e. an increase is observed in going from 8-hydroxyquinolinate to its halogenated derivatives. Calculations of the overlap integral J between the phosphorescence spectrum of the ligand and the absorption spectrum of Nd^{III} according to the Dexter exchange-interaction theory give large values as expected from the above discussion, confirming the reason for the intense NIR luminescence observed with all these complexes.

Lanthanides 8-hydroxyquinolinates are promising materials for the design of electroluminescent devices and further applications will be discussed in section 4.

3.2.3. *Terphenyl-based ligands*

Acyclic *m*-terphenyl-based ligands form another class of chelating agents which encapsulate efficiently Ln^{III} ions via the formation of 1:1 complexes (Ln = Nd, Sm, Eu, Gd, Tb, Dy, Er, and Yb) and, at the same time, act as antenna-chromophores since they have a high rate of intersystem crossing (Steemers et al., 1995). Their macrocyclic analogs (ligands **22b**, **c**, and **d**) have already been discussed in section 3.1.3. In search of suitable ligands for the sensitization of Ln^{III} NIR luminescence, F.C.J.M. Van Veggel and collaborators have synthesized *m*-terphenyl-based ligands bearing amido (ligands **58a**, **b**) and sulfonamido (ligand **58c**) functionalities (Klink et al., 2000b). Each of these ligands, which are represented on fig. 56, provides eight oxygen donor atoms: three ether and three carboxylate functions from the three oxyacetate groups, and two additional donors from amide or sulfonamide groups. Coordina-

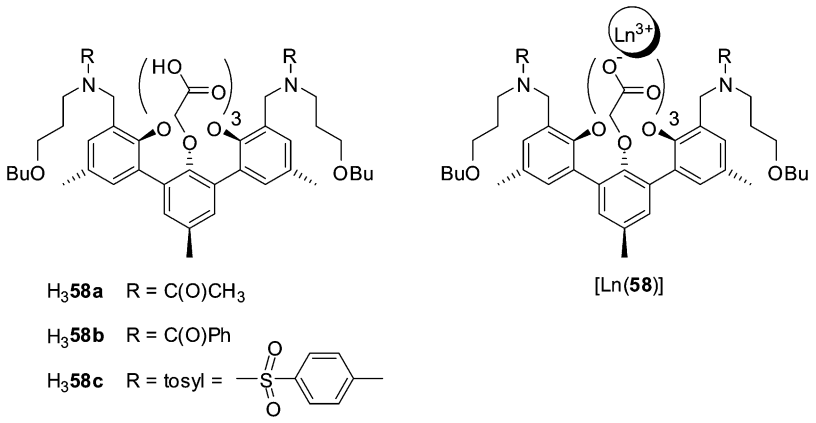

Fig. 56. Terphenyl-based ligands bearing amido and sulfonamido pendant arms and their corresponding Ln^{III} complexes.

tion of the latter to the lanthanide ion has been evidenced by NMR measurements of the Y^{III} complexes in dmso-d_6.

From the luminescence lifetimes obtained in methanol and methanol-d_1 for the Eu^{III} and Tb^{III} complexes, it has been established that only one methanol molecule is coordinated to the Ln^{III} ion in [Ln(**58a–b**)] complexes, leading to 9-coordinate complexes. For the compounds [Ln(**58c**)], q_{MeOH} is between one and two, which suggests the presence of an equilibrium between two differently solvated species. In spite of the high lying triplet states of the terphenyl-based ligands ($\approx$24 600 cm^{-1}), sensitized NIR emission of Nd^{III}, Er^{III} and Yb^{III} complexes with ligands **58b** and **58c** occurs in dmso after laser excitation at 350 nm. Using dmso-d_6 instead of dmso leads to a significant increase in the lifetimes, indicating that in such complexes C–H oscillators of the solvent molecules are effective quenchers of the Ln^{III} excited states. The quenching rate constants calculated for complexes [Ln(**58b–c**)] amount to $\approx 4.5 \times 10^5$, 1.5×10^5 and 6×10^4 s^{-1} for Ln = Nd^{III}, Er^{III}, and Yb^{III}, respectively. The same experiment has been repeated on Eu^{III} complexes and the calculated rate constants are two to three orders of magnitude smaller ($\approx$100 s^{-1}). These results are in agreement with the well-established energy gap law. Taking radiative lifetimes of 0.25, 14, and 2 ms for Nd, Er and Yb, respectively, gives intrinsic quantum yields of 0.84, 0.02, and 0.78% in dmso-d_6. These low values are caused essentially by the presence of C–H oscillators in the ligand. As a consequence, deuteration of the ligand H_3**59a** has been achieved to yield H_3**59b** (see fig. 57), where all the C–H groups that contribute to quenching have been deuterated (Hebbink et al., 2001b). In order to determine which C–H oscillators are responsible for the quenching, average distances between hydrogen atoms and the Ln^{III} ion have been calculated using molecular dynamics simulations. Since the quenching rate is exponentially related to the distance between donor and acceptor, C–H groups lying at 6 Å and further away from the Ln^{III} ion will not significantly contribute to the quenching and thus do not have to be deuterated. This is the case for all the hydrogen atoms of the *m*-terphenyl moiety, whereas all the other groups have to

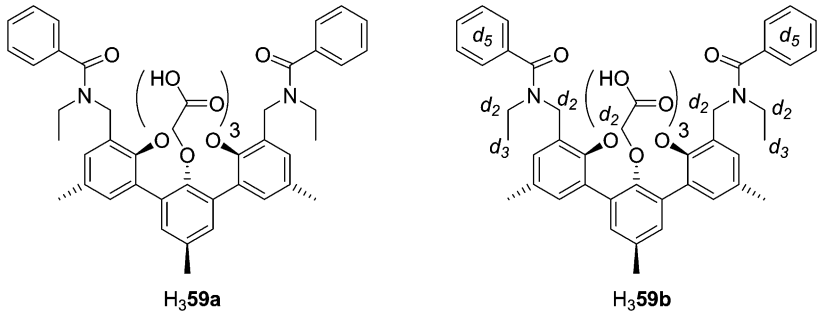

Fig. 57. Terphenyl-based ligand and its deuterated analog.

be deuterated. The lifetimes obtained in dmso-d_6 with non-deuterated ligand **59a** amount to 2.5, 3.3, and 19.0 μs for Nd, Er, and Yb, respectively, while the corresponding lifetimes for the deuterated ligand **59b** are 5.5, 5.4, and 52.3 μs, leading to intrinsic quantum yields of 2.0, 0.04, and 3.0%, assuming the same radiative lifetime as above, for Nd^{III}, Er^{III}, and Yb^{III}, respectively. The enhancement factor upon deuteration of the ligand is therefore 2- to 3-fold.

One great advantage of all these *m*-terphenyl-based ligands comes from their rather easy functionalization by incorporating different sensitizer units at the amide and sulfonamide positions, without changing either the synthetic route or the coordinating nature of the ligand. Therefore a series of new terphenyl-based ligands containing additional chromophoric units possessing relatively high intersystem crossing quantum yield, such as organic dyes (see fig. 58), have been synthesized in view of practical applications. Indeed, with this approach, it is hoped that the excitation wavelength can be shifted into the visible region up to around 530 or even 630 nm, where very compact and relatively cheap green or red diode lasers can be used as excitation sources. Moreover in such complexes the antenna chromophore is positioned in close proximity to the Ln^{III} ion because of the coordination of the amide carbonyl. The first example of a terphenyl-based ligand fitted with a dye antenna is derivative H_3**60a** depicted in fig. 59 (Klink et al. 1999, 2000a). It exhibits an isc quantum yield of 89%, but for this ligand, excitation has to be performed in the UV, between 300 and 350 nm.

Upon excitation of the triphenylene antenna, the typical line-like emission of NIR emitting Ln^{III} ions is observed for all [Ln(**60a**)] complexes in dmso-d_6 with lifetimes of 2.5, 3.4, and 18.6 μs for Ln = Nd, Er and Yb, respectively, whereas lifetimes measured in non-deuterated dmso are 1.4–2 times smaller. This decrease clearly shows the extreme sensitivity of NIR emitting Ln^{III} ions toward quenching by C–H oscillators, in this case from the solvent molecules. Quenching rate constants of these C–H oscillators range from 0.5 to 3.1×10^5 s^{-1} with the higher value for the [Nd(**60a**)] complex, in agreement with the energy gap law. The radiative rate constants calculated from the radiative lifetimes, amount to 4000, 71, and 500 s^{-1} for Nd, Er, and Yb, respectively. Since the observed rate constant k is the sum of both the radiative and nonradiative rate constants and in view of the values obtained, it is clear that for NIR emitting Ln^{III} ions the rate constant k is dominated by nonradiative deactivation of the luminescent state.

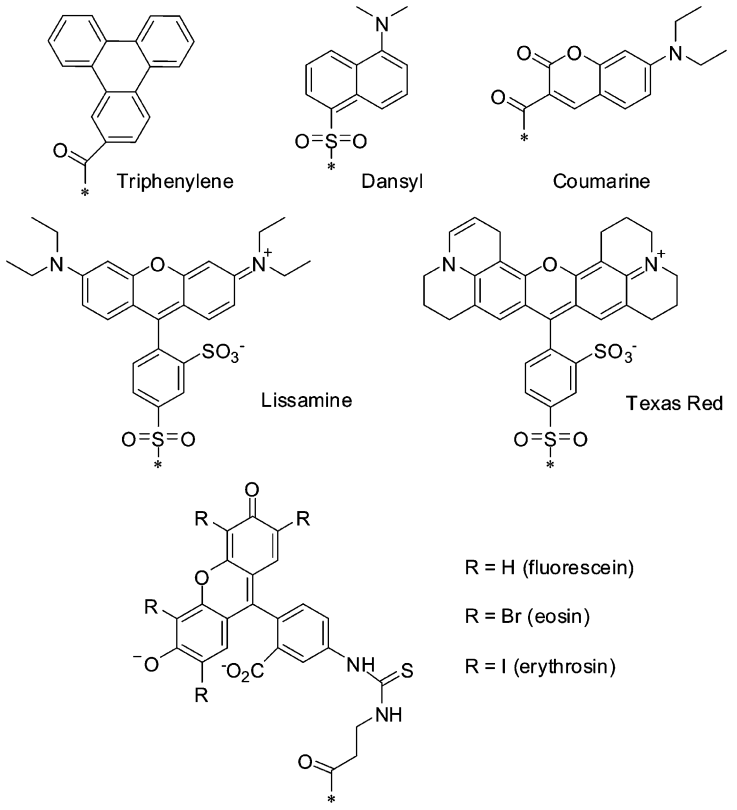

Fig. 58. Organic dyes used as antenna chromophore in terphenyl-based ligands.

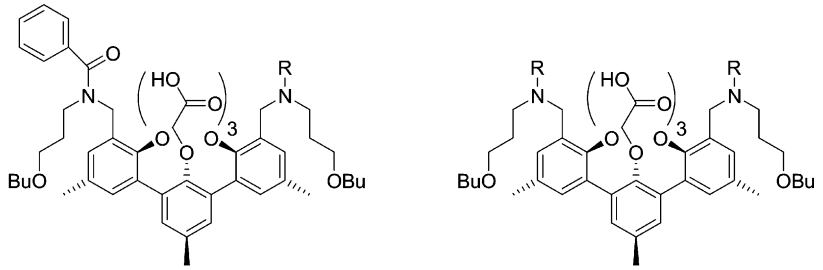

R = triphenylene (H_3**60a**), dansyl (H_3**60b**), coumarine (H_3**60c**), lissamine (H_3**60d**), Texas Red (H_3**60e**)

R = dansyl (H_3**60f**), coumarine (H_3**60g**)

Fig. 59. Dye-functionalized derivatives of terphenyl-based ligands.

Although an internal redox mechanism is possible for the sensitization of Yb^{III} luminescence, it has been shown that it cannot occur in such complexes and that as a consequence, the usual energy transfer pathway ($^1S \rightarrow {}^3T \rightarrow Ln^*$) is operative in these Yb^{III} complexes. Oxygen quenching of the triphenylene triplet state and energy transfer to the Ln^{III} ion are in competition. Therefore the luminescence intensity is enhanced by 35% for [Nd(**60a**)], 120% for [Er(**60a**)], and 90% for [Yb(**60a**)] upon de-oxygenation of the dmso-d_6 solutions. A good estimate of the energy transfer rate can be achieved from this oxygen dependence by using the following Stern–Volmer equation:

$$\frac{I_0}{I} = 1 + k_{\text{diff}} \cdot \tau_T \cdot [O_2], \tag{30}$$

where I_0 and I are the Ln^{III} luminescence intensities in the absence and presence of oxygen, respectively, k_{diff} is the diffusion-controlled quenching rate constant, τ_T, the lifetime of the triphenylene triplet state, and $[O_2]$, the oxygen concentration in dmso. Taking $k_{\text{diff}} = 10^{10}\ M^{-1}\ s^{-1}$ and $[O_2] = 0.47$ mM, and assuming that in deoxygenated solutions the lifetime of the triphenylene triplet state is mainly governed by the energy transfer rate constant $k_{et} = 1/\tau_T$. The energy transfer rate constants obtained for the different complexes reach 1.3×10^7, 3.8×10^6, and $5.1 \times 10^6\ s^{-1}$ for Nd, Er, and Yb, respectively. These values are of the same order of magnitude as the oxygen quenching rate ($\approx 5 \times 10^6\ s^{-1}$) so that the slowest the energy transfer is, the largest the oxygen quenching and thus the lowest energy transfer quantum yield. This is corroborated by the experimental observations. Thus the Nd^{III} complex, in which the energy transfer is the fastest, is less influenced by the presence of oxygen and exhibits the lowest luminescence enhancement after de-oxygenation, whereas the reverse situation is observed for the Er^{III} complex. As a consequence, the energy transfer quantum yields amount to 74, 45, and 53% for the Nd, Er, and Yb complexes, respectively. Although energy transfer is quite efficient in the Nd^{III} complex, the intrinsic quantum yield is relatively low, only 1% in dmso-d_6, meaning that the overall quantum yield is also low. For the Er^{III} and Yb^{III} complexes, intrinsic quantum yields of 0.02 and 0.93%, respectively, were calculated.

Keeping in mind the development of a polymer-based optical amplifier, for which Nd^{III} and Er^{III} ions are suitable as the optical active component, a series of six dye-functionalized Nd^{III} complexes have been synthesized and their luminescence properties investigated (Klink et al., 2001). The study focused on complexes with Nd^{III} since it exhibits larger intrinsic quantum yields than Er^{III} in organic environments. Four different fluorescent dyes, namely dansyl, coumarine, lissamine and Texas Red (see figs. 58 and 59) were used for the sensitization of the Nd^{III} luminescence. Bis-functionalized ligands with dansyl (H_3**60f**) and coumarine (H_3**60e**) have also been synthesized to investigate the influence of an additional chromophore on the efficiency of the sensitization process. All these fluorescent dyes have broad and intense bands ranging from the near-UV to the visible region, with absorption maxima at 345 nm for dansyl, 400 nm for coumarine, 568 nm for lissamine, and 590 nm for Texas Red. For the six Nd^{III} complexes, excitation of the antenna chromophore resulted in the observation of the typical NIR Nd^{III} emission, the lifetimes of which are around 2.2 μs in dmso-d_6. Taking into account the absorbance of the samples and differences in the excitation intensity as a function of the wavelength, the recorded emission intensities showed that in the series of investigated dyes,

dansyl (H_3**60b**) is the most efficient sensitizer, followed by lissamine (H_3**60d**) and Texas Red (H_3**60e**), while coumarine (H_3**60c**) is the least efficient one. Moreover, incorporation of a second antenna chromophore in ligands H_3**60f** and H_3**60g** does not increase the luminescence quantum yield of the system. For most of the complexes, oxygen has no influence on their luminescence intensities, except for [Nd(**60c**)] and [Nd(**60g**)] formed with coumarine functionalized ligands for which de-oxygenation of the samples leads to a 20% increase in luminescence intensity. According to the authors, this indicates that the transfer of energy from coumarine to Nd^{III} is slower than for the other antenna chromophores. The presence of the Nd^{III} ion leads to a significant reduction of the antenna fluorescence intensity in the complex when compared to the free ligand. The most important decrease is observed for dansyl chromophore (80%) whereas for coumarin only a 40% decrease occurs. At first, the authors explained the reduction in the fluorescence intensity of the antenna by an external heavy atom effect induced by the presence of the heavy and paramagnetic Nd^{III} ion, which enhances the intersystem crossing process and thus hinders the radiative process, i.e. the fluorescence of the antenna. However more detailed work performed on dansyl- and lissamine-functionalized Nd^{III} complexes clearly showed that this explanation is not correct and that the observation of sensitized Nd^{III} luminescence in such complexes results from a direct energy transfer from the singlet excited state of the dye to the lanthanide ion (Hebbink et al., 2002a). As seen previously, the dansyl chromophore is a better sensitizer with the emission intensity of the lissamine-functionalized complex [Nd(**60d**)] being approximately 70% of that of the dansyl one, [Nd(**60b**)]. Lifetimes are in the range 2.1–2.2 μs in dmso-d_6, whereas they are almost two times shorter in dmso (1.1–1.2 μs). Moreover as stated before, the luminescence of these two complexes is not influenced by oxygen, which is known as an efficient triplet-state quencher, implying two possible explanations; the triplet state is either (i) depopulated relatively fast, meaning that the energy transfer from the triplet state to the Ln^{III} ion is too fast ($>10^7\ s^{-1}$) to compete with oxygen quenching, or (ii) is not involved at all, indicating that the energy transfer occurs from the singlet state. Measurements performed on the Gd^{III} complexes show that quantum yields and lifetimes of the dye fluorescence are the same for the complexes and for free ligands H_3**60b** and H_3**60d**. This implies that no external heavy atom effect from the lanthanide ions is operative on the dansyl and lissamine moieties. As a consequence, the decrease of the antenna fluorescence in the Nd^{III} complexes can only be attributed to a direct energy transfer from the singlet state to the Nd^{III} ion. Furthermore no phosphorescence could be observed at 77 K in an ethanol/methanol glass, indicating that the formation of triplet states is insignificant.

Er^{III} and Yb^{III} complexes have also been studied, but upon antenna excitation no sensitized NIR luminescence was observed, and the lifetimes of the antenna fluorescence in these complexes are the same as those measured for the free ligands. It is obvious that for a fast energy transfer the antenna singlet excited state and the accepting Ln^{III} energy level should have a non-zero spectral overlap integral. Based on the large energy gap between the $Yb^{III}(^2F_{5/2})$ level lying at 10 200 cm^{-1} and the singlet excited state of both the dansyl ($E(^1\pi\pi^*) \approx 17200\ cm^{-1}$) and lissamine ($E(^1\pi\pi^*) \approx 23\,500\ cm^{-1}$) moieties, the energy transfer will be slow and cannot compete with the rate of radiative deactivation by fluorescence. Both Nd^{III} and Er^{III} ions possess several energy levels able to accept the excitation en-

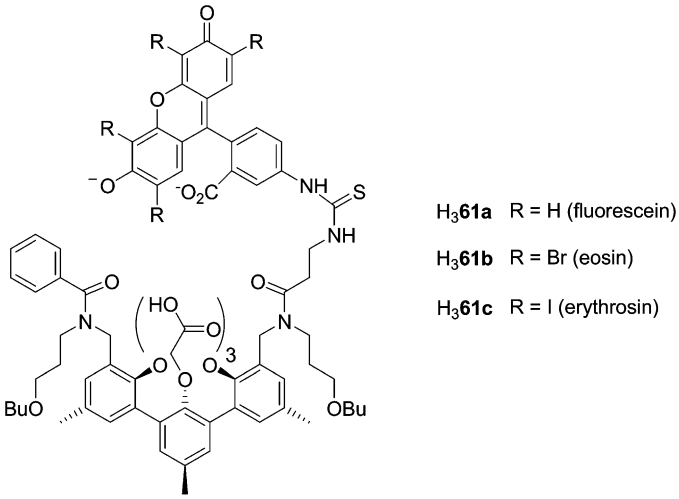

Fig. 60. Xanthene-functionalized terphenyl-based ligands for the sensitization of NIR emitting Ln^{III} ions.

ergy from the singlet excited state of dansyl and lissamine units. However these levels should satisfy the selection rules for 4f–4f transitions accompanying the energy transfer process. Since Dexter-type mechanisms have the highest probability, the selection rule $|\Delta J| = 0, 1$ ($J = J' = 0$ excluded) allowing this type of transfer has to be followed. In these conditions, only the Nd^{III} ion possesses levels allowing energy transfer from the lissamine and dansyl units. The only excited level of Er^{III} meeting this selection rule is $^4I_{15/2}$, lying at 6400 cm^{-1}, for which the energy gap is too large to allow fast energy transfer. Even though the best results were obtained with the dansyl-functionalized ligand H_3**60b**, the lissamine-containing ligand H_3**60d** is more suitable for applications since it allows excitation up to 570 nm, whereas with the dansyl unit the excitation window is limited to 400 nm.

Three other *m*-terphenyl-based ligands have been prepared which incorporate dyes that are structurally very similar to the xanthene moiety (Hebbink et al., 2003). The dyes used are fluorescein, eosin and erythrosin (see figs. 58 and 62) linked to the terphenyl moiety via a β-alanine spacer and possessing absorption maxima in methanol at 505, 535, and 545 nm, respectively. The great advantage of these dyes compared to the previous ones comes from their carboxylate group that coordinates to the Ln^{III} ion, reducing the distance between the donor and the acceptor, and thus allowing more efficient energy transfer. Furthermore, in such complexes the Ln^{III} ion is coordinated by four carboxylates, two amides, and three ether oxygen atoms, leading to a coordination number of 9, henceforth saturating the first coordination sphere and preventing solvent molecules to interact directly with the Ln^{III} ion. Molecular dynamics calculations clearly evidenced the coordination of the carboxylate anion, and the average distances between the Ln^{III} ion and the xanthene unit were found to be 6.1–6.2 Å.

The complexes of general formula [Ln(**61**)] (Ln = Nd, Er and Yb) (see fig. 60) exhibit the typical NIR luminescence of each Ln^{III} ion upon excitation in the antenna chromophore. The overall quantum yields have been determined in deuterated methanol and by using the Nd^{III}

Table 13
NIR emission properties of [Ln(**61**)] complexes in methanol-d_1

Ln	Ligand	Q_{Ln}^{L} (%)	Q_{Ln}^{Ln} (%)[b]	η_{sens} (–)
Nd	**61a**	0.03	0.16	0.19
	61b	0.014	0.16	0.09
	61c	0.012	0.15	0.08
Er	**61a**	1.0[a]	0.0065	
	61b	0.51[a]	nd[c]	
	61c	0.43[a]	nd[c]	
Yb	**61a**	0.23	0.55	0.42
	61b	0.14	0.56	0.25
	61c	0.17	0.58	0.29

[a]Relative quantum yields, $Q([Er(\mathbf{61a})]) = 1.0$.
[b]Calculated from $Q_{Ln}^{Ln} = \tau_{obs}/\tau_{rad}$, with $\tau_{rad} = 0.25$, 14, and 2 ms for Nd, Er, and Yb, respectively.
[c]Not determined, no accurate decay trace obtained.

and Yb^{III} complexes formed with fluorexon (Fx, see fig. 64 in section 3.2.4 below) as standards for the Nd^{III} and Yb^{III} complexes. For the Er^{III} complexes, the quantum yields are given relative to the complex [Er(**61a**)], for which the quantum yield has been fixed to unity. From data reported in table 13, it is clear that the highest quantum yields are obtained for complexes formed with H_3**61a** which contains the fluorescein antenna; this was difficult to predict since the intersystem crossing yield is much higher in erythrosin (82%) or eosin (18%) than in fluorescein (2%). In fact, the isc quantum yields of the antenna has less influence than expected since the external heavy atom effect provided by the Ln^{III} ion diminishes drastically this difference. Moreover, for Nd^{III} complexes the accepting energy level is $^4F_{9/2}$ (at 15 000 cm^{-1}) and not the $^4F_{7/2}$ level located at 13 400 cm^{-1}. Therefore, energy back transfer occurring from the accepting Nd^{III} level to the triplet state of eosin and erythrosin is more pronounced than for fluorescein, the energy gap being larger in the latter case. For Er^{III} complexes, the authors postulate that relaxation of the selection rules allows additional pathways, which may be the reason for the sensitization of this ion. For instance, the more efficient sensitization observed in the fluorescein complex [Er(**61a**)] can be attributed to a pathway involving the Er^{III} $^4F_{9/2}$ level at 15 500 cm^{-1}.

The quantum yields are rather low despite the fact that deuterated methanol-d_1 was used. This is mainly due to vibrational deactivations occurring in the complex itself, especially C–H oscillators as seen above. From the lifetimes obtained in methanol and deuterated methanol it is possible to calculate the rate constant of solvent quenching in these complexes. A value smaller or equal to 3×10^4 s^{-1} was found for the Yb^{III} complexes, whereas for the corresponding Yb^{III} complex formed with ligand H_3**58b** this quenching rate constant is one order of magnitude higher (3×10^5 s^{-1}). This shows that the ligand shield effectively the Ln^{III} ion from the solvent, which is in accordance with the molecular modeling studies. Rate constants of $\leqslant 1 \times 10^6$ s^{-1} were found for Nd^{III} complexes, caused by solvent molecules present in the second coordination sphere, whereas this value reaches 2.3×10^6 s^{-1} in the correspond-

ing complex [Nd(**58b**)], which has solvent molecules in the first coordination sphere. Thus, second-sphere solvent molecules play a greater role in the deactivation of Nd^{III} ions when compared to Yb^{III}, since the energy gap between the excited and ground states is much larger for the latter. Moreover Nd^{III} ions are slightly bigger than Yb^{III} ions allowing more space for second sphere quenchers. Concerning the energy transfer rate constant, it was estimated to be at least 10^8 s^{-1}.

3.2.4. *Polyaminocarboxylates*

Polyaminocarboxylates yield stable 1:1 complexes with lanthanide ions in view of the strong ionic bonds between the carboxylate anions and the Ln^{III} cation, and due to the formation of five-membered chelate rings. The simplest ligands belonging to this class are nitrilotriacetic acid (H_3nta), ethylenediaminetetraacetic acid (H_4edta), and diethylenetriaminepentaacetic acid (H_5dtpa), which are depicted in fig. 61. In the case of nta or edta, formation of 1:2 (Ln:L) complexes is also possible. The remarkable stability of the 1:1 complexes is exploited in complexometric titrations (Schwarzenbach, 1957), in the determination of stability constants by competitive measurements, or in the design of contrast agents for medical imaging.

In absence of chromophoric substituents, no sensitization of Ln^{III} luminescence occurs, either in the visible or in the near-infrared ranges (Beeby et al., 1997; Beeby and Faulkner, 1997). On the other hand, complexation of the chelating agent removed the inner-sphere water molecules, resulting in a considerably enhanced intrinsic quantum yield. Two strategies have been probed to improve the photophysical properties of lanthanide polyaminocarboxylates, (i) electrochemically generated luminescence (ECL) and (ii) the functionalization of polyaminocarboxylate with dyes. Conversely, aminocarboxylate groups are often grafted on luminescence sensitizers to improve their coordinative properties, as seen elsewhere in this review.

Ala-Kleme and collaborators have probed the ability of six heptadentate, one octadentate, and three nonadentate polyaminocarboxylates to sensitize Yb^{III} emission by an electrochemically generated process (fig. 62). In these experiments, peroxidisulfate is added to the chelate solutions and electric pulses generate hydrated electrons ($E^0 = -2.9$ V vs SHE) which trigger the following reactions:

$$S_2O_8^{2-} + e^-(aq) \rightarrow SO_4^{\bullet -} + SO_4^{2-}, \tag{31a}$$

$$YbL + SO_4^{\bullet -} \rightarrow Yb(L^{\bullet})^+ + SO_4^{2-}, \tag{31b}$$

$$YbLn(L^{\bullet})^+ + e^-(aq) \rightarrow YbL^* \rightarrow Yb^*L. \tag{31c}$$

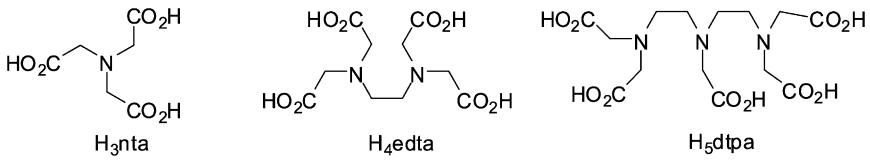

Fig. 61. Simple polyaminocarboxylic acids.

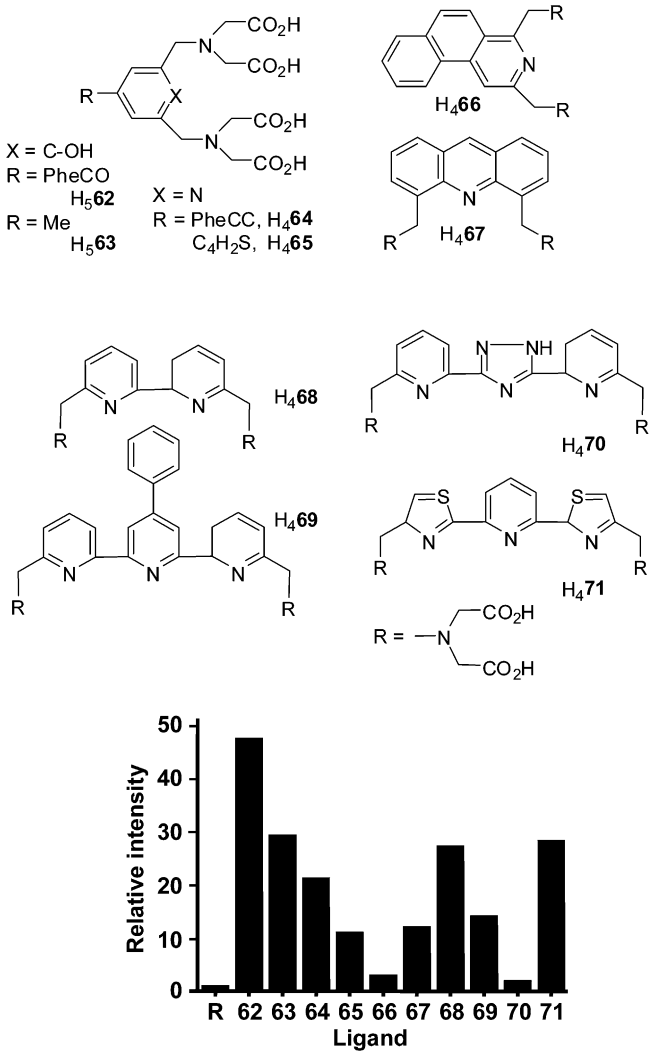

Fig. 62. Aromatic polyaminocarboxylate ligands for ECL (top) and relative ECL emission for Yb^{III} complexes 10^{-5} M at pH 9.2 (bottom); R is the reference edta chelate.

Sulfate radicals are formed ($E^0 = +3.49$ V vs SHE), which oxidize the aromatic moieties of the polyaminocarboxylate ligands into $Yb(L^{\cdot})^{+}$. In turn, the latter species is easily reduced by aqueous electrons leading to an excited ligand (YbL^{*}). This reaction is fast enough to produce the excited singlet or triplet states of the aromatic unit, provided that the net reaction enthalpy exceeds the energy difference between the ground state and the excited state of the organic ligand. This is effectively the case here, $-\Delta H^0$ being estimated to $\approx$4.1 eV, while

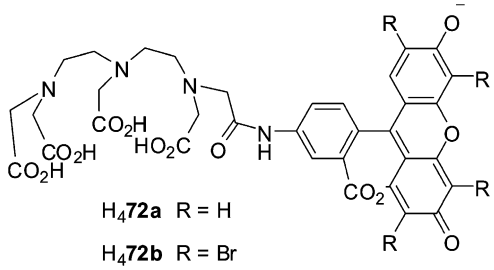

Fig. 63. Xanthene-modified diethylenetriaminepentaacetic acid (dtpa) derivatives.

$E(^1\pi\pi^*) \approx 3.7$–$4.1$ eV and $E(^3\pi\pi^*) \approx 2.8$–$3.3$ eV. The excited ligand subsequently transfers energy onto the metal ion (Yb^*L). The process is sometimes called "oxidation-initiated reductive excitation". Alternatively, a competing "reduction-initiated oxidative excitation" could occur in which the aqueous electron that reduces the chelate (YbL^-) is produced first and then reacts with the sulfate radical to produce YbL^*. Energy considerations, however, indicate that the preferred excitation is the first mechanism. Several of the tested chelates have sizeable Yb^{III}-centered ECL as shown on fig. 62 in which $[Yb(edta)]^-$ is taken as reference (R). The advantage of these systems, beside generating NIR ECL luminescence in water, is that the blank electrochemically generated luminescence of the oxide-covered aluminum cathode (the so-called F-center ECL) is practically zero in this spectral range leading to a high signal-to-noise ratio (Ala-Kleme et al., 1999).

Polyaminocarboxylates are often used as building blocks for designing more elaborate ligands in which, for instance, an antenna chromophore is grafted on one of the tertiary amine of the aliphatic skeleton. This results in a new type of receptors which are well suited for the sensitization of Ln^{III} luminescence since they combine the coordinating properties of polyaminocarboxylate moieties and the light harvesting efficiency of dyes. With a judicious choice of the chromophore, efficient sensitization of NIR emitting Ln^{III} ions can be achieved with visible light. For instance, xanthene derivatives such as fluorescein and eosin, which have absorption maxima near 500 nm, have been attached onto dtpa, yielding ligands H_4**72a** and H_4**72b** depicted on fig. 63 (Hofstraat et al., 1998; Werts et al., 1997). As expected, both ligands form stable, water-soluble 1:1 complexes with Ln^{III} ions (Ln = Nd, Er, and Yb), but the complexation does not change their absorption spectra, the maxima being still observed at 491 nm for the fluorescein-containing ligand and at 519 nm for the eosin-containing one. Excitation at 488 nm of 10^{-6} M solutions of the chelates in deuterated Tris-DCl buffer (Tris is 2-amino-2-(hydroxymethyl)propane-1,3-diol) leads to the typical NIR lanthanide emission. The relatively good sensitization of Ln^{III} NIR luminescence in [Ln(**72a**)] complexes, whereas the isc quantum yield of fluorescein is only 2% in water, can be explained by the heavy atom effect produced by the lanthanide ion. Enhancement of the isc yield could not be quantitatively determined, but it is confirmed by the large decrease in fluorescence intensity of the antenna upon complexation. The luminescence of all the solutions is more or less oxygen sensitive, clearly indicating the implication of the xanthene triplet state in the sensitization process. Luminescence enhancement factors of 1.1

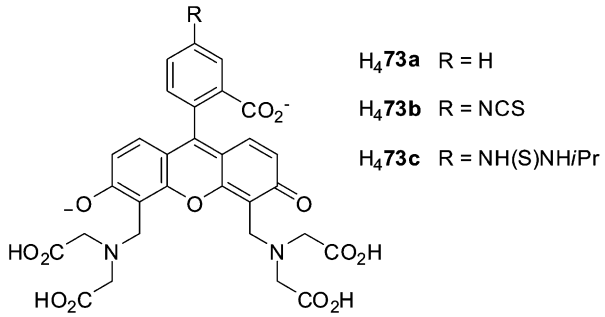

Fig. 64. 4′,5′-bis[*N*,*N*-bis(carboxymethyl)aminomethyl]fluorescein, also called fluorexon (fx, R = H) and thio-derivatives.

for [Er(**72a**)] to 5.8 and 6.4 for the Yb^{III} chelates with H_4**72a** and H_4**72b**, respectively, have been observed upon de-oxygenation of the solutions. Therefore, the ligand-to-metal energy transfer in the Yb^{III} complex is much slower than the corresponding process in the Nd^{III} and Er^{III} compounds. This is relatively easy to understand since energy transfer occurs between two states separated by a large energy gap ≈5000 cm^{-1}, the excited triplet state of the dye lying at ≈15000 cm^{-1}. In some cases $^1O_2$ ($^1\Delta_g \rightarrow {}^3\Sigma_g$) phosphorescence at 1275 nm has been detected, the latter species resulting from a triplet–triplet annihilation process occurring when the sensitizer triplet state interacts with molecular oxygen.

The lifetimes measured for Ln^{III} complexes with ligand H_4**72a** amount to 0.6, 1.0, and 8.5 μs for Nd^{III}, Er^{III}, and Yb^{III}, respectively, and are comparable to the lifetimes generally found for organic complexes, but still remain short compared to those obtained in inorganic glasses, which are in the millisecond range. This demonstrates once more the effectiveness of high-energy vibrational modes in deactivation of the excited states of those NIR emitting Ln^{III} ions. Multi-photon excitation mechanism is another way to further shift the excitation wavelength into the visible or near-infrared region, for which low-cost excitation sources can be used. The first case of sensitization of NIR emitting lanthanide via multi-photon excitation has been demonstrated on Nd^{III} and Yb^{III} complexes formed with H_4**72a** (Piszczek et al., 2002a). NIR emission is sensitized via two-photon excitation of the fluorescein-containing ligand at 800 or 840 nm for Yb^{III} and Nd^{III}, respectively. The four-fold decrease in the emission intensity when the excitation is attenuated two-fold clearly demonstrates two-photon absorption.

The xanthene dye sensitizers used in the studies cited above feature a fused three-ring system acting as the chromophoric unit which is oriented almost perpendicular to the phenyl ring. As a result, the distance between the chromophoric unit and the lanthanide ion is long, which is detrimental for the overall sensitization process, the exchange interaction being weakened. To circumvent this drawback, a fluorescein derivative, 4′,5′-bis[*N*,*N*-bis(carboxymethyl)aminomethyl]fluorescein, commonly named calcein or fluorexon (fx, H_4**73a**) has been prepared (Werts et al., 2000a). This ligand and related derivatives are depicted on fig. 64; they consist of a fluorescein dye, in which the xanthene moiety has been directly functionalized with polyaminocarboxylate arms. By doing so, the binding site of the

lanthanide ion is in closer proximity of the chromophore than in complexes with ligands H_4**72a** and H_4**72b**.

Under stoichiometric conditions, fluorexon and its derivatives form 1:1 complexes with Ln^{III} ions. However when the ratio Ln:Fx is increased, complexes with other stoichiometries are observed, the exact nature of which has not been determined. On the other hand, luminescence data of solutions with a ratio Yb^{III}:Fx $\leqslant 1$ clearly indicate the presence of only one luminescent species, the 1:1 complex. Monoexponential luminescence decays are observed corresponding to a lifetime of 1.9 μs, whereas multi-exponential decays are measured when the Yb^{III}:Fx ratio is increased. Further proof of the existence of 1:1 complexes has been brought by mass spectrometry. Competitive titration with edta has been followed by monitoring the Yb^{III} luminescence, since the edta complex is non-luminescent, contrary to the chelate formed with Fx. After addition of 5 equivalents of edta to a solution of [Yb(fx)] in Tris-HCl buffer, the Yb^{III} luminescence intensity decreases to 12% of its initial value. The thermodynamic stability of the fluorexon chelate is, therefore, comparable to $[Yb(edta)]^-$. In addition, the luminescence decay after addition of edta aliquots is relatively slow, the estimated rate constant being 7.1×10^4 s^{-1}, indicating a reasonably high kinetic stability of the fluorexon chelate.

As for the chelates formed with ligands H_4**72a** and H_4**72b**, the fluorescence intensity of the dye is drastically reduced upon complexation with Nd^{III}, Er^{III}, and Yb^{III}, the corresponding quantum yield decreasing from 85% for the free ligand to less than 1% in the complexes. The quenching of the antenna fluorescence can be explained by three different mechanisms; (i) energy transfer from the singlet state to the Ln^{III} ion, (ii) electron transfer (especially for Yb^{III} ion which is easily reduced) and (iii) improved intersystem crossing. Since the quenching is identical in the complexes with the three NIR-emitting ions and with Gd^{III}, the first two mechanisms can be discarded and thus an enhancement of the intersystem crossing due to the paramagnetic and heavy atom effects is the most likely cause of the fluorescence quenching. The intersystem crossing rate constant can be estimated to be $>10^{10}$ s^{-1}. Moreover, study of the photophysical properties of the Gd^{III} complex gives direct information on the triplet state of the chromophore, especially its lifetime, which is found to be short (3.1 μs). Deoxygenation of the solution, results in an increase of this lifetime to 21 μs. For the complexes with the NIR-emitting Ln^{III} ion, only the typical metal-centered luminescence is observed in each case, indicating an efficient energy transfer from the triplet state of the antenna to the Ln^{III} ion. Furthermore, the overall NIR luminescence quantum yield is independent of the oxygen concentration contrary to what was observed in complexes with H_4**72a**. This implies that both the intersystem crossing and the $^3\pi\pi^* \rightarrow Ln^{III}$ energy transfer rates are fast since oxygen quenching, which occurs at a rate of $\approx 10^7$ s^{-1}, cannot compete. This results in high sensitization efficiencies, which reach estimated values of 50, 100, and 90% for Ln = Nd^{III}, Er^{III}, and Yb^{III}, respectively. However the lifetimes are still in the microsecond range (0.25–10.4 μs) and similar to what is usually observed in other organic complexes, corresponding to small intrinsic quantum yields, so that despite the high sensitization efficacy, the overall quantum yields (table 14) remain small, the highest value reaching 0.09% for the Yb^{III} complex in Tris-HCl 0.1 M (0.45% in deuterated Tris-DCl).

Table 14
Lifetimes, intrinsic and overall quantum yields, and sensitization efficiency for 1:1 complexes formed with ligands H_4**73a** and H_4**74** in aqueous solution

Ln	Ligand[a]		τ (μs)	Q^{Ln}_{Ln} (%)[b]	Q^{L}_{Ln} (%)	η_{sens} (–)[c]
Nd	H_4**73a**	H_2O[a]	0.25	0.03	0.017	0.5
		D_2O[a]	0.58	0.07	0.038	0.5
	H_4**74**	H_2O	<0.2	<0.03[d]	0.004	0.1[d]
		D_2O	0.4	0.05[d]	0.02	0.4[d]
Er	H_4**73a**	H_2O[a]	–	–	–	–
		D_2O[a]	1.46	0.02	0.019	1.0
	H_4**74**	H_2O	–	–	–	–
		D_2O	1.2	0.02[d]	0.004	0.2[d]
Yb	H_4**73a**	H_2O[a]	1.91	0.1	0.089	0.9
		D_2O[a]	10.4	0.5	0.45	0.9
	H_4**74**	H_2O	2.5	0.13[d]	0.02	0.2[d]
		D_2O	10.0	0.50[d]	0.10	0.2[d]

[a]Tris-HCl and deuterated Tris-DCl 0.1 M solutions.
[b]Calculated from $Q^{Ln}_{Ln} = \tau_{obs}/\tau_{rad}$, with $\tau_{rad} = 0.8$, 8, and 2 ms for Nd^{III}, Er^{III}, and Yb^{III}, respectively.
[c]Calculated from $Q^{L}_{Ln} = \eta_{sens} \cdot Q^{Ln}_{Ln}$.
[d]Recalculated from the data of (Quici et al., 2005) using the radiative lifetimes given under[b].

This work clearly demonstrates that a fluorescent chromophore is not necessarily a bad antenna for lanthanide ions. Indeed, high fluorescence quantum yields indicate the absence of nonradiative deactivation and thus, if the Ln^{III} ion is sufficiently close to the chromophore, a significant intersystem crossing enhancement can occur, leading to an efficient sensitization of the Ln^{III} luminescence. The authors extended the study further by functionalizing ligand H_4**73a** with a reactive group, in this case isothiocyanate (see ligands H_4**73b** and **73c**, fig. 64) for coupling with biological molecules in view of developing near-infrared luminescent probes for fluoroimmunoassays and fluorescence microscopy, as discussed in section 4.3 (Werts et al., 2000b).

The simpler phenanthroline chromophore has also been tested by grafting it onto diethylenetriaminetetraacetic acid, H_4dtta or H_4**74**, depicted on fig. 65 (Quici et al., 2005). Stable, water-soluble 1:1 complexes form with Ln^{III} ions and ^{1}H NMR and luminescence studies performed on the [Eu(**74**)] chelate clearly indicate that the two nitrogen atoms of the phenanthroline are involved in the coordination of the lanthanide ion, thus that no solvent molecule is present in the first coordination sphere. As already observed with the previous ligands, complexation with lanthanide ions leads to a quenching of the antenna fluorescence and hence to an enhancement of the intersystem crossing process. In the case of phen, the high value of the isc quantum yield in the free ligand (85%) suggests that it should be close to unity in the chelates.

Upon excitation of phen in the UV, at 279 nm, the typical luminescence of Pr^{III}, Nd^{III}, Sm^{III}, Eu^{III}, Tb^{III}, Dy^{III}, Ho^{III}, Er^{III}, and Yb^{III} is observed. Thus ligand H_4**74** is able to sensitize the

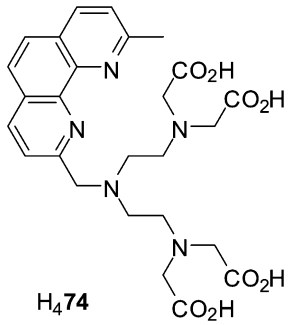

Fig. 65. Phenanthroline-functionalized diethylenetriaminetetraacetic acid (dtta).

whole range of emitting lanthanide ions in aqueous solution, which is quite exceptional especially for Sm^{III}, Dy^{III}, and Ho^{III}, the NIR luminescence of which is rarely observed in solution. Regarding NIR emitting Ln^{III} ions (Nd, Er, and Yb) the lifetimes of the Nd^{III}, Er^{III}, and Yb^{III} excited levels are exactly in the same range of values as those observed for complexes formed with H_4**73a**; i.e. from 0.2 to 10 µs (see table 14). However the overall quantum yields are smaller, with a maximum value of 0.1% in D_2O obtained for the [Yb(**74**)] chelate. It has to be noted that a potential cause of luminescence quenching for NIR emitting Ln^{III} ions in aqueous solutions can be water reabsorption of the emitted light. For instance, Er^{III} complexes with H_4**73a** and H_4**74** undergo complete quenching in water and their emission can only be detected in deuterated water.

Another completely different approach consists in choosing a dye, that already possesses aminocarboxylate functions (Meshkova et al., 1992a), such as triphenylmethane dyes. The latter can be used for selective luminescent determination of Nd^{III} and Yb^{III} in samarium oxide, for instance. As previously described in the section devoted to β-diketonates (section 3.2.1), the triplet excited states of β-diketonates lie at energies $>20\,000$–$25\,000$ cm^{-1}, above most of the accepting levels of Ln^{III} ions. As a consequence, determination of Nd^{III} and Yb^{III} in europium or samarium oxides is difficult using β-diketonates since these two ions exhibit luminescence in the NIR, especially Sm^{III} with emission lines at 908, 930, 950, and 1038 nm close to the analytical lines of Nd^{III} and Yb^{III}. Therefore, the detection limit of Nd^{III} and Yb^{III} in samarium compounds by luminescence of their ternary complexes with tta and phen is only 0.1–1 wt%.

In order to solve this problem, Meshkova et al. used triphenylmethane dyes, especially phthalexon S (PS, H_4**75a**, fig. 66) and xylenol orange (XO, H_4**75c**), since their triplet states ($12\,800$–$14\,600$ cm^{-1}) are higher in energy than the $^4F_{3/2}$ and $^2F_{5/2}$ excited levels of Nd^{III} and Yb^{III}, respectively, but lower than the $^4G_{5/2}$ excited state of the Sm^{III} ion. Following this strategy and using XO as colored reagent, detection limits of Nd^{III} and Yb^{III} in samarium oxide could be brought down to 2.5×10^{-3} and 3.0×10^{-4} wt%, respectively.

Ligands H_4**75a** and H_4**75c** form 1:1 and 1:2 complexes with Ln^{III} ions, and to avoid quenching by water molecules, a surfactant was added. The subsequent formation of micelles led to 7- to 12-fold increases in Nd^{III} luminescence intensity (Rusakova et al., 1984).

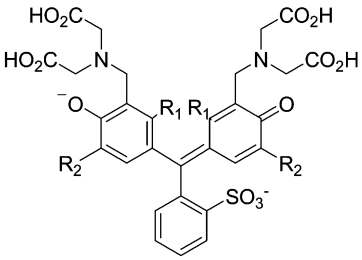

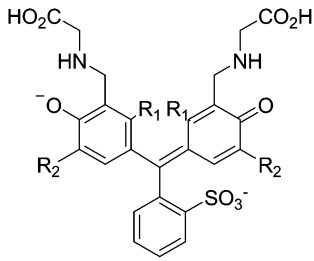

H_4**75a** $R_1 = R_2 = H$ (Phthalexon S, PS)

H_4**75b** $R_1 = H$, $R_2 = Br$

H_4**75c** $R_1 = H$, $R_2 = CH_3$ (xylenol orange, XO)

H_4**75d** $R_1 = CH_3$, $R_2 = i$-Pr (methylthymol blue)

H_4**76a** $R_1 = H$, $R_2 = CH_3$ (glycinecresol red)

H_4**76b** $R_1 = CH_3$, $R_2 = i$-Pr (glycinethymol blue)

Fig. 66. Triphenylmethane dyes.

Cationic surfactants cause the greatest increase, whereas anionic or nonionic surfactants influence the luminescence intensity to a much lesser extent. With PS or XO as colored reagent and the cationic surfactant Etonium (1,2-ethanediaminium, N,N'-bis[2-(decyloxy)-2-oxoethyl]-N,N,N',N'-tetramethyl-dichloride), the smallest concentration of Nd^{III} that yields observable NIR luminescence reaches 0.1 $\mu g\,ml^{-1}$. Further triphenylmethane dyes were tested, such as H_4**75b**, **d** and H_4**76a**, **b** (fig. 66), the two last ligands possessing iminoacetate functions instead of iminodiacetate ones (Rusakova and Meshkova, 1990). The solvent also influences the emission intensity and with respect to water, the largest enhancement occurs when dmso is added (up to 70%), followed by dmf and alcohols, whereas with acetone and acetonitrile, the emission is enhanced up to addition of 60% solvent and then drops due to decomposition of the complexes. In view of these results, a new selective method for determining Nd^{III} in rare-earth oxides has been proposed based on a Nd^{III} complex with xylenol orange in the presence of Etonium and dmso. The Nd^{III} detection limit in Sm^{III} and Pr^{III} oxides is 2.5×10^{-3} wt%, whereas in La^{III} and Y^{III} oxides it reaches 1×10^{-3} wt%. Similar results have been obtained for Yb^{III} (Meshkova et al., 1985; Poluektov et al., 1984) and the most important photophysical characteristics of the two series of complexes with ligands H_4**75** and H_4**76** in water and deuterated water are summarized in table 15.

Because of the higher sensitivity of Nd^{III} ions towards deactivation through O–H oscillators, the complexes with this lanthanide have much lower quantum yields and lifetimes when compared to Yb^{III}. The best photophysical properties are obtained with phthalexon S and since complexes with PS contain 4–5 water molecules, depending on the lanthanide ion, it is quite clear that exclusion of these water molecules from the first coordination sphere will lead to much enhanced luminescent properties. This is indeed demonstrated by bis(cyclen)-substituted PS, H_7**36** (see fig. 36), which increases quantum yields to 0.23 and 1.45% in D_2O for Nd^{III} and Yb^{III}, respectively (Korovin and Rusakova, 2002).

Table 15
Photophysical properties of some Nd^{III} and Yb^{III} complexes with triphenylmethane dyes in water (Korovin and Rusakova, 2002)

Ln	Ligand	$E(^3\pi\pi^*)$ (cm^{-1})	Q_{Ln}^{L} (%)[a]	τ (μs)	
				H_2O	D_2O
Nd	H_4**75a**	14 060	0.025	0.07	0.35
	H_4**75c**	13 950	0.021	0.06	0.30
	H_4**75d**	13 750	0.008	0.05	0.25
Yb	H_4**75a**	14 110	0.411	0.70	3.15
	H_4**75c**	14 030	0.496	0.60	2.70
	H_4**75d**	13 870	0.190	0.40	1.60
	H_4**76a**	14 015	0.020	0.15	0.80
	H_4**76b**	13 905	0.036	0.20	1.15

[a]Overall luminescence quantum yields of D_2O solutions determined with [ZnTPP] as standard ($Q = 3.15\%$ in ethanol).

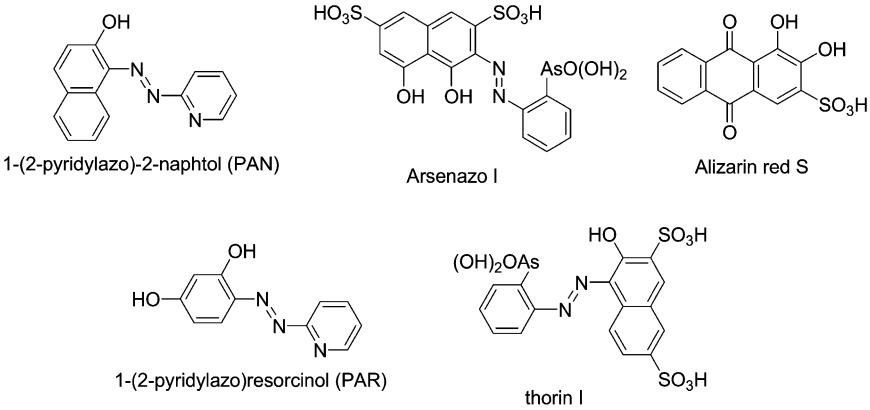

Fig. 67. Some of the dyes investigated as colored reagents.

3.2.5. *Other chelating agents*

3.2.5.1. *Dyes* Following a strategy similar to the one described above, other types of dyes have been proposed for analytical purposes. For instance, Korovin et al. have investigated the possibility of using a 1:2 (Yb:L) ytterbium complex with 1-(2-pyridylazo)-2-naphthol (PAN, fig. 67) for the determination of Yb^{III} in solutions of its salts. The luminescence intensity varies linearly over an Yb^{III} concentration range from 0.1 to 10.0 μg ml^{-1}, whereas the detection limit reaches 0.05 μg ml^{-1} (Korovin et al., 1984). One disadvantage of using dyes as ligands comes from the fact that most of the time the first coordination sphere of the Ln^{III} ion is not saturated, leaving space for one or several bound solvent molecules. This leads to a consequent quenching of the NIR luminescence and thus decreases the detection limit. To circumvent this problem, Meshkova et al. turned to ternary complexes, as often encountered

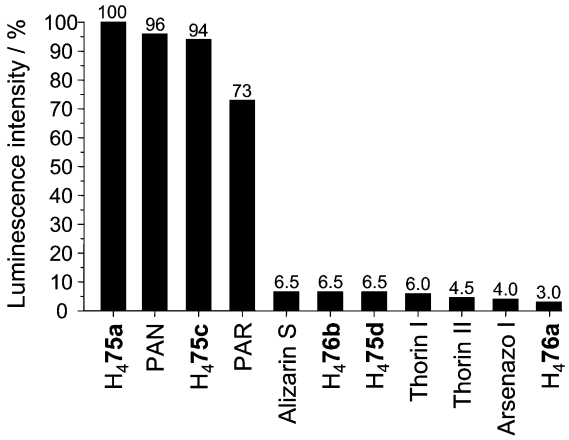

Fig. 68. Relative intensities of luminescence of Yb^{III} ion in complexes with colored organic reagents; values taken from (Poluektov et al., 1984).

with β-diketonates, using an organic base, such as phen, bpy or pyridine as second ligand (Meshkova et al., 1987).

The luminescence characteristics of four complexes formed with arsenazo (I and II) and thorin (I and II) dyes (fig. 67) as well as those of the corresponding ternary complexes with phen have been investigated in aqueous solution. In presence of Yb^{III} ions, 1:1 complexes are formed, except for thorin I, which yields a 1:2 (Yb:L) complex. As a consequence, for thorin I only one phen molecule is present, yielding a 1:2:1 (Yb:L:phen) ternary complex, while 1:1:2 stoichiometries are observed for the three other complexes. Addition of phen results in a significant enhancement (2- to 7-fold) of the luminescence quantum yields, which reach a maximum value of 0.13% for the complex with arsenazo I. As a consequence, the detection limits are lowered by similar factors, from 2 to 8.

Hydroxyanthraquinone derivatives, especially alizarine red S (fig. 67), also form 1:1 complexes with Yb^{III} ions (Korovin et al., 1988). The observed lifetimes are very short, around 0.3 μs, but comparable to those listed in table 15 for the complexes with triphenylmethane dyes. The relative luminescence intensities of Yb^{III} complexes with several different dyes are summarized in fig. 68. The intensities are given relative to the more luminescent complex, with phthalexon S. It is noteworthy that all these complexes have absorption maxima at wavelengths longer than 500 nm, between 505 nm for thorin I and 590 nm for methylthymol blue H_4**75d**, and can thus be excited by the 546 nm-emission line of a mercury lamp.

F.J. Steemers and coworkers followed a similar approach, but designing organic chromophores derived from azatriphenylene (fig. 69) instead of organic dyes (Steemers et al., 1998). In acetonitrile and in presence of Ln^{III} ions, formation of 1:1 complexes occurs with diazatriphenylene **77** and with two of the tetraazatriphenylene ligands, **78a** and **78b**, while ligand **78c** yields 1:2 (Ln:L) complexes. Sensitization of the NIR luminescence of Nd^{III}, Er^{III}, and Yb^{III} ions is achieved through excitation in the ligand absorption bands. Azatriphenylene

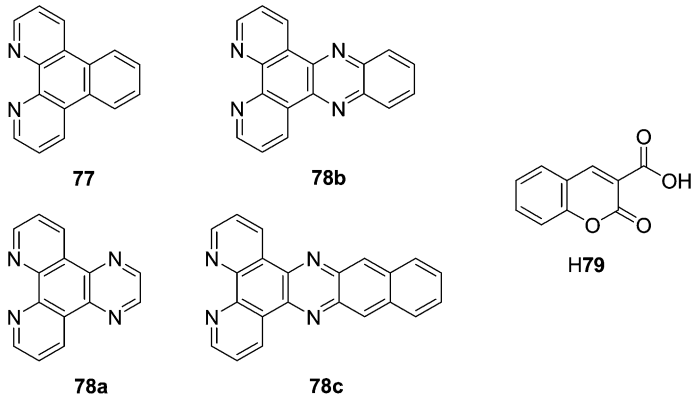

Fig. 69. Azatriphenylene (**77**–**78c**) and coumarin (H**79**) derivatives.

derivatives possess several absorption bands and can be excited in a spectral range extending from 280 to 375 nm, or even up to 450 nm for ligand **78c**. However their triplet excited states lie at relatively high energy, between 18 500 (**78b**) and 23 800 cm^{-1} (**77**) compared to the accepting levels of Nd^{III}, Er^{III}, and Yb^{III}. As a consequence, energy transfer to the Ln^{III} ion is not sufficiently fast to avoid competition with triplet state deactivation due to oxygen quenching. This is evidenced by an emission band appearing at 1275 nm, which is attributed to the phosphorescence of singlet oxygen, the latter resulting from energy transfer between the excited triplet state of the chromophore and molecular oxygen. Ln^{III} luminescence is, therefore, enhanced upon de-oxygenation of the samples. For tetraazatriphenylene **78c**, for which the triplet state lies at the lowest energy, the influence of oxygen is strongly reduced, indicating a faster energy transfer in complexes formed with this ligand. The lifetimes measured for all the complexes in acetonitrile are around 0.5, 2 and 8 μs for Nd^{III}, Er^{III}, and Yb^{III} ions, respectively.

A completely different approach consists in resorting to rather simple molecular frameworks functionalized with carboxylate groups, since these groups strongly coordinate Ln^{III} ions. The first example lies at the border of the two last approaches since the ligand H**79** (fig. 69) is based on a coumarin dye, functionalized in position 3 by a carboxylic acid (Roh et al., 2004b). In view of potential advanced photonic applications, interest has focused on the Er^{III} tris complex, $[Er(\mathbf{79})_3(H_2O)_3]$, in which three water molecules are needed to saturate the first coordination sphere. The photophysical properties of this chelate 10^{-5} M in dmso proved to be moderately interesting, the presence of the fluorescence band of the ligand between 375 and 550 nm indicating that energy transfer is not very efficient.

3.2.5.2. *Carboxylates* With the aim of developing highly luminescent Er^{III} complexes for advanced photonic applications, some of the research concentrates on the synthesis of new ligands, based on simple molecular frameworks such as alkyl chains or benzene rings fitted with carboxylate groups for coordination to the lanthanide ions. For instance, the photophys-

ical properties of Er^{III} complexes formed with ligands H**80** and H**81** (see fig. 70) have been studied in the solid state by direct excitation of the Er^{III} ion (Li et al., 2005). Ligand H**80**, commonly named stearic acid, possesses a long C_{18}-alkyl chain and forms a tris complex [Er(**80**)$_3$], which exhibits a Er($^4I_{13/2}$) lifetime of 2.69 μs. Assuming a radiative lifetime of 14 ms, which corresponds to the typical value observed for Er^{III} in silica, an intrinsic quantum yield of 0.02% can be calculated for this compound. Since C–H oscillators are efficient quenchers of Er^{III} luminescence, the authors tried to address this problem by synthesizing ligand H**81**, in which the C–H groups of the C_8-alkyl chain are completely fluorinated. As for ligand H**80**, one can expect the formation of a tris complex, but the photoluminescence decay of the Er^{III} compound with ligand H**81** turned to be a multi exponential function, indicating the presence of several species, which were assumed to be the tris and tetrakis species [Er(**81**)$_3$] and [Er(**81**)$_4$]$^-$. Depending on the pumping wavelength, intrinsic quantum yields ranging from 0.4 to 4.3% were obtained, again assuming a radiative lifetime of 14 ms. Therefore a considerable enhancement in the intrinsic quantum yield is observed compared to the typical value of 0.02% for usual Er^{III} organic complexes.

In a similar way, the luminescence properties of Er^{III} complexes with benzoic acid (H**82a**) and pentafluorobenzoic acid (H**82b**), as well as their ternary complexes with bipyridine (fig. 70) have been investigated (Roh et al., 2004a). Thermogravimetric analyses (TGA) performed on tris complexes clearly show the presence of three water molecules in the first coordination sphere of the Er^{III} ion, as was previously observed in complexes with coumarin-3-carboxylic acid, H**79**. In the corresponding ternary complexes with bpy, TGA revealed the absence of coordinated water molecule and thus the formation of saturated 8-coordinate Er^{III}

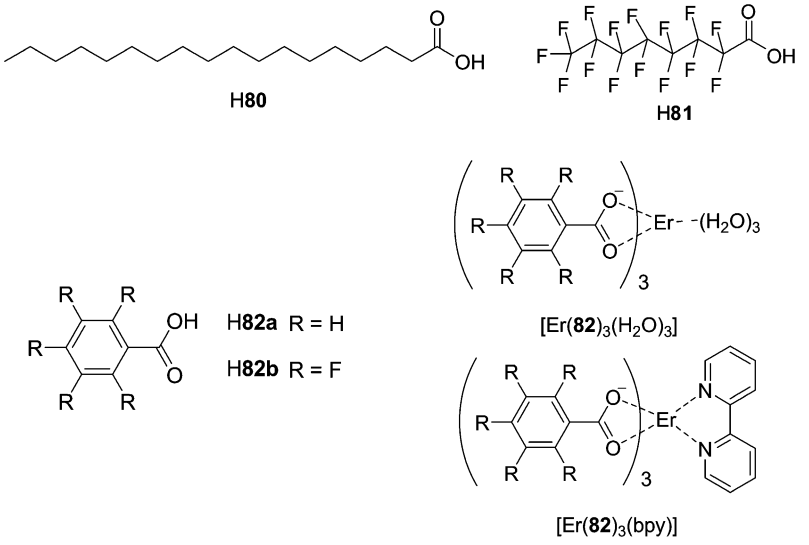

Fig. 70. (Top) Carboxylate-functionalized alkyl and perfluoroalkyl ligands; (bottom) benzoate and pentafluorobenzoate ligands and their tris and ternary complexes.

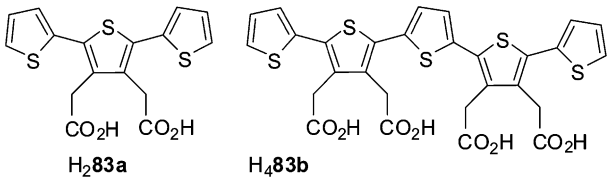

Fig. 71. Oligothiophene ligands.

complexes, [Er(**82**)$_3$(bpy)]. Upon excitation in the ligand levels, the typical NIR luminescence of Er^{III} ion is observed in both tris and ternary complexes. As expected, the luminescence intensity of ternary complexes is much higher than that of the hydrated tris chelates. NIR luminescence is also much more intense (up to 80 times in ternary complexes) when indirect excitation is performed instead of direct Er^{III} excitation at 488 nm. Furthermore the probability of multi-phonon relaxation is essentially related to the energy difference between the upper and lowers levels of the Ln^{III} ion ($\Delta E \approx 7000$ cm^{-1} for Er^{III}) and to the harmonic vibration energy of the metal ion surroundings. In complexes with pentafluorobenzoate, this probability is very low because the harmonic vibration energy of C–F bonds is much smaller than the energy gap, whereas one overtone of C–H vibration almost matches the energy difference, leading to a much higher probability in multi-phonon relaxation. As a consequence, the luminescence intensity is much stronger in fluorine-containing complexes. For instance [Er(**82b**)(bpy)] is four times more luminescent than its analog formed with ligand **82a**. The same photophysical study has been performed on the dimeric Er^{III} complex, [Er_2(**82a**)$_6$(bpy)$_2$], synthesized through a ligand-exchange reaction using erbium chloride in the presence of bipyridine and potassium benzoate salt. According to the crystal structure, four bridging and two chelating benzoate as well as two bipyridine ligands are involved in the coordination of the two 8-coordinate Er^{III} ions (Roh et al., 2005).

One of the problems pertaining to the development of Er^{III} electroluminescent devices is the relatively low solubility of lanthanide complexes. To overcome this drawback, organic polymers (PMMA, PVK) are used in the blend of the active luminescent materials, or organic ligands are attached onto polymeric chains. Examples of the latter are oligothiophene ligands with carboxylate functionalities (fig. 71) which have the following advantages: (i) good solubility in organic solvents, facilitating the production of devices, for instance by spin-coating, (ii) good transport properties, and (iii) efficient isc process combined with the possibility of excitation in the visible range for H_4**83b**.

Er^{III} complexes with 1:2 stoichiometries are isolated by reaction of the sodium salts of the two oligothiophene ligands with erbium chloride under anhydrous conditions. No analytical data are reported to prove this stoichiometry, but both compounds Na[Er(**83a**)$_2$] and Na_5[Er(**83b**)$_2$] display the 1.54 μm emission in anhydrous pyridine upon excitation at 353 nm. The emission intensity of [Er(**83a**)$_2$]$^-$ is comparable to the fluorescence intensity of [Er(8-Q)$_3$] recorded under the same experimental conditions, while emission intensity of the pentathiophene complex is about half that. This is explained by the more efficient triplet state production in shorter oligothiophenes than in longer ones (Destri et al., 2003).

2,6-Pyridine-dicarboxylic acid (H_2dpa) is a well known chelating agent for both d- and f-transition metal ions. It reacts in water with lanthanide ions to yield 9-coordinate tris complexes with D_3 symmetry. The tris complexes have appreciable stability, with $\log \beta_3$ in the range 18–22, and they are also highly luminescent upon excitation into the ligand level, so that they are used as luminescent stains in analytical processes, for instance $[Tb(dpa)_3]^{2-}$ for the detection of bacterial endospores, such as anthrax (Pellegrino et al., 1998). Crystals of $Na_3[Yb(dpa)_3]\cdot 13H_2O$ have an Yb($^2F_{5/2}$) lifetime of 2.5 μs at 15 K and the ligand-field splitting of the $^2F_{5/2}$ (3 sub-levels, total splitting 268 cm^{-1}) and $^2F_{7/2}$ (4 sub-levels, 348 cm^{-1}) is in line with the trigonal symmetry. In aqueous solution at room temperature, the lifetime decreases to 2 μs; no up-conversion process could be evidenced either for the crystals or for the solution (Reinhard and Güdel, 2002).

Substitution of the 4-position of the pyridine ring of dpa with OH or Cl has been achieved and the resulting Nd^{III} complexes formed with these derivatives showed better luminescence properties than the corresponding dpa complexes (Curry et al., 2005).

3.2.5.3. *Tropolonates* In view of their moderately low-lying excited triplet states (≈16 800 cm^{-1}), tropolone-based ligands are well-suited for efficient energy transfer to the low-energy accepting levels of several NIR emitting lanthanide ions such as Nd^{III}, Ho^{III}, Er^{III}, Tm^{III}, and Yb^{III}. Moreover tropolonates provide strong coordination to Ln^{III} ions since two oxygen donors are available, forming stable 5-membered chelate rings. Therefore 2-hydroxycyclohepta-2,4,6-trien-1-one, known as tropolone (H**84a**, fig. 72), has been chosen for the development of NIR emitting Ln^{III} complexes (Zhang et al., 2005). X-ray structures of $\{K[Ln(\mathbf{84a})_4]\cdot dmf\}_\infty$ (Ln = Tb, Dy, Ho, Er, Tm, Yb, Lu) clearly show the Ln^{III} ion being surrounded by four bidentate tropolonates, while the potassium ion plays a significant role in the packing pattern of the complexes in the crystal.

UV–vis titrations in dmso indicate that 1:1, 1:2, 1:3, and 1:4 (Ln:L) complexes are successively formed in solution. Under the conditions leading to tetrakis $[Ln(\mathbf{84a})_4]^-$ complexes and when excitation is performed in the ligand absorption band at 340 nm, typical NIR luminescence is monitored for all the complexes, indicating efficient sensitization of the Ln^{III} luminescence via energy transfer from the tropolonate moieties. Not only are the well-known emission bands from Nd^{III}, Er^{III}, and Yb^{III} ions observed, but also the less-common Tm^{III} bands at 796 ($^3F_4 \rightarrow {}^3H_6$) and 1465 nm ($^3F_4 \rightarrow {}^3H_4$), and the ones from Ho^{III} around 975, 1160, and 1479 nm, which are assigned to $^5F_5 \rightarrow {}^5I_7$, $^5I_6 \rightarrow {}^5I_8$, and $^5F_5 \rightarrow {}^5I_6$ transitions, respectively. However the presence of ligand-centered emission in all these complexes clearly indicates that the ligand-to-lanthanide energy transfer process is not complete. To quantify the intramolecular energy transfer, the overall luminescence quantum yields have been determined in different solvents and are summarized in table 16.

The $^4G_{5/2} \rightarrow {}^6H_{9/2}$ transition of Sm^{III} (2-hydroxyisophthalamide) macrobicyclic complex with $Q^L_{Ln} = 0.073\%$ in 0.01 M tris buffer (Petoud et al., 2003) has been used as a reference for the $[Yb(\mathbf{84a})_4]^-$ complex, this latter being itself taken as standard for the quantum yield measurements of Nd^{III} and Er^{III} complexes. For Ho^{III} and Tm^{III}, the $[Er(\mathbf{84a})_4]^-$ complex was used as standard because of their comparable luminescence intensities. The quantum yields obtained are clearly dependent on the nature of the solvent, suggesting that the Ln^{III}

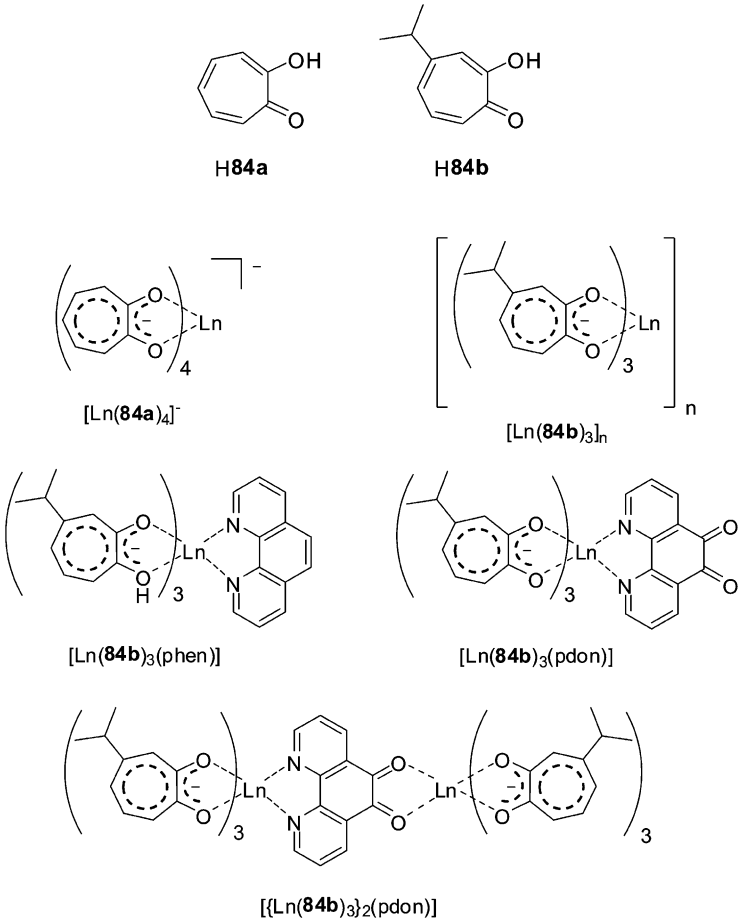

Fig. 72. (Top) Tropolone-based ligands and (bottom) their Ln^{III} complexes with and without secondary ligand.

Table 16
Overall luminescence quantum yields for $[Ln(\mathbf{84a})_4]^-$ in organic and aqueous media ($\lambda_{ex} = 340$ nm)

Ln	Solvent	Q^L_{Ln} (%)	Q^L_{Ln} (%)[a]
Nd	dmso	0.21	0.36
Ho	dmso	2.3×10^{-3}	2.4×10^{-3}
Er	dmso	1.7×10^{-2}	3.2×10^{-2}
Tm	dmso	3.8×10^{-3}	5.7×10^{-3}
Yb	dmso	1.9	2.2
	MeOH	0.13	1.6
	H_2O	2.4×10^{-2}	0.74

[a]Overall luminescence quantum yields measured in the corresponding deuterated solvent.

ion is not completely shielded from solvent molecules by the four tropolonate ligands. Using eq. (9a) with Yb^{III} lifetimes of 0.75 and 10.03 μs in H_2O and D_2O, respectively, one finds $q_{H_2O} = 1.1$; the same value is obtained for q_{CH_3OH}. Thus the structure in solution is different from that in the solid state in which no solvent molecules are coordinated to the lanthanide ion.

According to elemental, thermogravimetric and IR analyses, the tris-tropolonato Ln^{III} complexes of the 4-isopropyl derivative H**84b** (fig. 72), obtained by reaction of a methanolic solution of H**84b** with NaOH and $LnCl_3{\cdot}6H_2O$, have no coordinated solvent molecules (Bertolo et al., 2006). However, the authors suppose that, in order to complete the first coordination sphere of the Ln^{III} ion, the complexes are in the form $[Ln(\mathbf{84b})_3]_n$ ($n = 2$ or 3). These polymeric forms easily react with a secondary ligand to form ternary complexes with phen or 1,10-phenanthroline-5,6-dione (pdon) as secondary ligand. The latter is a suitable ditopic ligand for the formation of bimetallic complexes since it contains two well separated coordination sites. The various adducts, [Ln(**84b**)phen], [Ln(**84b**)pdon], and {[Ln(**84b**)]$_2$pdon} are depicted on fig. 72. Upon excitation in the absorption bands of the ligand at 355 nm, the characteristic Er^{III} emission is observed for all the complexes. The quantum yield of the IR emission is on the order of a few hundredths of percent, which is comparable with the data obtained for the tris 8-hydroxyquinolinate Er^{III} complex. On the other hand, the lifetimes measured in dmso are in the range 2.11–2.15 μs and are somewhat longer when compared to [Er(8-Q)$_3$] (1.80 μs). The tris-tropolonato Yb^{III} complex, $[Yb(\mathbf{84b})_3]_n$ exhibits the typical NIR emission near 1 μm when excited at 355 nm. Even though no quantitative data are presented in this work, the authors, in view of the luminescence intensity, estimated a quantum yield of about two orders of magnitude larger than the one measured for the corresponding Er^{III} complex. The photoluminescence decay is again monoexponential and lifetimes as long as 70–80 μs were obtained, suggesting a good protection of the Ln^{III} ion from nonradiative deactivation processes in this complex.

3.2.5.4. *Imidophosphinates* Sterically bulky bidentate imidodiphosphinates present an ideal framework for the minimization of nonradiative deactivation processes because of the formation of a lipophilic shell around the Ln^{III} ion avoiding the coordination of solvent molecules and the lack of high-energy oscillators in close proximity to the lanthanide ion. In view of these characteristics, Bassett et al. (2005) have synthesized a tetraphenyl imidodiphosphinate ligand, H**85a** (fig. 73), and studied the photophysical properties of its neutral tris Ln^{III} complexes (Ln = Nd, Er and Yb) in solution in CH_3CN or in the solid state. X-Ray analysis of single crystals of [Er(**85a**)$_3$] shows two symmetrically independent arrangements, in which the Er^{III} ion is hexa-coordinated by the oxygen atoms of the three ligands. The difference between these two complexes lies in the geometry around the Er^{III} ion, which is a distorted octahedron in one complex and a distorted trigonal prism in the other one. However in both cases, the three ligands are symmetrically equivalent around the Ln^{III} ion, as further demonstrated for all the complexes by ^{31}P NMR. It is also important to note that the presence of intramolecular CH–π interactions between the 12 phenyl rings of the same ligand may stabilize the hydrophobic shell around the Ln^{III} ion.

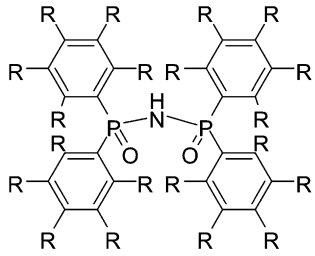

Fig. 73. Imidodiphosphinate ligand and its perfluorinated analog.

Upon excitation in the phenyl absorption band of the ligand at 266 nm, all the complexes exhibit near-infrared emission in both solution and solid state. The lifetimes measured in dry acetonitrile solutions are quite long, amounting to 2.7, 6.5, and 52.8 μs for Nd^{III}, Er^{III}, and Yb^{III}, respectively. These values are comparable with the ones obtained for complexes with fully fluorinated β-diketonate ligands, in line with an efficient shielding of the Ln^{III} ion by the three imidodiphosphinate ligands. Adding an excess of water ($[H_2O] = 10$ M) to the acetonitrile solutions results in a large decrease in the emission lifetimes reaching 81% for Nd^{III}, whereas the lifetimes diminish only by 17 and 24% for [Er(**85a**)$_3$] and [Yb(**85a**)$_3$], respectively. The corresponding data measured on powdered samples are 1.2, 2.3, and 17.8 μs for Nd^{III}, Er^{III}, and Yb^{III}, respectively. According to the authors, the shortening of the lifetimes with respect to solutions may be attributed to lattice vibrations or cross-relaxation mechanisms between the closely positioned lanthanide ions in the solid state. To further improve emission intensity, fluorination of the imidodiphosphinate ligand has been performed, yielding ligand H**85b** (Mancino et al., 2005). The authors investigated only the Er^{III} tris complexes formed with fluorinated and non-fluorinated ligands, in $CDCl_3$ and in the solid state both as powder and as 500 nm thin film. The intrinsic quantum yields of Er^{III} in [Er(**85b**)$_3$] complexes calculated using a radiative lifetime of 8 ms amount to 0.4% in solution and to 1.8 and 1.71% for powder and thin-film samples, respectively. These values are significantly larger (from 7, up to 43 times) than the ones obtained for the corresponding complex with the non-fluorinated ligand. However the luminescence decays for all the complexes is best described by a biexponential process, which is in contradiction with the monoexponential decays observed for [Er(**85a**)$_3$] by Bassett et al. (2005). Moreover the lifetime values for the Er^{III} powdered samples are not in agreement from one study to the other.

3.2.5.5. *Pyrazoylborates* Tetradentate (**86**) and hexadentate (**87**) pyrazoylborates (see fig. 74) form a range of 1:1 and 1:2 complexes with Ln^{III} ions, as well as ternary 1:1:1 adducts with dibenzoylmethanate, which have coordination number between 8 and 12. In the case of visible-emitting lanthanide ions, large quantum yields have been recorded, up to 50% for Tb^{III} for instance (Armaroli et al., 1997). With Nd^{III} and Yb^{III}, four types of complexes

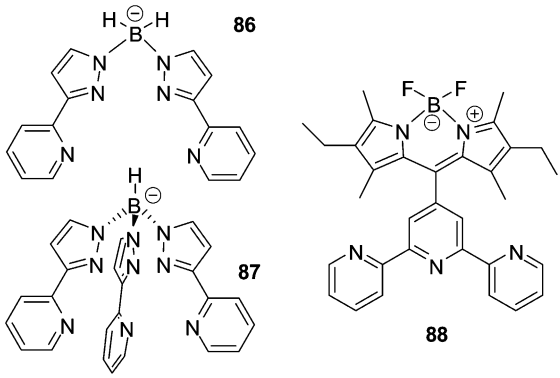

Fig. 74. Pyrazoylborate (left) and boradiazaindacene-substituted terpyridine (right).

have been characterized, 8-coordinate [Ln(**87**)(dbm)$_2$], 10-coordinate [Ln(**87**)(NO$_3$)$_2$] and [Ln(**86**)$_2$(NO$_3$)], and 12-coordinate [Ln(**87**)$_2$]BPh$_4$ in which the metal center is bound by two interpenetrating hexadentate podands (Beeby et al., 2002a). Lifetimes have been determined in methanol and are relatively long, 0.15–1.6 μs for Nd^{III} and 0.45–2.9 μs for Yb^{III}, in view of the few C–H vibrations close to the metal ion. Using relationships (9b) and (10b), solvation numbers have been calculating and, with the exception of [Yb(**87**)$_2$(NO$_3$)], they are in the range 0–1.

It was demonstrated later that [Nd(**87**)(dbm)$_2$] rearranges to [Nd(**87**)$_2$][Nd(dbm)$_4$] upon re-crystallization, with the latter entity having almost perfect O$_8$ coordination. Besides, Pr^{III} emission assigned to $^1D_2 \rightarrow {}^3F_4$ is observed at 1.02 μm for [Pr(**87**)(dbm)$_2$] in methanol (lifetime: 13 ns), as well as the 1.53 μm fluorescence (lifetime 0.85 μs) of the isostructural Er^{III} complex (Davies et al., 2004). In addition to visible emission from $^3P_0$, praseodymium luminescence at 1.44 μm was also detected in the case of [Pr(**87**)(NO$_3$)$_2$] and [Pr(**86**)$_2$(NO$_3$)] and was assigned to the $^1D_2 \rightarrow {}^1G_4$ transition which fits exactly with the expected energies of these levels; further evidence for this assignment comes from the lifetimes determined while monitoring the two NIR bands and which were found to be the same, within experimental errors; they amount to 54 and 73 ns for the complexes with **86** and **87**, respectively (Davies et al., 2005a).

The terpyridine-substituted difluoroborondipyrromethene dye **88** is a singlet emitter at 540 nm (18 500 cm^{-1}) and its triplet state emission extends from 550–750 nm (18 200–13 300 cm^{-1}), which makes it a potential sensitizer of lanthanide NIR luminescence. In [Yb(NO$_3$)$_3$(**88**)] (see fig. 75), the lanthanide ion is bound to the terdentate terpyridine and to three bidentate nitrate counterions, in a distorted tricapped antiprismatic geometry. The Ln^{III} complexes (Ln = La, Nd, Er, Yb) have large absorption coefficients (65 000 M^{-1} cm^{-1} at 529 nm) and upon complexation with lanthanide ions, the quantum yield of the $^1\pi\pi^*$ emission decreases from 79% for the free ligand in dichloromethane to 54% for the La^{III} complex, due to the heavy atom effect favoring the isc process. With Nd^{III}, Er^{III}, and Yb^{III} the quantum yield further decreases to 15–20% while NIR emission appears, indicating energy transfer

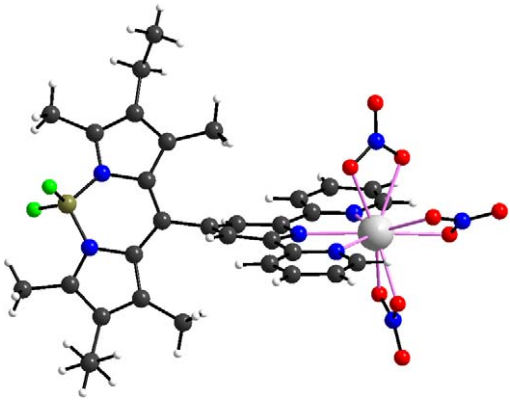

Fig. 75. Structure of [Yb$(NO_3)_3$(**88**)], redrawn from (Ziessel et al., 2006).

from the ligand to the metal ions. In the same solvent, at a concentration of 10^{-4}–10^{-7} M, the quantum yields of the metal-centered luminescence are 0.016 and 0.31% for Nd^{III}, and Yb^{III}, respectively. Calculations of the sensitization efficiency of the indacene dye moiety based on an estimate of the intrinsic quantum yields via lifetimes (τ_{rad} taken as 0.8 and 2.0 ms, respectively) lead to $\eta_{sens} = 47$ and 63%, respectively. These comparatively low values, despite favorable energy gaps, may be traced back to the relatively long distance between the metal ion and the indacene unit which can be estimated to be about 9 Å, and to the unfavorable orientation of the chromophore which is tilted by about 60° with respect to the terpyridine coordination unit (Ziessel et al., 2006).

3.2.6. *New synthetic strategies podands, dendrimers, self-assembly processes*
In addition to the systems described in sub-sections 3.2.1–3.2.5, some innovative strategies for sensitizing the luminescence of NIR-emitting lanthanide ions are emerging. We describe three of these new approaches in this section, which call on the design of podands or dendrimeric ligands, as well as on the use of self-assembly processes.

3.2.6.1. *Podands* A good way to reach efficient energy transfer from the ligand to the NIR-emitting metal ion while simultaneously achieving thermodynamic stability and kinetic inertness of the resulting molecular edifice is to resort to multidentate podands fitted with one or several sensitizer arms (Beeby et al. 2002a, 2002b). It is essential that the targeted chelating agents offer a good protection against solvent interactions and are devoid of coordinating groups possessing high energy vibrations. Until now, there are only few examples, most of them stemming out of our laboratory, of such a molecular construction in which a sensitizing unit is attached onto small backbones or on atoms.

A first example is heptadentate 2,2′,2″-tris(salicylideneimino)-triethylamine, H_3**89** (fig. 76), which forms an isomorphous series of complexes [Ln(**89**)] (Bernhardt et al., 2000). A crystal field analysis based on polarized absorption and emission spectra of the trigonal

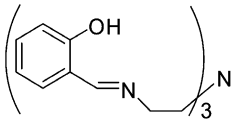

H_3**89**

Fig. 76. Salicylidene-imino podand.

crystals [Er(**89**)] was performed. The C_3 site symmetry of the metal ion requires eight ligand-field parameters for a full description within the one-operator model. All the 4f–4f transitions could be reliably assigned and the compound shows unusually large splittings of the multiplets. In fact, the heptadentate ligand imparts one of the largest ligand field reported for Er^{III} complexes with organic ligands (Flanagan et al., 2001). The ligand-field splitting was also interpreted in terms of the angular overlap model and a similar analysis was reported subsequently for Nd^{III} (Flanagan et al., 2002).

Another design for a tetrapodal ligand (H_8**90**, fig. 77) relies on a short 1,2-diaminoethane backbone fitted with four 8-hydroxyquinolinate moieties, the corresponding anion being known to be an efficient sensitizer of lanthanide NIR luminescence, as seen in section 3.2.2 (Kido and Okamoto, 2002; Rizzo et al., 2004). The spacer bears an amide coupling function and its length has been chosen to achieve a tight coordination around the Ln^{III} ion saturating its first coordination sphere; the same reason prevailed to the choice of a tetrapodal instead of a more common tripodal ligand. Finally, sulfonate groups have been grafted onto the 8-hydroxyquinoline building block to improve solubility in water (Imbert et al., 2005). The ligand possesses 14 protonation sites, four pyridinium nitrogen atoms, two tertiary amines, four hydroxyl groups (pK_a's in the range 1.8–12.2), and four sulfonate groups. It interacts fairly strongly with trivalent lanthanide ions in water yielding 1:1 podates with pLn values in the range 15–16.[7] Several species are in equilibrium and the speciation depends upon the pH. Fortunately, the 1:1 $[Ln(H_2$**90a**$)]^{3-}$ species is largely dominant in the pH range 6–8, and particularly at physiological pH 7.4, as shown from quantitative spectrophotometric and potentiometric data collected on the Eu^{III}/H_8**90a** system (fig. 77, bottom).

The Nd^{III} and Yb^{III} podates are quite luminescent, while Er^{III} gives rise to somewhat fainter emission. Their photophysical properties are gathered in table 17. The hydration numbers calculated from eqs. (10a) and (9a) are very small, 0.37 and 0.15 for Nd^{III} and Yb^{III}, respectively. They could arise either from partial dissociation of the (probably) 8-coordinate podates or from second-sphere interaction with diffusing water molecules and/or the N–H oscillators. To settle this point, the tetrapodal podand H_8**90b** in which the secondary amine groups are methylated has been synthesized. Its acid–base and coordination properties are not much changed with respect to H_8**90a**, but now, the calculated hydration numbers for both Nd^{III} and Yb^{III} are close to zero, being even slightly negative. In another experiment, the podates have been inserted into Triton X-100 micelles, which in principle protect the complex entities from interacting with water molecules and no changes at all were detected in lifetime data or in quantum yields. This clearly proves the deleterious action of the four secondary amine groups

[7] The pLn values are defined as $-\log_{10}[Ln]_{free}$ at pH 7.4 and for $[Ln]_{tot} = 10^{-6}$ M and $[L]_{tot} = 10^{-5}$ M (Raymond et al., 1984).

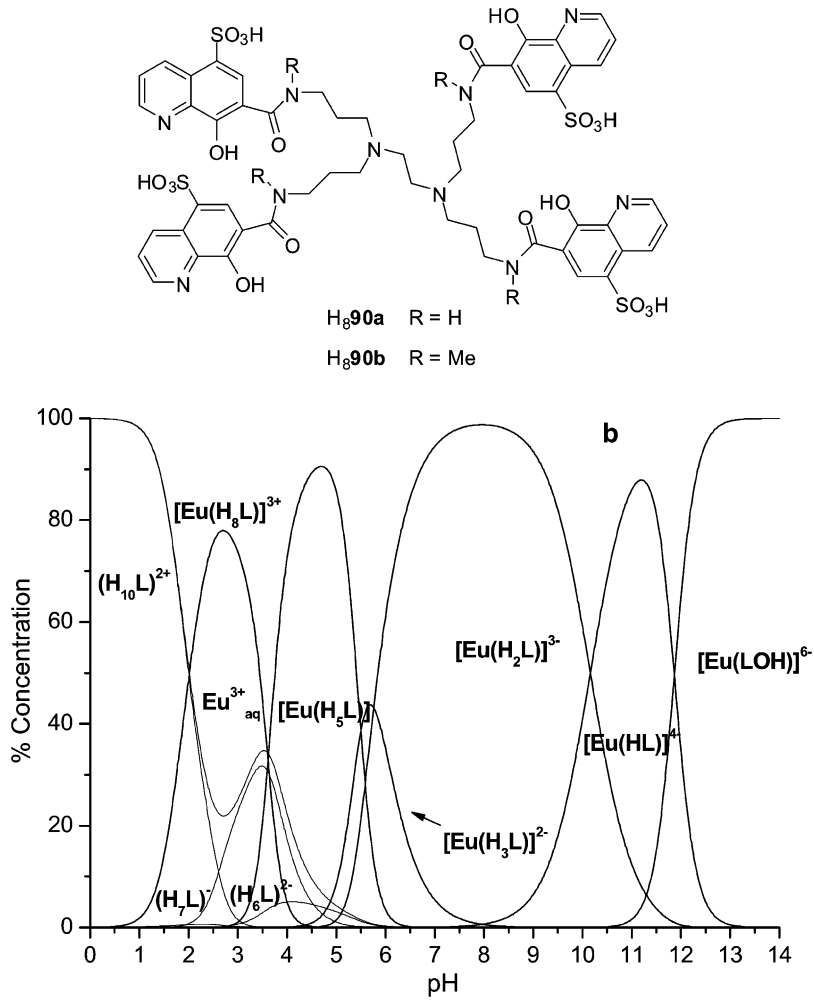

Fig. 77. (Top) Quinoline-fitted podands. (Bottom) Speciation for the Eu^{III}/H_8**90a** (= H_8L) system. Reproduced with permission from (Comby et al., 2006b).

on the emissive properties, as corroborated by the quantum yield values increasing by a factor of two when H_8**90a** is replaced with H_8**90b** in the Yb^{III} podates. Another conclusion is that the coordination environment provided by the podand is tight enough to effectively prevent solvent molecules to interact with the metal ion, as planned in the ligand design. The quantum yield obtained for Yb^{III} is so far the largest reported for a molecular compound in aqueous solution. It is 4- and 15-fold larger than the quantum yields reported for complexes with fluorexon (Werts et al., 2000b) and tropolonate (Zhang et al., 2005), for instance. The

Table 17
Absolute quantum yields measured upon ligand excitation (relative error: ±10%), lifetimes (standard deviation in parentheses), and associated hydration numbers of the $[Ln(H_2\mathbf{90})]^{3-}$ podates, 6×10^{-5} M in aqueous solutions at 295 K and pH 7.4 (Comby et al., 2006b)

Ln	λ_{an} (nm)	τ (μs) H_2O	Q^L_{Ln} (%) H_2O	τ (μs) D_2O	Q^L_{Ln} (%) D_2O	q[a]
H_8**90a**						
Nd	1063	0.13(1)	0.02	0.58(2)	0.10	0.37
Er	1540	0.23(1)	3.7×10^{-5}	1.39(2)	5.4×10^{-3}	–
Yb	976	2.21(1)	0.18	10.0(1)	0.81	0.15
H_8**90b**						
Nd	1063	0.25(3)	0.04	0.61(1)	0.11	−0.09
Er	1540	0.67(1)	4.0×10^{-5}	2.31(2)	7.1×10^{-3}	–
Yb	976	5.79(1)	0.37	14.6(1)	0.90	−0.1

[a]Calculated with eqs. (9a) (Yb^{III}, corrective factor $B = 0.2\ \mu s^{-1}$) and (10a) (Nd^{III}).

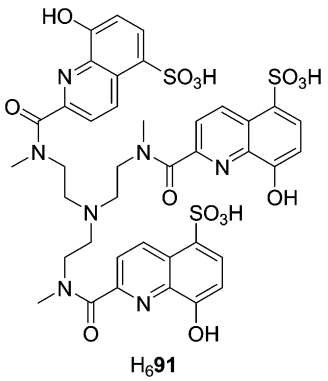

H6**91**

Fig. 78. Quinoline-containing tripodal ligand.

overall luminescence efficiency of the $[Yb(H_2\mathbf{90})]^{3-}$ podate, $\varepsilon \cdot Q^L_{Ln}$, reaches 70 $M^{-1}\,cm^{-1}$ for an excitation at 344 nm and excitation up to 580 nm is possible. On the other hand, methylation has far less influence on the quantum yields of the Nd^{III} and Er^{III} podates, which is understandable since other nonradiative deactivation processes are much more efficient than in the Yb^{III} complex (Comby et al., 2006b). The $[Yb(H_2\mathbf{90})]^{3-}$ podate has been successfully introduced into a glass matrix using a two-step sol–gel method and thin films of this material display even better photophysical properties than the aqueous solutions, with an average quantum yield of 0.45%, which is encouraging with respect to potential applications (Comby et al., 2006a).

Following a slightly different strategy, the same authors have designed another tripodal ligand, $H_6\mathbf{91}$ (fig. 78), consisting of a triamine anchor bearing three 8-hydroxyquinoline units

Table 18
Absolute quantum yields measured upon ligand excitation, lifetimes (standard deviation in parentheses), and associated hydration numbers of the Ln^{III} podates with H_6**91**, 6.5×10^{-5} M in aqueous solutions at 295 K and pH 7.4. From (Comby et al., 2007)

Ln	λ_{an} (nm)	τ (μs) H_2O	Q^L_{Ln} (%) H_2O	τ (μs) D_2O	Q^L_{Ln} (%) D_2O	q[a]
H_6**91**						
Nd	1063	0.15(1)	0.03	0.91(2)	0.08	0.31
Er	1540	0.24(1)	n.a.	2.55(1)	3.5×10^{-3}	–
Yb	976	2.47(3)	0.13	26.0(2)	1.5	0.16

[a]Calculated with eqs. (9a) (Yb^{III}, corrective factor $B = 0.2\ \mu s^{-1}$) and (10a) (Nd^{III}).

which are tailored to behave as tridentate receptors. As for ligands H_8**90a** and H_8**90b**, sulfonation of the 8-hydroxyquinoline subunits leads to relatively highly water-soluble podates. In addition to the three sulfonate groups, which are always deprotonated in the experimental conditions used, the ligand possesses seven protonation sites, three pyridinium nitrogen atoms, one tertiary amine, and three hydroxyl groups (pK_a's range from 3.7 to 10.2). In presence of Ln^{III} ions, stable and water-soluble 1:1 complexes are formed, as demonstrated by NMR titration of a tris-DCl solution of H_6**91** with Ln^{III} (Pr and Lu) solutions prepared in D_2O.

The three Nd^{III}, Er^{III}, and Yb^{III} chelates display sizeable metal-centered NIR luminescence in HBS-buffered (pH 7.4) aqueous solutions. Their photophysical characteristics are summarized in table 18. The hydration numbers calculated from eqs. (10a) and (9a) are very small, 0.31 and 0.16 for Nd^{III} and Yb^{III}, respectively, and compare well with the results obtained for the tetrapodal ligand H_8**90a**. The overall luminescence quantum yields in aqueous solution are comparable to those obtained for H_8**90a**, but smaller than those determined for chelates with H_8**90b** (compare tables 17 and 18). Upon deuteration of the solvent, from 3- to 10-fold increases are observed in the luminescence quantum yields. Moreover cytotoxicity studies on several cell lines have shown the Yb^{III} chelate to be non-toxic, opening the way for applications in cell imaging (Comby et al., 2007).

3.2.6.2. *Dendrimers* Dendrimer chemistry can be thought of as being a branch of polymer chemistry in which highly branched monomers are uniformly assembled to yield a tree-like or generational structure. Preparing such polymers demands a high level of synthetic control which is achieved through stepwise reactions, building the dendrimer one monomer layer, or "generation", at a time. Each dendrimer consists of a multifunctional core molecule with a dendritic wedge attached to each functional site. The core molecule is referred to as "generation 0". Each successive repeat unit along all branches forms the next generation, generation 1 (G1), generation 2 (G2), and so on until the terminating generation. Interest in lanthanide dendrimers stems from nuclear magnetic imaging for which contrasts agents with large molecular weight are thought to be more efficient (Fulton et al., 2006; Wiener et al., 1994). Few reports deal with visible (Cross et al., 2004; Kawa and Frechet, 1998) or NIR luminescence (Kim et al., 2005) and, generally speaking, lanthanide dendrimer chemistry is still in its infancy.

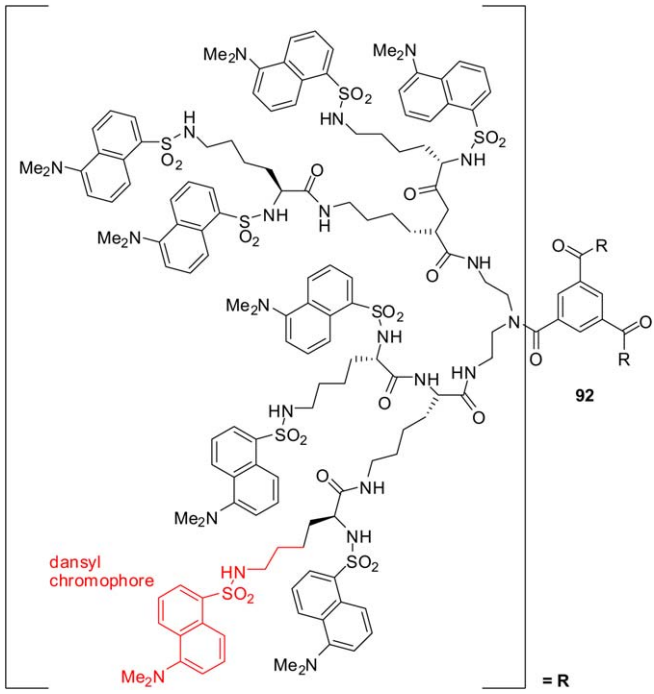

Fig. 79. Benzene-cored dendrimer fitted with dansyl chromophores.

The polylysin dendrimer depicted on fig. 79 consists of a benzene core branched in 1, 3, and 5 positions; each branch starts with a (dialkyl)carboxamide-type unit and carries six aliphatic amide groups and eight 5-dimethylamino-1-naphthalenesulfonamido (dansyl) chromophores. Therefore the interior of the dendrimer contains 18 amide groups which are known to strongly bind to lanthanide ions, as well as 24 light-harvesting moieties on the periphery, leading to molar absorption coefficients of 3×10^5 (253 nm) and 9.2×10^4 (338 nm) $M^{-1}\,cm^{-1}$. The photophysical properties of the dansyl groups in the dendrimer are close to those displayed by the monomeric dansyl group, so that little interaction between the chromophores is anticipated. Titration of a 4.2 μM solution of the dendrimer in acetonitrile/dichloromethane by Nd^{III} nitrate causes a quenching of the broad-band ligand fluorescence extending from 420 through 650 nm ($Q = 28\%$ in absence of metal ion) with decrease of the singlet state lifetime from 15 to 6 ns and a concomitant increase in the metal-centered NIR luminescence. The overall quantum yield of the metal-centered luminescence, obtained by a comparison method with $[Nd(hfa)]_3$ in D_2O, amounts to 0.27%. Combined with the large absorption coefficients of the dendrimer, this makes this dendrimeric complex a relatively efficient NIR emitter (Vögtle et al., 2001). Sensitized emission of Eu^{III}, Tb^{III}, Er^{III}, and Yb^{III} also occurs with this dendrimer, the latter two ions emitting only moderately (Vicinelli et al., 2002).

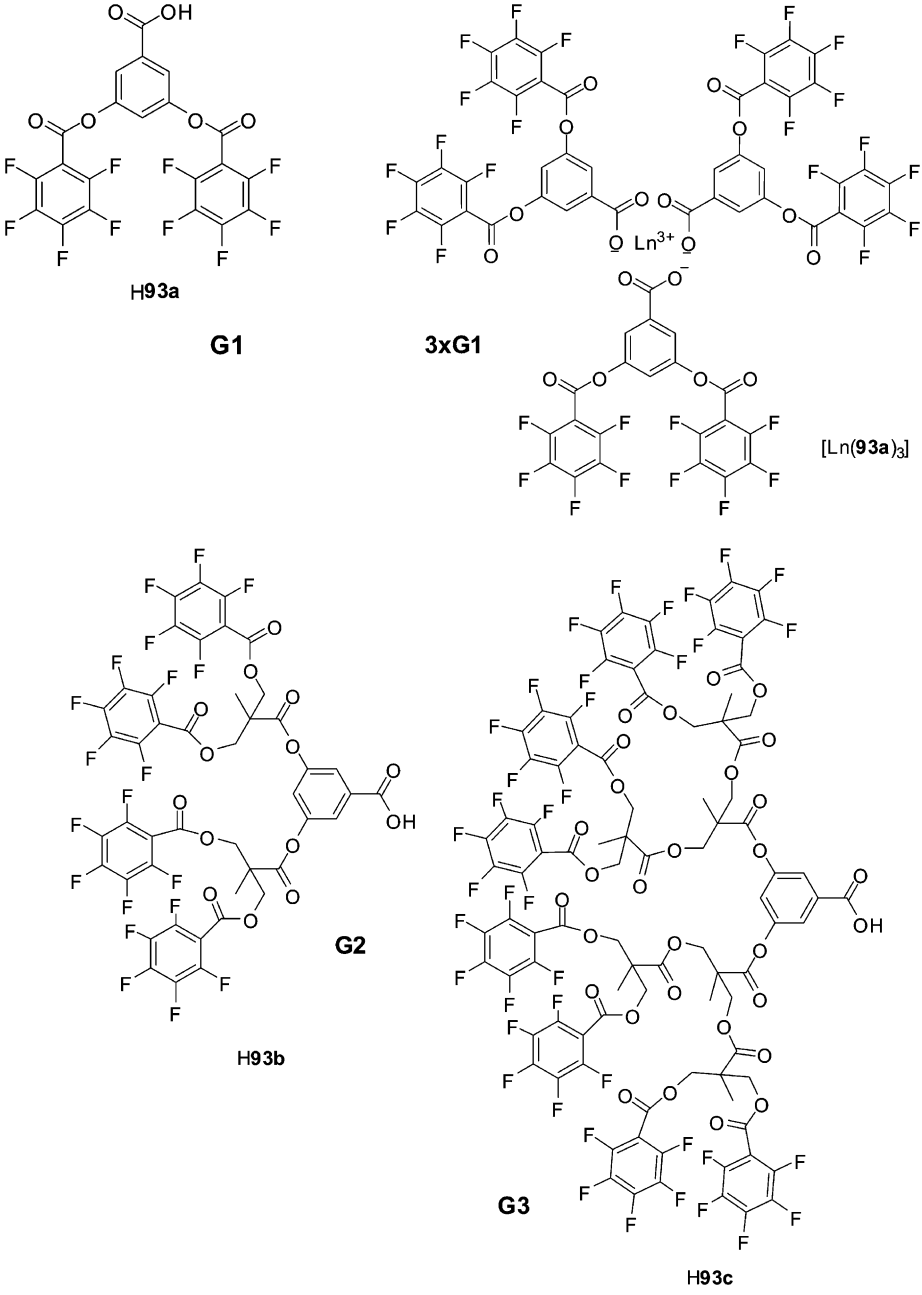

Fig. 80. Fluorinated dendrons and corresponding lanthanide dendrimer of first generation.

In order to minimize nonradiative losses, a fluorinated dendrimeric system has been designed in which the lanthanide ions act as the core. The dendrons are derived from benzenecarboxylic acid substituted in positions 3 and 5 by a pentafluorinated phenyl group, the linker being an ester group. First (H**93a**), second (H**93b**) and third (H**93c**) generations of these dendrons (see fig. 80) have been prepared. When reacted with lanthanide acetate in a dry and oxygen-free atmosphere, three dendrons assemble around the core Ln^{III} ion (Ln = Pr, Nd, Er). Sensitized luminescence was only observed for [Nd(**93b**)$_3$] and [Er(**93c**)$_3$], 2.7 and 0.73 mM, respectively, in methylene chloride. The former compound can be excited at 805 nm ($^4F_{5/2} \leftarrow {}^4I_{9/2}$ transition). On the other hand, no luminescence could be detected for the Pr^{III} dendrimers (Pitois et al., 2003) while the same systems sensitize Eu^{III} and Tb^{III} emission (Pitois et al., 2005).

Cyclam, or 1,4,8,11-tetraazacyclotetradecane is a popular macrocyclic ligand for d-transition metal coordination chemistry. It also coordinates to lanthanide ions, although much less strongly than the better size-adapted cyclen. As for the latter, however, derivatization of the amine functions by amide, carboxylate, or phosphinate groups considerably improves the coordination ability of the macrocycle.

Disregarding this aspect, and since cyclam is an interesting core for constructing dendrimers because it can be easily functionalized and because despite its absence of spectroscopic properties, it can interact in such a way with dendrons as to modify their photophysical properties, the interaction of lanthanide ions with cyclam-based dendrimers has been investigated. The dendrimers are constructed from the cyclam core fitted with four dimethoxybenzene and eight naphthyl units (generation 1, fig. 81); second generation introduces a total of 12 dimethoxybenzene and 16 naphthyl moieties. Coordination to Ln^{III} ions occurs in acetonitrile/methylene chloride (Ln = Nd, Eu, Gd, Tb, and Dy), but no sensitized Ln-luminescence was observed (Saudan et al., 2004). Another example of a macrocycle-based dendrimer is discussed below in section 3.3.2.

The large light-harvesting ability of dendrimeric ligands is an attractive asset and in an attempt to obtain highly emitting NIR systems, aryl ether dendrons have been combined with a carboxylic acid derivatized diphenyl anthracene coordinating unit. The resulting complexes are protected from nonradiative deactivation by further binding of an ancillary ligand, namely tpy (fig. 81, bottom). These elaborate ligands **G*n*An** are synthesized in five steps from 9,10-dibromoanthracene and **G*n***-Br. Efficient energy transfer is observed between the dendritic units and the anthracene moiety with photoluminescence quantum yields ranging from 62% for $n = 1$ to 80% for $n = 3$. Thin films of the resulting Ln^{III} complexes (Ln = Nd, Er, Yb) display NIR luminescence with concomitant decrease in the anthracene fluorescence intensity. The intensity of the metal-centered luminescence is independent of the presence of oxygen and no phosphorescence could be evidenced at low temperature for the corresponding Gd^{III} complexes. As a consequence, it is assumed that the ligand-to-metal energy transfer essentially involves singlet states of the dendritic ligands. The quantum yields of the [Ln(G3-An)$_3$(tpy)] dendrimers calculated from the lifetimes, assuming $\tau_{rad} = 0.25$, 8, and 2 ms for Nd^{III}, Er^{III}, and Yb^{III}, respectively, amount to 0.28, 0.025, and 0.55%, with $\tau_{obs} = 0.7$ (Nd^{III}), 2 (Er^{III}), and 11 (Yb^{III}) μs. These figures remain modest but in view of the large absorption displayed by the dendritic ligands, the overall emission intensity is large (Baek et al., 2006).

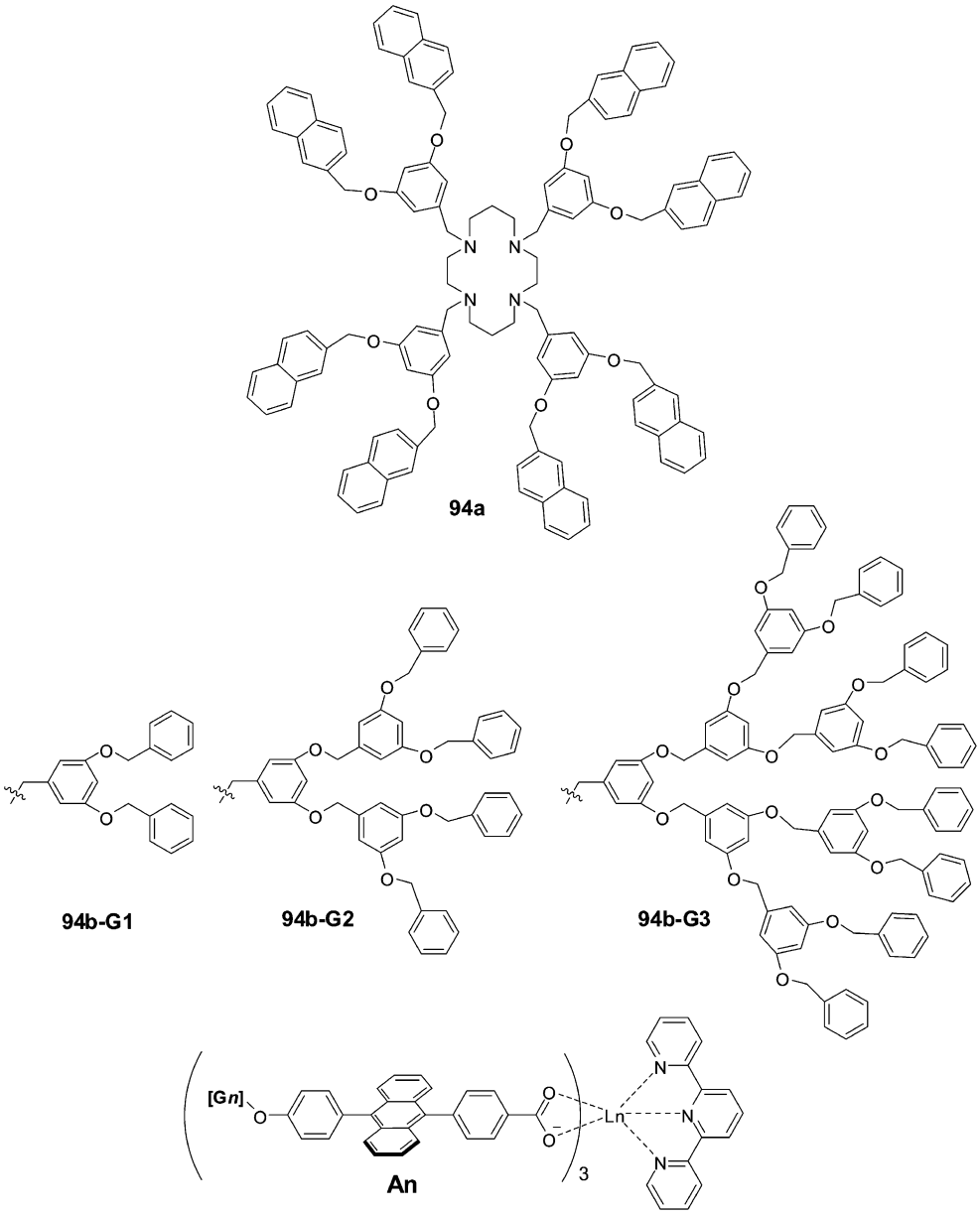

Fig. 81. (Top) Cyclam-based dendrimer of first generation. (Bottom) Dendritic 9,10-diphenylanthracene ligands and their Ln complexes.

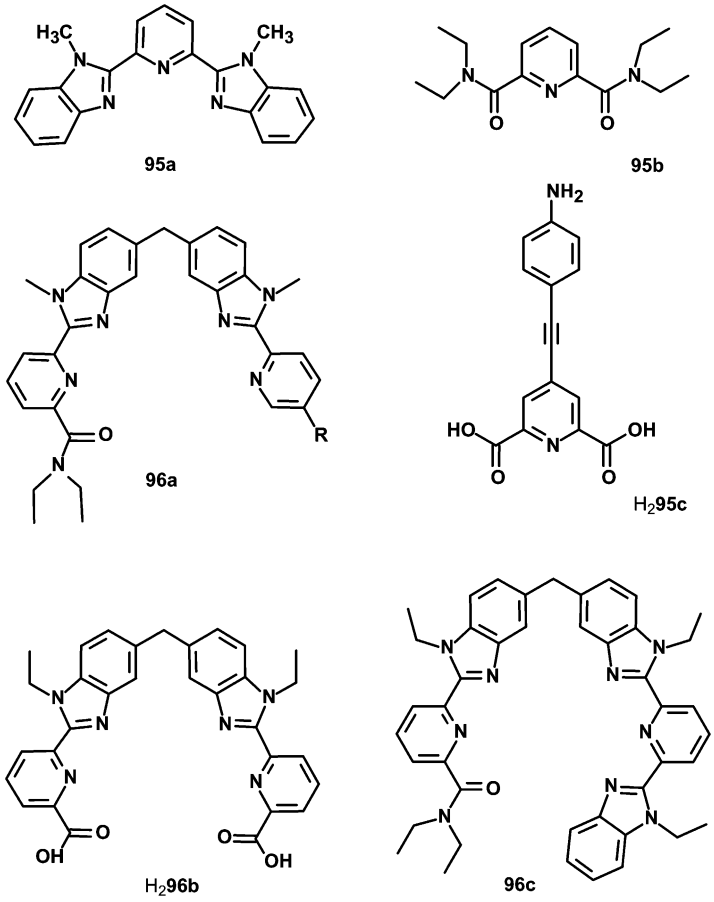

Fig. 82. Ligands for helical monometallic and bimetallic complexes.

3.2.6.3. *Self-assembly processes* Self-assembly processes imply the formation of an induced coordination cavity around the targeted metal ion from tailored ligand strands possessing adequate donor atoms and some conformational flexibility. The difference between a simple coordination reaction, e.g. formation of a tris(β-diketonate), and a self-assembly process is sometimes blurred and because self-assembly is fashionable, this term is often misused. An important factor in a self-assembly process is the concept of recognition: the induced cavity should be tailored for a specific metal ion. That is the targeted self-assembled species form preferentially among various possibilities. This is illustrated by the ligands described in fig. 82. For instance, three ligand strands **95a** self-assemble with lanthanide ions in acetonitrile to yield triple helical complexes which are stabilized by nine ion-dipole Ln^{III}–N bonds and by additional strong π-stacking interactions between ligand strands. As a result, the sys-

tem shows a larger selectivity for the cations in the middle of the lanthanide series than for the heavier lanthanide ions (Petoud et al., 1997). On the other hand, although the dipicolinic acid derivative **95b** also forms helical tris complexes, a simple electrostatic trend prevails for their stability constants, and no interstrand interaction contributes to their energetics; the resulting complexes are simple coordination compounds. This is also the case for the axial $[Ln(\mathbf{95c})_3]^{3-}$ complexes, the relatively low lying triplet state of which ($\approx$18 000 cm^{-1}) sensitizes Nd^{III} luminescence (Platas et al., 2001).

In contrast, the three ligands **96** are designed for the simultaneous recognition of a 4f–3d metal ion pair (**96a**) (Piguet et al., 1996), a homopair of 4f ions (H_2**96b**) (Elhabiri et al., 1999), or a heteropair of 4f ions (**96c**) (André et al., 2002). For instance, under stoichiometric conditions, $[M^{II}Ln^{III}(\mathbf{96a})_3]$ is the only species formed out of a potential mixture of at least six species (three M^{II}- and two Ln^{III}-containing complexes were identified in solutions with a single metallic species). The photophysical and energy-transfer properties of $Cr^{III}Ln^{III}$ and $Ru^{II}Ln^{III}$ (Ln = Nd, Yb) helicates is described below in section 3.3.4.

Stable triple-stranded homobimetallic helicates are self-assembled in water from H_2**96b**, which feature large thermodynamic stability and excellent protection of the nine-coordinate Ln^{III} ions lying in pseudo tricapped trigonal prismatic coordination environments. The $[Yb_2(\mathbf{96b})_3]^{3-}$ helicate is faintly emissive in water, so that its photophysical properties have been investigated in deuterated water in which the quantum yield of the metal-centered luminescence amounts to 1.8%, upon ligand excitation, and the $Yb(^2F_{5/2})$ lifetime is equal to 40 ± 2 μs. Analysis of the crystal-field splitting of both $^2F_{5/2}$ and $^2F_{7/2}$ levels confirm the D_3 symmetry of the self-assembled helicate. Up-conversion was looked for, but was not observed, possibly a consequence of the relatively large separation of the two Yb^{III} ions, 9.1–9.3 Å (Gonçalves e Silva et al., 2002).

A helical triple-decker complex of Yb^{III} has been self-assembled in 25% yield from ligand H_2**99b** (see fig. 84 below), $YbCl_3 \cdot 6H_2O$ and $Zn(OAc)_2 \cdot 2H_2O$ in methanol/acetonitrile (X.P. Yang et al., 2006a). The solid-state structure of this compound reveals a complex supramolecular architecture involving cross-linked one-dimensional strands of chiral trimetallic molecules linked by π–π stacking interactions. Each Yb^{III} ion is eight-coordinate and intermetallic distances range between 3.7 and 3.8 Å. A solid-state sample and a solution in acetonitrile exhibit metal-centered NIR luminescence while solutions in methanol and deuterated methanol are less luminescent, probably due to some dissociation of the complex. When compared to the emission of a solution of $[ZnYb(\mathbf{99b})(NO_3)_2(OAc)]$ in acetonitrile having the same absorbance, the fluorescence intensity of $[Yb_3(\mathbf{99b})Cl(OAc)_2]$ at 976 nm is larger by a factor 2.7, which supports the idea that the helical ligand framework in the trimetallic complex provides improved shielding of the metal ions.

Other examples of self-assembled, NIR-emitting triple helical complexes are described in section 3.3.4.

3.3. *Heterometallic functional assemblies: taking advantage of d-transition metal ions*

The synthesis of heteropolymetallic d–f complexes is well documented and understood because the two metal ions display highly different stereochemical preferences. Valence

d-orbitals are external and interact strongly with ligand orbitals, whereas the shielding of 4f-orbitals by the filled $5s^2$ and $5p^6$ subshells results in spherical Ln^{III} ions with little covalency in their binding with organic ligands. Heteropolymetallic d–f molecular edifices (or coordination polymers) are appealing because the communication between metal ions is an additional tool for the synthetic chemist for tuning the inner coordination sphere of the metal ions and therefore their electronic properties (Piguet et al., 2000). Three types of intermetallic interactions have been evidenced: mechanical coupling, interactions based on orbital overlap, and electrostatic communication. Intermolecular mechanical coupling between metallic centers is well established, particularly for Fe^{II}-containing discrete oligomers in which the triggering of the iron spin-crossover properties has been unambiguously demonstrated in heterobimetallic triple-stranded helicates (Edder et al., 2000). Orbital overlap is a route for intermetallic interaction; when 4f elements are involved though, the distance between the two metal ions must be short because the 4f–nd coupling is very small in view of the limited expansion of the 4f orbitals. This type of interaction is mainly involved in magnetic coupling (e.g., between Cu^{II} and Gd^{III}, with an exchange integral on the order of a few cm^{-1}), although it may also influence the flow of energy between the two metal ions (Bünzli and Piguet, 2002). Finally, long-distance energy transfer processes often occur via multipolar through-space mechanisms and both 4f $\rightarrow$ 3d and 3d $\rightarrow$ 4f energy transfer processes have been evidenced (Brayshaw et al., 1995; Cantuel et al., 2002; Edder et al., 2001); it is noteworthy that in solid-state devices, Cr^{III} acts as a good sensitizer of the luminescence of several Ln^{III} ions, including Nd^{III} in YAG lasers, Er^{III} or Tm^{III} (Shen et al., 2000; Tröster, 2003).

With respect to NIR luminescence, we are mostly interested in the latter communication mode, for two reasons. The first is that d-transition metal ions have larger molar absorption coefficients than 4f ions and, additionally, they may be excited through charge transfer states; subsequent directional transfer to 4f ions will consequently provide an efficient way of sensitizing their luminescence. Moreover, Ln^{III} ions displaying NIR luminescence have comparatively shorter lifetimes (10^{-9}–10^{-6} s) than the visible-emitting ions (10^{-3} s), which somewhat limits the efficiency of time-resolved experiments. This disadvantage can be overcome by the use of long-lived excited states of d-transition metal ions for populating the excited states of the 4f ions (Imbert et al., 2003; Torelli et al., 2005).

The various roles of d-transition metal ions in the elaboration of lanthanide-containing luminescent edifices, as well as some of the structural motifs described to date are schematically depicted in fig. 83. Among the heteropolymetallic d–f edifices reported to date, some make use of a transition metal ion because they build convenient counterions; this function discussed previously (cf. section 3.1.1, fig. 13) is not represented in fig. 83. In fig. 83a, the transition metal ion is a component of the ligand but assumes no essential role, apart from stabilizing the ligand structure. In the second case (fig. 83b), transition ion complexation affects the electronic properties of the ligand, allowing a better energy transfer or a more convenient excitation mode. In the molecular edifice sketched on fig. 83c, directional energy transfer from the d-transition metal ion populates the excited state of the 4f ion, therefore controlling its photophysical properties. The latter two situations are combined in fig. 83d, in that complexation of the d-transition metal ion induces ligand-to-metal charge transfer states which will

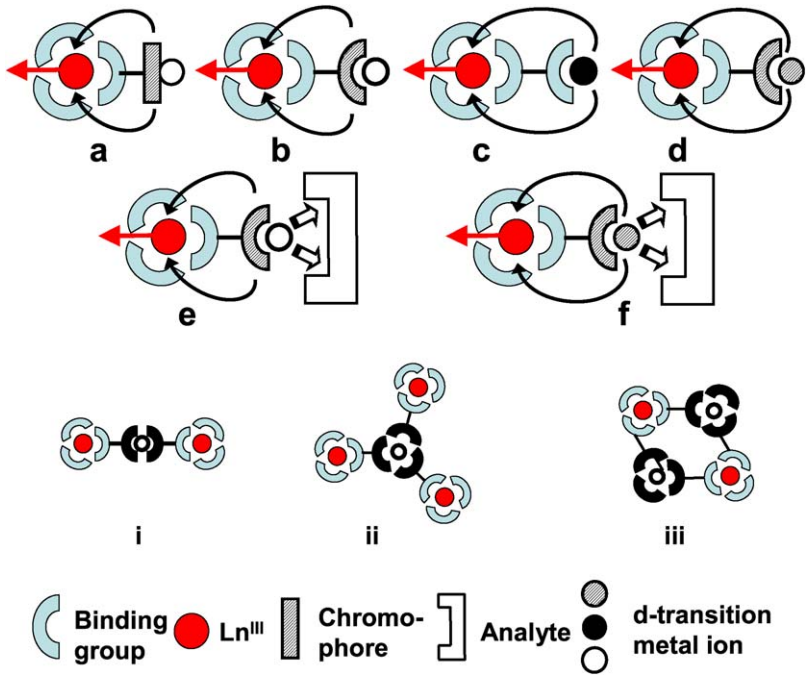

Fig. 83. Various roles (a through f) and structural motifs (i through iii) in d–f functional edifices.

transfer energy to the 4f ion. The last two cases (e, f) make use of the transition metal moiety of the edifice for the recognition of the analyte (e.g. DNA intercalation of Pt-complexes, see below); the d-transition metal ion can play no further role, or modify the electronic properties of the ligand (fig. 83e), or take part in the energy transfer through ^{3}MLCT states (fig. 83f). Depending on the edifices, intermediate situations between those described in fig. 83 can also be foreseen.

In view of the strong stereochemical preferences of the d-transition metal ions, several structural motifs are at hand, for instance with the d-metal ion unit acting as bridging ligand (i), or as templating agent for larger edifices (in fig. 83ii, a triangular motif is depicted, but others are possible, for instance, star-like or dendrimer-like arrangements), or with d- and f-metal ions arranging themselves in 2D grids as depicted in fig. 83iii, or in more elaborate 3D coordination polymers.

3.3.1. *Zn^{II} as structure stabilizer*

The zinc Schiff base complex N,N'-bis(3-methoxysalicylidene)ethylene-1,2-diamine, [Zn(**97a**)] fig. 84), reacts with lanthanide trinitrates giving neutral trimetallic complexes with formula [Zn(NO_3)(μ-**97a**)(Ln(NO_3)$_2$(H_2O)] (Ln = Nd, Ho, Er, Yb). X-ray crystallography of the Ho^{III} complex reveals that the Zn^{II} ion is located in the N_2O_2 cavity and is 5-coordinate,

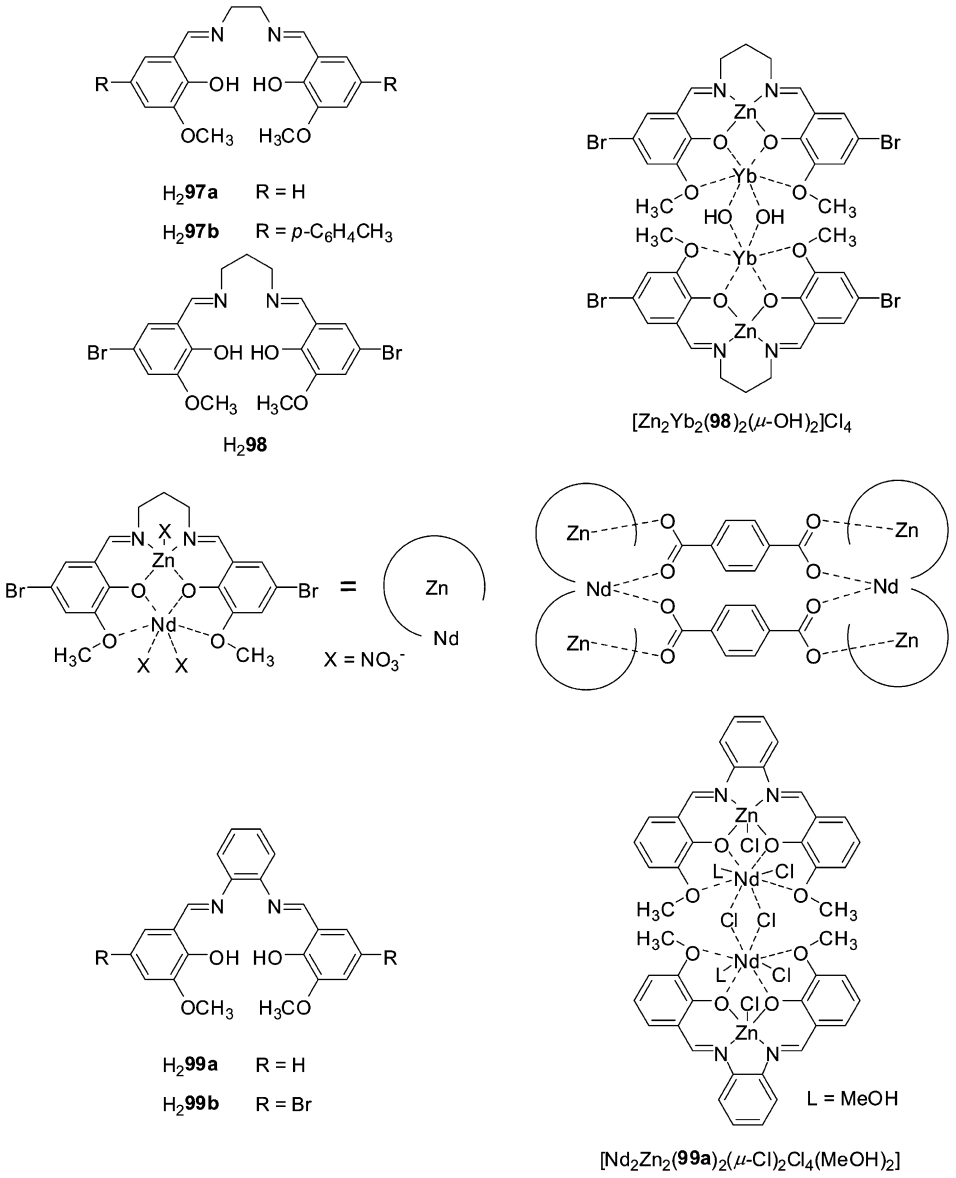

Fig. 84. Schiff-base derivatives for Zn–Ln heterometallic edifices.

with a distorted square pyramidal geometry, by the additional coordination of a monodentate nitrate ion. The Yb^{III} ion is 9-coordinate being bound to two bidentate nitrate ions, two bridging phenolate groups, two methoxy oxygen atoms and one water molecule. In methanol,

the complexes behave as 2:1 electrolytes, owing to the dissociation of two nitrate ions while they are non-electrolytes in acetonitrile. Upon excitation either at about 280 nm or 350 nm, ligand fluorescence occurs at 460–475 nm with a quantum yield of 3.37% for Ln = Gd. This quantum yield is smaller in the other complexes (0.72, 1.33, 2.77, and 1.37% for Nd, Ho, Er, and Yb, respectively) indicating energy transfer onto the Ln^{III} ion. Indeed, apart from the Ho^{III} compound, the complexes exhibit characteristic Ln^{III} NIR luminescence in methanol, with lifetimes of 1.33 μs for Nd^{III} and 1.31 μs for Yb^{III} (Wong et al., 2002). Similar complexes were isolated with H_2**97b**, $[Zn(NO_3)_{3-y}(\mu\text{-}$**97b**$)(Ln(NO_3)_y(H_2O)_x]$ ($x = 2$, $y = 3$, Ln = La, Nd; $x = 1$, $y = 2$, Ln = Gd, Ho, Er, and Yb). The molecular structures of La, Nd, Er, and Yb elucidated by X-ray crystallography are very similar to the structure of the Ho^{III} complex with H_2**97a**, except for the coordination number which varies from 9 (Er, Yb, one bound H_2O, two bidentate nitrate ions) to 10 (Nd, one bound H_2O, one monodentate and two bidentate nitrate ions) and 11 (La, one bound H_2O and three bound bidentate nitrate ions). In acetonitrile, the $Yb(^2F_{5/2})$ lifetime is larger than for the solid state samples, reaching 14.6 μs, while the Nd^{III} lifetime remains the same (Lo et al., 2004).

Modification of the Schiff-base ligand by introduction of two bromine substituents in H_2**98** resulted in the isolation of a tetrametallic species $\{[YbZn(\mathbf{98})]_2(\mu\text{-}OH)_2\}$ (fig. 84) when the zinc complex was treated with ytterbium trichloride. Typical $Yb(^2F_{5/2})$ emission takes place upon ligand excitation, both in acetonitrile and in methanol, with an intensity larger than the one exhibited by the related bimetallic complex $[Zn(\mathbf{98})(ac)Yb(NO_3)_2]$ (Yang et al., 2005).

The interest of ligand H_2**98** is its two dissimilar metal-binding sites. In bimetallic complexes, the metal ions are roughly located in a planar deprotonated ligand set. The mononegative ligand X (see middle of fig. 84) often occupies an axial site of the 3d metal ion, resulting in a distorted square-based pyramidal configuration. In $\{[YbZn(\mathbf{98})]_2(\mu\text{-}OH)_2\}$, this axial ligand has disappeared in favor of two bridging hydroxyl units spanning the two metal ions. This suggests that the nuclearity of the complexes could be increased by carefully choosing multidentate ligands able to occupy the axial and bridging sites of each 3d–4f pair. 1,4-Benzenedicarboxylate (bdc) fulfils these requirements, and reaction of equimolar quantities of H_2**98**, zinc acetate, neodymium nitrate and H_4bdc in ethanol afforded a remarkable hexametallic assembly comprised of two $Zn_2Nd(\mathbf{98})_2$ fragments connected by two bdc dianions each carboxylate unit of which spans a Zn–Nd pair. The assembly is stable in methanol and displays $Nd(^4F_{3/2})$ emission upon UV excitation (275–330 nm). In a semi-quantitative assay, the authors determine that the emission intensity is 5–6 times larger than the one exhibited by $[Zn(\mathbf{98})(ac)Yb(NO_3)_2]$ (X.P. Yang et al., 2006b).

Reaction of equimolar quantities of neodymium trichloride and Zn(**99a**) in methanol leads to the isolation of the tetrametallic species $\{[NdZn(\mathbf{99a})]_2(\mu\text{-}Cl)_2Cl_4(MeOH)_2\}$ in which the zinc Schiff base acts as a tetradentate ligand for 8-coordinate Nd^{III} (fig. 84, bottom right). Upon replacement of neodymium chloride with neodymium nitrate, bimetallic species are isolated—$[Zn(\mathbf{99a})(MeCN)Nd(NO_3)_3]$—featuring 10-coordinated Nd^{III}. On the other hand, trimetallic species form when the stoichiometric ratio is increased to 1:2 (Nd:Zn): $\{Nd[Zn(\mathbf{99a})(H_2O)(NO_3)]\cdot H_2O\cdot NO_3\cdot EtOH\}$, in which one methoxy group of each Schiff base binds Nd^{III} in addition to the two bridging phenolates, and $\{[Nd(Zn(\mathbf{99a}))_2Cl_2(H_2O)_3]\cdot Cl\cdot 2MeOH\cdot 5H_2O\}$ with 9-coordinate Nd^{III}. All these species are NIR emitters, the bet-

ter intensity being obtained for the bimetallic species (Wong et al., 2006). Finally, dibromination of **99a** does not seem to affect the luminescence intensity, since [Nd(Zn(**99b**)(μ-ac)$(NO_3)_2(H_2O)$] was found to be only weakly emitting (X.P. Yang et al., 2006c).

3.3.2. *Transition metal ions as modifiers of ligand electronic properties and/or recognition units*

Erbium-doped silica amplifiers are widely used in telecommunication systems. However, Er^{III} cations are poorly soluble in inorganic media, leading to poor amplification properties. One way to circumvent this problem is to develop polymer-based fiber optic systems, in which Er^{III} complexes would be fairly soluble. With this in mind, H.K. Kim has proposed to use a substituted tetraphenylporphyrin H_3**100a**, or more precisely the corresponding metalloporphyrins H**100b–c** in order to achieve complexation of the lanthanide ion by the carboxylic acid function and not by the porphyrinic core (fig. 85). Since the tris complex, which can be classified as a dendrimer (see section 3.2.6.2), would only fill six of the coordination sites of the lanthanide ion; a ternary complex with terpyridine has been prepared. In addition to the non-coordinating nature of the macrocyclic core, the another advantage of metalloporphyrins over free porphyrins lies in a larger symmetry resulting in only two components for the Q absorption band. The benefit of Pt^{II} over Zn^{II} is the occurrence of a strong interaction between the unoccupied 5d orbitals of the metal ion and the π orbitals of the porphyrin, resulting in appreciable shifts in both the UV absorption spectrum and the red emission. Upon excitation at 430 nm for instance, the Zn porphyrin H**100b** displays a moderate emission band at 596 nm and a strong band at 646 nm, while the photoluminescence spectrum of the platinum porphyrin H**100c** shows a strong band at 653 nm and a moderate one at 713 nm. The photoluminescence spectrum of the ternary complex [Er(**100c**)(tpy)] recorded under excitation at 488 nm displays the characteristic $^4I_{15/2} \rightarrow {}^4I_{13/2}$ emission at 1.525 μm while this band is hardly seen for the corresponding tris(hydrated) metalloporphyrinate or for the zinc-based ternary complex in thf (Oh et al. 2004, 2005). The quenching of this NIR luminescence by oxygen proves the role of the porphyrin triplet state in the sensitization process.

In addition to facile quenching by proximate vibrations, Er^{III} ions sustain concentration quenching that is well documented. This limits for instance the concentration of Er^{III} ions in doped silica optical fibers and consequently the maximum gain achievable (to about 30 dB). To minimize similar quenching process in the metalloporphyrinate complexes, the same authors have fitted the benzo substituents of the Pt-porphyrinate with a second generation aryl-ether dendron used to produce dendrimers, leading to receptor H**100d**. The resulting micelle-like entities with a Ln^{III} core effectively display a larger luminescence intensity when compared with [Er(**100c**)(tpy)], both in tetrahydrofuran (10^{-5} M) and in the solid state where it is 7-fold larger (Oh et al., 2005).

Palladium porphyrinates have appealing properties in that they feature long-lived triplet states: they are subject to very efficient quenching by molecular oxygen, they bind deoxyribonucleic acid (DNA), and this intercalation process curbs the oxygen quenching so that emission from the triplet state is enhanced considerably. In an effort to explore the sensitizing ability of the Pd-porphyrinate moiety, Beeby et al. (2000) has prepared a porphyrinate conjugate linked to a chiral lanthanide moiety (**101b**). Reaction of the porphyrinate iodoac-

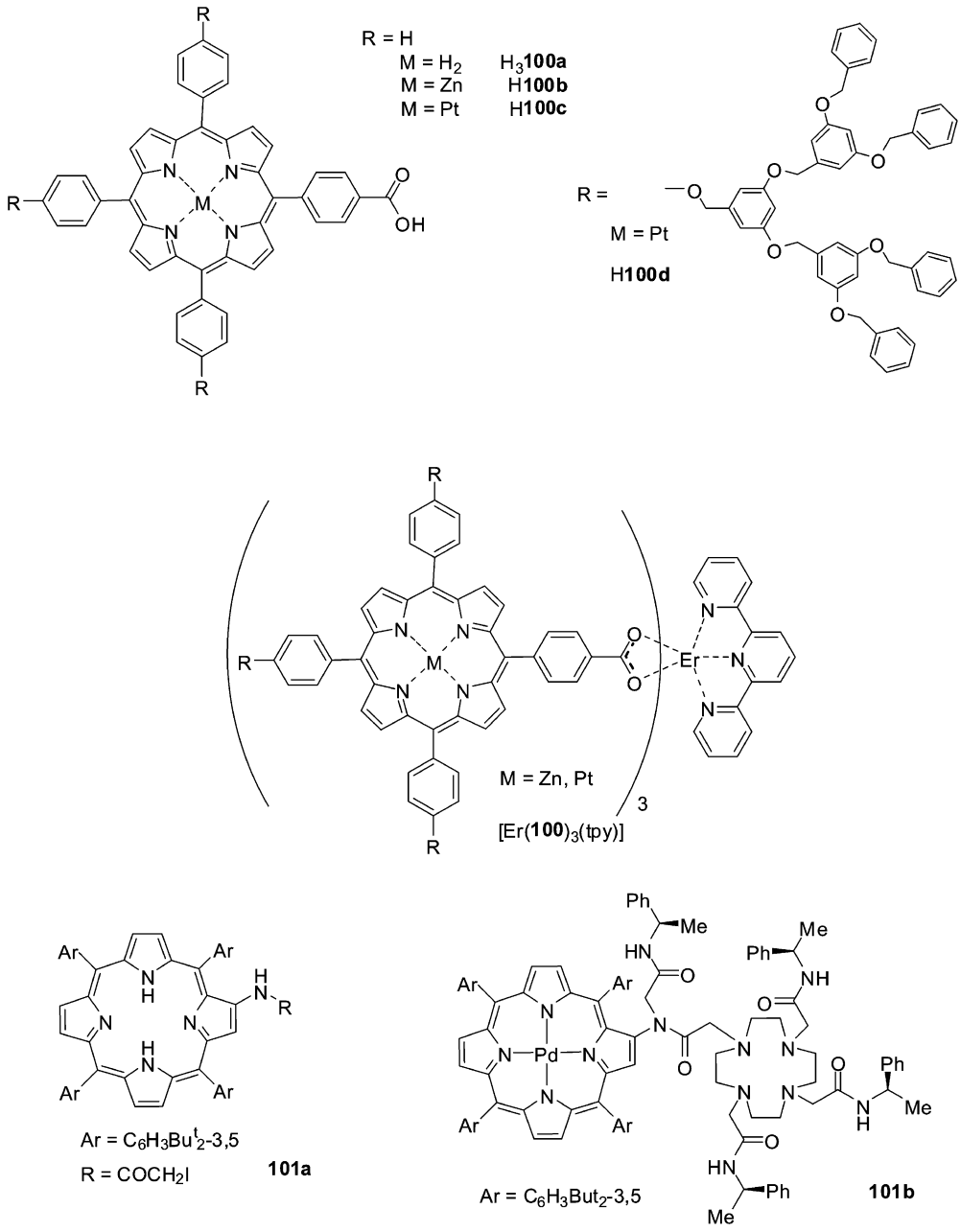

Fig. 85. (Top) Metalloporphyrins and corresponding Er^{III} complexes. (Bottom) Modified palladium metalloporphyrin.

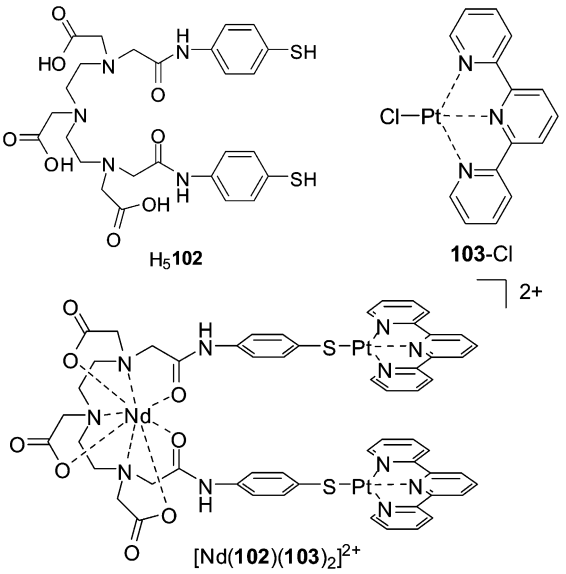

Fig. 86. Hairpin-shaped complex for DNA intercalative recognition (Glover et al., 2003).

etamide **101a** with an excess of cyclen in thf gave the monosubstituted Pd-porphyrinate in almost quantitative yield. The three chiral pendant arms were then introduced with either chirality (*RRR*) or (*SSS*) and subsequent reaction with lanthanide trifluoromethanesulfonates yielded the cationic complexes $[Ln(\mathbf{101b})]^{3+}$ (Ln = Nd, Yb). Their CD spectra are dominated by the porphyrinate chromophore, with g_{abs} values (eq. (24)) at 560 nm of $+1.7 \times 10^4$ for both the Nd and Yb complexes. With (*RRR*)-$[Yb(\mathbf{101b})]^{3+}$ weak CPL signals were observed at 985 nm ($g_{lum} = -0.04$, see eq. (23)) and 963 nm ($g_{lum} = +0.05$); the Nd^{III} complex exhibits an even weaker CPL signal ($g_{lum} = -0.006$ at 1055 nm). In de-aerated methanol–water (5 μM, CD_3OD/D_2O 80/20), the phosphorescence of the porphyrinate moiety appears as weak bands at 735 and 800 nm, in addition to metal-centered luminescence, which is not the case for aerated solutions. Removal of oxygen from the solutions results in an enhancement of the NIR luminescence by a factor 2 for Nd^{III} and 7 for Yb^{III}. Since excitation spectra nearly perfectly match the absorption spectra of the complexes, the ligand-to-metal energy transfer rate is competitive with the rate of triplet state quenching by oxygen; the latter is 10^9 s^{-1} for Pd-porphyrinate; monitoring the decay of the porphyrinate triplet emission as well as the grow-in and decay of the Ln^{III} luminescence by time-resolved experiments allowed the rate constant for oxygen quenching to be calculated as being 5×10^8 s^{-1} (Ln = Nd). The addition of an oligonucleotide such as $[(CG)_6]_2$ or of calf-thymus DNA to an aerated solution of (*RRR*)- or (*SSS*)-$[Yb(\mathbf{101b})]^{3+}$ leads to an increase of about 30% in the luminescence intensity of the porphyrinate and the Yb^{III} ion, with respect to a de-aerated solution. The sensitivity of Nd^{III} and Yb^{III} luminescence to pO_2 is of interest for potential mapping of regions of organisms with low oxygen pressure.

Following the same motivation of DNA tagging, but using a very different approach, Pikramenou and coworkers (Glover et al., 2003) have self-assembled a $LnPt_2$ complex featuring a hard binding core H_5**102** for Ln complexation via five oxygen and three nitrogen atoms and bearing two soft thiol substituents for coordination to Pt^{II} (see fig. 86). Platinum terpyridyl moieties **103** were chosen for their ability to intercalate in DNA. The reactants **102**, $NdCl_3 \cdot xH_2O$, and **103** were mixed into 1:1:2 stoichiometric ratio and the solution in methanol was simply refluxed during 2 h, yielding the desired heterotrimetallic complex in quantitative yield. The absorption spectrum of $[Nd(\mathbf{102})(\mathbf{103})_2]^{2+}$ is the sum of the spectra of the individual components, [Nd(H_2**102**)] and **103**–Cl, with a slight shift of the aromatic thiolate, plus a new band at 515 nm which is attributed to a ligand-to-ligand charge transfer (LLCT) state, $p\pi(RS^-) \rightarrow \pi^*$(tpy). Sensitization of the Nd^{III} luminescence occurs through this state (as well as through states centered on the thiophenyl units) and the relative emission intensity remains constant upon addition of calf-thymus DNA. The binding to the latter has been further evidenced by linear dichroism and the corresponding constant estimated to be on the order of 10^8 M^{-1}. The Nd^{III} unit acts as a luminescent reporter of the intercalation despite its relatively low quantum yield (0.25% in dmso-d_6, as estimated from eq. (7) with $\tau_{obs} = 670$ ns and assuming $\tau_0 = 270$ µs).

3.3.3. *d-Transition metal ions as luminescence sensitizers*

In the following, chromophores containing transition metal ions, namely Cr^{III}, Fe^{II}, Ru^{II}, Re^{I}, Os^{II}, and Pt^{II} are inserted into heterometallic edifices and sensitize Ln^{III}, mainly Nd^{III} and Yb^{III}, luminescence through either directional dipole–dipole transfer, MLCT states, or a sequential process involving both mechanisms. The energy of the MLCT states largely depends on the d-metal ion environment and can therefore be tuned by modifying the hosting ligands. The first excitation mode does not require a direct chemical link between the two communicating metals, whereas the second does and several bridging ligands have been described for this purpose. For instance, S. Kaizaki has developed a series of stable heterobimetallic complexes by linking lanthanide hydridotris(1-pyrazolyl)borates with a mixed Cr^{III} complex with acetylacetonate and oxalate: [Cr(acac)(µ-ox)Ln(Tp^H)$_2$] (fig. 87). Red emission arising from the Cr(^{2}E) excited state is seen for the complexes with Tb^{III} and Lu^{III}, but not with Yb^{III} for which the $Cr^{III} \rightarrow Yb^{III}$ transfer is complete owing to the ideal energy gap ($\approx$2500 cm^{-1}) between the Cr(^{2}E) and Yb($^2F_{5/2}$) levels (Sanada et al., 1998b); the lifetime of the Yb($^2F_{5/2}$) level amounts to 48 µs at 10 K. NIR emission also occurs for the complexes with Nd^{III}, Ho^{III} ($^5I_{5,4} \rightarrow {}^5I_8$, $^5I_7 \rightarrow {}^5I_8$ transitions, 1.2–1.6 µm), Er^{III}, and Tm^{III} ($^3F_3$, $^3H_4 \rightarrow {}^3H_6$, $\approx$800 nm), simultaneously with Cr^{III} luminescence (Subhan et al., 2003). The series of chiral complexes (Ln = Nd, Sm, Dy, Ho, Er, and Yb), has also been extensively studied by NIR circular dichroism and NIR magnetic circular dichroism (Subhan et al., 2001; Subhan et al., 2002). Replacing oxalate with trimethylenebis(oxamide) (tbo) and Cr^{III} by Ni^{II} resulted in the isolation of a trimetallic complex {[Ni(μ^2-tbo)][Yb(Tp^H)$_2$]$_2$}, the crystal structure of which was solved, but no metal-centered luminescence was detected (Sanada et al., 1998a). Another bridging ligand is 3,5-di(2-pyridyl)pyrazolate (bpypz) which yields [Cr(acac)$_2$(μ-bpypz)Ln(hfa)$_3$] complexes (fig. 87) in which the Ln ion (Ln = Yb) is 8-coor-

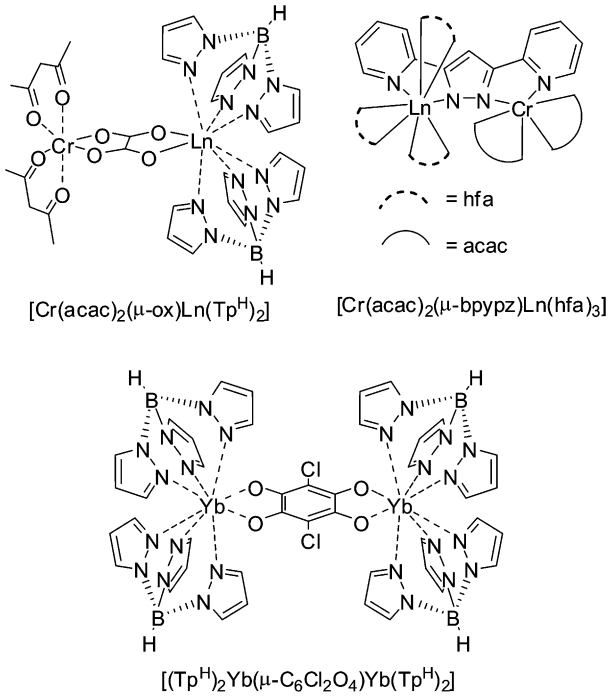

Fig. 87. Bridged Cr–Ln and Ln–Ln bimetallic complexes.

dinate in a bicapped trigonal prismatic geometry (Kawahata et al., 2003). Since the Cr–Yb distance is shorter (4.65 Å) in $[Cr(acac)_2(\mu\text{-bpypz})Yb(hfa)_3]$ than in $[Cr(acac)(\mu\text{-ox})Yb(Tp^H)_2]$, emission from the $Yb(^2F_{5/2})$ level only occurs for the former compound, even at 10 K and the corresponding lifetime amounts to 155 μs (solid state). The Nd^{III} analog also shows exclusively 4f–4f emission. When bpypz is replaced with chloranilate, a tetradentate ligand acting as bridging bis(bidentate)unit, a homobimetallic Yb^{III} complex forms, with formula $[(Tp^H)_2Yb(\mu\text{-}C_6Cl_2O_4)Yb(Tp^H)_2]$. The deep-violet complex crystallizes in the $P2_1/n$ space group and the two 8-coordinate Yb^{III} ions linked by the planar bis(bidentate) chloranilate are separated by 8.56 Å. The complex displays strong Yb-centered emission which is traced back to energy transfer from the triplet state of chloranilate: the excitation spectrum indeed presents a band at around 600 nm due to the intraligand singlet–singlet n–π^* transition of chloranilate, shifted from 568 nm in the absorption spectrum and from 511 nm in the absorption spectrum of free chloranilate (Abdus et al., 2004).

The first example of Nd^{III} and Yb^{III} luminescence sensitized by Ru^{II} and ferrocene appeared in 2000. The authors noticed that $[Ru(bpy)_3]^{2+}$ has an intersystem crossing yield near unity and that it enables excitation with visible light up to 500 nm. On the other hand, ferrocene has weaker absorption bands in the visible spectrum, but its low-lying triplet state (≈13 300 cm^{-1}) matches fairly well the Nd^{III} ($^4F_{3/2}$, 11 300 cm^{-1}) and Yb^{III} ($^2F_{5/2}$,

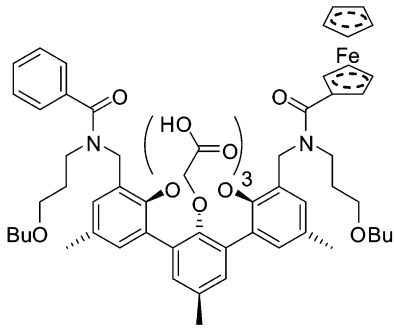

H_3**104**

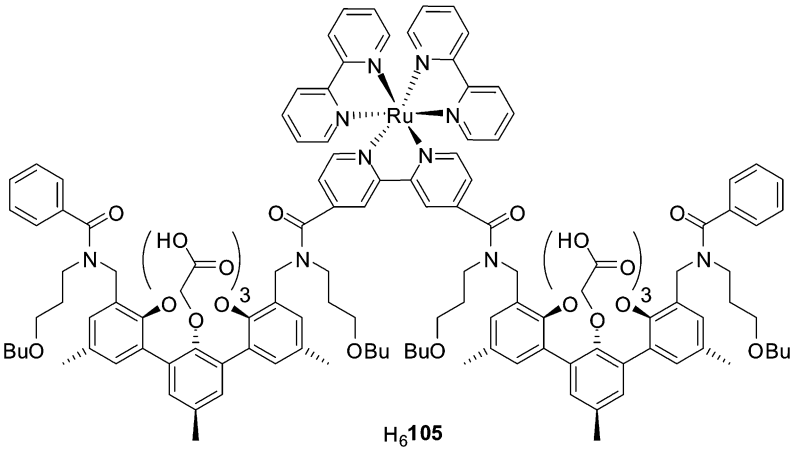

H_6**105**

Fig. 88. Ferrocene and Ru^{II} chromophore for the sensitization of Nd^{III} and Yb^{III} luminescence.

10 300 cm^{-1}) excited states. Terphenyl-based Ln^{III} complexes were covalently linked to the transition metal complexes (fig. 88). De-oxygenated solutions of dmso-d_6 of the ferrocene-functionalized complexes with Nd^{III} and Yb^{III} (10^{-4} M) display the typical metal-centered emission upon ferrocene excitation at 320 nm; the lifetimes are 2.0 ± 0.2 μs for [Nd(**104**)] and 18.8 ± 0.2 μs for [Yb(**104**)]. The trimetallic complexes [Ln_2(**105**)] also displayed metal-centered luminescence upon visible light excitation. Time-resolved luminescence data on the Nd^{III} system proved that energy transfer involves a ^{3}MLCT state of the Ru^{II} chromophore: the Nd^{III} luminescence intensity rises with a lifetime (420 ± 20 ns) equal to the lifetime of the chromophore triplet state (420 ± 10 ns, emission at 660 nm) and decays with a lifetime equal to 2.1 ± 0.2 μs. Both the intensity of the Ru^{II} chromophore luminescence and its lifetime (770 ± 20 ns) are larger in the corresponding Gd^{III} reference compound; the energy transfer rate to Nd^{III} can then be estimated to $k_{et} = 1.1 \times 10^6$ s^{-1}. On the other hand, both the triplet

state intensity and lifetime of the Yb^{III} trimetallic complex are equal to the corresponding data for Gd^{III}, meaning that the rate of the energy transfer process in [Yb_2(**105**)] is at least one order of magnitude smaller than the decay rate of the triplet state (i.e., $<10^5$ s^{-1}). This points to an electron transfer mechanism for the excitation of the $Yb(^2F_{5/2})$ state, the lifetime of which amounts to 18.2 ± 0.8 μs in dmso-d_6 (Klink et al. 2000c, 2002).

More elaborate molecular edifices have been proposed (fig. 89, note that the "outer"-sketched substituents of calix[4]arene are in fact located on the narrower rim). For instance, a star-like receptor featuring a central $[Ru(bpy)_3]^{2+}$ core unit to which six functionalized calixarene receptors are covalently linked (Beer et al., 2004). Addition of lanthanide nitrate (Ln = Nd, Eu, Tb) to solutions of the Ru^{II} complexes causes substantial changes in the absorption spectra, confirming complexation of the trivalent ions, although not always complete. Analysis of the UV–visible titrations yields the final following stoichiometries (Nd:L): 1:1 for receptor H_3**106** ($\log K = 5.2$ in acetonitrile), 2:1 for H_6**107** ($\log \beta_2 = 13.4$), and at least 5:1 for H_{18}**108** (no stability constant could be determined). During the titrations, a decrease of the ^{3}MLCT emission of ruthenium at 610 nm parallels an increase in the typical 4f–4f emission of Nd^{III} as the metal ion concentration increases. In the case of [Nd(**106**)], the rate constant for the ^{3}MLCT → $Nd(^4F_{3/2})$ could be estimated to be 2.4×10^6 s^{-1}. On the other hand, excitation spectrum of the Ru^{II} emission at 610 nm does not display the band corresponding to the calixarene receptor, while this band is markedly present in the excitation spectrum of Nd^{III}; in fact, since the latter ion lies closer to the calixarene than Ru^{II}, this proximity gives rise to a fast energy transfer to the 4f-metal ion.

Starting from the same $[Ru(bpy)_3]^{2+}$ chromophore, S. Faulkner and coworkers (Pope et al., 2004b) have modified one of the bipyridine moiety in L^1 = 4′-methyl-2,2′-bipyridyl-4-carboxylic acid, (H**109a**, fig. 89) and have extended the study to the $[Os(bpy)_2L^1]^{2+}$ antenna (H**109b**) as well as to the facial complex *fac*-$[ReCl(CO)_3L^1]$ (H**109c**). Ternary complexes of the type $\{[M(bpy)_2(L^1)][Ln(do3a)]\}^{2+}$ (M = Ru, Os) or $\{[ReCl(CO)_3(L^1)][Ln(do3a)]\}$, Ln = Nd, Er, Yb, are formed in methanol by simple mixing of the two metal-containing components. The idea behind this design was to complete the coordination sphere of the do3a complexes by the carboxylate moiety of L^1 and to be able to screen a large number of chromophores by simple interaction with the known stable complexes of do3a. If the latter idea proved to be successful, some residual solvation remains, as evidenced by the q values obtained on the basis of lifetime measurements in methanol and deuterated methanol: $q_{Yb} = 0.6$, (Re^I) 0.7 (Ru^{II}) and 1.1 (Os^{II}). Somewhat smaller values were obtained for Nd^{III}, which is surprising in view of the larger ionic radius of this ion, but relationship (10b) is known to be less reliable than the relationship for q_{Yb}. Er^{III} luminescence could hardly be detected in methanol and the short-emissive MLCT states based on Re^I and Os^{II} proved to be more suitable as donor chromophores when compared to the Ru^{II} moiety.

The ternary complex strategy is appealing, but the stability of the complexes may be a problem, a reason why the same authors have covalently grafted chromophores H**109a–c** on a dtpa core to yield ligands H_3**110a**, H_3**110b**, and H_3**111** (fig. 90). The existence of trimetallic complexes $[Ln(\mathbf{110})]^{n+}$ ($n = 4$, Ru^{II}, Os^{II}; $n = 0$, Re^I) in methanolic solution is ascertained by mass spectrometry. In the same solvent, the ^{3}MLCT emission maximum shifts from 630 in H_3**110a** to 637 nm in its complexes with Nd^{III}, Er^{III}, and Yb^{III}. In parallel, the ^{3}MLCT lifetime

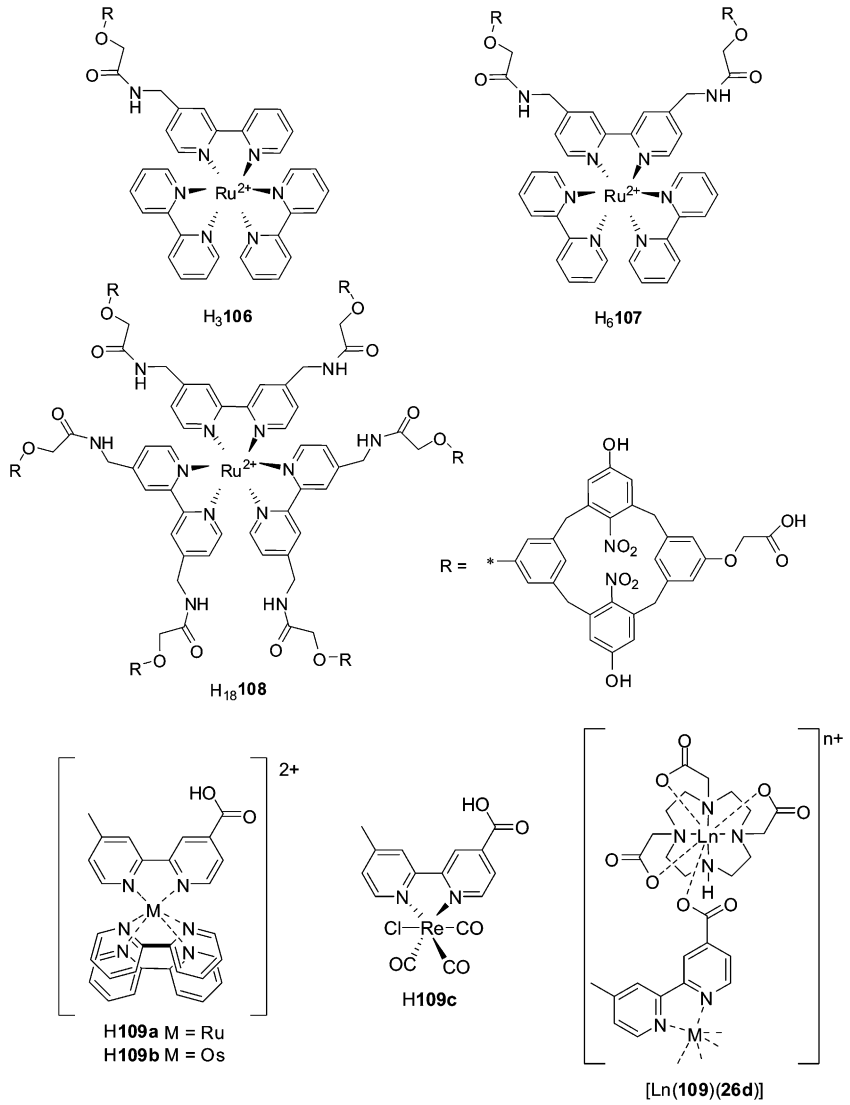

Fig. 89. (Top and middle) Calix[4]arene-fitted $[Ru(bpy)_3]^{2+}$. (Bottom) Ru^{II}, Os^{II}, and Re^{I} chromophores and ternary complexes with do3a.

(309 ns) decreases to 240, 275, and 294 ns, respectively, indicative of an energy transfer onto the lanthanide ion. From the measured rise time, ≈200 ns for both Nd^{III} and Er^{III}, this transfer is however rather inefficient. In the case of Yb^{III}, the NIR emission of ^{3}MLCT and the 4f ion could not be clearly separated so that no quantitative data are at hand. The Os^{II} trimetallic

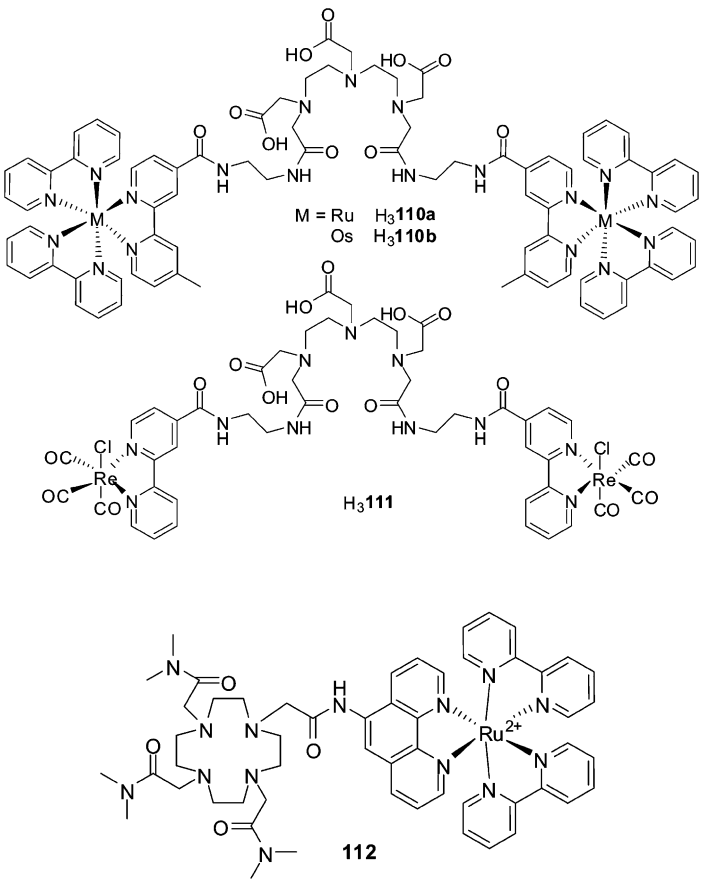

Fig. 90. d-Transition metal chromophores fitted on dtpa (top and middle) and do3a (bottom).

complexes also show attenuation of the ^{3}MLCT emission when compared to H_3**110b**, as well as a red shift from 745 to 757 nm. The triplet state lifetime of H_3**110b** (34 ns in methanol) is much shorter compared to H_3**110a** and it shortens to 24–26 ns in the trimetallic complexes. Again, the chromophore emission interferes with Yb^{III} luminescence so that deconvolution methods have to be used to extract the lifetimes. The *fac*-[$ReCl(CO)_3(L^1)$] complex emits at 625 nm, much as the Ru^{II} chromophore and this emission is not shifted in the trimetallic complexes. The ^{3}MLCT lifetime (13 ns) is also not much affected by lanthanide complexation (10–13 ns) but the emission intensity decreases by about 30%, again indicative of energy transfer. The lifetimes of the Ln^{III} excited states amount to 0.51, 0.54, and 8.3 μs for Nd^{III}, Er^{III}, and Yb^{III}, respectively. These values are comparable to those obtained with the other two chromophores, but the grow-in of the emission is very fast. The determination of hydration numbers leads to values between 0.1 and 0.3 for Nd^{III} in the three complexes, consistent

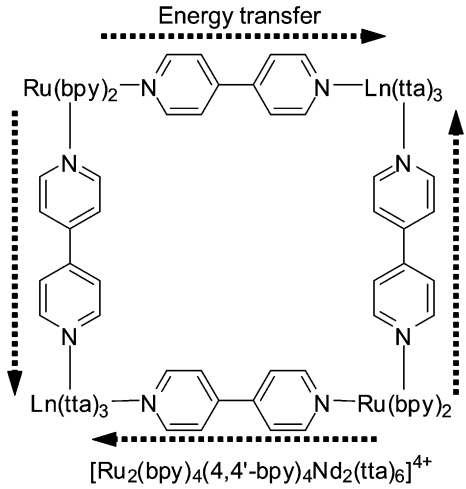

Fig. 91. Tetrametallic complex exhibiting Ru^{II}-to-Ln^{III} (Ln = Nd, Yb) directional energy transfer (Guo et al., 2004).

with an octadentate coordination environment. As for the ternary complexes, none of the Er^{III} complexes produces detectable emission in methanol, but emission is observed in deuterated methanol. An intriguing aspect of this work is the comparison of the apparent energy transfer efficiencies; energy transfer rates lie between 3.5 and 5.8×10^7 s^{-1} for the Re^I chromophore, almost one order of magnitude faster than for the Os^{II} chromophore ($6.2–9.4 \times 10^6$ s^{-1}) and two orders of magnitude larger when compared with Ru^{II} (3.8×10^5 s^{-1}). Since the energies of the donor ^{3}MLCT state are close for Re^I and Ru^{II} (15 700 and 16 000 cm^{-1}, respectively), and the linker between the dtpa coordination site and the transition metal ion chromophore comprises a saturated ethylene linker, rendering through bond energy transfer unlikely, the spatial proximity between the donor and the acceptor will play a key role. The less sterically hindered Re^I chromophore is therefore a better donor than the more crowded Ru^{II} one (Pope et al. 2004b, 2005).

Following a similar line, T. Gunnlaugsson has covalently attached the $[Ru(bpy)_2]^{2+}$ chromophore on a cyclen-amide derivative via a phenanthroline moiety (**112**, fig. 90). Excitation of the latter, at 285 nm, or of the ^{3}MLCT state, at 450 nm, results in sensitized emission. The Ru^{II} lifetime (202 ns) remains constant in water and deuterated water, which is not the case of the Nd($^4F_{3/2}$) level: its lifetime decreases from 192 ns in D_2O to 30 ns in water; similarly, τ(Yb^{III}) decreases from 6.4 to 2 μs, signifying a quenching by the solvent (Gunnlaugsson and Leonard, 2005).

In order to improve the Ru^{II}-to-Ln^{III} energy transfer, Guo et al. have proposed interesting tetrametallic square Ru_2Ln_2 complexes (fig. 91). The ^{3}MLCT emission at 610 nm is clearly visible in the reference Gd^{III} assembly, but fades considerably for Yb^{III} and even more for Nd^{III}, being ten times smaller than in the reference compound. In parallel, the metal-centered emission grows considerably, demonstrating the energy transfer (Guo et al., 2004); unfortunately, no quantitative data have been reported. This type of work on d–f complex prefigures

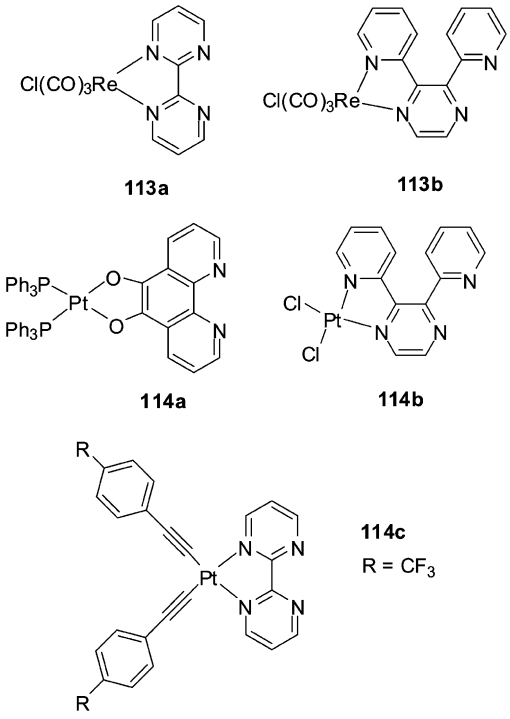

Fig. 92. Rhenium and platinum chromophores.

the development of coordination polymers in which sensitization of NIR luminescence occurs (see section 3.4).

Monovalent rhenium carbonyl complexes with 2,2′-bipyrimidine (**113a**, bpym) or 2,3-bis-(2-pyridyl)pyrazine (**113b**, bppz) have also been tested as potential sensitizing groups (fig. 92). The available bidentate coordination unit is simply coupled to a lanthanide β-diketonate complex, such [Ln(tta)$_3$] or [Ln(fod)$_3$]. The 650-nm emission of the ^{3}MLCT state is quenched in the ternary adducts with Nd^{III}, Er^{III}, and Yb^{III}, demonstrating the energy transfer (Shavaleev et al., 2002). Metal-centered luminescence is consequently observed in methylene chloride upon excitation at 460 nm with lifetimes of <0.5 μs (Nd^{III}, Er^{III}), and 6.7 μs (Yb^{III}); quantum yields for solid state samples remain very small, 0.24, 0.02, and 0.79% for Nd, Er, and Yb, respectively, estimated from lifetime measurements and assuming $\tau_{rad} = 0.25$, 14, and 2 ms, respectively (Shavaleev et al., 2005). The same authors have designed similar chromophores by replacing Re^{I} with Pt^{II} (**114a–c**, cf. fig. 92). The ternary complexes [Ln(tta)**114a**] display slightly improved photophysical properties with respect to the Re chromophore, with lifetimes, in methylene chloride, equal to 0.99 (Nd^{III}), 2.52 (Er^{III}), and 10.6 μs (Yb^{III}), and quantum yields (solid state, from lifetimes) of 0.4, 0.018, and 0.53%, respectively (Shavaleev et al., 2003a). Replacing chromophore **114a** with the pyrazine derivative **114b** and/or the β-diketonate tta with btfa, (benzoyltrifluoroacetonate) does not change sub-

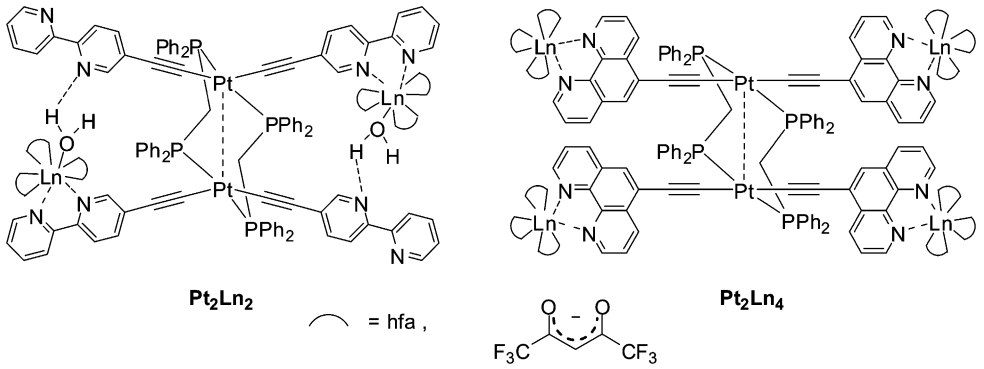

Fig. 93. Diplatinum chromophores forming tetra- and hexa-metallic complexes with Ln^{III} ions (Xu et al., 2006).

stantially the photophysical properties and both lifetimes and quantum yields remain close to the figures listed above (Shavaleev et al., 2003b). This is also true for chromophore **114c**: the lifetime of [Nd(hfa)$_3$**114c**] is smaller than 0.5 μs and the quantum yield estimated from the lifetime of a solid sample (1 μs, $\tau_{rad} = 0.36$ ms) amounts to 0.27% (Shavaleev et al., 2005).

Another example of bifunctional bridging ligand is the diplatinum alkynyl chromophore depicted on fig. 93 (Xu et al., 2006). It is based on an acetylide-functionalized diimine (a commonly used building block for the design of multicomponent assemblies featuring redox and/or photoactive units) and the coordination sphere of the Pt^{II} ion is completed by binding to bridging bis(diphenylphosphinomethane) (dppm) units. It forms 5d–4f heterometallic arrays with a nuclearity of four when reacted with luminescent lanthanide β-diketonates (hfa in this case, Ln = Nd, Eu, Yb). If the bipyridine unit is replaced with a 1,10-phenanthroline group, hexametallic arrays are isolated with the same lanthanide β-diketonates. In the case of Pt_2Eu_2, the association constant for the binding of the Eu^{III} diketonate to the bipyridyl sites is 3×10^7 M^{-2}. According to X-ray analysis, the Pt_2Nd_2 array is composed of [Pt_2(μ-dppm)$_2$(bpy-ethynyl)$_4$] units incorporating [Nd(hfa)$_3$(H_2O)$_2$] complexes through 2,2′-bipyridyl chelates; they are stabilized by strong intramolecular hydrogen bonds and the intramolecular Pt···Nd distance is 8.8 Å, that is favorable to dipole–dipole (through space) energy transfers. Upon irradiation in the diplatinum ^{3}MLCT band (250–450 nm), all of the isolated complexes exhibit metal-centered emission, both in the solid state and in methylene chloride. Lifetimes of the Nd($^4F_{3/2}$) level are 0.21 (Pt_2Nd_2) and 0.49 μs (Pt_2Nd_4) in the solid state (emission in solution is too weak for lifetime measurements), while Yb($^2F_{5/2}$) lifetimes amount to 11–13 μs for the two edifices, either in the solid state or in solution. The quantum yields of the solid samples calculated from the lifetimes, with $\tau_{rad} = 0.25$ ms (Nd) and 2 ms (Yb), are 0.08% for Pt_2Nd_2, 0.20% for Pt_2Nd_4, and 0.57 and 0.64% for the corresponding Yb^{III} complexes.

Building on their technique for assembling [2]pseudorotaxanes through anion templation, P.D. Beer and S. Faulkner have designed supramolecular d–f heterometallic assemblies in which the luminescence of the lanthanide ion is sensitized by a d-transition metal ion (fig. 94).

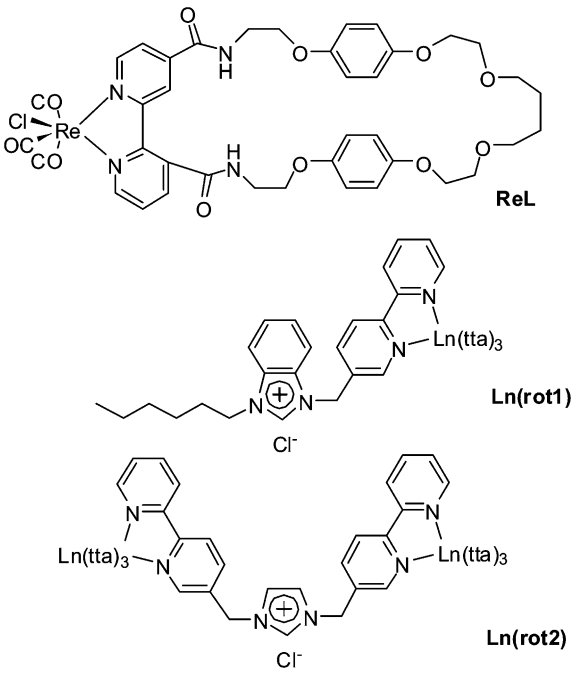

Fig. 94. Macrocycle (top) used to host the lanthanide-containing pseudo-rotaxane threads (middle and bottom) (Sambrook et al., 2006).

The threading component is comprised of a benzimidazolium or an imidazolium chloride stoppered by a tris(thenoyltrifluoroacetonate) lanthanide unit. The rhenium-containing macrocycle **ReL** contains a rhenium(I) bipyridyl group as sensitizer, in combination with an amide cleft for chloride recognition and electron rich hydroquinone groups for potential π–π stacking interactions. It allows the penetration of the benzimidazolium or imidazolium chloride into its cavity and therefore the formation of **Ln(rot)** $\subset$ **ReL** (Ln = Nd, Gd, Yb) occurs through anion recognition and is signaled by sensitized NIR emission (Sambrook et al., 2006). Association constants are log $K_a = 4.2$ and 4.8 in methylene chloride for **Gd(rot1)** $\subset$ **ReL** and **Gd(rot2)** $\subset$ **ReL**, respectively. Upon complexation to the Gd^{III} threads, the lifetime of the $Re^{I}(^3MLCT)$ emission increases from 31 ns for the free macrocycle to 215 ns. Replacement of Gd^{III} by Nd^{III} or Yb^{III} threads results in a severe quenching of the rhenium emission, when compared with the emission of the Gd^{III} analogs. This evidences energy transfer from the $Re^{I}(^3MLCT)$ state located at 25 900 cm^{-1} onto the emissive Ln^{III} states. The lifetimes of the latter amount to 0.8 µs for $Nd(^4F_{3/2})$ and 11.1 µs for $Yb(^2F_{5/2})$.

3.3.4. *d-Transition metal ions for extending the apparent Ln^{III} lifetime*

When the donor d-transition metal ion and the accepting Ln^{III} ion lie relatively close, typically at distances <5 Å, several mechanisms are operative to achieve the energy transfer,

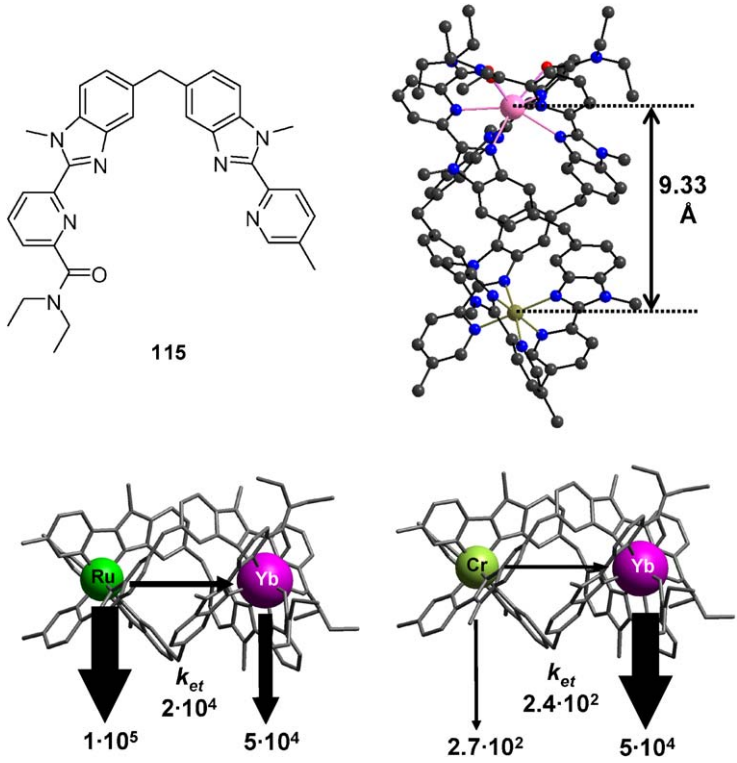

Fig. 95. (Top left) Ditopic ligand for the self-assembly of discrete M–Ln edifices. (Top right) Structure of $[CrYb(\mathbf{115})_3]^{6+}$, redrawn from (Imbert et al., 2003). (Bottom) Schematic representation of the energy migration paths occurring in the RuYb and CrYb edifices, with associated rate constants in s^{-1} (Torelli et al., 2005).

particularly in the case of Yb^{III} for which both an electron exchange pathway and phonon-assisted processes are feasible. The possible simultaneous occurrence of these mechanisms in the same heterobimetallic edifice, combined with the difficulty in separating the exchange from the multipolar contributions to the ligand-to-metal energy transfer limits the efficiency of molecular programming and the tuning of the electronic properties of the 4f ion, henceforth intensity of its NIR luminescence. In this context, discrete nd–4f heterobimetallic edifices have been designed and produced by strict self-assembly of a pentadentate ditopic ligand **115** based on benzimidazolepyridine units. The molecule belongs to a class of compounds comprising both hexadentate and pentadentate synthons, which self-assemble under stoichiometric conditions to produce Ln_2L_3, $LnLn'L_3$ or $MLnL_3$ triple-stranded helicates with approximate D_3 symmetry (Bünzli and Piguet, 2002). In these edifices, the three ligands are arranged in a head-to-head-to-head fashion (*HHH*), that is, the same three coordinating units are connected to the same metal ion. In the structure shown in fig. 95, Yb^{III} is 9-coordinate by six nitrogen atoms and three oxygen atoms from the three amide groups, in an approximate tricapped trig-

onal prismatic geometry, whereas the smaller Cr^{III} ion is 6-coordinate in a slightly distorted octahedral arrangement. The intermetallic distance of 9.33 Å ensures that the energy transfer mechanism is mainly of dipole–dipolar origin.

When one metal ion is used as a donor for sensitizing the emission of a second accepting metal ion, the characteristic lifetimes τ of their excited states, which are related to their deactivation rates by $\tau = k^{-1}$, are affected by the metal-to-metal communication process. This situation can be simply modeled for the special case of an isolated d–f pair, in which the d-block chromophore (M) sensitizes the neighboring lanthanide ion (Ln) thanks to an energy transfer process described by the rate constant $k_{et}^{M,Ln}$. In absence of energy transfer, excited states of the two isolated chromophores decay with their intrinsic deactivation rates k^{M} and k^{Ln}, respectively, which provides eqs. (32) and (33) yielding eqs. (34) and (35) after integration:

$$d\big[M^*(t)\big]/dt = -\big(k_{et}^{M,Ln} + k^{M}\big) \cdot \big[M^*(t)\big]^2, \tag{32}$$

$$d\big[Ln^*(t)\big]/dt = k_{et}^{M,Ln} \cdot \big[M^*(t)\big] - k^{Ln}\big[Ln^*(t)\big], \tag{33}$$

$$\big[M^*(t)\big] = \big[M^*(0)\big] \cdot e^{-(k_{et}^{M,Ln}+k^{M})\cdot t}, \tag{34}$$

$$\big[Ln^*(t)\big] = \big[M^*(0)\big] \cdot \frac{k_{et}^{M,Ln}}{k^{Ln} - (k_{et}^{M,Ln} + k^{M})} \cdot \Big(e^{-(k_{et}^{M,Ln}+k^{M})\cdot t} - e^{-k^{Ln}\cdot t}\Big). \tag{35}$$

The decay rate of the excited state of the d-block donor M^* increases when it transfers energy to an acceptor. The experimental decay rate thus corresponds to the sum of the two deactivation rate constants and translates into a reduced lifetime:

$$k_{obs}^{M} = k^{M} + k_{et}^{M,Ln}, \quad \tau^{M} = \big(k_{obs}^{M}\big)^{-1} = \big(k^{M} + k_{et}^{M,Ln}\big)^{-1}. \tag{36}$$

Interpretation of eq. (35) is less straightforward, because the magnitude of $k_{et}^{M,Ln}$ controls the feeding rate of the excited state of the acceptor. Therefore, the variation of [Ln*] over time, after initial excitation of the donor, strongly depends on the relative magnitudes of the rate constants k_{obs}^{M} and k^{Ln} and two limiting cases can be described:

(i) $k_{obs}^{M} > k^{Ln}$

The Ln^* level is almost completely populated before any significant Ln-centered deactivation occurs. As a consequence, the experimental Ln-centered deactivation rate k_{exp}^{Ln} mirrors that found in absence of metal-to-metal communication, k^{Ln}. Introducing the specific condition $k_{obs}^{M} \gg k^{Ln}$ in eq. (35) produces eq. (37), whereby the time dependence of the decay profile indeed corresponds to $k_{exp}^{Ln} = k^{Ln}$:

$$\big[Ln^*(t)\big] = \big[M^*(0)\big] \cdot \frac{k_{et}^{M,Ln}}{k_{et}^{M,Ln} + k^{M}} \cdot e^{-k^{Ln}\cdot t}. \tag{37}$$

This situation is encountered for a large number of d–f pairs, because the intrinsic deactivation rates of the d-block donor k^{M} are often considerably larger than the deactivation of the Ln-centered 4f excited states. For instance, it occurs for the Ru → Yb transfer in $[RuYb(\mathbf{115})_3]^{5+}$ (fig. 95). As expected, the experimental decay rate k_{obs}^{Ru} =

1.2×10^5 s^{-1} is larger compared to $k^{Ru} = 1.0 \times 10^5$ s^{-1} (in [RuGd(**115**)$_3$]$^{5+}$). Since $k^{Ru}_{obs} = 1.2 \times 10^5$ s^{-1} > $k^{Yb} = 5 \times 10^4$ s^{-1} (in [ZnYb(**115**)$_3$]$^{5+}$), eq. (35) predicts that the experimental Yb-centered decay rate recorded in [RuYb(**115**)$_3$]$^{5+}$ should roughly mirror k^{Yb}, and this is indeed observed with an experimental value of $k^{Yb}_{exp} = 4.4 \times 10^4$ s^{-1}.

(ii) $k^{M}_{obs} < k^{Ln}$

Here, the Ln-centered excited state relaxes almost instantaneously as long as it is slowly populated by the donor and deactivation of the d-block ion controls the overall deactivation process. As a consequence, the experimental Ln-centered deactivation rate k^{Ln}_{exp} should mirror k^{M}_{obs}. Introduction of the condition $k^{M}_{obs} < k^{Ln}$ into eq. (35), provides a simplified eq. (38), which demonstrates that the time dependence of the decay profile would indeed correspond to $k^{Ln}_{exp} = k^{M}_{obs}$:

$$\left[Ln^*(t)\right] = \left[M^*(0)\right] \cdot \frac{k^{M,Ln}_{et}}{k^{Ln}} \cdot e^{-(k^{M,Ln}_{et} + k^{M}) \cdot t} = \left[M^*(0)\right] \cdot \frac{k^{M,Ln}_{et}}{k^{Ln}} \cdot e^{-k^{M}_{obs} \cdot t}. \qquad (38)$$

The replacement of Ru^{II} with Cr^{III} as the donor in [CrYb(**115**)$_3$]$^{6+}$ illustrates this second situation. The combination of the intrinsic deactivation rate of the Cr-centered donor levels $k^{Cr} = 2.7 \times 10^2$ s^{-1} (in [CrGd(**115**)$_3$]$^{6+}$), with the rate of energy transfer $k^{Cr,Yb}_{et} = 2.4 \times 10^2$ s^{-1} gives $k^{Cr}_{obs} = k^{Cr} + k^{Cr,Yb}_{ET} = 5.1 \times 10^2$ s^{-1}. This remains small compared to the intrinsic rate of deactivation of Yb($^2F_{5/2}$) ($k^{Yb} = 5 \times 10^4$ s^{-1} in [ZnYb(**115**)$_3$]$^{5+}$), and therefore $k^{Yb} \gg k^{M}_{obs}$ (fig. 95). Experimentally, the decay rate of the Yb($^2F_{5/2}$) level amounts to $k^{Yb}_{exp} = 5.1 \times 10^2$ s^{-1}, which perfectly mirrors the slow deactivation of the Cr^{III} chromophore. These rate constants can be transformed into characteristic excited lifetimes, thus leading to $\tau^{Yb}_{exp} = 23$ µs, when Yb^{III} is sensitized by Ru^{II} in [RuYb(**115**)$_3$]$^{5+}$, and $\tau^{Yb}_{exp} = 1960$ µs (1.96 ms) when Yb^{III} is sensitized by Cr^{III} in the isostructural complex [CrYb(**115**)$_3$]$^{6+}$. Such apparent extension of the Ln-centered NIR luminescence, which is also observed for Nd^{III} (Imbert et al., 2003), by two or three orders of magnitude (from the microsecond to the millisecond range) may be valuable for improving the sensitivity of time-gated homogeneous luminescent immunoassays, provided a judicious choice of the donor chromophore is made.

3.3.5. *4f-Transition metal ions as luminescence sensitizers*

Energy transfers between lanthanide ions are well documented, either in solid state, for instance for the sensitization of laser materials, or in solution of metal-containing proteins in which the replacement of Ca^{II} or Zn^{II} with different Ln^{III} ions allows the determination of the metal-to-metal distances by measuring the yield of energy transfer. Diffusion limited energy transfer from Tb^{III} to NIR emitting ions, particularly Nd^{III} (Bünzli and Vuckovic, 1983; Kandpal et al., 1979) and Er^{III} (Kandpal and Tripathi, 1979), in organic solvents such as acetone, acetonitrile, dmf, or dmso is also well documented. On the other hand, energy transfer between 4f ions in discrete molecular assemblies has been less studied because of the lack of suitable synthetic methods for producing pure heteropolymetallic complexes; as a consequence, studies have often been performed on statistical mixtures (Froidevaux and Bünzli,

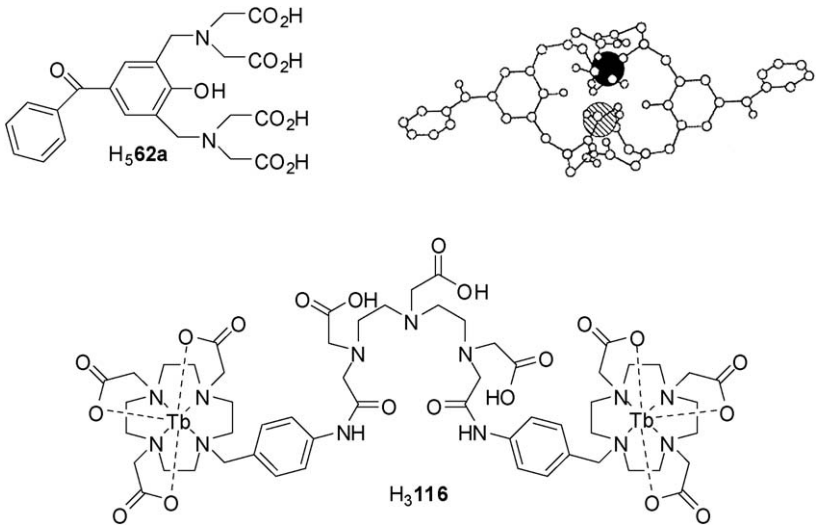

Fig. 96. (Top) Polyaminocarboxylic acid for producing $Ln^{III}Ln^{III}$ dimeric species, with a calculated structure; reproduced from (Ala-Kleme et al., 2000). (Bottom) Bis(do3a)-modified dtpa for sensitization of Yb^{III} by convergent energy transfers from two Tb^{III} ions.

1994; Piguet et al., 1993). One example pertains to the sensitization of Nd^{III} and Yb^{III} by energy transfer from Tb^{III} in dimeric polyaminocarboxylates. The dimeric species $Tb^{III}Tb^{III}$, $Ln^{III}Ln^{III}$, and $Tb^{III}Ln^{III}$ (Ln = Y, Nd, Dy, Yb) were prepared by diluting appropriate amounts of Ln^{III} ions in an equimolar solution of the potentially heptadentate ligand 2,6-bis[*N*,*N*-bis(carboxymethyl)-aminomethyl]-4-benzoylphenol, H_5**62a** (fig. 96), adjusted to pH 9.2 in a borate buffer in order to ensure complete deprotonation of the ligand (Ala-Kleme et al., 2000). The solutions were placed in a quartz cuvette containing an oxide-covered aluminum working electrode having a surface of ≈0.8 cm^2 and a thickness of ≈4 nm, as well as a platinum counter electrode; peroxodisulfate was added. Electrochemically generated luminescence was observed for Tb^{III} and Dy^{III}. Intensity of the Tb^{III} luminescence progressively decreases when the Ln^{III} (Ln = Nd, Yb) proportion is increased in the Tb^{III}/Ln^{III} systems, clearly pointing to energy transfer onto the NIR emitting ions. The corresponding luminescence was however not observed due to instrumental limitations.

It is only recently that S. Faulkner took advantage of the kinetic inertness of Ln^{III} cyclen macrocyclic complexes for producing the neutral pure heterotrimetallic compound [Yb(**116b**)] (fig. 96) in which convergent directional intramolecular $Tb^{III} \rightarrow Yb^{III}$ processes are responsible for the sensitization of the NIR $Yb(^2F_{5/2})$ emission (Faulkner and Pope, 2003). The complex is stable in water and according to the lifetime measured (1.83 and 4.22 μs in H_2O and D_2O, respectively), the hydration number of Yb^{III} is close to zero ($q_{Yb} = 0.2$) while $q_{Tb} = 1.4$ is obtained, in line with its complexation by the heptadentate cyclen derivative.

The $Yb(^2F_{5/2})$ lifetime is independent of the excitation mode, through the aryl chromophore or through the Tb^{III} ion (488 nm).

3.4. *NIR luminescence in extended structures and various materials*

The aim of this chapter is to review NIR-emitting *molecular* edifices. If the last complexes discussed belong to this category, while completely inorganic Nd:YAG materials are clearly excluded, there is a range of compounds and materials which are between these two aspects of lanthanide science. They include extended mono-dimensional or poly-dimensional structures, both inorganic or organic, composite porous materials, and nanoparticles. Since these compounds are more and more tested for practical applications, either in telecommunications, lighting, or medical diagnostic (bioanalyses and imaging), we discuss them here with varying extent of coverage, the more inorganic-like systems being less dealt with. We have also added a section on ionic liquids, another emerging field of today's chemistry.

3.4.1. *Coordination polymers*

The assembly of metal–organic infinite frameworks via the coordination of metal ions by multi-functional bridging ligands provides the possibility of bringing metal ions in close proximity, henceforth facilitating metal-to-metal communications, as well as of increasing the number of metal ions per unit cell, improving the performance of functional materials. Introduction of lanthanide ions in one- (1D-), two- (2D-), or three- (3D-) dimensional networks is expected to be more difficult to control than their d-block metal analogs due to the higher coordination numbers of lanthanide ions and the absence of strong specific steric requirements. On the other hand, the inherent flexibility of lanthanide coordination geometry leads to the synthesis of unprecedented structures.

The connecting ligand dictates, to some degree, the dimensionality of the array. For instance, cyanide or d-metal cyanides help constructing 1D arrays; a judicious combination of small ligands such as cyanide and carbonyl results in 2D grid-like materials, while benzene polycarboxylates or derivatized bipyridines often lead to 3D arrangements (Bünzli and Piguet, 2002). Although the number of reported lanthanide-containing coordination polymers (sometimes referred to as metal–organic frameworks, MOF) is steadily increasing (Guillou and Daiguebonne, 2004), relatively few have been specifically designed for NIR luminescence and all of these examples are fairly recent.

In order to bring Ru^{II} close to an NIR-emitting Ln^{III} ion, M. Ward and coworkers (Davies et al., 2005b; Miller et al., 2004) have co-crystallized the cyanoruthenate chromophore K_2(**117**) ($K_2[Ru(CN)_4(bpy)]$, fig. 97) with lanthanide chlorides (Ln = Pr, Nd, Gd, Er, Yb) in water, which afforded oligomers and networks in which the $[Ru(CN)_4(bpy)]^{2-}$ unit is connected to the lanthanide ion via Ru–CN–Ln bridges. Two main structural types of coordination polymers crystallize. In the first one, depicted in the middle of fig. 97, the chromophoric unit is connected to a single Ln^{III} ion by individual cyanide bridges, yielding trimetallic fragments, $\{[Ru(CN)_4(bpy)]_2[Ln(H_2O)_x][K(H_2O)_y]\cdot zH_2O\}_n$ (x = 7, 6, 6 for Ln = Pr, Er, Yb, respectively), denoted as RuLnK. The second type contains 2D sheets of interconnected, cyanide-bridged Ru_2Ln_2 squares and corresponds to the general formula

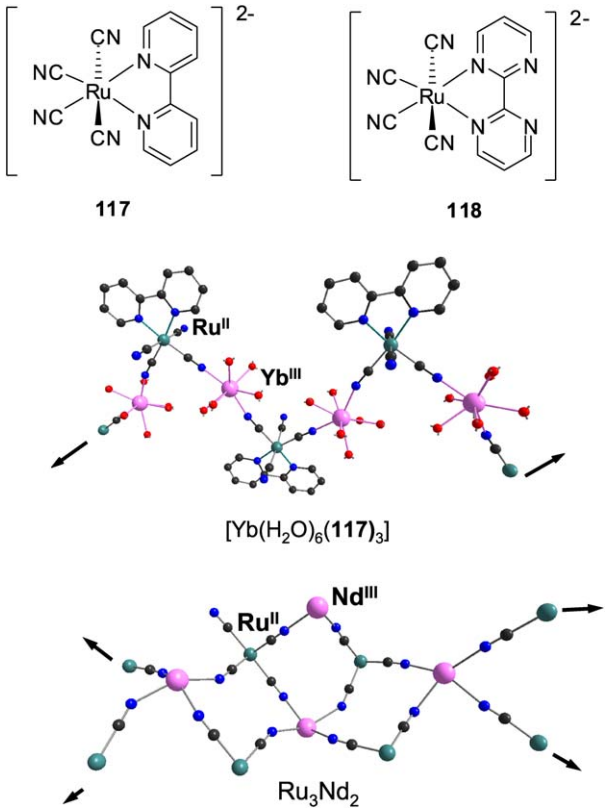

Fig. 97. (Top) Ru^{II} synthons for building coordination polymers; (middle) Ru–CN–Yb bridged coordination polymer. (Bottom) Sketch of the 2D sheet structure in the Ru_3Nd_2 compound. Redrawn from (Davies et al., 2005b; Miller et al., 2004).

$\{[Ru(CN)_4(bpy)]_3[Ln(H_2O)_4]_2{\cdot}zH_2O\}_n$ (Ln = Nd, Gd); it is denoted Ru_3Ln_2. The Ru^{II}-based luminescence observed upon excitation at 337 nm in the Ru_3Gd_2 largely fades off in the networks containing NIR-emitting Ln^{III} ions with concomitant appearance of the typical 4f–4f transitions, even the Pr^{III} ($^1D_2 \rightarrow {}^3F_4$) transition at 1.01 μm. For solid state samples, the ^{3}LMCT lifetime decreases from 550 ns in the Ru_3Gd_2 compound to 197 ns in Ru_2YbK, 76 ns in Ru_2ErK, 22 ns in Ru_2PrK and 5 ns in Ru_3Nd_2. The Ru^{II}-to-Ln^{III} energy transfer rates could be estimated and range from 3×10^6 s^{-1} in Ru_2YbK, to 1×10^7 s^{-1} in Ru_2ErK, 4×10^7 s^{-1} in Ru_2PrK, and 2×10^8 s^{-1} in Ru_3Nd_2. These fast rates are explained by the vicinity of the Ru–Ln pairs (5.4–5.5 Å in RuLnK and 5.4–5.7 Å in Ru_3Ln_2 polymers). Indeed they are about two orders of magnitude larger than those reported for the molecular complexes with receptors H_3**104**–H_6**105** (fig. 88). The increasing order of transfer rates, Nd > Pr > Er > Yb can further be rationalized on the basis of the overlap of the f–f absorption bands with the emission spectrum from the donor ^{3}MLCT state.

In an extension of this work, bipyridine in $[Ru(CN)_4(bpy)]^{2-}$ has been replaced with 2,2′-bipyrimidine (bpym, see formula **118**, fig. 97) for two reasons: bpym has a lower triplet state than bpy and its two additional nitrogen atoms may coordinate to Ln^{III} ions (Herrera et al., 2006a). Simple evaporation of an aqueous solution containing $K_2[Ru(CN)_4(bpym)]$ and hydrated $Ln(NO_3)_3$ in a 1:5 molar ratio results in the crystallization of two types of isostructural coordination polymers: (i) $\{[Ru(CN)_4(bpym)][Ln(NO_3)(H_2O)_5]\}_n$ for Ln = Nd, Sm, Gd (denoted RuLn), in which 1D helical chains along the *c* axis consist of alternating $[Ru(CN)_4(bpy)]^{2-}$ and $[Ln(NO_3)(H_2O)_5]$ units linked by cyanide bridges, and (ii) $\{[Ru(CN)_4(bpym)]_2[Ln(NO_3)(H_2O)_2][Ln(NO_3)_{0.5}(H_2O)_{5.5}](NO_3)_{0.5}(H_2O)_{5.5}\}_n$ for Ln = Er, Yb (denoted Ru_2Ln), which form complicated 2D networks. Sensitized NIR emission from Nd, Er, and Yb was observed for all of the crystalline samples grown in D_2O (to minimize quenching by O–H vibrations) upon excitation either at 337 nm or at 430 nm (^{1}MLCT state). For Nd^{III}, the lifetime of the lanthanide-based excited state is about the same in RuNd and Ru_2Nd (64 and 66 ns at room temperature), while it is much longer in RuYb (587 ns) than in Ru_2Yb (245 ns). For Er^{III}, the decay had to be fitted with a bi-exponential function (τ_{obs} = 43 and 300 ns). The ^{3}MLCT lifetime of the donor amounts to 80 ns, which means that the energy transfer rates are fast; they have been estimated to be larger than 10^8 s^{-1}, that is somewhat faster when compared to the rates determined for the coordination polymers based on the $[Ru(CN)_4(bpy)]^{2-}$ donor. A similar coordination polymer based on hexaaza-triphenylene (hat) with overall formula $\{Nd_2[Ru(CN)_4]_3(\mu^3\text{-hat})\cdot 23H_2O\}_n$ contains 9-coordinate Nd^{III} ions bound to five water molecules and four cyanide ions. It displays strong MLCT absorption and transfers energy onto the 4f-ion, the lifetime of the $^4F_{3/2}$ level being around 100 ns (Herrera et al., 2006b). Although interesting from the point of view of energy transfer efficiency, these materials however present a severe drawback in that several water molecules remain coordinated on the lanthanide ion and as a result, nonradiative deactivations stay important.

The influence of fluorination on Er^{III} luminescence has been demonstrated with 1,4-benzenedicarboxylate (bdc) and 2,3,5,6-tetrafluoro-1,4-benzenedicarboxylate (dbc-F_4) organic frameworks (Chen et al., 2006). A mixture of hydrated erbium nitrate and the desired dicarboxylic acid in dimethylformamide/ethanol is introduced into a vial which is sealed and heated for 24 h at 80 °C, yielding light purple crystals. The structure of $[Er_2(bdc)_3(dmf)_2(H_2O)_2]\cdot H_2O$ consists in bimetallic Er^{III} units as building blocks, bridged by two carboxylates from two bdc anions; the coordination sphere of each Er^{III} ion is completed through coordination from two bidentate carboxylates and terminal dmf and water molecules. The bimetallic units are connected by six bdc anions and form a 3D distorted primitive cubic framework. The structure of $[Er_2(bdc\text{-}F_4)_3(dmf)(H_2O)]\cdot dmf$ is different, consisting in a 1D rod-like framework, but the number of Er^{III} ions per unit volume, 1.14 per 1000 $Å^3$, is similar when compared to the un-fluorinated coordination polymer (1.24), so that comparing emission intensities has some meaning: the fluorescence intensity is four times larger for the fluorinated compound.

Amino–carboxylic and phosphonic acids are known to form open frameworks (i.e. porous materials), particularly with first-row transition metal ions. Lanthanide diphosphonates with 3D pillared-layer structure are also known and several classes of ligands such as sim-

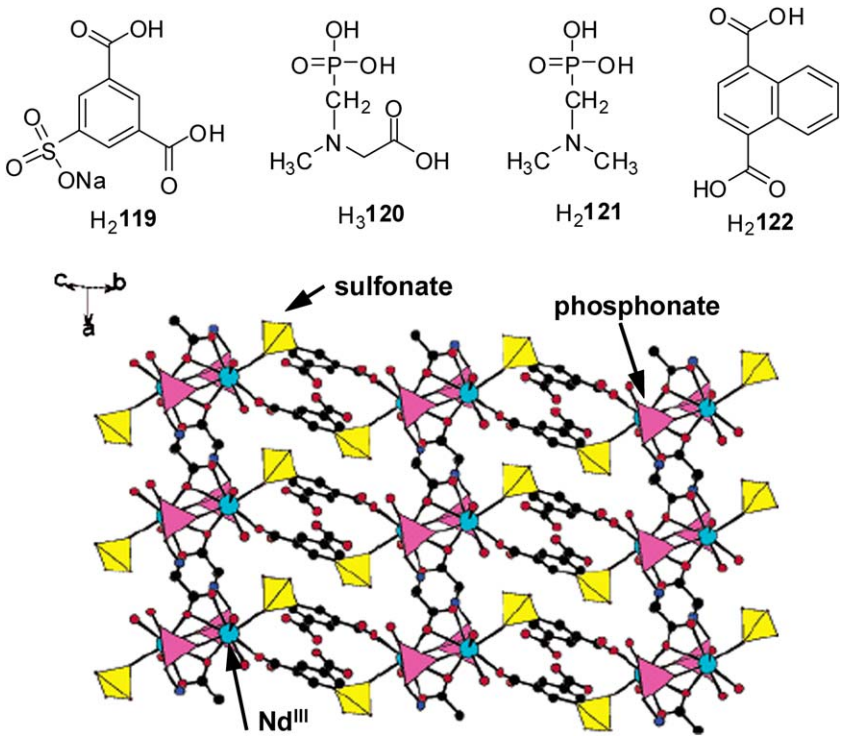

Fig. 98. (Top) Ligands based on sulfonic, phosphonic and carboxylic acids. (Bottom) ⟨011⟩ layer in [Nd(**119**)(H_2**120**)(H_2O)$_2$]·H_2O; reproduced with permission from (Song et al., 2004).

ple aromatic derivatives, aminoacids, calixarenes and cyclens have been decorated with phosphonate groups. Jiang-Gao Mao and his collaborators have chosen the sodium salt of 5-sulfoisophthalic acid (H_2**119**, fig. 98) and one carboxylic-phosphonic acid, *N*-(phosphonomethyl)-*N*-methylglycine (H_3**120**) to produce, by hydrothermal methods, phosphonate–sulfonate hybrids of general formula [Ln(**119**)(H_2**120**)(H_2O)$_2$] (Ln = La, Pr, Nd, Gd) and having an isomorphous layered architecture (see fig. 98 for an example). While the Gd compound possesses a single emission band at 416 nm arising from the ligand states, the Nd coordination polymer displays, in addition, its typical emission from the $^4F_{3/2}$ state, the intensity of which is much enhanced upon de-hydration of the hybrid material (Song et al., 2004). Replacing 5-sulfoisophthalate with oxalate (ox), results in the crystallization of three series of tridimensional networks with the following formulae: {[Ln(ox)(H_2**120**)]·0.5H_2O}$_n$ (Ln = Nd, Eu, Gd), {[Ln_4(ox)$_5$(**121**)$_2$(H_2O)$_4$]·2H_2O}$_n$ (Ln = La, Nd), and {[Ln_3(ox)$_4$(**121**)(H_2O)$_6$]·6H_2O}$_n$ (Ln = Gd, Er). Both Nd^{III}-containing materials, as well as the Er^{III} compound are luminescent, and the emission intensity again increases upon removal of the lattice water molecules. The advantages of these materials are their high

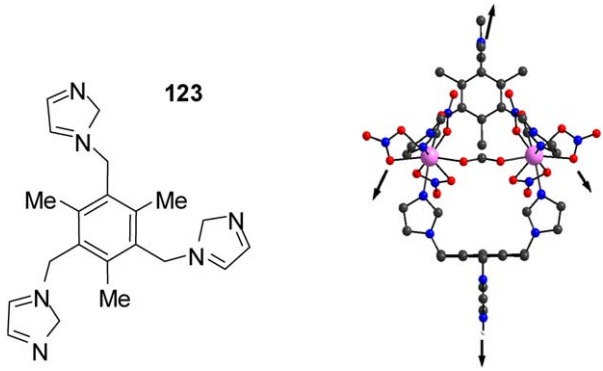

Fig. 99. (Left) Tripodal ligand for the building of a lanthanide–organic framework. (Right) Yb^{III} dimeric unit with arrows indicating the directions of the H-bonds in the 2D network. Redrawn from (Zhang et al., 2006).

solubility and good crystallinity due to the introduction of the oxalate anion (Song and Mao, 2005).

Aromatic polycarboxylates easily form 2D or 3D networks, for instance $[Nd_2(\mathbf{122})_3(dmf)_4]\cdot H_2O$ which present a 2D structure in which the 1,4-naphthalenedicarboxylate anions link Nd^{III} ions of two adjacent double chains keeping them at a short distance of about 4.1 Å (J. Yang et al., 2006). This allows up-conversion to take place, albeit with very low efficiency: a blue emission is seen at 449.5 nm upon excitation at 580 nm (corresponding to the $^4G_{5/2} \leftarrow {}^4I_{9/2}$ transition) and from the structure and the magnetic properties an energy-transfer up-conversion mechanism involving no excited state absorption is more likely.

Another way of realizing extended networks is to program weak interactions between discrete complex molecules, for instance hydrogen bonds or π–π stacking interactions. One example of such a network is given by W.-Y. Sun et al. (Zhang et al., 2006) who reacted the tripodal ligand 1,3,5-tris(imidazole-1-ylmethyl)-2,4,6-trimethylbenzene (**123**, fig. 99) with hydrated lanthanide nitrate in presence of triethylorthoformate in methanol and obtained bimetallic complexes $[Ln_2(NO_3)_6(\mu\text{-}HCO_2)(\mu\text{-}\mathbf{123})(\mu\text{-}\mathbf{123}H)]\cdot 3MeOH$ (Ln = Eu, Gd, Tb, Dy, Er, and Yb). The structure of the Gd^{III} compound reveals dimeric species in which the two metal ions are connected by bidentate bridging **123** units (fig. 99) and the formate ions. The tripodal ligand uses only two of the three imidazole groups, the third one being uncoordinated; one ligand adopt a *cis, cis, cis* conformation while the other one is protonated with a *cis, trans, trans* conformation. The dimeric units are connected into a 2D network by hydrogen bonds between the nitrate O-atoms and the C–H bonds of the methyl groups of the anchor, as well as between the protonated NH^+ and the unprotonated amine function of an uncoordinated imidazole (fig. 99); according to the authors, a further much weaker interaction between benzene rings ensures a 3D dimensionality (distance between aromatic cores ≈3.8–4 Å, far from the generally agreed upon distance of 3.5 Å). The cavity holes host three methanol molecules (not shown on fig. 99). Near-infrared emission is reported for the Yb^{III} complex 1 mM in dmso-d_6.

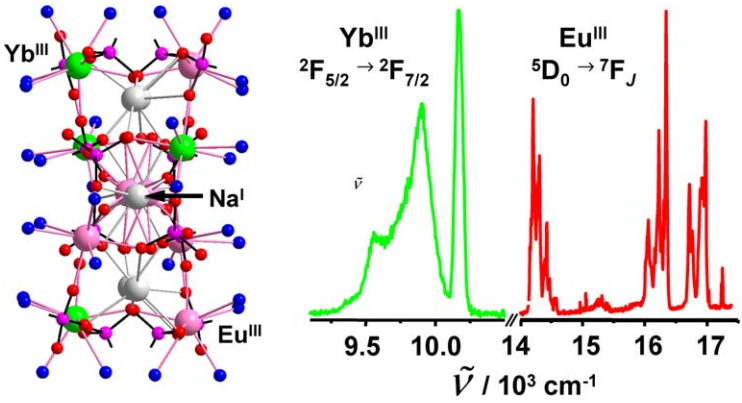

Fig. 100. (Left) Structure of the Eu ⊂ $Na_6Eu_{8-x}Yb_x$ cluster ($x = 4$) and (right) dual emission in the visible and NIR. Redrawn from (Comby et al., 2006c).

3.4.2. *Inorganic clusters*

The exploration of lanthanide-containing discrete polymetallic frameworks with high and controlled nuclearity is a field which is not yet mature, except maybe in the cases of dendrimeric structures for MRI contrast agents (Pierre et al., 2005) and of metallacrowns (Stemmler et al., 1999). Such clusters have, however, large potential interest as precursors for doped materials or for studying (and implementing) metal–metal interactions, e.g. energy transfers or magnetic interactions (Zaleski et al., 2004). Research on these clusters has usually focused in obtaining wheel- or cage-like edifices, some of them acting as supramolecular receptors for anions or cations. They can be assembled using different synthetic strategies, the key being to avoid the extension of the structure into a coordination polymer and, possibly, to control the nuclearity (i.e. the number of metal ions in the core, m) or the global complexity $m + n$ of $[Ln_mL_n]$ (Senegas et al., 2005). This can be achieved with simple polydentate ligands leaving some coordination vacancies around the metal ion, such as 5′-methyl-2,2′-bipyridyl-6-phosphonic acid (H_2L). Monoclinic crystals of composition $[Na_6Ln_9L_{16}(H_2O)_4]\cdot(OH)\cdot 47H_2O$ (Ln = Eu, Gd, Tb, Er) crystallize upon slow diffusion of acetone into aqueous solutions with a 1:3 Ln^{III}:H_2L stoichiometric ratio and adjusted to pH 7.4 (Comby et al., 2006c). The crystallization process is strictly controlled and any change in the experimental conditions fails to produce the desired material. The clusters contains eight eight-coordinate peripheral Ln_p^{III} ions arranged in the corners of two parallel parallelepipeds; the ninth Ln^{III} ion lies in the middle of the assembly, is also eight-coordinate, but four water molecules are bound in its inner coordination sphere. The Na_6Ln_9 clusters are held together by an intricate network of bridging phosphonate groups and sizeable π–π stacking interactions.

Mixed clusters Eu ⊂ $Na_6Eu_{8-x}Yb_x$, with $x = 4$ or 5 (see fig. 100), in which the central site is occupied by Eu^{III} whereas the Yb^{III} ions are statistically distributed in the peripheral sites, are isostructural with the Na_6Ln_9 species. They display dual luminescence from Eu^{III} and Yb^{III}, an interesting property despite the fact that the quantum yield of the Yb^{III} luminescence

remains modest at $0.22 \pm 0.02\%$ while the $^2F_{5/2}$ lifetime amounts to 9.3 ± 0.1 μs at room temperature (the quantum yield of the Eu^{III} luminescence is $20 \pm 2\%$).

Ytterbium luminescence has also been seen for a nonametallic cluster assembled from hexylsalicylate (hesa) and with overall formula $H_{10}[Yb_9(hesa)_{16}(\mu\text{-}O)_{10}(NO_3)]$. The cluster has two fused square-pyramidal pentametallic units assembled via an apical metal ion. The two square pyramids are twisted 45° and the cluster core is stabilized by hydroxide bridges. The luminescence decay of the Yb^{III} cluster is bi-exponential, with lifetimes of 0.2 and 0.6 μs, reflecting the two types of cations (Manseki et al., 2006).

Polyoxometalates are important reagents in analytical chemistry and they also find applications in catalysis, molecular biology, materials sciences, and medicine. A recent study of nine Nd^{III} polyoxometalates (POM) showed their aqueous 5 mM solutions to be weakly luminescent, whereas no luminescence at all is seen for the aquo ion. In particular, the bis(POM) complexes better protect the Nd^{III} ion from nonradiative deactivations, for instance $\tau(^4F_{3/2}) = 411 \pm 6$ ns for $[Nd(PW_{11}O_{39})_2]^{11-}$ and 67 ± 2 ns for $[Nd(As_4W_{40}O_{140})]^{25-}$ (But et al., 2005).

The 1.5 μm emission line of Er^{III} is useful for amplifying optical fiber signals. Its performance depends on a range of properties, stimulated emission cross section, effective bandwidth of the emission band, and fluorescence lifetime, i.e. intrinsic quantum yield. As seen previously, silica matrices in which the ion is simply doped have the disadvantage that the doping percentage must remain low to avoid concentration quenching; purely inorganic compounds are sparingly soluble in apolar solvents used to produce polymer-based devices. Organic complexes can transfer efficiently energy onto Er^{III} but the presence of numerous deactivating vibrational modes, mainly the energetic O–H, N–H, or C–H vibrations, is difficult to avoid without deuterating or fluorinating the molecules at high cost, and even in these cases, the result is not always rewarding. As an alternative, J.G. Brennan has proposed cluster compounds which are soluble in organic solvents and are relatively devoid of high-energy vibrational modes, while providing a reasonable concentration of Ln^{III} ions per unit volume. The most successful Ln cluster syntheses rely on chalcogenide derivatives, such as $Ln(EPh)_3$, which are oxidized by elemental E (E = S, Se, Te). Common to all the clusters is the presence of at least one ancillary, neutral ligand binding the Ln^{III} ion and therefore allowing the formation of discrete architectures.

In one synthesis, metallic Er, $PhSe_2Ph$, iodine, and mercury were combined in thf at room temperature; after all the lanthanide metal had reacted, elemental sulfur was added. Pink crystals of the hexametallic $[Er_6S_6I_6(thf)_{10}]\cdot 6thf$ cluster (**Er_6S_6**) crystallized out of the solution. The compound has a double cubane framework, with one face of an Er_4S_4 cubane cluster capped by an Er_2S_2 layer. Single terminal iodides are connected to all six Er^{III} ions while the remaining octahedral coordination sites are occupied by thf molecules (fig. 101). When the starting $Ln{:}I_2$ ratio is increased from 1:0.5 to 10:3 while simultaneously replacing S with a mixture of S and Se, a yellow decametallic cluster $[Er_{10}S_6(Se_2)_6I_6(thf)_{14}]\cdot 3thf$ (**$Er_{10}S_6$**) crystallized, in which the central Er_6S_6 core is capped on two opposite sides by $Er_2(Se_2)_3$ units (Kornienko et al., 2005b). The two inner Er^{III} ions are therefore entirely surrounded by chalcogenide ligands (4 S^{2-} and 4 Se^{-}). Absorption spectra of these two clusters in thf, as well as of $[Er(SC_6F_5)_3(dme)_2]$ (**ErS_3**) have been recorded and oscillator strengths calculated

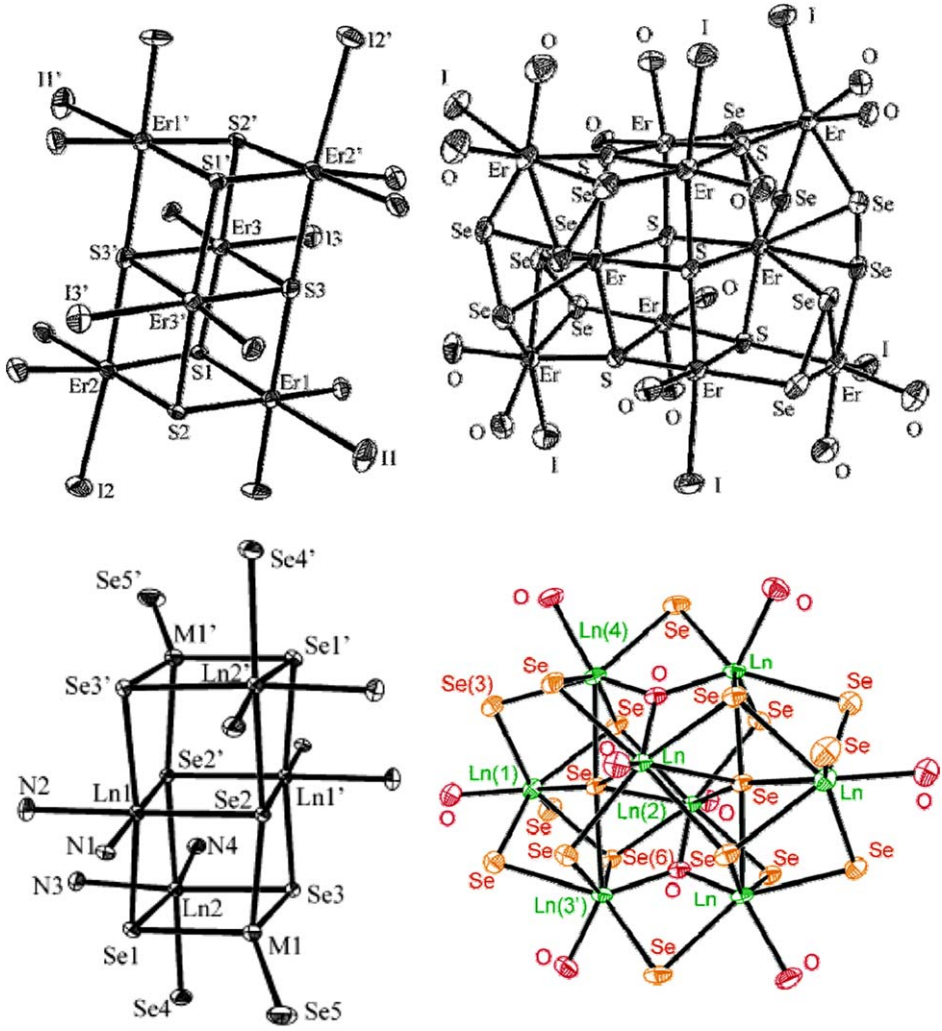

Fig. 101. (Top) Double cubane structures of the clusters $[Er_6S_6I_6(thf)_{10}]\cdot 6thf$ (left) and $[Er_{10}S_6(Se_2)_6I_6(thf)_{14}]\cdot 3thf$ (right). Reproduced with permission from (Kornienko et al., 2005b) ©2005 American Chemical Society. (Bottom) Double cubane structures of the cluster $[Ln_4M_2Se_6(SePh)_4(py)_8]$ (left) reproduced with permission from (Kornienko et al., 2005a) ©2005 American Chemical Society, and structure of $[Ln_8O_2Se_2(SePh)_{16}(thf)_8]$ (right), reproduced with permission from (Banerjee et al., 2005) ©2005 American Chemical Society.

(Kumar et al., 2005). In turn the Judd–Ofelt parameters were calculated and the radiative lifetime estimated from eqs. (14)–(18). It is noteworthy that Judd–Ofelt parameters reproduce the observed spectra well. Photophysical data are listed in table 19 along with the emission cross section and the lifetime of the $Er(^4I_{13/2})$ level. The emission spectra were obtained by exci-

Table 19
Photophysical parameters of the clusters with double cubane structure. Data are from (Kornienko et al., 2005b; Kumar et al., 2005)

Property	$\mathbf{Er_6S_6}$	$\mathbf{Er_{10}S_6}$	$\mathbf{ErS_3}$	$\mathbf{Er{:}LaF_3}$
Ions/cm^3	8.7×10^{20}	3.5×10^{20}	1.26×10^{18}	22.6×10^{20}
Emission cross section, σ_e (cm^2)	4.1×10^{-21}	1.6×10^{-20}	0.76×10^{-20}	3.3×10^{-21}
Emission bandwidth, $\Delta\lambda$ (nm)	61	76	104	73
Radiative lifetime, τ_{rad} (ms)	3.85	3.85	3.85	12.3
Observed lifetime, τ_{obs} (ms)	3.0	3.0	2.88	12.3
Intrinsic quantum yield (%)	78	78	75	100

tation either at 800 nm or at 980 nm (by a diode laser). All these properties are remarkable, particularly the large quantum yield, ranging between 75 and 78%, especially when compared to the corresponding data for Er-doped lanthanide trifluoride. These are the highest values reported for Er^{III}-containing molecular compounds and they are attributable to the absence of any O–H and C–H vibrations close to the emitting center: the second-order vibrational energy of the latter is indeed almost resonant with the energy of the $^4I_{13/2} \rightarrow {}^4I_{15/2}$ transition. In the clusters, the only C–H bonds are those of thf molecules; they are distant from the Er^{III} and, moreover, the solvent molecule is only loosely bound to the metal ion. The more luminescent cluster is $\mathbf{Er_{10}S_6}$ and comparing it with $\mathbf{ErS_3}$, this results from the higher ionic concentration in the unit cell. Analysis of the energy transfer between nearby Er^{III} ions in $\mathbf{Er_{10}S_6}$ by Monte-Carlo simulations reveals a strong multipolar interaction between these ions; the critical separation for the dipole–dipole interaction (R_0) is estimated to 15.5 Å. Because the shortest and the longest separation between two metal centers in this cluster (3.9 and 10.25 Å, respectively) are both shorter than this distance, there is always a multipolar interaction between two Er^{III} ions quenching part of the luminescence, which explains why the quantum yield is smaller than 100%. In fact the luminescence decay can be simulated taking into account both cooperative energy transfer up-conversion and excited state absorption (Kumar et al., 2005). It is noteworthy that the obtained photophysical properties compared very favorably with those reported for chalcogenide glasses, As_2O_3 and $As_{24}S_{38}Se_{38}$, doped with Er^{III}: due to their high refractive indices, the emission cross sections amount to 1.5×10^{-20}, but the lifetimes of the $^4I_{13/2}$ level is only 2.3 ms (Fick et al., 2000).

Similarly, hetero hexametallic clusters containing Ln^{III} ions (Ln = Er, Yb, Lu) and group 12 M^{II} divalent ions (M = Cd, Hg), $[Ln_4M_2Se_6(SePh)_4(py)_8]$ (Ln = Er, Yb and M = Cd, Hg), $\mathbf{Ln_4M_2Se_6}$, have been isolated (Kornienko et al., 2005a). Their structure (fig. 101, bottom left) is also derived from a double cubane framework. With respect to $\mathbf{Er_{10}S_6}$, the emission intensity of $\mathbf{Ln_4Cd_2Se_6}$ and $\mathbf{Ln_4Hg_2Se_6}$ is 45% smaller and the observed lifetimes are shorter (1.41 and 0.71 ms, respectively). This is attributed to a lesser number of Er^{III} ions per unit volume and the quenching effect of the C–H vibrations of the SePh units.

Ln_xE_y clusters are air-sensitive, a definite obstacle in composite materials synthesis. Air-stable O-containing ligands (e.g. O^{2-}) could be another solution but the resulting clusters react with water to form hydroxides. Selenium oxide is an alternative soluble source of oxo ligands, giving for instance $[Ln_8(\mu_3\text{-}O)_2(\mu_5\text{-}Se)_2(SePh)_{16}(thf)_8]\cdot 6thf$ clusters (fig. 101, bot-

tom right), in which the strong Ln–O bond does not impact negatively the Nd^{III} emissive properties (Banerjee et al., 2005). On the contrary, the emission intensity of this oxoseleno cluster (upon 800-nm pumping) is larger when compared to $[Nd(SC_6F_5)_3(dme)_3]$. In particular, the transitions to $^4I_{15/2}$ (1.8 μm) and $^4I_{13/2}$ (1.35 μm) are clearly visible, the latter being relevant to the telecommunication windows. However, strong luminescence quenching still occurs in the cluster (quantum yield = 16%), again, because of interactions between Nd^{III} ions and the presence of C–H vibrations in thf, dme, and SePh.

3.4.3. *Zeolites and composite mesoporous materials (inorganic–organic hybrids)*
This section describes systems which are at the border of what has been defined as being the scope of this review and therefore does not pretend to be comprehensive. Indeed, if there is a wealth of strictly inorganic materials and glasses into which NIR-emitting lanthanide ions have been incorporated and which are clearly excluded from the review, there also exist a continuum between these materials and molecular entities, for instance coordination polymers and clusters which have been described in the two preceding sections. In continuity with these concepts are micro- and mesoporous materials into which lanthanide salts or complexes can be incorporated or attached. These are essentially zeolites and sol–gel materials, either conventional or the so-called inorganic–organic hybrids, as well as polymers.

3.4.3.1. *Zeolites* The zeolites are framework silicates consisting of interlocking tetrahedrons of SiO_4 and AlO_4 with a ratio (Si + Al)/O equal to 1/2. The alumino-silicate structure is negatively charged and has large vacant spaces or cages that allow space for large cations, such as alkali, alkaline-earth or lanthanide cations and even relatively large molecules such as water, ammonia, carbonate ions and nitrate ions. In the more useful zeolites, the spaces are interconnected and form long wide channels of varying sizes depending on the mineral, which allow easy movement of the guest ions and molecules into and out of the structure. Zeolites are characterized by their ability to lose and absorb water without damage to their crystal structures. The term zeolite includes natural silicate zeolites, synthetic materials, and phosphate minerals that have a zeolite like structure. The complexity of this combined group is extensive with over 120 structural variations and more are being discovered or made every year. Zeolites should be suitable host materials for NIR emitting lanthanide ions because their walls consist of Si–O–Al and Si–O–Si framework with low vibrational energies; on the other hand, their ability to host hydroxyl groups or water molecules may be detrimental to the sought after property. A series of interesting zeolites are faujasites (FAU) which have a 3-dimensional structure with pores running perpendicular to each other in the x, y, and z directions. The pore (supercage) entrance is large with a diameter of 7.4 Å, being defined by a 12-member oxygen ring; it leads into a larger cavity of diameter 12 Å (fig. 102) which is surrounded by smaller sodalite cages. S. Yanagida has prepared nanocrystalline faujasite containing tetramethylammonium cations (TMA^+) and with particles sizes 50–80 nm (n-FAU-TMA). Treatment of these particles in water containing neodymium chloride yielded a Nd-exchanged zeolite, 85–95% of the sodium ions being replaced with Nd^{III} ions. The TMA^+ cations remain in the smaller sodalite cages and prevents lanthanide ions to penetrate into these voids. Further treatment included the replacement of the anions with bis(perfluoromethylsulfonyl)aminate

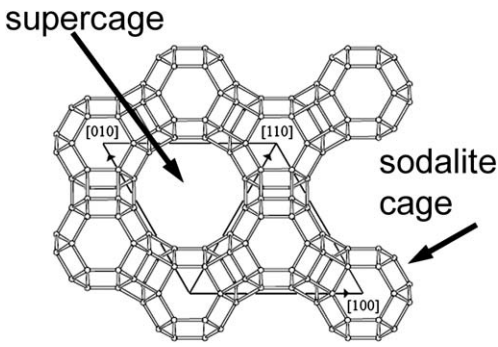

Fig. 102. Schematic representation of a Faujasite.

(pms)[8] and exposition to D_2O vapor to convert O–H oscillators. The number of complexes was estimated to 1–2 per supercage and excitation of the Nd($^2G_{7/2}$) level at 585 nm of both powdered samples and dispersions in dmso-d_6 resulted in characteristic Nd^{III} emission. Dispersions of the doped nanocrystalline particles into dmso-d_6 have a high quantum yield of $9.5 \pm 1\%$, compared to 3.3% for solutions of [Nd(pms)$_3$] in the same solvent. The former yield is the highest reported for a "molecular" neodymium compound (Ryo et al., 2004; Wada et al., 2000). The Nd($^4F_{3/2}$) lifetime of the powdered samples depends on the Nd^{III} loading level: at low level, water molecules remain coordinated to the metal ion ($\tau < 40$ µs); when more neodymium salt is inserted, the lifetime increases to 100 µs, which is assigned to anhydrous [Nd(pms)$_3$] entities. Concentration quenching then occurs through energy migration among the Nd^{III} ions, which are separated by 8 Å when two molecules are inserted into the same cage. At this distance, cross relaxation is suppressed (it is operative at distances <4 Å), but energy migration is still effective. This concentration quenching can be removed by diluting the Nd^{III} ions with La^{III} (Ryo et al., 2003). The variation of Judd–Ofelt parameters, particularly Ω_2 versus the temperature treatment of the samples indicates a lowering in site symmetry when the temperature is increased from 293 to 473 K; a higher symmetry is regained at temperatures between 473 and 623 K (Ryo et al., 2002).

U. Kynast has proposed another strategy adapted from works on visible Ln^{III} luminescence, in which Ln^{III}-loaded faujasite in absence of TMA^+ cations is thermally converted into sodalite (the so-called Hauyne phase) by heating at 660–1000 °C in presence of molybdate MoO_4^{2-} (Ln = Eu) or tungstate WO_4^{2-} (Ln = Tb). Excitation of the luminescent centers via the LMCT state (O → W^{VI}, 254 nm) results in high quantum yields (e.g. 55% for [$Eu_4(Al_8SAl_4O_{24})(MoO_4)_2$]). [$La_xLnYb_{3-x}(Al_8SAl_4O_{24})(WO_4)_2$] (Ln = Ho, Er, $x = 1, 2$) samples have been prepared by the same method (Lezhnina and Kynast, 2004). Unfortunately, excitation into the LMCT band did not result in NIR luminescence. On the other hand, upconversion was observed upon excitation at 980 nm. For the Yb^{III}/Er^{III} couple, twofold resonant energy transfers initially yield an excited Er^{III} ion ($^4F_{7/2}$), which vibronically relaxes to Er($^2H_{11/2}$). Subsequent emission from this state is observed at 526 nm (see fig. 103). Some

[8] This anion is also designated NTf_2 and named bis(trifluoromethanesulfonyl)imide.

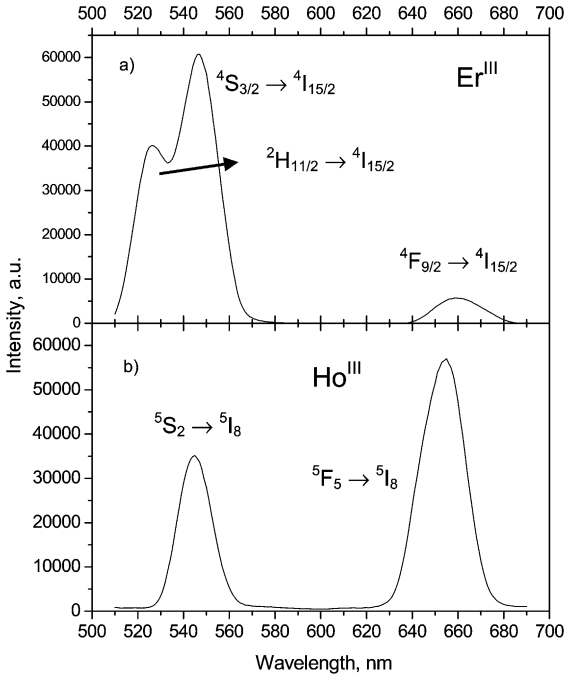

Fig. 103. Up-conversion spectra obtained under excitation at 980 nm of the Yb($^2F_{5/2}$) level for (a) [$La_2ErYb(Al_8SAl_4O_{24})(WO_4)_2$] and (b) [$LaHoYb_2(Al_8SAl_4O_{24})(WO_4)_2$]. Reproduced from (Lezhnina and Kynast, 2004). © 2004 with permission from Elsevier

of the energy is transferred onto the green emitting $^4S_{3/2}$ state (548 nm, most intense band in the up-conversion spectrum) while further relaxation ends to the red-emitting state $^4F_{9/2}$ (648 nm). In the corresponding Ho^{III} sodalite, excitation of Yb($^2F_{5/2}$) at 980 nm is followed by a transfer onto Ho($^5I_6$) which, in turn, populates the luminescent Ho($^5S_2$) state emitting at 544 ($^5S_2 \rightarrow {}^5I_8$) and 654 ($^5F_5 \rightarrow {}^5I_8$) nm. The internal relaxation $^5S_2 \rightarrow {}^5F_5$ is quite efficient, as proved by the larger intensity of the red emission when compared to the green one.

Similar up-conversion also takes place for fluoride complexes inserted in zeolites and luminescence from Nd^{III} occurs for [$La_2Nd_xGd_{2-x}(Al_8SAl_4O_{24})(WO_4)_2$] or [$La_{4-x}Nd_x(Al_8SAl_4O_{24})(WO_4)_2$] sodalites upon pulsed diode laser excitation at 803 nm. The optimum content of neodymium maximizing the 1.06 μm emission in the second material is 0.2 Nd^{III} ion per unit cell (Lezhnina et al., 2006; Lezhnina and Kynast, 2005).

3.4.3.2. *Simple silica matrices* To further illustrate the limit of this chapter, we briefly discuss one type of materials that will not be systematically reviewed: layered lanthanide silicates obtained by hydrothermal synthesis. An alkaline solution of sodium silicate and lanthanide chlorides was stirred to produce a gel which was subsequently put into an autoclave under pressure at 230 °C during seven days, a procedure during which lamellar photoluminescent silicates

form, $K_3[Ln'_{1-a}\,Ln_a\,Si_3O_8(OH)_2]$ (Ln′ = Y, Eu, Gd, Tb, Er; Ln = Eu, Gd, Tb, Er), which are denoted Ln-AV-22. The materials contain crystallographically unique LnO_6 centers with slightly distorted octahedral geometry and connected to six SiO_4 tetrahedra. The photoluminescence spectra of homometallic Er-AV-22 at 300 and 75 K display well resolved ligand-field split emission bands. Interestingly, the integrated intensity increases with increasing temperature, particularly above 225 K, for a 2.7-fold total increase between 75 and 300 K, due to redistribution of population between the Stark levels of the fundamental multiplet (Ananias et al., 2004).

Attempts to incorporate relatively large lanthanide complexes in silica matrix by sol–gel procedure have also been successful. For instance, neodymium tris(dipicolinate), $Na_3[Nd(dpa)]_3$), has been encapsulated into a silicate sol–gel monolith at room temperature. The Nd^{III} ions are shielded from hydroxyl interaction by the dipicolinate anions. The emission of the doped gels exhibit inhomogeneous broadening typical of metal ions in a disordered environment and the longest lifetime recorded is around 3 μs (Lai et al., 1996). Other examples are erbium (Clark et al., 1999) and neodymium (Cervantes et al., 2002) tetraphenylporphyrinates, [Ln(TPP)(acac)], which have been introduced in a tetraethylorthosilicate matrix with, as a result, the production of gels having high optical quality. They present both visible and near IR emission and the bandwidth of the erbium emission is five- to six-fold narrower in the gel when compared to solutions or to silica glasses. Dibenzoylmethanate ternary complexes with phenanthroline, $[Ln(dbm)_3phen]$, Ln = Nd, Yb, have been introduced in the same matrix by an in situ sol–gel synthesis with the aim of designing laser materials (Sun et al., 2005). A Judd–Ofelt analysis of the radiative properties performed on the Nd^{III}-containing material revealed that the stimulated emission cross section of the $^4F_{3/2} \rightarrow {}^4I_{11/2}$ transition (1.06 μm) amounts to 1.4×10^{-20} cm^2, a value comparable to those found in glasses, while its radiative lifetime is 0.52 ms, making this transition a potential candidate for laser action.

Sol–gel chemistry leads to inorganic polymerization reactions and offers a possibility of controlling both the micro- and macro-structures of the host matrix. It presents great potential for manufacturing low cost optical devices because large areas can be covered with good homogeneity and surface planarity. A common synthetic method is the hydrolysis of a silane derivative, such as diethoxymethylsilane, $[SiH(OEt)_2(CH_3)]$ referred to as DEMS, in presence of a metal alkoxide. This leads to the formation of a siloxane network with concomitant evolution of hydrogen gas as a result of the cleavage of Si–H bonds. The advantage of the method is that the synthesis is performed at lower temperature compared with conventional chemical reactions and therefore organic components can be inserted in the oxide gel matrix without decomposition. It is particularly well suited when coatings or thin films are needed. In an early study on luminescent coatings, sols were prepared by reacting DEMS in ethanol with $Zr(OPr^n)_4$ and a lanthanide methoxyethoxide (Ln = Nd, Sm, Dy, Er, Tm), generating Zr–Ln-containing particles embedded in the siloxane structure (fig. 104). Thin layers of 50–100 μm were then deposited on a glass plate, and all of the coatings presented photoluminescence, including those containing the NIR emitting Nd^{III} and Er^{III} ions (Koslova et al., 1993). In the case of Nd^{III} both the absorption and emission spectra were analyzed in details in terms of Judd–Ofelt theory and the $Nd(^4F_{3/2})$ lifetime was shown to decrease from 160 μs for 4×10^{19} ions cm^{-3} (quantum yield estimated from the lifetimes was 35%)

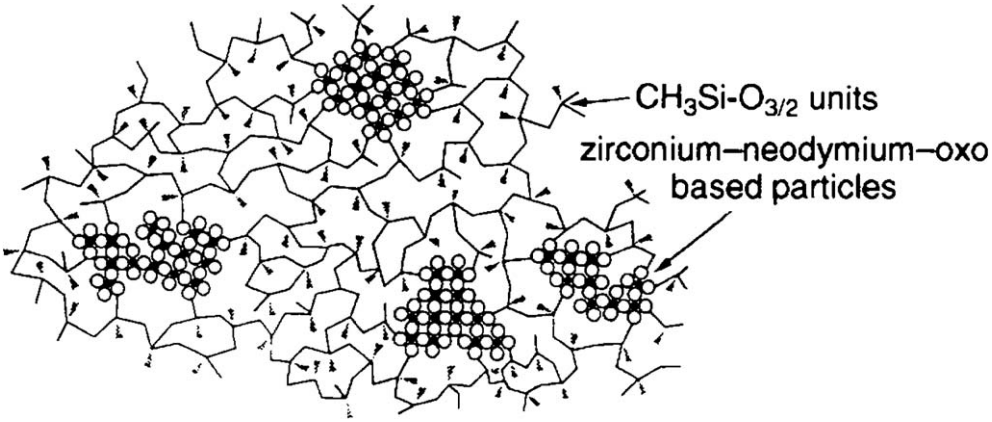

Fig. 104. Schematic structure of hybrid siloxane–metal oxide materials. From (Viana et al., 1995), reproduced with permission from the Royal Society of Chemistry.

to 0.2 μs for a concentration of 4×10^{21} ions cm^{-3} (quantum yield $< 0.01\%$) in view of cross-relaxation processes; in addition, the Nd^{III} ions are well encapsulated inside the Zr-oxo core at low concentrations and are therefore far from the surface and protected from interactions with the residual hydroxy groups (Viana et al., 1995). Co-doping the Nd^{III}-containing particles with rhodamine 6G which emits a broad band centered at 570 nm, results in energy transfer from the latter to the 4f ion. The process is however not efficient because rhodamine 6G is hydrophobic and interacts with the methyl groups of the siloxane polymer, so that the dye molecules lie too far away from the acceptor ion.

Despite the inherent advantages of the sol–gel procedure no commercial waveguides based on this technology are available at the time of the writing of this review, despite numerous attempts made around the world. Two reasons can be invoked, the layer thickness (1–2 μm is needed) and the difficulty in handling large volumes of solution at the industrial scale. The first issue is not easy to address because 25–35 successive coatings are necessary to reach the desired thickness and mechanical problems can arise during the process. In order to obtain crack-free thick films, an improved method has been proposed in which the films are obtained by dispersion of silica–hafnia nanoparticles into a binder solution, spin-coating followed by thermal treatment. The hafnia nanoparticles allow a control of the refractive index. The resulting films present good optical quality and the required thickness for a fiber matching single mode waveguide. Thick films obtained by this method and doped with 0.3 mol% erbium and 0.7 mol% ytterbium (as sensitizer) support two transversal electric modes at 1.55 μm and possess low birefringence, as indicated by the very small difference between the transversal electric and magnetic modes, with corresponding refractive indices equal to 1.4730 and 1.4735, respectively. The ligand-field splitting reflected in the $Er(^4I_{13/2} \rightarrow {}^4I_{15/2})$ transition is typical of a cubic environment for the metal ion, henceforth indicating the presence of erbium in the cubic phase of HfO_2 nanoparticles. Up-conversion of the $Er(^4F_{3/2} \rightarrow {}^4I_{15/2})$ transition has been obtained upon continuous wave excitation at 980 nm (Sigoli et al., 2006).

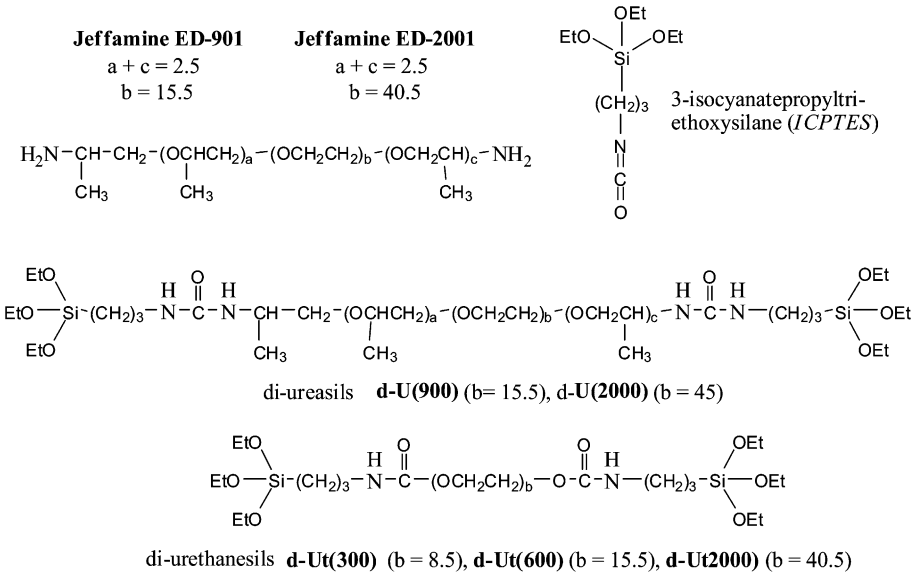

Fig. 105. Some components and precursors of di-ureasil inorganic–organic hybrids.

Silica-polyethyleneglycol (PEG) hybrids present an increased solubility for lanthanide complexes. In view of the large ability of dipicolinate (dpa) and calcein, 4′,5′-bis-[*N*,*N*-bis(carboxymethyl)aminomethyl]fluorescein (H_4**73a**, fig. 64), to sensitize the NIR luminescence of lanthanide ions, the corresponding complexes $[Ln(dpa)_3]^{3-}$ and $[Ln(calcein)]^{2-}$ (Ln = Pr, Nd, Sm, Dy, Er, Ho, Yb) have been doped in a matrix prepared from tetramethylorthosilicate and PEG-200 (Driesen et al., 2004b). Intense Yb^{III} luminescence was observed for both complexes, while only calcein sensitized Nd^{III} and Er^{III} luminescence to an acceptable extent, especially when the gel was dried. Indeed, the produced gels contain unreacted silanol groups as well as water molecules which reduce strongly the NIR emission and shorten the lifetime. The lifetime of the Nd($^4F_{3/2}$) level is 139 ± 4 ns (280 ± 4 ns after drying the gel), as compared to 250 ns for the same complex in water. For the calcein complex, the lifetime of the Yb($^2F_{5/2}$) level is 1.83 ± 0.02 μs (3.72 ± 0.02 μs after drying), as compared to 1.9 μs in water.

3.4.3.3. *Xerogels: ureasilicates and urethanesilicates* One class of investigated compounds in the development of polymeric electrolytes for various types of electrochemical devices (fuel cells, rechargeable batteries, solar cells, for instance) are ureasilicates, also termed di-ureasils, di-urethanesils, or ormosils. They possess good mechanical and thermal stability in addition to being optically transparent. In these materials, urea (or urethane) bridges are used to graft diamines containing oxyethylene segments of two different molecular weights onto a silica network (fig. 105). The preparation of lanthanide-doped materials goes through the reaction of 3-isocyanatepropyltriethoxysilane with a diamine, α,ω-diaminepoly(oxyethylene-co-oxypropylene), commercially designated as Jeffamine ED-Y (Y = 901 or 2001, for in-

Table 20
Lifetimes (ms, at 14 K) of the di-ureasils emitting centers and efficiency (%) of the energy transfer to the Nd^{III} ion in **d-U(Y)$_n$Nd(Otf)$_3$** xerogels; percentages within parentheses indicate the Nd^{III} content with respect to the total mass (Sa Ferreira et al., 2003)

	U(900)$_n$Nd(Otf)$_3$				**U(2000)$_n$Nd(Otf)$_3$**			
	$n = \infty$	$n = 100$ (1.5%)	$n = 60$ (2.4%)	$n = 40$ (3.4%)	$n = \infty$	$n = 100$ (2.1%)	$n = 60$ (3.4%)	$n = 40$ (4.7%)
τ_{NH}	122 ± 7	103 ± 12	38 ± 5	21 ± 7	160 ± 7	98 ± 9	79 ± 5	49 ± 4
τ_{Si}	3.7 ± 0.4	3.1 ± 0.2	3.2 ± 0.1	2.8 ± 0.2	3.6 ± 0.1	2.1 ± 0.4	0.9 ± 0.3	0.5 ± 0.1
η_{NH}	–	16	69	83	–	39	51	70
η_{Si}	–	5	8	35	–	40	74	86

stance) in thf, to yield ureapropyltriethoxysilane or urethanepropyltriethoxysilane precursors. A lanthanide salt LnX_3 (usually a triflate) dissolved in ethanol/water is then added to the solution of the precursor. Slow evaporation of the solvent results in gelation and after drying and aging for a sufficient time (3–4 weeks), a rigid and brittle elastomeric film is obtained, which is called a xerogel. The designation codes for the materials are as follows: **d-U(Y)$_n$LnX$_3$** or **d-Ut(Y)$_n$LnX$_3$** where **d-U** and **d-Ut** stand for di-ureasil and di-urethanesil, respectively, **Y** depends on the stoichiometric coefficient b (see fig. 105) and indirectly indicates the length of the oxyethylene chains, and $\boldsymbol{n}$ = O/Ln represents the ratio of ($O–CH_2–CH_2–$) monomers units per Ln ion (Bermudez et al., 1998).

The undoped xerogels are luminescent by themselves. For instance, **d-U(2000)** emits a blue-green band with a maximum around 540 nm, but extending from 375 to 630 nm, upon excitation at 460 nm. The luminescence originates both from the urea moiety (NH-emission, due to photoinduced proton transfer between NH_2^+ and N^- defects) and from electron–hole recombinations in the inorganic siliceous backbone. When neodymium triflate is doped into the material (with $\boldsymbol{n}$ = 100, 60, 40, and 20) dips appear in this emission band, which correspond to absorptions from the Nd^{III} ion. As a result, $Nd(^4F_{3/2})$ emission is detected in the NIR range, the intensity of which shows an intricate dependence upon Nd^{III} concentration and temperature (Carlos et al., 2000). The lifetimes of the di-ureasil emitting centers and the efficiency of the energy transfer between them and Nd^{III}, calculated according to eq. (4a), have been determined for a series of **d-U(Y)$_n$Nd(Otf)$_3$** xerogels (**Y** = 900, 2000, $\boldsymbol{n}$ = 40, 60, 100, and ∞). They are reported in table 20. The efficiency of the two energy transfer processes increases with the concentration of incorporated Nd^{III} ions for both host materials. At the doping concentration tested, no or little concentration quenching occurs (Sa Ferreira et al., 2003).

Room-temperature NIR emission has also been reported for the di-urethanesils **Ut(600)$_3$-Er(Otf)$_3$** and **Ut(900)$_n$Nd(Otf)$_3$** ($\boldsymbol{n}$ = 80, 60), indicating that this hybrid framework protects the lanthanide ions from nonradiative deactivation processes equally efficiently when compared with the di-ureasils (Carlos et al., 2004). In fact, the most noticeable difference between the Nd^{III}-doped di-ureasils and di-urethanesils is the energy difference between the undoped host and the doped hybrids which, in the case of **Ut(600)$_n$**, for instance, is concentration dependent (Gonçalves et al., 2005).

Ormosil spin-coated thin films obtained from vinyltriethoxysilane and doped with β-diketonates have been recently investigated by H. Wang and collaborators. Both hydrated chelates and ternary complexes with phen and tppo were doped at a concentration of 5 mol% (relative to Si) by a multi step sol–gel method. Out of the 12 compounds tested, $[Nd(tta)_3(tppo)_2]$ yielded the best results but no quantitative luminescence data are given, preventing comparison with materials of known properties (Wang et al., 2005).

3.4.3.4. *Covalently-linked luminescent hybrid materials* Hybrid materials combine inorganic, organic, and even biochemical properties in a tailored matrix. They possess inorganic pores with adjustable size and their surface can be modified by organic or bio-active functions. The possibility of processing mesoporous hybrid materials into thin films adds to their applicability, especially when optical devices are targeted. The chemical synthesis of hybrid materials implies essentially a combination between sol–gel chemistry of the inorganic precursors (alkoxide or inorganic salts, for instance) and the self-assembly features of the organic pore templates, e.g. surfactants (Soler-Illia and Innocenzi, 2006).

One of the problems with the previously described systems is the presence of either water molecules or hydroxyl groups which can induce de-complexation of the doping complexes. Moreover, the lanthanide-containing compounds are only bonded to the matrix through weak interactions (van der Waals forces, hydrogen bonds or weak electrostatic effects, for instance), which gives little control over the clustering of emitting centers and leads to inhomogeneous dispersion, itself a cause of leaching of the photoactive centers in the material. A strategy to overcome these difficulties consists in attaching a coordinating group onto the porous framework which simultaneously acts as a sensitizer. Several such examples deal with ternary complexes of lanthanide β-diketonates (fig. 106). In one example, the glass matrix was prepared by first reacting 5-amino-1,10-phenanthroline with 3-(triethoxysilyl) propyl isocyanate. The resulting compound, tetramethoxysilane (TMOS) and diethoxydimethylsilane (DEDMS) were hydrolyzed and condensed at a neutral pH to a sol–gel glass. A tris(2-thenoyltrifluoroacetonato) europium(III) dihydrate complex was then covalently attached to the phen groups on the silica gel (fig. 106a). The sol–gel glass doped with Sm^{III} shows luminescence both in the visible ($^4G_{5/2} \rightarrow {}^6H_J$, $J = 5/2$–$9/2$) and in the near-infrared range ($^4G_{5/2} \rightarrow {}^6H_{15/2}$, $^6F_{5/2–9/2}$ transitions), with a lifetime of 65 μs. Luminescence from the other NIR-emitting ions could also be detected: Nd^{III}, lifetime of $^4F_{3/2} = 0.26$ μs, Er^{III}, lifetime of $^4I_{13/2} = 0.99$ μs, and Yb^{III}, lifetime of $^2F_{5/2} = 13$ μs after drying the sample (Lenaerts et al., 2005b). In order to simplify the cumbersome synthesis of the 1,10-phenanthroline-derivatized matrix, the same authors have resorted to a 2-substituted imidazo[4,5-f]1,10-phenanthroline linking group (fig. 106b), which allowed them to detect NIR luminescence from Nd^{III} ($^4F_{3/2} \rightarrow {}^4I_{9/2–13/2}$, lifetime = 0.32 μs), Sm^{III} ($^4G_{5/2} \rightarrow {}^6H_{15/2}$, $^6F_{5/2–9/2}$ lifetime = 40 μs), Ho^{III} ($^5S_2 \rightarrow {}^5I_6$, 975 and 1020 nm), Er^{III} ($^4I_{13/2} \rightarrow {}^4I_{15/2}$, lifetime = 0.95 μs), and Yb^{III} ($^2F_{5/2} \rightarrow {}^2F_{7/2}$, lifetime = 12 μs) at room temperature and from Pr^{III} ($^1D_2 \rightarrow {}^3F_4$, 1.03 μm) at 77 K. Emission from the Ho^{III} compound was too weak to measure the lifetime. Thin films were produced by spin-coating and displayed more intense luminescence than the bulk materials: the Er($^4I_{13/2}$) lifetime could be determined as being 1 μs (Lenaerts et al., 2005c). The same β-diketonates were covalently attached to a cross-linked chloromethylated polystyrene (Mer-

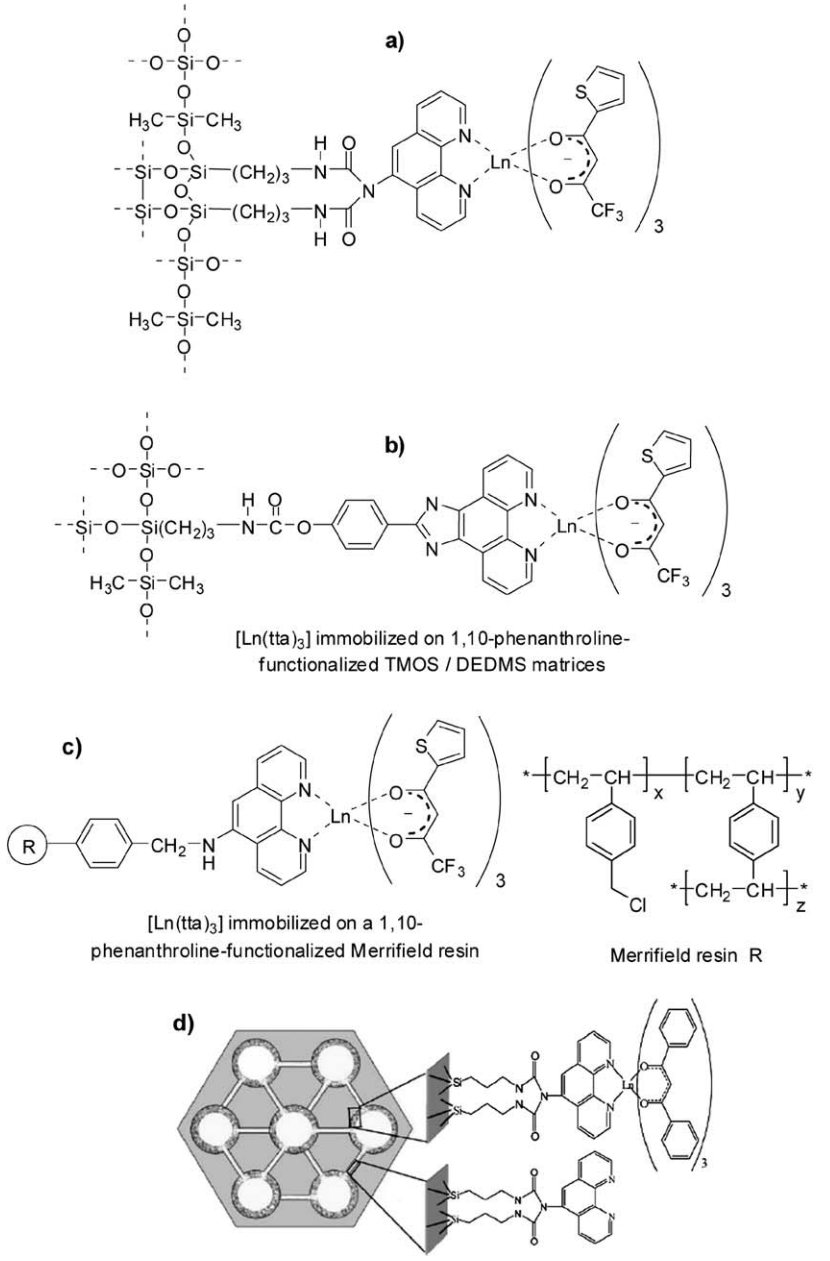

Fig. 106. Immobilized β-diketonate complexes in mesoporous materials. Part (d) is reproduced with permission from (Sun et al., 2006).

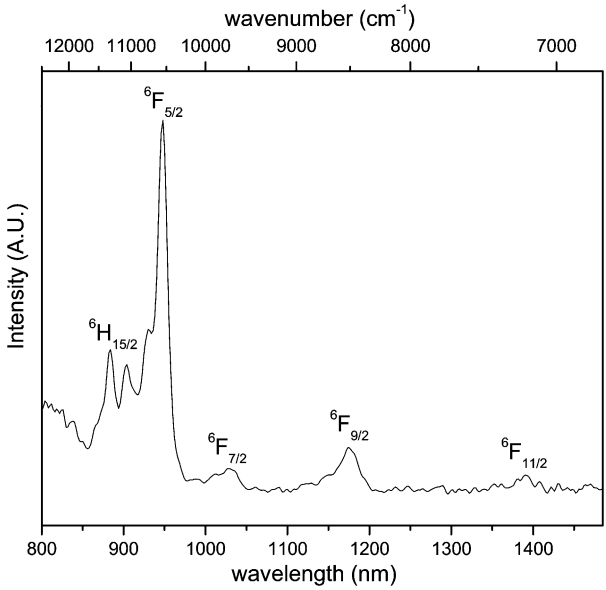

Fig. 107. NIR region of the photoluminescence spectrum ($\lambda_{exc} = 370$ nm) of [$Sm(tta)_3$] immobilized on a phen-derivatized Merrifield resin (fig. 106c). Reproduced with permission from (Lenaerts et al., 2005a).

rifield resin) through a 1,10-phenanthroline linker (fig. 106, bottom) and again, NIR emission could be detected at room temperature from Nd^{III}, Sm^{III} (fig. 107), Er^{III}, and Yb^{III} with lifetimes longer than the previous ones: 0.4, 70, 1.4, and 10 μs, respectively (Lenaerts et al., 2005a).

Mesoporous materials similar to the one described in fig. 106a, but possessing a hexagonally-ordered silicate structure, have been described in 1992 (Kresge et al., 1992). A typical example is MCM-41 which is obtained by reacting the surfactants hexadecyltrimethylammonium hydroxide with tetramethylammonium silicate in presence of alumina and precipitated silica at 150 °C during 2 days, followed by calcination at 540 °C. The resulting material shows regular hexagonal arrays of uniform channels similar to the arrangement found in lyotropic liquid crystals. Its pores have a diameter of about 40 Å, that is, much larger than those found in zeolites, and can be tuned by varying the size of the surfactant alkyl chain. The MCM-41 material has been functionalized by 1,10-phenanthroline units in order to bind lanthanide β-diketonates and the resulting compounds are written [$Ln(dbm)_3$phen-MCM-41_{XY}] with X denoting the Ln^{III}/phen-MCM-41 molar ratio and Y the reaction time (in hours) for the complexation to the mesoporous material; $X = 12$ and $Y = 6$ proved to be optimum (Sun et al., 2006). A similar functionalization has been performed on a related material, SBA-15, obtained from alkyl poly(ethylene oxide) oligomeric surfactants and poly(alkylene oxide) block copolymers (Zhao et al., 1998), yielding [$Ln(dbm)_3$phen-SBA-15] compounds. The excitation spectra of Er^{III}-doped materials are very similar and extend from 250 to 450 nm; they

are narrower than for the parent β-diketonate and blue shifted, due to the change in polarity in the mesoporous materials. The $^4I_{13/2} \rightarrow {}^4I_{15/2}$ transitions are broad with a full width at half height (fwhh) equal to 76 and 72 nm for MCM-41 and SBA-15, respectively, enabling wide gain bandwidth for optical amplification. The Nd^{III}- and Yb^{III}-doped materials present the same excitation spectra. The [Ln(dbm)$_3$phen-SBA-15] materials which have a lower lanthanide ion content present slightly longer lifetimes of the NIR luminescence (0.28 vs 0.23 μs for Nd^{III}, 2.40 vs 2.29 μs for Er^{III}, and 12.3 vs 12.1 μs for Yb^{III}) and higher emission intensity per lanthanide ion (factor 9.6, 7, and 3.9 for Nd^{III}, Er^{III}, and Yb^{III}, respectively) than the corresponding [Ln(dbm)$_3$phen-MCM-41], probably in view of the larger number of residual surface silanol groups in the latter (Sun et al., 2006).

3.4.4. *Microspheres and nanoparticles*

Silica-based glasses doped with lanthanide ions are optically active materials widely used for photonic applications. As mentioned previously, their properties are however limited, for instance, by concentration quenching, and several alternative solutions are being investigated, including the materials described in the preceding section. One of these solutions is the synthesis of nanoscale particles doped with Ln^{III} luminescent centers. The main advantage of such an approach is that physical and electronic properties of the particles can be modulated by varying their size and shape, a definite plus for the design of microlasers, thin-film devices or active photonic band-gap materials, or luminescent nanosensors. Moreover, this approach opens the way for the use of luminescent inorganic compounds in organic environment since most of the nanoparticles can be dispersed in apolar organic solvents and/or in polymers. As for the previous section, description of nanoparticle-based NIR luminescent materials is not intended to be comprehensive since the field is at the border of the matter covered in this chapter. Selected examples will be presented, highlighting their fundamental aspects, while a more detail account can be found in another chapter of this volume (Liu and Chen, 2007). The substrates used in the various studies range from simple silica microspheres to lanthanide fluorides, phosphates, oxides, borates, vanadates, and titanium oxide. They will be described in this order. The parameters influencing the optical properties are the size and size distribution of the particles, the doping rate of the luminescent centers, as well as the presence of a co-dopant. As far as excitation mode is concerned the nanoparticles described up to now fall into two classes: those for which direct 4f–4f excitation is required and those for which excitation makes use of a sensitization process involving TiO_2 or vanadate (e.g. $LaVO_4$).

Control of the particle size is critical and heavily depends on the preparation method. Sonochemistry has been tried, for instance for the reaction of lanthanide nitrates with tetraethyl orthosilicate (TEOS), but a large fraction of the nanoparticles agglomerated in clusters with irregular shapes and sizes, while the doping density could not be controlled satisfyingly. Despite this somewhat deceptive result, silica (and alumina) particles doped with Eu^{III} and Tb^{III} displayed emission intensities comparable to those of the commercial phosphors (Patra et al., 1999). Ion implantation is an alternative, but only a few particles can be doped at one time and the level of doping is not homogeneous. Therefore chemical methods were tested which proceed either by base- or by acid-catalyzed growth of silica particles. In fact, base-catalyzed growth is inadequate because of the easy formation of lanthanide hydroxides. On the other

hand, the acid-catalyzed method proved to be quite successful. First, 0.5–2% of $LnCl_3 \cdot 6H_2O$ are dissolved into an aqueous solution of acetic acid and TEOS is rapidly added; after initial stirring during a few seconds, the solution is left reacting for half an hour and the doped nanoparticles sediment and are separated by centrifugation. To eliminate unreacted TEOS, the particles are re-dispersed several times in ethanol before being thermally treated to 750 °C; this treatment not only eliminates solvents and acetate groups, but it also promotes more complete condensation of the surface and interior silanol groups, which should reduce the luminescence quenching by O–H vibrations. On the other hand, the treatment leaves enough hydroxyl groups on the surface to maintain the hydrophilic nature of the particles and to allow for future surface functionalization (e.g. surface coating by alkoxysilanes). In absence of lanthanide dopant, most of the particles (up to 85%) are "necked", whereas spherical, discrete particles are obtained in presence of the lanthanide salt. For a given ratio TEOS: acetic acid: water, usually in the range 1:(4–8):(1.5–5), the polydispersity of the particles is controlled by the concentration of the lanthanide salts and the reaction time. At a concentration of 1% $LnCl_3 \cdot 6H_2O$ a sample of doped microparticles with an average size of 2.8 μm and a standard deviation of less than 10% was isolated after only 5 min. In fact, if the reaction is stopped after the nucleation and growth of the first generation of nuclei, more monodisperse (or, better, uniform) samples can be obtained. The resulting Ln-doped (Ln = Pr, Er) samples were highly luminescent, with emission from $^1D_2$ and $^3P_0$ for Pr^{III} and from $^4I_{13/2}$ in the NIR for Er^{III} (Moran et al., 2001). The same synthetic route has been used by M.J.A. de Dood for producing monodisperse Er-doped colloidal silica microspheres. In addition, a seeded growth process is described in which a thin shell of Er-doped silica is grown on existing monodisperse silica colloids (de Dood et al., 2002). The luminescence decay of the annealed particles is a single exponential function and the associated lifetime amounts to 13.2 ms which corresponds to an estimated intrinsic quantum yield of ≈70%.

Lanthanide trifluoride has very low vibrational energies, with the highest phonon energy around 350 cm^{-1}, and is thus an ideal host for the study of lanthanide spectroscopy, particularly erbium (Hüfner, 1978; Weber, 1967a; Weber, 1967b). The LaF_3 nanoparticles are prepared by heating a solution of ammonium di-*n*-octadecyldithiophosphate with NaF in ethanol/water and adding a solution of lanthanum nitrate and of the desired lanthanide nitrate. After centrifugation and re-dispersion in dichloromethane for purification purposes, the particles with diameter between 5 and 10 nm are simply dried in vacuum for two days. They can be dispersed in apolar solvent such as chloroform, dichloromethane, or toluene. Near-infrared emission was observed for the dispersed particles doped with 5% of Ln^{III}: for Nd^{III}, upon excitation at 514 nm, the luminescence decay is bi-exponential corresponding to lifetimes of the $^4F_{3/2}$ level equal to 240 and 40 μs; for Ho^{III}, under excitation at 448 nm, both $^5F_5 \rightarrow {}^5I_7$ (966 nm) and $^5F_5 \rightarrow {}^5I_6$ (1.46 μm) transitions are observed (lifetimes: 340 and 30 μs); for Er^{III}, upon excitation at 488 nm, the emission at 1.53 μm shows a wide bandwidth, but the decay is a single exponential function corresponding to a lifetime of 220 μs. The authors explain the occurrence of two lifetimes by the presence of luminescent ions in the center and at the surface of the nanoparticles; a possible explanation for observing only one lifetime in the case of erbium is that the metal ions are located closer to the surface due to a stronger ligand–Er^{III} interaction (Stouwdam and Van Veggel, 2002). Using Eu^{III} as structural local

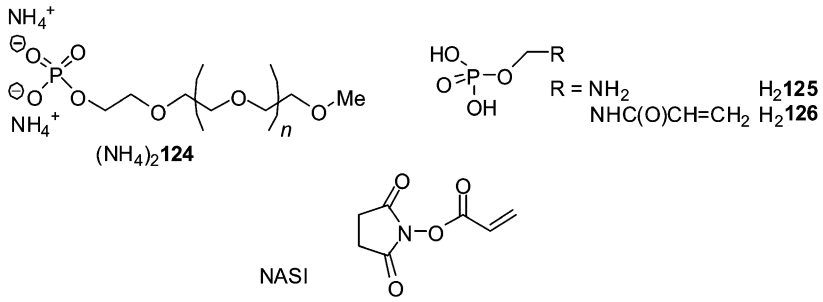

Fig. 108. Ligands used for the formation of Ln^{III}-doped LaF_3 nanoparticles.

probe, the site symmetry of the dopant ion has been established to be C_2 and the luminescence decays were calculated theoretically with a shell model considering the quenching at the surface by the solvent (10 shells were taken into account) and which reproduced correctly the longer lifetime of the core–shell nanoparticles (Stouwdam et al., 2003). Further improvement of the photophysical properties, particularly of Er^{III}, could be obtained by preparing, by sol–gel technique, thin films with Ln^{III}-doped LaF_3 nanoparticles stabilized by citrate. Lifetimes of the $Er(^4I_{13/2})$ level up to 10.9 ms could be obtained (Sudarsan et al., 2005), indicating the absence of clustering of the Er^{III} ions. This value is close to the 17 ms lifetime measured for Er^{III} in ion-implanted (350 keV) silica colloidal particles with a size of 240–360 nm and for which the intrinsic quantum yield was estimated to be around 80% based on a radiative lifetime of 20–22 ms (Slooff et al., 2000a).

In view of potential applications as biolabels, F.C.J.M. van Veggel and collaborators have prepared six types of water-soluble, highly luminescent Ln^{III}-doped (5 mol%, Ln = Eu, Er) LaF_3 nanoparticles from one-pot syntheses using the ligands reported in the upper part of fig. 108 (Diamente and Van Veggel, 2005). The phosphate monoester group limits the size of the nanoparticles to <20 nm in view of the electrostatic repulsion generated by the doubly charged anion, while the PEG substituent in **124** is intended for covalently attaching the nanoparticles to biological macromolecules. In addition to the hydrophilic nature of PEG, rendering the nanoparticles water soluble, this group suppresses antigenic and immunogenic epitopes, preventing recognition and degradation of the nanoparticles by proteolytic enzymes. Ligand H_2**125** was tested to demonstrate that with an amine-terminated ligand, the nanoparticles can be modified at their surface, for instance with *N*-acryloxysuccinimide (NASI) while retaining their photophysical properties. The optical properties of the PEG-based nanoparticles in water were investigated using Eu^{III} as a spectroscopic probe and according to luminescence decay analysis three different metal ion environments (core and surface) are present; one with a long lifetime (2.7 ms) corresponds to the luminescent centers embedded in the particle cores while the other two arise from surface-located Eu^{III} ions ($\tau = 0.6$ and 0.2 ms). For Er^{III}, NIR luminescence is only seen in deuterated water and the corresponding decay is also tri-exponential, with the longer lifetime equal to 50 μs, indicating still significant quenching (compare $\tau_{rad} \approx 20$ ms). Nanoparticles grown with H_2**125** have bi-exponential luminescence decay with longer lifetimes, 118 and 17 μs. When these nanoparticles are reacted with NASI,

their solubility in water decreases due to the presence of vinyl groups, but the overall photophysical properties are maintained.

Although lanthanum phosphate possesses higher energy phonons ($\approx$1050 cm^{-1}) than lanthanide fluoride it is also a convenient medium for preparing Ln-doped nanoparticles, starting from tris(2-ethylhexyl)phosphate and following a procedure similar to that used for the fluoride nanoparticles. Some transitions not seen in the fluoride materials could be recorded in the phosphate medium, possibly because the metal ion sites have lower symmetry, C_1 (Stouwdam et al., 2003). This is the case of the 980-nm emission from erbium ($^4I_{11/2} \rightarrow {}^4I_{15/2}$) and of Pr^{III} emission not observed in the fluoride particles upon excitation at 476 nm. For the latter, transitions from the $^1D_2$ level to the ^3F_J manifold ($J = 2$, 3, and 4, in the range 800–1100 nm) and to the $^1G_4$ level (1.4–1.55 μm) were identified; incorporation of $LnPO_4$:Ln nanoparticles in poly(methylmethacrylate) is feasible and the photophysical properties are retained (Hebbink et al., 2002b). Similarly, the $LaPO_4$ nanoparticles can be incorporated into 3-(trimethoxysilyl)propyl methacrylate (Jung et al., 2005). On the other hand, Ho^{III} emission could not be observed in $LaPO_4$ particles, contrary to the fluoride medium while co-doping Yb^{III} and Er^{III} led to increased erbium emission in both materials in view of the energy transfer process discussed previously (Jung et al., 2005; Lehmann et al., 2003; Stouwdam et al., 2003).

Since oxide materials are extensively used in practical devices such as lamp phosphors or laser materials, their behavior at the nanoscale level has also been investigated. The size of yttrium oxide nanoparticles Y_2O_3:Ln can be finely tuned by glycine-nitrate combustion synthesis. The overall equation of the exothermic reaction can be expressed as:

$$6\,Ln(NO_3)_3 + 10\,NH_2CH_2CO_2H + 18\,O_2 \rightarrow 3\,Ln_2O_3 + 5\,N_2 + 18\,NO_2 + 20\,CO_2 + 25\,H_2O. \quad (39)$$

Combustion of the lanthanide nitrate and glycine spontaneously starts at 240 °C and the resulting voluminous powder is annealed at 600 °C. The particle size depends on the annealing temperature and time, as well as on the glycine/$Ln(NO_3)_3$ ratio and can be tuned accordingly between 15 and 70 nm, the smallest particles being the most luminescent. Thin films of these particles inserted into PMMA polymer matrix obtained by spin-coating have been produced and the authors showed that the optimal parameters with respect to integrated emission intensity are a concentration of 1 mol% of Er^{III} (to minimize ESA) and co-dopant concentrations of 1 mol% Ce^{III} or 5 mol% Yb^{III} (see fig. 8). The net gain of the PMMA/Er:Yb:Y_2O_3 system reaches 30 dB cm^{-1} for a pump intensity of 12.5 W cm^{-2} (Le Quang et al., 2005).

Lamellar nanohybrids composed of Ln_2O_3 layers regularly separated from each other by organic layers of intercalated benzoate molecules can be obtained by a one-pot procedure (Karmaoui et al., 2006), the benzyl alcohol route. Lanthanide isopropoxides are simply dissolved in benzyl alcohol and reacted at high temperature (250–300 °C), resulting in the isolation of nanoparticles of 50-nm mean size. Eu^{III}-doped nanohybrids have better radiance characteristics than the standard phosphor Y_2O_3:Eu while both yttrium- and gadolinium-based nanomaterials doped with Nd^{III} display intense NIR luminescence, with a Nd($^4F_{3/2}$) lifetime of 49 μs in the case of the yttrium nanohybrid (Sa Ferreira et al., 2006).

Yttrium orthoborate nanoparticles $Y_{1-x}Nd_xBO_3$ have been less studied. They can be prepared by hydrothermal synthesis from boric acid, urea, yttrium nitrate, and neodymium

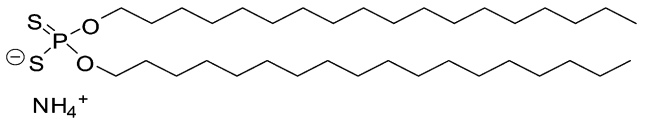

Fig. 109. Dithiophosphate ligand used in the synthesis of $LaVO_4$:Ln nanoparticles.

sesquioxide in dilute nitric acid. The Nd^{III} ions lie in two different metal ion sites with the same C_3 symmetry and therefore have similar emission properties, leading to narrow emission bands. The luminescence intensity of these particles having diameter in the range 40–60 nm is maximized when the Nd^{III} doping concentration reaches 10 mol% (F. Wang et al., 2004).

Concentrated aqueous colloidal solutions of well dispersed YVO_4:Ln (Ln = Nd, Yb) nanocrystals with an average size of 8 nm were obtained by precipitation of lanthanide citrates with sodium orthovanadate and heating at 60 °C for 30 min (Buissette et al., 2003). Aqueous suspensions of these nanocrystals have luminescence properties which are not as good compared to the bulk materials (e.g. smaller lifetimes). Thermal treatment at 600 °C yields silica-capped nanoparticles for which the initial luminescent properties are restored. In particular, the co-doped YVO_4:Er,Yb material exhibits green up-conversion luminescence, in addition to the 1.55 μm NIR emission. The two-photon process is demonstrated by the square-power dependence of the green emission intensity at 550 nm. A noteworthy result is that the up-conversion efficiency (0.4%) is not affected by the nanometric size of the crystallites. To make vanadate nanoparticles soluble in organic solvents, F.C.J.M. van Veggel et al. have proposed to coordinate negatively charged ligands at their surface, such as dithiophosphate substituted with a C_{18} alkyl chain (fig. 109). The doped vanadate nanoparticles are synthesized by heating a solution of the dithiophosphate with sodium orthovanadate, lanthanum nitrate, and 5 mol% of the dopant lanthanide nitrate in ethanol/water at 75 °C, followed by the usual treatment, re-dispersion, and drying at room temperature.

One advantage of the vanadate system is its V–O charge-transfer state around 35 700 cm^{-1} (280 nm) which can be used to populate the Ln^{III} excited states. In this way, NIR emission form Nd^{III}, Ho^{III}, and Er^{III} is observed in chloroform solutions, upon excitation at 280 nm (Stouwdam et al., 2005).

Stable luminescent suspensions of Er^{III}-doped titania (TiO_2) nanoparticles with an average size of 50 nm display only faint luminescence from the $^4I_{13/2}$ level upon pumping at 795 nm if no thermal treatment is applied. Simple drying at 100 °C improves their photophysical properties and treatment at 500 °C results in further luminescence enhancement. The nanoparticles can be assembled into thin films and inserted into photonic crystals (Jeon and Braun, 2003). Energy transfer from titania is also instrumental in exciting the Ln^{III} levels, as demonstrated on very small (3–5 nm) TiO_2 nanoparticles doped with NIR-emitting Ln^{III} ions and prepared from thermal decomposition of an organometallic precursor in trioctylphosphine oxide. Diluted dispersions in dichloromethane of the particles doped with Nd^{III}, Er^{III}, or Yb^{III} emit the characteristic NIR luminescence and the corresponding excitation spectra show the same broad band with an onset at 350 nm, proving sensitization by the inorganic matrix (Stouwdam and Van Veggel, 2004).

3.4.5. *Fullerenes*

The fact that fullerenes may host additional atoms in their structure, particularly metal atoms, has been demonstrated by mass spectrometry on samples obtained by laser vaporization of lanthanum-impregnated graphite. Another method of obtaining lanthanide-containing fullerenes is arc vaporization of cored carbon rods packed with lanthanide oxide and graphite powder, followed by extraction by carbon disulfide or 1,2-dichlorobenzene and purification by high performance liquid chromatography (HPLC). Rare earth atoms do not enter easily into C_{60} although $La@C_{60}$, has been evidenced, as well as a few other compounds. They are more likely to be found in larger cages, such as C_{82} and C_{84}, the former being favored because its tri-anionic form is stabilized by the additional electrons. Despite the stunning properties of the metallofullerenes (magnetic properties, superconductivity for instance) few spectroscopic studies are reported, mainly because of the difficulty in producing pure materials in reasonable yield (Bethune et al., 1993). Undoped fullerenes dissolved in toluene have a deep red appearance and the onset of absorption shift to longer wavelengths when the cage becomes larger. For instance, C_{60} starts to absorb strongly at 400 nm while the corresponding absorption onset lies at 500 nm for C_{82}. In the case of $La@C_{82}$, two isomers have been identified which present extended absorption spectra to the NIR range down to 2 μm, with a weak and broad absorption at 1.5 μm for the major isomer and 1.35 μm for the minor isomer. In addition, other sharp feature are seen at about 1 μm and 700 nm (Yamamoto et al., 1994). As far as NIR luminescence is concerned the most studied ion is Er^{III} trapped in endohedral fullerenes and we shall limit the discussion to these systems.

Thin films of a mixture of fullerenes are reported to present an emission spectrum at 20 K in the range 700–1400 nm upon excitation with an argon laser (457 nm). Two sets of vibrational progressions could be identified, the relative intensities of which change drastically from sample to sample, which were assigned to C_{60}. When the fullerenes are doped with Er^{III}, the general shape of this emission remains similar, although the intensities of the vibrational features are modified; in addition a very well resolved $^4I_{13/2} \rightarrow {}^4I_{15/2}$ transition appears in the range 1.45–1.65 μm. The authors however could not identify the species ($Er@C_{60}$ or $Er@C_{82}$) responsible for this emission spectrum (Hoffman et al., 1995). In a subsequent study, the same authors produced $Er@C_{82}$ and $Er_2@C_{82}$ by the carbon arc method. Time-of-flight mass spectrometry suggested that the bimetallic species is the most abundant metallofullerene in the samples. Low-temperature photoluminescence spectra display at least three lines attributable to lanthanide emission (1.520, 1.526, and 1.545 nm). It was concluded from molecular orbital calculations that this emission arises mainly from the bimetallic species, because the lowest unoccupied molecular orbital (LUMO) of the C_{82}^{3-} fullerene lies at 5000 cm^{-1}, that is lower than the $Er(^4F_{13/2})$ level. This is not the case for C_{82}^{6-} for which the energy of the LUMO has been measured at 9000 cm^{-1} for a Sc^{II} fullerene, $Sc_3@C_{82}$, so that energy transfer from the cage to the metal ion is feasible for $Er_2@C_{82}$ (Hoffman et al., 1998). This result has been confirmed later by two other groups (Ding et al., 1997a; Ding et al., 1997b; MacFarlane et al., 1997). In particular, MacFarlane produced three different isomers of $Er_2@C_{82}$, separated by repeated HPLC passes. One isomer was isolated with >96% purity and was dissolved in carbon disulfide and in a mixture of *cis* and *trans* decalin (decahydro-naphthalene) which forms a glass when frozen. The room-temperature

absorption spectrum of the carbon disulfide solution extends down to 1.3 μm, with distinct features at 1.1 μm, 900 nm, and 700 nm. The emission spectra of the decalin glass and of the frozen CS_2 solution at 1.6 K exhibit the characteristic Er^{III} emission centered at 1.57 μm. A fine structure assigned to an exchange coupling between the two encaged Er^{III} ions has been identified on the 1.51 μm component of the transition. Although the $Er(^4I_{13/2})$ lifetime could not be measured, an upper limit, <50 μs, could be determined, corresponding to an intrinsic quantum yield of less than 0.1% (MacFarlane et al., 1997). In fact, it has been shown that vacuum sublimation of the soot at low temperature (350–430 °C) leads to a mixture with $Er@C_{60}$ as the main component. The metallofullerene can then be isolated in good purity by HPLC, as shown by time-of-flight mass spectrometry (Ogawa et al., 2000). In light of this result, Hoffman and Conley re-investigated their initial system, producing thin films under various conditions, avoiding any contact with air. Fluorescence from two samples generated by vacuum sublimation at 430 and 850 °C was compared to the emission of a sample obtained directly from the toluene extract. The latter clearly shows a line at 1.519 μm, typical of $Er_2@C_{82}$ while the film obtained at high-temperature displays, in addition, two lines at 1.511 and 1.526 μm, typical of $Er@C_{60}$. The film sublimated at low temperature is devoid of the line corresponding to $Er_2@C_{82}$ (Hoffman and Conley, 2001). This demonstrates that sample preparation is very crucial for metallofullerene and sometimes difficult to control precisely, especially that the purity of the isolated samples is rarely larger than 95%, opening the way to artifacts generated by minor species.

Erbium has also been introduced into another family of endohedral fullerenes, namely $Ln_xSc_{3-x}N@C_{80}$. This system is interesting because it possesses icosahedral I_h symmetry, as demonstrated for $Sc_3N@C_{80}$ by NMR spectroscopy (Stevenson et al., 1999). Moreover, the synthesis mainly produces one isomer and the entire $Er_xSc_{3-x}@C_{80}$ is available for $x = 0-3$. The crystal structure of $ErSc_2N@C_{80}$ points to triangular tri-metal nitride R_3N^{6+} groups inside C_{80}^{6}-cages (Olmstead et al., 2000); extended Hückel calculations indicate that the C_{80} edifice is greatly stabilized by the addition of six electrons. Lifetimes of the $Er(^4I_{13/2})$ levels have been measured at 1.6, 77, and 300 K for the three compounds with $x = 1$, 2, and 3; they lie between 1.1 and 1.6 μs, with a marked difference between the species with $x = 3$ and the two other compounds. Analysis of the narrow multiplet arising from ligand-field splitting allows one to further characterize each particular species. The quantum yield estimated from the lifetimes is on the order of 10^{-4}, that is comparable to the one determined for glassy or crystalline hosts (MacFarlane et al., 2001).

3.4.6. *Ionic liquids and liquid crystal phases*

Room temperature ionic liquids (RTIL) are non-flammable, non-volatile liquids which can potentiality replace usual organic solvents in almost every field of chemistry (e.g. catalysis, synthesis, or electrochemistry). A working definition of an ionic liquid is a salt with a melting temperature below the boiling point of water. Both the cationic and the anionic components of these liquids can be easily varied and they can therefore be tailored for specific applications or sets of properties. As a consequence, RTIL's represent an environmental-friendly, "green" alternative to volatile organic solvents. They were discovered at the beginning of the 19th century but they remained laboratory curiosities until the 1960's when

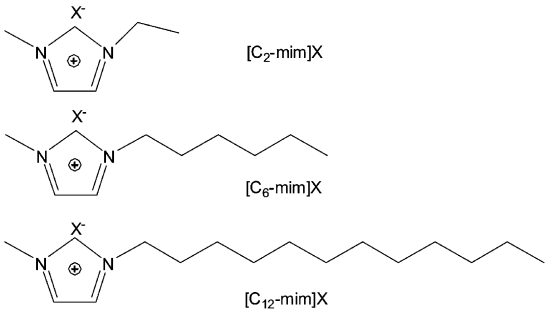

Fig. 110. Examples of methylimidazolium ionic liquids.

aluminates were developed as electrolytes for fuel cells and batteries. The interest for these compounds with respect to broader applications only developed in the 1990's but today a large number of these compounds have been synthesized and tested (Moutiers and Billard, 2004; Wasserscheid and Welton, 2005). Several ionic liquids are colorless and are transparent through almost the whole visible and NIR spectral ranges. Together with their excellent chemical stability, this makes them quite adequate as optical solvents. The spectroscopy of lanthanide ions in these media is not yet well known, but initial studies demonstrated novel aspects, with, in addition, the ability of some RTILs to stabilize Ln^{II} divalent states (Billard et al. 2003, 2004). One of the most studied classes of ionic liquid derives from the 3-methylimidazolium cation substituted in position 1 by an alkyl chain of variable length (fig. 110). Another advantage of the RTILs is that a wide range of anions can be tested, particularly large non-coordinating anions, such as triflate (Otf), bis(trifluoromethanesulfonyl)imide (Tf_2N) or bis(perfluorobutylsulfonyl)imide, $[C_4F_9SO_2]_2N^-$ (pbs). On the other hand, precautions have to be taken in that the properties of RTILs are very sensitive to their water content and most of the ionic liquids are highly hygroscopic.

Neodymium salts with Br^-, Otf^-, and Tos^- (tosylate) as anions have been dissolved in the ionic liquids with the corresponding anions, [C_6-mim]Br and [C_2-mim]X (X = Otf, and Tos), and the Judd–Ofelt parameters Ω_2, Ω_4, and Ω_6 were calculated from the absorption spectra. The Ω_2 parameter is associated with short-range coordination effects, while the two other parameters depend on long-range effects. The first parameter for the investigated salts amounts to 5.2, 4.8, and 8.5×10^{-20} cm^2 for Br, Otf, and Tos, respectively that is 2–3 fold larger than for the aquo ion (2.25×10^{-20} cm^2, cf. table 4), despite the weak binding properties of the anions. NIR luminescence was observed for the three systems upon direct excitation in the $^4G_{5/2} \leftarrow {}^4I_{9/2}$ transition at 586 nm (Driesen et al., 2004a) and the lifetimes of the Nd($^4F_{3/2}$) level are 1.51, 0.38, and 0.80 μs for Br, Otf, and Tos, respectively. Neutral and anionic lanthanide complexes are also stable in ionic liquids as demonstrated by an extensive physico-chemical study of $[Ln(tta)_n]^{(n-3)-}$ ($n = 3, 4$) in [C_4-mim]Tf_2N/water biphasic system (Jensen et al., 2003): the $[Nd(tta)_4]^-$ absorption and emission spectra in this RTIL match those recorded for the same species in *o*-xylene, for instance. Similarly, the tetrakis(β-diketonate) complex of Nd^{III} with 4,4,4-trifluoro-1-(2-naphthyl)-1,3-butanedionate, $[Nd(NTA)_4]^-$, in [C_6-mim]Br

displays the characteristic Nd^{III} NIR emission under excitation into the diketonate levels, and a similar observation has been made for [Nd(pbs)$_3$(phen)] in [C_6-mim]pbs (Driesen et al., 2004a).

With respect to the water content of RTILs, the detrimental influence of water on the spectroscopic properties of LnI_3 salts (Ln = Nd, Er) dissolved in [C_{12}-mim] Tf_2N is evidenced by the disappearance of the NIR luminescence as soon as the samples are exposed to air. On the other hand, the quantum yield of an anhydrous solution of the Nd^{III} salt amounts to $1.5 \pm 0.2\%$, a quite high value, which compares favorably with those obtained in *deuterated* organic solvents (see table 21 below). The corresponding lifetime is $\tau(^4F_{3/2}) = 15.3$ μs; the luminescence intensity of the Er^{III} salt was too low to determine the quantum yield, but the $^4I_{13/2}$ lifetime is in the microsecond range, 10.4 μs (Arenz et al., 2005). Interestingly, the dysprosium NIR absorption $^6F_{11/2}$, $^6H_{9/2} \leftarrow {}^6H_{15/2}$ in the range 7000–9000 cm^{-1} is seen in this solvent and the lifetime of the visible emitting level $^6H_{15/2}$ is similar to the one found in deuterated water, 63 μs (Mudring et al., 2006).

Other ionic liquids of interest are those displaying simultaneously liquid crystalline properties (Binnemans, 2005a). Indeed, liquid crystalline phases provide anisotropic media which are used in displays (LCD) and succeeding in producing emissive LCDs by rendering the liquid crystalline phase luminescent would be a definitive advantage. Several strategies have been proposed for the design of lanthanide-containing liquid crystalline phases (Terazzi et al., 2006). With respect to the NIR spectral range, mesomorphic materials could be useful in optical communications by acting as switchable light-converting devices. The first near-infrared photoluminescent liquid–crystalline material has been made by doping the nematic liquid–crystalline matrix *N*-(*p*-methoxybenzylidene)-*p*-butylaniline (MBBA) with [Ln(dbm)$_3$(phen)], Ln = Nd, Er, Yb. The photoluminescence intensity of the Yb^{III} sample increases by 100% when the isotropic phase is cooled to the nematic phase, due to the birefringence nature of the liquid crystalline phase, which better diffuses light and leads to enhanced excitation of the lanthanide ion (Van Deun et al., 2003b). Imidazolium chlorides with long alkyl chains, e.g. [C_{12}-mim]Cl, form lamellar arrays in the crystalline phase and an enantiomeric smectic crystalline phase (termed SmA_2) at room temperature. The crystal-to-SmA_2 transition temperature depends on the hydration of the ionic liquid, ranging from −2.8 °C for anhydrous [C_{12}-mim]Cl to +44.5 °C for the monohydrated species. Lanthanide salts, such as chlorides, nitrates, triflates, or perchlorates can be doped into the liquid crystalline phases without disturbing the mesomorphic properties of the ionic liquid, up to a concentration of 10 mol% (Guillet et al., 2004). A similar strategy was adopted to insert 1 mol% of highly luminescent β-diketonate complexes [Ln(tta)$_3$phen] (Ln = Nd, Er, Yb) into the same ionic liquid (Puntus et al., 2005). Due to the relative sensitivity of the complexes to thermal decomposition, thermal treatment of the resulting materials could not be made at temperatures allowing complete dehydration and the transition temperature was in the range 6–12 °C. On the other hand, the smectic A_2 phase is retained after introduction of the complexes, as ascertained by differential scanning calorimetry and small-angle X-ray diffraction data. Despite the low concentration of the lanthanide complexes, all three samples displayed NIR luminescence with an intensity comparable or larger than the one exhibited by the solid state samples. This is particularly true for the Yb^{III} mesophase, with an associated quantum yield

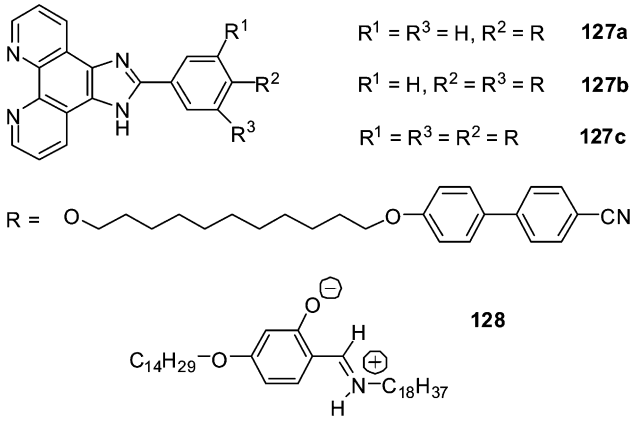

Fig. 111. (Top) Imidazo[4,5-f]1,10-phenanthroline ligands for metallomesogens. (Bottom) Salicylaldimine Schiff base for low temperature lanthanidomesogens.

of $2.1 \pm 0.3\%$, as compared to $1.6 \pm 0.2\%$ for microcrystalline [Yb(tta)$_3$phen] (Puntus et al., 2005) or to $1.1 \pm 0.1\%$ for its solution in toluene (Meshkova et al., 1999). Interestingly, these NIR-emitting mesophases can be excited up to 410 nm, in the visible.

Liquid crystalline phases containing lanthanide ions are also obtained by the design of suitable ligands. The resulting complexes are termed lanthanidomesogens and the nature of the liquid crystalline phases obtained depends on the ligand design (Piguet et al., 2006). Few systems deal with luminescent lanthanidomesogens and among them only a couple report NIR luminescence. To obtain nematic phases containing lanthanide ions, K. Binnemans and coworkers (Cardinaels et al., 2005) have decoupled the mesogenic groups from the metal-coordinating group by a flexible spacer (fig. 111). The lanthanide β-diketonates [Ln(tta)$_3$] are simply dissolved in the liquid–crystal host and phase separation is prevented by the covalent link between the metal ion and the mesogenic moiety (here through the phenanthroline group). All of the [Ln(tta)$_3$**127**] complexes present a crystalline-to-nematic transition around 75–92 °C depending on the metal ion and mesogenic ligand; the nematic phases exist over a temperature range of 35–50 °C. The Nd^{III} ternary complex with **127a** and the Er^{III} and Yb^{III} ternary complexes with **127b** display an intense and well characterized NIR emission at room temperature. NIR luminescence is also seen for [Sm(tta)$_3$**127b**] in the range 880–950 nm, corresponding to the $^4G_{5/2} \rightarrow {}^6F_J$ transitions ($J = 7/2, 5/2$), and around 1180 nm, assigned to $^4G_{5/2} \rightarrow {}^6F_{9/2}$. In order to obtain lanthanide mesophases close to room temperature, the same authors have prepared β-diketonate ternary complexes with a salicylaldimine Schiff base derivative, [Ln(tta)$_3$(**128**)$_2$] and [Ln(btfa)$_3$(**128**)$_2$]. The transition temperatures from initial glassy states to smectic A phases occur between 20 and 24 °C for La^{III} to Er^{III} complexes with thenoyltrifluoroacetonates while the corresponding benzoyltrifluoroacetonates display somewhat lower transition temperature, around 18–19 °C. Thin films of [Nd(tta)$_3$(**128**)$_2$] and [Nd(btfa)$_3$(**128**)$_2$] emit in the NIR and the lifetimes of the Nd($^4F_{3/2}$) level amount to 0.44 and 0.38 μs, respectively. The luminescence from the Er^{III} compounds is much weaker but can

nevertheless be observed at room temperature, with lifetime of 0.66 μs (tta) and 0.56 μs (btfa) for the $^4I_{13/2}$ level (Y.T. Yang et al., 2006).

4. Overview of potential applications

Potential applications of lanthanide-induced NIR emission essentially lie in two main fields: optical and electro-optical devices on one hand, including laser materials, amplifiers, and light emitting diodes, and biomedical analysis on the other hand. While the latter field is in its infancy, optical applications are numerous and we do not intend to cover them thoroughly. Moreover, keeping to our working principle, purely inorganic systems, such as glasses or nanocrystalline silicon thin films which have generated a wealth of publications during the last 30 years or so, are excluded from the review, and we concentrate on systems using lanthanide chelates.

4.1. *Inorganic liquid lasers*

Crystals and glasses containing trivalent neodymium ion have been widely used as laser materials. Since single-crystal growing and shaping were complicated techniques at the end of the 1960's and beginning of the 1970's, many researchers focused on lanthanide-doped liquids exhibiting laser action at room temperature, and thus providing a potential alternative to solid-state lasers (Batyaev, 1971; Heller, 1968a). Some initial studies focused on solutions of β-diketonates (Binnemans, 2005b) or fluorinated propionates (Heller, 1967), but it became rapidly evident that efficient nonradiative deactivation by vibrations of the organic ligands was difficult to overcome, so that researchers turned to purely inorganic systems. This field of research appears now to be abandoned, but we nevertheless review it, at least as far as neodymium lasers are concerned, so as to bring some of the accumulated data to the knowledge of younger readers.

In order to allow the accumulation of ions in the metastable state, for instance, the Nd($^4F_{3/2}$) level, and thus achieve population inversion, a fundamental requirement for these liquids is minimization of radiationless relaxation paths. Deactivation through vibrations can be prevented following two different strategies. The first one consists in using laser active materials possessing strongly allowed transitions, like fluorescent organic dyes. In this case the radiative deactivation occurs at rates which are fast relative to the nonradiative ones. The second strategy is based on the weakening of the vibrations in the environment of the laser active ion so that they do not compete with the lanthanide transitions. This can be achieved either by totally excluding high-energy vibrations from the system or by shielding the ion from its environment by the coordination of one or several ligands having no such high-energy vibrations.

4.1.1. *Neodymium in selenium oxychloride*

A number of solvent systems have been screened for potential ionic (uncomplexed) Nd^{3+}-based liquid lasers. These systems must meet several requirements: they should (i) not contain

light atoms, particularly hydrogen and deuterium, (ii) be devoid of vibrations with frequency exceeding 2000 cm^{-1}, (iii) have high dielectric constants to allow the complete dissolution of the lanthanide salts and (iv) be transparent in the pumping range (500–900 nm) and emission range (1000–1400 nm) of Nd^{3+}. Selenium oxychloride, $SeOCl_2$, meets all these requirements and has therefore been used in numerous studies. Since no lighter atoms than oxygen is present, there are no vibrations of sufficient energy to accept the energy corresponding to the gap between the excited and ground multiplets. Indeed the highest vibration of selenium oxychloride is 955 cm^{-1}, whereas the smallest possible gap for Nd^{III} amounts to 5500 cm^{-1}. In spite of the high dielectric constant of selenium oxychloride, neodymium oxide and chloride dissolve only to a limited extent in this solvent. One way to increase the concentration of Nd^{3+} in such systems consists in designing neutral or acidic solutions, by adding aprotic acids, like $SnCl_4$, $TiCl_4$, $SbCl_5$, for instance. This leads to the formation of a Lewis acid–selenium oxychloride adduct, $(MCl_6)^{n-}(SeOCl^+)_n$, which further decomposes to provide the strong acid species $SeOCl^+$. This species then reacts with neodymium oxide or chloride, solubilizing it:

$$SnCl_4 + 2SeOCl_2 \rightleftharpoons SnCl_6^{2-} + 2SeOCl^+,$$

$$SbCl_5 + SeOCl_2 \rightleftharpoons SbCl_6^- + SeOCl^+,$$

$$6SeOCl^+ + Nd_2O_3 \rightleftharpoons 2Nd^{3+}(solv) + 3SeOCl_2 + 3SeO_2,$$

$$3SeOCl^+ + NdCl_3 \rightleftharpoons Nd^{3+}(solv) + 3SeOCl_2,$$

where $Nd^{3+}(solv)$ represents in fact the solvated ion with several selenium oxychloride molecules coordinated in the first coordination sphere, that is $[Nd(SeOCl_2)_m]^{3+}$. The anions $(MCl_6)^{n-}$ of the aprotic acid are coordinated in the outer sphere of $Nd^{3+}(solv)$. Indirect evidence for this outer shell coordination is given by the electronic absorption spectra of the Nd^{3+} f–f transitions which are independent of the aprotic acid used.

In such laser solutions the most undesirable impurities are hydrogen-containing compounds, since hydrogen atoms are known to provide highly energetic oscillators (O–H or N–H, for instance). As a consequence these compounds have to be eliminated and this can be done either by using extremely pure solvents or by separating the undesired products during the preparative steps (Heller, 1968c). Since the extreme solvent purification techniques required are tedious, the second way is generally followed and hydrogen-containing compounds are removed by distillation along with part of the solvent. The obtained mixture is usually deep brown owing to the presence of reduction products such as selenium or diselenium dichloride Se_2Cl_2. The brown products interfere with the optical pumping of the laser solutions and are eliminated by oxidation with $KClO_3$. Finally, vacuum removal of the dissolved gases (chlorine or chlorine dioxide) formed during the chlorate treatment yields solutions that contain only selenium dioxide, tetrachloride, or oxychloride, which do not absorb in the spectral range used for optical pumping.

The laser liquids prepared by these techniques possess properties, such as high gain and sharpness of the emission, that are more characteristic of crystalline hosts (Nd^{3+}:$CaWO_4$ or Nd^{3+}:YAG) than glass lasers (Heller, 1966; Heller, 1968a; Lempicki and Heller, 1966). Moreover, under identical excitation conditions, the solutions have $^4F_{3/2} \rightarrow {}^4I_{11/2}$ emission

intensity exceeding the emittance of the best neodymium-doped sodium-compensated calcium tungstate laser crystals. In systems containing $SeOCl_2$, the lifetimes of the Nd($^4F_{3/2}$) level ranges between 150 and 255 μs, depending on the conditions used for preparing the solution. Basic solutions, prepared without addition of Lewis acids, exhibit the lowest lifetime, whereas the system $SbCl_5$:$SeOCl_2$ possesses the longest one (255 ± 10 μs). Tin tetrachloride gives a very similar lifetime of 240 ± 10 μs. Since the viscosity of the solutions are quite high, and increases with increasing amounts of neodymium salt and Lewis acid, attempts have been made to reduce it. For the system $SnCl_4$:$SeOCl_2$, this can be done by removing the excess of acid by fractional distillation, leading to solutions with lower viscosity, referred to as "neutral" solutions. However, the luminescence characteristics of these neutral solutions are not as good as the ones of acidic solutions. This can be explained by the enhancement of diffusion-assisted quenching processes since the liquid is less viscous. The best lifetimes obtained for the neutral solutions reach only 200 ± 10 μs.

The quantum yields of fluorescence of the different systems have also been determined relative to a single crystal of neodymium-doped YAG for which a quantum yield of unity has been assumed (Heller, 1968a). The quantum yields obtained, even if they are accurate only within a factor of two, follow the same trend as for the lifetimes, with the highest values for the acidic solutions; 0.70 and >0.75 in presence of $SnCl_4$ and $SbCl_5$, respectively. Neutral and basic solutions are less luminescent and have quantum yields of 0.5 and 0.4, respectively. Identical measurements performed on a sodium-compensated neodymium-doped calcium tungstate crystal lead to a value of 0.5. The high quantum efficiency and the low threshold (between 2 and 40 J) of these Nd^{3+}:$SeOCl_2$ systems clearly demonstrate that liquids are not inherently inferior to solids as laser materials.

In all the studies described above, the stimulated emission originates in the $^4F_{3/2} \rightarrow {}^4I_{11/2}$ transition of Nd^{3+} ion near 1.06 μm. The possibility of observing stimulated emission from other Nd^{3+} transitions has also been explored (Heller and Brophy, 1968). Stimulated emission from the $^4F_{3/2} \rightarrow {}^4I_{13/2}$ transition at 1.33 μm can indeed be achieved at room temperature whereas such a phenomenon is not observed for the $^4F_{3/2} \rightarrow {}^4I_{9/2}$ transition. However the cross section for stimulated emission at 1.33 μm is 11-fold smaller than the stimulated emission at 1.06 μm and the threshold required is one order of magnitude larger.

From a more technical point of view, liquid lasers solutions containing Nd^{3+} in $SeOCl_2$ display an unusual and interesting phenomenon, referred to as self Q-switching. It consists in the generation of highly energetic pulses with peak powers in the range of 300–500 MW (Samelson et al. 1968b, 1968a; Samelson and Lempicki, 1968). Such output powers are achieved without the aid of any devices, like Pockel or Kerr cells, saturable absorbers, for instance.

4.1.2. *Neodymium in phosphorus oxychloride*

Selenium oxychloride is not the only inorganic solvent used for liquid lasers, several studies use as solvent phosphorus oxychloride, $POCl_3$ (Blumenthal et al., 1968; Brecher and French, 1969; Brinkschulte et al., 1972). Although this solvent is a worse host for ionic salts due to its lower dielectric constant, it is much more attractive for liquid laser uses since it is far less toxic and corrosive than $SeOCl_2$. The approach for the preparation of $POCl_3$ solutions is slightly

different from that described for $SeOCl_2$. With $POCl_3$, the dissolution of neodymium oxide can be described by the following equation:

$$Nd_2O_3 + 3SnCl_4 + 6POCl_3 \rightleftharpoons 2Nd^{3+}(solv) + 3SnCl_6^{2-} + 3P_2O_3Cl_4.$$

However, due to the much lower solubility of rare earth salts in $POCl_3$, concentrations of Nd^{3+} needed for laser solutions cannot be achieved in pure and completely anhydrous solvent. The addition of water to acidified $POCl_3$ in a molar ratio of about 1:10 increases dramatically the solubility of Nd^{3+}. It is believed that one of the compounds resulting from the reaction of water with phosphorus oxychloride enhances the solubility of Nd^{3+} in $POCl_3$:$SnCl_4$. The difficulty consists in returning to the aprotic state without destroying the compound responsible for the solubility enhancement. This has been done by boiling off a sufficient fraction of the solution to remove all the residual HCl and H_2O and finally by adding anhydrous $POCl_3$ and $SnCl_4$ to reach the desired concentration. A 0.3 M Nd^{3+} solution in $POCl_3$:$SnCl_4$ prepared in this way has a fluorescence decay time of 245 μs whereas the corresponding laser solution with $SeOCl_2$:$SnCl_4$ has a lifetime of 260 μs. The comparison of the $SeOCl_2$ and $POCl_3$ aprotic solvents leads to the conclusion that the differences between the two liquid laser systems are not large (Brecher and French, 1969). In addition to its lower corrosiveness and toxicity the $POCl_3$ system has the advantage over selenium oxychloride solutions that the $^4F_{3/2} \rightarrow {}^4I_{11/2}$ has larger intensity whereas the resonant $^4F_{3/2} \rightarrow {}^4I_{9/2}$ transition is less intense. Thus the proportion of energy reaching the $^4F_{3/2}$ excited state and being emitted in the desired spectral range is much greater for $POCl_3$ solutions. This leads to a decrease of the overall transition probability from this state and hence makes potentially a more efficient laser system. However, comparison of the measured lifetime with the one calculated from spectroscopic considerations shows it to be about 20% smaller than the calculated value (310 μs) and thus points to nonradiative losses from the emitting state. For the $SeOCl_2$ system, the measured and calculated lifetimes are nearly identical (280 μs), indicating the absence of losses and hence a quantum efficiency close to unity. Vibrational coupling is a possible explanation for nonradiative deactivation in the $POCl_3$ system. Indeed a rather intense absorption is present in the infrared spectrum in the region of the first overtone of the P–O stretching vibration, whereas only a very weak second overtone of the Se–O vibration is observed in the corresponding $SeOCl_2$ system. Except for these differences, the two systems are quite similar and the choice of one or the other depends mainly on experimental conditions.

Different Lewis acids are used to facilitate the dissolution of relatively high amounts of Nd^{3+} salts in the inorganic phosphorus oxychloride. Except well-known tin tetrachloride, acids such as $TiCl_4$, $AlCl_4$, $ZrCl_4$ or BBr_3 have been used to develop suitable systems showing laser action (Brinkschulte et al., 1972; Schimitscheck, 1968). The $POCl_3$:$ZrCl_4$ system has been studied in more details in the work of Hongyo et al. (1972) and Brecher and French (1973).

4.1.3. *Other lasing ions*

Erbium and ytterbium ions also display NIR emission in selenium oxychloride (Heller, 1968b). Simple $Nd^{3+} \rightarrow Yb^{3+}$ and double $Nd^{3+} \rightarrow Yb^{3+} \rightarrow Er^{3+}$ energy transfers have been investigated. In selenium oxychloride solutions, energy transfer processes depend to a

greater extent of the acidity of the medium, the more acidic solutions exhibiting the poorer energy transfer efficiency. In this respect, basic solutions are most suited. However, due to the lower solubility of rare earth salts in basic media, neutral solutions were preferred. Upon excitation at 578 nm, a wavelength absorbed only by Nd^{3+}, the characteristic Yb^{3+} fluorescence is observed in parallel to Nd^{3+} emission in the binary solution. Using the same excitation wavelength for the ternary solution, simultaneous emission of the three ions, Nd^{3+}, Yb^{3+} and Er^{3+} occurs. The Er^{3+} luminescence is particularly well sensitized by the Yb^{III} $^2F_{5/2} \rightarrow {}^2F_{7/2}$ transition, which fully overlaps the Er^{III} ($^4I_{11/2} \leftarrow {}^4I_{15/2}$) absorption band. In absence of sensitizing ion, no Er^{3+} luminescence is observed.

4.1.4. *A second try*

Although numerous studies have been performed on selenium oxychloride or phosphorus oxychloride as inorganic solvent for liquid lasers, systems based on these solvents have no longer been developed and utilized for almost twenty years because of their high toxicity and corrosiveness toward structural materials. At the end of the 1980's, attempts have been made in order to develop inorganic liquid lasers with low toxicity, using mixtures of bromides (e.g. $AlBr_3$–$SbBr_3$–PBr_3–$NdBr_3$) or chlorides ($SOCl_2$–$AlCl_3$, $SOCl_2$–$GaCl_3$). The lasing properties of $NdCl_3$ in $SOCl_2$–$GaCl_3$ are comparable ($\tau = 240$ μs) to the $SeOCl_2$- or $POCl_3$-based lasers, but with lower toxicity and viscosity (Batyaev et al., 1989b). The same binary aprotic solvent has been used to study energy transfer in solution occurring between Yb^{III} and Er^{III} ions (Batyaev et al., 1989a). In 1995, Han et al. (1995) studied the possible use of a Nd^{3+} solution in ethyleneglycol as amplifier gain medium for a Nd^{3+}:YLF (yttrium lithium fluoride) laser. Since this study, no improvement has been achieved anymore.

4.2. *Optical fiber amplifiers and waveguides*

In optical telecommunication systems, light carries information between several users. Optical links consisting in single-mode silica optical fibers are now used in telecommunications and have the ability of providing high-bandwidth and long-distance communication. The manipulation of the optical signals on a local scale requires splitters, couplers, multiplexers, de-multiplexers, and amplifiers. These devices are easy to make and can be integrated on one planar substrate with a technology called integrated optics, a basic element of which is the planar optical waveguide. It consists of a high refractive index guiding core layer of typical dimension 2×1 μm^2, sandwiched between two lower-index cladding layers (fig. 112 gives an example for a PMMA device). The optical signal travels in the guiding layer and total internal reflection at the interface between the core and cladding maintains it in the waveguide. The increasing demand for optical links in the office and at home is generating interest for cheap optical devices which can be directly installed by the end-user, a reason why plastic optical fibers receive presently a lot of attention. Indeed, they have clear technical advantages over glass fibers: a better flexibility and a large core diameter enabling efficient coupling. If the guiding layer of an optical fiber is doped with an active element, optical gain results upon adequate pumping. Typical low-cost plastic optical fibers of 100 m length have an attenuation of 100 dB km^{-1} and a bandwidth around 5.1 GHz. More importantly, fluorinated fibers are

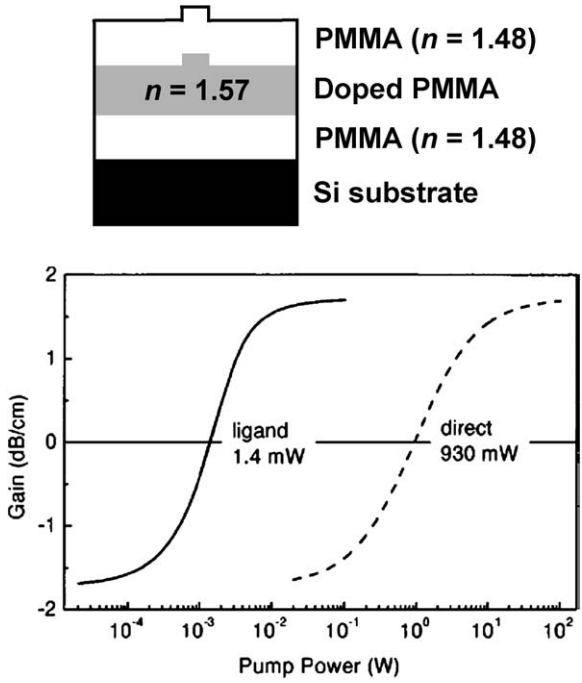

Fig. 112. (Top) Polymer channel waveguide for optical gain. (Bottom) Calculated differential optical gain for an Er-doped devices (organic complex, $2 \times 1\ \mu m^2$ core section) as a function of pump power for direct (- - -) and ligand (—) excitation; reproduced with permission from (Slooff et al., 2002).

at hand, with an optical transmission range extending in the NIR range (Kuriki et al., 2002). This has triggered a large number of projects aiming at developing polymers containing highly luminescent lanthanide complexes, mostly β-diketonates.

Under direct Ln^{III} excitation and assuming that the population of the ground state (N_g) of the emitting 4f ion decays rapidly to populate the first excited state (N_e), the rate equations reduce to those of a two-level system, and further assuming steady state, one gets

$$N_g = \frac{W_e}{W_e + R} \cdot N \quad \text{and} \quad N_e = \frac{R}{W_e + R} \cdot N \quad \text{with } R = \frac{\sigma_a P \lambda}{hca}, \tag{40}$$

where W_e is the Ln^{III} decay rate, N the Ln^{III} concentration, P the pump power in the waveguide, σ_a the absorption cross section, λ the excitation wavelength, and a the waveguide core cross section. The differential optical gain (OG, in dB cm^{-1}) is given by:

$$\mathrm{OG} = 10 \times {}^{10}\log\frac{I}{I_0} = 10 \times {}^{10}\log\left(e^{kx}\right) \quad \text{with } k = \sigma_e \cdot (N_e - N_g) \cdot \alpha, \tag{41}$$

in which I_0 is the light intensity at the beginning of the waveguide and I the intensity along the waveguide, k is the optical gain factor, σ_e the emission cross section, and α the fraction

of incident light confined in the core of the waveguide. In the case of Er^{III}, Slooff et al. (2002) have calculated the gain factor versus the pump power with the following parameters: $W_e = 1.25 \times 10^6\ s^{-1}$ (corresponding to $\tau_{obs} = 0.8\ \mu s$), $\sigma_a = 1.1 \times 10^{-20}\ cm^2$ at $\lambda = 488$ nm, $\sigma_e = 1.1 \times 10^{-20}\ cm^2$ at 1.54 μm, $a = 2\ \mu m^2$, $N = 9 \times 10^{19}\ cm^{-3}$, $\alpha = 0.4$. The threshold power, that is the power at which k becomes positive is 930 mW (fig. 112, dashed curve) which is much higher than the minimum power needed in Er^{III}-doped glasses or alumina amplifiers. This can be traced back to the very small quantum yield of Er^{III} in organic media. But this threshold power can be dramatically reduced if excitation is made in the ligand levels for which the absorption cross section is much larger ($\approx 10^3$-fold). Taking the ligand-to-Ln^{III} ion energy transfer into consideration and assuming than the isc ($^1S \rightarrow {}^3T$) process is fast, calculation of the gain proceeds as follows:

$$\frac{dN_\ell}{dt} = R_\ell N_{g\ell} - W_{\ell r} N_\ell - W_{\ell nr} N_\ell N_g \quad \text{with } R_\ell = \frac{\sigma_\ell P \lambda}{hca}, \tag{42}$$

$$\frac{dN_e}{dt} = -W_e N_e + W_{\ell nr} N_\ell N_g, \tag{43}$$

in which N_ℓ and N_e are the population fractions of the excited states of the ligand and Ln^{III} ion, respectively, while $N_{g\ell}$ and N_g are the corresponding values for the ground states, $W_{\ell n}$ is the ligand radiative decay rate, $W_{\ell nr}$ is the ligand nonradiative (transfer) rate, and σ_ℓ is the ligand absorption cross section. In the case of the triphenylene-based organic complexes of Er^{III} (see section 3.2.3), $\sigma_\ell = 8.5 \times 10^{-18}\ cm^2$, $W_{\ell r} = 2 \times 10^8\ s^{-1}$, and $W_{\ell nr} = 10^9\ s^{-1}$, resulting in the plain curve in fig. 112 and in a threshold power of only 1.4 mW. Note however that these calculations do not take up-conversion and excited state absorption into account, which may increase the pump power needed for amplification (Polman and Van Veggel, 2004; Slooff et al., 2002).

The main problem for lanthanide-containing NIR optical fibers is the minimization of non-radiative deactivation of the excited states. Several groups, including industrial laboratories, have devoted a large effort to develop strategies addressing this problem along several lines: (Hasegawa et al., 2004; Slooff et al., 2002; Yanagida et al., 1998).

(i) Suppression of vibrational deactivation (including the one induced by water molecules). This problem has been discussed in section 3.2.1 and is usually dealt with by adding long perfluorinated lateral chains on the β-diketonate, by deuterating the C–H bridge and by working in deuterated solvents. The longer the perfluorinated chain, the less water molecules penetrate into the inner coordination sphere. They are also expelled by coordination of strong donor such as dmso. Despite these improvements, the intrinsic quantum yields remain small, for instance, they do not exceed 3% for Nd^{III} in acetone, a solvent with C–H vibrations.

(ii) Inhibition of energy migration between luminescent centers and of up-conversion processes. Diffusion of Ln^{III} chelates in solution induces collisions between molecules, leading to energy transfer via cross-relaxation and excitation migration (see fig. 113 for an illustration in the case of Nd^{III}). Both processes are based on dipole–dipole interactions. In cross relaxation, energy is partially transferred to a neighboring ion, leaving

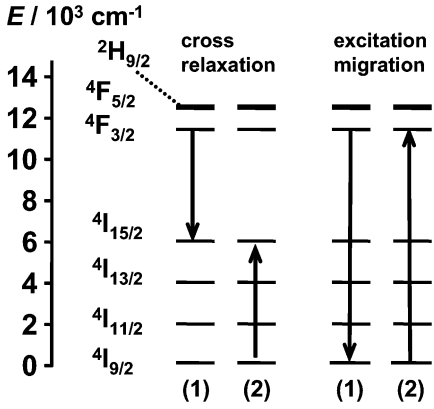

Fig. 113. Radiationless transitions via energy migration in Nd^{III} samples.

both ions in a lower energy level, e.g. Nd($^4I_{15/2}$), from which they relax easily in a nonradiative way to the ground level. Migration of energy by hopping onto a neighboring ion does not quench luminescence by itself, but it enhances the probability of quenching by permitting the energy to finally migrate onto a site where more rapid nonradiative decay takes place. The only way of avoiding this "concentration quenching" is to keep luminescent centers enough apart ($r_{Ln-Ln} > R_0$) so that the probability of transfer is reduced. This can be done either by having large complexes, e.g. [Nd(pom)$_3$] (fig. 48) which possesses long fluorinated alkyl chains, or by dispersing them into polymer matrices.

One problem with polymers such as polymethylmethacrylate (PMMA) though is the presence of C–H bonds so that the use of polymers with low percentages of C–H bonds is recommended. One example is polyhexafluoroisopropylmethacrylate (P-FiPMA). Additionally, dmso-d_6 can be added to improve the quantum yield. For instance, the intrinsic quantum yield of [Nd(hfa-d_1)$_3$(D_2O)$_2$] incorporated in PMMA (weight percentage of H-atom: 8%) is only 0.1%, that is comparable to the yield measured in methanol-d_4 (see table 11). When 6.6 wt% of dmso-d_6 is added, it increases to 0.5%, and finally, reaches 0.7% with P-FiPMA/dmso-d_6 (containing 2.5 wt% of C–H bonds), a value still lower than in pure dmso-d_6, 1.1%, see table 11 (Hasegawa et al., 1999; Yanagida et al., 2000b). The chelates [Nd(pms)$_3$] and [Nd(pes)$_3$] (fig. 50) have been similarly incorporated into PMMA/dmso-d_6 and P-FiPMA/dmso-d_6 leading to intrinsic quantum yields of $0.9 \pm 0.2\%$ for both complexes in the first matrix and of 1.3 ± 0.1 and $1.6 \pm 0.1\%$, respectively, in the second matrix. The authors judge that these values are large enough to prepare working devices for the 1.3 μm telecommunication window (Hasegawa et al., 2003).

Up-conversion and excited state absorption are the main gain-limiting factors in Er^{III}-doped planar optical amplifiers, either glass- or polymer-based. Up-conversion increases the pump power required to achieve a certain degree of population inversion, up to factors

5–10. The ESA cross section is strongly material dependent and this phenomenon also increases the pump power needed, so that when both gain-limiting factors are present, pump powers of 10–100 mW are required, which considerably increases the cost of optical amplifiers. It is hoped that the introduction of sensitizers such as Yb^{III}, Ag^{I} or silicon nanocrystals into inorganic optical fibers will help solving this problem. Organic chelates in polymer fibers may also be an alternative (Polman and Van Veggel, 2004).

(iii) Optimization of the sensitization ability of the ligand and of the emission intensity. As seen in section 3.2.1, η_{sens} is between 20 and 30% and is larger with unsymmetrical ligands compared with symmetrical ones. Adding a second ligand to form a ternary complex, or a dye to transfer energy on the metal ion, can improve the sensitization, although it is difficult to go beyond a factor of two, possibly three. An example of such a strategy is the use of dichromated gelatin, a water-soluble volume hologram emulsion with a wide transmission bandwidth between 300 and 2700 nm. This photolime gelatin was doped by neodymium chloride hexahydrate (6.7×10^{19} ions cm^{-3}) and chlorophenol red (23%). All the active components were dissolved in a mixed solvent and no aggregation was observed in the obtained waveguide. The latter consisted in a layer of the doped gel sandwich between an Al layer deposited on glass, and an indium tin oxide (ITO) layer covered with glass. The waveguide was pumped by a tunable Ti:sapphire laser, while the signal beam was provided by a Nd:YAG laser (1.06 μm) and an optical gain of 3.8 dB was obtained at this wavelength. The optical gain heavily depends on the Nd^{III} concentration, reaching a peak in the range 4–8 $\times 10^{19}$ cm^{-3}. The waveguide also generated an optoelectronic effect (An et al., 1998). Therefore, the real problem resides in the low intrinsic quantum yields (see the two points above).

(iv) Choice of an adequate host medium and defect-free fabrication of the waveguide. The ideal host should disperse the luminescent centers sufficiently to avoid concentration quenching while simultaneously allowing high enough concentration of these centers and minimizing optical losses. Losses can come from several sources: scattering is a major one and arises from imperfections in the waveguide, such as rough sidewalls or defects in the core material. Another loss mechanism is the mismatch between the device waveguide mode and the incident light source mode. Finally, in a waveguide doped with a chromophoric organic complex, absorption of both the chromophore and the polymer backbone also contributes to the loss. The host material should also not modify the complex, or at least not the inner coordination sphere, and not provide nonradiative deactivation paths, henceforth the many fluorinated polymers and functionalized zeolites were tested.

Interestingly, attempts are also made to use optical fibers in nuclear power plants, especially for monitoring radioactivity. However, when measurements of high rate radioactive doses are performed in this way, this induces losses in the optical fibers. To remedy this problem, the use of NIR emission from rare earths ions instead of visible light has been suggested, particularly when they are inserted into inorganic matrices, such as $Gd_2O_2S:Ln^{III}$ (Ln = Pr, Nd, Yb). For instance, linear relationship between dose rate and peak counts has been demonstrated in the case of Pr^{III} (Takada et al., 1998).

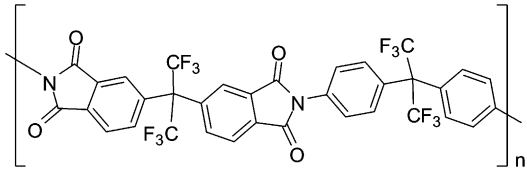

Fig. 114. Generic formula for the polyimide Ultradel®-9000.

4.2.1. *Neodymium-doped polymers*

Optical amplification in a silica fiber containing Nd^{III} has been demonstrated in 1961 (Snitzer, 1961) and since many active high-performance integrated optical devices have been fabricated in purely inorganic matrices. The first organic Nd^{III}-containing optical amplifier appeared in 1993 and was built from photolime gel doped with 5 wt% of neodymium chloride leading to a concentration of Nd^{III} ions equal to 1.03×10^{20} cm^{-3}: a gain of 8.5 dB was observed over a waveguide length of 2.2 cm using a tunable Ti:sapphire laser as the pump and a Nd:YAG laser as the source (Chen et al., 1993). Contrary to the system described under point (iii) above, no sensitizing dye was used.

Among other systems tested, neodymium octanoate doped into PMMA shows a high-transmission window between 50 and 620 nm, with the minimum loss occurring at 570 nm (27 dB km^{-1}). The fibers made with a fiber-drawing method have a coupling efficiency of 20% for a 25-cm length and a core diameter of 60 μm. Neodymium fluorescence at 575 nm occurs through a three-level system, the pump light (514.5 nm) populating the Nd($^4G_{7/2}$, $^4G_{9/2}$) levels, which decay rapidly to the $^4G_{5/2}$ level emitting orange light. Excited state absorption from the $^4G_{5/2}$ to the $^2F_{5/2}$ level has a much smaller transition probability. The threshold pump energy is relatively large, at 85 mW and the transition originating from $^4F_{3/2}$ are not seen, mainly because the transmission window of the fiber is not suitable under the experimental conditions used (Zhang et al., 1998). Observation of the orange emission from Nd^{III} has, however, been challenged and assigned to dye impurities in the fiber (Werts et al., 1999a). On the other hand, photoluminescence from the Nd($^4F_{3/2}$) level has been reported for [Nd(hfa-d_1)$_3$] doped into all-deuterated PMMA under pumping by a dye laser at 580 nm (Kuriki et al., 2000).

Since hermetic packaging of polymer optical devices is expensive, manufacturers prefer environmentally stable polymers such as epoxy or polyimide polymers, which are not water soluble. However, incorporating the Ln^{III} ion under the form of a salt into such matrices is often difficult, even with techniques such as spin- or spray-coating. This is easier with organic chelates, which dissolve in the polymer solution. A combination of choices, meeting many of the requirements for an optimum optical device, is the incorporation of [Nd(hfa)$_3$] into fluorinated polyimides such as Ultradel®-9000 (fig. 114). The doped fluorinated polyimide was spin coated and the film baked at 100 °C for a few minutes to remove the solvents before being exposed to a UV mercury lamp to crosslink the polymer. A final heat treatment under nitrogen (175 °C during 30 min) afforded a uniform film of 3 μm thickness. Several kinds of single-mode and multi-mode devices were prepared having N_{Nd} in the range 0.2–1.0 × 10^{20} cm^{-3} (about half the value in glass hosts), which have an absorption cross section of

about 10^{-20} cm^2 at 799 nm. The photoluminescence signal is about 20 dB higher than the pump power (Lin et al., 1996).

A multilayer waveguide structure with alternate layers of undoped and Nd^{III}-doped Ultradel® polyimides of the series 9000 was fabricated. Ultradel® 9020 was chosen for the top layer since it has a refractive index lower than Ultradel® 9120 used for the doped layer. The layer of undoped polyimide renders the doped polyimide layer more planar, thus reducing surface scattering losses. Channels in the active layer (50 μm × 7 μm × 5 cm) were defined by photolithography. Photoluminescence spectra are broad (fwhh = 27 nm) which is beneficial to the operation of the waveguide. A gain of 8 dB has been obtained when a continuous-wave Ti–sapphire laser operating at 800 nm was used as the pump source and a cw Nd-YAG laser operating at 1.06 μm as the signal beam. The channels were multimode at the pump and probe wavelengths and the density of Nd^{III} ions was about 10^{20} per cm^3, corresponding to 2.2 wt% (Karve et al., 2000).

As seen above, one way to improve the properties of optical amplifiers is to increase the ligand cross section, e.g. by grafting dye moieties on the chelating agent. For example, a terphenyl-based chelating agent has been functionalized with lissamine, a derivative of rhodamine, and the photophysical properties of both [Nd(**58b**)] (fig. 56) 10^{-2} M and [Nd(**60d**)] (fig. 59) 10^{-6} M were determined in dmso-d_6. When monitored at 1.06 μm, the photoluminescence intensity of the lissamine-modified chelate is very different from the reference compound, particularly in the range 475–525 nm clearly indicating energy transfer from the xanthene unit of the dye. The measured absorption cross section is in the range 10^{-17} cm^2, that is, four orders of magnitude higher than the typical intra-4f transitions of Nd^{III} (at 515 nm, the optical absorption is almost identical for the two solutions). The lissamine-functionalized chelate was introduced into fluorinated polycarbonate waveguides at concentrations varying between 1 and 10 wt%. Partially fluorinated polycarbonates are ideally suited for planar waveguide applications because the background loss at the Nd^{III} emission wavelengths is <0.05 dB cm^{-1} at 1.06 μm and 0.08 dB cm^{-1} at 1.34 μm. The waveguides were made by spin-coating a solution of polycarbonate and the chelate onto a silicon substrate covered with a 3 μm thick, thermally grown layer of silica, followed by thermal annealing at 190 °C in vacuum for one hour. The absorption cross section at 580 nm, as determined from ellipsometry and refractive index measurements, amounts to 4.5×10^{-16} cm^2, while the lifetime of the Nd($^4F_{3/2}$) level is only 0.8 μs, a substantial reduction from the 2.2 μs observed in dmso-d_6. Since the emission is not quenched by the presence of oxygen, the authors estimated that the rate of energy transfer between lissamine and Nd^{III} is faster than 10^7 s^{-1}. The distance between lissamine and the Nd^{III} ion is about 7–8 Å, whereas the effective Bohr radius for the excited lissamine and unexcited metal ion is about 2.5 Å. According to Dexter theory, this means that only 3% of the maximum possible energy transfer is reached. There are two ways of improving this figure, either by shortening the lissamine–Nd^{III} distance, which is not easy to achieve, or by increasing the spectral overlap between the donor and the acceptor. In the present case, the energy of the lissamine $^3\pi\pi^*$ state matches with the 14 600 cm^{-1} absorption band of the metal ion, which has a low cross section. Red-shifting the triplet state energy by 1000 cm^{-1} would result in an overlap with the much stronger absorption $^4S_{3/2} \leftarrow {}^4I_{9/2}$. Another problem to address is the strong photo-degradation occurring upon continuous illumination, which might be due to the

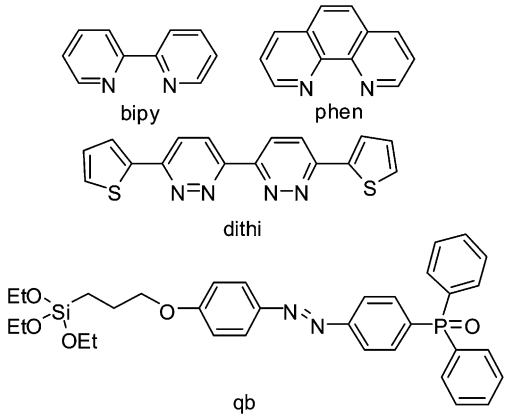

Fig. 115. Aza aromatic ligands.

presence of oxygen in the polymer film or to radicals formed upon photo-excitation (Slooff et al., 2000b).

4.2.2. *Erbium-doped polymers*

Thin films of simple Er^{III} complexes with aza aromatic ligands such as 2,2′-bipyridine (bpy), 1,10-phenanthroline (phen) or 2-dithienyl-2,2′-bipyridazine (dithi, fig. 115) doped into polymethylmethacrylate (PMMA), or polyl[2-methoxy-5-(3′,7′-dimethyl-octyloxy)]-*p*-phenylene vinylene (MDMO-PPV) have been fabricated. The dithi complex is the most promising, with the strong luminescence of the MDMO-PPV matrix quenched by a factor 100 upon doping (Koppe et al., 2001). No other quantitative data are however reported.

In an erbium-doped planar optical amplifier, pump and signal beams are coupled into the device through separate input waveguides and combined into a wavelength division multiplexer (WDM) to which a few-centimeter long Er^{III}-doped waveguide section is hooked. The latter is rolled up on a small area forming a spiral structure (amplifying waveguide spiral, AMP). After this section, signal and pump are separated in a second WDM and a splitter is added. The total device area is mostly determined by the size of the AMP. By using high refractive index waveguide cores, the spiral dimension can be kept as small as 1 mm^2; for instance, a 4-cm spiral of Er^{III}-doped alumina has a net gain of 2.3 dB for a pumping power of 10 mW at 1.48 μm and a signal wavelength of 1.53 μm (Polman and Van Veggel, 2004).

The photophysical properties of terphenyl-based acyclic (**22a**) and cyclic hemispherands (**22c**, **22d**, see fig. 27) have been investigated in organic solvents and in KBr pellets (1 wt%) with the purpose of introducing them later in optical amplifiers (Slooff et al., 1998). Absorption cross sections for the 1.54 μm emission, which is quite broad with fwhh = 70 nm, amount to 0.62, 1.1, and 0.93 $\times$ 10^{-20} cm^2 for [Er(**22a**)], [Er(**22c**)] and [Er(**22d**)], respectively. The best photoluminescence intensities are obtained with the cyclic ligands. The optical gain of the complexes doped into a polymer channel waveguide is on the order of 1.7 dB cm^{-1}, while the threshold power is as low as 1.4 mW.

Hybrid organic–inorganic channel waveguides can also be envisaged and the proof of principle has been given for an Er-doped material prepared by using a highly reactive siloxane precursor, methyl-trimethoxysilane or methyl-diethoxysilane, associated with colloidal silica stabilized into tripropylene glycol diacrylate. The Er^{III} β-diketonate (2,4-pentanedionate) was introduced in 1.6 wt% and buried channel waveguides were made of a three-layer structure deposited by dip-coating on a silicon substrate: a buffer layer, the active guiding layer, and a protective layer. The resulting waveguides were typically from 2 to 10 μm wide and 2.5-cm long. Light is highly confined in these structures and compensation of energy losses was reached (Etienne et al., 2000).

To solubilize Er^{III} in a transparent matrix while minimizing interactions between adjacent metal ions by keeping them sufficiently apart, complex $[Er(NO_3)_3(qb)_3]$ has been designed (see fig. 115) and introduced into PMMA. Polymer thin films have been obtained by spin coating, as well as single-mode waveguides, and their physical and photophysical properties have been investigated versus erbium concentration. With a 980-nm excitation, the intensity of the 1.542 μm emission from erbium increases regularly with doping concentration, up to ten weight percent (wt%), and then decreases, indicating self-quenching. The fluorescence decay significantly deviates from single exponential behaviour at concentration larger than 10 wt% and analysis of the lifetimes of $Er(^4I_{13/2})$ versus concentration yields a quenching concentration (i.e. the concentration at which the actual lifetime is half that for the zero concentration limit) of 13.4 wt%; the zero concentration lifetime amounts to 4.6 ms, while the lifetime at ten weight percent concentration is 3.46 ms (Le Quang et al., 2007).

The widespread distribution of fiber optics built from Er^{III}-doped fiber amplifiers has stirred a need for predicting the characteristics of such materials, in particular their gain, noise factor and absorption and emission spectra of erbium. Several models are available, among them a so-called "black-box" model for which a detailed knowledge of the structure of the optical material is not needed. With this model, determination of the gain is a simple one-parameter problem. A recent extension of this model has been proposed in which the "input noise approach" used for calculating the characteristics of active electronic devices has been implemented. This allowed the calculation of the limiting spectral efficiency of information transfer, which is in the range 6.0–6.7 bits per second and per Hz for an erbium amplifier with 20 dB signal-to-noise ratio (Varaksa et al., 2006a; Varaksa et al., 2006b).

4.3. *NIR organic light-emitting diodes (OLEDs)*

A landmark in the development of OLED is the finding in 1987 of the bright green emission of aluminum tris(8-hydroxyquinolinate), $[Al(8\text{-}Q)_3]$, in thin organic layers (Tang and Van Slyke, 1987). This device has a luminance of 1000 $cd\,m^{-2}$ below 10 V and a quantum efficiency of 1 photon per 100 electrons injected. Presently, electroluminescent devices can be made of a single layer of a π-conjugated polymer, such as poly(phenylene–vinylene), PVV, between two electrodes (Kido and Okamoto, 2002). Thin films OLEDs consist of multiple organic and/or metallic layers on an indium–tin oxide (ITO) covered glass deposited by various known methods, plasma deposition, thermal evaporation, Langmuir–Blodgett deposition, or spin-coating from solutions. It is important that the layers are chemically stable

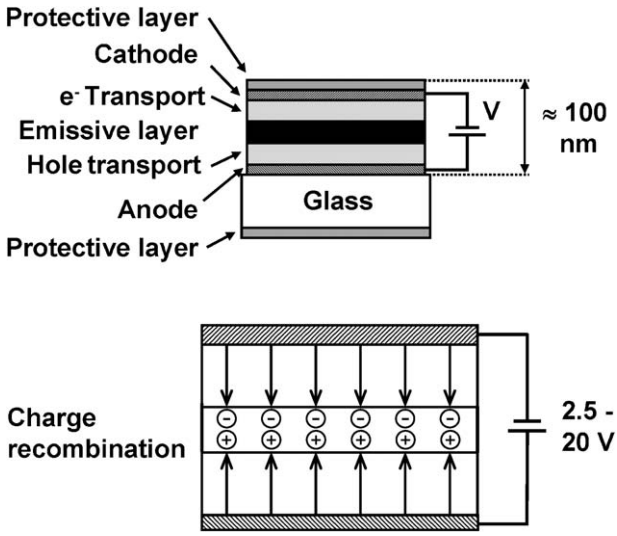

Fig. 116. Scheme of a typical electroluminescent device (OLED).

and highly transparent to the emitted light. The devices can have a single or a triple active layer. The latter case is shown on fig. 116: a voltage bias is applied to the ITO electrodes and electrons and holes are injected in the electron- and hole-transport layers by the cathode and anode, respectively. The voltage bias is not large, but since the layers are very thin (typically a few nm thick) the electric field is in the range 10^5–10^7 V cm^{-1}. Therefore, the injected charges migrate against each other, meet and recombine in the emissive layer. The hole-transport layer mainly transports holes within the highest occupied molecular orbital (HOMO) and to a lesser degree within the lowest unoccupied molecular orbital (LUMO). Consequently the corresponding materials should have a high hole mobility and a low ionization potential. Additionally, after charge recombination, the hole-transporting layer should also block the migration of excitons from the emitting layer, that is, it should have higher exciton energy than the emissive layer. Finally, it should also be transparent to the radiation emitted by the emissive layer. Among potential materials are poly-(*N*-vinylcarbazole) (PVK) and *N*,*N*-diphenyl-*N*,*N*-bis(3-methylphenyl)-[1,1′-biphenyl]-4,4′-diamine (TPD). Electron-transporting materials widely used are 2-(4-biphenyl)-5-(4-*tert*-butylphenyl)-1,3,4-oxadiazole or the tris(8-hydroxyquinolinate)aluminum complex. The charge recombination energy is transferred to the material of the emissive layer, a polymer doped with luminescent centers. In OLEDs, 25% of the excitation energy leads to singlet states and 75% to triplet states. As a consequence, it is desirable that the luminescent centers are good triplet quenchers, which is the case of some transition metal ions and of lanthanide ions. Amazingly the exploitation of the triplet state energy was ignored until 1998 (Baldo et al., 1998) but is now a major goal in the development of these lighting devices. A main challenge in OLEDs is the design of efficient, white-emitting diodes and a recent example demonstrated the feasibility of

a lanthanide-based device using up-conversion to produce simultaneous emission of Tm^{III} at 475 nm, Er^{III} at 525, 550, and 675 nm, as well as of Eu^{III} at 590 and 620 nm, upon excitation at 980 nm. The device consists in a sol–gel derived thin film made with Ln^{III}-doped lanthanum fluoride nanoparticles (Ln = Eu, Er, Tm, Yb); the Yb^{III} ions serve as Er^{III} sensitizer (Sivakumar et al., 2005). Here we concentrate on NIR emission and the following descriptions are classified according to the Ln^{III} luminescent ion. In several instances, the emissive layer and the electron-transporting layers are combined into a single thin film built up from the luminescent complex. The performances of OLEDs are tested by measuring the current density–voltage and the luminance–voltage characteristics. The turn-on voltage is defined as the voltage needed to produce a luminance of 1 $cd\,m^{-2}$. The luminance increases with increasing bias voltage up to a certain value from which saturation occurs leading ultimately to a decrease in luminance. Finally, the external electroluminescence quantum efficiency is defined as the ratio of the emitted photons to the number of charge carriers generated in the device.

4.3.1. *Neodymium OLEDs*

The feasibility of room-temperature Nd^{III} electroluminescence was demonstrated on a doped gallium arsenide semiconductor; the external quantum yield of 5×10^{-7} is close to the one exhibited by similar Er^{III}-doped LED, but about three orders of magnitude smaller than for Yb:InP (Chang, 1995). To our knowledge, the first Nd^{III}-containing three-layer OLED has been proposed by S. Yanagida and collaborators. The 50-nm thick hole-transporting layer is a diamine derivative, TPD, the electron-transporting layer (50 nm thick) is [Al(8-Q)$_3$], and the emitting layer (25 nm thick) contains the ternary β-diketonate [Nd(dbm)$_3$bath], where bath is monobathophenanthroline (fig. 117). The device not only emits the characteristic Nd^{III} light with a threshold voltage of about 15 V, but also a pale bluish-green luminescence arising from [Al(8-Q)$_3$]. The luminescence properties of the device are very sensitive to the layer thickness. When the emitting layer is thinner than 15 nm, the dominant emission is from [Al(8-Q)$_3$], for instance. Moreover, the device degrades fairly rapidly upon illumination at 390 nm (Kawamura et al., 1999).

A similar ITO/TPD (see fig. 117) OLED was built, with [Nd(8-Q)$_3$] as luminescent active layer; the device has an operative voltage of 30 V, corresponding to a current density of 78 $mA\,cm^{-2}$; the threshold voltage is 13 V ($\approx$0.23 $mA\,cm^{-2}$) and no visible luminescence is emitted (Khreis et al., 2000).

Another early system for Nd^{III} OLED relies on a tetrakis(pyrazolonate) complex the negative charge of it is compensated by an hemicyanine-based cation (fig. 118), (**130**)[Nd(**129**)$_4$]. The complex has very good film-forming as well as second-harmonic generation properties (Pavier et al., 1996). Electroluminescence of 15-Langmuir–Blodgett monolayers deposited on ITO and fitted with an Al electrode occurs with voltage thresholds in the range 4–7 V. The corresponding complex with Dy^{III} also displays electroluminescence. These materials can be used to produce OLEDs (Weaver et al., 1996).

9-Hydroxyphenalen-1-ones have been employed as sensitizer ligands because they are soluble in a wide range of organic solvents and possess adequate photophysical properties. For instance, the isc efficiency is nearly equal to one, due to the α,β-conjugated carbonyl groups.

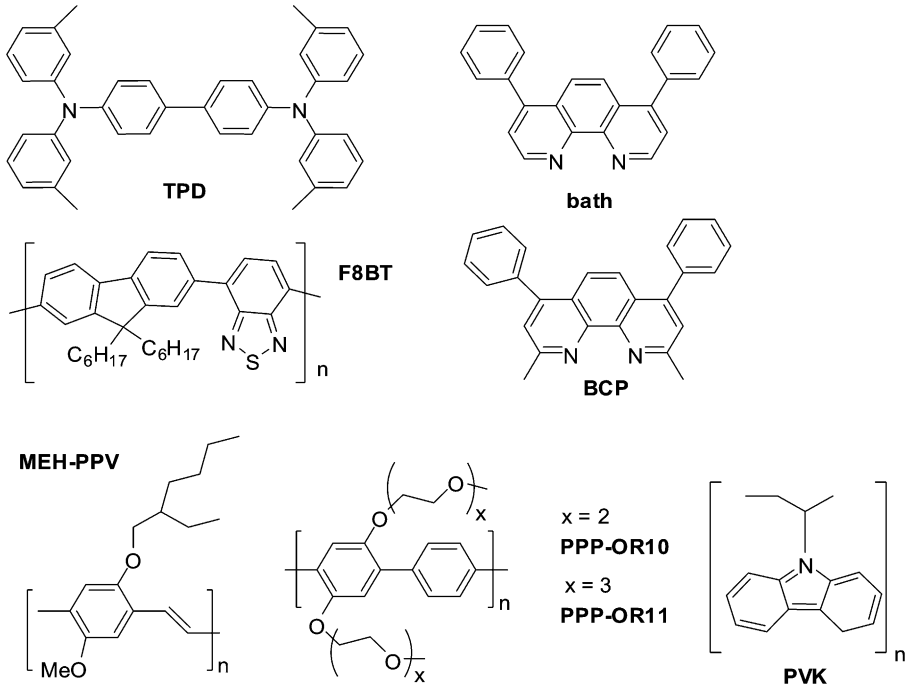

Fig. 117. Formula of various hole- and electron-injection and transport materials, as well as of the ancillary ligand bath used in Ln^{III}-containing OLEDs.

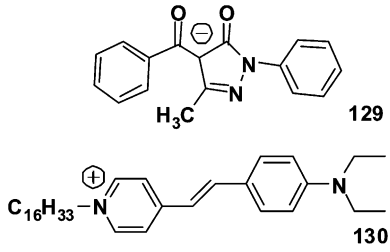

Fig. 118. Pyrazolonate ligand and hemicyanine-based counterion.

Doped PVK thin films display intense electroluminescence from the Nd^{III} ion and OLED devices fabricated with this active material have a maximum irradiance of 8.5 nW mm^{-2} and an external quantum yield of 0.007%. Further refinement of the processing will hopefully lead to a still better optimization of the performance of these Nd^{III}-doped polymeric emissive layers (O'Riordan et al., 2006).

The lissamine-sensitized terphenyl Nd^{III} chelate [Nd(**60d**)] (fig. 59) has been introduced in the host polymer F8BT (fig. 117) and the latter is efficiently quenched by the chelate. Lis-

samine acts as a charge trapping site owing to its low energy gap between HOMO and LUMO and, moreover, has a fast isc rate (4.4×10^8 s^{-1}). A device made of ITO electrodes, poly(3,4-ethylene dioxythiophene), PEDOT, doped with polystyrene sulfonate, PSS, as hole injection layer, and of the Nd^{III} chelate in F8BT as emissive layer shows intense electroluminescence; F8BT has very high photoluminescence efficiency in the solid state (≈60%), a good solubility in common organic solvents, and a high electron affinity (≈2.9 eV), which facilitates electron injection. Finally, there is considerable overlap between its emission spectrum and the absorption spectrum of Nd^{III}, so that efficient Förster-type energy transfers are operative in this doped material. For a 2 mm^2 area and an 80-nm thick active layer, the threshold voltage is around 15 V at ≈0.01 cd m^{-2}. The electroluminescence is about four-fold larger than photoluminescence of the lissamine-functionalized chelates in polycarbonate waveguides (Slooff et al., 2001).

The β-diketonate [$Nd(dbm)_3$bath] (see figs. 41 and 117) has a photoluminescence quantum efficiency of 0.33% in dmso-d_6 solution at a 1 mM concentration. It has been introduced as the active 20-nm thick layer into an OLED having an ITO electrode with a sheet resistance of 40 Ω cm^{-2}, TPD as hole transporting layer with a thickness of 40 nm, and bathocuproine (BCP) (40 nm) as the electron injection and transporting layer (see fig. 117). The electroluminescence spectrum is identical to the photoluminescence emission; the luminescence intensity at 1.07 μm versus current density curve deviates from linearity from approximately 10 mA cm^{-2} on, due to triplet–triplet annihilation. Near-IR electroluminescent efficiency Q_{EL} has been determined by comparison with [$Eu(dbm)_3$bath] for which the total photoluminescence quantum yield in dmso-d_6 at a concentration of 1 mM is $Q_{PL} = 6\%$ upon ligand excitation, while its external electroluminescence efficiency is 0.14% (3.2 cd m^{-2} at 1 mA cm^{-2}):

$$Q_{EL} = \eta_e \cdot \eta_r \cdot Q_{PL}, \tag{44}$$

where η_e is the fraction of emitted photons coupled out of the device and η_r is the fraction of injected charge carriers that form excitons. Therefore, for similar devices:

$$Q_{EL}(Ln) = Q_{EL}(Eu) \cdot \frac{Q_{PL}(Ln)}{Q_{PL}(Eu)}. \tag{45}$$

In the case of the [$Nd(dbm)_3$bath] OLED, the estimated $Q_{EL}(Nd)$ amounts to 7×10^{-5} neglecting deactivation effects at the metal cathode; this figure is low but larger than the quantum efficiency of the Nd:GaAs LED, 5×10^{-7} at 77 K (Kawamura et al., 2001).

Electroluminescence of [$Nd(TPP)CoP^{Me}$] (see figs. 18 and 19) dispersed in a polystyrene host in a 2:1 (complex:host) ratio has also been reported (Kang et al., 2003b).

4.3.2. *Erbium OLEDs*

The systems of interest here entail either 8-hydroxyquinolinate, β-diketonate, or porphyrin complexes. Upon excitation at 351 nm, tris(8-hydroxyquinolate) [$Er(8\text{-}Q)_3$] shows a broad emission band at room temperature in the range 380–750 nm, with a maximum at 600 nm, which is red-shifted by about 80 nm with respect to group III (e.g. Al^{III}) quinolinates. In addition, a bright 1.54-nm emission is seen upon excitation with an argon laser at 457 nm the intensity of which varies linearly with the excitation power in the range 1–100 mW (Gillin

and Curry, 1999). The same bands, although narrower, are emitted by a multi-layer device containing an ITO-coated glass with a sheet resistance of 20 $\Omega\,cm^{-2}$, a 60-nm thick TPD hole-transporting layer (see fig. 117), a 60-nm film of [Er(8-Q)$_3$], and an aluminum electrode, upon excitation by a driving voltage of 25 V. Interestingly, the blue electroluminescence is considerably weaker when compared to the one observed under the same operating conditions for OLEDs with groups III chelates. The current–voltage characteristics of the Er-containing OLED point to a relatively high turn-on voltage of 12 V, which is indicative of poor injection at the contact electrode. The device appears to be robust, not breaking down under reverse voltages up to −30 V (Curry and Gillin, 1999). The use of silicon as the hole injection contact is also feasible (Curry et al. 2000, 2001). On the other hand, the electroluminescent properties of the Er-containing OLED are dependent on the deposition conditions (Curry and Gillin, 2000). As for many similar devices, a decrease in efficiency with increasing current is explained by the quenching of the excited lanthanide ion state with injected charge carriers (polarons). Triplet–triplet annihilation plays an important role in this process (Curry and Gillin, 2001). [Er(8-Q)$_3$]-doped monodisperse microparticles (≈20 μm) seem to have some potential for OLED devices as well, besides organic red-emitting dyes (Suzuki et al., 2004; Suzuki, 2004).

A single-layer OLED with [Er(acac)$_3$phen] doped into a 80-nm thick film of PVK (see fig. 117) prepared by spin-coating and deposited on an ITO electrode, and with a 100-nm lithium-doped (0.1%) aluminum cathode has also been tested and shows an onset voltage of about 12 V for electroluminescence (Sun et al., 2000). [Er(dbm)$_3$bath] has a photoluminescence quantum yield of 0.007% in dmso-d_6 at 1 mM concentration; the OLED based on this compound and similar to the one described above for Nd^{III} has a NIR external electroluminescence efficiency of 1×10^{-6} (Kawamura et al., 2001).

Another approach takes advantage of the high degree of spectral overlap between the emission band of MEH-PPV (fig. 117) and the Q-absorption bands of tetraphenylporphyrin (TPP) to transfer energy from the host polymer to [Ln(TPP)(acac)], Ln = Er, Yb, or between the fluorescence of PPP-OR11 (fig. 117) and the Soret band of the same complexes. Near-IR electroluminescent devices were fabricated starting with an ITO glass electrode coated with a special hole-transporting layer; the polymer:[Ln(TPP)(acac)] (5 mol%) blend was then spin-coated from a 1% solution in toluene. After drying under vacuum, a 5-nm thick layer of calcium, followed by a 150-nm layer of aluminum were deposited and the whole OLED was encased in epoxy to minimize exposure to air, i.e. oxygen and moisture. Erbium electroluminescence is clearly seen when a 13 V voltage is applied for both MEH-PPV (Harrison et al., 2001) or PPP-OR11 devices (Schanze et al., 2003).

4.3.3. *Ytterbium OLEDs*

Proposed Yb^{III}-containing OLEDs contain either β-diketonates or porphyrin complexes. With respect to the first class of compounds, [Yb(dbm)$_3$bath] (see figs. 41 and 117), which has a photoluminescence quantum yield of 1.4% in dmso-d_6 at a 1 mM concentration, has been introduced into a three-layer electroluminescent device, TPD (50 nm thick)/[Yb(dbm)$_3$bath] (25 nm)/[Al(8-Q)$_3$] (50 nm), with ITO and Mg:Al (10:1) electrodes. Bright luminescence is recorded with a threshold voltage of 15 V and only saturates when the voltage reaches 24 V.

One drawback of the device though is the poor charge injection ability of the Yb^{III} diketonate, so that at 20 V bias, the current density only reaches 9.7 mA cm^{-2} (Kawamura et al., 2000). Replacing [Al(8-Q)$_3$] with BCP increases the efficiency of the device, although it shows a more marked decrease in emitted intensity and electroluminescence efficiency with current density, when compared to the corresponding Nd^{III} OLED (see above). For instance, the current densities giving 10% of the initial efficiency are 55 and 230 mA cm^{-2} for Yb^{III} and Nd^{III}, respectively. On the other hand, the external electroluminescent efficiency is the largest for Yb^{III} (3×10^{-4}) in comparison with Nd^{III} (7×10^{-5}) and Er^{III} (1×10^{-6}) (Kawamura et al., 2001). Another design using the same emissive complex, ITO/TPD (40 nm)/[Yb(dbm)$_3$bath]:TPD (weight ratio 1:1, 40 nm)/[Yb(dbm)$_3$bath] (60 nm)/Ag:Mg (150 nm) has a onset voltage of about 6 V while saturation starts around 12 V, corresponding to a current density of about 250 mA cm^{-2}; in fact the maximum emission efficiency is in the range 1–10 mA cm^{-2} (Hong et al., 2001b). Similarly to the Nd^{III} OLED, Yb^{III} tris(hydroxyquinolinate) emissive material was used in an ITO/TPD/[Yb(8-Q)$_3$]/Al device, in which the luminescent layer was deposited on ITO by sublimation at 10^{-6} mbar pressure. The electroluminescence spectrum is turned on at current densities above 5 mA cm^{-2}, which corresponds to a drive voltage of 17 V; it displays a sharp peak at 977 nm on top of a broader feature (Khreis et al., 2001). Further treatment of the ITO layer by oxygen plasma may considerably lower the turn-on voltage, as observed for the corresponding devices with Nd^{III} (Khreis et al., 2000) and Er^{III} (Curry and Gillin, 1999).

The performances of two Yb^{III} complexes, [Yb(dbm)$_3$phen] and [Yb(dnm)$_3$phen] (dnm is dinaphthoylmethanate) have been compared in OLEDs based on two blue emitting oligoether-functionalized poly(*p*-phenylenes), PPP-OR10 with $Q_{PL} = 44\%$ and PPP-OR11 with $Q_{PL} = 92\%$ (fig. 117). The structure of the electroluminescent devices comprises an Al:Ca electrode, the emissive complex (1–20 mol%): PPP-OR11 layer, a hole-injection film of poly(3,4-ethylene dioxythiophene), PEDOT doped with polystyrene sulfonate, and an ITO glass electrode. Quenching of the polymer fluorescence as well as the NIR irradiance are clearly more important with dnm than with dbm. The turn-on voltage is only 5 V for 10 mol% [Yb(dnm)$_3$phen] doped into PPP-OR11, but the emissive layer must contain more than 10 mol% of the dnm complex for the NIR emission to be larger than the blue polymer fluorescence. Depending on the conditions used, the external quantum efficiencies are between 10^{-5} and 10^{-4}, which is comparable to the previous device (Kang et al., 2003a).

On the other hand, external electroluminescence efficiencies about ten times larger are obtained with the PPP-OR11-based OLED doped with 5 mol% [Yb(TPP)CoP^{Me}] and which has an onset voltage of 6 V: at 7 V, $Q_{EL}(Yb) = 4 \times 10^{-4}$ (Schanze et al., 2003). This device has better characteristics than the one based on [Yb(TPP)acac] (Harrison et al., 2001). Possible reasons are the higher photoluminescence quantum yield of [Yb(TPP)CoP^{Me}] (3.2% in $CHCl_3$) compared to [Yb(dnm)$_3$phen] (0.1% in the same solvent), an improved host fluorescence/dopant absorption spectral overlap, and an enhanced carrier transport through the porphyrin (Kang et al., 2003a). The porphyrinate complex has been blended into polystyrene and PVK at concentrations of 50–80 wt%. The devices with the first polymer have a turn-on voltage of only 4 V and near-IR irradiance of 0.2–0.6 μW cm^{-2} for bias voltages between 10 and 15 V. The external electroluminescence efficiency peaks at about 10^{-3} for very low

current density, on the order of 1 mA cm^{-2}, and with the lowest loading of the emissive complex (50 wt%); as soon as current density is increased the efficiency drops to a constant value of 2×10^{-4}, a phenomenon likely due to saturation effects caused by the long 50 μs lifetime of Yb($^2F_{5/2}$). Conversion of electron–hole pair recombination events into luminescence is estimated to approximately 10% in these devices. Replacing polystyrene with PVK does not alter the characteristics of the OLEDs, meaning that charge transport in both devices is dominated by the [Yb(TPP)CoP^{Me}] complex, regardless of its electroactive host (Kang et al., 2003b). The same authors have fabricated OLEDs based on [Yb(TPP)CoP^{Me}] blended into PPP-OR11 and investigated energy-transfer processes in the corresponding devices from the polymer to the luminescent complex. If a dipole–dipole transfer is assumed to be the main operative mechanism, the donor–acceptor distance for 50% transfer amounts to 4.6 nm. Light absorbed by PPP-OR11 produces a singlet exciton on the host which transfers energy on the TPP complex and generates the TPP $^1\pi\pi^*$ state; in turn, the latter rapidly decays by isc to the TPP $^3\pi\pi^*$ state, followed by transfer onto the 4f-centered excited state. The OLED tested, ITO/PEDOT-PSS/PPP-OR11:[Yb(TPP)CoP^{Me}]/Ca:Al, turns on between 4 and 5 V bias voltage and the electroluminescence intensity peaks at 9 V. The NIR irradiance at 9 V depends on the doping concentration and ranges from 1.6 (5 mol%) to 10.0 (15 mol%) μW cm^{-2} at current densities of 100 and 315 mA cm^{-2}, respectively. At a current density of 100 mA cm^{-2}, the external electroluminescence efficiency is around 10^{-4} for doping concentrations equal or larger than 10%. The efficiency of the electron–hole recombinations converted into light is between 1 and 10%. The authors explain these values by the hole injection being more efficient and the hole transport more rapid compared to electron injection and transport, henceforth a mismatch detrimental to the overall efficiency of the OLED. The ability of non-conjugated polymers such as PMMA to produce OLEDs with similar properties has been demonstrated, which opens up opportunities for lowering the cost of the devices with these inexpensive polymers (Harrison et al., 2004).

4.3.4. *OLEDs with other lanthanide ions*

Both metal-centered visible (608 nm, $^1D_2 \rightarrow {}^3H_6$) and near-IR (890 nm, $^1D_2 \rightarrow {}^3F_2$; 1.015 μm, $^1D_2 \rightarrow {}^3F_3$; 1.065 μm, $^1D_2 \rightarrow {}^3F_4$; 1.55 μm, $^1D_2 \rightarrow {}^1G_4$) light is emitted by [Pr(dbm)$_3$bath] in bi- and tri-layer devices containing TPD, in addition to broad exciplex fluorescence from the polymer host. The visible emission at 608 nm is favored when the concentration of the Pr^{III} complex is increased and NIR emission starts when the voltage bias is 8 V corresponding to a current density of 4.5 mA cm^{-2} (Hong et al., 2001a). When the Ho^{III} β-diketonate is doped into TPD, near-IR luminescence is observed at 980 nm ($^5F_5 \rightarrow {}^5I_7$), 1.20 μm ($^5I_6 \rightarrow {}^5I_8$), and 1.50 μm ($^5F_5 \rightarrow {}^5I_6$), the turn-on voltage being around 10 V (Zang et al., 2004b). Similarly, the 1.2 μm emission was observed with the PPP-OR11:[Ho(TPP)CoP^{Me}] OLED (Schanze et al., 2003). Thulium electroluminescence at 800 nm ($^3F_4 \rightarrow {}^3H_4$) and 1.4 μm ($^3F_4 \rightarrow {}^3H_6$) is generated in OLEDs containing one of the β-diketonates, [Tm(dbm)$_3$phen], [Tm(dbm)$_3$bath], [Tm(acac)$_3$phen], or [Tm(acac)$_3$bath]. Electroluminescence from the latter two complexes is, however, very weak because the triplet state of acetylacetonate lies at about 25 500 cm^{-1}, resulting in a preferred population of the $^1G_4$ level which radiatively relaxes by emitting 480 nm photons. In the case of dbm, the en-

ergy of the triplet state is smaller than the energy of the $^1G_4$ level and the $^3F_{4,3,2}$ levels are populated by the energy transfer process, despite a relatively large energy mismatch. Simultaneous introduction of [Tm(dbm)$_3$bath] and [Er(dbm)$_3$bath] in the emissive layer resulted in a broad band emission extending from 1.4 to 1.6 μm, an interesting property for applications in optical communications (Zang et al., 2004a).

4.4. *Analytical applications*

In addition to the elemental analyses performed with β-diketonates and mentioned in section 3.2.1, NIR luminescent lanthanide complexes start to be used as responsive probes for the analysis of cations and anions.

Ligand **131** contains both cryptate and crown ether binding units. It reacts with neodymium triflate to give a 1:1 cryptate [Nd $\subset$ **131**]$^{3+}$ exhibiting NIR luminescence upon excitation at 355 nm. The lifetime of the Nd($^4F_{3/2}$) level is 347 and 711 ns in methanol and methanol-d_4, respectively, which translates to $q_{MeOH} \approx 0$ using eq. (10b). When barium ions are added to a solution of this complex in acetonitrile, the intensity of the 1.06 μm emission band is reduced substantially, while the lifetime of the Nd($^4F_{3/2}$) level remains unchanged at about 470 ns. The Nd^{III} ion is therefore not displaced from the cryptand cavity, while its luminescence is modulated by the presence of the Ba^{2+} ions bound by the crown ether (Coldwell et al., 2006).

Anion sensing using visible-emitting lanthanide probes has proven successful (Tsukube et al., 2006) and this work is now being extended to Yb^{III} probes, particularly for the detection of thiocyanate. The latter is the principal metabolite of cyanide anion and exists in human serum, saliva, and urine. The luminescent probe is a complex of hexadentate tetrakis(2-pyridylmethyl)ethylenediamine (tpen, see fig. 119) which bears two water molecules, [Yb(tpen)(H_2O)$_2$](Otf)$_3$. In absence of anion coordination, the 980-nm luminescence is quenched, but the replacement of the water molecules with thiocyanate or other anions such as acetate, nitrate or halogenides removes the quenching, which makes the complex a responsive probe. The largest effect (a six-fold increase in luminescence) is obtained for thiocyanate, followed by acetate and nitrate (3.5-fold) and chloride (two-fold).

A more elaborate sensor consists in a dendrimeric-like complex featuring eight quinoline units **132** (fig. 119, bottom), allowing the complexation of four Yb^{III} ions and yielding a 8.5-fold increase in the 980-nm emission upon thiocyanate complexation (Tsukube and Shinoda, 2006).

Asymmetrically substituted cyclen derivatives (**133**, see fig. 119) have been developed to prepare a series of photoactive donor–acceptor quencher triads based on Nd^{III} and Yb^{III} complexes. Two successive nitrogen atoms of the cyclen scaffold are fitted with a rhodamine B antenna and a nucleoside quencher serving as chelator for the metal ion. This ensures close proximity of the antenna-quencher pair, facilitating their interaction. The rhodamine antenna can be excited in its whole absorption range, from 355 to 700 nm, which is a definite advantage. The remaining two nitrogen atoms are alkylated with coordinating arms to enhance the stability of the complexes. The resulting complexes, [Ln(**133-B**)]Cl_3 (Ln = Nd, Yb; B = U, A), display essentially no luminescence in methanol, because the uridine or adenosine group quenches the emission from rhodamine B, preventing energy transfer onto the 4f ion. When

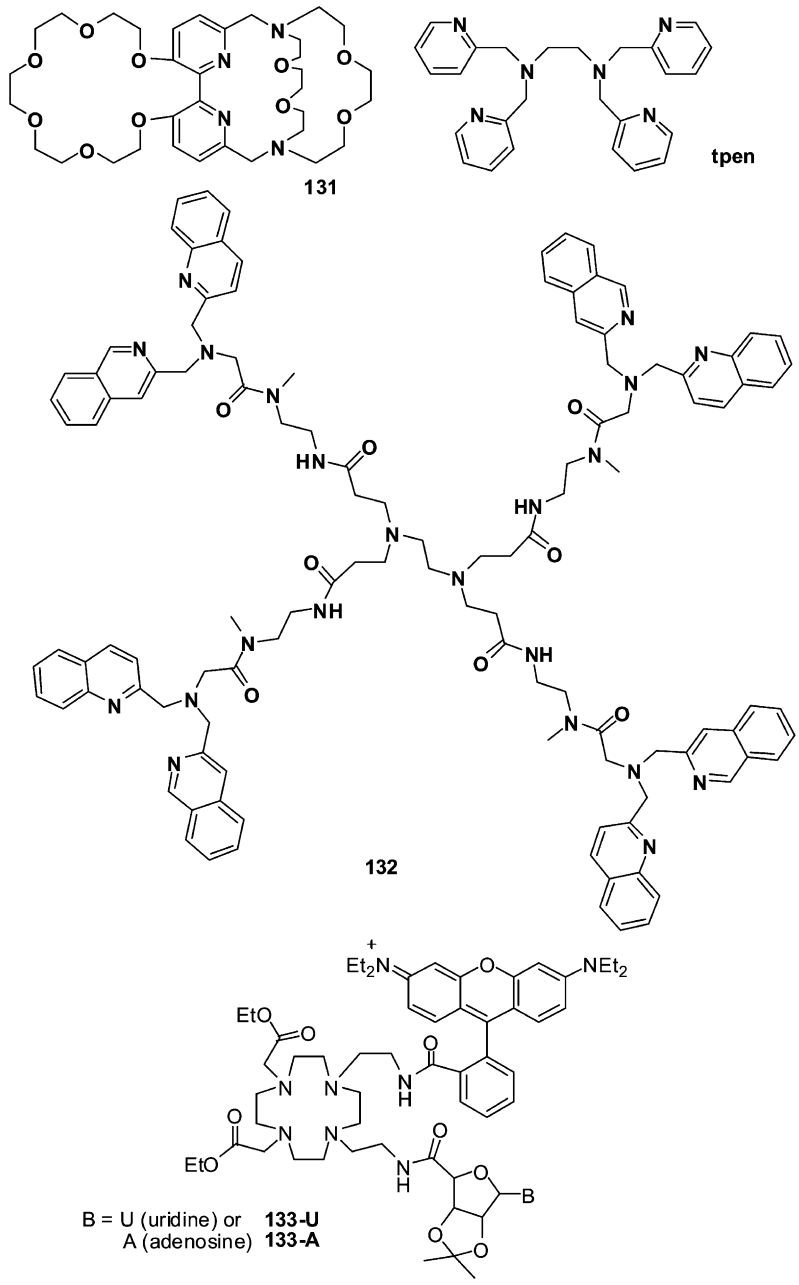

Fig. 119. (Top) Crown-cryptand for the analysis of barium and ethylenediamine ligand for anion sensing (tpen). (Bottom) Dendrimer-like ligand for anion sensing.

a complementary nucleoside base, uridine or adenosine, was added to the solution, quenching of the rhodamine fluorescence decreased and energy transfer between rhodamine and the Ln^{III} ion was restored. For the Nd complexes this also translated into a longer lifetime. For instance, in the case of $[Nd(\mathbf{133\text{-}A})]^{3+}$, $\tau(^4F_{3/2})$ increased from non-measurable (too short) in absence of complementary base to 0.23 μs in presence of one equivalent of complementary base. The change in lifetime was more marked when uridine was present (increasing from 0.09 to 0.47 μs). For Yb^{III} complexes, an opposite trend was observed and has been attributed by the authors to the susceptibility of Yb^{III} to reduction by the added nucleoside (Supkowski et al., 1999). In conclusion, this work demonstrates the possibility of regulating the extent of energy transfer between the antenna and the lanthanide by an external chemical stimulus (Borbas and Bruce, 2006).

4.5. *Biomedical applications*

Although bioanalyses and bio-imaging have been the driving force of many investigations during the last ten years, very few systems have made it up to real applications at least as far as NIR luminescence is concerned (Faulkner et al., 2005). On the other hand, the use of CD spectroscopy of Yb^{III} for determining the configuration of chiral diols (Di Bari et al., 2002; Tsukube and Shinoda, 2002) or biological substrates is well established. We have also described the CPL properties of some Yb^{III} complexes with cyclen derivatives in section 3.1.4. There are two major applications for which NIR probes are being developed: luminescent immunoassays and diagnosis of tumors (cell imaging). Immunoassays rely on a biochemical reaction between an antigen (analyte) and a specific antibody. In luminescent assays, the latter is labeled by a lanthanide chelate. There are two types of luminescent immunoassays, heterogeneous and homogeneous (fig. 120). In the first ones, the Ln-labeled antibody is reacted with the antigen (step 1), the non-reacted reagents are washed, and the pH is lowered to de-complex the Ln^{III} probe before re-complexing it with another chelating agent (step 2), inserting it into a micelle and reading the luminescence intensity in time-resolved mode. Homogeneous assays necessitate less handling: the antigen is reacted with two different but specific antibodies, one labeled with the Ln^{III} luminescent chelate and the other with an (organic) acceptor. Upon excitation (often by UV light), energy is transferred first from the triplet state of the chelating agent onto the Ln^{III} ion and subsequently onto the acceptor molecule which emits characteristic light. The resonant energy transfer only occurs when the Ln^{III} chelate (the donor) and the acceptor lie at a reasonably short distance, i.e. when they are attached to the same antigen molecule, so that there is no need to separate the various chemical species in solution before reading the luminescence intensity. The same principle can be used to detect protein-protein interactions and DNA hybridization (Bünzli and Piguet, 2005). The most usual Ln^{III} probes used to date are visible-emitting Ln^{III} ions with detection limit in time-resolved mode as low as 10^{-15} M (Matsumoto and Yuan, 2003). Since Yb^{III} is the NIR-emitting ion having usually the best quantum yield, all the biomedical applications published to date use this ion. One incentive for trying to use NIR-emitting probes rather than visible-emitting ones is the fact that the former may be more easily excited by visible light, instead of UV-light which may damage biological molecules.

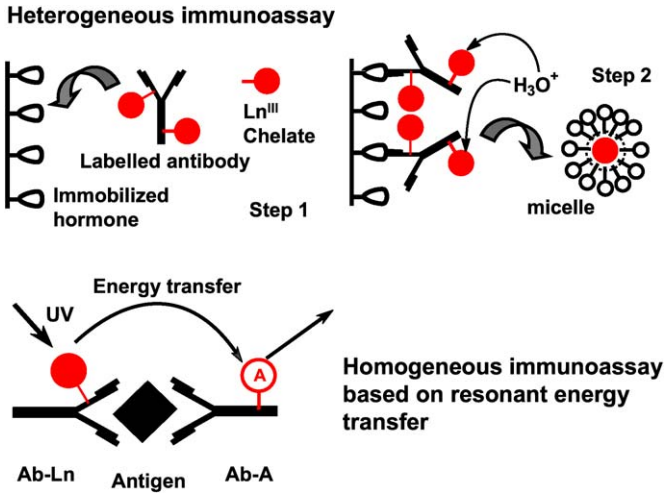

Fig. 120. Principle of heterogeneous (top) and homogeneous (bottom) immunoassays.

To allow coupling with biological material, the fluorescein-substituted polyaminocarboxylate ligand H_4**73a** has been functionalized with an isothiocyanate group, leading to H_4**73b** (see fig. 64). The latter is reactive towards amine functions, allowing easy coupling to proteins. Avidin was chosen for a proof of principle (Werts et al., 2000b). This glycoprotein of molecular weight 68 kDa is synthesized in the hen oviduct and represents about 0.05% (w/w) of the total protein content of the hen egg white. The great affinity of avidin for biotin ($K_{\text{assoc}} = 10^{15}$ M) results in a great number of applications in biochemistry, immunoassays, receptor and histochemical studies, bacteriophage inhibitions, for instance. Excitation at 514 nm of the avidin-[Yb(**73b**)] conjugate containing on average 3.2 labels per protein leads to metal-centered luminescence with a quantum yield and a lifetime (2.0 μs) equal to those of [Yb(**73a**)]. The quantum yield drops by 20% however when the number of labels per protein is increased to 5.2. The authors point out that the Yb^{III} label compares favorably with the Eu^{III} luminescent cryptate used in a commercial diagnostic and for which the product $\varepsilon \cdot Q$ amounts to 100 M^{-1} cm^{-1} when light from a nitrogen laser (337 nm) is used for excitation: the avidin-[Yb(**73b**)] conjugate achieves the same figure for excitation at 514 nm. The robustness of the Yb^{III} label was also tested in a known medical pregnancy test making use of a heterogeneous immunoassay of human chorionic gonadotropin (hCG). The analyte containing 5 international units of hCG was sandwiched between an anti hCG antibody immobilized on a nitrocellulose membrane and an antibody labeled with [Yb(**73b**)]. Luminescence was observed with a scanning near-IR microscope and clearly revealed the spots corresponding to a positive test. On the other hand, an attempt to conjugate Nd^{III}- and Er^{III}-doped LaF_3-based nanoparticles with avidin proved unsuccessful, since no metal-centered luminescence was observed (Diamente et al., 2006).

Protein concentration in solutions and in physiological fluids such as blood plasma can be determined by the changes occurring in the NIR fluorescence intensity during the highly specific reaction between an antigen and an antibody in Langmuir–Blodgett (LB) films. An immunosensor based on LB films of ytterbium tetraphenylporphyrinate, [Yb(TPP)(X)] (the nature of X is not specified in the article) has been proposed by G.K. Chudinova and the antigen–antibody reaction tested used rabbit immunoglobulin G (IgG), which is a polyclonal antibody against human serum albumin (HSA). IgG was labeled with benzoyltrifluoroacetone isothiocyanate, while HSA was conjugated with [Yb(TPP)(X)]. Labeled IgG was mixed with a lipid (phosphatidylcholine), a monolayer produced and transferred onto a quartz plate coated with stearic acid. Depending on the number of stearic acid layers, the working surface is either polar (10 layers) or non-polar (11 layers). The interaction between the immobilized and labeled IgG and the HSA-[Yb(TPP)(X)] conjugate results in an amplification of the Yb^{III} luminescence intensity due to energy transfer from benzoyltrifluoroacetone and the non-polar system gives the best results. In fact, due to concentration quenching, the luminescence intensity increases when the concentration of the conjugate decreases from 10^{-7} to 10^{-11} M. The sensitivity achieved by the sensor for protein detection in blood plasma is 10^{-11} M. As a comparison, enzyme-linked immunosorbent assays (ELISA) have a detection limit of 10^{-9} M and require a much longer reaction time, 2 h versus 6 min. In addition to serum albumin, the immunosensor described here can be adapted to the detection of other proteins, provided that the corresponding specific antibody can be immobilized in an LB film (Nagovitsyn and Chudinova, 2002).

We would also like to mention the elegant technology proposed by a group from Leiden University who has developed a luminescent reporter for the sensitive detection of antigens in tissue sections or on cell membranes, although it does not use NIR luminescence but rather NIR excitation followed by up-conversion. It consists of phosphor microcrystals (0.2–0.4 μm) made of yttrium oxysulfide doped with two different lanthanides exhibiting strong emission in the visible (blue, green, and red). The microparticles are surface-labeled with avidin or antibodies and can bind specifically to antigens on intact cells or in tissue sections. The phosphor microparticles exhibit visible luminescence by up-converting infrared to visible light. The method is termed up-converting phosphor technology (UPT) and has been tested on the prostate-specific antigen in tissue sections and the CD4 membrane antigen on human lymphocytes (Zijlmans et al., 1999), as well as for various other assays (Kuningas et al., 2006).

The possibility of using Yb^{III} luminescence from porphyrinate complexes for the diagnosis of tumors has been described in 1989 already, but does not seem to have been followed by practical applications (see section 3.1.1, fig. 11). The affinity of porphyrin for cancer cells increases when metalloporphyrin-albumin conjugates are used and therefore, [Yb(H_3**4c**)$(im)_2$] (see fig. 11, im is imidazole) has been conjugated with bovine serum albumin (BSA) which contains free amino groups from lysine residues located at its surface. Conjugation was achieved in two steps, the first being the preparation of the succinimide ester of the porphyrinate under anhydrous conditions. The second step involved conjugation with the protein in water–organic medium at pH 9–9.3. The number of porphyrin molecules per protein is in the range 5.4–6.6. With respect to [Yb(H_3**4c**)$(im)_2$], which has a quantum yield of 0.6% in

water at pH 9.2 and at a concentration of 0.1 M, which doubles in Triton X-100 micelles, the fluorescence of the BSA conjugate is three-fold larger (Chudinov et al., 2004).

5. Comparison of the chromophores

In order to evaluate the efficacy of the chromophores used by various authors for the sensitization of the NIR emission of Ln^{III} ions, the photophysical properties, lifetimes and quantum yields, of the complexes described in the previous sections are listed in table 21 for Nd^{III}, table 22 for Er^{III}, and table 23 for Yb^{III}. Within a table, data are listed in order of increasing excitation wavelength. *Only ligands substituted by a specific chromophore are listed in these tables*. That is for instance, parent calix[n]resorcinarenes and calix[n]arenes are not included since relevant data are given in tables 7 and 8. The same remark is valid for simple tris(β-diketonates) for which quantitative data are listed in figs. 42, 45, and 46, tables 10 and 11, as well as for triphenylmethane dyes (tables 14 and 15).

5.1. *Note on quantum yields*

Complete data are not available for all the chromophores. Moreover, one has to exercise some care with quantum yield data. They are among the most difficult photophysical parameters to determine experimentally and require adequate standards when a comparative method is used, which are not always easily at hand as far as NIR luminescence is concerned. It is of course essential that the same detector is used for measuring the luminescence from the standard and from the unknown solution. If these two solutions are not in the same solvent, the refractive index correction has to be applied (Chauvin et al., 2004). Sometimes all the NIR bands of Nd^{III} are not measured because of detector response: few detectors are able to measure simultaneously the three $^4F_{3/2} \rightarrow {}^4I_J$ transitions ($J = 13/2, 11/2, 9/2$), so that *partial quantum yields* are given taking into account only one or two transitions. There is also some confusion about the nature of the quantum yield and a clear distinction has to be made between the overall quantum yield obtained upon ligand excitation and the intrinsic quantum yield obtained upon direct metal-ion excitation (see eq. (11)). Henceforth all the quantum yields estimated using lifetime measurements are intrinsic quantum yields. Moreover, the value of the radiative lifetime is not a constant for a given lanthanide ion and it varies depending on the compound and emitting level. It should therefore be calculated from eq. (17) and not taken from "literature data". Intrinsic quantum yields estimated in this way are highly susceptible to bear larger errors.

The best procedure for quantum yield determination is the absolute method of Wrighton, using an integration sphere (de Mello et al., 1997; Wrighton et al., 1974) and which is operative for both powdered samples and solutions (Gumy and Bünzli, 2006). In any case, whether a comparative or absolute method is used, excellent instrumental functions should be at hand to correct the measured spectra. These functions should be re-determined often, especially if excitation is in a spectral range in which the lamp has a low luminance or if the emission lines fall in a low-response range of the detector. In photon counting mode, saturation of the

Table 21
Photophysical properties of Nd^{III}-containing compounds

Nd			Experimental conditions					
Antenna[a]	Major unit		λ_{ex} (nm)	Nature/solvent	Q^{L}_{Ln} (%)	$Q^{Ln}_{Ln\ or\ rel}$ (%)[b,c,d,e,f,g]	τ (μs)[h,i,j]	Reference
Complexes for which quantum yields (Q^{L}_{Ln}, $Q^{Ln}_{Ln\ or\ rel}$) have been measured or estimated								
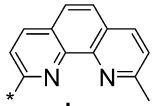 **phen**	Polyamino-carboxylates	H_4**74**	279	H_2O	4×10^{-3}		<0.2	(Quici et al., 2005)
				D_2O	0.02		0.4	
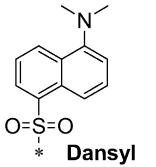 **Dansyl**	Dendrimer	**92**	297	CH_3CN/ CH_2Cl_2 (5:1)	0.27		–	(Vögtle et al., 2001)
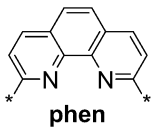 **phen**	Crown ether	**14**	300	Acetone	0.07[k]		0.64	(Korovin et al., 2002d)
				Acetone-d_6	0.10[k]		1.17	
		H_6**15**		H_2O	0.09[k]		0.72	
				D_2O	0.18[k]		1.34	
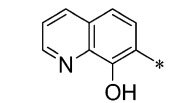 **8-Hydroxyquinoline**	Podands	H_8**90a**	344	H_2O	0.02	0.03[c]	0.13[j]	(Imbert et al., 2005)
				D_2O	0.10	0.14[c]	0.58[j]	
		H_8**90b**	344	H_2O	0.04	0.06[c]	0.25[j]	(Comby et al., 2006b)
				D_2O	0.11	0.15[c]	0.61[j]	

continued on next page

Table 21, *continued*

Nd			Experimental conditions					
Antenna[a]	Major unit		λ_{ex} (nm)	Nature/solvent	Q^{L}_{Ln} (%)	$Q^{Ln}_{Ln\ or\ rel}$ (%)[b,c,d,e,f,g]	τ (μs)[h,i,j]	Reference
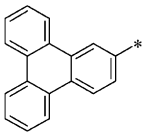 **Triphenylene**	Terphenyl-based ligands	H_3**60a**	350	dmso-h_6		0.56[b]	1.4[i]	(Klink et al. 1999, 2000a)
				dmso-d_6		1.00[b]	2.5[i]	
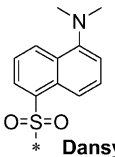 **Dansyl**	Terphenyl-based ligands	H_3**60b**	350	dmso-h_6		–	1.10[i]	(Klink et al., 2001; Hebbink et al., 2002a)
				dmso-d_6		1.0[g]	2.21[i]	
		H_3**60f**		dmso-d_6		0.95[g]	2.15[i]	
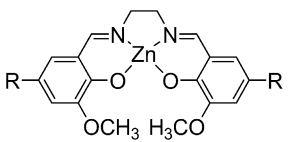	Zn Schiff base	H_2**97a**	355	CH_3OH		–	1.33	(Wong et al., 2002; Lo et al., 2004)
		H_2**97b**		CH_3CN		0.52[b]	1.31	
[**G3-An**] (cf. fig. 81)	Dendrimer	**94b-G3**	390	thin film		0.28[b]	0.7	(Baek et al., 2006)
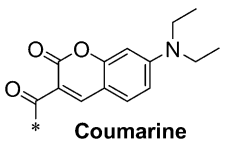 **Coumarine**	Terphenyl-based ligands	H_3**60c**	400	dmso-d_6		0.29[g]	2.16[i]	(Klink et al., 2001)
		H_3**60g**				0.26[g]	2.39[i]	
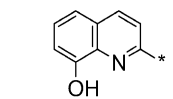 **8-Hydroxyquinoline**	Podands	H_6**91**	410	H_2O	0.03		0.15[j]	(Comby et al., 2007)
				D_2O	0.08		0.91[j]	

continued on next page

Table 21, *continued*

Nd			Experimental conditions					
Antenna[a]	Major unit		λ_{ex} (nm)	Nature/solvent	Q^{L}_{Ln} (%)	$Q^{Ln}_{Ln\ or\ rel}$ (%)[b,c,d,e,f,g]	τ (μs)[h,i,j]	Reference
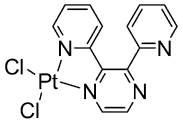 **114b**	β-Diketonates (Ternary complex)	**tta**	440	CH_2Cl_2		–	–	(Shavaleev et al., 2003b)
				Solid		–	0.94	
		btfa		CH_2Cl_2		0.33[b]	0.82	
				Solid		–	1.02	
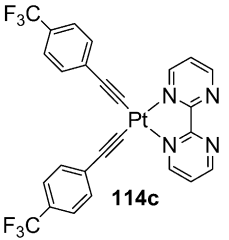 **114c**	β-Diketonates (Ternary complex)	**hfa**	460	CH_2Cl_2		–	<0.5[j]	(Shavaleev et al., 2005)
				Solid		0.27[b]	1.0[j]	
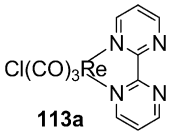 **113a**	β-Diketonates (Ternary complex)	**fod**	460	CH_2Cl_2		–	<0.5[j]	(Shavaleev et al., 2005)
				Solid		0.24[b]	0.9[j]	
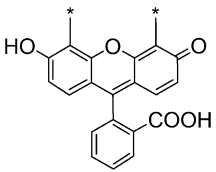	Polyamino-carboxylates	H_4**73a**	480	H_2O	0.017	0.031[d]	0.25[i]	(Werts et al., 2000a)
				D_2O	0.038	0.073[d]	0.58[i]	

continued on next page

Table 21, *continued*

Nd			Experimental conditions					
Antenna[a]	Major unit		λ_{ex} (nm)	Nature/solvent	Q^{L}_{Ln} (%)	$Q^{Ln}_{Ln\ or\ rel}$ (%)[b,c,d,e,f,g]	τ (μs)[h,i,j]	Reference
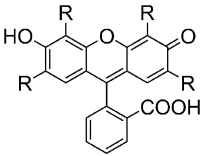 R = Br **Eosin**	Polyamino-carboxylates	H_4**72b**	488	D_2O		1.0[f]	–	(Werts et al., 1997;
				Degassed D_2O		1.5[f]	–	Hofstraat et al., 1998)
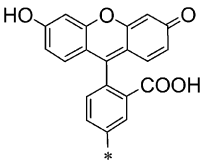 **Fluorescein**	Polyamino-carboxylates	H_4**72a**	488	D_2O		0.71[f]	0.6	(Werts et al., 1997;
				Degassed D_2O		0.86[f]	–	Hofstraat et al., 1998)
	Terphenyl-based ligands	H_3**61a**	505	CH_3OH	–	0.10[b]	0.24[i]	(Hebbink et al., 2003)
				CH_3OD	0.030	0.16[b]	0.41[i]	
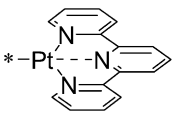	Polyamino-carboxylates	H_5**102**	515	H_2O		0.25[e]	0.670[i]	(Glover et al., 2003)
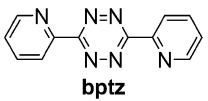 **bptz**	β-Diketonates (Ternary complex)	**tta**	520	CH_2Cl_2		0.3[b]	0.76[i]	(Shavaleev et al.,
				CH_2Cl_2			0.78	2003c)
				Solid			1.25[i]	
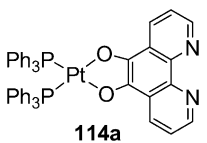 **114a**	β-Diketonates (Ternary complex)	**tta**	520	CH_2Cl_2		0.40[b]	0.99	(Shavaleev et al.,
				Solid		–	0.95	2003a, 2003b)

continued on next page

Table 21, *continued*

Nd Antenna[a]	Major unit		Experimental conditions λ_{ex} (nm)	Nature/solvent	Q^{L}_{Ln} (%)	$Q^{Ln}_{Ln\ or\ rel}$ (%)[b,c,d,e,f,g]	τ (μs)[h,i,j]	Reference
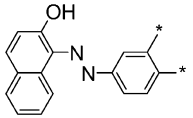 **1-phenylazo-2-naphtol**	Crown ether	**13a**	532	D_2O	0.09		0.8	(Korovin et al., 2002c; Korovin and Rusakova, 2004)
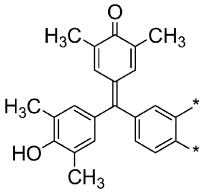 **Xylenol Blue derivative**	Crown ether	**XB**	532	D_2O	–		–	(Korovin et al., 2002c; Korovin and Rusakova, 2004)
		13b			0.12		0.9	
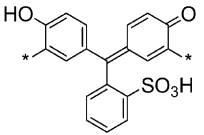 **Phthalexon S derivative**	Cyclen	**PS**	532	H_2O	–		0.07	(Korovin and Rusakova, 2002, 2004)
				D_2O	0.07		0.35	
		H_7**36**		H_2O	–		0.75	
				D_2O	0.23		1.45	
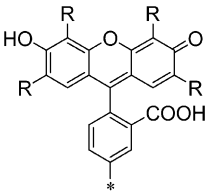 **b** R = Br **Eosin** **c** R = I **Erythrosin**	Terphenyl-based ligands	H_3**61b**	535	CH_3OH	–	0.14[b]	0.36[i]	(Hebbink et al., 2003)
				CH_3OD	0.014	0.16[b]	0.41[i]	
		H_3**61c**	545	CH_3OH	–	0.10[b]	0.25[i]	
				CH_3OD	0.012	0.15[b]	0.37[i]	

continued on next page

Table 21, *continued*

Nd			Experimental conditions					
Antenna[a]	Major unit		λ_{ex} (nm)	Nature/solvent	Q^{L}_{Ln} (%)	$Q^{Ln}_{Ln\ or\ rel}$ (%)[b,c,d,e,f,g]	τ (μs)[h,i,j]	Reference
 **lissamine**	Terphenyl-based ligands	H_3**60d**	570	dmso-h_6		–	1.16[i]	(Klink et al., 2001; Hebbink et al., 2002a; Slooff et al., 2000b)
				dmso-d_6		0.75[g]	2.21[i]	
				Polymer host		–	0.8[i]	
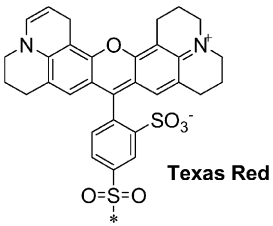 **Texas Red**	Terphenyl-based ligands	H_3**60e**	590	dmso-d_6		0.53[g]	2.26[i]	(Klink et al., 2001)
Complexes for which only lifetimes have been determined								
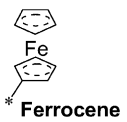 **Ferrocene**	Terphenyl-based ligands	H_3**104**	320	dmso-d_6	–		2.0[i]	(Klink, et al. 2000c, 2002)
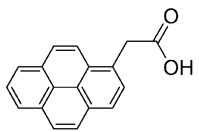 **Pyrene acetic acid (H34)**	Cyclen	**do3a**	337	H_2O	–		0.15	(Faulkner et al., 2004)
	(Ternary complex)			D_2O			0.75	

continued on next page

Table 21, *continued*

Nd			Experimental conditions					
Antenna[a]	Major unit		λ_{ex} (nm)	Nature/solvent	Q^{L}_{Ln} (%)	$Q^{Ln}_{Ln\ or\ rel}$ (%)[b,c,d,e,f,g]	τ (μs)[h,i,j]	Reference
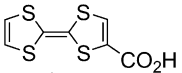 H**35a**	Cyclen (Ternary complex)	**do3a**	337	CH_3OH CD_3OD	–		0.12 0.46	(Pope et al., 2006)
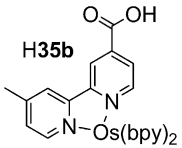 H**35b**	Cyclen (Ternary complex)	**do3a**	337	CH_3OH CD_3OD	–		0.24 0.57	(Pope et al., 2006)
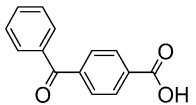 H**35c**	Cyclen (Ternary complex)	**do3a**	337	CH_3OH CD_3OD	–		0.13 0.59	(Pope et al., 2006)
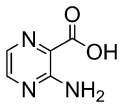 H**35d**	Cyclen (Ternary complex)	**do3a**	337	CH_3OH CD_3OD	–		0.11 0.55	(Pope et al., 2006)
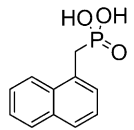 H_2**35e**	Cyclen (Ternary complex)	**do3a**	337	CH_3OH CD_3OD	–		0.16 0.60	(Pope et al., 2006)

continued on next page

Table 21, *continued*

Nd			Experimental conditions					
Antenna[a]	Major unit		λ_{ex} (nm)	Nature/solvent	Q^{L}_{Ln} (%)	$Q^{Ln}_{Ln\ or\ rel}$ (%)[b,c,d,e,f,g]	τ (μs)[h,i,j]	Reference
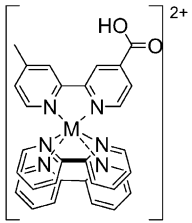 M = Ru (H**109a**), Os (H**109b**)	Cyclen (Ternary complex)	H**109a**	337	CH_3OH	–		0.174	(Pope et al., 2004b)
				CD_3OD			0.413	
		H**109b**		CH_3OH			0.237	
				CD_3OD			0.565	
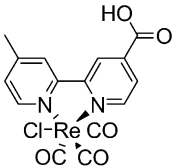 H**109c**	Cyclen (Ternary complex)	H**109c**	337	CH_3OH	–		0.353	(Pope et al., 2004b)
				CD_3OD			0.754	
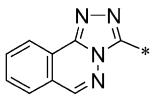 **Triazolophthalazine**	Cyclen	H_3**33**	337	H_2O	–		0.09	(Burton-Pye et al., 2005)
				D_2O			0.33	
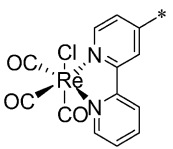	Polyamino-carboxylates	H_3**111**	337	CH_3OH	–		0.237	(Pope et al., 2004a, 2005)
				CD_3OD			0.512	

continued on next page

Table 21, *continued*

Nd			Experimental conditions					
Antenna[a]	Major unit		λ_{ex} (nm)	Nature/solvent	Q^{L}_{Ln} (%)	$Q^{Ln}_{Ln\ or\ rel}$ (%)[b,c,d,e,f,g]	τ (μs)[h,i,j]	Reference
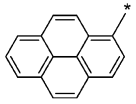 **Pyrene**	Cyclen	H_3**30a**	355	H_2O D_2O	–		0.080 0.320	(Faulkner et al., 2004)
	Cyclen	H_3**30b**	355	H_2O D_2O	–		0.220 0.310	(Faulkner et al., 2004)
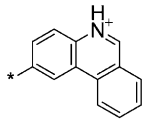 **Phenanthridinium**	Cyclen	**29**	355	H_2O H_2O degassed D_2O D_2O degassed	–		0.189 0.182 0.357 0.345	(Beeby et al., 2001)
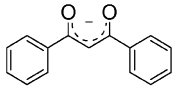 **dbm, 48b**	Calix[4]arene (Ternary complex)	H_2**46**	360	CD_2Cl_2	–		0.9	(Hebbink et al., 2001a)
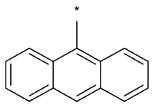 **anthryl**	β-Diketonates	**47j**	366	dmf $CHCl_3$ Me-thf	–		0.93 0.63 0.87	(Nah et al., 2006)
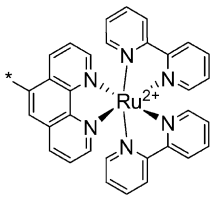	Cyclen	**112**	450	H_2O D_2O	–		0.03 0.192	(Gunnlaugsson and Leonard, 2005)

continued on next page

Table 21, *continued*

Nd			Experimental conditions					
Antenna[a]	Major unit		λ_{ex} (nm)	Nature/solvent	Q^{L}_{Ln} (%)	$Q^{Ln}_{Ln\ or\ rel}$ (%)[b,c,d,e,f,g]	τ (μs)[h,i,j]	Reference
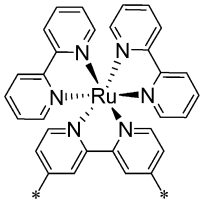 **[Ru(bpy)$_3$]$^{2+}$**	Terphenyl-based ligands	H_6**105**	450	dmso-d_6	–		2.1	(Klink et al., 2000c, 2002)
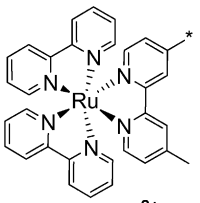 **[Ru(bpy)$_3$]$^{2+}$**	Polyamino-carboxylates	H_3**110a**	450	CH_3OH CD_3OD	–		0.22 0.50	(Pope et al., 2005)
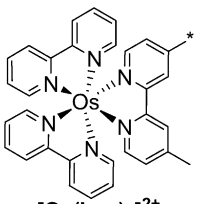 **[Os(bpy)$_3$]$^{2+}$**	Polyamino-carboxylates	H_3**110b**	490	CH_3OH CD_3OD	–		0.27 0.55	(Pope et al., 2005)

continued on next page

Table 21, *continued*

Nd			Experimental conditions					
Antenna[a]	Major unit		λ_{ex} (nm)	Nature/solvent	Q^{L}_{Ln} (%)	$Q^{Ln}_{Ln\ or\ rel}$ (%)[b,c,d,e,f,g]	τ (μs)[h,i,j]	Reference
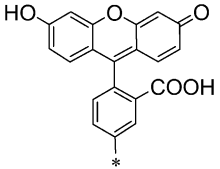 **Fluorescein**	Calix[4]arene	H_5**43a**	515	CD_3OD	–		0.86[i]	(Wolbers et al.,
				dmso			1.23[i]	1998a;
		H_5**43b**		CD_3OD			0.80[i]	Hofstraat et al., 1998)
				dmso			1.26[i]	
		H_2**43c**		CH_3CN			0.73[i]	

[a]The attachment point of the antenna is indicated by —∗; in case of ternary complexes, the sketched molecule acts both as the ternary ligand and antenna.
[b]Intrinsic quantum yields (Q^{Ln}_{Ln}) estimated from a radiative lifetime τ_0(Nd) = 0.25 ms.
[c]Intrinsic quantum yields (Q^{Ln}_{Ln}) estimated from a radiative lifetime τ_0(Nd) = 0.42 ms.
[d]Intrinsic quantum yields (Q^{Ln}_{Ln}) estimated from a radiative lifetime τ_0(Nd) = 0.8 ms.
[e]Intrinsic quantum yields (Q^{Ln}_{Ln}) estimated from a radiative lifetime τ_0(Nd) = 0.27 ms.
[f]Quantum yields relative to the one of [Nd (**72b**)] (Q^{Ln}_{rel}) in aerated D_2O (Tris-DCl buffer); fixed to unity.
[g]Quantum yields relative to the one of [Nd (**60b**)] (Q^{Ln}_{rel}) in dmso-d_6; fixed to unity.
[h]Measured under excitation at the wavelength given in column 3, or otherwise stated.
[i]λ_{ex} = 337 nm.
[j]λ_{ex} = 355 nm.
[k]Partial quantum yields ($^4F_{3/2} \rightarrow {}^4I_{9/2}$ and $^4F_{3/2} \rightarrow {}^4I_{11/2}$ transitions).

Table 22
Photophysical properties of Er^{III}-containing compounds

Er			Experimental conditions					
Antenna[a]	Major unit		λ_{ex} (nm)	Nature/solvent	Q^{L}_{Ln} (%)	$Q^{Ln}_{Ln\ or\ rel}$ (%)[b,c,d,e,f]	τ (μs)[g,h,i]	Reference
Complexes for which quantum yields (Q^{L}_{Ln}, $Q^{Ln}_{Ln\ or\ rel}$) have been measured or estimated								
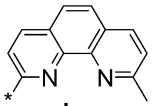 **phen**	Cyclen	H_3**31**	278	D_2O	5×10^{-4}		–	(Quici et al., 2004)
	Polyamino-carboxylates	H_4**74**	279	H_2O	–		–	(Quici et al., 2005)
				D_2O	4×10^{-3}		1.2	
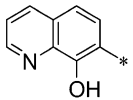 **8-Hydroxyquinoline**	Podands	H_8**90a**	344	H_2O	3.7×10^{-5}	0.035[c]	0.23[i]	(Imbert et al., 2005; Comby et al., 2006b)
				D_2O	5.4×10^{-3}	0.21[c]	1.39[i]	
		H_8**90b**	344	H_2O	4.0×10^{-5}	0.10[c]	0.67[i]	
				D_2O	7.1×10^{-3}	0.35[c]	2.31[i]	
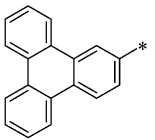 **Triphenylene**	Terphenyl-based ligands	H_3**60a**	350	dmso-h_6		0.02[b]	2.4[h]	(Klink et al., 1999, 2000a)
				dmso-d_6		0.02[b]	3.4[h]	
[**G3-An**] (cf. fig. 81)	Dendrimer	**94b-G3**	390	thin film		0.025[d]	2	(Baek et al., 2006)
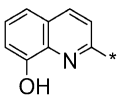 **8-Hydroxyquinoline**	Podands	H_6**91**	410	H_2O	–		0.24[i]	(Comby et al., 2007)
				D_2O	3.5×10^{-3}		2.55[i]	

continued on next page

Table 22, *continued*

Er			Experimental conditions					
Antenna[a]	Major unit		λ_{ex} (nm)	Nature/solvent	Q^{L}_{Ln} (%)	$Q^{Ln}_{Ln\ or\ rel}$ (%)[b,c,d,e,f]	τ (μs)[g,h,i]	Reference
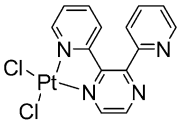 **114b**	β-Diketonates (Ternary complex)	**tta**	440	CH_2Cl_2		–	–	(Shavaleev et al., 2003b)
				Solid		–	1.59	
		btfa		CH_2Cl_2		0.011[b]	1.50	
				Solid		–	1.41	
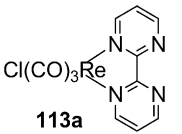 **113a**	β-Diketonates (Ternary complex)	**fod**	460	CH_2Cl_2		–	<0.5[i]	(Shavaleev et al., 2005)
				Solid		0.02[b]	1.6[i]	
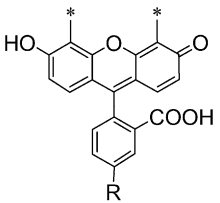 **Fluorescein**	Polyamino-carboxylates	H_4**73a**	480	H_2O	–	–	–	(Werts et al., 2000a)
				D_2O	0.019	0.018[d]	1.46[h]	
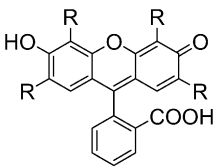 R = Br **Eosin**	Polyamino-carboxylates	H_4**72b**	488	D_2O		0.083[e]	–	(Werts et al., 1997; Hofstraat et al., 1998)
				Degassed D_2O		0.30[e]	–	

continued on next page

Table 22, *continued*

Er Antenna[a]	Major unit		Experimental conditions λ_{ex} (nm)	Nature/solvent	Q^{L}_{Ln} (%)	$Q^{Ln}_{Ln\ or\ rel}$ (%)[b,c,d,e,f]	τ (μs)[g,h,i]	Reference
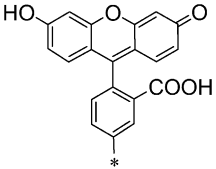 **Fluorescein**	Polyamino-carboxylates	H_4**72a**	488	D_2O		0.28[e]	1.0	(Werts et al., 1997;
				Degassed D_2O		0.31[e]	–	Hofstraat et al., 1998; Hebbink et al., 2003)
	Terphenyl-based ligands	H_3**61a**	505	CH_3OD		1.0[f]	0.91	
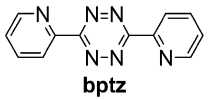 **bptz**	β-Diketonates (Ternary complex)	**tta**	520	CH_2Cl_2		0.012[b]	1.70[h]	(Shavaleev et al., 2003c)
				CH_2Cl_2			1.69	
				solid			2.0[h]	
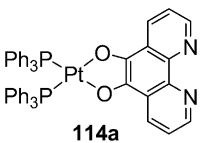 **114a**	β-Diketonates (Ternary complex)	**tta**	520	CH_2Cl_2		0.018[b]	2.52	(Shavaleev et al., 2003a, 2003b)
				Solid		–	1.56	
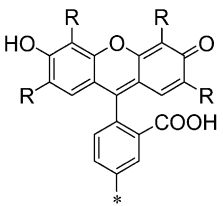 **b** R = Br **Eosin** **c** R = I **Erythrosin**	Terphenyl-based ligands	H_3**61b**	535	CH_3OD		0.51[f]	–	(Hebbink et al., 2003)
		H_3**61c**	545	CH_3OD		0.43[f]	–	

continued on next page

Table 22, *continued*

Er			Experimental conditions					
Antenna[a]	Major unit		λ_{ex} (nm)	Nature/solvent	Q^{L}_{Ln} (%)	$Q^{Ln}_{Ln\ or\ rel}$ (%)[b,c,d,e,f]	τ (μs)[g,h,i]	Reference
Complexes for which only lifetimes have been determined								
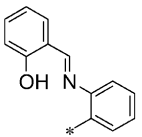 **2-salicylal-diminobenzyl**	Crown ether	**17c**	337	CH_3CN CH_3OH CD_3OD	-		0.78 0.42 0.78	(Gonzales-Lorenzo et al., 2005)
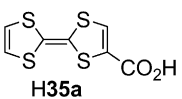 **H35a**	Cyclen (Ternary complex)	**do3a**	337	CH_3OH CD_3OD	–		– 0.44	(Pope et al., 2006)
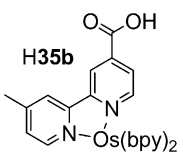 **H35b**	Cyclen (Ternary complex)	**do3a**	337	CH_3OH CD_3OD	–		– 0.49	(Pope et al., 2006)
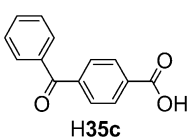 **H35c**	Cyclen (Ternary complex)	**do3a**	337	CH_3OH CD_3OD	–		– 0.41	(Pope et al., 2006)
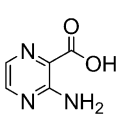 **H35d**	Cyclen (Ternary complex)	**do3a**	337	CH_3OH CD_3OD	–		– 0.56	(Pope et al., 2006)

continued on next page

Table 22, *continued*

Er			Experimental conditions					
Antenna[a]	Major unit		λ_{ex} (nm)	Nature/solvent	Q^{L}_{Ln} (%)	$Q^{Ln}_{Ln\ or\ rel}$ (%)[b,c,d,e,f]	τ (μs)[g,h,i]	Reference
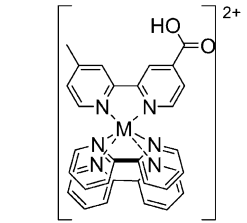 M = Ru (H**109a**), Os (H**109b**)	Cyclen (Ternary complex)	H**109a**	337	CH_3OH	–		–	(Pope et al., 2004b)
				CD_3OD			0.427	
		H**109b**		CH_3OH			–	
				CD_3OD			0.490	
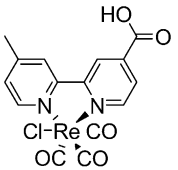 H**109c**	Cyclen (Ternary complex)	H**109c**	337	CH_3OH	–		–	(Pope et al., 2004b)
				CD_3OD			0.398	
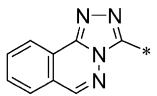 **Triazolophthalazine**	Cyclen	H_3**33**	337	H_2O	–		<0.02	(Burton-Pye et al., 2005)
				D_2O			1.3	
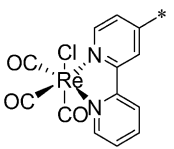	Polyamino-carboxylates	H_3**111**	337	CH_3OH	–		–	(Pope et al., 2004a, 2005)
				CD_3OD			0.54	

continued on next page

Table 22, *continued*

Er Antenna[a]	Major unit		Experimental conditions λ_{ex} (nm)	Nature/solvent	Q^{L}_{Ln} (%)	$Q^{Ln}_{Ln\ or\ rel}$ (%)[b,c,d,e,f]	τ (μs)[g,h,i]	Reference
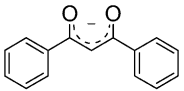 dbm, 48b	Calix[4]arene (Ternary complex)	H_2**46**	360	CD_2Cl_2	–		1.3	(Hebbink et al., 2001a)
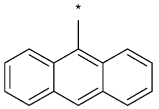 anthryl	β-Diketonates	**47j**	366	dmf $CHCl_3$ Me-thf	–		1.53 1.57 1.87	(Nah et al., 2006)
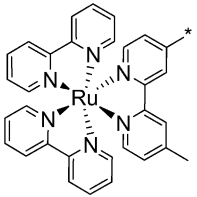 $[Ru(bpy)_3]^{2+}$	Polyamino-carboxylates	H_3**110a**	450	CH_3OH CD_3OD	–		–[h] 0.85[h]	(Pope et al., 2005)
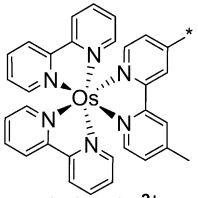 $[Os(bpy)_3]^{2+}$	Polyamino-carboxylates	H_3**110b**	490	CH_3OH CD_3OD	–		–[h] 1.16[h]	(Pope et al., 2005)

continued on next page

Table 22, *continued*

Er			Experimental conditions					
Antenna[a]	Major unit		λ_{ex} (nm)	Nature/solvent	Q^{L}_{Ln} (%)	$Q^{Ln}_{Ln\ or\ rel}$ (%)[b,c,d,e,f]	τ (μs)[g,h,i]	Reference
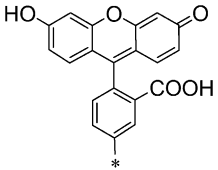 **Fluorescein**	Calix[4]arene	H_5**43a**	515	CD_3OD	–		0.76[h]	(Wolbers et al., 1998a; Hofstraat et al., 1998)
				dmso			1.71[h]	
		H_5**43b**		CD_3OD			0.88[h]	
				dmso			1.63[h]	
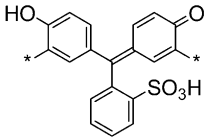 **Phthalexon S derivative**	Cyclen	H_7**36**	532	dmso-d_6	–		1.8	(Korovin and Rusakova, 2004)

[a]The attachment point of the antenna is indicated by —∗; in case of ternary complexes, the sketched molecule acts both as the ternary ligand and antenna.
[b]Intrinsic quantum yields (Q^{Ln}_{Ln}) estimated from a radiative lifetime $\tau_0(Er) = 14$ ms.
[c]Intrinsic quantum yields (Q^{Ln}_{Ln}) estimated from a radiative lifetime $\tau_0(Er) = 0.66$ ms.
[d]Intrinsic quantum yields (Q^{Ln}_{Ln}) estimated from a radiative lifetime $\tau_0(Er) = 8$ ms.
[e]Quantum yields relative to the one of [Nd (**72b**)] (Q^{Ln}_{rel}) in aerated D_2O (Tris-DCl buffer); fixed to unity.
[f]Quantum yields relative to the one of [Nd (**61a**)] (Q^{Ln}_{rel}) in CH_3OD; fixed to unity.
[g]Measured under excitation at the wavelength given in column 3, or otherwise stated.
[h]$\lambda_{ex} = 337$ nm.
[i]$\lambda_{ex} = 355$ nm.

Table 23
Photophysical properties of Yb^{III}-containing compounds

Yb			Experimental conditions					
Antenna[a]	Major unit		λ_{ex} (nm)	Nature/solvent	Q^{L}_{Ln} (%)	$Q^{Ln}_{Ln\ or\ rel}$ (%)[b,c]	τ (μs)[d,e,f]	Reference
Complexes for which quantum yields (Q^{L}_{Ln}, $Q^{Ln}_{Ln\ or\ rel}$) have been measured or estimated								
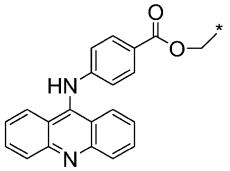 **9-(4-carboxyphenyl-amino)acridine**	Crown ether	**12g**	254	H_2O–C_2H_5OH	0.022		–	(Korovin et al., 2002e)
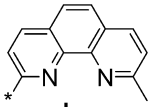 **phen**	Polyamino-carboxylates	H_4**74**	279	H_2O	0.02		2.5	(Quici et al., 2005)
				D_2O	0.10		10.0	
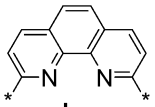 **phen**	Crown ether	**14**	300	Acetone	0.39		2.20	(Korovin et al., 2002d)
				Acetone-d_6	0.58		3.86	
		H_6**15**		H_2O	0.53		4.55	
				D_2O	0.86		8.86	
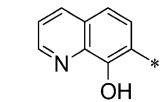 **8-Hydroxyquinoline**	Podands	H_8**90a**	344	H_2O	0.18	0.11[b]	2.21[f]	(Imbert et al., 2005; Comby et al., 2006b)
				D_2O	0.81	0.50[b]	10.0[f]	
		H_8**90b**	344	H_2O	0.37	0.29[b]	5.79[f]	
				D_2O	0.90	0.73[b]	14.6[f]	

continued on next page

Table 23, *continued*

Yb			Experimental conditions					
Antenna[a]	Major unit		λ_{ex} (nm)	Nature/solvent	Q^{L}_{Ln} (%)	$Q^{Ln}_{Ln\ or\ rel}$ (%)[b,c]	τ (μs)[d,e,f]	Reference
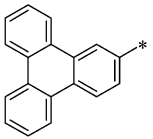 **Triphenylene**	Terphenyl-based ligands	H_3**60a**	350	dmso-h_6		0.47[b]	9.4[e]	(Klink et al., 1999;
				dmso-d_6		0.93[b]	18.6[e]	Klink et al., 2000a)
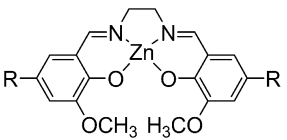	Zn Schiff base	H_2**97a**	355	CH_3OH		–	1.31	(Wong et al., 2002;
		H_2**97b**		CH_3CN		0.73[b]	14.59	Lo et al., 2004)
[**G3-An**] (cf. fig. 81)	Dendrimer	**94b-G3**	390	Thin film		0.55[b]	11	(Baek et al., 2006)
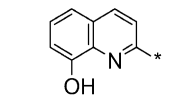 **8-Hydroxyquinoline**	Podands	H_6**91**	410	H_2O	0.13		2.47[f]	(Comby et al., 2007)
				D_2O	1.5		26.0[f]	
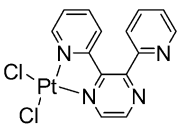 **114b**	β-Diketonates (Ternary complex)	**tta**	440	CH_2Cl_2		0.37[b]	7.30	(Shavaleev et al.,
				Solid		–	11.5	2003b)
		btfa		CH_2Cl_2		0.48[b]	9.50	
				Solid		–	11.0	

continued on next page

Table 23, *continued*

Yb			Experimental conditions					
Antenna[a]	Major unit		λ_{ex} (nm)	Nature/solvent	Q^{L}_{Ln} (%)	$Q^{Ln}_{Ln\ or\ rel}$ (%)[b,c]	τ (μs)[d,e,f]	Reference
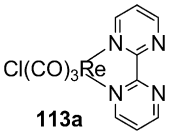 **113a**	β-Diketonates (Ternary complex)	**fod**	460	CH_2Cl_2 Solid		– 0.79[b]	6.7[f] 9.6[f]	(Shavaleev et al., 2005)
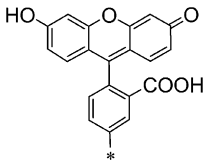 **Fluorescein**	Polyamino-carboxylates	H_4**72a**	488	D_2O Degassed D_2O		0.08[c] 0.46[c]	8.5 –	(Werts et al., 1997; Hofstraat et al., 1998)
	Terphenyl-based ligands	H_3**61a**	505	CH_3OH CH_3OD	– 0.23	0.49[b] 0.55[b]	9.8[e] 11.1[e]	(Hebbink et al., 2003)
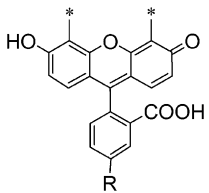	Polyamino-carboxylates	H_4**73a**	480	H_2O D_2O	0.09 0.45	0.10[b] 0.52[b]	1.91[e] 10.4[e]	(Werts et al., 2000a, 2000b)
		H_4**73c**	510	H_2O	≈0.05	0.09[b]	1.8[e]	
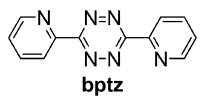 **bptz**	β-Diketonates (Ternary complex)	**tta**	520	CH_2Cl_2 CH_2Cl_2 solid		0.70[b]	13.3[e] 14.5 14.1[e]	(Shavaleev et al., 2003c)
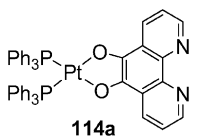 **114a**	β-Diketonates (Ternary complex)	**tta**	520	CH_2Cl_2 Solid		0.53[b] –	10.6 11.0	(Shavaleev et al., 2003a, 2003b)

continued on next page

Table 23, *continued*

Yb			Experimental conditions					
Antenna[a]	Major unit		λ_{ex} (nm)	Nature/solvent	Q^{L}_{Ln} (%)	$Q^{Ln}_{Ln\ or\ rel}$ (%)[b,c]	τ (μs)[d,e,f]	Reference
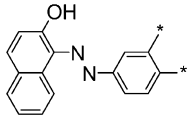 **1-phenylazo-2-naphtol**	Crown ether	**13a**	532	D_2O	0.66		3.8	(Korovin et al., 2002c; Korovin and Rusakova, 2004)
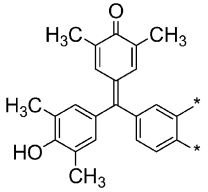 **Xylenol Blue derivative**	Crown ether	**XB**	532	D_2O	0.11		0.6	(Korovin et al., 2002c; Korovin and Rusakova, 2004)
		13b			0.88		4.2	
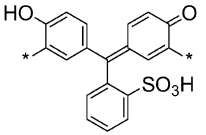 **Phthalexon S derivative**	Cyclen	**PS**	532	H_2O	–		0.70	(Korovin et al., 2002c; Korovin and Rusakova, 2004)
				D_2O	0.41		3.15	
		H_7**36**		H_2O	–		6.80	
				D_2O	1.45		12.60	
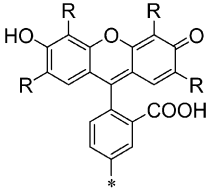 **b** R = Br **Eosin** **c** R = I **Erythrosin**	Polyamino-carboxylates	H_4**72b**	488	D_2O		1.4[c]	–	(Werts et al., 1997; Hofstraat et al., 1998)
				D_2O degassed		9.0[c]	–	
	Terphenyl-based ligands	H_3**61b**	535	CH_3OH	–	0.58[b]	11.6[e]	(Hebbink et al., 2003)
				CH_3OD	0.14	0.56[b]	11.2[e]	
		H_3**61c**	545	CH_3OH	–	0.51[b]	10.2[e]	
				CH_3OD	0.17	0.58[b]	11.5[e]	

continued on next page

Table 23, *continued*

Yb			Experimental conditions					
Antenna[a]	Major unit		λ_{ex} (nm)	Nature/solvent	Q^{L}_{Ln} (%)	$Q^{Ln}_{Ln\ or\ rel}$ (%)[b,c]	τ (μs)[d,e,f]	Reference
Complexes for which only lifetimes have been determined								
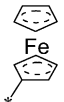 **Ferrocene**	Terphenyl-based ligands	H_3**104**	320	dmso-d_6	–		18.8[e]	(Klink et al., 2000c, 2002)
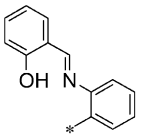 **2-salicylal-diminobenzyl**	Crown ether	**17c**	337	CH_3CN CH_3OH CD_3OD	–		4.34 2.92 4.65	(Gonzales-Lorenzo et al., 2005)
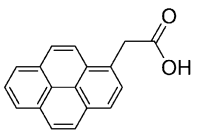 **Pyrene acetic acid (H34)**	Cyclen (Ternary complex)	**do3a**	337	H_2O D_2O	–		0.72 2.52	(Faulkner et al., 2004)
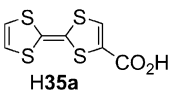 **H35a**	Cyclen (Ternary complex)	**do3a**	337	CH_3OH CD_3OD	–		2.02 3.49	(Faulkner et al., 2002; Pope et al., 2006)
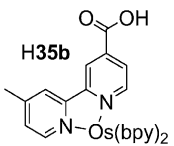 **H35b**	Cyclen (Ternary complex)	**do3a**	337	CH_3OH CD_3OD	–		1.38 8.19	(Pope et al., 2006)

continued on next page

Table 23, *continued*

Yb			Experimental conditions					
Antenna[a]	Major unit		λ_{ex} (nm)	Nature/solvent	Q^{L}_{Ln} (%)	$Q^{Ln}_{Ln\ or\ rel}$ (%)[b,c]	τ (μs)[d,e,f]	Reference
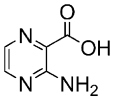 H**35d**	Cyclen (Ternary complex)	**do3a**	337	CH_3OH CD_3OD	–		1.43 7.02	(Pope et al., 2006)
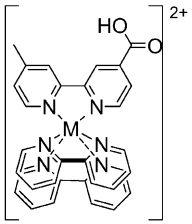 M = Ru (H**109a**), Os (H**109b**)	Cyclen (Ternary complex)	H**109a** H**109b**	337	CH_3OH CD_3OD CH_3OH CD_3OD	–		2.00 9.60 1.38 8.19	(Pope et al., 2004b)
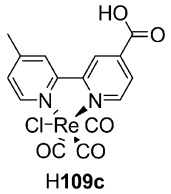 H**109c**	Cyclen (Ternary complex)	H**109c**	337	CH_3OH CD_3OD	–		1.85 4.76	(Pope et al., 2004b)
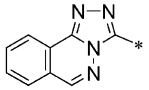 **Triazolophthalazine**	Cyclen	H_3**33**	337	H_2O D_2O	–		1.87 7.88	(Burton-Pye et al., 2005)

continued on next page

Table 23, *continued*

Yb			Experimental conditions					
Antenna[a]	Major unit		λ_{ex} (nm)	Nature/solvent	Q^{L}_{Ln} (%)	$Q^{Ln}_{Ln\ or\ rel}$ (%)[b,c]	τ (μs)[d,e,f]	Reference
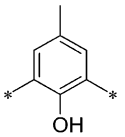 **phenol**	Cyclen	H_7**37a**	337	H_2O site I	–		1.67	(Pope et al., 2003b)
				H_2O site II			0.51	
				D_2O site I			4.95	
				D_2O site II			1.17	
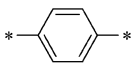 **p-xylene**	Cyclen	H_6**37b**	337	H_2O	–		1.45	(Pope et al., 2003a)
				D_2O			6.07	
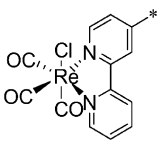	Polyamino-carboxylates	H_3**111**	337	CH_3OH	–		1.88	(Pope et al., 2004a, 2005)
				CD_3OD			8.30	
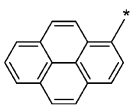 **Pyrene**	Cyclen	H_3**30a**	355	H_2O	–		0.74	(Faulkner et al., 2004)
				D_2O			7.45	
		H_3**30b**		H_2O	–		1.34	
				D_2O			7.40	
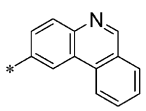 **Phenanthridine**	Cyclen	**29**	355	H_2O	–		5.0	(Beeby et al., 2002c)
				H_2O degassed			24.4	
				D_2O			5.9	
				D_2O degassed			26.3	
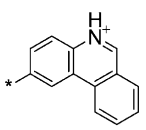 **Phenanthridinium**				H_2O	–		0.9	
				H_2O degassed			0.9	
				D_2O			7.7	
				D_2O degassed			7.7	

continued on next page

Table 23, *continued*

Yb			Experimental conditions					
Antenna[a]	Major unit		λ_{ex} (nm)	Nature/solvent	Q^{L}_{Ln} (%)	$Q^{Ln}_{Ln\ or\ rel}$ (%)[b,c]	τ (μs)[d,e,f]	Reference
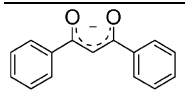 **dbm, 48b**	Calix[4]arene (Ternary complex)	H_2**46**	360	CD_2Cl_2	–		12.5	(Hebbink et al., 2001a)
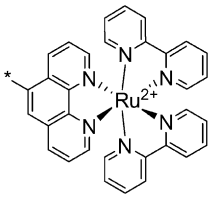	Cyclen	**112**	450	H_2O D_2O	–		2.0 6.37	(Gunnlaugsson and Leonard, 2005)
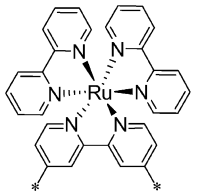 **$[Ru(bpy)_3]^{2+}$**	Terphenyl-based ligands	H_6**105**	450	dmso-d_6	–		18.2	(Klink, et al. 2000c, 2002)
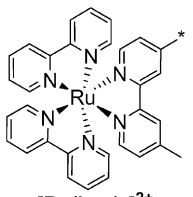 **$[Ru(bpy)_3]^{2+}$**	Polyamino-carboxylates	H_3**110a**	450	CH_3OH CD_3OD	–		–[e] 7.39[e]	(Pope et al., 2005)

continued on next page

Table 23, *continued*

Yb			Experimental conditions					
Antenna[a]	Major unit		λ_{ex} (nm)	Nature/solvent	Q^{L}_{Ln} (%)	$Q^{Ln}_{Ln\ or\ rel}$ (%)[b,c]	τ (μs)[d,e,f]	Reference
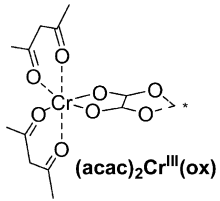 **$(acac)_2Cr^{III}(ox)$**	Cr^{III}–Ln^{III} assembly		488	Solid	–		48	(Subhan et al., 2003)
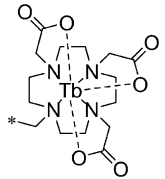	Polyamino-carboxylates	H_3**116**	337 488	H_2O D_2O D_2O	–		1.83 4.22 4.22	(Faulkner and Pope, 2003)
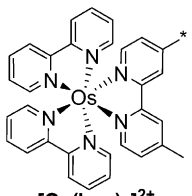 **$[Os(bpy)_3]^{2+}$**	Polyamino-carboxylates	H_3**110b**	490	CH_3OH CD_3OD	–		–[e] 5.33[e]	(Pope et al., 2005)

[a]The attachment point of the antenna is indicated by —∗; in case of ternary complexes, the sketched molecule acts both as the ternary ligand and antenna.

[b]Intrinsic quantum yields (Q^{Ln}_{Ln}) estimated from a radiative lifetime $\tau_0(Yb) = 2$ ms.

[c]Quantum yields relative to the one of [Nd(**72b**)] (Q^{Ln}_{rel}) in aerated D_2O (Tris-DCl buffer); fixed to unity.

[d]Measured under excitation at the wavelength given in column 3, or otherwise stated.

[e]$\lambda_{ex} = 337$ nm.

[f]$\lambda_{ex} = 355$ nm.

detected signal should also be avoided (signal $<5\times10^5$ cps). Accuracies better than $\pm$10–20% are anyway difficult to achieve.

For Nd^{III}, the overall quantum yields exhibited by molecular complexes with organic ligands remain small. The best chromophores seem to be un-symmetric fluorinated β-diketonates, for which partial quantum yields up to 1.2% are obtained in organic solvents that are boosted to 3–4% in the corresponding ternary complexes. The largest quantum yields for complexes with calixarenes and calixresorcinarenes are in the range 0.1–0.2% in dmf. The use of sensitization groups such as 8-hydroxyquinolinate, 1,10-phenanthroline, dansyl or phthalexon S, or xylenol blue leads to quantum yields in the range of 0.1 to 0.3% in deuterated water or acetonitrile and 0.04 to 0.09% in water. It should be stressed here that the intrinsic quantum yield rarely exceeds 2–4%, so that the sensitization process is not the only limiting factor.

Quantum yields for Er^{III} are much smaller and no data are reported for β-diketonates. Among the few other quantitative figures reported, we note a quantum yield of 0.02% in deuterated water with fluorescein as the antenna chromophore, while all the other quantum yields are far below 10^{-3}%. As for neodymium, 1,10-phenanthroline and 8-hydroxyquinolinate are among the best sensitizers.

Ytterbium is a more rewarding ion in that quantum yields in the range 0.2–0.5% are reported in water, these values reaching 0.4–1.45% in deuterated water and in some organic solvents. Calixarene derivatives have quantum yields in the range 0.1–0.6% in dmf and ternary complexes with β-diketonates reach quantum yields of 1–2% in organic solvents and up to 6% in deuterated solvents and when the C–H bridge of the diketonate unit is deuterated. As far as sensitizing moieties are concerned, the best ones are again 1,10-phenanthroline and 8-hydroxyquinolinate and the best dyes are fluorescein, 1-phenylazo-2-naphthol, phthalexon S, and xylenol blue.

6. Conclusions

The number and variety of molecular systems tested for the encapsulation and sensitization of the NIR-emitting trivalent lanthanide ions Nd^{III}, Er^{III}, and Yb^{III} which are described in sections 3 and 4 of this review are vivid proofs of the interest for these luminescent centers triggered by potential applications in telecommunications, lighting devices, and more recently medical diagnostic and analyses. The starting point of NIR luminescence in lanthanide-containing complexes with organic ligands is the report by Crosby and Kasha (1958) on the sensitization of ytterbium luminescence by β-diketonates, followed by the report of Gurevich and Solev'ev (1961) on the luminescence of ytterbium porphyrinate, but the field really took off in the mid 1970's only so that most of the information described in this chapter has been gathered during the last twenty years. We note that the contribution of Bill Carnall, to whom this volume of the Handbook is dedicated, on the NIR transitions of trivalent lanthanide ions in solution which appeared in 1962 has also to be considered as one of the activators of this research field (Carnall et al., 1962).

6.1. *Is sensitization of the NIR luminescence a problem?*

When designing a host system for NIR-emitting lanthanide ions, chemists have two problems to solve: (i) sensitization of the lanthanide luminescence, taken in a restrictive sense that is optimization of the ligand-to-metal energy transfer, and (ii) protection against nonradiative deactivation. The first problem is not difficult to cope with, and the answer to the question stated above is clearly no, since η_{sens} values larger than 60% can routinely be obtained with many chromophoric ligands. The numerous detailed photophysical studies performed on many systems have clearly evidenced the various mechanisms for energy transfer, which depend on the specific lanthanide ion, and they have also demonstrated that the simplistic scheme $^1S \rightarrow {}^3T \rightarrow Ln^*$ is not the only mechanism to take into account. This has fruitful consequences in that the simplistic model calls for organic ligands having as little fluorescence as possible and a large intersystem crossing yield. In fact, ligands with large fluorescence intensity and poor isc yield may also be excellent sensitizers for two reasons. The first one is that some ions, particularly the fluorescent Nd^{III} ion, can be easily excited by direct transfer from the singlet state. The second is that complexation of paramagnetic lanthanide ions to the organic chromophore results in a large "heavy atom" effect favoring the isc process to the expense of ligand fluorescence. Furthermore, in the case of Yb^{III} excitation, more elaborate mechanisms are operative, involving either a phonon-assisted transfer or a double electron exchange mechanism in which the ytterbium ion is momentarily reduced into its divalent oxidation state. And to render this mechanism operative, considerations other than singlet and triplet state energies have to be included, especially free Gibbs energy of the redox processes. Finally, Er^{III} excitation is also an example for which alternative mechanisms may be developed, such as up-conversion. Additionally, two-photon absorption, which has yet to be demonstrated for organic complexes of the NIR emitting Ln^{III} ions, may also be considered in the future.

6.2. *Preventing nonradiative deactivation: the real problem*

All organic ligands possess a large distribution of phonon states. Careful tailoring of the ligands to meet the criteria of thermodynamic stability (and possibly kinetic inertness), protection from inner-sphere solvent interaction, as well as efficient energy transfer onto the metal ion excited state is not sufficient to produce a highly luminescent lanthanide complex. The inner coordination sphere must be devoid of high energy vibrations such as O–H and N–H and C–H and, worse, these vibrations should ideally also be absent from the second and subsequent coordination spheres. This is especially true for Nd^{III} and Er^{III} complexes since the energy gap for these ions is very small. If O–H and N–H vibrations can be reasonably well dealt with, see for instance the replacement of water molecules with non O–H donors in β-diketonate ternary complexes (Rusakova et al., 1992a) or the substitution of N–H by N–Me demonstrated for quinolinate-based podands (Comby et al., 2006b), C–H vibrations are much more difficult to eliminate. In the case of Er^{III}, recent modeling of their quenching effect indicates that the environment of the metal ion must be devoid of C–H vibrators up to distances ranging between 20 and 30 Å for the radiative rate constant to be larger than the nonradiative one (Quochi et al., 2006; Winkless et al., 2006). The only alternative is either deuteration or fluorination of the ligands and both methods are expensive and time-consuming. In

addition if the ligands are deuterated, then deuterated solvents should be used to avoid hydrogen exchange. Similarly, deactivation by the solvent can be curtained only by replacing C–H containing solvents with halogenated solvents such as carbon tetrachloride or by deuterating them.

6.3. *Best complexation agents and chromophores*

Amid the relatively simple chelating agents, aminocarboxylates, β-diketonates, and 8-hydroxyquinolinate are the best. The advantage of aminocarboxylates is their large stability in water, but unless suitably substituted, they do not provide any antenna effect. On the other hand, β-diketonates are among the best sensitizers of NIR luminescence, but they are not stable enough in water. The ideal compromise seems to stem from 8-hydroxyquinolinates, the stability of which in water is only slightly smaller than the one of polyaminocarboxylates and which provide an antenna effect comparable or better than the sensitization afforded by β-diketonates. Generally speaking, macrocyclic receptors have not produced highly luminescent entities, with a few exceptions, and they must be considered for special applications only. For instance, the ability of porphyrins and related compounds to selectively bind cancer cells is important for the development of cancer imaging or for the monitoring of cancer cell apoptosis. Another promising application of porphyrinates is electroluminescence owing to their electron conducting ability. Other applications of macrocycles could involve the encapsulation of ions in the kinetically inert environment of cyclen derivatives, or the design of luminescent sensors with a special compartment for the complexation of alkali cations, for instance. When dealing with more elaborate ligands, one wishes to substitute a strong complexing agent with chromophores having low-energy singlet and triplet states. The best molecules and dyes tested so far are clearly the dansyl chromophore, fluorescein, phthalexon S, 1-phenylazo-2-naphthol, and xylenol blue; in any case, the sensitizing moiety has to be brought close to the Ln^{III} ion in order to maximize the efficiency of the energy transfer process.

Excitation of the Ln^{III} ion by a d-transition metal ion is an alternative to chromophore-substituted ligands, and proof of principle has been demonstrated for several systems. The lack of quantitative data, however does not allow an evaluation of their real potential, except for their main advantage, which is the control of the luminescent properties of the 4f-metal ion by directional energy transfer. In this context, we note the emergence of self-assembly processes to build new edifices, particularly bi-metallic edifices, by the simultaneous recognition of two metal ions. This relatively unexplored area has already resulted in the design of edifices in which the rate of population, and therefore the apparent lifetime, of a 4f-excited state can be fine-tuned by energy transfer from a d-transition metal ion (Torelli et al., 2005).

6.4. *The future of NIR-emitting Ln^{III} ions in applications*

There is no doubt that despite the low quantum yields achieved to date for Nd^{III} and Er^{III} organic materials, polymer optical fibers will be an alternative to silica fibers in the telecommunication windows, mainly in view of their intrinsic advantages cited in section 4, including low cost. A similar conclusion can be drawn for NIR-emitting OLEDs and the availability of fluorinated polymers and β-diketonates with low vibrations will certainly help boosting

developments in this area. Encaging the luminescent centers in porous materials has proved rewarding as well, with the astonishingly large quantum yield of 9.5% attained for $[Nd(pms)_3]$ doped into TMA^+-containing faujasite zeolite nanocrystallites dispersed in dmso-d_6 (Ryo et al., 2004).

While we do not foresee wide applications of Nd^{III} and Er^{III} for biology-related problems, except for up-converting phosphor technology (Kuningas et al., 2006), Yb^{III} probes are luminescent stains with a large potential in this field. Technical developments in instrumentation for imaging of NIR-emission signals are still ongoing, but some proofs of principle are at hand, for instance, the NIR-image of a [Yb(TPP)Trp] device in polystyrene captured using a commercial video camera with NIR capability (Harrison et al., 2004). Indeed, the possibility of exciting NIR luminescent probes by visible light makes it inevitable that NIR-labels will be accepted as bioprobes in a near future, much as their visible counterparts, especially if quantum yields of 1–3% can be achieved for Yb^{III} under physiological conditions. This target should be within reach in a near future, possibly with 8-hydroxyquinolinate-based systems. Another direction for future research in NIR biolabels is *in cellulo* probing and imaging. The prerequisite is that the complex must be non-toxic and cell-permeable with, preferably, targeting ability. That is, the complex should localize in a given organelle. Bio-conjugation is a major tool towards this goal since the localization of the probe in the cell will then be determined by the nature of the protein or peptide vector used. The problem of localization is however relatively complex since the bio-conjugates often recognize a cell surface receptor, so that the conjugates reside then in an endosome or a related vesicle structure. Solving this problem is a real challenge which will only be met by a close collaboration between biochemists and chemists.

6.5. *Concluding statement*

The wealth and variety of results reviewed in this chapter show both the potential of organic complexes and materials for NIR-luminescent probes and the difficulty in achieving reasonable emission efficiency, especially with the very difficult-to-solve problem of C–H vibrations. Alternatives between purely inorganic systems such as glasses and organic complexes and polymers may well be clusters which combine the advantages of both, as demonstrated with Er^{III} polymetallic assemblies having a double cubane structure (Kumar et al., 2005), or functionalized nanoparticles, e.g. doped LaF_3 nanoparticles (Slooff et al., 2000a). In these systems, intrinsic quantum yields reach values as high as 70–80% and therefore the main problem hindering the development of NIR-emitting lanthanide-containing probes is elegantly overcome. Furthermore, the possibility of derivatizing nanoparticles and their binding to biomolecules opens the way for their application in targeted biomedical analyses, including multiplexed detection of protein cancer markers, and cell imaging (Diamente et al., 2006). Other promising systems for inclusion of NIR-emitting Ln^{III} ions are ionic liquids in which tetrakis(β-diketonates) act as the anion or doped ionogels generated by the confinement of ionic liquids within a porous silica matrix. Not only do these gels have excellent mechanical, thermal and optical properties but in addition, they feature high ionic conductivity, a key factor for electroluminescent devices (Neouze et al., 2005).

References

Abdus, S., Kawahata, R., Nakata, H., Fuyuhiro, A., Tsukuda, T., Kaizaki, S., 2004. Inorg. Chim. Acta **357**, 3139.

Aime, S., Botta, M., Parker, D., Williams, J.A.G., 1996. J. Chem. Soc., Dalton Trans., 17.

Aime, S., Batsanov, A.S., Botta, M., Dickins, R.S., Faulkner, S., Foster, C.E., Harrison, A., Howard, J.A.K., Moloney, J.M., Norman, T.J., Parker, D., Royle, L., Williams, J.A.G., 1997. J. Chem. Soc., Dalton Trans., 3623.

Ala-Kleme, T., Haapakka, K., Latva, M., 1999. Anal. Chim. Acta **395**, 205.

Ala-Kleme, T., Latva, M., Haapakka, K., 2000. Anal. Chim. Acta **403**, 161.

Albota, M., Beljonne, D., Bredas, J.L., Ehrlich, J.E., Fu, J.Y., Heikal, A.A., Hess, S.E., Kogej, T., Levin, M.D., Marder, S.R., McCord-Maughon, D., Perry, J.W., Rockel, H., Rumi, M., Subramaniam, C., Webb, W.W., Wu, X.L., Xu, C., 1998. Science **281**, 1653.

An, D.C., Yue, Z.Z., Chen, R.T., 1998. Appl. Phys. Lett. **72**, 2806.

Ananias, D., Kostova, M., Almeida Paz, F.A., Ferreira, A., Carlos, L.D., Klinowski, J., Rocha, J., 2004. J. Am. Chem. Soc. **126**, 10410.

André, N., Scopelliti, R., Hopfgartner, G., Piguet, C., Bünzli, J.-C.G., 2002. Chem. Commun., 214.

Archer, R.D., Chen, H.Y., Thompson, L.C., 1998. Inorg. Chem. **37**, 2089.

Arenz, S., Babai, A., Binnemans, K., Driesen, K., Giernoth, R., Mudring, A.-V., Nockemann, P., 2005. Chem. Phys. Lett. **402**, 75.

Armaroli, N., Balzani, V., Barigelletti, F., Ward, M.D., McCleverty, J.A., 1997. Chem. Phys. Lett. **276**, 435.

Artizzu, F., Deplano, P., Marchio, L., Mercuri, M.L., Pilia, L., Serpe, A., Quochi, F., Orru, R., Cordella, F., Meinardi, F., Tubino, R., Mura, A., Bongiovanni, G., 2005. Inorg. Chem. **44**, 840.

Asano-Someda, M., Kaizu, Y., 2001. J. Photochem. Photobiol. A Chem. **139**, 161.

Asfari, Z., Böhmer, V., Harrowfield, J.M., Vicens, J., 2001. Calixarenes 2001. Kluwer Academic Publishers, Dordrecht.

Auzel, F., 2004. Chem. Rev. **104**, 139.

Baek, N.S., Kim, Y.H., Roh, S.G., Kwak, B.K., Kim, H.K., 2006. Adv. Funct. Mater. **16**, 1873.

Baldo, M.A., O'Brien, D.F., You, Y., Shoustikov, A., Sibley, S., Thompson, M.E., Forrest, S.R., 1998. Nature **395**, 151.

Banerjee, S., Huebner, L., Romanelli, M.D., Kumar, G.A., Riman, R.E., Emge, T.J., Brennan, J.G., 2005. J. Am. Chem. Soc. **127**, 15900.

Bassett, A.P., Magennis, S.W., Glover, P.B., Lewis, D.J., Spencer, N., Parsons, S., Williams, R.M., De Cola, L., Pikramenou, Z., 2004. J. Am. Chem. Soc. **126**, 9413.

Bassett, A.P., Van Deun, R., Nockemann, P., Glover, P.B., Kariuki, B.M., Van Hecke, K., Van Meervelt, L., Pikramenou, Z., 2005. Inorg. Chem. **44**, 6140.

Batsanov, A.S., Beeby, A., Bruce, J.I., Howard, J.A.K., Kenwright, A.M., Parker, D., 1999. Chem. Commun., 1011.

Batyaev, I.M., 1971. Russ. Chem. Rev. (Engl. Transl.) **40**, 622.

Batyaev, I.M., Danil'chuk, N.V., Kabatskii, Y.A., Shapovalov, V.N., Shilov, S.M., 1989a. J. Appl. Spectrosc. (Engl. Transl.) **51**, 1262.

Batyaev, I.M., Kabatskii, Y.A., Mokhova, E.A., Sviridov, V.V., 1989b. J. Appl. Spectrosc. (Engl. Transl.) **50**, 394.

Becker, A., Hessenius, C., Licha, K., Ebert, B., Sukowski, U., Semmler, W., Wiedenmann, B., Grotzinger, C., 2001. Nat. Biotechnol. **19**, 327.

Beeby, A., Faulkner, S., 1997. Chem. Phys. Lett. **266**, 116.

Beeby, A., Dickins, R.S., Faulkner, S., Parker, D., Williams, J.A.G., 1997. Chem. Commun., 1401.

Beeby, A., Clarkson, I.M., Dickins, R.S., Faulkner, S., Parker, D., Royle, L., de Sousa, A.S., Williams, J.A.G., Woods, M., 1999. J. Chem. Soc., Perkin Trans. **2**, 493.

Beeby, A., Dickins, R.S., FitzGerald, S., Govenlock, L.J., Maupin, C.L., Parker, D., Riehl, J.P., Siligardi, G., Williams, J.A.G., 2000. Chem. Commun., 1183.

Beeby, A., Faulkner, S., Parker, D., Williams, J.A.G., 2001. J. Chem. Soc., Perkin Trans. **2**, 1268.

Beeby, A., Burton-Pye, B.P., Faulkner, S., Motson, G.R., Jeffery, J.C., McCleverty, J.A., Ward, M.D., 2002a. J. Chem. Soc., Dalton Trans., 1923.

Beeby, A., Bushby, L.M., Maffeo, D., Williams, J.A.G., 2002b. J. Chem. Soc., Dalton Trans., 48.

Beeby, A., Faulkner, S., Williams, J.A.G., 2002c. J. Chem. Soc., Dalton Trans., 1918.

Beer, P.D., Szemes, F., Passaniti, P., Maestri, M., 2004. Inorg. Chem. **43**, 3965.

Bermudez, V.D., Carlos, L.D., Duarte, M.C., Silva, M.M., Silva, C.J.R., Smith, M.J., Assuncao, M., Alcacer, L., 1998. J. Alloys Compd. **277**, 21.

Bernhardt, P.V., Flanagan, B.M., Riley, M.J., 2000. Aust. J. Chem. **53**, 229.

Bertolo, L., Tamburini, S., Vigato, P.A., Porzio, W., Macchi, G., Meinardi, F., 2006. Eur. J. Inorg. Chem., 2370.

Bethune, D.S., Johnson, R.D., Salem, J.R., de Vries, M.S., Yannoni, C.S., 1993. Nature **366**, 123.

Billard, I., Mekki, S., Gaillard, C., Hesemann, P., Moutiers, G., Mariet, C., Labet, A., Bünzli, J.-C.G., 2004. Eur. J. Inorg. Chem., 1190.

Billard, I., Moutiers, G., Labet, A., El Azzi, A., Gaillard, C., Mariet, C., Lützenkirchen, K., 2003. Inorg. Chem. **42**, 1726.

Binnemans, K., 2005a. Chem. Rev. **105**, 4148.

Binnemans, K., 2005b. Rare earth β-diketonate complexes: functionalities and applications. In: Gschneidner Jr., K.A., Bünzli, J.-C.G., Pecharsky, V.K. (Eds.), Handbook on the Physics and Chemistry of Rare Earths, vol. **35**. Elsevier, Amsterdam (chapter 225).

Blumenthal, N., Ellis, C.B., Grafstei, D., 1968. J. Chem. Phys. **48**, 5726.

Bol'shoi, D.V., Meshkova, S.B., Topilova, Z.M., Lozinskii, M.O., Shapiro, Y.E., 1997. Opt. Spectrosc. (Engl. Transl.) **83**, 627.

Borbas, K.E., Bruce J.I., 2006. Chem. Commun., 4596.

Brayshaw, P.A., Bünzli, J.-C.G., Froidevaux, P., Harrowfield, J.M., Kim, Y., Sobolev, A.N., 1995. Inorg. Chem. **34**, 2068.

Brecher, C., French, K.W., 1969. J. Phys. Chem. **73**, 1785.

Brecher, C., French, K.W., 1973. J. Phys. Chem. **77**, 1370.

Breen, P.J., Hild, E.K., deW. Horrocks Jr., W., 1985. Biochemistry **25**, 4991.

Brinkschulte, H., Fill, E., Lang, R., 1972. J. Appl. Phys. **43**, 1807.

Buissette, V., Huignard, A., Gacoin, T., Boilot, J.P., Aschehoug, P., Viana, B., 2003. Surf. Sci. **532**, 444.

Bünzli, J.-C.G., 1987. Complexes with synthetic ionophores. In: Gschneidner Jr., K.A., Eyring, L. (Eds.), Handbook on the Physics and Chemistry of Rare Earths, vol. **9**. Elsevier Science Publ., Amsterdam, pp. 321–394 (chapter 60).

Bünzli, J.-C.G., 1989. Luminescent probes. In: Bünzli, J.-C.G., Choppin, G.R. (Eds.), Lanthanide Probes in Life, Chemical and Earth Sciences. Theory and Practice. Elsevier Science B.V., Amsterdam, pp. 219–293 (chapter 7).

Bünzli, J.-C.G., 1998. Coordination chemistry of the trivalent lanthanide ions: an introductory overview. In: Saez Puche, R., Caro, P. (Eds.), Rare Earths. Editorial Complutense, Madrid, pp. 223–259.

Bünzli, J.-C.G., 2004. Luminescent lanthanide probes as diagnostic and therapeutic tools. In: Sigel, A., Sigel, H. (Eds.), Metal Complexes in Tumor Diagnosis and as Anticancer Agents, vol. **42**. Marcel Dekker, New York, pp. 39–75 (chapter 2).

Bünzli, J.-C.G., 2005. Rare earth luminescent centers in organic and biochemical compounds. In: Liu, G.K., Jacquier, B. (Eds.), Spectroscopic Properties of Rare Earths in Optical Materials. Springer Verlag, Berlin, pp. 462–499 (chapter 11).

Bünzli, J.-C.G., Besançon, F., 2005. Phys. Chem. Chem. Phys. **7**, 2191.

Bünzli, J.-C.G., Piguet, C., 2002. Chem. Rev. **102**, 1897.

Bünzli, J.-C.G., Piguet, C., 2005. Chem. Soc. Rev. **34**, 1048.

Bünzli, J.-C.G., Pilloud, F., 1989. Inorg. Chem. **28**, 2638.

Bünzli, J.-C.G., Vuckovic, M.M., 1983. Inorg. Chim. Acta **73**, 53.

Bünzli, J.-C.G., Vuckovic, M.M., 1984. Inorg. Chim. Acta **95**, 105.

Bünzli, J.-C.G., Besançon, F., Ihringer, F., 2000. Bimetallic lanthanide supramolecular edifices with calixarenes. In: Lumetta, G.J., Rogers, R.D., Gopalan, A. (Eds.), Calixarenes for Separations, vol. **757**. American Chemical Society, Washington, DC, pp. 179–194 (chapter 14).

Burton-Pye, B.P., Heath, S.L., Faulkner, S., 2005. Dalton Trans., 146.

But, S., Van Deun, R., Parac-Vogt, T.N., Görller-Walrand, C., Binnemans, K., 2005. Spectrochim. Acta A **62**, 478.

Cantuel, M., Bernardinelli, G., Imbert, D., Bünzli, J.-C.G., Hopfgartner, G., Piguet, C., 2002. J. Chem. Soc., Dalton Trans., 1929.

Cardinaels, T., Driesen, K., Parac-Vogt, T.N., Heinrich, B., Bourgogne, C., Guillon, D., Donnio, B., Binnemans, K., 2005. Chem. Mater. **17**, 6589.

Carlos, L.D., Ferreira, R.A.S., Bermudez, V.D., 2000. Electrochim. Acta **45**, 1555.

Carlos, L.D., Ferreira, R.A.S., Silva, N.J.O., Amaral, V.S., Goncalves, M.C., Bermudez, V.D., 2004. Adv. Mater. Forum **455–456**, 564.

Carnall, W.T., 1979. The absorption and fluorescence spectra of rare earth ions in solution. In: Gschneidner Jr., K.A., Eyring, L. (Eds.), Handbook on the Physics and Chemistry of Rare Earths, vol. **3**. North Holland, Amsterdam, pp. 172–208 (chapter 24).

Carnall, W.T., Gruen, D.M., McBeth, R.L., 1962. J. Phys. Chem. **66**, 2159.

Carnall, W.T., Fields, P.R., Wybourne, B.G., 1965. J. Chem. Phys. **42**, 3797.

Carnall, W.T., Fields, P.R., Rajnak, K., 1968. J. Chem. Phys. **49**, 4424.

Carnall, W.T., Hessler, J.P., Wagner, F.J., 1978. J. Phys. Chem. **82**, 2152.

Carnall, W.T., Beitz, J.V., Crosswhite, H.M., Rajnak, K., Mann, J.B., 1983. Spectroscopic properties of the f-elements in compounds and solutions. In: Sinha, S.P. (Ed.), Systematics and the Properties of Lanthanides. Reidel, Dordrecht, pp. 389–450 (chapter 9).

Carnall, W.T., Crosswhite, H., Crosswhite, H.M., 1997. Energy Level Structure and Transition Probabilities of the Trivalent Lanthanides in LaF_3. Argonne National Laboratory, Argonne, USA.

Casnati, A., Sansone, F., Sartori, A., Prodi, L., Montalti, M., Zaccheroni, N., Ugozzoli, F., Ungaro, R., 2003. Eur. J. Org. Chem., 1475.

Cervantes, M., Clark, A., Terpugov, V., Medrano, F., 2002. J. Opt. Technol. **69**, 61.

Chang, C.A., Francesconi, L.C., Malley, M.F., Kumar, K., Gougoutas, J.Z., Tweedle, M.F., Lee, D.W., Wilson, L.J., 1993. Inorg. Chem. **32**, 3501.

Chang, C.A., Liu, Y.-L., Chen, C.-Y., Chou, X.-M., 2001. Inorg. Chem. **40**, 3448.

Chang, S.J., 1995. J. Appl. Phys. **78**, 4279.

Chauvin, A.-S., Gumy, F., Imbert, D., Bünzli, J.-C.G., 2004. Spectrosc. Lett. **37**, 517. Erratum: 2007, **40**, 193.

Chen, B., Yang, Y., Zapata, F., Qian, G., Luo, Y., Zhang, J., Lobkovsky, E.B., 2006. Inorg. Chem. **45**, 8882.

Chen, R.T., Lee, M., Natarajan, S., Lin, C., Ho, Z.Z., Robinson, D., 1993. IEEE Phot. Technol. Lett. **5**, 1328.

Choppin, G.R., 1989. Chemical properties of the rare earth elements. In: Bünzli, J.-C.G., Choppin, G.R. (Eds.), Lanthanide Probes in Life, Chemical and Earth Sciences. Theory and Practice. Elsevier Science, Amsterdam, pp. 1–41 (chapter 1).

Chudinov, A.V., Rumyantseva, V.D., Lobanov, A.V., Chudinova, G.K., Stomakhin, A.A., Mironov, A.F., 2004. Russ. J. Bioorg. Chem. (Engl. Transl.) **30**, 89.

Clark, A., Terpugov, V., Medrano, F., Cervantes, M., Soto, D., 1999. Opt. Mater. **13**, 355.

Coldwell, J.B., Felton, C.E., Harding, L.P., Moon, R., Pope, S.J.A., Rice, C.R., 2006. Chem. Commun., 5048.

Comby, S., Gumy, F., Bünzli, J.-C.G., Saraidarov, T., Reisfeld, R., 2006a. Chem. Phys. Lett. **432**, 128.

Comby, S., Imbert, D., Chauvin, A.-S., Bünzli, J.-C.G., 2006b. Inorg. Chem. **45**, 732.

Comby, S., Scopelliti, R., Imbert, D., Charbonnière, L.J., Ziessel, R., Bünzli, J.-C.G., 2006c. Inorg. Chem. **45**, 3158.

Comby, S., Imbert, D., Vandevyver, C., Bünzli, J.-C.G., 2007. Chem. Eur. J. **13**, 936.

Crosby, G.A., Kasha, M., 1958. Spectrochim. Acta **10**, 377.

Cross, J.P., Lauz, M., Badger, P.D., Petoud, S., 2004. J. Am. Chem. Soc. **126**, 16278.

Crosswhite, H.M., Moos, H.W., 1967. Optical Properties of Ions in Crystals. Interscience Publishers, New York.

Curry, R.J., Gillin, W.P., 1999. Appl. Phys. Lett. **75**, 1380.

Curry, R.J., Gillin, W.P., 2000. Synth. Met. **111**, 35.

Curry, R.J., Gillin, W.P., 2001. Curr. Opin. Solid State Mater. Sci. **5**, 481.

Curry, R.J., Gillin, W.P., Knights, A.P., Gwilliam, R., 2000. Appl. Phys. Lett. **77**, 2271.

Curry, R.J., Gillin, W.P., Knights, A.P., Gwilliam, R., 2001. Opt. Mater. **17**, 161.

Curry, R.J., George, M.R., Grossel, M.C., 2005. The potential of pyridine-2,6-dicarboxylic acid based organolanthanide complexes for efficient near infrared emission. In: Zajya, H., Kafafi, H., Lane, P.A. (Eds.), Proc. SPIE, pp. 59371R-1–59371R-9.

Davies, G.M., Aarons, R.J., Motson, G.R., Jeffery, J.C., Adams, H., Faulkner, S., Ward, M.D., 2004. Dalton Trans., 1136.

Davies, G.M., Adams, H., Pope, S.J.A., Faulkner, S., Ward, M.D., 2005a. Photochem. Photobiol. Sci. **4**, 829.

Davies, G.M., Pope, S.J.A., Adams, H., Faulkner, S., Ward, M.D., 2005b. Inorg. Chem. **44**, 4665.

de Dood, M.J.A., Berkhout, B., van Kats, C.M., Polman, A., van Blaaderen, A., 2002. Chem. Mater. **14**, 2849.

de Mello, J.C., Wittmann, H.F., Friend, R.H., 1997. Adv. Mater. **9**, 230.

de Sá, G.F., Malta, O.L., Donega, C.D., Simas, A.M., Longo, R.L., Santa-Cruz, P.A., da Silva, E.F., 2000. Coord. Chem. Rev. **196**, 165.

De Silva, A.P., Fox, D.B., Huxley, A.J.M., Moody, T.S., 2000. Coord. Chem. Rev. **205**, 41.

Destri, S., Porzio, W., Meinardi, F., Tubino, R., Salerno, G., 2003. Macromolecules **36**, 273.

deW. Horrocks Jr., W., Bolender, J.P., Smith, W.D., Supkowski, R.M., 1997. J. Am. Chem. Soc. **119**, 5972.

Di Bari, L., Pintacuda, G., Salvadori, P., 2000a. J. Am. Chem. Soc. **122**, 5557.

Di Bari, L., Pintacuda, G., Salvadori, P., Dickins, R.S., Parker, D., 2000b. J. Am. Chem. Soc. **122**, 9257.

Di Bari, L., Lelli, M., Pintacuda, G., Salvadori, P., 2002. Chirality **14**, 265.

Diamente, P.R., Van Veggel, F.C.J.M., 2005. J. Fluoresc. **15**, 543.

Diamente, P.R., Burke, R.D., Van Veggel, F.C.J.M., 2006. Langmuir **22**, 1782.

Dickins, R.S., Howard, J.A.K., Maupin, C.L., Moloney, J.M., Parker, D., Peacock, R.D., Riehl, J.P., Siligardi, G., 1998. New J. Chem. **22**, 891.

Dickins, R.S., Howard, J.A.K., Maupin, C.L., Moloney, J.M., Parker, D., Riehl, J.P., Siligardi, G., Williams, J.A.G., 1999. Chem. Eur. J. **5**, 1095.

Dickins, R.S., Parker, D., Bruce, J.I., Tozer, D.J., 2003. Dalton Trans., 1264.

Dieke, G.H., 1968. Spectra and Energy Levels of Rare Earth Ions in Crystals. Interscience Publishers, New York.

Ding, X.Y., Alford, J.M., Wright, J.C., 1997a. Chem. Phys. Lett. **269**, 72.

Ding, X.Y., Geng, L., Lascola, R., Wright, J.C., 1997b. J. Lumin. **72–74**, 553.

Dorenbos, P., 2003. J. Phys.: Condens. Matter **15**, 575.

Dossing, A., 2005. Eur. J. Inorg. Chem., 1425.

Driesen, K., Nockemann, P., Binnemans, K., 2004a. Chem. Phys. Lett. **395**, 306.

Driesen, K., Van Deun, R., Görller-Walrand, C., Binnemans, K., 2004b. Chem. Mater. **16**, 1531.

Edder, C., Piguet, C., Bernardinelli, G., Mareda, J., Bochet, C.G., Bünzli, J.-C.G., Hopfgartner, G., 2000. Inorg. Chem. **39**, 5059.

Edder, C., Piguet, C., Bünzli, J.-C.G., Hopfgartner, G., 2001. Chem. Eur. J. **7**, 3014.

Elhabiri, M., Scopelliti, R., Bünzli, J.-C.G., Piguet, C., 1999. J. Am. Chem. Soc. **121**, 10747.

Ermolaev, V.L., Sveshnikova, E.B., 1979. J. Lumin. **20**, 387.

Etienne, P., Coudray, P., Porque, J., Moreau, Y., 2000. Opt. Commun. **174**, 413.

Faulkner, S., Pope, S.J.A., 2003. J. Am. Chem. Soc. **125**, 10526.

Faulkner, S., Beeby, A., Dickins, R.S., Parker, D., Williams, J.A.G., 1999. J. Fluoresc. **9**, 45.

Faulkner, S., Beeby, A., Carrié, M.-C., Dadabhoy, A., Kenwright, A.M., Sammes, P.G., 2001. Inorg. Chem. Commun. **4**, 187.

Faulkner, S., Burton-Pye, B.P., Khan, T., Martin, L.R., Wray, S.D., Skabara, P.J., 2002. Chem. Commun., 1668.

Faulkner, S., Carrié, M.-C., Pope, S.J.A., Squire, J., Beeby, A., Sammes, P.G., 2004. Dalton Trans., 1405.

Faulkner, S., Pope, S.J.A., Burton-Pye, B.P., 2005. Appl. Spectrosc. Rev. **40**, 1.

Fick, J., Knystautas, E.J., Villeneuve, A., Schiettekatte, F., Roorda, S., Richardson, K.A., 2000. J. Non-Cryst. Sol. **272**, 200.

Flanagan, B.M., Bernhardt, P.V., Krausz, E.R., Luthi, S.R., Riley, M.J., 2001. Inorg. Chem. **40**, 5401.

Flanagan, B.M., Bernhardt, P.V., Krausz, E.R., Luthi, S.R., Riley, M.J., 2002. Inorg. Chem. **41**, 5024.

Floquet, S., Borkovec, M., Bernardinelli, G., Pinto, A., Leuthold, L.-A., Hopfgartner, G., Imbert, D., Bünzli, J.-C.G., Piguet, C., 2004. Chem. Eur. J. **10**, 1091.

Foley, T.J., Abboud, K.A., Boncella, J.M., 2002. Inorg. Chem. **41**, 1704.

Foley, T.J., Harrison, B.S., Knefely, A.S., Abboud, K.A., Reynolds, J.R., Schanze, K.S., Boncella, J.M., 2003. Inorg. Chem. **42**, 5023.

Froidevaux, P., Bünzli, J.-C.G., 1994. J. Phys. Chem. **98**, 532.

Fu, L.M., Wen, X.F., Ai, X.C., Sun, Y., Wu, Y.S., Zhang, J.P., Wang, Y., 2005. Angew. Chem. Int. Ed. **44**, 747.

Fulton, D.A., Elemento, E.M., Aime, S., Chaabane, L., Botta, M., Parker, D., 2006. Chem. Commun.

Furphy, B.M., Harrowfield, J.M., Kepert, D.L., Skelton, B.W., White, A.H., Wilner, F.R., 1987. Inorg. Chem. **26**, 4231.

Gaiduck, M.I., Grigoriants, V.V., Mironov, A.F., Roitman, L.D., Chissov, V.I., Rumiantseva, V.D., Sukhin, G.M., 1989. Dokl. Acad. Nauk SSSR **309**, 980.

Gaiduck, M.I., Grigoriants, V.V., Mironov, A.F., Rumyantseva, V.D., Chissov, V.I., Sukhin, G.M., 1990. J. Photochem. Photobiol. B Biol. **7**, 15.

Gaiduck, M.I., Grigoriants, V.V., Mironov, A.F., Rumyantseva, V.D., 1991. Eesti Teaduste Akadeemia Toimetised, Fuusika, Matemaatika **40**, 198.

Gao, X.C., Cao, H., Huang, C.H., Li, B.G., Umitani, S., 1998. Appl. Phys. Lett. **72**, 2217.

Gillin, W.P., Curry, R.J., 1999. Appl. Phys. Lett. **74**, 798.

Glover, P.B., Ashton, P.R., Childs, L.J., Rodger, A., Kercher, M., Williams, R.M., De Cola, L., Pikramenou, Z., 2003. J. Am. Chem. Soc. **125**, 9918.

Gonçalves e Silva, F.R., Malta, O.L., 1997. J. Alloys Compd. **250**, 427.

Gonçalves e Silva, F.R., Longo, R.L., Malta, O.L., Piguet, C., Bünzli, J.-C.G., 2000. Phys. Chem. Chem. Phys. **2**, 5400.

Gonçalves e Silva, F.R., Malta, O.L., Reinhard, C., Güdel, H.U., Piguet, C., Moser, J.E., Bünzli, J.-C.G., 2002. J. Phys. Chem. A **106**, 1670.

Gonçalves, M.C., Silva, N.J.O., de Zea Bermudez, V., A sà Ferreira, R., Carlos, L.D., Dahmouche, K., Ostrovskii, D., Correia Vilela, I.C., Craievich, A.F., 2005. J. Phys. Chem. B, 20093.

Gonzales-Lorenzo, M., Platas-Iglesias, C., Avecilla, F., Geraldes, C.F.G.C., Imbert, D., Bünzli, J.-C.G., de Blas, A., Rodriguez-Blas, T., 2003. Inorg. Chem. **42**, 6946.

Gonzales-Lorenzo, M., Platas-Iglesias, C., Avecilla, F., Faulkner, L.R., Pope, S.J.A., de Blas, A., Rodriguez-Blas, T., 2005. Inorg. Chem. **44**, 4254.

Gouterman, M., Schumaker, C.D., Srivastava, T.S., Yonetani, T., 1976. Chem. Phys. Lett. **40**, 456.

Guillet, E., Imbert, D., Scopelliti, R., Bünzli, J.-C.G., 2004. Chem. Mater. **16**, 4063.

Guillou, O., Daiguebonne, C., 2004. Lanthanide-containing coordination polymers. In: Gschneidner Jr., K.A., Bünzli, J.-C.G., Pecharsky, V.K. (Eds.), Handbook on the Physics and Chemistry of Rare Earths, vol. **34**. Elsevier North Holland, Amsterdam (chapter 221).

Gumy, F., Bünzli, J.-C.G., 2006, unpublished results.

Gunnlaugsson, T., Leonard, G.A., 2005. Chem. Commun., 3114.

Guo, D., Duan, C., Lu, F., Hasegawa, Y., Meng, Q., Yanagida, S., 2004. Chem. Commun., 1486.

Gurevich, M.G., Solev'ev, K.N., 1961. Dokl. Acad. Nauk SSSR **5**, 291.

Gutierrez, F., Tedeschi, C., Maron, L., Daudey, J.P., Poteau, R., Azéma, J.L., Tisnes, P., Picard, C., 2004. Dalton Trans., 1334.

Gutsche, C.D., 1998. Calixarenes Revisited. Monographs in Supramolecular Chemistry. The Royal Society of Chemistry, Cambridge.

Hall, J., Häner, R., Aime, S., Botta, M., Faulkner, S., Parker, D., de Sousa, A.S., 1998. New J. Chem. **22**, 627.

Han, K.G., Kong, H.J., Kim, H.S., Um, G.Y., 1995. Appl. Phys. Lett. **67**, 1501.

Harrison, B.S., Foley, T.J., Bouguettaya, M., Boncella, J.M., Reynolds, J.R., Schanze, K.S., Shim, J., Holloway, P.H., Padmanaban, G., Ramakrishnan, S., 2001. Appl. Phys. Lett. **79**, 3770.

Harrison, B.S., Foley, T.J., Knefely, A.S., Mwaura, J.K., Cunningham, G.B., Kang, T.-S., Bouguettaya, M., Boncella, J.M., Reynolds, J.R., Schanze, K.S., 2004. Chem. Mater. **16**, 2938.

Hasegawa, Y., Kimura, Y., Murakoshi, K., Wada, Y., Kim, J.-H., Nakashima, N., Yamanaka, T., Yanagida, S., 1996a. J. Phys. Chem. **100**, 10201.

Hasegawa, Y., Murakoshi, K., Wada, Y., Kim, J.H., Nakashima, N., Yamanaka, T., Yanagida, S., 1996b. Chem. Phys. Lett. **260**, 173.

Hasegawa, Y., Murakoshi, K., Wada, Y., Yanagida, S., Kim, J.-H., Nakashima, N., Yamanaka, T., 1996c. Chem. Phys. Lett. **248**, 8.

Hasegawa, Y., Iwamuro, M., Murakoshi, K., Wada, Y., Arakawa, R., Yamanaka, T., Nakashima, N., Yanagida, S., 1998. Bull. Chem. Soc. Jpn. **71**, 2573.

Hasegawa, Y., Sogabe, K., Wada, Y., Kitamura, T., Nakashima, N., Yanagida, S., 1999. Chem. Lett., 35.

Hasegawa, Y., Ohkubo, T., Sogabe, K., Kawamura, Y., Wada, Y., Nakashima, N., Yanagida, S., 2000. Angew. Chem. Int. Ed. **39**, 357.

Hasegawa, Y., Sogabe, K., Wada, Y., Yanagida, S., 2003. J. Lumin. **101**, 235.

Hasegawa, Y., Wada, Y., Yanagida, S., 2004. J. Photochem. Photobiol. C: Photochem. Rev. **5**, 183.

He, H., Wong, W.-K., Guo, J., Li, K.-F., Wong, W.-Y., Lo, W.-K., Cheah, K.-W., 2004a. Inorg. Chim. Acta **357**, 4379.

He, H., Wong, W.-K., Guo, J., Li, K.-F., Wong, W.-Y., Lo, W.-K., Cheah, K.-W., 2004b. Aust. J. Chem. **57**, 803.

He, H., Zhu, X., Hou, A., Guo, J., Wong, W.-K., Wong, W.-Y., Li, K.-F., Cheah, K.-W., 2004c. Dalton Trans., 4064.

He, H.S., Zhao, Z.X., Wong, W.K., Li, K.F., Meng, J.X., Cheah, K.W., 2003. Dalton Trans., 980.

He, H.S., Guo, J.P., Zhao, Z.X., Wong, W.K., Wong, W.Y., Lo, W.K., Li, K.F., Luo, L., Cheah, K.W., 2004a. Eur. J. Inorg. Chem., 837.

He, H.S., Wong, W.K., Li, K.F., Cheah, K.W., 2004b. Synth. Met. **143**, 81.

He, H.S., Wong, W.K., Li, K.F., Cheah, K.W., 2004c. Synth. Met. **145**, 103.

Hebbink, G.A., Klink, S.I., Oude Alink, P.G.B., Van Veggel, F.C.J.M., 2001a. Inorg. Chim. Acta **317**, 114.

Hebbink, G.A., Reinhoudt, D.N., Van Veggel, F.C.J.M., 2001b. Eur. J. Org. Chem., 4101.

Hebbink, G.A., Klink, S.I., Grave, L., Alink, P.G.B.O., Van Veggel, F.C.J.M., 2002a. Chem. Phys. Chem. **3**, 1014.

Hebbink, G.A., Stouwdam, J.W., Reinhoudt, D.N., Van Veggel, F.C.J.M., 2002b. Adv. Mater. **14**, 1147.

Hebbink, G.A., Grave, L., Woldering, L.A., Reinhoudt, D.N., Van Veggel, F.C.J.M., 2003. J. Phys. Chem. A **107**, 2483.

Heller, A., 1966. Appl. Phys. Lett. **9**, 106.

Heller, A., 1967. J. Am. Chem. Soc. **89**, 167.

Heller, A., 1968a. J. Mol. Spectrosc. **28**, 101.

Heller, A., 1968b. J. Mol. Spectrosc. **28**, 208.

Heller, A., 1968c. J. Am. Chem. Soc. **90**, 3711.

Heller, A., Brophy, V., 1968. J. Appl. Phys. **39**, 4086.

Herrera, J.M., Pope, S.J.A., Adams, H., Faulkner, S., Ward, M.D., 2006a. Inorg. Chem. **45**, 3895.

Herrera, J.M., Ward, M.D., Adams, H., Pope, S.J.A., Faulkner, S., 2006b. Chem. Commun., 1851.

Hoffman, K.R., Conley, W.G., 2001. J. Lumin. **94–95**, 187.

Hoffman, K.R., DeLapp, K., Andrews, H., Sprinkle, P., Nickels, M., Norris, B., 1995. J. Lumin. **66–67**, 244.
Hoffman, K.R., Norris, B.J., Merle, R.B., Alford, M., 1998. Chem. Phys. Lett. **284**, 171.
Hofstraat, J.W., Wolbers, M.P.O., Van Veggel, F.C.J.M., Reinhoudt, D.N., Werts, M.H.V., 1998. J. Fluoresc. **8**, 301.
Hong, Z.R., Liang, C.J., Li, R.G., Zang, F.X., Fan, D., Li, W.L., Hung, L.S., Lee, S.T., 2001a. Appl. Phys. Lett. **79**, 1942.
Hong, Z.R., Liang, C.J., Li, R.G., Zhao, D., Fan, D., Li, W.L., 2001b. Thin Solid. Films **391**, 122.
Hongyo, M., Ueda, K., Sasaki, T., Yamanaka, C., Nagao, Y., 1972. IEEE J. Quantum Electron. QE **8**, 192.
Huang, C.H., Wang, K.Z., Xu, G.X., Zhao, X.S., Xie, X.M., Xu, Y., Liu, Y.Q., Xu, L.G., Li, T.K., 1995. J. Phys. Chem. **99**, 14397.
Hüfner, S., 1978. Optical Spectra of Transparent Rare Earth Compounds. Academic Press, New York.
Imbert, D., Cantuel, M., Bünzli, J.-C.G., Bernardinelli, G., Piguet, C., 2003. J. Am. Chem. Soc. **125**, 15698.
Imbert, D., Comby, S., Chauvin, A.-S., Bünzli, J.-C.G., 2005. Chem. Commun., 1432.
Isobe, T., Misumi, S., 1974. Bull. Chem. Soc. Jpn. **47**, 281.
Iwamuro, M., Adachi, T., Wada, Y., Kitamura, T., Yanagida, S., 1999. Chem. Lett., 539.
Iwamuro, M., Hasegawa, Y., Wada, Y., Murakoshi, K., Nakashima, N., Yamanaka, T., Yanagida, S., 1998. J. Lumin. **79**, 29.
Iwamuro, M., Adachi, T., Wada, Y., Kitamura, T., Nakashima, N., Yanagida, S., 2000a. Bull. Chem. Soc. Jpn. **73**, 1359.
Iwamuro, M., Wada, Y., Kitamura, T., Nakashima, N., Yanagida, S., 2000b. Phys. Chem. Chem. Phys. **2**, 2291.
Izatt, R.M., Bradshaw, J.S., Nielsen, S.A., Lamb, J.D., Christensen, J.J., 1985. Chem. Rev. **85**, 271.
Izatt, R.M., Pawlack, K., Bradshaw, J.S., Bruening, R.L., 1991. Chem. Rev. **91**, 1721.
Jensen, M.P., Neuefeind, J., Beitz, J.V., Skanthakumar, S., Soderholm, L., 2003. J. Am. Chem. Soc. **125**, 15466.
Jeon, S., Braun, P.V., 2003. Chem. Mater. **15**, 1256.
Judd, B.R., 1962. Phys. Rev. **127**, 750.
Jung, H.K., Oh, J.S., Seok, S.I., Lee, T.H., 2005. J. Lumin. **114**, 307.
Kachura, T.F., Sevchenko, A.N., Solov'ev, K.N., Tsvirko, M.P., 1974. Dokl. Acad. Nauk SSSR **217**, 1121.
Kaizaki, S., Shirotani, D., Tsukahara, Y., Nakata, H., 2005. Eur. J. Inorg. Chem., 3303.
Kaizu, Y., Asano, M., Kobayashi, H., 1986. J. Phys. Chem. **90**, 3906.
Kaminski, A.A., Li, L., 1974. Phys. Status Solidi A **26**, K21.
Kandpal, H.C., Tripathi, H.B., 1979. Solid State Commun. **29**, 139.
Kandpal, H.C., Agarwal, A.K., Tripathi, H.B., 1979. J. Lumin. **20**, 207.
Kang, T.S., Harrison, B.S., Bouguettaya, M., Foley, T.J., Boncella, J.M., Schanze, K.S., Reynolds, J.R., 2003a. Adv. Funct. Mater. **13**, 205.
Kang, T.S., Harrison, B.S., Foley, T.J., Knefely, A.S., Boncella, J.M., Reynolds, J.R., Schanze, K.S., 2003b. Adv. Mater. **15**, 1093.
Karmaoui, M., Ferreira, R.A.S., Mane, A.T., Carlos, L.D., Pinna, N., 2006. Chem. Mater. **18**, 4493.
Karve, G., Bihari, B., Chen, R.T., 2000. Appl. Phys. Lett. **77**, 1253.
Kawa, M., Frechet, J.M.J., 1998. Thin Solid Films **331**, 259.
Kawahata, R., Tsukuda, T., Yagi, T., Subhan, M.A., Nakata, H., Fuyuhiro, A., Kaizaki, S., 2003. Chem. Lett. **32**, 1084.
Kawamura, Y., Wada, Y., Hasegawa, Y., Iwamuro, M., Kitamura, T., Yanagida, S., 1999. Appl. Phys. Lett. **74**, 3245.
Kawamura, Y., Wada, Y., Iwamuro, M., Kitamura, T., Yanagida, S., 2000. Chem. Lett., 280.
Kawamura, Y., Wada, Y., Yanagida, S., 2001. Jpn. J. Appl. Phys. I **40**, 350.
Kazakov, V.P., Voloshin, A.I., Shavaleev, N.M., 1998. J. Photochem. Photobiol. A Chem. **119**, 177.
Keller, B., Bukietynska, K., Jezowska-Trzebiatowska, B., 1982. Chem. Phys. Lett. **92**, 541.
Khreis, O.M., Curry, R.J., Somerton, M., Gillin, W.P., 2000. J. Appl. Phys. **88**, 777.
Khreis, O.M., Gillin, W.P., Somerton, M., Curry, R.J., 2001. Org. Electron. **2**, 45.
Kido, J., Okamoto, Y., 2002. Chem. Rev. **102**, 2357.
Kim, H.K., Oh, J.B., Baek, N.S., Roh, S.G., Nah, M.K., Kim, Y.H., 2005. Bull. Korean Chem. Soc. **26**, 201.
Kim, J.-H., Park, Y.-P., 2003. J. Korean Phys. Soc. **43**, 277.
Kim, S., Lim, Y.T., Soltesz, E.G., De Grand, A.M., Lee, J., Nakayama, A., Parker, J.A., Mihaljevic, T., Laurence, R.G., Dor, D.M., Cohn, L.H., Bawendi, M.G., Frangioni, J.V., 2004. Nat. Biotechnol. **22**, 93.
Kimura, T., Kato, Y., 1995. J. Alloys Compd. **225**, 284.
Klink, S.I., Hebbink, G.A., Grave, L., Van Veggel, F.C.J.M., Reinhoudt, D.N., Slooff, L.H., Polman, A., Hofstraat, J.W., 1999. J. Appl. Phys. **86**, 1181.

Klink, S.I., Grave, L., Reinhoudt, D.N., Van Veggel, F.C.J.M., Werts, M.H.V., Geurts, F.A.J., Hofstraat, J.W., 2000a. J. Phys. Chem. A **104**, 5457.

Klink, S.I., Hebbink, G.A., Grave, L., Peters, F.G.A., Van Veggel, F.C.J.M., Reinhoudt, D.N., Hofstraat, J.W., 2000b. Eur. J. Org. Chem. **10**, 1923.

Klink, S.I., Keizer, H., Van Veggel, F.C.J.M., 2000c. Angew. Chem. Int. Ed. **39**, 4319.

Klink, S.I., Alink, P.O., Grave, L., Peters, F.G.A., Hofstraat, J.W., Geurts, F.A.J., Van Veggel, F.C.J.M., 2001. J. Chem. Soc., Perkin Trans. **2**, 363.

Klink, S.I., Keizer, H., Hofstraat, H.W., Van Veggel, F.C.J.M., 2002. Synth. Met. **127**, 213.

Koeppen, C., Yamada, S., Jiang, G., Garito, A.F., Dalton, L.R., 1997. J. Opt. Soc. Am. B Opt. Phys. **14**, 155.

Koppe, M., Brabec, C.J., Sariciftci, N.S., Eichen, Y., Nakhmanovich, G., Ehrenfreund, E., Epstein, O., Heiss, W., 2001. Synth. Met. **121**, 1511.

Kornienko, A., Banerjee, S., Kumar, G.A., Riman, R.E., Emge, T.J., Brennan, J.G., 2005a. J. Am. Chem. Soc. **127**, 14008.

Kornienko, A., Emge, T.J., Kumar, G.A., Riman, R.E., Brennan, J.G., 2005b. J. Am. Chem. Soc. **127**, 3501.

Korovin, Y.V., Rusakova, N.V., 2001. Rev. Inorg. Chem. **21**, 299.

Korovin, Y.V., Rusakova, N.V., 2002. J. Fluoresc. **12**, 159.

Korovin, Y.V., Rusakova, N.V., 2004. J. Alloys Compd. **374**, 311.

Korovin, Y.V., Meshkova, S.B., Poluektov, N.S., 1984. J. Anal. Chem. USSR (Engl. Transl.) **39**, 234.

Korovin, Y.V., Meshkova, S.B., Poluektov, N.S., 1988. Zh. Prikl. Spektrosk. (Engl. Transl.) **48**, 45.

Korovin, Y.V., Shevchuk, S.V., Bacherikov, V.A., Rusakova, N.V., Alekseeva, E.A., Gren', A.I., 2000. Russ. J. Inorg. Chem. (Engl. Transl.) **45**, 1383.

Korovin, Y.V., Zhilina, Z., Rusakova, N.V., Kuz'min, V., Vodzinsky, S., Ishkov, Y., 2001. J. Porphyrins Phthalocyanines **5**, 481.

Korovin, Y.V., Rusakova, N.V., Kostenchuk, M., Rusakova, M., Suveyzdis, Y., 2002a. Pol. J. Chem. **76**, 901.

Korovin, Y.V., Rusakova, N.V., Popkov, Y.A., 2002b. J. Appl. Spectrosc. (Engl. Transl.) **69**, 89.

Korovin, Y.V., Rusakova, N.V., Popkov, Y.A., 2002c. Russ. Chem. Bull. (Engl. Transl.) **51**, 2303.

Korovin, Y.V., Rusakova, N.V., Popkov, Y.A., Dotsenko, V.P., 2002d. J. Appl. Spectrosc. (Engl. Transl.) **69**, 841.

Korovin, Y.V., Rusakova, N.V., Suveyzdis, Y.I., 2002e. Russ. J. Inorg. Chem. (Engl. Transl.) **47**, 1398.

Korovin, Y.V., Rusakova, N.V., Zhilina, Z.I., Ishkov, Y.V., Vodzinsky, S.V., Dotsenko, V.P., 2002f. Mendeleev Commun., 151.

Korovin, Y.V., Lozitskaya, R.N., Rusakova, N.V., 2003. Russ. J. Gen. Chem. (Engl. Transl.) **73**, 1641.

Koslova, N.I., Viana, B., Sanchez, C., 1993. J. Mater. Chem. **3**, 111.

Kresge, C.T., Leonowicz, M.E., Roth, W.J., Vartuli, J.C., Beck, J.S., 1992. Nature **359**, 710.

Kumar, G.A., Riman, R.E., Torres, L.A.D., Garcia, O.B., Banerjee, S., Kornienko, A., Brennan, J.G., 2005. Chem. Mater. **17**, 5130.

Kuningas, K., Ukonaho, T., Pakkila, H., Rantanen, T., Rosenberg, J., Lovgren, T., Soukka, T., 2006. Anal. Chem. **78**, 4690.

Kuo, R.L., Paterson, R.F., Siqueira, T.M., Derdak, S., Steele, R.E., Simmons, G.R., Lingeman, J.E., 2002. J. Urol. **167**, 295.

Kuriki, K., Kobayashi, T., Imai, N., Tamura, T., Nishihara, S., Tagaya, A., Koike, Y., Okamoto, Y., 2000. IEEE Phot. Technol. Lett. **12**, 989.

Kuriki, K., Koike, Y., Okamoto, Y., 2002. Chem. Rev. **102**, 2347.

Lai, D.C., Dunn, B., Zink, J.I., 1996. Inorg. Chem. **35**, 2152.

Lakowicz, J.R., Piszczek, G., Maliwal, B.P., Gryczynski, I., 2001. ChemPhysChem **2**, 247.

Latva, M., Takalo, H., Mukkala, V.-M., Matachescu, C., Rodriguez-Ubis, J.-C., Kankare, J., 1997. J. Lumin. **75**, 149.

Le Quang, A.Q., Besson, E., Hierle, R., Mehdi, A., Reyé, C., Corriu, R., Ledoux, I., 2007. Opt. Mater. **29**, 941.

Le Quang, A.Q., Zyss, J., Ledoux, I., Truong, V.G., Jurdyc, A.M., Jacquier, B., Le, D.H., Gibaud, A., 2005. Chem. Phys. **318**, 33.

Lehmann, O., Meyssamy, H., Kompe, K., Schnablegger, H., Haase, M., 2003. J. Phys. Chem. B **107**, 7449.

Lehn, J.-M., 1995. Supramolecular Chemistry. Concepts and Perspectives. VCH, Weinheim.

Lempicki, A., Heller, A., 1966. Appl. Phys. Lett. **9**, 108.

Lenaerts, P., Driesen, K., Van Deun, R., Binnemans, K., 2005a. Chem. Mater. **17**, 2148.

Lenaerts, P., Ryckebosch, E., Driesen, K., Van Deun, R., Nockemann, P., Görller-Walrand, C., Binnemans, K., 2005b. J. Lumin. **114**, 77.

Lenaerts, P., Storms, A., Mullens, J., D'Haen, J., Görller-Walrand, C., Binnemans, K., Driesen, K., 2005c. Chem. Mater. **17**, 5194.

Lezhnina, M., Kynast, U., 2004. J. Alloys Compd. **380**, 55.

Lezhnina, M., Laeri, F., Benmouhadi, L., Kynast, U., 2006. Adv. Mater. **18**, 280.

Lezhnina, M.M., Kynast, U.H., 2005. Phys. Sol. State **47**, 1485.

Li, Y.G., Yang, H., He, Z., Liu, L.Y., Wang, W.C., Li, F.Y., Xu, L., 2005. J. Mater. Res. **20**, 2940.

Lin, S.H., Feuerstein, R.J., Mickelson, A.R., 1996. J. Appl. Phys. **79**, 2868.

Lincoln, S.F., 1997. Coord. Chem. Rev. **166**, 255.

Lis, S., Kimura, T., Yoshida, Z., 2001. J. Alloys Compd. **323**, 125.

Lisowski, J., Ripoli, S., Di Bari, L., 2004. Inorg. Chem. **43**, 1388.

Liu, G.K., Chen, X.Y., 2007. Spectroscopic properties of lanthanides in nano materials. In: Gschneidner Jr., K.A., Bünzli, J.-C.G., Pecharsky, V.K. (Eds.), Handbook on the Physics and Chemistry of Rare Earths, vol. **37**. Elsevier, Amsterdam (chapter 233).

Lo, W.-K., Wong, W.-K., Guo, J., Wong, W.-Y., Li, K.-F., Cheah, K.-W., 2004. Inorg. Chim. Acta **357**, 4510.

Lukes, I., Kotek, J., Vojtisek, P., Hermann, P., 2001. Coord. Chem. Rev. **216**, 287.

MacFarlane, R.M., Wittmann, G., vanLoosdrecht, P.H.M., de Vries, M., Bethune, D.S., Stevenson, S., Dorn, H.C., 1997. Phys. Rev. Lett. **79**, 1397.

MacFarlane, R.M., Bethune, D.S., Stevenson, S., Dorn, H.C., 2001. Chem. Phys. Lett. **343**, 229.

MacGillivray, L.R., Reid, J.L., Ripmeester, J.A., 2001. Chem. Commun., 1034.

Magennis, S.W., Ferguson, A.J., Bryden, T., Jones, T.S., Beeby, A., Samuel, I.D.W., 2003. Synth. Met. **138**, 463.

Malta, O.L., Gonçalves e Silva, F.R., Longo, R.L., 1999. Chem. Phys. Lett. **307**, 518.

Mancino, G., Ferguson, A.J., Beeby, A., Long, N.J., Jones, T.S., 2005. J. Am. Chem. Soc. **127**, 524.

Manseki, K., Hasegawa, Y., Wada, Y., Ichida, H., Kanematsu, Y., Kushida, T., 2006. J. Lumin. **122–123**, 262.

Mathis, G., 1993. Clin. Chem. **39**, 1953.

Mathis, G., 1998. Biological applications of rare earth cryptates. In: Saez Puche, R., Caro, P. (Eds.), Rare Earths. Editorial Complutense, Madrid, pp. 285–297.

Matsumoto, K., Yuan, J.G., 2003. Lanthanide chelates as fluorescent labels for diagnostics and biotechnology. In: Sigel, A., Sigel, H. (Eds.), Metal Ions in Biological Systems, vol. **40**. Marcel Dekker, New York, pp. 191–232 (chapter 6).

Maupin, C.L., Parker, D., Williams, J.A.G., Riehl, J.P., 1998. J. Am. Chem. Soc. **120**, 10563.

Maupin, C.L., Dickins, R.S., Govenlock, L.G., Mathieu, C.E., Parker, D., Williams, J.A.G., Riehl, J.P., 2000. J. Phys. Chem. A **104**, 6709.

Meinardi, F., Colombi, N., Destri, S., Porzio, W., Blumstengel, S., Cerminara, M., Tubino, R., 2003. Synth. Met. **137**, 959.

Meng, J.X., Li, K.F., Yuan, J., Zhang, L.L., Wong, W.K., Cheah, K.W., 2000. Chem. Phys. Lett. **332**, 313.

Meshkova, S.B., 2000. J. Fluoresc. **10**, 333.

Meshkova, S.B., Rusakova, N.V., 1990. J. Anal. Chem. USSR (Engl. Transl.) **45**, 737.

Meshkova, S.B., Korovin, Y.V., Poluektov, N.S., 1985. Russ. J. Phys. Chem. (Engl. Transl.) **59**, 1012.

Meshkova, S.B., Korovin, Y.V., Poluektov, N.S., Demeshko, D.V., 1987. J. Anal. Chem. USSR (Engl. Transl.) **42**, 385.

Meshkova, S.B., Rusakova, N.V., Bol'shoi, D.V., 1992a. Acta Chim. Hung. **129**, 317.

Meshkova, S.B., Rusakova, N.V., Topilova, Z.M., Lozinskii, M.O., Kudryavtseva, L.S., 1992b. Russ. J. Coord. Chem. (Engl. Transl.) **18**, 183.

Meshkova, S.B., Topilova, Z.M., Lozinskii, M.O., Rusakova, N.V., Bol'shoi, D.V., 1997. J. Anal. Chem. USSR (Engl. Transl.) **52**, 852.

Meshkova, S.B., Shapiro, Y.E., Kuz'min, V.E., Artemenko, A.G., Rusakova, N.V., Pykhteeva, E.G., Bol'shoi, D.V., 1998. Russ. J. Coord. Chem. (Engl. Transl.) **24**, 669.

Meshkova, S.B., Topilova, Z.M., Bol'shoi, D.V., Beltyukova, S.V., Tsvirko, M.P., Venchikov, V.Y., 1999. Acta Phys. Pol. A **95**, 983.

Miller, T.A., Jeffery, J.C., Ward, M.D., Adams, H., Pope, S.J.A., Faulkner, S., 2004. Dalton Trans., 1524.

Mondry, A., Starynowicz, P., 1995. J. Alloys Compd. **225**, 367.

Moran, C.E., Hale, G.D., Halas, N.J., 2001. Langmuir **17**, 8376.

Moutiers, G., Billard, I., 2004. Techniques de l'Ingénieur, Report AF 6, 712.

Mudring, A.V., Babai, A., Arenz, S., Giernoth, R., Binnemans, K., Driesen, K., Nockemann, P., 2006. J. Alloys Compd. **418**, 204.

Nagovitsyn, I.A., Chudinova, G.K., 2002. Dokl. Biochem. Biophys. **382**, 16.

Nah, M.K., Cho, H.G., Kwon, H.J., Kim, Y.J., Park, C., Kim, H.K., Kang, J.G., 2006. J. Phys. Chem. A **110**, 10371.

Neouze, M.A., Le Bideau, J., Leroux, F., Vioux, A., 2005. Chem. Commun., 1082.

Ng, D.K.P., 2001. Half-sandwich tetrapyrrole complexes of rare earths and actinides. In: Gschneidner Jr., K.A., Eyring, E.M., Lander, G.H. (Eds.), Handbook on the Physics and Chemistry of Rare Earths, vol. **32**. Elsevier Science B.V., Amsterdam, pp. 611–653 (chapter 210).

Nielson, C.W., Koster, G.F., 1963. Spectroscopic Coefficients for p^n, d^n, and f^n Configurations. MIT Press, Cambridge, MA.

O'Riordan, A., O'Connor, E., Moynihan, S., Nockemann, P., Fias, P., Van Deun, R., Cupertino, D., Mackie, P., Redmond, G., 2006. Thin Solid Films **497**, 299.

Ofelt, G.S., 1962. J. Chem. Phys. **37**, 511.

Ogawa, T., Sugai, T., Shinohara, H., 2000. J. Am. Chem. Soc. **122**, 3538.

Oh, J.B., Paik, K.L., Ka, J.-W., Roh, S.-G., Nah, M.K., Kim, H.K., 2004. Mater. Sci. Eng. C, Biomimet. Supramol. Syst. **C24**, 257.

Oh, J.B., Kim, Y.H., Nah, M.K., Kim, H.K., 2005. J. Lumin. **111**, 255.

Olmstead, M.M., de Bettencourt-Dias, A., Duchamp, J.C., Stevenson, S., Dorn, H.C., Balch, A.L., 2000. J. Am. Chem. Soc. **122**, 12220.

Olmstead, M.M., Sigel, G., Hope, H., Xu, X., Power, P.P., 1985. J. Am. Chem. Soc. **107**, 8087.

Oueslati, I., Sa Ferreira, R.A., Carlos, L.D., Baleizao, C., Berberan-Santos, M.N., de Castro, B., Vicens, J., Pischel, U., 2006. Inorg. Chem. **45**, 2652.

Page, R.H., Schaffers, K.I., Payne, S.A., Krupke, W.F., 1997. J. Lightwave Technol. **15**, 786.

Patra, A., Sominska, E., Ramesh, S., Koltypin, Y., Zhong, Z., Minti, H., Reisfeld, R., Gedanken, A., 1999. J. Phys. Chem. B **103**, 3361.

Pavier, M.A., Weaver, M.S., Lidzey, D., Richardson, T., Searle, T.M., Bradley, D.D.C., Huang, C.H., Li, H., Zhou, D., 1996. Thin Solid Films **285**, 644.

Pavlovsky, V.I., Kulikov, O.V., Rusakova, N.V., Andronati, S.A., Korovin, Y.V., 2004. Russ. Chem. Bull. (Engl. Transl.) **53**, 791.

Pellegrino, P.M., Fell, N.F., Rosen, D.L., Gillespie, J.B., 1998. Anal. Chem. **70**, 1755.

Perkins, W.G., Crosby, G.A., 1965. J. Chem. Phys. **42**, 407.

Petoud, S., Bünzli, J.-C.G., Renaud, F., Piguet, C., Schenk, K.J., Hopfgartner, G., 1997. Inorg. Chem. **36**, 5750.

Petoud, S., Cohen, S.M., Bünzli, J.-C.G., Raymond, K.N., 2003. J. Am. Chem. Soc. **125**, 13324.

Pettinari, C., Marchetti, F., Pettinari, R., Drozdov, A., Troyanov, S., Voloshin, A.I., Shavaleev, N.M., 2002. J. Chem. Soc., Dalton Trans., 1409.

Pierre, V.C., Botta, M., Raymond, K.N., 2005. J. Am. Chem. Soc. **127**, 504.

Piguet, C., Bünzli, J.-C.G., 1999. Chem. Soc. Rev. **28**, 347.

Piguet, C., Bünzli, J.-C.G., Bernardinelli, G., Hopfgartner, G., Williams, A.F., 1993. J. Am. Chem. Soc. **115**, 8197.

Piguet, C., Bünzli, J.-C.G., Bernardinelli, G., Hopfgartner, G., Petoud, S., Schaad, O., 1996. J. Am. Chem. Soc. **118**, 6681.

Piguet, C., Edder, C., Rigault, S., Bernardinelli, G., Bünzli, J.-C.G., Hopfgartner, G., 2000. J. Chem. Soc., Dalton Trans., 3999.

Piguet, C., Borkovec, M., Hamacek, J., Zeckert, K., 2005. Coord. Chem. Rev. **249**, 705.

Piguet, C., Bünzli, J.-C.G., Donnio, B., Guillon, D., 2006. Chem. Commun., 3755.

Pirtea, Th.I., 1936. Z. Anal. Chem. **107**, 191.

Piszczek, G., Gryczynski, I., Maliwal, B.P., Lakowicz, J.R., 2002a. J. Fluoresc. **12**, 15.

Piszczek, G., Maliwal, B.P., Gryczynski, I., Dattelbaum, J., Lakowicz, J.R., 2002b. J. Fluoresc. **11**, 101.

Pitois, C., Vestberg, R., Rodlert, M., Malmstrom, E., Hult, A., Lindgren, M., 2003. Opt. Mater. **21**, 499.

Pitois, C., Hult, A., Lindgren, M., 2005. J. Lumin. **111**, 265.

Pizzoferrato, R., Lagonigro, L., Ziller, T., Di Carlo, A., Paolesse, R., Mandoj, F., Ricci, A., Lo Sterzo, C., 2004. Chem. Phys. **300**, 217.

Platas, C., Avecilla, F., de Blas, A., Rodriguez-Blas, T., Geraldes, C.F.G.C., Tóth, E., Merbach, A.E., Bünzli, J.-C.G., 2000. J. Chem. Soc., Dalton Trans., 611.

Platas, C., Piguet, C., André, N., Bünzli, J.-C.G., 2001. J. Chem. Soc., Dalton Trans., 3084.

Polman, A., Van Veggel, F.C.J.M., 2004. J. Opt. Soc. Am. B Opt. Phys. **21**, 871.

Poluektov, N.S., Meshkova, S.B., Korovin, I.V., 1984. Dokl. Acad. Nauk SSSR (Engl. Transl.) **273**, 960.

Pope, S.J.A., Kenwright, A.M., Boote, V.A., Faulkner, S., 2003a. Dalton Trans., 3780.

Pope, S.J.A., Kenwright, A.M., Heath, S.L., Faulkner, S., 2003b. Chem. Commun., 1550.

Pope, S.J.A., Coe, B.J., Faulkner, S., 2004a. Chem. Commun., 1550.

Pope, S.J.A., Coe, B.J., Faulkner, S., Bichenkova, E.V., Yu, X., Douglas, K.T., 2004b. J. Am. Chem. Soc. **126**, 9490.

Pope, S.J.A., Coe, B.J., Faulkner, S., Laye, R.H., 2005. Dalton Trans., 1482.

Pope, S.J.A., Burton-Pye, B.P., Berridge, R., Khan, T., Skabara, P.J., Faulkner, S., 2006. Dalton Trans., 2907.

Pratisto, H., Ith, M., Frenz, M., Weber, H.P., 1995. Appl. Phys. Lett. **67**, 1963.

Puntus, L., Schenk, K.J., Bünzli, J.-C.G., 2005. Eur. J. Inorg. Chem., 4739.

Quici, S., Cavazzini, M., Marzanni, G., Accorsi, G., Armaroli, N., Ventura, B., Barigelletti, F., 2005. Inorg. Chem. **44**, 529.

Quici, S., Marzanni, G., Forni, A., Accorsi, G., Barigelletti, F., 2004. Inorg. Chem. **43**, 1294.

Quochi, F., Orru, R., Cordella, F., Mura, A., Bongiovanni, G., Artizzu, F., Deplano, P., Mercuri, M.L., Pilia, L., Serpe, A., 2006. J. Appl. Phys. **99**, 053520-1.

Raymond, K.N., Müller, G., Matzanke, F., 1984. Top. Curr. Chem. **123**, 49.

Reinhard, C., Güdel, H.U., 2002. Inorg. Chem. **41**, 1048.

Reisfeld, R., Jorgensen, C.K., 1977. Lasers and Excited States of Rare Earths. Springer-Verlag, Berlin.

Renaud, F., Piguet, C., Bernardinelli, G., Bünzli, J.-C.G., Hopfgartner, G., 1999. J. Am. Chem. Soc. **121**, 9326.

Riehl, J.P., Muller, G., 2005. Circularly polarized luminescence spectroscopy from lanthanide systems. In: Gschneidner Jr., J.-C.G., Bünzli, K.A., Pecharsky, V.K. (Eds.), Handbook on the Physics and Chemistry of Rare Earths, vol. **34**. Elsevier, Amsterdam, pp. 289–357 (chapter 220).

Rizzo, F., Papagni, A., Meinardi, F., Tubino, R., Ottonelli, M., Musso, G.F., Dellepiane, G., 2004. Synth. Met. **147**, 143.

Rodriguez-Cortinas, R., Avecilla, F., Platas-Iglesias, C., Imbert, D., Bünzli, J.-C.G., de Blas, A., Rodriguez-Blas, T., 2002. Inorg. Chem. **41**, 5336.

Roh, S.G., Oh, J.B., Nah, M.K., Baek, N.S., Lee, Y., Kim, H.K., 2004a. Bull. Korean Chem. Soc. **25**, 1503.

Roh, S.G., Baek, N.S., Hong, K.-S., Kim, H.K., 2004b. Bull. Korean Chem. Soc. **25**, 343.

Roh, S.G., Nah, M.K., Oh, J.B., Baek, N.S., Park, K.M., Kim, H.K., 2005. Polyhedron **24**, 137.

Roundhill, D.M., 1995. Prog. Inorg. Chem. **43**, 533.

Rusakova, N.V., Meshkova, S.B., 1990. J. Anal. Chem. USSR (Engl. Transl.) **45**, 1371.

Rusakova, N.V., Meshkova, S.B., Poluektov, N.S., 1984. Dokl. Acad. Nauk SSSR (Engl. Transl.) **279**, 404.

Rusakova, N.V., Meshkova, S.B., Venchikov, V.Y., Pyatosin, V.E., Tsvirko, M.P., 1992a. J. Appl. Spectrosc. (Engl. Transl.) **56**, 488.

Rusakova, N.V., Topilova, Z.M., Meshkova, S.B., Lozinskii, M.O., Gevaza, Y.I., 1992b. Russ. J. Inorg. Chem. (Engl. Transl.) **37**, 63.

Rusakova, N.V., Korovin, Y.V., Zhilina, Z.I., Vodzinskii, S.V., Ishkov, Y.V., 2004a. J. Appl. Spectrosc. (Engl. Transl.) **71**, 506.

Rusakova, N.V., Popkov, Yu.A., Dotsenko, V.P., 2004b. J. Appl. Spectrosc. (Engl. Transl.) **69**, 841.

Rusakova, N.V., Pavlovsky, V.I., Kulikov, O.V., Andronati, S.A., Korovin, Y.V., Kost, S.S., 2005. Russ. J. Inorg. Chem. (Engl. Transl.) **50**, 1516.

Ryo, M., Wada, Y., Okubo, T., Nakazawa, T., Hasegawa, Y., Yanagida, S., 2002. J. Mater. Chem. **12**, 1748.

Ryo, M., Wada, Y., Okubo, T., Hasegawa, Y., Yanagida, S., 2003. J. Phys. Chem. B **107**, 11302.

Ryo, M., Wada, Y., Okubo, T., Yanagida, S., 2004. Res. Chem. Intermed. **30**, 191.

Sa Ferreira, R.A., Carlos, L.D., de Zea Bermudez, V., Molina, C., Dahmouche, K., Messaddeq, Y., Ribeiro, S.J.L., 2003. J. Sol–Gel Technol. **26**, 315.

Sa Ferreira, R.A., Karmaoui, M., Nobre, S.S., Carlos, L.D., Pinna, N., 2006. ChemPhysChem **7**, 2215.

Sambrook, M.R., Curiel, D., Hayes, E.J., Beer, P.D., Pope, S.J.A., Faulkner, S., 2006. New J. Chem. **30**, 1133.

Samelson, H., Lempicki, A., 1968. J. Appl. Phys. **39**, 6115.

Samelson, H., Lempicki, A., Brophy, V., 1968a. J. Appl. Phys. **39**, 4029.

Samelson, H., Lempicki, A., Brophy, V.A., 1968b. IEEE J. Quantum Electron. **4**, 849.

Sanada, T., Suzuki, T., Kaizaki, S., 1998a. J. Chem. Soc., Dalton Trans., 959.

Sanada, T., Suzuki, T., Yoshida, T., Kaizaki, S., 1998b. Inorg. Chem. **37**, 4712.

Sastri, V.S., Bünzli, J.-C.G., Rao, V.R., Rayudu, G.V.S., Perumareddi, J.R., 2003. Modern Aspects of Rare Earths and Complexes. Elsevier B.V., Amsterdam.

Saudan, C., Ceroni, P., Vicinelli, V., Maestri, M., Balzani, V., Gorka, M., Lee, S.K., van Heyst, J., Vögtle, F., 2004. Dalton Trans., 1597.

Schanze, K.S., Reynolds, J.R., Boncella, J.M., Harrison, B.S., Foley, T.J., Bouguettaya, M., Kang, T.S., 2003. Synth. Met. **137**, 1013.

Schimitscheck, E.J., 1968. J. Appl. Phys. **39**, 6120.

Schwarzenbach, G., 1957. Complexometric Titrations. Chapman & Hall, London.

Seltzer, M.D., 1995. J. Chem. Educ. **72**, 886.

Seltzer, M.D., Fallis, S., Hollins, R.A., Prokopuk, N., Bui, R.N., 2005. J. Fluoresc. **15**, 597.

Senegas, J.-M., Koeller, S., Bernardinelli, G., Piguet, C., 2005. Chem. Commun., 2235.

Shavaleev, N.M., Bell, Z.R., Ward, M.D., 2002. J. Chem. Soc., Dalton Trans., 3925.

Shavaleev, N.M., Moorcraft, L.P., Pope, S.J.A., Bell, Z.R., Faulkner, S., Ward, M.D., 2003a. Chem. Commun., 1134.

Shavaleev, N.M., Moorcraft, L.P., Pope, S.J.A., Bell, Z.R., Faulkner, S., Ward, M.D., 2003b. Chem. Eur. J. **9**, 5283.

Shavaleev, N.M., Pope, S.J.A., Bell, Z.R., Faulkner, S., Ward, M.D., 2003c. Dalton Trans., 808.

Shavaleev, N.M., Accorsi, G., Virgili, D., Bell, Z.R., Lazarides, T., Calogero, G., Armaroli, N., Ward, M.D., 2005. Inorg. Chem. **44**, 61.

Shen, Y.R., Riedener, T., Bray, K.L., 2000. Phys. Rev. B **61**, 11460.

Sherry, A.D., Ren, J., Huskens, J., Brucher, E., Tóth, E., Geraldes, C.F.G.C., Castro, M.M.C.A., Cacheris, W.P., 1996. Inorg. Chem. **35**, 4604.

Shevchuk, S.V., Rusakova, N.V., Turianskaya, A.M., Korovin, Y.V., Nazarenko, N.A., Gren, A.I., Shapiro, Y.E., 1997. Anal. Commun. **34**, 201.

Shevchuk, S.V., Alekseeva, E.A., Rusakova, N.V., Korovin, Y.V., Bacherikov, V.A., Gren, A.I., 1998a. Mendeleev Commun., 112.

Shevchuk, S.V., Rusakova, N.V., Turianskaya, A.M., Korovin, Y.V., Nazarenko, N.A., Gren, A.I., 1998b. J. Fluoresc. **8**, 225.

Shevchuk, S.V., Rusakova, N.V., Turianskaya, A.M., Korovin, Y.V., Nazarenko, N.A., Gren, A.I., 1999. Asian J. Spectrosc. **3**, 155.

Shionoya, S., Yen, W.M., 1999. Principal phosphor materials and their optical properties. In: Shionoya, S., Yen, W.M. (Eds.), Phosphor Handbook. CRC Press Inc., Boca Raton, FL 33431, USA, pp. 177–230 (chapter 3).

Shushkevich, I.K., Dvornikov, S.S., Kachura, T.F., Solov'ev, K.N., 1981. J. Appl. Spectrosc. (Engl. Transl.) **35**, 1109.

Sigoli, F.A., Gonçalves, R.R., Messaddeq, Y., Ribeiro, S.J.L., 2006. J. Non-Cryst. Solids **352**, 5194.

Sivakumar, S., van Veggel, F.C.J.M., Raudsepp, M., 2005. J. Am. Chem. Soc. **127**, 12464.

Slooff, L.H., Polman, A., Wolbers, M.P.O., Van Veggel, F.C.J.M., Reinhoudt, D.N., Hofstraat, J.W., 1998. J. Appl. Phys. **83**, 497.

Slooff, L.H., de Dood, M.J.A., van Blaaderen, A., Polman, A., 2000a. Appl. Phys. Lett. **76**, 3682.

Slooff, L.H., Polman, A., Klink, S.I., Hebbink, G.A., Grave, L., Van Veggel, F.C.J.M., Reinhoudt, D.N., Hofstraat, J.W., 2000b. Opt. Mater. **14**, 101.

Slooff, L.H., Polman, A., Cacialli, F., Friend, R.H., Hebbink, G.A., Van Veggel, F.C.J.M., Reinhoudt, D.N., 2001. Appl. Phys. Lett. **78**, 2122.

Slooff, L.H., van Blaaderen, A., Polman, A., Hebbink, G.A., Klink, S.I., Van Veggel, F.C.J.M., Reinhoudt, D.N., Hofstraat, J.W., 2002. J. Appl. Phys. **91**, 3955.

Snitzer, E., 1961. Phys. Rev. Lett. **7**, 444.

Soler-Illia, G.J.A.A., Innocenzi, P., 2006. Chem. Eur. J. **12**, 4478.

Solovev, K.N., Tsvirko, M.P., Kachura, T.F., 1976. Opt. Spectrosc. (Engl. Transl.) **40**, 391.

Song, J.L., Lei, C., Mao, J.G., 2004. Inorg. Chem. **43**, 5630.

Song, J.L., Mao, J.G., 2005. Chem. Eur. J. **11**, 1417.

Steemers, F.J., Verboom, W., Hofstraat, J.W., Geurts, F.A.J., Reinhoudt, D.N., 1998. Tetrahedron Lett. **39**, 7583.

Steemers, F.J., Verboom, W., Reinhoudt, D.N., Vandertol, E.B., Verhoeven, J.W., 1995. J. Am. Chem. Soc. **117**, 9408.

Stemmler, A.J., Kampf, J.W., Kirk, M.L., Atasi, B.H., Pecoraro, V.L., 1999. Inorg. Chem. **38**, 2807.

Stetter, H., Frank, W., 1976. Angew. Chem. **88**, 760.

Stevenson, S., Rice, G., Glass, T., Harich, K., Cromer, F., Jordan, M.R., Craft, J., Hadju, E., Bible, R., Olmstead, M.M., Maitra, K., Fisher, A.J., Balch, A.L., Dorn, H.C., 1999. Nature **401**, 55.

Stewart, D.R., Gutsche, C.D., 1999. J. Am. Chem. Soc. **121**, 4136.

Stouwdam, J.W., Van Veggel, F.C.J.M., 2002. Nano Lett. **2**, 733.

Stouwdam, J.W., Van Veggel, F.C.J.M., 2004. Chem. Phys. Chem. **5**, 743.

Stouwdam, J.W., Hebbink, G.A., Huskens, J., Van Veggel, F.C.J.M., 2003. Chem. Mater. **15**, 4604.

Stouwdam, J.W., Raudsepp, M., Van Veggel, F.C.J.M., 2005. Langmuir **21**, 7003.

Subhan, M.A., Suzuki, T., Kaizaki, S., 2001. J. Chem. Soc., Dalton Trans., 492.

Subhan, M.A., Suzuki, T., Kaizaki, S., 2002. J. Chem. Soc., Dalton Trans., 1416.

Subhan, M.A., Nakata, H., Suzuki, T., Choi, J.H., Kaizaki, S., 2003. J. Lumin. **101**, 307.

Sudarsan, V., Sivakumar, S., Van Veggel, F.C.J.M., Raudsepp, M., 2005. Chem. Mater. **17**, 4736.

Sun, L.N., Zhang, H.J., Meng, Q.G., Liu, F.Y., Fu, L.S., Peng, C.Y., Yu, J.B., Zheng, G.L., Wang, S.B., 2005. J. Phys. Chem. B **109**, 6174.

Sun, L.N., Zhang, H.J., Peng, C.Y., Yu, J.B., Meng, Q.G., Fu, L.S., Liu, F.Y., Guo, X.M., 2006. J. Phys. Chem. B **110**, 7249.

Sun, R.G., Wang, Y.Z., Zheng, Q.B., Zhang, H.J., Epstein, A.J., 2000. J. Appl. Phys. **87**, 7589.

Supkowski, R.M., deW. Horrocks Jr., W., 2002. Inorg. Chim. Acta **340**, 44.

Supkowski, R.M., Bolender, J.P., Smith, W.D., Reynolds, L.E.L., deW. Horrocks Jr., W., 1999. Coord. Chem. Rev. **186**, 307.

Suzuki, H., 2004. J. Photochem. Photobiol. A Chem. **166**, 155.

Suzuki, H., Hattori, Y., Iizuka, T., Yuzawa, K., Matsumoto, N., 2003. Thin Solid Films **438**, 288.

Suzuki, H., Yokoo, A., Notomi, M., 2004. Polym. Adv. Technol. **15**, 75.

Sveshnikova, E.B., Timofeev, N.T., 1980. Opt. Spektrosk. **48**, 503.

Takada, E., Hosono, Y., Kakuta, T., Yamazaki, M., Takahashi, H., Nakazawa, M., 1998. IEEE Trans. Nucl. Sci. **45**, 556.

Tanabe, S., 2002. Comptes Rendus Chim. **5**, 815.

Tang, C.W., Van Slyke, S.A., 1987. Appl. Phys. Lett. **51**, 913.

Terazzi, E., Suárez, S., Torelli, S., Nozary, H., Imbert, D., Mamula, O., Rivera, J.-P., Guillet, E., Benech, J.-M., Bernardinelli, G., Scopelliti, R., Donnio, B., Guillon, D., Bünzli, J.-C.G., Piguet, C., 2006. Adv. Funct. Mater. **16**, 157.

Topilova, Z.M., Gerasimenko, G.I., Kudryavtseva, L.S., Lozinskii, M.O., Meshkova, S.B., 1989. Russ. J. Inorg. Chem. (Engl. Transl.) **34**, 1265.

Topilova, Z.M., Rusakova, N.V., Meshkova, S.B., Lozinskii, M.O., Kudryavtseva, L.S., Kononenko, L.I., 1991. J. Anal. Chem. USSR (Engl. Transl.) **46**, 618.

Topilova, Z.M., Meshkova, S.B., Bol'shoi, D.V., Lozinskii, M.O., Shapiro, Y.E., 1997. Zh. Neorg. Khim. **42**, 99.

Torelli, S., Imbert, D., Cantuel, M., Bernardinelli, G., Delahaye, S., Hauser, A., Bünzli, J.-C.G., Piguet, C., 2005. Chem. Eur. J. **11**, 3228.

Tröster, T., 2003. Optical studies of non-metallic compounds under pressure. In: Gschneidner Jr., K.A., Bünzli, J.-C.G., Pecharsky, V.K. (Eds.), Handbook on the Physics and Chemistry of Rare Earths, vol. **33**. Elsevier, Amsterdam, pp. 515–589 (chapter 217).

Tsukube, H., Shinoda, S., 2002. Chem. Rev. **102**, 2389.

Tsukube, H., Shinoda, S., 2006. Near infrared emissive lanthanide complexes for anion sensing. ICFE'6 Conference, Wroclaw, September 4–9, 2006, paper AI-5.

Tsukube, H., Onimaru, A., Shinoda, S., 2006. Bull. Chem. Soc. Jpn. **79**, 725.

Tsvirko, M.P., Kachura, T.F., 1975. J. Appl. Spectrosc. (Engl. Transl.) **23**, 907.

Tsvirko, M.P., Stelmakh, G.F., Pyatosin, V.E., Solovyov, K.N., Kachura, T.F., 1980. Chem. Phys. Lett. **73**, 80.

Tsvirko, M.P., Stelmakh, G.F., Pyatosin, V.E., Solovyov, K.N., Kachura, T.F., Piskarskas, A.S., Gadonas, R.A., 1986. Chem. Phys. **106**, 467.

Tsvirko, M.P., Meshkova, S.B., Venchikov, V.Y., Bol'shoi, D.V., 1999. Opt. Spectrosc. (Engl. Transl.) **87**, 866.

Tsvirko, M.P., Meshkova, S.B., Venchikov, V.Y., Topilova, Z.M., Bol'shoi, D.V., 2001. Opt. Spectrosc. (Engl. Transl.) **90**, 669.

Ungaro, R., Pochini, A., Andreetti, G.D., Domiano, P., 1985. J. Chem. Soc., Perkin Trans. **2**, 197.

Van Deun, R., Fias, P., Driesen, K., Binnemans, K., Görller-Walrand, C., 2003a. Phys. Chem. Chem. Phys. **5**, 2754.

Van Deun, R., Moors, D., De Fre, B., Binnemans, K., 2003b. J. Mater. Chem. **13**, 1520.

Van Deun, R., Fias, P., Nockemann, P., Schepers, A., Parac-Vogt, T.N., Van Hecke, K., Van Meervelt, L., Binnemans, K., 2004a. Inorg. Chem. **43**, 8461.

Van Deun, R., Nockemann, P., Görller-Walrand, C., Binnemans, K., 2004b. Chem. Phys. Lett. **397**, 447.

Varaksa, Y.A., Sinitsyn, G.V., Khodasevich, M.A., 2006a. J. Appl. Spectrosc. (Engl. Transl.) **73**, 309.

Varaksa, Y.A., Sinitsyn, G.V., Khodasevich, M.A., 2006b. Opt. Spectrosc. (Engl. Transl.) **100**, 946.

Venchikov, V.Y., Tsvirko, M.P., 2000. J. Appl. Spectrosc. (Engl. Transl.) **67**, 745.

Viana, B., Koslova, N.I., Haschehoug, P., Sanchez, B., 1995. J. Mater. Chem. **5**, 719.

Vicinelli, V., Ceroni, P., Maestri, M., Balzani, V., Gorka, M., Vögtle, F., 2002. J. Am. Chem. Soc. **124**, 6461.

Vigato, P.A., Tamburini, S., 2004. Coord. Chem. Rev. **248**, 1717.

Vögtle, F., Gorka, M., Vicinelli, V., Ceroni, P., Maestri, M., Balzani, V., 2001. Chem. Phys. Chem. **2**, 769.

Voloshin, A.I., Shavaleev, N.M., Kazakov, V.P., 2000a. J. Lumin. **91**, 49.

Voloshin, A.I., Shavaleev, N.M., Kazakov, V.P., 2000b. J. Photochem. Photobiol. A Chem. **131**, 61.

Voloshin, A.I., Shavaleev, N.M., Kazakov, V.P., 2000c. J. Photochem. Photobiol. A Chem. **136**, 203.

Voloshin, A.I., Shavaleev, N.M., Kazakov, V.P., 2000d. J. Photochem. Photobiol. A Chem. **134**, 111.

Voloshin, A.I., Shavaleev, N.M., Kazakov, V.P., 2001a. J. Lumin. **93**, 199.

Voloshin, A.I., Shavaleev, N.M., Kazakov, V.P., 2001b. J. Lumin. **93**, 115.

Wada, Y., Okubo, T., Ryo, M., Nakazawa, T., Hasegawa, Y., Yanagida, S., 2000. J. Am. Chem. Soc. **122**, 8583.

Wang, F., Fan, X.P., Pi, D.B., Wang, M.Q., 2004. J. Solid State Chem. **177**, 3346.

Wang, H., Qian, G., Zhang, J., Luo, Y., Wang, Z., Wang, M., 2005. Thin Solid Films **479**, 216.

Wang, H.S., Qian, G.D., Wang, M.Q., Zhang, J.H., Luo, Y.S., 2004. J. Phys. Chem. B **108**, 8084.

Wang, Q.Y., Zhang, S.Y., Jia, Y.Q., 1993. J. Alloys Compd. **202**, 1.

Wasserscheid, P., Welton, T., 2005. Ionic Liquids in Synthesis. Wiley–VCH, Weinheim.

Weaver, M.S., Lidzey, D.G., Pavier, M.A., Mellor, H., Thorpe, S.L., Bradley, D.D.C., Richardson, T., Searle, T.M., Huang, C.H., Lui, H., Zhou, D., 1996. Synth. Met. **76**, 91.

Weber, J.K.R., Felten, J.J., Cho, B., Nordine, P.C., 1998. Nature **393**, 769.

Weber, M.J., 1967a. Phys. Rev. **157**, 262.

Weber, M.J., 1967b. Phys. Rev. **156**, 231.

Weber, M.J., 1968. Phys. Rev. **171**, 283.

Weissleder, R., 2001. Nat. Biotechnol. **19**, 316.

Weissleder, R., Ntziachristos, V., 2003. Nat. Med. **9**, 123.

Weissleder, R., Tung, C.H., Mahmood, U., Bogdanov, A., 1999. Nat. Biotechnol. **17**, 375.

Weissman, S.I., 1942. J. Chem. Phys. **10**, 214.

Werts, M.H.V., Hofstraat, J.W., Geurts, F.A.J., Verhoeven, J.W., 1997. Chem. Phys. Lett. **276**, 196.

Werts, M.H.V., Verhoeven, J.W., Hofstraat, J.W., 1999a. Appl. Phys. Lett. **74**, 3576.

Werts, M.H.V., Duin, M.A., Hofstraat, J.W., Verhoeven, J.W., 1999b. Chem. Commun., 799.

Werts, M.H.V., Verhoeven, J.W., Hofstraat, J.W., 2000a. J. Chem. Soc., Perkin Trans. **2**, 433.

Werts, M.H.V., Woudenberg, R.H., Emmerink, P.G., van Gassel, R., Hofstraat, J.W., Verhoeven, J.W., 2000b. Angew. Chem. Int. Ed. **39**, 4542.

Werts, M.H.V., Jukes, R.T.F., Verhoeven, J.W., 2002. Phys. Chem. Chem. Phys. **4**, 1542.

Wiener, E.C., Brechbiel, M.W., Brothers, H., Magin, R.L., Gansow, O.A., Tomalia, D.A., Lauterbur, P.C., 1994. Magn. Reson. Med. **31**, 1.

Winkless, L., Tan, R.H.C., Zheng, Y., Motevalli, M., Wyatt, P.B., Gillin, W.P., 2006. Appl. Phys. Lett. 89, Art. 111115, Sept. 11, 2006.

Wolbers, M.P.O., Van Veggel, F.C.J.M., Heeringa, R.H.M., Hofstraat, J.W., Geurts, F.A.J., Vanhummel, G.J., Harkema, S., Reinhoudt, D.N., 1997a. Liebigs Ann. Chem., 2587.

Wolbers, M.P.O., Van Veggel, F.C.J.M., Hofstraat, J.W., Geurts, F.A.J., Reinhoudt, D.N., 1997b. J. Chem. Soc., Perkin Trans. **2**, 2275.

Wolbers, M.P.O., Van Veggel, F.C.J.M., Snellink-Rüel, B.H.M., Hofstraat, J.W., Geurts, F.A.J., Reinhoudt, D.N., 1997c. J. Am. Chem. Soc. **119**, 138.

Wolbers, M.P.O., Van Veggel, F.C.J.M., Peters, F.G.A., Van Beelen, E.S.E., Hofstraat, J.W., Geurts, F.A.J., Reinhoudt, D.N., 1998a. Chem. Eur. J. **4**, 772.

Wolbers, M.P.O., Van Veggel, F.C.J.M., Snellink-Rüel, B.H.M., Hofstraat, J.W., Geurts, F.A.J., Reinhoudt, D.N., 1998b. J. Chem. Soc., Perkin Trans. **2**, 2141.

Wong, C.-P., Venteicher, R.F., deW. Horrocks Jr., W., 1974. J. Am. Chem. Soc. **96**, 7149.

Wong, W.K., Hou, A.X., Guo, J.P., He, H.S., Zhang, L.L., Wong, W.Y., Li, K.F., Cheah, K.W., Xue, F., Mak, T.C.W., 2001. J. Chem. Soc., Dalton Trans., 3092.

Wong, W.K., Liang, H.Z., Wong, W.Y., Cai, Z.W., Li, K.F., Cheah, K.W., 2002. New J. Chem. **26**, 275.

Wong, W.K., Yang, X., Jones, R.A., Rivers, J.H., Lynch, V., Lo, W.K., Xiao, D., Oye, M.M., Holmes, A.L., 2006. Inorg. Chem., 4340.

Wrighton, M.S., Ginley, D.S., Morse, D.L., 1974. J. Phys. Chem. **78**, 2229.

Wu, S.L., deW. Horrocks Jr., W., 1995. Inorg. Chem. **34**, 3724.

Xu, H.-B., Shi, L.-X., Ma, E., Zhang, L.-Y., Wei, Q.-H., Chen, Z.-N., 2006. Chem. Commun., 1601.

Yamamoto, K., Funasaka, H., Takahashi, T., Akasaka, T., Suzuki, T., Maruyama, Y., 1994. J. Phys. Chem. **98**, 12831.

Yanagida, S., Hasegawa, Y., Murakoshi, K., Wada, Y., Nakashima, N., Yamanaka, T., 1998. Coord. Chem. Rev. **171**, 461.

Yanagida, S., Hasegawa, Y., Iwamuro, M., Kawamura, Y., Wada, Y., 2000a. J. Org. Synth. Chem. Jpn. **58**, 945.

Yanagida, S., Hasegawa, Y., Wada, Y., 2000b. J. Lumin. **87–89**, 995.

Yang, J., Yuo, Q., Li, G.D., Cao, J.J., Li, G.H., Chen, J.S., 2006. Inorg. Chem. **45**, 2857.

Yang, L.F., Gong, Z.L., Nie, D.B., Lou, B., Bian, Z.Q., Guan, M., Huang, C.H., Lee, H.J., Baik, W.P., 2006. New J. Chem. **30**, 791.

Yang, X.P., Jones, R.A., Lynch, V., Oye, M.M., Holmes, A.L., 2005. Dalton Trans., 849.

Yang, X.P., Jones, R.A., Oye, M.M., Holmes, A.L., Wong, W.-K., 2006a. Cryst. Growth Des. **6**, 2122.

Yang, X.P., Jones, R.A., Wong, W.K., Lynch, V., Oye, M.M., Holmes, A.L., 2006b. Chem. Commun., 1836.

Yang, X.P., Jones, R.A., Wu, Q.Y., Oye, M.M., Lo, W.K., Wong, W.K., Holmes, A.L., 2006c. Polyhedron **25**, 271.

Yang, Y.T., Driesen, K., Nockemann, P., Van Hecke, K., Van Meervelt, L., Binnemans, K., 2006. Chem. Mater. **18**, 3698.

Zaleski, C.M., Depperman, E.C., Kampf, J.W., Kirk, M.L., Pecoraro, V.L., 2004. Angew. Chem. Int. Ed. **43**, 3912.

Zang, F.X., Hong, Z.R., Li, W.L., Li, M.T., Sun, X.Y., 2004a. Appl. Phys. Lett. **84**, 2679.

Zang, F.X., Li, W.L., Hong, Z.R., Wei, H.Z., Li, M.T., Sun, X.Y., Lee, C.S., 2004b. Appl. Phys. Lett. **84**, 5115.

Zhang, J., Badger, P.D., Greib, S.J., Petoud, S., 2005. Angew. Chem. Int. Ed. **44**, 2508.

Zhang, Q.J., Wang, P., Sun, X.F., Zhai, Y., Dai, P., Yang, B., Hai, M., Xie, J.P., 1998. Appl. Phys. Lett. **72**, 407.

Zhang, X.X., Li, K.F., Cheah, K.W., Zhou, X.J., Tanner, P.A., 2004. Chem. Phys. Lett. **400**, 331.

Zhang, Z.H., Song, Y., Okamura, T., Hasegawa, Y., Sun, W.Y., Ueyama, N., 2006. Inorg. Chem. **45**, 2896.

Zhao, D., Huo, Q., Feng, J., Chmelka, B.F., Stucky, G.D., 1998. J. Am. Chem. Soc. **120**, 6024.

Zhong, Q., Wang, H., Qian, G., Wang, Z., Zhang, J., Qiu, J., Wang, M., 2006. Inorg. Chem. **45**, 4537.

Zhu, X.J., Wong, W.K., Lo, W.K., Wong, W.Y., 2005. Chem. Commun., 1022.

Ziessel, R., Ulrich, G., Charbonnière, L.J., Imbert, D., Scopelliti, R., Bünzli, J.-C.G., 2006. Chem. Eur. J. **12**, 5060.

Zijlmans, H.J.M.A., Bonnet, J., Burton, J., Kardos, K., Vail, T., Niedbala, R.S., Tanke, H.J., 1999. Anal. Biochem. **267**, 30.